MONTANA BUREAU OF MINES AND GEOLOGY
SPECIAL PUBLICATION 96

CONF-8808218--Suppl.

MBMG
1988

DO NOT MICROFILM
COVER

Precambrian and Mesozoic
PLATE MARGINS

DISTRIBUTION OF THIS DOCUMENT IS UNLIMITED

MONTANA COLLEGE OF MINERAL SCIENCE AND TECHNOLOGY
Lindsay Norman, *President*

MONTANA BUREAU OF MINES AND GEOLOGY
Edward T. Ruppel, *Director and State Geologist*

BOARD OF REGENTS
Ex Officio
Ted Schwinden, *Governor*
Carrol Krause, *Commissioner of Higher Education*
Ed Argenbright, *Superintendent of Public Instruction*

Appointed
Dennis E. Lind, Chairman, *Missoula*
Burt Hurwitz, *White Sulphur Springs*
Scott Birkenbuel, Student Regent, *Bozeman*
William L. Mathers, *Miles City*
Beatrice C. McCarthy, *Anaconda*
Jim Caze, *Havre*
Elsie Redlin, *Lambert*

BUREAU STAFF

Butte Office

*David D. Alt, *Geologist*
Mervin J. Bartholomew, *Chief, Geology and Mineral Resources Division*
Richard B. Berg, *Economic Geologist*
Robert N. Bergantino, *Hydrogeologist*
Sharon M. Burt, *Editorial Assistant*
Robert Dal Porto, *Drafter II*
Janet Deutsch, *Administrative Aide II*
Terence E. Duaime, *Hydrogeologist*
John Dunstan, *Chief, Administrative Division*
Carole Durkin, *Accounting Technician II*
Wanda Hislop, *Accounting Technician I*
Roger Holmes, *Cartographic Supervisor*
*Donald W. Hyndman, *Geologist*
H. L. James, *Geologist/Editor*
Gayle LaBlanc, *Chemist II*
Sharon E. Lewis, *Geologist*
Robin McCulloch, *Staff Field Agent*
Betty McManus, *Administrative Aide II*
Marvin R. Miller, *Chief, Hydrology Division*
Herman R. Moore, *Hydrologist II*
*Diane D. Nugent, *Graphics Technician II*
Wayne Olmstead, *Acting Chief, Analytical Division*
Thomas W. Patton, *Hydrogeologist*
Judy St. Onge, *Sales Clerk I*
Fred A. Schmidt, *Hydrogeologist*
Brenda C. Sholes, *Data Base Technician*
Mark A. Sholes, *Coal Geologist*
John L. Sonderegger, *Hydrogeologist*
Michael C. Stickney, *Director, Earthquake Studies Office*
Colleen Strizic, *Adminstrative Secretary I*
Mayrose E. Tompkins, *Administrative Aide I*
Susan M. Vuke-Foster, *Geologist*
*Lester Zeihen, *Adjunct Curator, Mineral Museum*

Billings Office

Teresa Donato, *Administrative Aide I*
Joseph J. Donovan, *Hydrogeologist*
Joseph Lalley, *Research Assistant II*
Jon C. Reiten, *Hydrogeologist*
Wayne A. Van Voast, *Senior Hydrogeologist*

*Adjunct and part-time.

First printing, 1988

Published by authority of State of Montana, Class II State Contract
Printed by Advanced Litho Printing, Great Falls, July 1988

Available from Montana Bureau of Mines and Geology, Main Hall,
Montana College of Mineral Science and Technology, Butte, Montana 59701

DISCLAIMER

This report was prepared as an account of work sponsored by an agency of the United States Government. Neither the United States Government nor any agency thereof, nor any of their employees, makes any warranty, express or implied, or assumes any legal liability or responsibility for the accuracy, completeness, or usefulness of any information, apparatus, product, or process disclosed, or represents that its use would not infringe privately owned rights. Reference herein to any specific commercial product, process, or service by trade name, trademark, manufacturer, or otherwise does not necessarily constitute or imply its endorsement, recommendation, or favoring by the United States Government or any agency thereof. The views and opinions of authors expressed herein do not necessarily state or reflect those of the United States Government or any agency thereof.

DISCLAIMER

Portions of this document may be illegible in electronic image products. Images are produced from the best available original document.

Special Publication 96

MONTANA COLLEGE OF MINERAL SCIENCE & TECHNOLOGY

De Re Metallica

DOE/ER/13962--1

DE90 002940

Precambrian and Mesozoic PLATE MARGINS: Montana, Idaho and Wyoming *with field guides* for the 8th International Conference on Basement Tectonics

August 8-12, 1988

Sharon E. Lewis
Richard B. Berg

Technical Editors

mineral and ground-water research
MBMG
•Butte
......since 1919

OBES-DOE

ARCO

1988

MASTER

DISTRIBUTION OF THIS DOCUMENT IS UNLIMITED

Contents

Preface iv

Articles

Geology of the Stillwater Complex, Montana: An overview .... *I. S. McCallum* 1

Age and Composition of a Late Archean magmatic complex, Beartooth Mountains, Montana-Wyoming .... *Paul A. Mueller, Robert D. Shuster, Michael A. Graves, Joseph L. Wooden and Donald R. Bowes* 7

A Review of the geochemistry and geochronology of Archean rocks of the Beartooth Mountains, Montana and Wyoming .... *Joseph L. Wooden, Paul A. Mueller, David W. Mogk and Donald R. Bowes* 23

Archean allocthonous units in the northern and western Beartooth Mountains, Montana .... *David W. Mogk* 43

Geochronologic and isotopic studies in the Yankee Jim and Lamar Canyon areas, Montana and Wyoming .... *R. E. Guy and A. K. Sinha* 53

Late Archean thin-skinned thrusting of the Cherry Creek metamorphic suite in the Henrys Lake Mountains, southern Madison Range, Montana and Idaho .... *Wendolyn Sumner and Eric A. Erslev* 69

An Early Proterozoic gneiss dome in the Highland Mountains, southwestern Montana .... *J. Michael O'Neill, Mack S. Duncan and Robert E. Zartman* 81

Sedimentation and tectonic setting of the Middle Proterozoic LaHood Formation, Belt Supergroup, southwestern Montana .... *James G. Schmidt* 89

The northern Idaho batholith and associated high-grade metamorphic rocks ... *Donald W. Hyndman and David A. Foster* 97

The Salmon River suture, western Idaho: An island arc-continent boundary .. *Karen Lund* 103

Geology of The Iron Dyke mine, Baker County, Oregon .... *Steven Bussey* 111

Field guides

An overview of some of the Precambrian crystalline rocks of southwestern Montana and northwestern Wyoming

Field guide to the Mountain View and West Fork areas, Stillwater Complex, Montana .... *I. S. McCallum* 121

Field guide to an Archean transect, eastern Beartooth Mountains, Montana-Wyoming .... *Paul A. Mueller and Joseph L. Wooden* 131

Field guide to pre-Beltian geology of the southern Madison and Gravelly ranges, southwest Montana .... *Eric A. Erslev* 141

Field guide to the Highland Mountains, southwest Montana .... *J. Michael O'Neill* 151

Field guide to mesoscopic features in the LaHood Formation, Jefferson Canyon area, southwest Montana .... *Sharon E. Lewis* 155

An overview from the continent into the Mesozoic suture zone, central Idaho and northeastern Oregon

Field guide to a section through the northern Idaho batholith and surrounding high-grade metamorphic rocks . . . . *Donald W. Hyndman and David A. Foster* 159

Field guide to deformation and sense of displacement in mylonitic rocks near Orofino, Idaho . . . . *Luther M. Strayer, IV* 165

Field guide to variations in lithologies and deformation styles of metamorphic and plutonic rocks west of Orofino, Idaho . . . . *Gary F. Davidson* 171

Field guide to a traverse (Slate Creek) across the Salmon River suture zone, west-central Idaho . . . . *Karen Lund* 175

Field guide to a transect across an island arc-continent boundary in west-central Idaho . . . . *Elaine A. Aliberti and Cathryn Allen Manduca* 181

Field guide to the Iron Dyke mine, Baker County Oregon . . . . *Steven Bussey* 191

Appendix

Access road logs to field guides 193

Pen sketches
by
Diane Nugent

DISCLAIMER

This report was prepared as an account of work sponsored by an agency of the United States Government. Neither the United States Government nor any agency thereof, nor any of their employees, makes any warranty, express or implied, or assumes any legal liability or responsibility for the accuracy, completeness, or usefulness of any information, apparatus, product, or process disclosed, or represents that its use would not infringe privately owned rights. Reference herein to any specific commercial product, process, or service by trade name, trademark, manufacturer, or otherwise does not necessarily constitute or imply its endorsement, recommendation, or favoring by the United States Government or any agency thereof. The views and opinions of authors expressed herein do not necessarily state or reflect those of the United States Government or any agency thereof.

Front cover
Beartooth Mountains
by
H. L. James, MBMG

Twin Lakes area. Cirque basin and glacial lakes carved in Precambrian Long Lake granite. View is to the northeast from Beartooth Plateau (Wyoming) across canyon of Rock Creek to Hellroaring Plateau (Montana).

Preface

Two field trips held in conjunction with the 8th International Conference on Basement Tectonics are the *raison d'etre* for this volume, which would perhaps otherwise seem an eclectic association. The unifying theme is an investigation of the nature of plate margins in time and space, consonant with the main theme of the conference, *Characterization and Comparison of Precambrian Through Mesozoic Continental Margins*. Papers presented at the conference will be published in a separate volume by the International Basement Tectonics Association, Inc.

The first field trip is at least a preliminary attempt at an overview of the Precambrian (predominantly Archean) crystalline basement of southwestern Montana. A number of interesting investigations have been focused on this region in recent years. Thus, papers in the first part of this volume take the reader from the Stillwater Complex across the Beartooth Plateau, to the northern borders of Yellowstone National Park, on to the southern Madison Range, and finally to some of the westernmost (probable) Archean exposures in the Highland Mountains south of Butte.

Moving considerably forward on the geologic time scale, the other broad topic dealt with in a second field trip and complementary articles is a relatively recent collisional terrane in central Idaho and eastern Oregon. Examined are portions of the Idaho batholith and its enigmatic and fascinating marginal rocks, and to the west, the heart of the suture zone itself in the Wallowa-Seven Devils terrane with its group of exotic intrusive, metavolcanic, and metasedimentary rocks.

Sharon E. Lewis
Richard B. Berg

Butte
May 2, 1988

GEOLOGY OF THE STILLWATER COMPLEX, MONTANA: AN OVERVIEW

I. S. McCallum
Department of Geological Sciences
University of Washington
Seattle, Washington 98195

Introduction

The Stillwater Complex, a stratiform layered mafic/ultramafic intrusion, crops out along the northern margin of the Beartooth Mountains of southern Montana. The complex, which has a crystallization age of 2.7 Ga (DePaolo and Wasserburg, 1979), extends for 48 kilometers along the Beartooth front and has a maximum exposed thickness of ~6 kilometers in the Contact Mountain area (**Figure 1**). The strike of the layering is approximately N 70° W with a steep, but variable, dip towards the northeast. The original size and shape of the complex are unknown, although there is geophysical and geological evidence that the exposed portion represents the upturned edge of a large saucer-shaped intrusion that extends to the north beneath the Paleozoic sediments. A Proterozoic (1.8-1.6 Ga) low grade, regional metamorphism has resulted in the localized development of greenschist facies mineral assemblages in the complex.

In the western part of the map area, between the Boulder and the East Boulder rivers, the complex is intrusive into Archean metasedimentary rocks along its lower contact, while between the East Boulder River and the West Fork of the Stillwater River, the complex is in fault contact with these same metasediments. Thermal metamorphism by the intrusion has converted the metasediments to cordierite-pyroxene hornfels in the inner zone of the contact aureole and to cordierite-anthophyllite hornfels in the outer zone. In the section exposed between the West

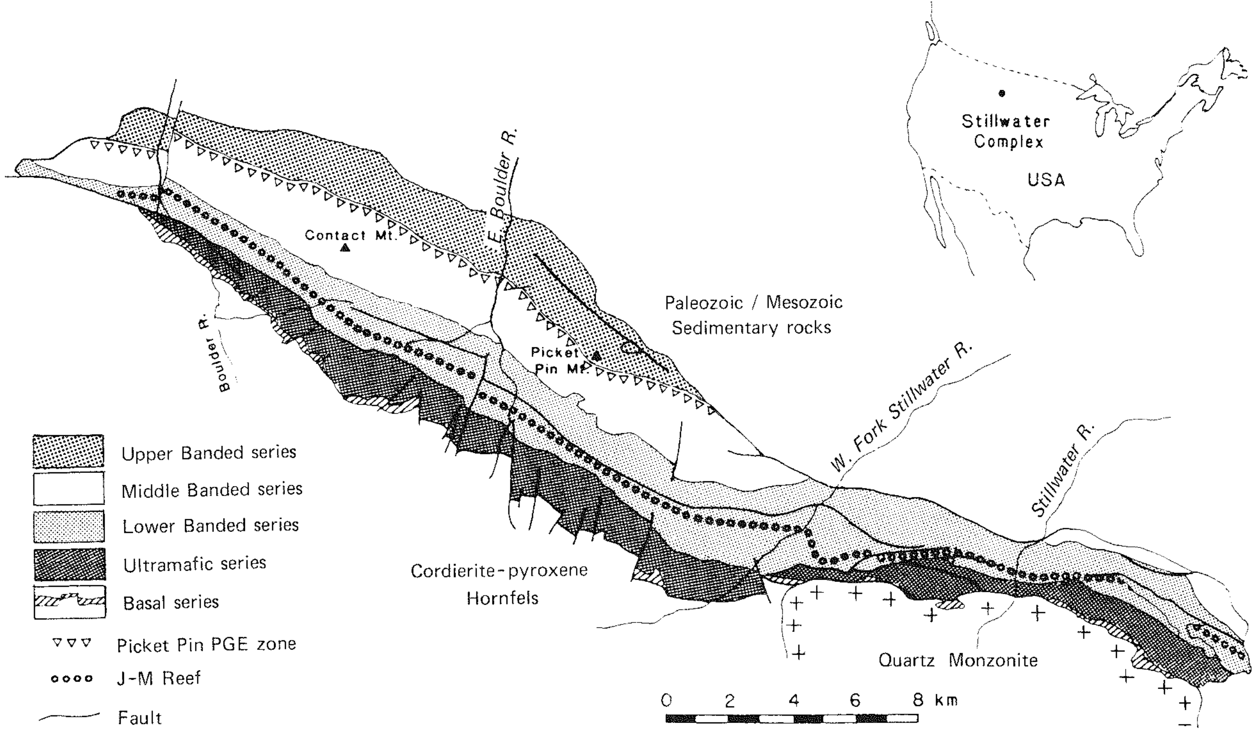
Stillwater Complex
USA
Contact Mt.
E. Boulder R.
Boulder R.
Picket Pin Mt.
Paleozoic / Mesozoic Sedimentary rocks
W. Fork Stillwater R.
Stillwater R.
Upper Banded series
Middle Banded series
Lower Banded series
Ultramafic series
Basal series
▽▽▽ Picket Pin PGE zone
oooo J-M Reef
Fault
Cordierite-pyroxene Hornfels
Quartz Monzonite
0 2 4 6 8 km

Figure 1—Generalized map of the Stillwater Complex showing major subdivisions and the location of mineralized zones (*after* Boudreau and McCallum, 1986).

Fork and the Stillwater River, the lower contact is a low-angle fault (the Bluebird thrust) along which Archean gneisses and quartz monzonites have been thrust over the complex during Laramide deformation. In the Mountain View area, located on the west side of the Stillwater River canyon, part of the original intrusive contact is preserved in a rotated block between the Bluebird thrust and the Lake fault. Between the Stillwater River and Fishtail Creek, quartz monzonite is intrusive into the lower part of the complex. The quartz monzonite has also been dated at 2.7 Ga (Nunes and Tilton, 1971) although it is clearly younger than the Stillwater Complex. The upper part of the complex is unconformably overlain by Paleozoic and Mesozoic sedimentary rocks on the west and is in fault contact with these same sedimentary rocks in the east.

The Stillwater Complex has attracted the attention of geologists and prospectors for over a century, not only because of the superb exposures of magmatic structures and textures but also because it is a major repository of magmatic ore deposits. The complex contains large reserves of chromite (~80% of the known reserves in the United States) in the Ultramafic series rocks, significant deposits of Cu/Ni sulfides in the Basal series rocks and underlying hornfelses, and a laterally extensive zone of platinum group element (PGE) mineralization (the J-M/Howland Reef) in the Lower Banded series. Platinum-bearing rocks are presently being mined from the reef along the west side of the Stillwater River valley. As might be anticipated, there is a very large amount of published information on the geology and mining/exploration activities in the complex; a comprehensive bibliography has been compiled by Bennett (1985). Extensive work has been carried out by geologists of the U.S. Geological Survey, Princeton University, University of Washington, and mining and exploration companies, particularly Anaconda and Johns-Manville. In 1985 an excellent guide to the Stillwater Complex was compiled by Gerald Czamanske and Michael Zientek of the U.S. Geological Survey and published by the Montana Bureau of Mines and Geology as Special Publication 92. Anyone interested in more detailed descriptions and additional field trips should consult this volume. A field trip guide (McCallum, this volume) is based in large part on the material published in Special Publication 92.

In this article, the terminology used to describe cumulate rocks is basically that recommended by Irvine (1982). The stratigraphic subdivisions of the complex used are those proposed by McCallum and others (1980) and Raedeke and McCallum (1984) with modifications proposed by Zientek and others (1985).

Stratigraphic units

The major subdivisions of the Stillwater Complex are the Basal series, the Ultramafic series, and the Lower, Middle and Upper Banded series (**Figure 2**). These have been further divided into a number of zones (**Figure 2**) and subzones.

Basal series and associated rocks

The Basal series comprises that part of the intrusion below the horizon where olivine appears as a major cumulus mineral. The series, locally more than 100 meters in thickness, is composed of a lower zone of heterogeneous norite plus a variety of multiphase "cumulates" containing variable amounts of orthopyroxene, plagioclase, augite and olivine. Individual members are of limited lateral extent. The upper zone of the basal series is a relatively uniform bronzitite cumulate. Ni/Cu sulfides are distributed throughout the Basal series, but, in general, decrease in abundance from the bottom to the top. Hornfels xenoliths are locally common.

Closely associated with the Basal series rocks is a suite of coeval sills and dikes that are particularly well developed in the eastern part of the intrusion (Zientek, 1983). The bulk of these fall into two compositional groups, diabase and mafic norite. The mafic norites are believed to be closely related to the parental magmas that produced the cumulates of the Ultramafic series. Massive sulfides are commonly associated with the mafic norite suite.

The country rock adjacent to the complex is dominantly composed of quartz-bearing and quartz-free cordierite-pyroxene hornfels, with lesser amounts of metamorphosed iron formation and quartzite. Mineral assemblages in the hornfels and iron-formation indicate temperatures up to 825° C and pressures of 3-4 kilobars during the peak of contact metamorphism (Labotka, 1985). The latter value provides the most reliable constraint on the depth of emplacement of the initial batches of Stillwater magma. The most extensive exposures of hornfels occur in the western region where a triangular wedge extends from the base of the complex to the Mill Creek-Stillwater fault zone, a maximum width of 10 kilometers.

Ultramafic series

The base of the Ultramafic series (UMS) is marked by the first appearance of significant amounts of cumulus olivine. This series is subdivided into a lower Peridotite zone containing olivine ± orthopyroxene ± chromite cumulates, and an upper Bronzitite zone. The Peridotite zone is made up of a variable number of cyclic units, a complete cycle being olivine cumulate (oC), overlain by olivine-bronzite

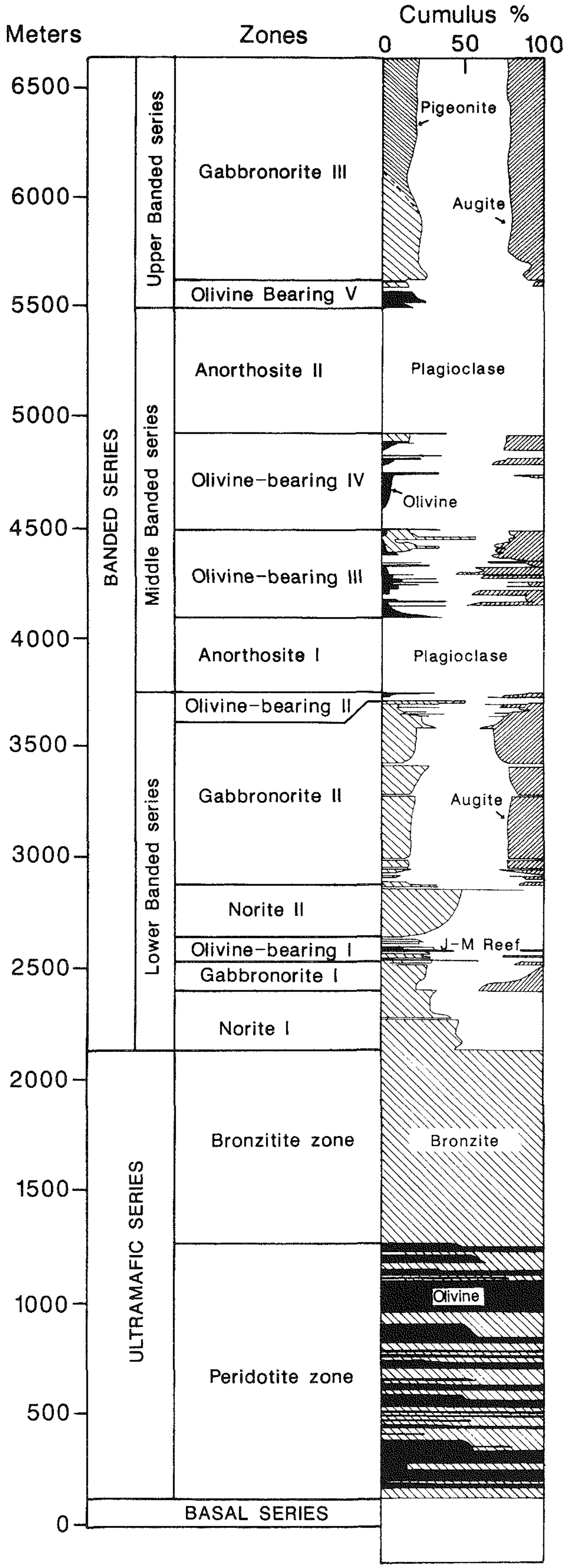
Meters
Zones
Cumulus %
0
50
100
6500
6000
5500
5000
4500
4000
3500
3000
2500
2000
1500
1000
500
0
BANDED SERIES
Upper Banded series
Middle Banded series
Lower Banded series
ULTRAMAFIC SERIES
Gabbronorite III
Olivine Bearing V
Anorthosite II
Olivine-bearing IV
Olivine-bearing III
Anorthosite I
Olivine-bearing II
Gabbronorite II
Norite II
Olivine-bearing I
Gabbronorite I
Norite I
Bronzitite zone
Peridotite zone
BASAL SERIES
Pigeonite
Augite
Plagioclase
Olivine
Plagioclase
Augite
J-M Reef
Bronzite
Olivine

Figure 2—Section through the Stillwater Complex showing the major zones and the modal abundances of cumulus minerals within zones. The Ultramafic series section is from the Mountain View area (*after* Raedeke and McCallum, 1984) and the Banded series section is from the Contact Mountain area (*after* McCallum and others, 1980).

cumulate (obC), in turn overlain by bronzite cumulate (bC). Olivine-chromite cumulate (ocC) occurs as layers within olivine cumulate. Incomplete cyclic units, in which one or more of the three members is missing, are fairly common. In a published model (Raedeke and McCallum, 1984), it was postulated that each cycle marked the influx of a batch of primitive, olivine-saturated magma into a chamber containing a liquid undergoing fractionation. Injection was followed by accumulation of suspended olivine, mixing between the new and the resident magma, and the reinitiation of fractional crystallization. The multiple injections of primitive magma into the chamber had the effect of buffering the magma composition and preventing extensive fractionation from occurring, as shown by the lack of compositional variation in the cumulus minerals.

A detailed stratigraphic section through the Ultramafic series in the Mountain View area was measured by Raedeke and McCallum (1984) and is shown as **Figure 3**. The left column represents a standard stratigraphic section superimposed on which are the compositions (in terms of Mg/Mg + Fe ratios) of olivines and orthopyroxenes. The right-hand column shows the modal variations of the cumulus minerals and sample locations. Not shown are the modal abundances of postcumulus minerals. Twenty cyclic units are present. In the olivine cumulates (dunites and harzburgites), postcumulus bronzite occurs as oikocrysts enclosing rounded and embayed olivine, clearly indicating a reaction relationship. Postcumulus plagioclase, occurring as interstitial fillings, is present in small amounts (2-10%) along with minor amounts of postcumulus augite and phlogopite, and trace amounts of pargasite and apatite. Chromite is commonly disseminated in the olivine cumulates or may form seams near the base of oC units. Minor amounts of sulfides are concentrated in the chromite-rich layers.

The contact between the olivine cumulates and overlying olivine-bronzite cumulates (granular harzburgite) is marked by an abrupt increase in modal bronzite. However, the textural change across this contact is not always sharp; the habit of bronzite changes from poikilitic to granular over a stratigraphic thickness of a few meters. Textures are complex and varied in the harzburgites. In some rocks both olivine and bronzite show secondary overgrowths to form a granular texture, while in others, olivine may be resorbed or rimmed by a bronzite overgrowth.

Bronzite cumulate (bronzitite), which forms the uppermost member of the cyclic unit, contains significant amounts of postcumulus plagioclase and augite. Bronzite usually shows secondary enlargement but may also show resorption textures against augite indicating some type of reaction relationship with

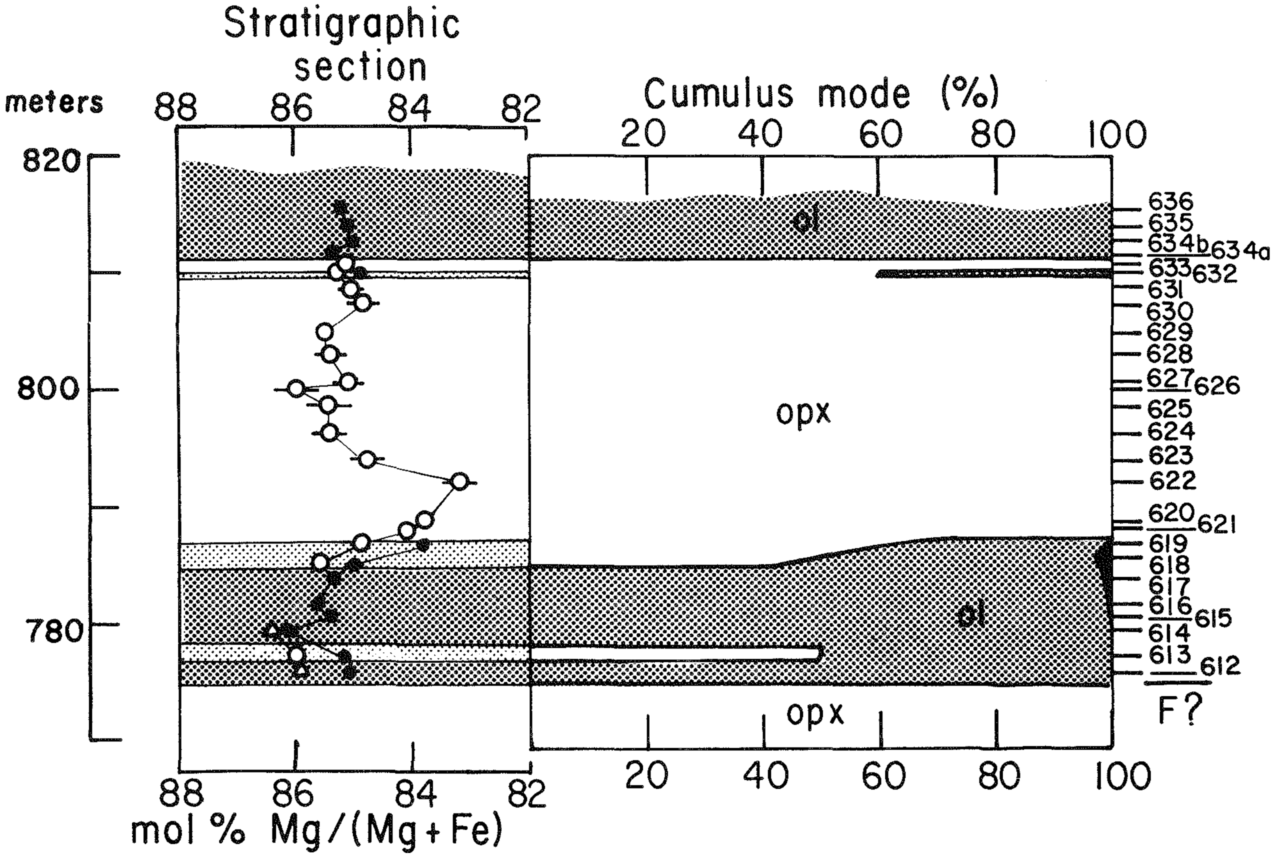

Figure 3—Stratigraphic section through the Ultramafic series in the Mountain View area (*after* Raedeke and McCallum, 1984). The left-hand column shows the stratigraphic distribution of lithologic units. Heavy shading (olivine cumulates), light shading (olivine-bronzite cumulates), no shading (bronzite cumulates). Also plotted are the Mg/Mg+Fe ratios of mafic minerals: open circles—cumulus bronzite; open triangles—postcumulus bronzite; closed circles—cumulus olivine. The right-hand column shows the modal abundances of cumulus minerals as a function of stratigraphic height. Shaded areas (olivine), unshaded (bronzite), black (chromite).

augite. Grain size variations with stratigraphic height are common in otherwise uniform bronzitites. Also, sharp breaks between competent and friable bronzitite occur along conformable contacts.

The upper Bronzitite zone consists almost entirely of bronzite cumulate (bC) with variable amounts of postcumulus plagioclase and augite, the latter forming distinctive emerald-green oikocrysts. As seen in **Figure 3**, there is no evidence of any systematic variation in the composition of cumulus bronzites in this zone.

Fine-scale layering is not conspicuously developed in the Ultramafic series, but it is not uncommon to find abrupt variation in grain size within lithologically homogeneous units. Pegmatitic rocks, which occur sporadically throughout the Ultramafic series, are spectacularly developed in the vicinity of the major chromitite seams. A distinctive rock type, called discordant dunite by Raedeke and McCallum (1984), occurs sporadically throughout the Ultramafic series. It is best developed in the Chrome Mountain and Iron Mountain areas. This unit is a true dunite (>90% olivine) and is associated with pegmatitic bronzitite. It might represent remobilized olivine cumulate or, in our preferred model, secondary dunite formed by the incongruent dissolution of pyroxene in response to the addition of water at supersolidus temperatures. There is a wide variation in the thickness of the Ultramafic series with the thickest exposed section (~2,100 m) occurring in the Mountain View area.

Banded series

The Banded series is made up of a thick sequence (approximately 4,500 meters in the Contact Mountain-Picket Pin area) of plagioclase-rich cumulates. A detailed stratigraphic section showing modal variation in the Contact Mountain area is shown in **Figure 2**. (For additional details of this area, see McCallum and others, 1980.) Plagioclase, orthopyroxene, augite and olivine are the chief cumulus minerals. The same minerals may also occur as postcumulus minerals along with phlogopite (restricted to olivine-bearing rocks), rare pargasite, quartz, apatite, magnetite, ilmenite, chromite and sulfides. This series has been subivided into a Lower Banded series (LBS), a Middle Banded series (MBS), and an Upper Banded series (UBS).

The Lower Banded series is composed dominantly of norite (pbC) and gabbronorite (pbaC) with minor troctolite (poC), peridotite (oC), anorthosite (pC), and bronzitite (bC) members. The olivine-bearing rocks, which are restricted to a zone (OB I) about 400 meters above the base of the series, are the host of the J-M/Howland Reef, a 1 to 3 meter-thick subzone containing disseminated sulfides rich in PGE. The reappearance of olivine as a cumulus mineral at this level in the intrusion is most likely due to the influx of a batch of primitive magma. Spectacular layering structures are developed in the LBS, particularly in the noritic members.

The Middle Banded series is dominantly composed of anorthosite (pC), troctolite (poC), and olivine gabbro (paoC). The crystallization sequence (plagioclase and augite before bronzite) in the MBS differs from that in the rest of the complex (bronzite before plagioclase and augite) leading to the speculation that a magma of significantly different composition might have been involved in the crystallization of the cumulates in the MBS. A sulfide-bearing interval, the Picket Pin deposit, occurs in a thick anorthosite near the top of the MBS. This deposit, known in the field as the "poor man's deposit," contains subeconomic amounts of PGE. This zone is of interest because the sulfide mineralization forms pods and pipes which are clearly transgressive to the layering leading Boudreau and McCallum (1986) to postulate that the sulfides were deposited from supersolidus, internally generated, hydrothermal solutions.

The Upper Banded series is composed of troctolite overlain by a thick sequence of uniform gabbronorite (pbaC) which contains inverted pigeonite in its upper part. The gabbronorites show a well developed igneous lamination and the mineral compositions vary in a manner consistent with fractional crystallization.

Acknowledgement

This work was supported by the National Aeronautics and Space Administration through Grant NAG 9-84.

References

Bennett, P. C., 1985, Stillwater Complex bibliography, *in* The Stillwater Complex, Montana: Geology and guide, G. K. Czamanske and M. L. Zientek, *(eds.)*: Montana Bureau of Mines and Geology Special Publication 92, p. 373-394.

Boudreau, A. E., and McCallum, I. S., 1986, Investigations of the Stillwater Complex, part III, The Picket Pin Pt/Pd deposit: Economic Geology, v. 81, p. 1953-1975.

Czamanske, G. K., and Zientek, M. L., *(eds.)*, 1985, The Stillwater Complex, Montana: Geology and guide: Montana Bureau of Mines and Geology Special Publication 92, 396 p.

DePaolo, D. J., and Wasserburg, G. J., 1979, Sm-Nd age of the Stillwater Complex and the mantle evolution curve for neodymium: Geochimica et Cosmochimica Acta, v. 43, p. 999-1008.

Irvine, T. N., 1982, Terminology for layered intrusions: Journal of Petrology, v. 23, p. 127-162.

Labotka, T. C., 1985, Petrogenesis of the metamorphic rocks beneath the Stillwater Complex: Assemblages and conditions of metamorphism, *in* The Stillwater Complex, Montana: Geology and guide, G. K. Czamanske and M. L. Zientek, *(eds.)*: Montana Bureau of Mines and Geology Special Publication 92, p. 70-76.

McCallum, I. S., Raedeke, L. D., and Mathez, E. A., 1980, Investigations of the Stillwater Complex, part I, Stratigraphy and structure of the Banded zone: American Journal of Science, v. 280A, p. 59-87.

Nunes, P. D., and Tilton, G. R., 1971, Uranium-lead ages of minerals from the Stillwater Igneous Complex and associated rocks, Montana: Geological Society of America Bulletin, v. 82, p. 2231-2249.

Raedeke, L. D., and McCallum, I. S., 1984, Investigations in the Stillwater Complex, part II, Petrology and petrogenesis of the Ultramafic series: Journal of Petrology, v. 25, p. 395-420.

Zientek, M. L., 1983, Petrogenesis of the Basal zone of the Stillwater Complex, Montana [Ph.D. dissertation]: Stanford University, Palo Alto, California, 246 p.

Zientek, M. L., Czamanske, G. K., and Irvine, T. N., 1985, Stratigraphy and nomenclature for the Stillwater Complex, *in* The Stillwater Complex, Montana: Geology and guide, G. K. Czamanske and M. L. Zientek, *(eds.)*: Montana Bureau of Mines and Geology Special Publication 92, p. 21-32.

Rock Creek canyon in the Beartooth Mountains southwest of Red Lodge, Montana. (H. L. James photo.)

AGE AND COMPOSITION OF A LATE ARCHEAN MAGMATIC COMPLEX, BEARTOOTH MOUNTAINS, MONTANA-WYOMING

Paul A. Mueller
Department of Geology
University of Florida
Gainesville, Florida 32611

Robert D. Shuster
Department of Geography and Geology
University of Nebraska-Omaha
Omaha, Nebraska 68182

Michael A. Graves
Department of Geology
University of Florida
Gainesville, Florida 32611

Joseph L. Wooden
U.S. Geological Survey
Menlo Park, California 94025
and
Donald R. Bowes
Department of Geology
University of Glasgow
Glasgow 612 8QQ
Scotland

Introduction

One of the critical aspects of interpreting the Archean rock record in terms of modern tectonic analogs is the resolution of the time frame applicable to the development of Archean rock associations. In the case of magmatic rocks, for example, rock units are often grouped according to their relative degrees of deformation or metamorphism, or their petrologic or geochemical affinities. Without age control, however, groupings of this nature are inadequate for resolving tectonic or orogenic processes. Differences of tens of millions of years yield much different models than differences of hundreds of millions of years. Consequently, high-resolution geochronology is essential to the development of realistic tectonic and petrogenetic models for Archean rock associations. The only geochronologic system that appears capable of consistently providing the necessary resolution is the U-Pb system in zircons (Krogh 1982). Such studies have demonstrated that age resolution of a few million years is possible for Archean rocks.

Geological setting

The Beartooth Mountains of Montana and Wyoming (**Figure 1**) lie within the Archean Wyoming province (Condie 1976; Peterman 1979; Wooden and others, 1988) and contain exposures of more than 5,000 km^2 of Archean rocks. The range lies astride a major Late Archean lithologic discontinuity in the province. To the south and east, Archean exposures are dominantly granitoids in the range of 2500-3000 Ma old (Peterman 1979; Wooden and others, 1988). To the north and west, Archean exposures are domi-

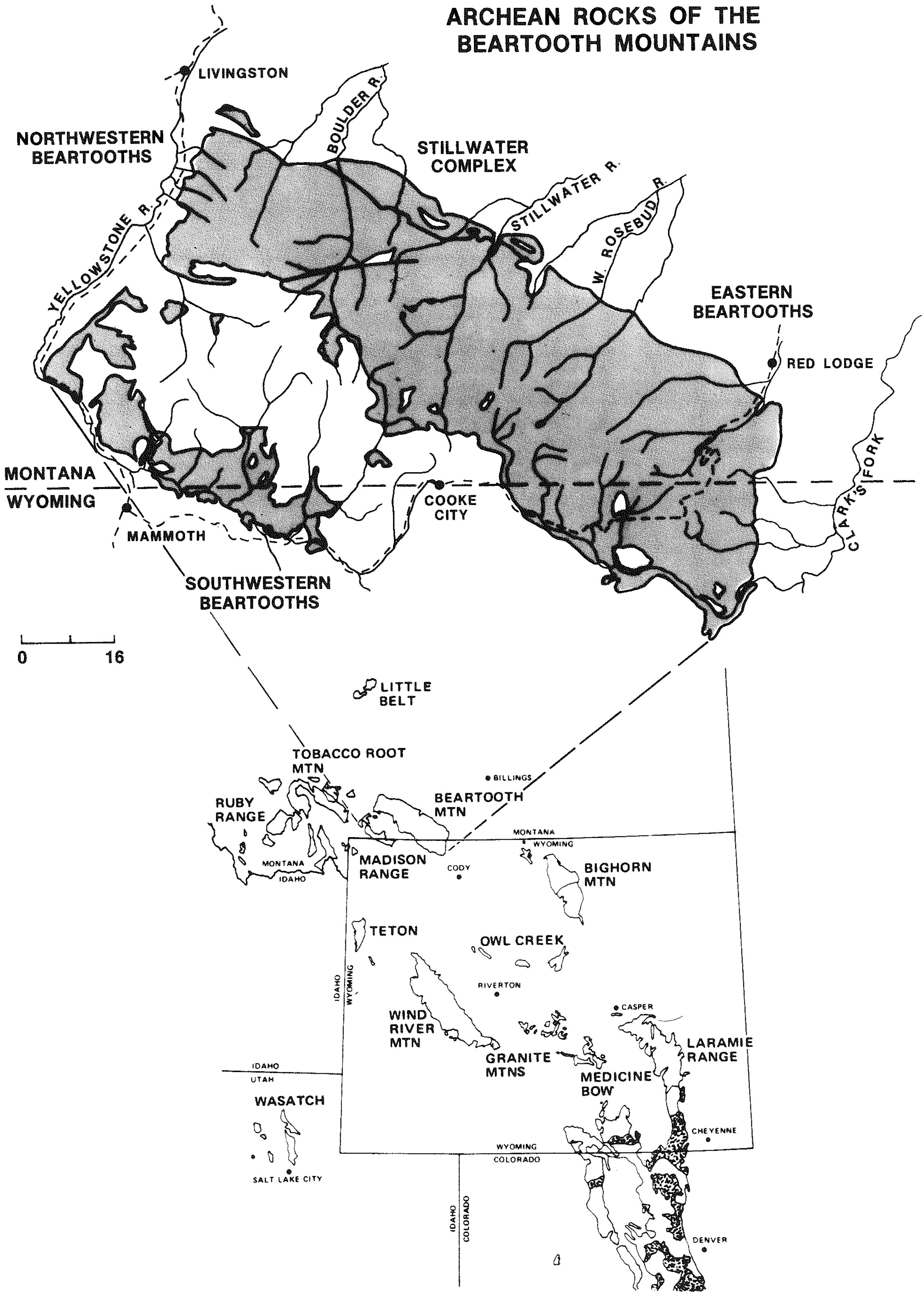
ARCHEAN ROCKS OF THE BEARTOOTH MOUNTAINS
LIVINGSTON
BOULDER R.
NORTHWESTERN BEARTOOTHS
STILLWATER COMPLEX
STILLWATER R.
W. ROSEBUD R.
YELLOWSTONE R.
EASTERN BEARTOOTHS
RED LODGE
CLARK'S FORK
MONTANA
WYOMING
COOKE CITY
MAMMOTH
SOUTHWESTERN BEARTOOTHS
0
16
LITTLE BELT
TOBACCO ROOT MTN
BILLINGS
RUBY RANGE
BEARTOOTH MTN
MONTANA
WYOMING
MONTANA
IDAHO
MADISON RANGE
CODY
BIGHORN MTN
TETON
OWL CREEK
IDAHO
WYOMING
RIVERTON
CASPER
WIND RIVER MTN
LARAMIE RANGE
GRANITE MTNS
MEDICINE BOW
IDAHO
UTAH
WASATCH
CHEYENNE
WYOMING
COLORADO
SALT LAKE CITY
IDAHO
COLORADO
DENVER

Figure 1—Index map showing the Beartooth Mountains and their relation to other major ranges of the Wyoming province.

nated by meta-supracrustal rocks that are primarily sedimentary in origin. Limited geochronologic work in this northwestern area, summarized by James and Hedge (1980), suggests mostly Late Archean ages for this terrane as well. This study represents part of an ongoing investigation into the nature of this lithologic discontinuity and its relation to Late Archean tectonics and crustal evolution (Mogk and others, 1988; Wooden and Mueller, 1988; Mueller and others, 1985).

The Beartooth Mountains can be subdivided into several generally distinct regions which include: 1) the granitoid-dominated areas in the eastern and central Beartooth Mountains, 2) the Stillwater Complex with its metasedimentary contact aureole, 3) the northwestern part of the range containing a gneissic basement overthrust by younger metasedimentary rocks, and 4) the southwestern portion of the range that is underlain primarily by metasedimentary rocks (Figure 1, Casella and others, 1982; Mueller and Wooden, 1982). As summarized in Wooden and others (1982), Warner and others (1982), and Mueller and others (1985), the eastern Beartooth Mountains contain remnants of an older (>3.4 Ga) granulite facies terrane (Henry and others, 1982) that served as the basement upon which a Late Archean sequence of calc-alkaline to sodic plutonic and volcanic rocks was developed. The three major Late Archean rock types recognized in the eastern Beartooth Mountains are a group of amphibolites of andesitic composition (AA), a granodioritic series informally known as the Long Lake granodiorite (LLGd), and a tonalitic to granitic series called the Long Lake granite (LLG). Samples of these units for this study were taken along U.S. Highway 212 between Red Lodge and Cooke City, Montana (Figure 1, Mueller and Wooden, this volume).

Analytical procedures

Zircons were separated by standard hydraulic, heavy liquid and magnetic methods. The separated zircons were washed in warm 7N HNO_3 for no longer than 30 minutes to partially remove pyrite. Samples were further separated according to size and/or magnetic susceptibility utilizing a Franz Isodynamic Magnetic Separator (**Table 1 A, B, C**). All fractions were purified by hand sorting. Zircon fractions were then loaded into teflon dissolution vessels with ultrapure HF and HNO_3 and the bomb assembly was heated for 5 days at 195°C. Samples were then dried, treated with HCl, and returned to the oven for conversion to chlorides. After total dissolution, samples were aliquotted and spiked with a mixed $^{208}Pb/^{235}U$ spike.

Lead and uranium were separated using a modification of the method of Krogh (1973). Mass spectrometry was done on a VG 354 automated mass spectrometer. Lead was loaded in phosphoric acid on a single Re filament with a silica-gel bed. Uranium was also loaded in phosphoric acid on a single Re filament, but was loaded with carbon in order to produce a U+ metal ion beam. Analytical precision is estimated at better than $\pm 0.1\%$ (2σ) for $^{207}Pb/^{206}Pb$ and $^{208}Pb/^{206}Pb$ ratios, ± 1 to 3% (2σ) for $^{206}Pb/^{204}Pb$ ratios, and $\pm 0.5\%$ (2σ) for U/Pb ratios. Decay constants and isotopic abundances used are those recommended by the IUGS Subcommission on Geochronology (Steiger and Jager, 1977). Analytical blanks determined concurrently with samples analyzed during the period of this study decreased from 3 ng to 0.2 ng total Pb as cleaning and separation techniques improved. The isotopic composition of the blank was: $^{204}Pb:^{206}Pb:^{207}Pb:^{208}Pb: = 1:18.67:15.66:38.39$. All lead isotopic data were corrected for 0.05% per amu mass discrimination based upon multiple analyses of SRM 981. The data were reduced and evaluated for uncertainties using the method of Ludwig (1980). Concordia intercepts were determined using the method of Ludwig (1985), which reports all age errors at 2σ. Model I assumes all error is analytical and weights all points according to analytical error. Models II and IV are used for data sets which scatter outside of analytical error and along with Model I use a student's T multiplier which significantly increases the intercept error for small populations. All procedures were performed in the isotope geology laboratory at the University of Florida. All chemical data were produced by standard XRF techniques in the Department of Geology at the University of Glasgow, Scotland.

Petrology and geochemistry

Andesitic amphibolites (AA)

Amphibolites of generally andesitic or dioritic composition are found throughout the eastern and central Beartooth Mountains and appear to be the oldest of three main Late Archean rock types. Field relations may be complex in certain areas (Fred Barker, personal communication, 1988), and the variety of metamorphosed mafic to intermediate rocks makes it impossible to consistently distinguish geo-

Table 1A—Major-and trace-element data for the andesitic amphibolites.

		Weight percent															ppm										
Sample	Type	SiO_2	TiO_2	Al_2O_3	Fe_2O_3	FeO	MnO	MgO	CaO	Na_2O	K_2O	P_2O_5	H_2O	CO_2	Total	Sample	Ba	Rb	Sr	Zr	Ce	Pb	Th	Y	Cr	Ni	Sample
BTR-39	Thol.	55.37	1.27	14.95	4.51	5.53	0.18	3.70	6.49	3.57	1.74	0.55	1.32	0.31	99.49	BTR-39	1571	40	824	229	218	21	22	28	74	47	BTR-39
BTR-43	Thol.	56.63	1.35	14.12	4.48	4.98	0.15		6.38	3.05	2.62	0.73	1.44	0.11	99.25	BTR-43	2455	58	989	217	267	13	17	34	67	25	BTR-43
BTR-37	Thol.	57.42	1.47	14.23	5.13	5.02	0.16	3.22	6.26	3.07	2.43	0.78	1.17	0.14	100.50	BTR-37	1782	60	880	259	288	18	26	36	55	20	BTR-37
BTR-52	Thol.	57.80	1.64	13.92	3.51	5.51	0.20	2.98	5.40	3.47	2.40	0.78	1.20	0.27	99.08	BTR-52	1435	48	718	217	211	14	12	37	51	17	BTR-52
BTR-51	Thol.	58.16	1.70	14.66	2.99	5.54	0.18	3.05	5.32	3.53	2.30	0.77	1.77	0.22	100.19	BTR-51	1490	40	728	204	198	17	13	33	47	16	BTR-51
BTR-27	Trans.	54.87	0.78	15.64	2.99	4.95	0.12	5.21	7.45	3.68	2.03	0.33	1.36	0.07	99.48	BTR-27	855	60	791	179	118	20	18	16	138	74	BTR-27
BTR-26	Trans.	55.10	0.73	16.18	3.18	4.75	0.11	4.58	7.78	3.25	1.93	0.29	1.46	0.43	99.77	BTR-26	949	57	766	104	127	16	24	16	84	47	BTR-26
BTR-25	Trans.	55.77	0.88	15.37	2.61	6.17	0.13	4.50	7.14	3.48	1.31	0.30	1.54	0.22	99.42	BTR-25	629	50	482	150	95	12	8	23	117	55	BTR-25
BTR-34	Trans.	56.11	0.84	15.07	3.78	5.22	0.16	4.85	6.77	3.46	1.55	0.39	0.88	0.10	99.18	BTR-34	491	76	431	156	91	28	11	21	140	40	BTR-34
BTR-38	Trans.	57.25	0.95	15.58	2.99	5.13	0.11	4.01	6.60	4.42	1.22	0.37	1.27	0.16	100.06	BTR-38	1066	32	522	240	133	16	11	29	96	43	BTR-38
BTR-154	CA	54.37	0.45	17.12	2.48	4.68	0.14	5.82	8.20	3.54	1.01	0.06	1.43	0.20	99.50	BTR-154	405	18	545	87	30	9	3	13	139	62	BTR-154
BTR-69	CA	55.38	0.69	14.86	2.64	5.01	0.16	6.85	6.10	3.20	2.30	0.24	2.17	0.28	99.88	BTR-69	575	90	346	127	92	9	2	26	250	78	BTR-69
BTR-91	CA	55.53	0.65	16.43	2.83	5.49	0.16	5.30	5.20	4.42	2.00	0.16	2.19	0.16	100.52	BTR-91	330	83	304	87	45	7	7	12	81	40	BTR-91
HT-6	CA	55.58	0.56	17.50	2.63	4.71	0.15	4.88	7.53	4.18	1.38	0.21	0.96	0.22	100.49	HT-6	619	56	554	129	101	13	5	23	140	58	HT-6
BTR-70	CA	55.66	0.63	16.18	2.80	4.93	0.13	5.00	7.05	3.43	1.47	0.18	2.13	0.17	99.76	BTR-70	505	51	468	6	55	6	7	10	130	52	BTR-70
BTR-163	CA	56.50	0.17	18.25	1.01	3.91	0.10	7.46	7.58	3.08	1.00	0.03	1.25	0.14	100.48	BTR-163	204	38	376	53	31	10	8	6	247	124	BTR-163
BTR-56	CA	57.92	1.13	15.37	2.63	5.33	0.16	4.07	5.70	3.60	2.20	0.50	1.04	0.17	99.82	BTR-56	1020	59	557	243	151	7	8	29	115	53	BTR-56
BTR-151	CA	57.98	0.61	17.27	2.41	4.51	0.11	3.56	6.82	4.07	1.07	0.17	1.05	0.30	99.93	BTR-151	580	22	600	195	63	6	2	16	45	28	BTR-151
BTR-158	CA	58.79	0.34	18.59	3.16	4.12	0.09	2.74	6.46	4.53	0.89	0.09	0.92	0.09	100.81	BTR-158	203	17	378	48	28	11	1	37	17	8	BTR-158
HT-7	CA	58.90	0.50	17.55	2.22	3.66	0.11	3.78	6.62	4.06	1.36	0.17	0.82	0.18	99.93	HT-7	638	54	569	98	77	13	3	13	97	44	HT-7
BTR-68	CA	59.32	0.84	15.38	2.40	4.41	0.13	3.93	5.20	3.67	1.82	0.52	1.28	0.23	99.13	BTR-68	810	62	522	80	180	12	11	41	127	50	BTR-68
HT-12	CA	59.68	0.79	15.42	2.61	4.79	0.14	3.97	5.89	3.53	1.54	0.26	1.03	0.21	99.86	HT-12	845	79	541	146	83	11	6	22	126	52	HT-12
BTR-36	CA	59.72	0.42	14.62	1.49	4.29	0.11	6.59	5.96	3.63	1.85	0.05	1.59	0.24	100.56	BTR-36	255	79	204	60	39	21	6	16	256	117	BTR-36
BTR-4	CA	61.48	0.33	15.39	0.98	4.32	0.09	4.91	5.80	3.79	0.97	0.03	1.17	1.22	100.48	BTR-4	199	24	277	100	29	14	4	18	92	55	BTR-4

Table 1B—Major-and trace-element data for the Long Lake granodiorite.

	Weight percent														ppm								
Sample	SiO_2	TiO_2	Al_2O_3	Fe_2O_3	FeO	MnO	MgO	CaO	Na_2O	K_2O	P_2O_5	H_2O	CO_2	Total	Ba	Rb	Sr	Zr	Ce	Pb	Th	Y	Sample
BTR-7	67.70	0.56	15.83	1.30	2.64	0.06	1.48	3.30	4.00	2.68	0.20	0.72	0.12	100.59	1087	140	228	196	118	23	29	13	BTR-7
BTR-15	66.35	0.54	17.08	0.61	2.39	0.03	1.42	4.09	4.07	1.64	0.16	1.51	0.05	99.94	1262	68	305	354	148	26	50	8	BTR-15
BTR-28	70.46	0.53	13.90	2.03	1.58	0.03	0.92	1.80	3.57	4.56	0.13	0.79	0.13	100.43	3699	117	313	367	395	28	50	43	BTR-28
BTR-32	67.71	0.76	13.57	2.63	2.68	0.06	1.33	3.18	4.06	2.41	0.35	0.58	0.03	99.35	1189	93	361	310	150	25	16	17	BTR-32
BTR-35	69.43	0.80	13.61	2.67	2.00	0.06	1.07	3.06	3.44	3.34	0.31	0.93	0.26	100.98	2464	101	458	301	203	21	20	69	BTR-35
WRS71/40	67.23	0.62	15.64	0.93	2.79	0.06	2.88	1.50	4.57	1.86	0.25	1.68	0.05	100.06	900	90	205	320	250	-	-	-	WRS71/40
WRS71/45	69.39	0.61	14.52	1.84	1.77	0.06	1.15	2.44	3.10	3.75	0.22	0.60	0.06	99.51	1620	215	360	290	150	-	-	-	WRS71/45
WRS71/17	63.33	0.90	15.08	2.94	3.65	0.11	2.30	4.25	3.42	2.60	0.46	0.88	0.15	100.07	1530	55	570	260	180	-	-	-	WRS71/17
WRS71/66	65.47	0.83	15.69	1.81	2.46	0.08	1.58	2.86	3.33	4.17	0.29	1.17	0.16	99.90	2470	95	490	350	200	-	-	-	WRS71/66
WRS70/5	68.46	0.82	15.05	1.41	2.32	0.08	1.35	3.07	3.30	3.59	0.21	0.28	0.00	99.94	1940	197	460	305	215	-	-	-	WRS70/5
WRS70/7	65.99	0.82	15.51	2.10	2.56	0.09	1.35	3.18	3.40	3.59	0.27	0.63	0.18	99.67	2210	207	415	360	230	-	-	-	WRS70/7
WRS70/11	64.75	1.11	16.45	2.10	3.20	0.09	1.70	3.60	3.98	1.93	0.34	0.46	0.00	99.71	570	182	420	295	170	-	-	-	WRS70/11
WRS70/31	64.78	0.93	16.10	2.47	2.63	0.09	1.53	3.33	3.30	3.66	0.30	0.43	0.00	99.55	2620	195	510	405	255	-	-	-	WRS70/3

Table 1C—Major-and trace-element data for the Long Lake granite.

	Weight percent														ppm								
Sample	SiO_2	TiO_2	Al_2O_3	Fe_2O_3	FeO	MnO	MgO	CaO	Na_2O	K_2O	P_2O_5	H_2O	CO_2	Total	Ba	Rb	Sr	Zr	Ce	Pb	Th	Y	Sample
High Na Series																							
UHR-51	67.49	0.28	18.28	0.44	1.19	0.03	0.68	3.24	6.16	1.55	0.05	0.52	0.26	100.17	175	46	343	168	25	26	15	4	UHR-51
UHR-32	68.79	0.30	17.20	0.60	1.57	0.02	1.02	2.72	5.50	2.06	0.03	0.75	0.32	100.88	311	94	293	178	32	29	18	5	UHR-32
UHR-31	69.35	0.30	17.04	0.59	1.47	0.03	0.93	2.68	5.29	1.92	0.03	0.71	0.12	100.46	302	90	303	181	24	24	11	6	UHR-31
UHR-30	70.79	0.24	16.25	0.47	1.12	0.02	0.73	2.62	5.33	1.83	0.03	0.66	0.12	100.21	288	77	295	175	18	26	9	7	UHR-30
BTR-21	70.89	0.32	15.61	0.96	1.71	0.04	0.92	2.49	5.63	1.36	0.03	0.67	0.15	100.78	126	73	248	156	83	29	34	8	BTR-21
UHR-20	71.46	0.19	16.24	0.45	0.94	0.03	0.50	2.64	5.75	1.17	0.03	1.05	0.17	100.62	132	55	326	195	48	29	25	10	UHR-20
BTR-46	71.93	0.25	13.84	1.05	1.01	0.00	0.68	2.42	4.57	2.60	0.06	0.52	0.21	99.14	1193	72	315	130	74	27	31	2	BTR-46
BTR-42	72.14	0.23	15.54	0.63	1.03	0.02	0.50	2.39	5.50	1.81	0.03	0.46	0.26	100.54	529	49	291	200	85	32	33	5	BTR-42
HT-3	72.53	0.13	16.35	1.03	0.56	0.01	0.30	2.36	4.61	3.58	0.02	0.25	0.22	101.95	1041	92	362	114	21	21	6	4	HT-3
BTR-20	73.27	0.18	14.74	0.57	0.99	0.02	0.46	1.86	4.53	2.98	0.03	0.44	0.14	100.21	911	84	250	148	51	40	25	5	BTR-20
BTR-45	73.59	0.21	14.73	0.37	0.70	0.02	0.37	2.01	5.13	3.07	0.06	0.47	0.18	100.91	1088	68	278	173	72	37	26	7	BTR-45
HT-11	73.66	0.22	14.88	1.09	0.88	0.03	0.23	1.67	4.29	3.81	0.03	0.53	0.17	101.49	949	115	242	131	66	30	16	9	HT-11
BTR-54	74.20	0.31	13.82	0.33	0.83	0.04	0.36	1.80	4.28	3.78	0.03	0.18	0.08	100.04	1355	98	252	72	42	32	20	2	BTR-54
BTR-17	74.64	0.18	13.63	0.80	0.80	0.03	0.59	0.69	4.46	3.21	0.03	0.72	0.13	99.91	918	73	149	141	53	25	27	7	BTR-17
HR-116	74.97	0.06	14.75	0.13	0.20	0.02	0.00	1.77	4.83	3.31	0.03	0.40	0.17	100.64	1056	65	311	93	7	33	6	3	HR-116
BTR-24	75.46	0.08	13.58	0.35	0.40	0.01	0.37	1.80	3.94	3.92	0.04	0.56	0.17	100.68	1267	94	237	51	52	36	22	4	BTR-24
Low Na Series																							
BTR-62	70.29	0.58	13.64	1.50	1.72	0.06	0.79	2.75	3.62	4.26	0.17	0.87	0.22	100.47	2760	82	196	252	87	27	11	7	BTR-62
BTR-89	70.59	0.38	13.77	1.24	1.61	0.04	0.76	2.45	3.66	3.75	0.11	0.74	0.29	99.39	991	111	158	195	58	24	18	3	BTR-89
BTR-88	71.10	0.38	14.20	1.28	1.46	0.05	0.98	2.50	3.92	3.51	0.10	0.70	0.23	100.41	905	107	155	191	91	30	20	4	BTR-88
BTR-11	71.95	0.27	14.53	0.90	1.06	0.02	0.79	2.79	3.35	4.22	0.11	0.53	0.04	100.56	2174	118	118	149	74	28	14	1	BTR-11
BTR-86	72.94	0.22	13.85	0.59	0.74	0.04	0.53	3.05	3.25	4.14	0.04	0.34	0.09	99.82	1580	96	398	45	44	25	17	1	BTR-86
BTR-105	73.13	0.34	13.26	0.77	0.71	0.04	0.47	2.48	3.08	4.53	0.04	0.45	0.10	99.40	2765	121	402	87	73	29	13	-	BTR-105
BTR-22	73.25	0.05	14.47	0.19	0.21	0.00	0.36	1.32	3.51	6.33	0.04	0.58	0.23	100.54	2115	135	246	0	29	45	10	1	BTR-22
BTR-8	73.25	0.22	14.11	0.62	1.07	0.05	0.56	2.04	3.50	4.16	0.09	0.50	0.15	100.32	1490	136	190	156	36	29	13	8	BTR-8
BTR-92	74.19	0.48	12.00	1.02	0.53	0.04	0.14	0.80	2.16	8.76	0.08	0.55	0.20	100.95	1643	212	194	113	29	35	11	12	BTR-92
BTR-90	74.27	0.28	13.07	0.88	0.81	0.03	0.53	1.62	3.08	5.04	0.05	0.58	0.21	100.45	1210	134	131	139	62	38	30	3	BTR-90
BTR-9	75.55	0.16	13.59	0.61	0.68	0.03		1.66	2.89	4.46	0.04	0.48	0.12	100.65	1636	128	188	116	9	30	4	5	BTR-9

chemical types in the field. Samples for this study were taken primarily from large rafts of amphibolite that have been intruded by later granitoids in the Long Lake and Chain Lakes areas of the eastern Beartooth Mountains (Figure 1, Mueller and Wooden, this volume).

These rocks have been recognized by Armbrustmacher and Simonds (1977) and Warner and others (1982) and are coarse to fine-grained amphibolites composed of plagioclase and quartz with both biotite and amphibole. Although homogeneous and coarse grained in many instances, some samples exhibit strong lineation and foliation. All samples are presently in the amphibolite facies and all major minerals are metamorphic. Morphology and U-Pb systematics, however, suggest the zircons have been little modified by metamorphic processes.

The geochemistry of these rocks has been discussed previously by Mueller and others (1983), as well as in a variety of earlier studies (Harris, 1959; Armbrustmacher and Simonds, 1977; Wooden and others, 1982). Mueller and others (1983) reported major and trace element data that clearly showed two major groups of amphibolites, one tholeiitic and one calc-alkaline **(Table 1A, Figure 2)**. In general, these rocks are distinguished by their high concentrations of incompatible elements **(Figure 3)** and their overall andesitic chemistry **(Table 1A)**. In addition, both calc-alkaline and tholeiitic types exhibit the relative depletion in the high-field strength elements (HFSE; e.g., Ta, Nb) that characterize modern subduction related andesites **(Figure 4)**. These compositional traits suggest that this suite of rocks may have also been generated by subduction-like processes.

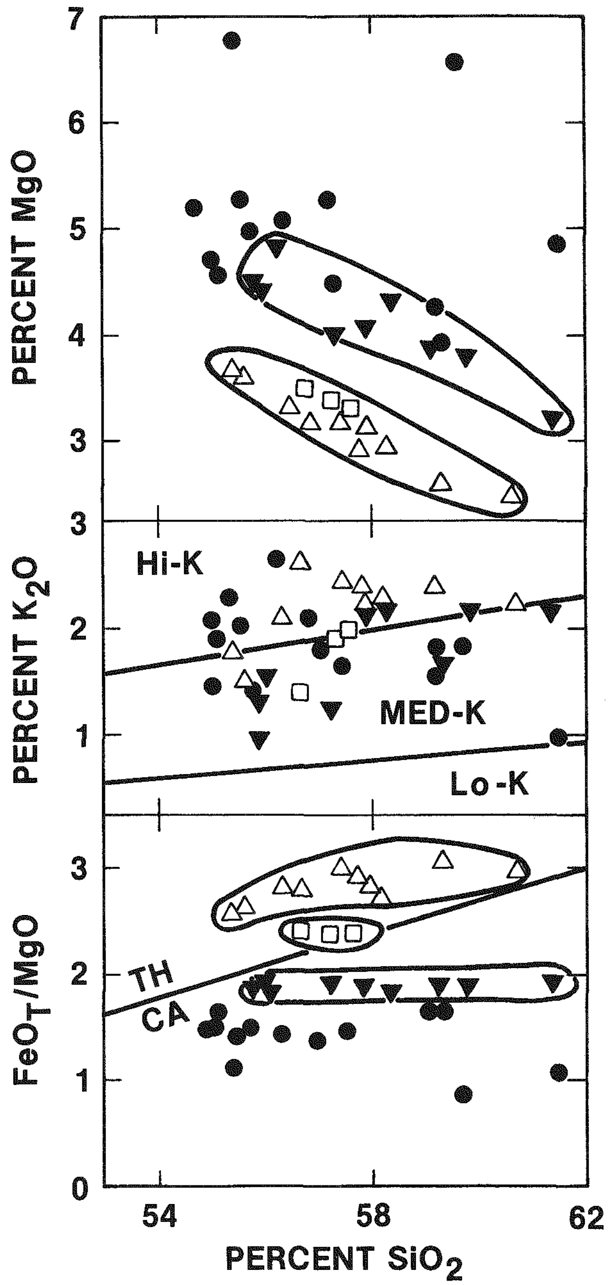

Figure 2—Major-element plots showing calc-alkaline and tholeiitic aspects of the andesitic amphibolite group. Filled symbols are calc-alkaline and open symbols are tholeiitic; other symbols represent potential subgroups.

Long Lake granodiorite (LLGd)

Field relations in the Long Lake area clearly show members of the andesitic amphibolite group were intruded by a later granodioritic magma. Wooden and others (1982), and Warner and others (1982) described this unit as a quartz-plagioclase-biotite rock with variable amounts of microcline which produces a range of compositions from tonalite to granite. The majority of samples analyzed, however, are granodiorite **(Table 1B)**. In general, this group exhibits igneous textures and mineralogy, but can exhibit strong foliation in some areas. The rock is interpreted as being late synkinematic relative to the metamorphic-deformational event that produced the andesitic amphibolites.

Geochemically, the rock is characterized by SiO_2 contents between 65 and 70 weight percent and K_2O/Na_2O *ratios less than one. In addition, this group* exhibits steep REE patterns **(Figure 3)** with strong light rare-earth enrichment and negative europium anomalies. As in the case of the andesitic amphibolites, the HFSEs are also relatively depleted in these rocks. Though not as reliable an indicator of subduction related magmatism in rocks of this silica content, the HFSE depletion and other trace element values suggest that these rocks are more likely to be related to the andesitic rocks than the later granites.

Long Lake granite (LLG)

The group of rocks described by Wooden and others (1982), and Warner and others (1982) as the Long Lake granite is the most abundant in the east-

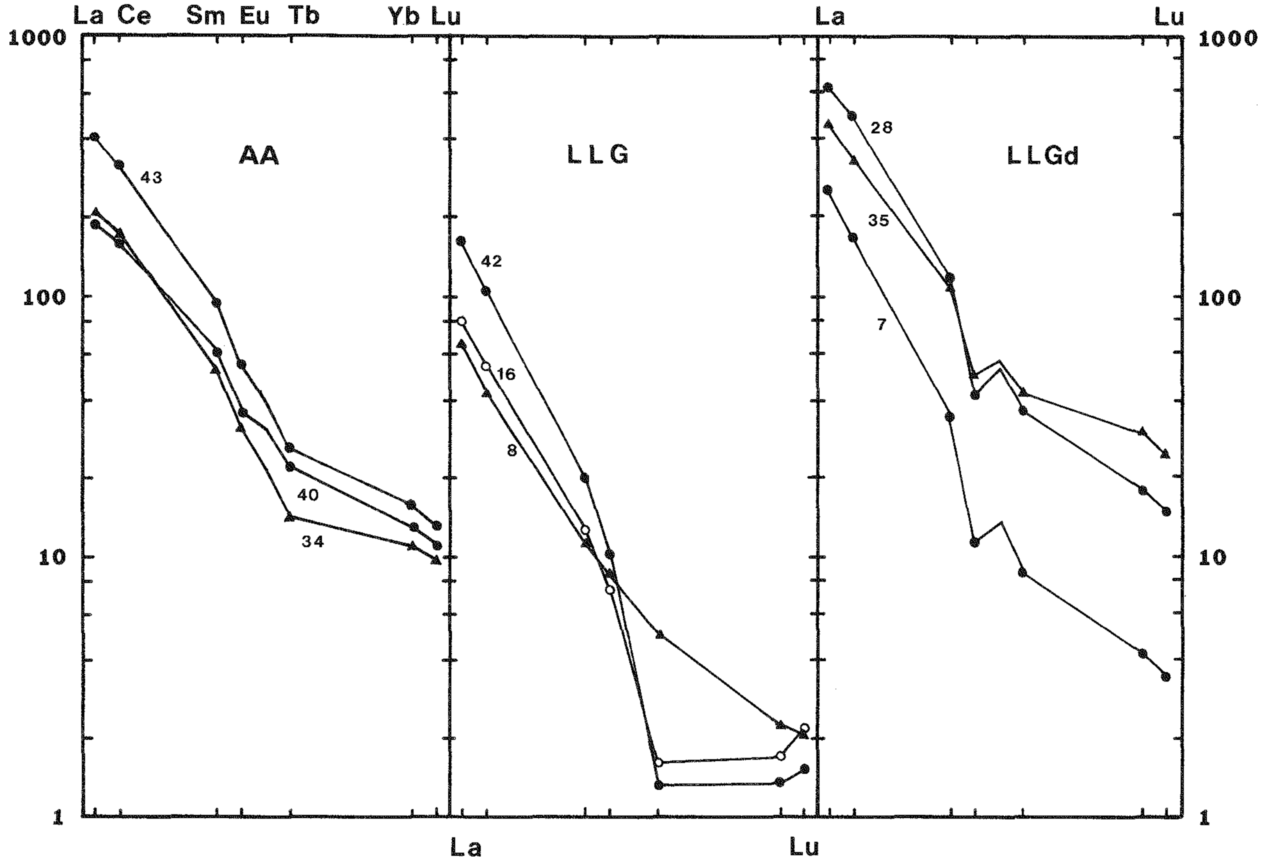

Figure 3—Chondrite normalized rare-earth element diagrams showing distinctions between main Late Archean rock types.

ern Beartooth Mountains. Field relations clearly show this group to be younger than the granodioritic or andesitic rocks in the area around Long Lake. Texturally, the rocks are igneous with very limited foliation developed near inclusions which are very abundant in this series. Rock types range from tonalite to granite and, therefore, overlap the compositional range of the granodioritic suite. The granite series, however, is distinguished by lower modal abundances of biotite, higher degrees of alteration of plagioclase, generally larger microcline crystals, and lack of sphene as an accessory phase.

Geochemically, this series is characterized by high silica, generally greater than 70 weight percent, and containing high soda (**Table 1C, Figure 5**). Trace-element abundances can be very high (e.g., Ba), and the rare-earth elements are generally lower in abundance than for the granodioritic series (**Figure 3**). In particular, these rocks are strongly depleted in the heavy rare-earth elements (**Figure 3**) and are unlikely to have a direct petrogenetic relation to either of the older rock types. In terms of the HFSE, they also show relative depletion. This suggests that some indirect relation between this series and the less silicic rocks may exist, such as short term recycling of subduction derived materials as might be expected in an arc or continental margin environment.

Geochronology

Previous geochronologic studies (Gast and others, 1958; Catanzaro and Kulp, 1964; Wooden and others, 1982) have established a generally Late Archean age for a majority of the rocks exposed in the eastern Beartooth Mountains. For the three main rock groups discussed here, whole-rock Rb-Sr, Sm-Nd, and Pb-Pb studies have all shown an inability to distinguish separate ages or initial ratios for the three series (Wooden and Mueller, 1988). For example, whole-rock Rb-Sr data reported by Wooden and others (1982) showed that the andesitic, granodioritic, and granitic series yielded an age of 2790 ± 35 Ma with an initial $^{87}Sr/^{86}Sr$ of 0.7022 ± 2. The Long Lake granite samples alone regressed to yield an age of 2800 ± 45 Ma with an initial ratio of 0.7019 ± 3. Similarly, the andesitic and granodioritic suites yielded essentially identical ages, but with larger errors related to their more limited range of Rb/Sr ratios. Sm-

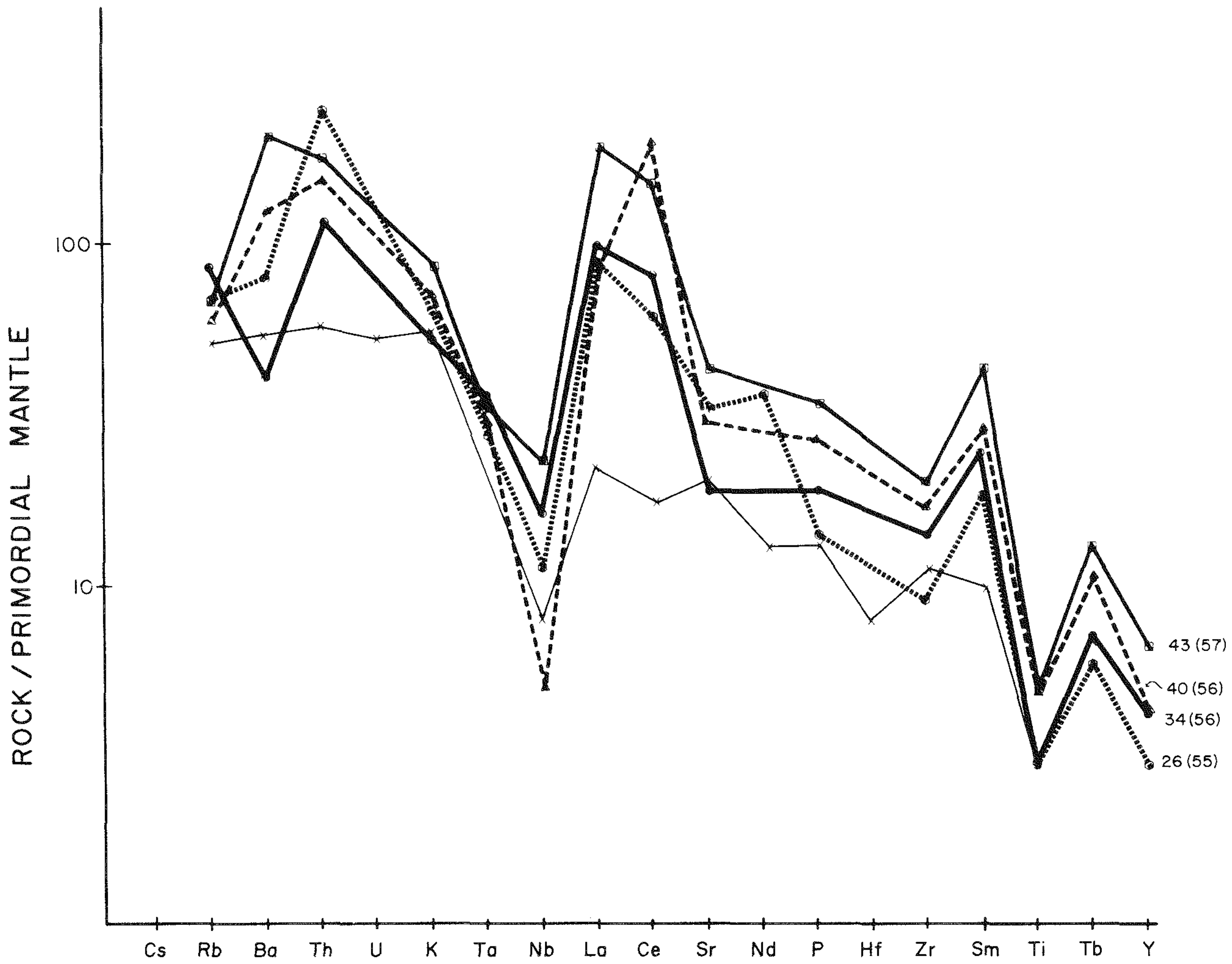

Figure 4—Normalized (primordial mantle) incompatible element plot for calc-alkaline (26,34) and tholeiitic (40,43) member of the andesitic amphibolite group; both show relative depletion of high-field strength elements (i.e., Nb, Ti).

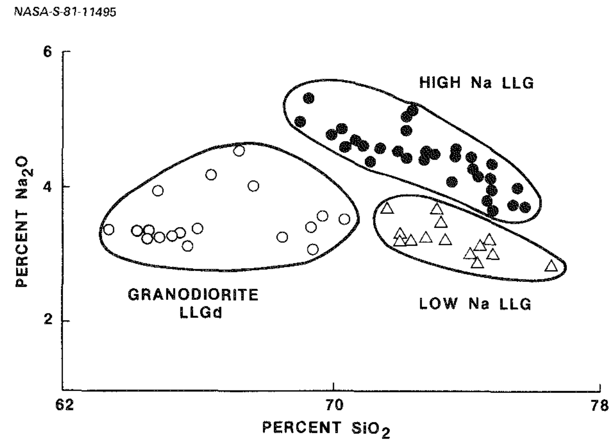

Figure 5—SiO_2 versus Na_2O showing overall high values for both oxides in the Long Lake granite. The Long Lake granodiorite overlaps with some members of the LLG suite.

Nd (Mueller and others, 1985) and Pb-Pb (Wooden and Mueller, 1988) also produced a series of statistically indistinguishable ages and initial ratios. From a petrologic and geochemical perspective, it is clearly important to ascertain whether the observed similarities in age and isotopic composition of these diverse rocks were related to overprinting by the volumetrically dominant granitic rocks or were inherent characteristics of the different suites. This can not be done without refined chronologic data. Consequently, a U-Pb zircon-based geochronologic investigation of the andesitic amphibolite, granodioritic, and granitic rock series was conducted.

Andesitic amphibolite

Zircons were obtained from four separate samples of AA. Two (BTR-27,57) are from the calc-alkaline suite, and two (BTR-43,52) are from the more enriched tholeiitic suite (Mueller and others, 1983). U-Pb isotopic and age data are presented in **Tables 2, 3**. Despite the variation in chemical types, samples 27, 57 and 52 appear to contain a single population of zircons (**Figure 6A**) that are nominally 100-600 microns long with length/width ratios of 2:1 to 5:1 and

Table 2—Zircon analyses.

SAMPLE	FRACTION[3]	SAMPLE WEIGHT (mg)	CONCENTRATIONS[1] (ppm) U	Pb	MEASURED RATIOS[1] $^{206}Pb/^{204}Pb$	$^{207}Pb/^{206}Pb$	$^{208}Pb/^{206}Pb$	ATOMIC RATIOS[2] $^{207}Pb/^{235}U$	$^{206}Pb/^{238}U$	$^{207}Pb/^{206}Pb$	AGE(Ma)[2] $^{207}Pb/^{206}Pb$
GRANITES											
BTR-21	small	1.2	1440	606	194	0.24833	0.6391	6.0961	0.2396	0.18453	2694
	medium	1.5	1190	456	582	0.21098	0.3717	7.1695	0.2740	0.18977	2740
	large	1.0	1210	438	613	0.21178	0.2322	7.4786	0.2830	0.19169	2757
BTR-33	small	1.2	727	250	163	0.26323	0.3420	5.8626	0.2268	0.18744	2720
	medium	0.9	518	324	96	0.31811	0.5247	8.7876	0.3349	0.19033	2745
	large	0.6	1020	324	82	0.34072	0.5885	4.1571	0.1581	0.19072	2748
BTR-46	m0°	0.8	867	375	867	0.20261	0.1819	9.2747	0.3571	0.18837	2728
	m2°	1.5	737	195	800	0.20582	0.2240	5.5522	0.2115	0.19042	2746
	m6°(light)	2.2	1090	356	567	0.20739	0.8170	4.6814	0.1830	0.18552	2703
	m6°(dark)	1.5	827	178	736	0.20881	0.2253	4.5374	0.1708	0.19271	2765
BTR-200	nm1°	0.2	669	335	1132	0.20102	0.1232	11.396	0.4347	0.19013	2743
	m1°	0.3	628	314	1010	0.19862	0.1653	10.787	0.4196	0.18636	2710
	m2°	0.5	475	208	1420	0.20012	0.1404	9.9218	0.3759	0.19145	2755
	large (dark)	4.5	700	218	386	0.22414	0.3209	5.9610	0.2248	0.19239	2762
	a.a.	0.6	675	205	697	0.21653	0.2518	6.4153	0.2355	0.19769	2806
GRANDODIORITES											
BTR-32	m0°	2.2	270	196	806	0.20930	0.3767	13.978	0.5224	0.19407	2777
	m1°	2.0	237	163	487	0.21913	0.4158	12.709	0.4753	0.19394	2776
	m2°	1.0	247	157	339	0.22903	0.4917	10.874	0.4093	0.19271	2765
BTR-62	m-1°	1.7	280	177	3620	0.19748	0.3726	12.429	0.4645	0.19409	2777
	m0°	2.6	375	230	1841	0.20006	0.4040	11.760	0.4410	0.19339	2771
	m1°	3.1	380	206	1026	0.20227	0.3937	10.194	0.3886	0.19027	2745
	m2°	1.3	526	252	693	0.20680	0.3552	9.0877	0.3488	0.18898	2733
BTR-64	m-1°	1.3	204	134	3282	0.19761	0.3582	13.005	0.4865	0.19387	2775
	m0°	3.6	215	135	3922	0.19724	0.3637	12.521	0.4678	0.19411	2777
	m1°	3.3	270	161	470	0.21919	0.4165	10.928	0.4106	0.19305	2768
	m2°	3.0	264	148	2568	0.19796	0.3750	10.990	0.4126	0.19318	2769
ANDESITIC AMPHIBOLITES											
BTR-57 (CA)	m0°	2.4	221	127	5438	0.19813	0.2125	12.668	0.4691	0.19588	2792
	m1°	2.5	383	206	2621	0.20044	0.2282	11.748	0.4352	0.19577	2791
	m2°	2.0	279	135	2492	0.20059	0.2361	10.483	0.3885	0.19568	2791
	m3°	1.6	440	201	1886	0.20207	0.2575	9.6986	0.3597	0.19557	2790
BTR-27 (CA)	m0°	3.5	397	250	3814	0.19837	0.1786	14.212	0.5282	0.19516	2786
	m1°	2.9	433	268	1871	0.20044	0.2226	13.387	0.5008	0.19388	2775
	m2°	2.6	544	316	1263	0.20101	0.2749	11.899	0.4512	0.19126	2753
BTR-52 (T)	m-1°	3.4	220	134	2403	0.19854	0.2461	12.981	0.4867	0.19343	2772
	m0°	4.3	261	153	3343	0.19648	0.2508	12.403	0.4666	0.19280	2766
	m1°	2.1	307	174	2549	0.19707	0.2607	11.888	0.4485	0.19224	2761
BTR-43 (T)	m-1°	1.0	256	138	11695	0.18774	0.2104	11.491	0.4464	0.18669	2713
	m0°	2.1	453	233	6060	0.18820	0.2377	10.729	0.4180	0.18616	2709
	m1°	0.9	592	266	3493	0.18419	0.2585	8.9746	0.3604	0.18062	2659
	m2°	1.1	591	238	1019	0.19284	0.3009	7.6707	0.3080	0.18061	2659

1) Corrected for analytical blank and mass fractionation.
2) Ratios corrected for blank and common Pb. Common Pb corrections for all samples were made by using feldspar Pb values determined for samples from the Long Lake region by Wooden and Mueller (in press). These values were $^{206}Pb/^{204}Pb = 13.84$, $^{207}Pb/^{204}Pb = 14.96$, and $^{208}Pb/^{204}Pb = 34.20$.
3) nm = nonmagnetic; m = magnetic at side tilt indicated (1.5A) for Franz Isodynamic Separator; small, medium, and large refer to populations separated by zircon size; dark = fraction consisting of large dark-brown grains from secondary population; a.a. = air abraded; CA = Calc-alkaline suite; T = Tholeiitic suite.

Table 3—Summary of U-Pb ages.

Sample	N	Concordia intercepts Upper (Ma)	Lower (Ma)	Model
ANDESITIC AMPHIBOLITES				
BTR-57	4	2793 ± 2	18 ± 4	1
BTR-57	4	2793 ± 2	18 ± 4	1
BTR-27	3	2791 ± 2	462 ± 30	1
BTR-52	3	2783 ± 5	271 ± 63	2
BTR-43	4	2734 ± 71	304 ± 370	2
GRANODIORITES				
BTR-32	3	2779 ± 30	110 ± 430	2
BTR-62	4	2797 ± 21	304 ± 140	2
BTR-64	4	2781 ± 11	102 ± 130	2
GRANITES				
BTR-21	3	2912 ± 240	390 ± 390	2
BTR-33	3	2743 ± 300	11 ± 620	2
BTR-46	4	2725 ± 97	-20 ± 210	2
BTR-200				
(minus abraded sample)	4	2727 ± 82	-80 ± 470	2
(with abraded sample)	5	2726 ± 60	-120 ± 230	2

Errors on concordia intercepts are 2σ.

are red to orange brown in color. Sample BTR-43, however, contained two morphologically different types of zircon. The most abundant type consists of dark, reddish-brown grains roughly 100-350 microns long with length/width ratios of about 1.5/1. These grains contain numerous inclusions and zoning is obvious in many grains. The less abundant group is also reddish brown in color, but has length/width ratios of about 4/1. Both groups are subhedral with few, if any, preserved crystal faces.

Although zircons from BTR-43 are less well formed than those from the other AA samples (and yield less precise age information), all AA zircons are considered to be primarily of igneous origin. An igneous origin appears likely in view of the generally prismatic shapes of the zircons and the high Zr contents of the rocks (Mueller and others, 1983), which suggest zircon as a probable liquidus phase. In addition, metamorphic zircon is unlikely to be produced at middle amphibolite grade and, if produced, would probably not have the size and shape of zircons found in the AA.

Zircons from three of the four samples studied provided well-defined upper intercept ages on a U-Pb concordia diagram **(Table 3)**. The two calc-alkaline samples (27 and 57) agree at the 95% confidence interval with ages of 2791 ± 2 Ma and 2793 ± 2 Ma **(Figure 7)**, respectively. Lower intercepts for these two samples, however, were distinct at the 95% confidence level and indicate substantially different Pb-loss patterns. Of the tholeiitic group, sample BTR-52 generated a precise discordia intercept age of 2783 ± 5 Ma. The other tholeiitic sample (BTR-43) exhibits the least precise age, 2734 ± 71 Ma. The reason for the scatter of the data for this sample is not clear, although the nature of the zircons themselves (two populations) suggests a different history than the other samples. In addition, this sample also exhibited the highest degree of Pb-loss, up to 44%, but does not have appreciably higher U contents **(Table 2)**.

Discounting the age of BTR-43 because of its uncertain upper intercept, the other three samples yield upper intercepts in the range 2778-2795 at the two sigma limit with well-defined individual upper intercepts. In particular, the upper intercept ages of the two calc-alkaline samples agree even at the one sigma level and strongly suggest this group of rocks was emplaced 2792 ± 3 Ma. The age of the tholeiitic suite is more difficult to assess. Field relations are not definitive concerning the relative ages of the tholeiitic and calc-alkaline suites and it is possible that at least some of the tholeiitic rocks are younger, although both types apparently experienced the same metamorphic event.

Long Lake granodiorite

Zircon separates were obtained from three different samples of the LLGd, BTR-32, 62 and 64 **(Tables 2, 3)**. All samples contained a single population of zircons. This population is composed of orange-brown to light red-brown-colored grains on the order of 100-450 microns long with length/width ratios of approximately 2.5-6/1 **(Figure 6B)**. Most grains, however, were roughly 200 microns long with length/width ratios of 2.5-3.5/1. Grains are euhedral to subhedral with few showing any inclusions, overgrowths, or zonation.

Individual samples produced both upper and lower intercept ages that agree with each other at the 95% confidence level **(Table 3)**. Upper intercept ages for individual samples are 2779 ± 30 Ma, 2797 ± 21 Ma, and 2781 ± 11 Ma. Considering the agreement among these samples for both upper and lower intercepts **(Table 3)**, it is not unreasonable to consider that the zircons from these samples may represent a single population. A combined Model IV regression (weighting proportional to degree of concordancy, Ludwig, 1985) on all eleven separates yields an age of 2779 ± 4 Ma with a lower intercept of 240 ± 75 Ma **(Figure 8)**. This composite age probably offers the best estimate of the time of intrusion of the granodiorite, although it is also clearly possible that granodioritic rocks were produced over a wider span of time as suggested by the individual ages.

Accepting the composite age as correct, 2779 Ma becomes a firm lower limit for the time of the amphibolite facies metamorphism that affected the AA. Considering that both members of the AA are in fact distinctly metamorphosed rocks while the LLGd is only slightly foliated with little evidence of metamor-

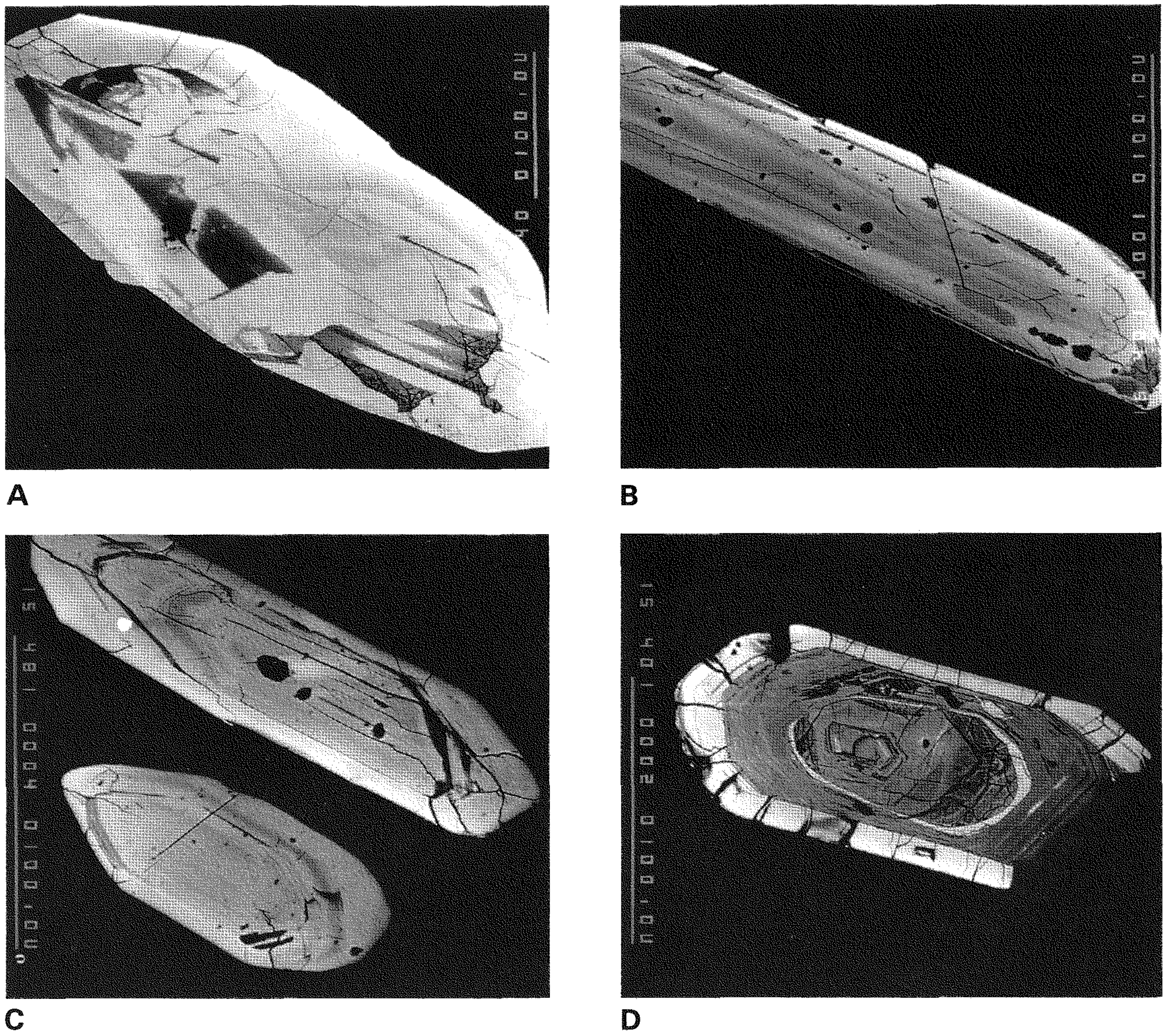

Figure 6—Back-scattered electron images of typical zircons from the main rock series. Tonal variations are primarily related to differences in Hf contents. See text for discussion of sizes. (A), Andesitic amphibolite (BTR-57); (B), Long Lake granodiorite (BTR-62); (C) Long Lake granite, primary population (BTR-200); (D) Long Lake granite, secondary population (BTR-200).

phism, it is clear that an episode of middle amphibolite grade-metamorphism occurred in this area in Late Archean time, probably between 2779 and 2795 Ma. Previous studies (Gast and others, 1958; Mueller and others, 1982; Wooden and others, 1982) had inferred this general time frame for a metamorphic event, but had not been able to precisely constrain its timing.

Long Lake granite

In view of the compositional variety and areal extent of this unit, zircon separates were obtained from four different samples of the LLG. All samples contained two populations of zircons. The primary population (95%) of pale to dark hyacinth-colored grains were generally euhedral and ranged from 75-200 microns with length to width ratios of approximately 3-4/1 (**Figure 6C**). These primary grains are often zoned and contain numerous inclusions, overgrowths and outgrowths; some of the smallest grains appear to have cores. Brown to dark red, stubby grains with pronounced cores composed the secondary population (5%). Separates of this population were made from samples BTR-46 and 200 (**Figure 6D**) and one fraction of the separate from 200 was abraded by about 50% prior to analysis (Goldich and Fisher, 1986). All members of this secondary population were also removed from all samples of the primary population prior to analysis.

Results of the isotopic analyses of the LLG separates (**Tables 2, 3**) show that their systematics are considerably different from those in the AA and

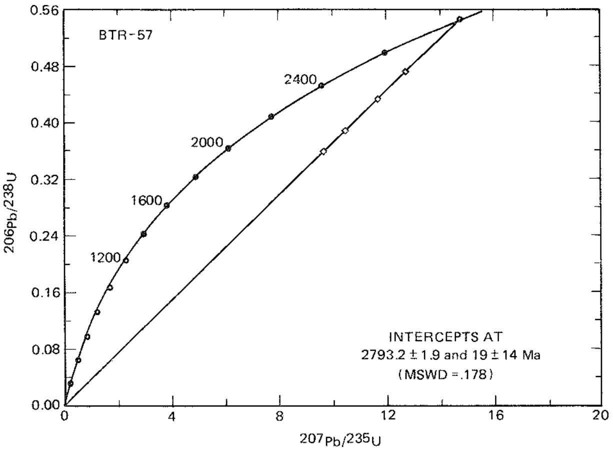

Figure 7—U-Pb concordia diagram for BTR-57 (AA) utilizing Model I of Ludwig (1985).

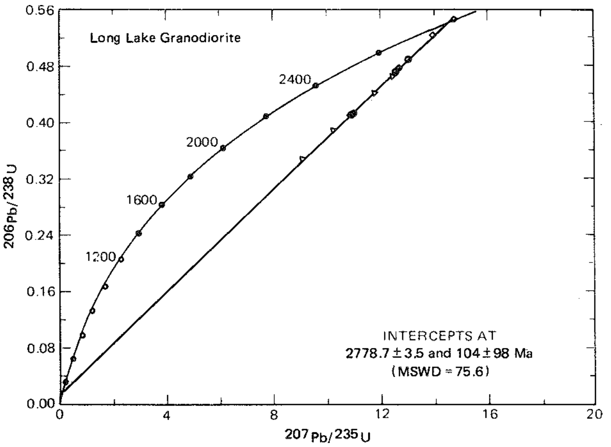

Figure 8—U-Pb concordia diagram for all samples of the Long Lake granodiorite (△ = BTR-62, □ = BTR-32, 0 = BTR-64) utilizing Model IV of Ludwig (1985) which weights points according to their proximity to the upper intercept with concordia. Cluster of data points along discordia represent one BTR-32 and two BTR-64 points.

LLGd. Regressions for individual samples show much more scatter and the entire data set is characterized by higher degrees of discordancy. Although the least magnetic fractions tend to produce the least discordant data, these fractions do not always have the lowest levels of common Pb or U as might be expected. This can be seen in **Figures 9 and 10** which show relations between common Pb and thorogenic Pb, and between common Pb and $^{207}Pb/^{206}Pb$ ages, respectively. The negative correlation of $^{206}Pb/^{204}Pb$ and $^{208}Pb/^{206}Pb$ mimics that of the abraded and unabraded samples from BTR-200 and suggests common Pb and Th are concentrated in the overgrowth material and that this component may be present in all zircons to some degree. The fact that both cores and overgrowths have lost approximately the same percentage of Pb, suggests the high contents of common Pb, thorogenic Pb, and Th are not solely the result of metamictization in the secondary population and probably not in the main population. The positive correlation between $^{206}Pb/^{204}Pb$ and $^{207}Pb/^{206}Pb$ age seen for most samples, consequently, must also be interpreted as an indigenous aspect of these zircons. Common Pb compositions determined from feldspar separates (Wooden and Mueller, 1988) were used to correct the data prior to calculating the ages used in **Figure 10**. In this case, the relation between the abraded/unabraded sample and the general trend for all zircons is also the same. The core exhibits higher $^{206}Pb/^{204}Pb$ and an older age relative to the rim. The fact that the abraded core from BTR-200 is only 45 Ma older than the mean age of the LLG supports the argument made earlier that the LLG was not produced by melting of significantly older crust (Wooden and Mueller, 1988).

These two diagrams exemplify the difficulty of interpreting a precise and accurate age for the LLG. The ages calculated are sensitive both to the amount of common Pb and its isotopic composition, as well as the amount of inherited component. The high degrees of Pb loss compounds these problems by making it difficult to resolve the age(s) of cores. Consequently, it is impossible to assign an age to the LLG that is not to some degree arbitrary. In general, samples with the lowest common Pb contents that have $^{206}Pb/^{204}Pb$ values higher than those of the core material would seem the most likely to yield a useful estimate of the age of the LLG. Any logical combination of samples such as the four highest $^{206}Pb/^{204}Pb$ samples (x = 2734 Ma) or the split from each sample with the highest $^{206}Pb/^{204}Pb$ (x = 2740 Ma) yield approximately the same value as the average of all $^{207}Pb/^{206}Pb$ ages exclusive of the composite grains (2732 ± 42 Ma, 2σ) or a Model II (Ludwig, 1985) regression for the same data (2738 ± 21 Ma, 2σ, **Figure 11**). Consequently, an age of approximately 2740 Ma seems most reasonable for the time of emplacement of the LLG. The error to be assigned to this estimate is difficult to determine because it is quite likely that a large, complex granitoid such as the LLG was intruded over a span of time. Further studies of more samples with more concordant zircons would be required to separate analytical errors from the real variations in age(s) of intrusion.

Discussion

The ages of magmatic and metamorphic events that occurred in the eastern Beartooth terrane (EBT) during the Late Archean are restricted to a period of approximately 50-100 Ma. Though not definitive, this relatively restricted interval has important implications for resolving the tectonic environment which

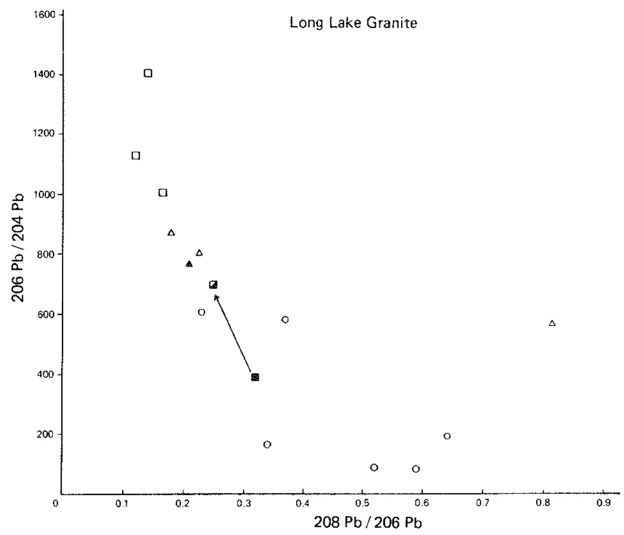

Figure 9—A plot of ^{206}Pb/^{204}Pb vs ^{208}Pb/^{206}Pb for individual zircon fraction; symbols are: BTR-21 (○), BTR-33 (○), BTR-46 (△), and BTR-200 (□). Filled symbols are for secondary population and half-filled are abraded. Data plotted are blank corrected only.

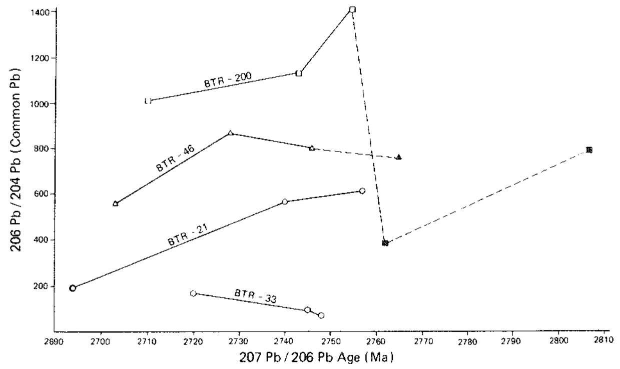

Figure 10—A plot of ^{206}Pb/^{204}Pb vs ^{207}Pb/^{206}Pb age for individual zircon fractions; symbols are: BTR-21 (○), BTR-33 (○), BTR-46 (△), and BTR-200 (□). ^{206}Pb/^{204}Pb ratios are blank corrected only, while ages are based on blank and common lead corrected 207/206 ratios.

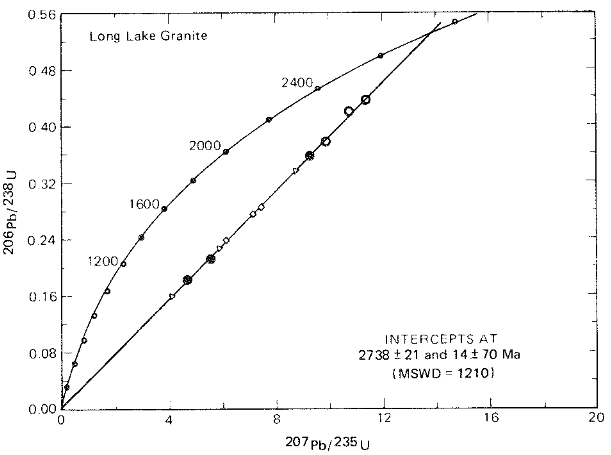

Figure 11—U-Pb concordia diagram utilizing Model II of Ludwig (1985) for all samples of Long Lake granite (● = BTR-46; □ = BTR-21; △ = BTR-33; ○ = BTR-200).

generated this terrane. In terms of modern analogs, this rapidly produced assortment of mantle- and crustally-derived tholeiitic, calc-alkaline and sodic rock series (variously affected by an episode of metamorphism and compressive deformation), is reminiscent of modern convergent margins (Reymer and Schubert, 1986; Marsh, 1982).

In particular, trace element and isotopic data for the Late Archean rocks strongly support analogies with modern convergent magmatic processes. From a trace element perspective, the depletion in the high field strength elements (HFSE), relative to other incompatible elements, suggests that the magmatic processes which produced the andesitic protoliths to the AA group are very similar to those that produce the same signature in modern convergent margin environments. The retention of this signature throughout all of the major Late Archean rock series also suggests that the more differentiated rocks share at least a partially consanguineous relation. In this regard, it is also clear from the isotopic data for these later rocks that they were not produced by partial melting of any of the exposed older rocks (Wooden and Mueller, 1988). In addition, Wooden and Mueller (1988) showed that all of these rocks series share the same initial Pb (206/204 = 13.86, 207/204 = 14.96, 208/204 = 34.01, Nd (C= -2). The Sr (0.7022) isotopic compositions also supports a consanguineous relation. Similar initial isotopic compositions for a large volume of crustally and mantle-derived rocks suggests large-scale, crust-mantle mixing similar to that proposed for many modern convergent margins (Wooden and Mueller, 1988).

Mueller and others (1985), Wooden and Mueller (1988), and Mogk and others (1988) have utilized more comprehensive geochemical, isotopic, and structural arguments respectively to further substantiate this analogy. Chronologic and chemical data reported here are compatible with these previous suggestions and support the contention that the major lithologic transition seen in southwestern Montana is the consequence of a Late Archean episode of plate convergence (Mogk, this volume). These data also help to substantiate earlier suggestions that Late Archean granitic plutonism becomes generally older from southeast to northwest in the Wyoming province (Peterman, 1979).

In addition to these tectonic implications, age data from the EBT calls attention to some of the general problems associated with classifying Archean terranes without the aid of detailed chronologic data. Traditionally, Archean terranes have been subdivided based upon first-order lithologic associations, metamorphic grade and structural style (Windley, 1982). Accumulations of eugeoclinal supracrustal rocks at low-metamorphic grade that are relatively mildly deformed and intruded by extensive granitoids (mostly tonalitic) were designated granite-greenstone terranes. These terranes have been variously interpreted in terms of modern tectonic environments such as sea-floor or mid-ocean volcanism, island arcs and ensialic rifts (Condie, 1981). Any of these alternatives may ultimately prove applicable for individual terranes. The remainder of Archean terranes were generally grouped as granite-gneiss or high-grade terranes. These were characterized by vast quantities of tonalitic to granitic gneisses at amphibolite to granulite grade with inclusions of miogeoclinal rocks that are also at high metamorphic grade. The lithologic association found in the EBT is clearly more similar to the granite-gneiss terranes than to the granite-greenstone terranes.

The association seen in the EBT is actually composed of large areas of 2740 Ma granitoids with inclusions of high-grade miogeoclinal rocks which are much older (Henry and others, 1982), and some of lower grade (middle amphibolite) that are only slightly older (e.g., AA, 2790 Ma) than the granitoids. Consequently, this high-grade terrane actually contains remnants of at least two separate tectonic environments that must be evaluated independently. High precision U-Pb chronology by Krogh and Turek (1982) refined the understanding of the stratigraphy and tectonics of granite-greenstone terranes of the Canadian Shield. Although this is obviously a more difficult proposition for granite-gneiss terrains, it seems reasonable to expect that important distinctions will also be revealed by detailed geochronologic and geochemical investigations of these terranes. In the case of the EBT, the record of an 3.4-3.6 Ga mature continent is apparent in early quartzites, psammites and iron-formations. These rocks were metamorphosed to granulite facies shortly thereafter, probably as the result of continental collision (Henry and others, 1982; Mueller and others, 1985). Roughly 500 Ma, evidence points to an episode of plate convergence and subduction along a continental margin (Mueller and others, 1985; Wooden and Mueller, 1988; Mogk and others, 1988). This is a very different scenario than could have been developed without the available chronologic data. Such data are essential, therefore, in resolving the important record of crustal development preserved in all Archean terranes. In particular, it points out the feasibility of recognizing rock associations in granite-gneiss terranes that are compatible with plate tectonic processes as has been proposed for many low-grade Archean terranes (Condie, 1981).

Conclusions

Zircons separated from Late Archean igneous and metamorphic rocks of the eastern Beartooth Mountains record the times of emplacement of three chemically distinct rock series. Both calc-alkaline and tholeiitic varieties of the only true metamorphic rock, the andesitic amphibolite, yield the oldest ages. These ages (excluding BTR-43) range from 2783-2793 Ma and suggest an emplacement age of approximately 2792 Ma for the protoliths of the calc-alkaline series; the tholeiitic rocks may be the same age, but also may be slightly younger. The Long Lake granodiorite exhibits some chronologic overlap and geochemical similarities with the AA, but its age is probably best evaluated in terms of a composite regression on all samples that yielded an age of 2779 ± 4 Ma. These age relations are generally compatible with field observations that show the LLGd as a late synkinematic rock intruding the thoroughly metamorphosed AA. The time of this metamorphic event is constrained to the interval 2779-2792 Ma. The youngest unit, the Long Lake granite, yields the youngest and least precise ages of the Late Archean suite, despite its lack of metamorphic effects. The imprecision of the ages is probably related to the presence of inherited older cores and a poorly constrained isotopic composition for common Pb in the zircons. Eliminating obviously composite grains and combining data from four different samples yields a discordia intercept age of 2738 ± 21 Ma, which is considered the best estimate of the age of this unit. These ages, together with geochemical data, particularly HFSE values and isotopic data, suggest that the eastern Beartooth Mountains may have been the site of a Late Archean episode of magmatic and tectonic activity similar to that expected for a modern convergent continental margin.

Acknowledgements

The authors wish to acknowledge the financial support of this study rendered by the U.S. Geological Survey (DI-14-08-0001-G-657), the NSF (EAR 8211828) and NASA (NAG-9-91). Laboratory assistance was provided by R. Ernst, M. MacKenzie and T. Acosta.

References

Armbrustmacher, T. J., and Simons, F. S., 1977, Geochemistry of amphibolites from the central Beartooth Mountains, Wyoming-Montana: U.S. Geological Survey Journal of Research v. 5, p. 53.

Casella, C. J., Levay, J., Eble, E., Hirst, B., Huffman, K., Lahti, V., and Metzger, R., 1982, Precambrian geology of the southwestern Beartooth Mountains, Yellowstone National Park, Montana and Wyoming: Montana Bureau Mines and Geology Special Publication 84, p. 1-24.

Catanzaro, E. J., and Kulp, J. L., 1964, Discordant zircons from the Little Belt Mountains (Montana), Beartooth Mountains (Montana), and Santa Catalina Mountains (Arizona): Geochimica et Cosmochimica Acta 28, 87 p.

Condie, K. C., 1976, The Wyoming Archean province in the western United States, *in* The Early History of The Earth, B. F. Windley, *(ed.)*: John Wiley & Sons, New York, p. 499-510.

______ 1981, Archean Greenstone Belts, Elsevier, Amsterdam, 434 p.

Gast, P. W., Kulp, J. L., and Long, L. E., 1958, Absolute age of the early Precambrian rocks in the Bighorn basin of Wyoming and Montana, and southeastern Manitoba: American Geophysical Union Transactions v. 39, p. 322.

Goldich, S. S., and Fisher, L. B., 1986, Air-abrasion experiments in U-Pb dating of zircon: Chemical Geology v. 58, p. 195-215.

Harris, R. L., Jr., 1959, Geologic evolution of the Beartooth Mountains, Montana and Wyoming; part 3, Gardner Lake area, Wyoming: Geological Society of America Bulletin 70, p. 1185-1216.

Henry, D. J., Mueller, P. A., Wooden, J. L., Warner, J. L., and Lee-Berman, R., 1982, Granulite grade supracrustal assemblages of the Quad Creek area, eastern Beartooth Mountains, Montana: Montana Bureau Mines and Geology Special Publication 84, p. 147-156.

James, H. L. and Hedge, C. E., 1980, Age of the basement rocks of southwest Montana: Geological Society of America Bulletin 91, p. 11-15.

Krogh, T. E., 1973, A low-contamination method for hydrothermal decomposition of zircon and extraction of U and Pb for isotopic age determinations: Geochimica et Cosmochimica Acta, v. 37, p. 485-494.

______ 1982, Improved accuracy of U-Pb zircon ages by the creation of more concordant systems using an air abrasion technique: Geochimica et Cosmochimica Acta, v. 46, p. 637-649.

Krogh, T. E. and Turek, A., 1982, Precise U-Pb zircon ages from the Granitagama greenstone belt, southern Superior province: Canadian Journal of Earth Sciences, v. 19, p. 859-867.

Ludwig, K. R., 1980, Calculation of uncertainties of U-Pb isotope data: Earth Planetary Science Letters, v. 46, p. 212-220.

______ 1985, ISOPLOT200: A plotting and regression program for isotope geochemists for use with HP200 series computers: U.S. Geological Survey Open-File Report No. 85-513, 28 p.

Marsh, B. D., 1982, The Aleutians, *in* Andesites, R. S. Thorpe, *(ed.)*: John Wiley & Sons, New York, p. 99-114.

Mogk, D. W., Mueller, P. A., and Wooden, J. L., 1988, Tectonic aspects of Archean continental development in the North Snowy block, Beartooth Mountains, Montana: Journal of Geology, v. 96, p. 125-141.

Mueller, P. A., and Wooden, J. L., *(compilers)*, 1982, Precambrian geology of the Beartooth Mountains, Montana and Wyoming: Montana Bureau of Mines and Geology Special Publication 84, 167 p.

Mueller, P. A., Wooden, J. L., Odom, A. L., and Bowes, D. R., 1982, Geochemistry of the Archean rocks of the Quad Creek and Hellroaring Plateau areas of the eastern Beartooth Mountains: Montana Bureau Mines and Geology Special Publication 84, p. 69-82.

Mueller, P. A., Wooden, J. L., Schulz, K., and Bowes, D. R., 1983, Incompatible element-rich andesitic amphibolites from the Archean of Montana and Wyoming: Evidence for mantle metasomatism: Geology, v. 11, p. 203-206.

Mueller, P. A., Wooden, J. L., and Bowes, D. R., 1985, Archean crustal evolution of the eastern Beartooth Mountains, Montana-Wyoming: Montana Bureau Mines and Geology Special Publication 92, p. 9-21.

Peterman, Z. E., 1979, Geochronology and the Archean of the United States: Economic Geology, v. 74, p. 1544-1562.

Reymer, A., and Schubert, G., 1986, Rapid growth of some major segments of continental crust: Geology, v. 14, p. 299-302.

Steiger, R. H., and Jager, E., 1977, Subcommission on Geochronology: Convention on the use of decay constants in geo- and cosmochronology: Earth Planetary Science Letters, v. 36, p. 359-362.

Warner, J. L., Lee-Berman, R., and Simonds, C. H., 1982, Field and petrologic relations of some Archean rocks near Long Lake, eastern Beartooth Mountains, Montana and Wyoming: Montana Bureau Mines and Geology Special Publication 84, p. 57-68.

Windley, B. F., 1982, The Evolving Continents: John Wiley & Sons, New York, 399 p.

Wooden, J. L., and Mueller, P. A., 1988, Pb, Sr, and Nd isotopic compositions of suite of Late Archean igneous rocks, eastern Beartooth Mountains: Implications for crust-mantle evolution: Earth Planetary Science Letters, v. 87, p. 59-72.

Wooden, J. L., Mueller, P. A., and Mogk, D. W., 1988, A review of the geochemistry and geochronology of the Archean rocks of the northern Wyoming province, *in* Metamorphism and Crustal Evolution in the Western United States, W. G. Ernst, *(ed.)*: Prentice-Hall, New York, p. 383-410.

Wooden, J. L., Mueller, P. A., Hunt, D. K., and Bowes, D. R., 1982, Geochemistry and Rb-Sr geochronology of Archean rocks from the interior of the southeastern Beartooth Mountains, Montana and Wyoming: Montana Bureau Mines and Geology Special Publication 84, p. 45-50.

©DIANE NUGENT 1988

A REVIEW OF THE GEOCHEMISTRY AND GEOCHRONOLOGY OF ARCHEAN ROCKS OF THE BEARTOOTH MOUNTAINS, MONTANA AND WYOMING

Joseph L. Wooden
U.S. Geological Survey
Menlo Park, California 94025

Paul A. Mueller
Department of Geology
University of Florida
Gainesville, Florida 32611

David A. Mogk
Department of Earth Science
Montana State University
Bozeman, Montana 59717
and
Donald R. Bowes
Department of Geology
University of Glasgow
Glasgow, Scotland 612 8QQ

Introduction

The two major exposures of Archean rocks in the United States are the southern extension of the Superior province into Minnesota, northern Michigan and Wisconsin, and the Wyoming province of Wyoming, southwestern Montana, and minor parts Idaho, Utah and western South Dakota. This paper will concentrate on the Beartooth Mountains in the northern part of the Wyoming province (**Figure 1**). The reader is refered to the work of Peterman (1979) and Condie (1976) for general reviews of the geology and geochronology of the Wyoming province. A more comprehensive review and update of the Wyoming province is described by Wooden and others (1988).

The exposures of Archean rocks in the Wyoming province differ from those of most other shield areas in that they consist of discrete blocks uplifted during the Laramide orogeny. Unlike the Superior province where there is little relief and continuous exposures, except for masking by glacial deposits, the Archean rocks of the Wyoming province are characterized by more than one kilometer of topographic relief and as much as ten kilometers of structural relief and form less than a third of the exposure. The wide separation of the exposures poses a major problem for interpretation of the Archean history. It prevents widespread correlation of structural or lithologic trends and makes it impossible to divide the area into subprovinces similar to those distinguished in the Superior province. The general lithologic character of the province is also difficult to assess. As presently exposed, the province would seem to be dominated by gneisses and granitoids with only minor exposures of supracrustal, low-metamorphic grade rocks. As discussed by Peterman (1979) however, given the exposure pattern in the Wyoming province, this lithologic distribution could easily be compatible with alternating greenstone-granite and granite-gneiss terranes such as those seen in the Superior province.

Because of the relatively small and inaccessible exposures of Archean rocks in the mountainous terrains of the Wyoming province, they have not been extensively studied. Archean shields in other parts of the world have received more extensive study for two major reasons. First, major economic deposits in Archean rocks are generally concentrated in greenstone-granite belts. Such terranes are rare in the

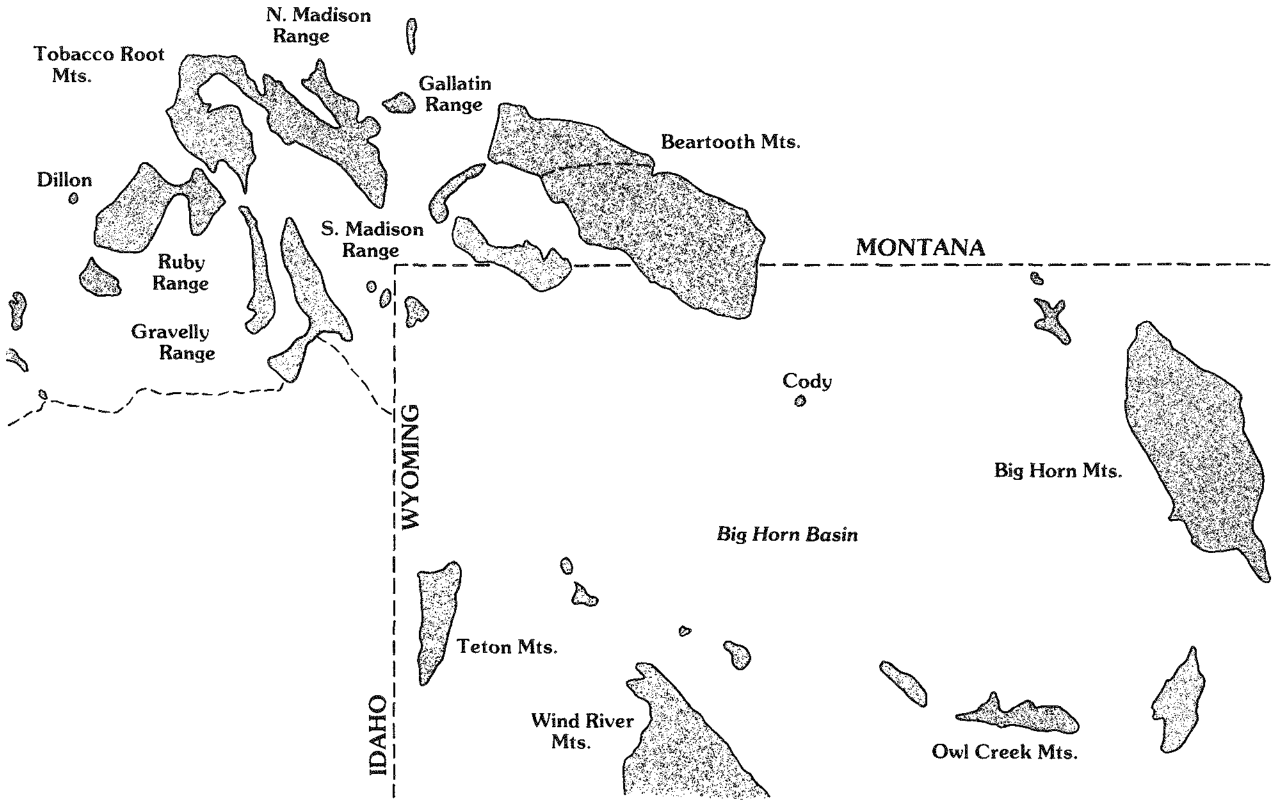

Figure 1—Location of Archean rocks in the northern Wyoming province.

Wyoming province. Secondly, a major interest in the presence of Early Archean rocks which provide information about the earliest geologic history of the earth have not been widely associated with the Wyoming province. Although there is growing evidence that rocks 3.4 Ga or older must exist in the Wyoming province, the oldest unambiguously dated rocks in the Wyoming province are only 3.2 Ga (e.g., Fisher and Stacey, 1986; Shuster and others, 1987). Aleinikoff and others (1987), however, have reported ion microprobe analyses of zircons from the Wind River Mountains that suggest ages as old as 3.8 Ga.

Beartooth Mountains

The Beartooth Mountains of Montana and Wyoming (**Figure 2**) lie immediately north of Yellowstone National Park and are roughly a W-NW-trending block underlain by over 5000 km² of Archean rocks. The Beartooth block can be divided into four areas: 1) Late Archean granitoids of the eastern and central portions that contain kilometer-size inclusions of older supracrustal rocks (Mueller and others, 1982a, b, 1985; Wooden and others, 1982; Mueller and Wooden, 1982), 2) metasedimentary rocks of the north-central area into which the Stillwater Complex and younger granitoids were intruded (Page, 1977), 3) metasedimentary rocks plus minor granitoids of the southwestern area (Casella and others, 1982), and 4) metamorphosed supracrustal and igneous rocks of the northwestern area that have been tectonically interleaved by faulting (Reid and others, 1975; Mogk, 1982, 1984; Mogk and others, 1988). Because the geology of each area is significantly different, individual areas will be discussed separately. It is not clear at this time what the relationships of individual areas are to each other, and it is possible that fundamentally different areas were tectonically juxtaposed in the Late Archean.

Eastern and central Beartooth Mountains

The eastern and central Beartooth Mountains were studied in detail by Eckelman and Poldervaart (1957); Harris (1959); Larsen and others (1966); and Casella (1969). The dominant granitic rocks of the area, along with associated metasedimentary rocks, were attributed to incomplete granitization of a sequence of folded sedimentary rocks. Later models from this group recognized the probable role of igneous processes, multiple deformation and metamorphism. Work by Mueller and others (1985) has led to

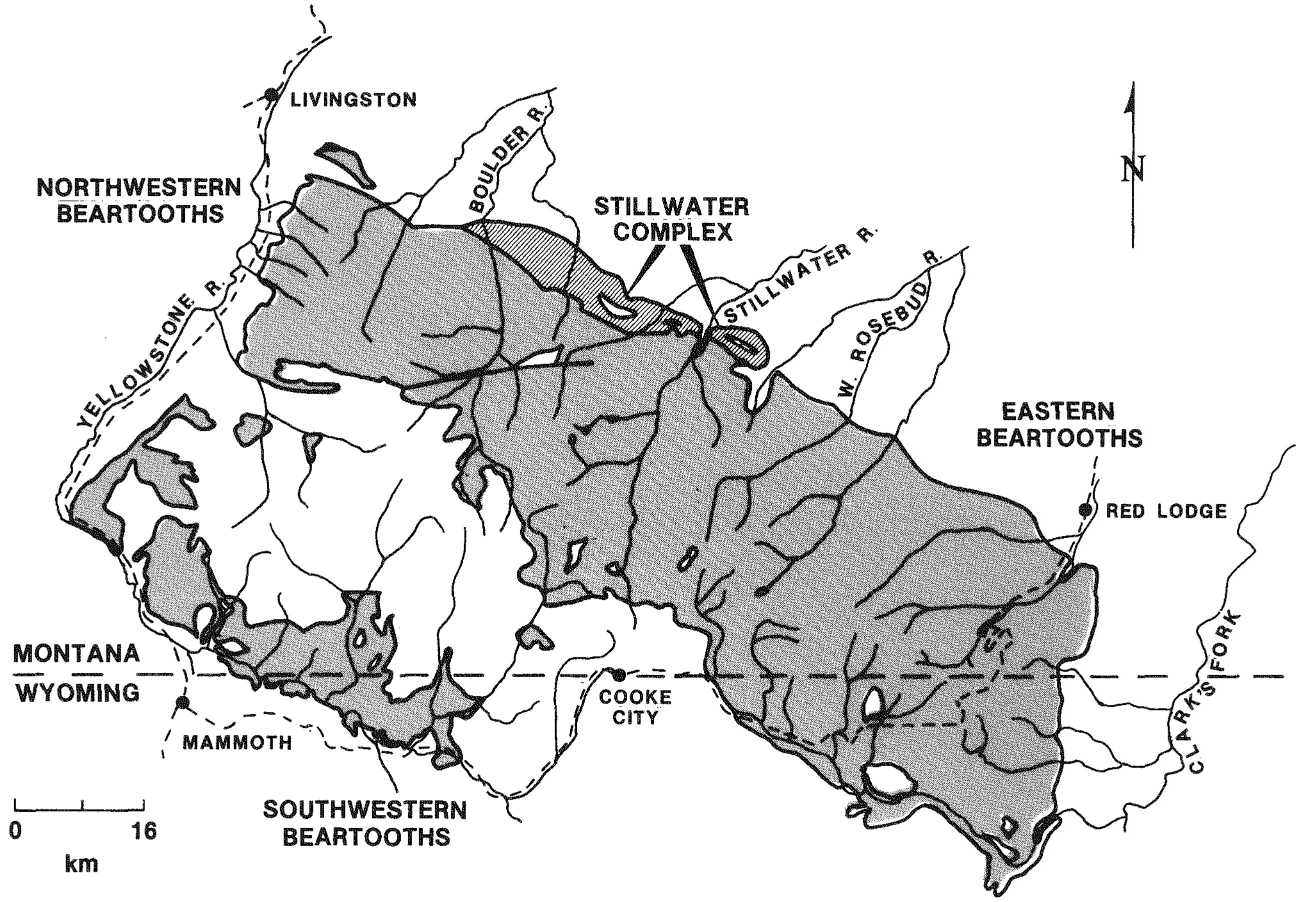
LIVINGSTON
NORTHWESTERN BEARTOOTHS
BOULDER R.
STILLWATER COMPLEX
STILLWATER R.
W. ROSEBUD R.
YELLOWSTONE R.
N
EASTERN BEARTOOTHS
RED LODGE
CLARK'S FORK
MONTANA
WYOMING
COOKE CITY
MAMMOTH
SOUTHWESTERN BEARTOOTHS
0
16
km

Figure 2—Distribution of Archean rocks in the Beartooth Mountains, Montana and Wyoming.

a model involving the intrusion of a group of Late Archean rocks into a Middle to Early Archean supracrustal sequence; parts of which had experienced a granulite-facies metamorphic event (Henry and others, 1982).

Geochemistry of Late Archean rocks

There are at least three distinctive compositional members of the Late Archean complex (**Figure 3**; also Mueller and others, this volume for compositional data). These three main series have been given the following informal names—andesitic amphibolite, Long Lake granodiorite, and Long Lake granite. Field relationships indicate that the andesitic amphibolite is the oldest member of this group and that these rocks experienced an amphibolite-grade metamorphism before the other members of the complex were emplaced. The present mineralogy of these amphibolites is biotite, hornblende, plagioclase and quartz. The andesitic amphibolite is found as meter- to kilometer-size inclusions in the younger granitoids. The Long Lake granodiorite is intermediate in age being found in some places as weakly foliated inclusions in the Long Lake granite. The Long Lake granodiorite is compositionally distinct, but very difficult to distinguish in the field from the Long Lake granite. Both of these rocks are leucocratic, medium to coarse grained, two feldspar plus quartz rocks, with biotite as the only mafic mineral (Wooden and others, 1982; Warner and others, 1982). It is difficult, therefore, to estimate the relative abundance of the granodiorite vs the granite in the field. Geochemical sampling indicates, however, that the granite is much more abundant.

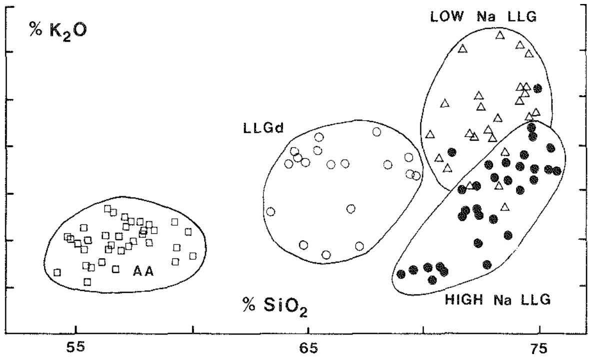

Figure 3—Weight percent K_2O vs weight percent SiO_2 for Late Archean rocks of the eastern and central Beartooth Mountains. Three major suites are distinguished: Andesitic amphibolites, Long Lake granodiorite, and Long Lake granite, which is subdivided into high Na and low Na groups.

Andesitic amphibolites (AA)

The major-element composition of the andesitic amphibolites is restricted to the andesitic or dioritic field (**Figure 3**). There is, however, a large variation in major-element abundances in this group, and several subgroups can be distinguished that exhibit regular elemental changes that may be related to fractionation processes. According to the classification developed by Gill (1981) for modern orogenic andesites, the andesitic amphibolites have major-element compositions that fall into both the calc-alkaline and tholeiitic fields. The calc-alkaline types dominate and are found over a wide geographic area in the eastern and central Beartooth Mountains; the tholeiitic types appear to be restricted to the eastern portion of the mountains. Because these rocks have been recrystallized in the middle amphibolite facies, it is not reasonable to classify them according to their alkali contents. Nonetheless, major-element compositions of these rocks, including alkalis, are not unusual with respect to modern or Archean andesites (Gill 1981; Condie, 1976, 1982).

The trace-element concentrations in the andesitic amphibolites deserve special mention. Although the range and abundance of the compatible trace elements in these rocks is within the normal range found in andesitic rocks, those of the incompatible trace elements are not. Sr concentrations range from 200-1000 ppm, Zr from 40-300 ppm, Ce from 20-300 ppm, and Ba 200-1500 ppm. In addition, the abundances of these incompatible elements are well correlated with each other (**Figure 4**). This is particularly unusual for Sr which typically shows little variation within an andesitic suite, even when fractionation has produced obvious variations in other elements. The best explanation for these chemical characteristics is a model that involves the interaction of an incompatible element-rich fluid with a partial melting process (Mueller and others, 1983). Variable degrees of partial melting can explain the range of major-element compositions and some of the trace-element variation. An incompatible element-rich fluid is needed to produce the unusually high concentrations of these elements in many of the rocks. Because Sr acts as an incompatible element, these processes must be occurring in a plagioclase-free environment, possibly the mantle.

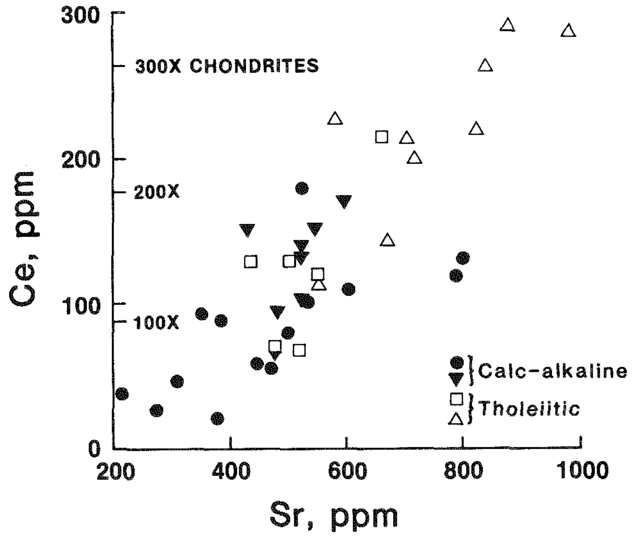

Figure 4—Ppm Ce vs ppm Sr for andesitic amphibolites of the eastern and central Beartooth Mountains.

Long Lake granodiorite (LLGd)

The Long Lake granodiorite has the major-element composition (**Figure 3**) of a typical calc-alkaline granodiorite (63-70% SiO_2). Although it overlaps the Long Lake granite in SiO_2 content, it maintains a lower Na_2O concentration. In keeping with its lower SiO_2 contents, the granodiorite is generally a more mafic rock than the granite with higher FeO, MgO and CaO concentrations. It is the incompatible trace-element contents of the granodiorite, however, that really distinguish it from the granite. The granodiorite has higher Sr, Ba and REE concentrations than the granite. The REE pattern of the granodiorite is particularly distinctive because it is higher in both the LREE and HREE and has a noticeable negative Eu anomally (**Figure 5**). The high contents of incompatible trace elements in the granodiorite suggest that it also could have had a trace-element-enriched fluid involved in its genesis. The negative Eu anomally, however, indicates that plagioclase was important as either a source or fractionating mineral; consequently, at least part of its genesis occurred at crustal P and T.

Long Lake granite (LLG)

The Long Lake granite is the volumetrically dominant rock type in the eastern Beartooth Mountains. It is divisible into at least two subgroups on the basis of Na_2O vs SiO_2 relationships (**Figure 6**). The high Na group is volumetrically more important and compositionally more coherent than the low Na group. Although the silica content of the Long Lake granite is restricted, the variation in Na_2O and K_2O concentrations (and modal plagioclase and K feldspar) indicate that the rock types vary from high-silica tonalite to average granite (IUGS). The negative correlation between Na and Si in both subgroups is unusual in modern calc-alkaline rocks, but is typical of Archean tonalitic and trondhjemitic suites. The genesis of tonalitic and trondhjemitic suites is best explained as the result of partial melting and/or fractionation of a basaltic parent. The lack of sodic suite rocks with intermediate compositions strongly favors an origin by

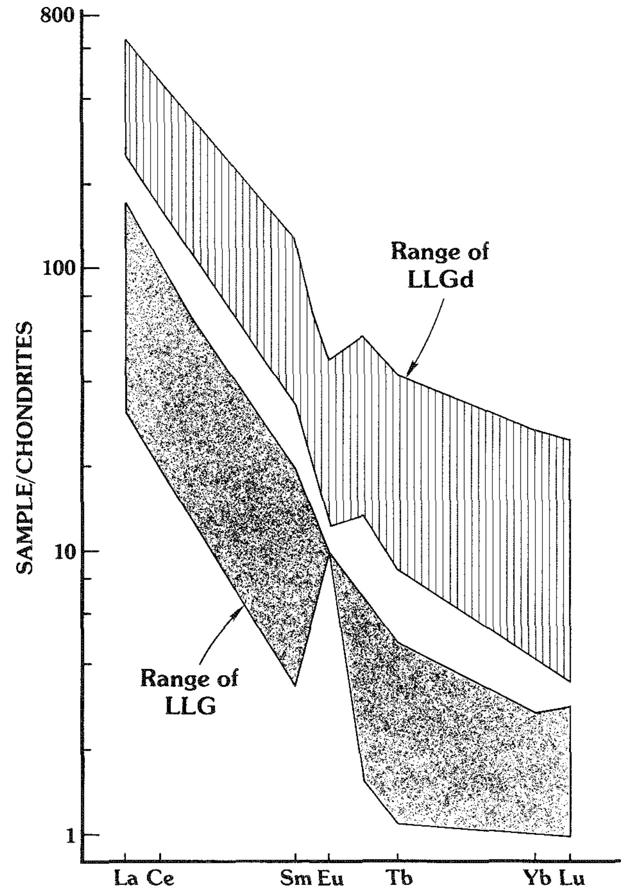

Figure 5—Comparison of rare-earth element patterns for the Long Lake granite and Long Lake granodiorite.

partial melting of a mafic source (basaltic and/or mafic andesite) that contained garnet, amphibole, or clinopyroxene to hold the HREE concentrations at 4X chondrites or lower. The strong LREE vs HREE fractionation seen in these rocks, along with the relatively low Sr and Rb contents, the low Rb/Sr ratios, and the high average K/Rb ratio (350) relative to other granitic rocks, are compatible with derivation from a mafic source.

Geochronology and isotopic systematics of Late Archean rocks

A range of isotopic data is now available for Late Archean rocks of the eastern and central Beartooth Mountains. Recently obtained U-Pb zircon data (Mueller and others, this volume) provide chronologic information for this group. These data are in agreement with previously discussed field relationships and give the following ages: Andesitic amphibolite, 2793 ± 2 Ma, 2791 ± 2 Ma, and 2783 ± 5 Ma; Long Lake granodiorite, 2779 ± 4 Ma; Long Lake granite, 2738 ± 21 Ma. The imprecise age of the Long Lake granite results from the zircons being at least 60% discordant. Within confidence limits, this group of rocks covers a time period of 35 to 80 Ma. Previously available Rb-Sr whole-rock data (Wooden and others, 1982) gave a composite isochron for all three major groups of 2790 ± 35 Ma (**Figure 7**). The initial Sr ratio of this isochron is 0.7022 ± 2. The common Pb isotopic data (**Figure 8**) for whole rocks and feldspars from the same three groups give an age of 2775 ± 50 Ma (Wooden and Mueller, 1988). The feldspar separates provide a good estimate of the initial Pb isotopic ratio in the rocks at the time of their formation. These ratios are 13.86 for $^{206}Pb/^{204}Pb$, 14.97 for $^{207}Pb/^{204}Pb$, and 34.00 for $^{208}Pb/^{204}Pb$ (average of 7). Sm-Nd chondritic model ages vary from 2.88-3.02 Ga, and initial epsilon Nd values calculated for an age of 2.78 Ga range from -1.5 to -3.1 for five samples (Wooden and Mueller, 1988).

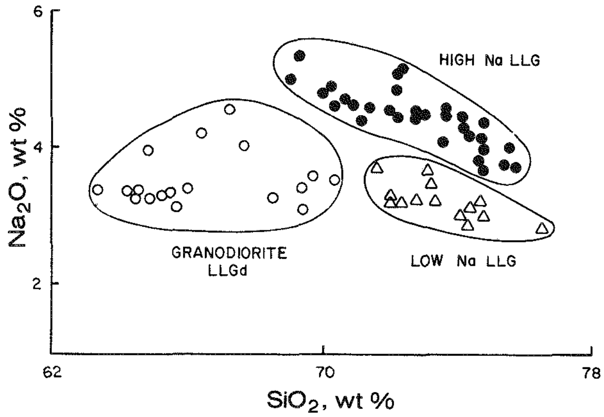

Figure 6—Weight percent SiO_2 vs weight percent Na_2O for the Long Lake granite and granodiorite. Diagram shows the distinction between high Na and low Na groups within the granite suite.

The chronologic and isotopic data for the Late Archean rocks clearly show that they are restricted to a relatively small time interval and are remarkably homogeneous in their initial Sr, Nd and Pb isotopic ratios. A time interval of 10-50 Ma for andesitic volcanism, deformation and metamorphism, and additional major plutonism is not remarkable for the Archean or the Phanerozoic. It is unusual, however, that such a compositionally diverse group of rocks would have the same initial isotopic ratios. These ratios are not what would be expected for new crust that was forming from primitive or depleted mantle. Initial Sr, Nd and Pb ratios in this case would be approximately 0.7010, epsilon Nd of 0 - +2, and $^{206}Pb/^{204}Pb$ = 13.40, $^{207}Pb/^{204}Pb$ = 14.58, $^{208}Pb/^{204}Pb$ = 33.16, respectively (Zartman and Doe, 1981). The difference between these values and those observed in the Late Archean complex suggest either an enriched mantle source or contamination of the rocks by older Archean crust. The very high Pb ratios strongly favor the involvement of older Archean crust in whatever process was responsible because it is only in crustal environments that the necessary high U/Pb could be

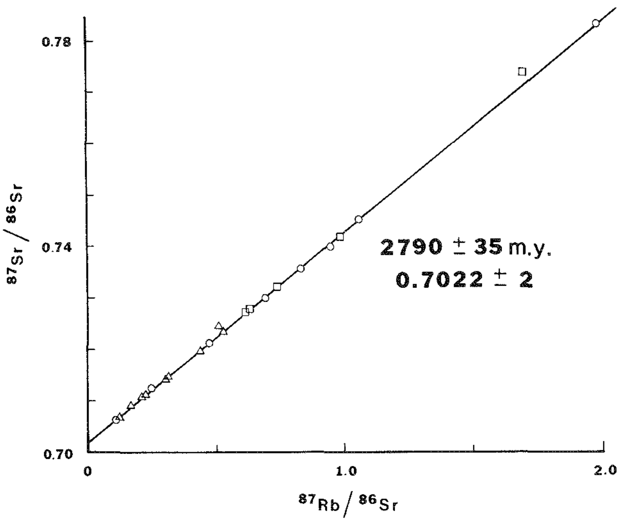

Figure 7—Composite Rb-Sr isochron diagram for Late Archean rocks of the eastern and central Beartooth Mountains. Long Lake granite, (circles); granodiorite, (squares); and andesitic amphibolite, (triangles).

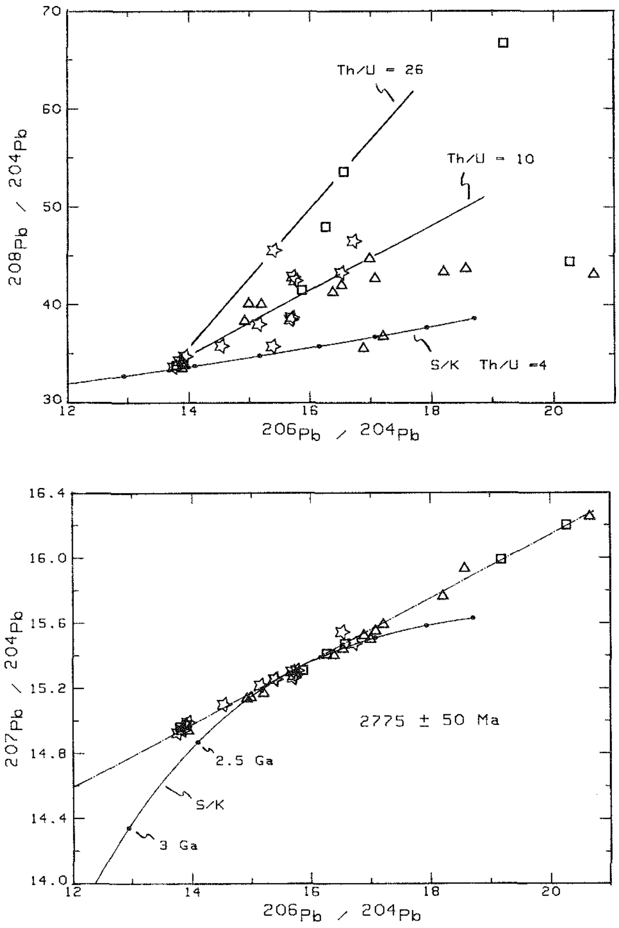

Figure 8—Pb-Pb isotopic data for whole-rock and feldspar samples from Late Archean rocks of the eastern and central Beartooth Mountains. The cluster of samples with the lowest $^{206}Pb/^{204}Pb$ ratios are the feldspars. Long Lake granite, (stars); granodiorite, (squares); and andesitic amphibolite, (triangles).

produced to allow the $^{206}Pb/^{204}Pb$ and $^{207}Pb/^{204}Pb$ to grow as high as needed. If crustal contamination occurred during emplacement of these rocks into an older, isotopically heterogeneous crust, it is difficult to understand how the necessary homogeneity was acheived. It seems most probable that a portion of the mantle itself was contaminated, possibly by introduction of crustal material through subduction, dewatering of the slab, and penetration of the overlying mantle wedge by fluids carrying Pb, Sr and Nd with a crustal signature (Wooden and Mueller, 1988). The crust could have been made from this contaminated mantle by first extracting basaltic material and then remelting it to produce more silicic rocks. The crust would have the necessary isotopic values and be isotopically homogeneous across a whole spectrum of compositional types, particularly if the crust-forming cycle was confined to a short time period that limited further radiogenic growth.

Geochemistry of the older Archean rocks

Enclosed in the Late Archean rocks of the eastern Beartooth Mountains are meter to several kilometer-sized inclusions of metamorphosed supracrustal rocks. At least some of these rocks have experienced both a granulite-grade metamorphic event (Henry and others, 1982) and the Late Archean amphibolite grade event discussed above. This granulite event was characterized by temperatures of about 800°C and pressures of about 6 kb, which suggest a geothermal gradient similar to those of modern orogenic zones (about 40-45°C/km). These rocks are strongly deformed and isoclinally folded; many lithologic layers exist only as boudins of various lengths. Metamorphic rocks with compositions equivalent to those of ironstones, basalts, andesites, ultramafic rocks, pelites, wackes, quartzites and felsic volcanic rocks can all be found in the supracrustal assemblages. To date no older plutonic rocks have been unequivocally identified, but the high and low K granitic rocks in the Quad Creek sections are potential examples (Mueller and others, 1982).

In spite of the deformation and metamorphism that has affected these rocks, they appear to have largely retained their original bulk chemistries **(Tables 1-4)**. The variation diagrams **(Figure 9, 10)** have no unusual features. If the samples with obvious and strongly fractionated sedimentary compositions are not considered (high Si quartzites, low Na pelites, high Fe ironstones), the remaining samples show the expected compositional variations of an igneous calc-alkaline sequence. Most of this sequence has moderate K_2O contents (2% or less) and K_2O/Na_2O (less than 1). Only samples with SiO_2 in the mid-70s have K_2O/Na_2O of 1 or greater.

Specific compositional features of some of the rock types in the older Archean sequence are worth emphasizing. The basaltic amphibolites are close to average basalt in composition and show little to moderate Fe enrichment. Rare-earth patterns are generally unfractionated and less than 20X chondrites. Sr contents are about 100 ppm, and Cr and Ni contents are about 250 and 100 ppm, respectively. The samples with SiO_2 contents between 65-73 weight % are comparable to moderate-K dacites. These samples have strongly fractionated REE patterns and no Eu anomalies. There is a group of rocks of rhyolitic composition with $K_2O/Na_2O \simeq 1$ that have fractionated REE patterns and strong negative Eu anomalies. The quartzites range in SiO_2 from 80-97%, are locally fuchsitic with up to 100 ppm Cr, and contain obvious detrital zircons. Iron-rich rocks vary in SiO_2 from 47-61% and in total Fe as FeO from 30-40%. Their compositional characteristics favor a continental shelf rather than a eugeoclinal depositional environment. Pelitic rocks in the section have SiO_2 contents in the low 60s, with very low CaO and NaO_2 contents. The combination of quartzites, iron-rich rocks and pelitic rocks strongly indicate that at least part of the history of this sequence involved a continental shelf environment.

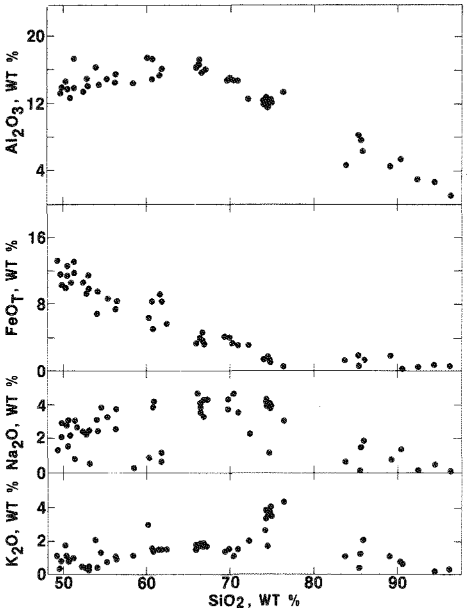

Figure 9—Compositional diagram for older Archean, supracrustal rocks of the eastern Beartooth Mountains.

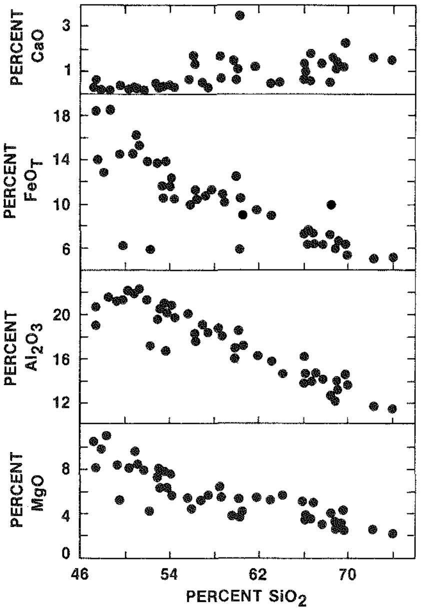

Figure 10—Compositional diagram for older Archean, supracrustal rocks of the Stillwater Complex.

Although there are general similarities among the various older Archean supracrustal packages, compositional differences do exist from location to location. In particular, there are differences between the Hellroaring Plateau **(Table 3)** and Quad Creek **(Tables 1, 2)** locations. The Hellroaring sequence contains more mafic and intermediate compositions. Among samples that fall into the andesitic field, the Hellroaring examples have much lower Sr concentrations. The average Sr concentration of all samples of Hellroaring is lower than that of Quad Creek. Na, K and Ca contents in the Hellroaring samples are more variable and less likely to conform to an unaltered igneous model. The samples with strong negative Eu anomalies mentioned above are common only in the Hellroaring suites. It is difficult to interpret the significance of these differences. They may represent protoliths of greatly different age, of a limited range in age, or of no significant range in age. They may suggest a change in tectonic environment, or juxtaposition of rocks from different environments. It is clear, however, that these rocks jointly underwent a final strong deformational event and were then intruded by the Late Archean granitoids.

Geochronology of the older Archean rocks

The age of the older Archean sequence is problematical and will remain so until new U-Pb zircon studies are completed. The zircon data that are available now (Mueller and others, 1982) indicate a minimum age ($^{207}Pb/^{206}Pb$ age) of 3295 Ma for a quartzite and 3220 Ma for a granitic migmatite from the Hellroaring Plateau. These data are produced by acid leaching of zircons that fell on a discordia line that intersected concordia at about 3100 Ma. The 3100 Ma age may have no geological meaning because it may be a point along an episodic cord between the true age of the zircons and the time of new zircon growth and/or Pb loss. The lower end of this episodic cord is represented by clear, acicular zircons with an age of

Table 1—Major- and trace-element data for older Archean rocks from upper Quad Creek.

		Weight percent															ppm																
Sample	Type	SiO2	TiO2	Al2O3	Fe2O3	FeO	MnO	MgO	CaO	Na2O	K2O	P2O5	H2O+	CO2	Total	Sample	Ba	Ce	Co	Cr	Cu	Ga	La	Ni	Pb	Rb	Sr	Th	U	Y	Zn	Zr	Sample
QC-84	MUM	41.85	0.25	5.98	5.48	5.87	0.13	28.90	4.88	0.20	0.16	0.01	4.17	0.51	98.39	QC-84	48	0	125	3200	1	5	5	820	0	4	6	1	0	9	72	24	QC-84
QC-83	MUM	51.55	0.22	4.81	2.40	8.40	0.20	27.03	3.29	0.01	0.20	0.01	0.54	0.66	99.32	QC-83	45	0	98	1940	12	4	5	742	0	7	8	0	1	8	50	24	QC-83
QC-63	MIS	42.17	0.14	3.81	23.70	22.00	0.88	3.46	2.53	0.00	0.13	0.02	0.11	0.11	99.06	QC-63	155	197	42	227	20	6	31	48	0	0	15	3	3	7	44	43	QC-63
QC-52	MIS	53.19	0.61	14.34	10.14	11.53	1.29	5.12	0.19	0.15	1.65	0.02	1.23	0.16	99.62	QC-52	467	67	35	422	84	20	16	131	3	100	15	11	2	204	80	109	QC-52
QC-85	MB	48.09	0.74	14.82	1.98	10.72	0.21	9.01	12.53	1.11	0.30	0.05	0.72	0.33	100.61	QC-85	81	0	57	528	7	11	16	134	1	11	101	0	1	20	71	35	QC-85
QC-60	MB	49.82	0.52	14.01	3.44	7.26	0.21	8.23	11.16	2.88	0.80	0.03	1.36	0.44	100.16	QC-60	63	24	50	249	28	14	1	133	10	6	79	4	1	16	83	37	QC-60
QC-89	MB	50.21	0.65	14.43	1.82	7.82	0.23	6.72	11.51	3.17	0.67	0.03	1.30	0.53	99.09	QC-89	70	0	55	553	100	11	11	144	6	9	111	0	1	17	93	41	QC-89
QC-87	MA	51.53	1.00	16.35	3.21	5.29	0.14	4.99	7.10	3.56	1.98	0.52	1.61	0.65	97.93	QC-87	1681	180	51	85	34	21	95	42	15	106	625	22	2	40	96	261	QC-87
QC-81	MA	57.38	0.55	16.74	1.24	5.80	0.11	4.23	8.05	2.45	0.75	0.09	1.08	0.12	98.59	QC-81	855	40	62	101	22	19	16	49	12	23	635	3	4	12	65	101	QC-81
QC-55	MP	60.23	0.73	17.38	0.84	5.39	0.08	4.53	5.10	0.84	2.97	0.11	1.61	0.21	100.02	QC-55	449	37	30	66	44	22	18	52	9	160	207	7	2	12	68	109	QC-55
QC-62	MP	61.87	0.75	16.03	1.96	6.44	0.16	3.35	5.92	1.17	1.55	0.11	1.16	0.19	100.66	QC-62	712	49	39	47	43	21	28	50	8	65	250	9	2	17	78	128	QC-62
QC-57	MD	60.70	0.61	17.30	0.91	4.17	0.93	2.95	6.09	3.89	1.51	0.10	1.05	0.31	100.52	QC-57	578	48	27	42	18	21	26	26	14	64	417	6	1	14	66	121	QC-57
QC-91	MD	62.64	0.67	15.00	2.12	2.99	0.09	2.72	4.44	3.71	1.82	0.19	1.17	0.44	98.00	QC-91	708	153	32	81	51	18	87	39	14	116	368	24	1	22	79	328	QC-91
QC-50A	MD	66.43	0.39	17.09	0.67	2.87	0.05	1.64	3.94	3.91	1.65	0.03	1.07	0.37	100.11	QC-50A	357	51	15	15	17	22	30	15	24	82	294	16	2	12	37	67	QC-50A
QC-58	MD	70.96	0.42	14.68	0.71	2.33	0.04	1.23	3.34	3.59	1.50	0.08	0.74	0.18	99.80	QC-58	263	58	14	11	10	19	28	10	16	79	286	14	1	7	47	190	QC-58
QC-86	MQ	80.05	0.10	10.08	0.03	0.32	0.02	1.34	1.35	2.20	2.69	0.00	0.63	0.32	99.13	QC-86	333	27	38	77	0	10	20	3	15	79	44	4	2	4	8	167	QC-86
QC-56	MQ	89.10	0.32	4.38	0.29	1.49	0.02	1.40	0.66	0.87	1.07	0.00	0.72	0.21	100.53	QC-56	235	5	15	106	0	8	2	14	7	62	47	2	1	3	30	205	QC-56

Rock types based entirely on compositional characteristics.
MUM = meta-ultramafic MA = meta-andesitic MD = metadacitic
MIS = meta-ironstone MP = metapelitic MQ = metaquartzite
MB = metabasaltic

Table 2—Major- and trace-element data for older Archean rocks from lower Quad Creek.

		Weight percent															ppm																
Sample	Type	SiO2	TiO2	Al2O3	Fe2O3	FeO	MnO	MgO	CaO	Na2O	K2O	P2O5	H2O+	CO2	Total	Sample	Ba	Ce	Co	Cr	Cu	Ga	La	Ni	Pb	Rb	Sr	Th	U	Y	Zn	Zr	Sample
QC-124	MB	49.79	0.61	13.95	2.78	8.07	0.29	7.29	12.56	2.36	0.75	0.03	1.19	0.55	100.22	QC-124	35	bd	48	422	85	13	5	89	1	12	96	bd	1	15	75	40	QC-124
QC-116	MB	51.09	1.03	13.44	5.73	8.42	0.27	5.08	9.27	2.15	0.89	0.10	1.22	0.27	98.96	QC-116	121	14	44	96	32	18	6	53	7	9	139	bd	1	29	105	101	QC-116
QC-110	MA	55.06	0.99	15.30	3.25	5.24	0.15	4.33	6.61	3.03	1.94	0.45	1.64	0.27	98.26	QC-110	1313	139	27	156	48	18	71	66	13	73	614	9	1	27	80	251	QC-110
QC-112	MD	64.66	0.82	15.28	1.83	3.00	0.11	1.84	3.94	4.13	1.70	0.43	0.96	0.40	99.10	QC-112	719	91	17	3	54	16	45	5	8	92	410	13	3	26	64	202	QC-112
QC-133	MD	69.12	0.35	15.80	0.80	2.36	0.04	1.77	3.96	3.34	1.44	0.06	0.75	0.37	100.16	QC-133	326	61	33	23	17	18	32	10	8	55	492	11	2	8	34	96	QC-133
QC-118	MD	69.89	0.29	16.03	0.58	1.50	0.03	1.12	3.64	4.58	1.18	0.07	0.35	0.19	99.45	QC-118	443	13	7	9	4	17	14	0	12	49	388	0	1	5	23	87	QC-118
QC-114	MD	73.58	0.15	14.44	0.42	0.59	0.02	0.54	2.10	4.15	2.82	0.03	0.12	0.15	99.11	QC-114	477	40	18	2	0	14	18	bd	23	64	162	11	1	8	13	117	QC-114
QC-125	MR	71.18	0.27	14.72	0.41	1.10	0.02	0.74	2.10	2.96	4.30	0.04	0.60	0.19	98.63	QC-125	1412	62	40	13	8	18	38	bd	19	97	556	10	1	5	15	186	QC-125
QC-117	MR	74.34	0.15	13.99	0.53	0.62	0.03	0.58	1.82	3.50	3.81	0.02	0.04	0.14	99.57	QC-117	696	32	14	2	1	13	27	bd	20	91	172	12	0	9	12	101	QC-117
QC-130	MQ	79.36	0.19	10.51	0.31	0.68	0.02	0.88	0.89	1.80	3.72	0.02	1.00	0.28	99.66	QC-130	974	36	28	136	bd	10	20	4	18	57	255	9	2	5	4	312	QC-130

Rock types based entirely on compositional characteristics.
MB = metabasaltic MR = metarhyolitic
MA = meta-andesitic MQ = metaquartzite
MD = metadacitic

Table 3—Major- and trace-element data for older Archean rocks from lower Hellroaring Plateau.

		Weight percent															ppm																
Sample	Type	SiO_2	TiO_2	Al_2O_3	Fe_2O_3	FeO	MnO	MgO	CaO	Na_2O	K_2O	P_2O_5	H_2O+	CO_2	Total	Sample	Ba	Ce	Co	Cr	Cu	Ga	La	Ni	Pb	Rb	Sr	Th	U	Y	Zn	Zr	Sample
HR-156	MB	48.71	0.74	13.26	2.86	9.41	0.27	9.07	10.62	2.56	0.82	0.04	1.20	0.36	99.92	HR-156	397	5	64	549	18	9	6	240	3	15	138	2	0	14	86	53	HR-156
HR-159	MB	50.03	0.85	13.05	2.61	9.41	0.29	6.94	10.62	2.69	0.76	0.05	1.06	0.60	98.96	HR-159	127	15	52	198	76	12	8	149	0	14	130	bd	2	14	83	66	HR-159
HR-165	AM	54.88	1.58	15.33	4.13	7.46	0.12	3.54	4.42	0.58	3.88	0.35	2.70	1.20	100.17	HR-165	475	38	40	28	16	20	20	73	7	186	130	6	2	18	24	157	HR-165
HR-152	MA	57.32	0.71	12.92	2.02	9.70	0.28	5.60	4.33	1.98	1.34	0.11	2.33	0.28	98.92	HR-152	2547	41	43	22	46	17	20	49	7	57	98	8	1	18	108	128	HR-152
HR-145	MA	57.83	0.91	16.50	1.18	7.52	0.08	5.36	3.19	2.90	1.44	0.07	1.39	0.54	98.91	HR-145	110	13	33	330	7	17	11	127	20	44	129	6	3	18	100	90	HR-145
HR-155	MD	64.16	0.56	17.23	0.75	2.95	0.07	1.96	4.19	4.55	1.14	0.12	1.65	0.14	99.47	HR-155	826	45	16	21	11	20	29	13	4	49	379	3	2	5	51	154	HR-155
HR-142	MD	69.71	0.21	16.26	0.44	1.42	0.03	1.75	1.42	6.95	0.47	0.05	1.07	0.04	99.82	HR-142	86	12	12	28	9	16	3	9	2	10	157	bd	2	3	11	83	HR-142
HR-153	MR	70.84	0.18	15.50	0.21	0.83	0.02	0.68	2.32	4.23	3.44	0.05	0.11	0.00	98.41	HR-153	1345	36	6	2	1	17	14	bd	17	80	408	2	1	5	12	102	HR-153
HR-158	MQW	75.97	0.41	8.60	0.99	2.01	0.26	2.09	4.08	1.33	1.94	0.04	1.18	0.30	99.20	HR-158	1180	bd	36	1341	54	7	5	117	0	71	31	bd	1	9	22	37	HR-158
HR-167	MQ	83.37	0.08	7.44	0.26	0.59	0.06	1.98	1.98	1.16	1.22	0.02	1.10	0.17	99.43	HR-167	200	24	16	47	bd	7	20	3	0	63	38	4	1	10	6	94	HR-167

Rock types based entirely on compositonal charcateristics.

MB = metabasaltic
AM = altered mafic
MA = meta-andesitic
MD = metadacitic
MR = metarhyolitic
MQW = metaquartzwacke
MQ = metaquartzite

Table 4—Major- and trace-element data for older Archean rocks from the Christmas Lake and Wyoming Creek areas.

		Weight percent															ppm																
Sample	Type	SiO_2	TiO_2	Al_2O_3	Fe_2O_3	FeO	MnO	MgO	CaO	Na_2O	K_2O	P_2O_5	H_2O+	CO_2	Total	Sample	Ba	Ce	Co	Cr	Cu	Ga	La	Ni	Pb	Rb	Sr	Th	U	Y	Zn	Zr	Sample
CL-10	MB	49.21	0.88	14.00	3.55	7.78	0.22	6.87	10.57	2.40	0.81	0.07	1.46	0.42	98.24	CL-10	115	bd	46	263	30	14	2	95	6	11	95	1	1	23	77	66	CL-10
CL-2	MB	50.54	0.78	13.58	4.19	8.83	0.21	6.99	10.44	3.04	0.92	0.05	1.35	0.04	100.96	CL-2	31	35	57	204	92	18	9	80	3	7	88	4	2	19	95	51	CL-2
CL-7	MB	52.86	0.34	14.83	2.75	6.11	0.18	6.56	9.38	3.22	0.78	0.05	1.26	0.39	98.71	CL-7	152	2	57	286	3	14	15	100	8	14	137	0	0	16	58	58	CL-7
CL-6	MA	55.27	0.34	14.88	2.46	6.37	0.15	6.76	9.07	3.47	0.74	0.05	1.37	0.06	100.99	CL-6	93	30	45	267	25	15	4	104	15	5	117	5	3	17	76	59	CL-6
CL-4	MA	56.27	0.32	15.43	2.39	5.18	0.16	5.74	7.99	3.82	1.09	0.05	1.60	0.04	100.08	CL-4	36	28	44	128	29	16	4	79	13	37	178	5	3	18	77	74	CL-4
CL-9	MA	61.16	0.52	15.90	2.38	3.04	0.10	3.35	5.12	3.78	1.59	0.10	1.24	0.46	98.74	CL-9	483	39	38	117	34	17	15	47	7	72	404	4	2	11	56	134	CL-9
CL-8	MD	64.05	0.42	14.41	1.84	4.04	0.13	3.38	4.00	3.12	2.08	0.12	1.39	0.12	99.10	CL-8	334	71	29	167	bd	16	35	56	9	129	215	13	1	18	60	118	CL-8
CL-3	MD	66.84	0.59	15.64	1.64	3.12	0.10	1.78	3.20	4.41	1.86	0.15	0.82	0.03	100.18	CL-3	178	55	16	11	33	21	9	19	21	132	208	16	2	17	89	162	CL-3
CL-13	MD	68.08	0.28	16.97	0.77	1.60	0.05	1.16	3.43	5.28	1.28	0.06	0.85	0.30	100.11	CL-13	128	51	19	6	8	19	29	11	19	74	249	5	4	9	30	142	CL-13
CL-12	MD	68.38	0.30	16.82	1.00	1.51	0.04	1.03	3.56	5.04	1.30	0.08	0.50	0.10	99.66	CL-12	155	30	17	16	2	17	32	6	14	72	265	3	3	6	23	127	CL-12
CL-11	MQW	69.57	0.62	14.36	1.70	1.55	0.04	1.14	2.16	2.98	4.21	0.16	0.61	0.09	99.19	CL-11	1811	95	44	33	24	16	49	16	28	122	209	58	2	17	38	399	CL-11
CL-1	MD	70.29	0.37	14.83	1.78	1.72	0.05	0.78	3.22	4.74	1.07	0.11	0.52	0.00	99.48	CL-1	102	43	10	0	23	16	13	6	21	60	218	13	4	10	57	229	CL-1
CL-5	HKS	76.40	0.06	13.30	0.15	0.20	0.02	0.15	1.43	3.14	4.40	0.01	0.45	0.00	99.71	CL-5	1097	8	15	14	14	15	4	6	30	104	200	5	2	2	10	42	CL-5
WC-3	MB	48.79	1.06	14.37	3.08	9.38	0.20	7.26	10.89	2.65	0.90	0.08	1.36	0.06	100.08	WC-3	109	5	56	242	2	16	3	124	7	16	104	0	2	26	116	72	WC-3
WC-6	MB	48.95	0.97	14.17	3.36	8.91	0.16	6.57	10.72	2.49	0.86	0.06	1.50	0.14	98.86	WC-6	92	0	49	195	10	15	8	119	5	10	93	0	2	28	107	66	WC-6
WC-1	MB	50.30	0.86	15.27	3.00	8.28	0.19	7.66	11.18	2.50	0.74	0.07	1.41	0.06	101.52	WC-1	84	4	46	207	0	17	5	123	4	10	94	1	0	24	96	71	WC-1
WC-5	MA	57.79	0.56	16.94	1.76	4.25	0.09	4.73	7.39	3.87	1.24	0.14	1.22	0.30	100.28	WC-5	598	40	81	163	42	19	23	60	10	48	435	4	1	19	70	126	WC-5
WC-2	MD	65.51	0.62	14.19	3.13	4.32	0.12	1.74	3.35	2.81	1.73	0.12	0.80	0.07	98.51	WC-2	854	62	36	95	36	23	29	45	15	99	227	14	5	49	110	365	WC-2
WC-4	MD	65.73	0.47	15.20	1.08	3.66	0.09	2.80	2.83	3.48	2.38	0.17	0.77	0.04	98.70	WC-4	1348	64	48	190	44	19	32	86	12	106	373	11	3	14	59	163	WC-4
WC-7	MQW	69.29	0.39	14.25	0.82	3.34	0.03	2.42	2.34	2.66	3.35	0.11	0.98	0.04	100.02	WC-7	1134	70	56	195	6	18	42	78	19	157	312	15	2	14	50	148	WC-7

Rock types based entirely on compositional characteristics.

MB = metabasalt
MA = meta-andesite
MD = metadacite
MQW = metaquartzwacke
HKS = high-K silicic

about 2.8 Ga. The 2.8 Ga age is consistent with the amphibolite facies metamorphic event that is recorded in the andesitic amphibolites, although it could also be related to an event that preceded the crystallization of the protoliths at 2790 Ma.

Rb-Sr, Sm-Nd and common Pb data also provide information concerning the age of the older Archean rocks. A Rb-Sr isochron for the granitic migmatite discussed above gives an age of 2830 ± 130 Ma and an initial ratio of 0.738 ± 7. The high initial ratio of the isochron clearly shows that it represents the time at which a much older rock had its Rb-Sr system reset. A model age based on the average Rb and Sr contents and Sr isotopic values of this rock is approximately 3500 Ma, if an initial Sr ratio of 0.700 is used. The Rb-Sr data for other rocks in the older complex also indicate an Early Archean age. Henry and others (1982) reported data for many of the lithologic types discussed above, and they fall along a 3350 Ma reference isochron with an initial ratio of 0.700 (**Figure 11**). These data do not define an isochron because samples scatter both above and below the reference line. This scatter may be caused by many factors related to the complicated geologic history of these rocks. Possibilities include Rb or ^{87}Sr loss during high-grade metamorphism, Rb addition during metamorphism or later plutonism, mixing of different age rocks during plutonism or deformation, or improper identification of younger rocks included in the older complex. Although the samples with lower Rb-Sr ratios could represent mixing between Late and Early Archean materials, the samples with high Rb-Sr ratios on the reference line provide clear evidence that some Early Archean material must be present.

The implication for ages of 3.3 Ga from the Rb-Sr system is supported by Sm-Nd and Pb-Pb isotopic data. Four samples have Sm-Nd chondritic model ages between 3.3-3.5 Ga. Three other samples have model ages between 3.1-3.2 Ga. Common Pb studies (Wooden and Mueller, 1987) show that the same samples that have high Rb-Sr and Sm-Nd model ages have very radiogenic Pb compositions that are consistent with a minimum age of 3.4 Ga and very high U/Pb ratios. Most of the samples from the Hellroaring Plateau define a Pb-Pb WR isochron of 3390 ± 80 Ma (**Figure 12**). Samples from the Quad Creek area scatter around either 2.8 or 3.1 Ga Pb-Pb reference isochrons. All of these Pb-Pb isochrons lie above the Stacey and Kramers (1975) modal curve for average crust, requiring that the sources for these rocks were already very radiogenic at 2.8-3.4 Ga. Closer analysis of the Hellroaring Plateau data on an outcrop basis shows that samples from individual outcrops define ages from 3.06-3.2 Ga. If some very radiogenic samples from the Hellroaring area are considered, even younger model ages from 2.9-2.7 Ga are defined. This pattern of Pb isotopic systematics indicates that rocks significantly older than 3.2 Ga had their Pb isotopic systematics partially to com-

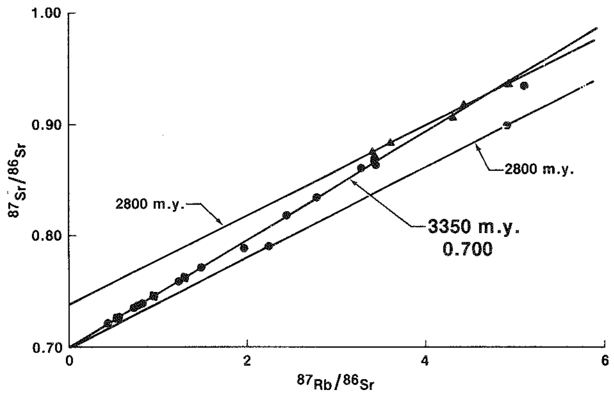

Figure 11—Rb-Sr isochron diagram for older Archean rocks of the eastern Beartooth Mountains. Most samples lie close to the 3.35 Ga reference isochron. Some samples have been reset or rehomogenized at about 2.8 Ga.

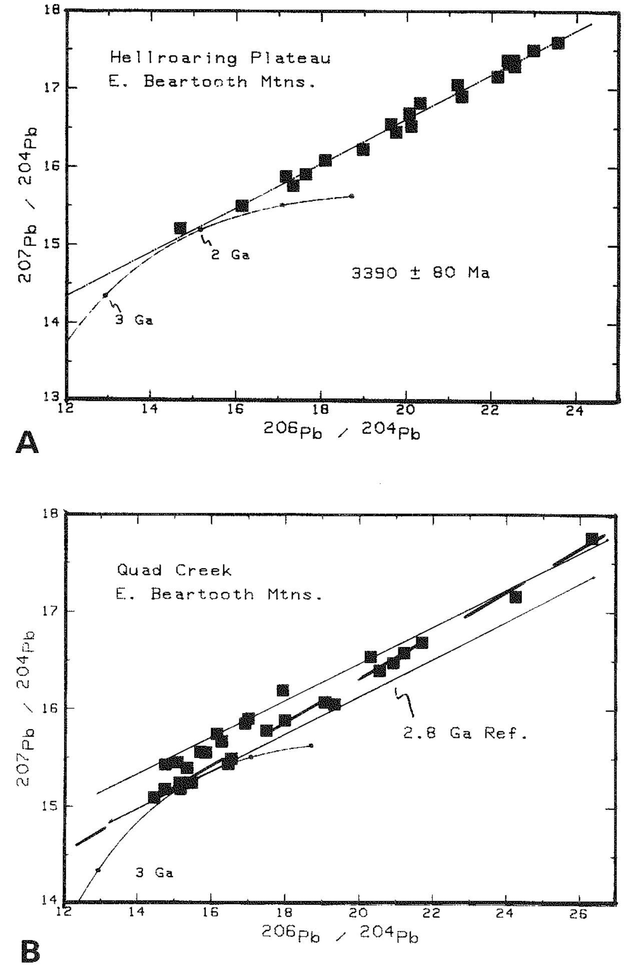

Figure 12—Pb-Pb isochron diagrams for older Archean rocks from (A), Hellroaring Plateau; (B), Quad Creek. Dashed line on Quad Creek plot is a 3.1 Ga reference isochron.

pletely homogenized at the outcrop scale during the Middle to Late Archean. A few samples must also have experienced significant U addition during this time. It is difficult to interpret the actual age of these resetting events, but two distinct events at about 3.1 and 2.8 Ga are strongly implied. The 2.8 Ga event may be the amphibolite-grade metamorphism and deformation associated with the andesitic amphibolites. The 3.1 Ga event may be the granulite event recorded in the Quad Creek area (Henry and others, 1982). Although the timing is uncertain, the Pb isotopic data require a high-grade metamorphic event later than the 3.3-3.4 Ga age originally suggested for the event at Quad Creek (Henry and others, 1982). In order to obtain the very radiogenic initial Pb isotopic compositions required by the reset isochrons, rocks 3.5 Ga and older with moderate to high U/Pb ratios must be involved. The high initial Pb ratios of the Late Archean complex (see above) also require the presence of older Archean material. Therefore, strong inferential, coupled with some direct evidence, suggests that rocks at least 3.3-3.5 Ga exist in the eastern and central Beartooth Mountains. Further studies are needed to provide details of their complex history.

North-central Beartooth Mountains

The area surrounding the Stillwater Complex has been of special interest to geologists studying the origin of this famous layered mafic igneous body. Unfortunately, the field relationships in this area are complicated by major faults that separate the Stillwater Complex and the metasedimentary rocks that it intrudes from the main exposures of Archean rocks in the remainder of the Beartooth Mountains. Butler (1966) was one of the first studies to consider the transition from the Stillwater Complex and its contact metamorphosed border rocks into the dominately crystalline Archean rocks that lie to the south. Page (1977), Wooden and others (1982), and Czemanske and Zientek (1985) contain more recently published information on the area.

The Stillwater Complex intruded a sequence of metasedimentary rocks (Page, 1977; Page and Zientek, 1985) about 2700 Ma (DePaolo and Wasserburg, 1979; Mueller and Wooden, 1976). These metasedimentary rocks are variable in composition with SiO_2 ranging between 45-80 percent. Low Na and Ca contents across this range indicate that all of these rocks experienced a strong weathering cycle. High Fe, Mg, Cr and Ni contents throughout this range also indicate that the provenance lithologies for these rocks contained both quartz- and Mg-rich components. Nunes and Tilton (1971) reported U-Pb zircon ages for rocks from the aureole of 3060 and 3090 Ma (**Figure 13**). DePaolo and Wasserburg (1979) reported a single Sm-Nd chondritic model age of 3130 Ma for a hornfels. It is clear, therefore, that these rocks contain materials that are at least 3.1 Ga. The only rocks compositionally similar to these are those found in the southwestern Beartooth Mountains, particularly in the Jardine mining district (Thruston, 1986).

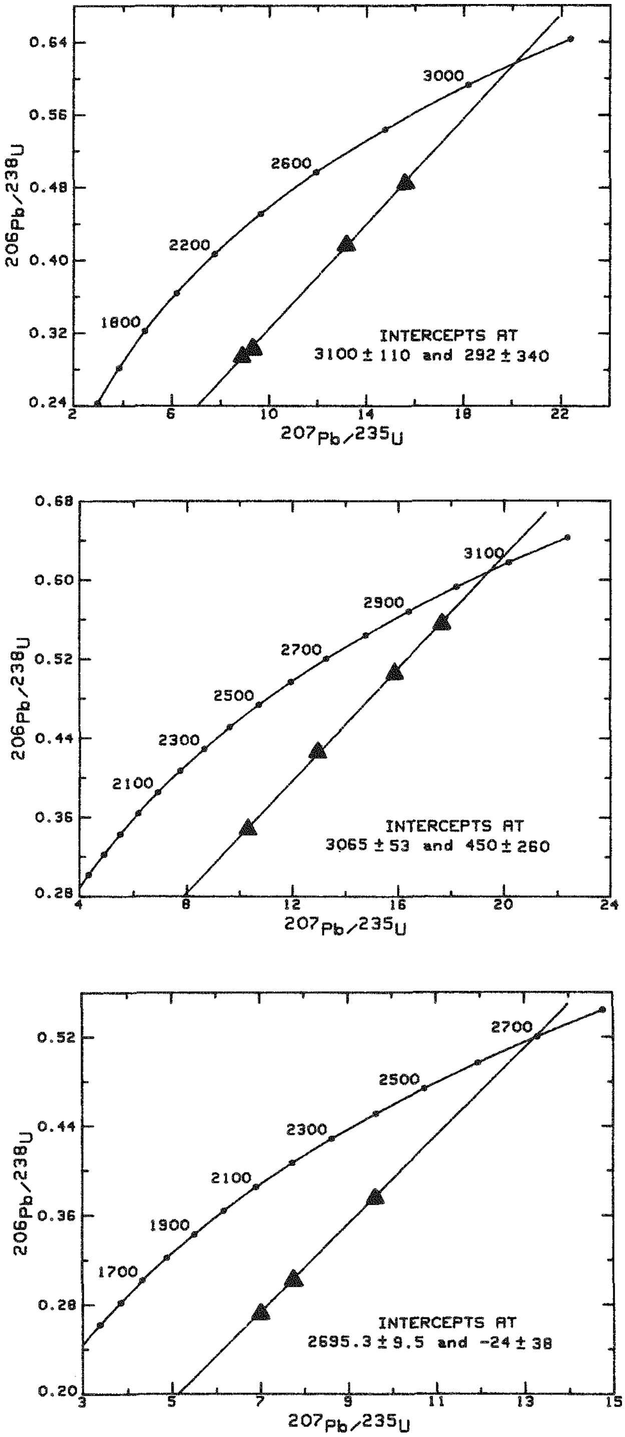

Figure 13—U-Pb concordia diagrams for granitoids at base of the Stillwater Complex, schists south of the complex, and hornfels produced by the complex. *Data from* Nunes and Tilton (1971).

The metasedimentary rocks of the aureole are separated from the crystalline rocks of the Beartooth Mountains by faults. Geissman and Mogk (1986) and Mogk (this volume) present evidence for the juxtaposition of the Stillwater block against these crystalline rocks along the Mill Creek—Stillwater fault zone. Briefly, the evidence involves a strong discontinuity in metamorphic grade (800°C and 2-3 kb for the Stillwater block vs 600°C and 7-8 kb for the crystalline rocks), structural style (preserved sedimentary structures in the aureole vs strongly developed schistose and gneissic textures in inclusions in the granitoids), and composition of supracrustal rocks (high Cr-Ni sediments vs andesitic amphibolites). This crystalline complex, however, is similar in many ways to the Late Archean complex of the eastern Beartooth Mountains. The granitoid rocks are dominated by high SiO_2, high Na members that have variable Na_2O/K_2O ratios (**Figure 14**). Some low Na granitoids are also present and rare crosscutting relationships suggest that at least some of these rocks are younger than the high Na suite. The granitoids also contain numerous inclusions of amphibolitic and schistose rocks that have dioritic/andesitic compositions or of metaplutonic rocks that have granodioritic compositions (**Tables 5, 6**). The style of intrusion for the granitic rocks seems to be one of numerous thin sheets that produce a *lit-par-lit* appearance. Pegmatite and aplite veins are the latest intrusions and account for about 20% of the rock volume (Richmond, 1987). A composite Rb-Sr isochron for the granitoid rocks in the Stillwater River valley gives an age of 2700 ± 100 Ma with an initial Sr ratio of 0.7023 (**Figure 15**). Common Pb isotopic data for the granitoids from the Stillwater River valley fall along the Pb-Pb isochron for the eastern Beartooth Late Archean complex. A U-Pb zircon age for the Hawley Peak biotite granite is 2752 ± 14 Ma (Lafrenz and others, 1986). Thus, the presently available data suggest that these rocks are generally equivalent to those of the eastern Beartooth Mountains in both age and composition.

A small body of coarse-grained granite occurs at the contact between the Stillwater Complex and the metasedimentary rocks. This granite may be a member of a larger suite of medium-grained granitoids (Page and others,1972). Nunes and Tilton (1971) obtained a zircon age of 2700 Ma on the coarse-grained granite (**Figure 13**). This is the youngest reliable Archean age for a granitoid in the Beartooth Mountains and another distinction between the Stillwater block and the adjoining crystalline terrane.

Compositional data for granitoids from the East Rosebud Creek area are presented in **Table 7**. This area is geographically situated between the eastern Beartooth Mountains and the Stillwater River valley. The porphyritic texture of many of the granitoids in the East Rosebud Creek area is distinctive relative to the granitoids in the other two areas. However, the compositional data for the East Rosebud Creek granitoids shows that most of these rocks also have the characteristics of the typical granitoids of the eastern and central Beartooth Mountains. In particular, the low Na suite of the Stillwater River valley is similar to the porphyritic samples from East Rosebud Creek.

Southwestern Beartooth Mountains

The Archean geology of the southwestern Beartooth Mountains is known from the work of Casella and others (1982). In addition, Thurston (1986) has examined the Gardiner area, where metasedimentary units are the dominant rock type. The metasedimentary units were intruded synkinematically by a variety of granitoids. The synkinematic intrusions contributed to the development of migmatite zones along contacts. The metasedimentary rocks occur as thinly bedded units of schist, quartzite, meta-conglo-

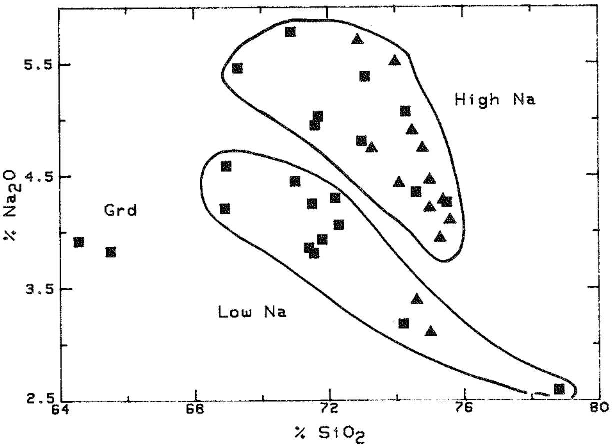

Figure 14—Weight percent SiO_2 vs weight percent Na_2O for Late Archean granitoids from the Stillwater River valley (squares) and Lake Plateau (triangles).

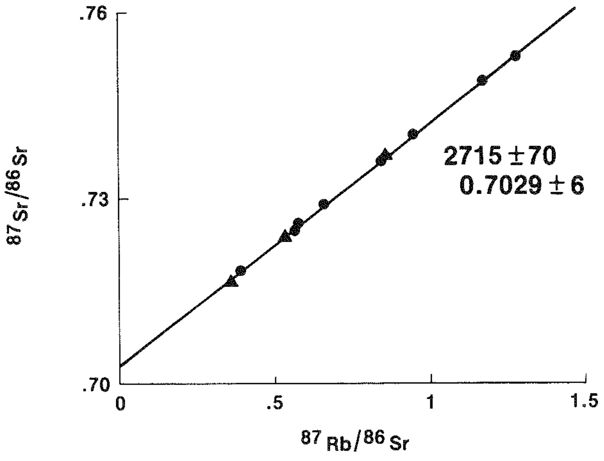

Figure 15—Rb-Sr isochron diagram for granitoids from the Stillwater River valley (circles) and East Rosebud Creek (triangles).

Table 5—Major- and trace-element data for granitoids along the Stillwater River.

		Weight percent															ppm												
Sample	Type	SiO2	TiO2	Al2O3	Fe2O3	FeO	MnO	MgO	CaO	Na2O	K2O	P2O5	H2O	CO2	Total	Sample	Ba	Rb	Sr	Zr	Ce	La	Pb	Th	Y	Cr	Ni	Sample
SW-11	LNG	68.88	0.30	15.23	1.11	1.78	0.03	0.96	2.86	4.21	2.52	0.12	0.86	0.05	98.91	SW-11	703	108	358	83	22	8	25	7	5	3	4	SW-11
SW-6	LNG	68.95	0.36	15.62	1.34	2.15	0.06	1.25	3.28	4.59	1.86	0.10	0.76	0.12	100.44	SW-6	296	95	317	49	85	49	23	15	6	8	7	SW-6
SW-8	LNG	71.00	0.30	15.01	1.35	1.69	0.05	0.86	2.96	4.45	1.77	0.08	0.55	0.00	100.07	SW-8	428	78	335	99	24	14	23	8	4	bd	5	SW-8
SW-10	LNG	72.18	0.17	15.54	0.00	1.76	0.03	0.40	2.80	4.29	2.58	0.06	0.53	0.07	100.41	SW-10	820	78	375	163	10	6	27	11	4	12	1	SW-10
SW-4	LNG	71.37	0.27	14.23	1.14	1.60	0.06	0.76	2.34	3.86	3.36	0.11	0.36	0.19	99.65	SW-4	1060	132	268	154	31	21	27	13	8	7	5	SW-4
SW-1	LNG	71.49	0.29	14.07	1.51	1.14	0.05	0.61	2.29	4.25	3.14	0.09	0.40	0.22	99.55	SW-1	1649	141	328	136	42	24	34	14	6	24	5	SW-1
SW-3	LNG	71.55	0.27	14.41	0.50	1.96	0.05	0.68	2.40	3.81	3.14	0.09	0.60	0.07	99.53	SW-3	912	111	281	150	50	26	26	12	8	4	3	SW-3
SW-2	LNG	71.83	0.28	14.39	1.12	1.48	0.06	0.63	2.31	3.93	3.14	0.09	0.41	0.17	99.84	SW-2	916	115	273	143	39	26	27	13	7	2	4	SW-2
SR-4	LNG	72.32	0.15	15.24	1.20	0.62	0.03	0.39	2.23	4.06	3.32	0.03	0.57	0.12	100.28	SR-4	1459	84	436	115	18	4	28	2	4	8	0	SR-4
SW-7	LG	78.81	0.05	11.94	0.26	0.19	0.01	0.00	1.15	2.59	4.75	0.06	0.29	0.11	100.21	SW-7	1740	120	263	76	3	3	31	8	4	11	bd	SW-7
SW-9	LG	74.19	0.16	14.41	0.65	0.55	0.02	0.16	1.84	3.18	4.66	0.04	0.29	0.14	100.29	SW-9	1739	118	341	151	10	8	34	11	4	bd	1	SW-9
SR-6	HNG	69.32	0.25	16.31	1.09	1.18	0.05	0.51	2.71	5.46	1.54	0.08	0.76	0.10	99.36	SR-6	389	36	537	185	42	21	19	10	8	6	0	SR-6
SR-2	HNG	70.90	0.25	16.49	1.16	1.10	0.03	0.19	2.66	5.78	1.49	0.07	0.67	0.07	100.86	SR-2	378	35	547	190	42	26	17	9	7	6	1	SR-2
SR-5	HNG	71.63	0.24	15.78	0.82	1.50	0.04	0.47	2.45	4.95	1.95	0.03	0.85	0.20	100.91	SR-5	290	86	264	103	42	16	28	16	7	19	0	SR-5
SW-23	HNG	71.67	0.16	15.26	0.53	0.95	0.03	0.47	2.25	5.03	2.18	0.11	0.97	0.10	99.71	SW-23	847	109	408	140	27	19	29	16	13	4	bd	SW-23
SW-21	HNG	73.00	0.18	14.87	0.70	0.97	0.03	0.39	1.85	4.81	2.36	0.07	0.58	0.20	100.01	SW-21	706	79	378	126	28	14	30	13	7	4	2	SW-21
SW-22	HNG	73.08	0.15	14.85	0.70	0.71	0.03	0.33	2.24	5.38	1.00	0.06	0.61	0.16	99.30	SW-22	163	53	375	131	25	18	24	16	7	26	bd	SW-22
SW-20	HNG	74.34	0.16	14.91	0.54	0.82	0.04	0.28	1.81	5.07	2.31	0.04	0.44	0.06	100.82	SW-20	801	71	399	112	20	14	30	12	5	0	bd	SW-20
SW-18	HNG	74.57	0.14	13.63	1.02	1.03	0.03	0.45	2.96	4.35	0.81	0.07	1.42	0.12	100.60	SW-18	129	40	303	135	14	6	20	6	7	7	6	SW-18
SR-1	HNG	75.48	0.10	14.58	1.00	0.33	0.03	0.15	1.73	4.26	3.22	0.01	0.37	0.02	101.28	SR-1	1108	89	312	80	32	18	22	12	4	2	0	SR-1
SW-16	AA	56.18	0.45	16.28	1.92	4.77	0.11	5.26	6.65	2.97	1.89	0.10	1.47	0.33	98.38	SW-16	459	90	455	100	50	23	13	9	13	171	83	SW-16
SW-17	AA	56.82	0.47	16.94	2.00	4.66	0.12	5.47	7.74	3.28	1.32	0.10	1.47	0.15	100.54	SW-17	523	43	567	108	51	18	9	6	13	171	79	SW-17
SW-5	AA	59.06	0.52	15.82	2.25	4.14	0.15	4.77	6.07	4.48	1.41	0.13	1.27	0.17	100.24	SW-5	123	79	304	119	63	28	14	12	14	155	68	SW-5
SW-19	AA	59.16	0.57	16.72	2.32	4.57	0.10	4.15	6.47	3.46	1.53	0.10	1.41	0.28	100.84	SW-19	558	53	509	110	46	19	14	10	11	85	44	SW-19
SW-12	AA	59.31	0.55	16.33	2.05	4.28	0.09	3.77	6.20	4.03	1.41	0.11	0.75	0.11	98.99	SW-12	530	75	491	123	39	12	14	9	12	76	44	SW-12
SW-13	AA	60.42	0.59	17.52	2.08	3.97	0.08	2.61	6.26	3.93	1.33	0.11	0.95	0.09	99.94	SW-13	575	60	447	124	40	14	13	6	15	7	8	SW-13
SW-14	AA	60.80	0.54	15.52	2.09	4.63	0.10	4.54	4.95	3.16	2.28	0.10	1.42	0.14	100.27	SW-14	547	126	406	108	28	15	13	8	13	211	89	SW-14
SR-3	AA?	62.61	0.42	16.40	2.44	3.57	0.12	2.53	5.22	3.97	1.39	0.08	1.03	0.18	99.96	SR-3	305	59	383	76	28	4	6	0	22	26	7	SR-3
SR-7	GRD	65.49	0.43	16.93	1.38	2.91	0.06	1.46	5.18	3.83	1.30	0.20	0.80	0.26	100.23	SR-7	342	76	150	200	42	20	10	8	28	18	14	SR-7
SW-15	GRD	64.55	0.47	16.62	1.84	2.91	0.08	2.49	5.01	3.92	1.61	0.11	0.96	0.13	100.70	SW-15	326	81	370	111	48	24	16	8	16	42	17	SW-15

HNG = high Na granitoid
LNG = low Na granitoid
LG = leucocratic granitoid
GRD = granodioritic granitoid
AA = andesitic amphibolite

Table 6—Major- and trace-element data for samples from Lake Plateau.

		Weight percent													ppm									
Sample	Type	SiO2	TiO2	Al2O3	Fe2O3T	MnO	MgO	CaO	Na2O	K2O	P2O5	LOI	Total	Sample	Ba	Sr	Zr	Nb	Y	Sc	V	Cr	Ni	Sample
LP-50	HNG	72.94	0.12	15.97	0.84	0.01	0.21	2.43	5.70	1.36	0.01	0.83	100.42	LP-50	870	406	77	22	5	3	14	13	16	LP-50
LP-23	HNG	73.35	0.21	14.95	1.80	0.03	0.35	1.84	4.74	2.83	0.01	0.37	100.48	LP-23	965	268	105	18	8	4	16	12	12	LP-23
LP-7	HNG	74.03	0.24	14.92	1.92	0.03	0.42	1.87	5.51	1.35	0.09	-	100.38	LP-7	502	340	115	-	10	6	23	13	15	LP-7
LP-35	HNG	74.07	0.15	15.12	1.37	0.01	0.36	1.81	4.43	2.71	0.09	-	100.12	LP-35	812	317	86	-	14	4	16	12	15	LP-35
LP-25	HNG	74.50	0.18	14.47	1.46	0.02	0.27	1.43	4.90	2.61	0.09	-	99.93	LP-25	941	319	96	-	12	7	33	26	33	LP-25
LP-42	HNG	74.83	0.19	14.51	1.29	0.02	0.32	2.10	4.74	2.06	0.07	-	100.13	LP-42	1420	339	72	20	4	3	14	13	14	LP-42
LP-1	HNG	74.96	0.14	13.97	1.28	0.02	0.17	1.26	4.21	3.47	0.09	-	99.57	LP-1	1250	221	76	35	9	4	17	13	17	LP-1
LP-56	HNG	75.38	0.12	14.09	0.77	0.02	0.10	0.99	4.28	4.33	0.01	-	100.09	LP-56	1280	225	56	-	4	2	3	3	3	LP-56
LP-8	HNLSG	75.64	0.08	13.79	0.81	0.03	0.03	0.81	4.11	4.20	0.01	0.31	99.82	LP-8	860	127	53	17	8	4	11	11	13	LP-8
LP-54	HNLSG	75.05	0.11	13.92	0.79	0.02	0.05	0.71	4.46	4.46	0.04	-	99.61	LP-54	580	99	47	11	9	5	3	5	4	LP-54
LP-26	HNLSG	75.28	0.08	13.97	0.51	0.01	0.01	0.71	3.94	5.13	0.16	-	99.80	LP-26	195	90	49	13	8	5	16	16	21	LP-26
LP-33	LNG	74.57	0.17	14.22	1.25	0.02	0.36	0.91	3.39	5.32	0.05	-	100.26	LP-33	1560	170	149	6	13	3	9	3	1	LP-33
LP-18	LNG	74.99	0.18	13.13	1.69	0.02	0.23	0.80	3.09	5.10	0.07	-	99.30	LP-18	1090	154	134	-	15	4	15	8	11	LP-18
LP-17	GRD	61.78	0.94	15.50	7.65	0.14	3.12	4.41	2.92	2.62	0.40	-	99.48	LP-17	1220	316	185	18	20	17	131	99	56	LP-17
LP-14	GRD	62.36	0.93	14.94	7.40	0.10	2.43	4.89	3.22	3.06	0.53	-	99.86	LP-14	3330	641	204	18	22	15	143	31	28	LP-14
LP-13	GRD	63.03	0.89	15.40	7.19	0.10	2.33	4.53	3.19	3.50	0.49	-	100.65	LP-13	3180	594	204	17	18	14	133	27	27	LP-13
LP-11	GRD	63.42	0.85	14.99	6.59	0.10	2.48	4.62	3.05	3.13	0.30	-	99.53	LP-11	1870	419	140	15	27	14	115	65	39	LP-11
LP-12	GRD	63.91	0.88	15.13	6.80	0.10	2.17	4.49	3.09	3.61	0.45	-	100.63	LP-12	3530	594	238	17	22	14	126	26	25	LP-12
LP-16	GRD	64.15	0.85	15.29	7.14	0.09	2.64	2.92	3.41	2.68	0.36	0.76	100.29	LP-16	733	237	160	22	24	15	105	70	62	LP-16
LP-15	GRD	65.26	0.76	14.91	6.32	0.08	2.17	3.82	2.85	3.31	0.28	-	99.76	LP-15	2250	428	144	12	28	14	99	56	32	LP-15
LP-55	AA	53.46	0.36	18.62	6.97	0.10	6.53	8.94	3.01	0.62	0.09	-	98.70	LP-55	291	600	44	10	7	18	103	171	105	LP-55
LP-45	AA	54.32	0.48	18.01	8.38	0.12	5.91	7.18	2.99	1.56	0.21	1.44	100.60	LP-45	473	552	36	-	7	12	135	115	65	LP-45
LP-24A	AA	56.90	0.80	16.07	9.26	0.14	4.78	7.22	3.58	1.41	0.22	-	100.38	LP-24A	677	514	70	16	13	22	187	109	77	LP-24A
LP-24B	AA	56.91	0.79	16.11	9.28	0.15	4.71	7.13	3.58	1.50	0.22	-	100.38	LP-24B	902	491	81	13	14	22	188	100	77	LP-24B
LP-21	AA	57.77	0.58	17.01	8.02	0.14	4.24	7.14	4.01	1.19	0.16	-	100.26	LP-21	536	535	67	14	13	20	145	83	57	LP-21
LP-19	AA	58.22	0.41	17.10	6.50	0.09	5.40	7.46	3.56	1.10	0.14	-	99.98	LP-19	400	473	63	13	8	16	103	120	79	LP-19
LP-52	AA	59.68	0.57	17.18	6.77	0.10	3.35	6.67	3.68	1.29	0.23	-	99.52	LP-52	528	425	98	-	14	18	140	73	68	LP-52
LP-41	AA	59.91	0.58	16.64	6.26	0.09	4.29	7.04	3.49	1.29	0.21	-	99.80	LP-41	845	526	71	23	15	17	122	19	50	LP-41
LP-51	AA	61.72	0.49	17.04	6.21	0.10	2.84	6.32	3.80	1.28	0.15	-	99.95	LP-51	456	423	69	20	12	16	122	44	46	LP-51
LP-57	AA	61.95	0.67	15.95	6.69	0.09	2.46	5.26	3.55	1.82	0.32	1.37	100.13	LP-57	389	430	158	-	23	17	142	30	39	LP-57

LNG = low Na granitoid
HNG = high Na granitoid
HNLSG = high Na low Sr granitoid
GRD = metagranodiorite
AA = andesitic amphibolite

merate and rare iron-formation. Sedimentary structures, including graded bedding, cross bedding and channel cut and fill, have been preserved in spite of the multiple periods of deformation and metamorphism that these rocks suffered. Thurston (1986) suggested that these sedimentary structures were most compatible with deposition by turbidity currents along an active continental margin. The major period of deformation produced isoclinal folds and was accompanied by amphibolite-grade metamorphism. A second period of amphibolite-grade metamorphism is associated with only minor deformation and the intrusion of two mica granites. These granites have a minimum Rb-Sr age of 2740 Ma and a high initial Sr ratio indicating that they are probably partial melts of upper crustal rocks (Wooden, 1979). Bulk compositional data for the metasedimentary rocks suggest that they were originally graywackes with a minor shale component. Thurston (1986) concluded that the petrographic and geochemical data required two sources for these rocks—mafic-ultramafic and tonalitic-trondhjemitic. These two sources are necessary to account for some samples with high transition element concentrations at high SiO_2 contents. In this respect, these rocks are very similar to those of the Stillwater block. The age of the metasedimentary sequence is uncertain, but seems to be in the range of 2.9-3.1 Ga based on model Rb-Sr data and a single model Sm-Nd age (Montgomery and Lytwyn, 1984). U-Pb ages of about 3.2 Ga for zircons in samples from the Gardiner area have been determined.

The metasedimentary sequence is intruded along the eastern edge of its exposure by granitoids. The earliest of these granitoids is a quartz-hornblende diorite that appears to be similar to the andesitic amphibolites of the eastern and central Beartooth Mountains. Intrusive into these rocks is a composite batholith with phases varying from tonalite to granite, but with granodiorite dominating. The bulk compositions of some of these rocks are similar to the granitoids of the eastern and central Beartooth Mountains. However, the majority of these rocks have higher K_2O/Na_2O ratios at the same SiO_2 level, and a greater number of the samples have weight% SiO_2 contents in the 60s, in keeping with their granodioritic modal classification. The Rb-Sr and U-Pb zircon data (Montgomery, 1982; Montgomery and Lytwyn, 1984; Wooden, 1979) are consistent with these rocks being the same age as the granitoids of the eastern and central Beartooth Mountains, but a significant reheating of this area in the Proterozoic has complicated the Rb-Sr systematics of these rocks.

Northwestern Beartooth Mountains

The northwestern part of the Beartooth Mountains is commonly referred to as the North Snowy block. This area was first described in detail by Reid and others (1975). Subsequent work by Mogk (1982, 1984) has added to the structural and geochemical knowledge of the area and allowed for new interpretations. Mogk and others (1988) show that this area is composed of a series of lithologically and metamorphically distinct packages that have been juxtaposed by tectonic processes. There are seven major units which can be defined from east to west.

(1) The *Mount Cowen augen gneiss* **(Figure 16)** contains augen-textured granitoids that occur marginal to the paragneiss unit (see below). The augen texture disappears to the east suggesting that these rocks may be only a textural variant of the massive granitoids to the east. Rock types range from granodiorite to granite **(Table 8)**. Unlike the granitoids of the eastern and central Beartooth Mountains, this unit has Na_2O/K_2O ratios consistently less than one, and higher Rb/Sr ratios. Although these rocks are similar in some respects to the low Na suites to the east, there are too many significant compositional differences to assign them directly to those low Na groups. A Rb-Sr isochron for samples from this unit gives an age of 2740 ± 50 Ma and an initial ratio of 0.7023, both of which are within error of the data for the eastern and central granitoids. In addition, common Pb isotopic data for these samples either lie along (or slightly above) the 2780 Ma isochron for Late Archean rocks of the eastern and central Beartooth Mountains (Wooden and Mueller, 1988).

(2) The *paragneiss unit* contains a heterogeneous assemblage of supracrustal rocks, including quartzofeldspathic gneisses, pelitic schists, amphibolites and banded-iron formation.

(3) The *augen gneiss sill* that is texturally and compositionally similar to some members of the Mount Cowan augen gneiss. This unit has intrusive contacts with the paragneiss and the Davis Creek schist (see below), and has a U-Pb zircon age of 2564 ± 13 Ma (Mogk and others, 1988). It is interpreted as

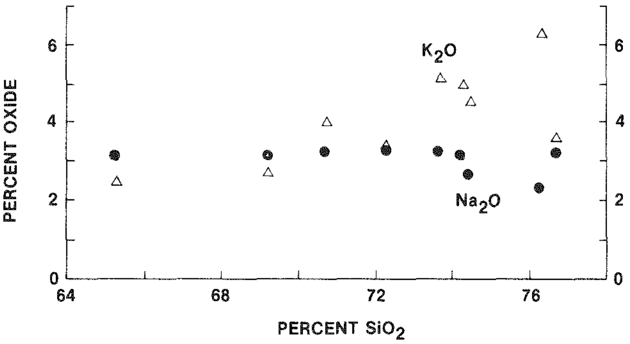

Figure 16—Weight percent SiO_2 vs weight percent NaO_2 and K_2O for the Mount Cowen granitic gneiss of the northwestern Beartooth Mountains.

Table 7—Major- and trace-element data for granitoids along East Rosebud Creek.

Sample	Type	Weight percent														ppm											
		SiO_2	TiO_2	Al_2O_3	Fe_2O_3	FeO	MnO	MgO	CaO	Na_2O	K_2O	P_2O_5	H_2O	CO_2	Total	Ba	Rb	Sr	Zr	Ce	La	Pb	Th	Y	Cr	Ni	Sample
ER-11	CGMG	62.86	0.68	16.88	2.21	2.76	0.03	2.26	4.73	4.70	1.63	0.20	0.86	0.44	100.24	745	62	565	95	28	14	4	0	3	66	26	ER-11
ER-15	LGR	67.57	0.36	16.76	0.81	1.57	0.00	1.15	3.33	5.59	1.62	0.05	0.24	0.22	99.27	279	39	283	230	43	25	16	18	6	12	8	ER-15
ER-6	DPRG	68.21	0.42	15.68	1.55	1.96	0.06	1.35	3.74	4.07	1.84	0.12	0.46	0.18	99.64	1621	35	435	172	40	22	8	3	7	32	12	ER-6
ER-2	PRG	68.27	0.50	15.70	1.95	1.86	0.05	1.50	3.27	4.89	1.99	0.15	0.62	0.11	100.86	799	56	429	162	67	42	9	3	8	25	9	ER-2
ER-5	DPRG	68.29	0.43	15.73	1.75	1.73	0.06	1.28	3.54	3.70	2.30	0.10	0.55	0.16	99.62	2012	44	410	171	39	24	10	1	9	25	14	ER-5
ER-13	GREL	68.99	0.27	16.31	0.67	0.93	0.02	0.80	3.16	6.67	1.46	0.09	0.66	0.31	100.34	1393	241	225	241	343	193	71	109	33	0	7	ER-13
ER-3	PRG	69.28	0.38	15.80	0.86	1.50	0.04	0.86	2.93	4.22	2.43	0.10	0.63	0.30	99.33	946	58	308	169	37	20	15	5	8	13	3	ER-3
ER-8	BGN	69.59	0.39	15.88	1.48	1.70	0.06	1.20	3.63	4.84	1.37	0.11	0.40	0.14	100.79	423	66	284	131	52	30	11	9	16	32	4	ER-8
ER-12	GREL	69.72	0.34	15.25	0.51	1.09	0.04	1.12	3.64	4.46	1.33	0.08	3.50	0.32	101.40	392	44	373	194	22	20	12	2	4	20	7	ER-12
ER-4	DPRG	70.04	0.31	14.83	1.12	1.29	0.05	0.61	1.63	3.89	4.89	0.09	0.52	0.14	99.41	855	169	145	140	114	66	20	15	8	9	6	ER-4
ER-1	PRG	70.97	0.29	15.14	1.25	1.17	0.04	0.76	2.63	4.15	2.84	0.09	0.65	0.05	100.03	1117	102	372	129	53	35	14	4	6	12	2	ER-1
ER-18	GRRL	73.97	0.13	13.91	0.07	0.64	0.04	0.52	1.47	3.77	4.01	0.02	0.42	0.23	99.20	1095	80	237	119	27	21	23	10	4	0	1	ER-18
ER-7	LUGR	74.40	0.12	13.82	0.94	0.44	0.00	0.00	1.38	3.55	4.47	0.01	0.22	0.11	99.46	890	87	166	76	28	19	21	12	3	1	0	ER-7
ER-14	BGN	77.06	0.28	11.86	0.13	0.93	0.04	1.47	1.82	3.61	2.35	0.03	0.77	0.18	100.53	1668	73	104	168	41	27	12	9	6	52	15	ER-14

PRG = porphyritic granitoid
DPRG = deformed porphyritic granitoid
CGMG = coarse-grained mafic granitoid
LUGR = leucocratic granitoid
BGN = banded gneiss
LGR = lavender colored granitoid
GREL = granitoid at Elk Lake
GRRL = granitoid at Rimrock Lake

Table 8—Major- and trace-element data for the Mount Cowan augen gneiss along West Boulder River.

Sample	Weight percent														Sample	ppm											Sample
	SiO_2	TiO_2	Al_2O_3	Fe_2O_3	FeO	MnO	MgO	CaO	Na_2O	K_2O	P_2O_5	H_2O	CO_2	Total		Ba	Rb	Sr	Zr	Ce	La	Pb	Th	Y	Cr	Ni	
MG-5	65.29	0.72	15.00	2.30	3.28	0.07	2.20	4.31	3.11	2.47	0.23	1.22	0.15	100.35	MG-5	979	100	379	217	109	63	15	15	18	40	18	MG-5
MG-8	69.22	0.51	14.15	1.76	2.41	0.05	1.49	3.45	3.11	2.71	0.16	0.84	0.12	99.98	MG-8	863	95	290	183	141	81	15	24	19	25	14	MG-8
MG-7	70.56	0.45	14.36	1.60	1.84	0.05	1.04	2.45	3.13	3.96	0.15	1.02	0.09	100.70	MG-7	854	150	222	186	116	61	25	30	18	18	6	MG-7
MG-3	72.25	0.38	13.48	1.21	1.95	0.07	0.91	2.16	3.39	3.48	0.12	0.96	0.15	100.51	MG-3	793	72	189	200	40	22	18	7	13	16	7	MG-3
MG-4	73.58	0.22	13.96	0.47	1.34	0.04	0.38	1.22	3.19	5.17	0.05	0.47	0.07	100.16	MG-4	676	173	101	201	131	70	51	54	16	5	4	MG-4
MG-6	74.18	0.20	13.84	0.00	1.84	0.03	0.37	0.89	3.19	4.98	0.08	0.87	0.12	100.59	MG-6	712	228	110	137	87	47	45	28	16	0	0	MG-6
MG-9	74.45	0.25	13.46	0.26	1.45	0.02	0.65	1.55	2.63	4.56	0.07	0.76	0.14	100.25	MG-9	1180	109	209	106	72	46	22	18	10	11	7	MG-9
MG-2	76.32	0.10	13.45	0.29	0.33	0.03	0.09	0.95	2.25	6.34	0.04	0.60	0.15	100.94	MG-2	1276	141	160	61	24	16	60	13	7	0	0	MG-2
MG-1	76.72	0.18	13.14	0.32	0.74	0.02	0.15	1.66	3.34	3.67	0.03	0.41	0.20	100.58	MG-1	904	93	159	91	41	24	46	21	8	8	1	MG-1

a synkinematic intrusion, and as such, would establish a minimum age for the juxtaposition of the units in this terrane.

(4) The *Davis Creek schist* is a phyllitic metapelite with minor layers of quartzite.

(5) The *trondhjemite-amphibolite complex* consists of trondhjemitic gneisses interlayered with a variety of amphibolites that range in composition from basalt to anorthositic gabbro. The trondhjemitic gneisses are similar to those found in other Archean terranes, with high SiO_2 (68-76%) and Na_2O (8-4%), low in K_2O (<2.5%), total Fe (<2%), and MgO (<1%). Unfortunately, these rocks are in a ductile shear zone metamorphosed in the epidote-obligoclase facies, which probably explains why the Rb-Sr whole-rock data are scattered (**Figure 17**). The majority of data lie close to a 3.4 Ga reference line, but a significant number of samples lie to the left of the line indicating unrealistically old ages. An Early Archean age for this unit is supported by two Sm-Nd chondritic model ages of 3.26 and 3.59 Ga. U-Pb zircon data have not yielded simple patterns. The oldest Pb-Pb ages from these zircons range from 2885-3050 Ma in spite of being strongly discordant and are therefore supportive of a minimum Middle Archean age.

(6) The *Pine Creek nappe complex* is cored by the Barney Creek amphibolite that is enclosed by symmetrically disposed beds of Jewel Lake quartzite and George Lake marble. The amphibolite ranges in composition from basaltic to andesitic. A single chondritic Sm-Nd model age of 3.2 Ga suggests a Middle Archean protolith for at least part of this unit. A U-Pb sphene age of 2568 Ma from the amphibolite is very similar to the zircon age of the augen gneiss sill. The sphene age establishes that this unit has not been above 400-500°C since that time.

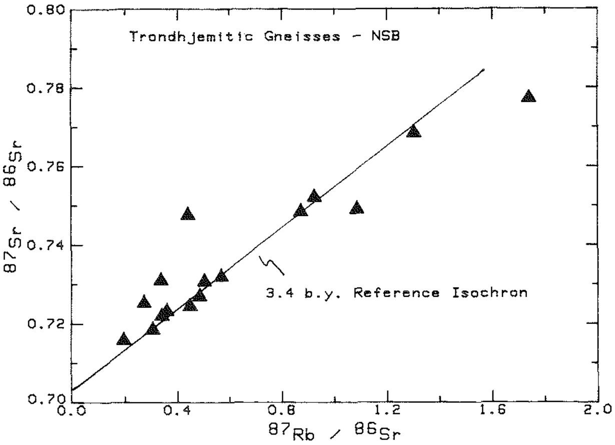

Figure 17—Rb-Sr isochron diagram for trondhjemitic gneisses of the North Snowy block.

(7) The *supracrustal—migmatite complex* consists of a supracrustal package with quartzites, amphibolites and minor schists that contains gneisses of granitic to tonalitic composition that appear to have been injected into the supracrustal rocks. The Rb-Sr whole-rock data for the gneisses indicate that these rocks are approximately 3.4 Ga. The data lie along the reference isochron for the trondhjemitic gneiss discussed above and there are compositonal similarities between some members of the heterogeneous gneiss and the trondhjemitic gneiss.

Summary

The Archean rocks of the Beartooth Mountains can be divided into four distinct terranes. Approximately two-thirds of the range is composed of Late Archean granitoids that intruded slightly older (2.74 Ga vs 2.79 Ga) amphibiolites of andesitic composition and foliated granitoids of granodioritc composition. The andesitic amphibolites are at middle amphibolite grade and are usually well foliated, indicating a period of metamorphism and deformation that occurred after 2.79 Ga, but before the main mass of the later granitoids was emplaced. The andesitic rocks have a range of major- and trace-element compositions indicating that they are composed of a complex suite of rocks. The major-element compositions are completely compatible with modern andesitic suites; however, incompatible trace elements show a wide range from typical to extremely enriched, implying variable involvement of a trace-element-enriched fluid in the genesis of these rocks. Many of the granodioritic rocks have this same trace-element-enriched character. The intruding granitoids are dominantly siliceous and Na rich and have variable K contents. These granitoids were emplaced mainly as sheets with individual plutons being difficult to recognize. The isotopic data indicate that all of the Late Archean rocks represent a single, major, crust-forming cycle that sampled a mantle source with an enriched isotopic character. All characteristics of this crust-forming cycle are compatible with a tectonic environment similar to that found in a modern zone of plate convergence.

Older Archean rocks are found in all four areas of the range although they seem limited to the edge of the exposed area dominated by the Late Archean granitoids and amphibolites. In the eastern and central Beartooth Mountains several packages of layered, gneissic rocks occur with extremely variable compositions. These compositions vary from ultramafic to dacitic and rhyolitic and from ironstone to quartzite, but no carbonates are present. Most of the rocks have experienced at least one period of granulite grade metamorphism and all have been isoclinally folded; rocks with meta-igneous compositions dominate. The compositional characteristics among packages do vary, which suggests that differences in age and/or origin may exist. The isotopic data do not establish well-defined ages, but do indicate probable ages of 3.2 to 3.6 Ga.

The older Archean rocks in the Stillwater block and the southwestern Beartooth Mountains are dominantly metasedimentary. These metasedimentary rocks share several common features, including preservation of sedimentary structures; low to moderate pressure metamorphism; high Ni and Cr contents (even high Si samples), and very low Ca and Na contents. The U-Pb geochronology indicates zircons from samples from both areas have ages of about 3.1-3.2 Ga. A tentative correlation between the metasedimentary rocks in these two areas is suggested, although the later Archean history of the two areas is different.

Finally, the North Snowy block is a very different terrane. Seven varied lithologic packages are juxtaposed there, perhaps as the result of collisional tectonics similar to those seen in modern plate tectonics. Many of the rocks in the various packages may be Middle to Early Archean in age. Several lithologic types, including a trondhjemitic and a carbonate unit, are not found elsewhere in the Beartooth Mountains. The present interpretation is that much of this area is allochthonous, having been moved from the west in the Late Archean (Mogk and others, 1988).

Acknowledgements

Much of the information presented here was originally compiled for a paper by Wooden and others (1988). The section of that paper on the Beartooth Mountains has been significantly updated and supplemented with compositional data for this volume. The authors wish to thank Gary Ernst who stimulated the writing of the original paper, and Fred Barker whose review improved the manuscript and whose present work in the eastern Beartooths has stimulated new ideas. The authors acknowledge the contributions of earlier workers in the Beartooth Mountains and to the basic geologic interpretations of the area which provided the framework for this study. This research has been funded by the National Science Foundation, the U.S. Geological Survey, NASA's Crustal Genesis Program, National Research Council, and NASA RTOP's to Larry Nyquist.

References

Aleinikoff, J. N., Williams, I. S., Compston, W., Stuckless, J. S., and Worl, R. G., 1987, Conventional and ion microprobe U-Pb ages of Archean rocks from the Wind River Range, Wyoming: Geological Society of America Abstracts with Programs, v. 19, p. 569.

Arth, J. G., Barker, F., and Stern, T. W., 1980, Geochronology of Archean gneisses in the Lake Helena area, southwestern Bighorn Mountains, Wyoming: Precambrian Geology, v. 11, p. 11-22.

Barker, F., Arth, J. G., and Millard, H. T., 1979, Archean trondhjemites of the southwestern Bighorn Mountains, Wyoming: A preliminary report, *in* Trondhjemites, Dacites, and Related Rocks, Fred Barker, *(ed.)*: Elsevier, Amsterdam, p. 401-414.

Bulter, J. R., 1966, Geologic evolution of the Beartooth Mountains, Montana and Wyoming, part 6, Cathedral Peak area, Montana: Geological Society of America Bulletin, v. 77, p. 45-64.

______ 1969, Origin of Precambrian granitic gneiss in the Beartooth Mountains, Montana and Wyoming: Geolological Society of America Memoir 115, p. 73-101.

Casella, C. J., 1964, Geologic evolution of the Beartooth Mountains, Montana and Wyoming, part 4, Relationship between Precambrian and Laramide structures in the Line Creek area: Geological Society of America Bulletin, v. 75, p. 969-986.

______ 1969, A review of the Precambrian geology of the eastern Beartooth Mountains, Montana and Wyoming: Geological Society of America Memoir 115, p. 53-71.

Casella, C. J., Levay, J., Eble, E., Hirst, B., Huffman, K., Lahti, V., and Metzer, R., 1982, Precambrian geology of the southwestern Beartooth Mountains, Montana and Wyoming: Montana Bureau of Mines and Geology Special Publication 84, p. 1-24.

Condie, K. C., 1976, The Wyoming Archean province in the western United States, *in* The Early History of the Earth, B. F. Windley, *(ed.)*, John Wiley & Sons, New York, p. 499-510.

______ 1982, Trace element geochemistry of Archean greenstone belts: Earth Science Reviews, v. 112, p. 393-417.

Czamanske, G. K., and Zientek, M. L., *(eds.),* 1985, The Stillwater Complex, Montana: Geology and guide: Montana Bureau Mines and Geology Special Publication 92, 396 p.

DePaolo, D. J., and Wasserburg, G. J., 1979, Sm-Nd age of the Stillwater Complex and the mantle evolution curve for neodymium: Geochimica et Cosmochimica Acta, v. 43, p. 999-1008.

Eckelmann, F. D., and Poldervaart, A., 1957, Geologic evolution of the Beartooth Mountains, Montana and Wyoming, part 1, Archean history of the Quad Creek area: Geological Society of America Bulletin, v. 68, p. 1225-1262.

Fischer, L. B., and Stacey, J. C., 1986, Uranium-lead zircon ages and common lead measurements for the Archean gneisses of the Granite Mountains, Wyoming: U.S. Geological Survey Bulletin 1622, p. 13-24.

Gill, J. B., 1981, Orogenic Andesites and Plate Tectonics: Springer-Verlag, New York, 390 p.

Harris, R. L., 1959, Geologic evolution of the Beartooth Mountains, Montana and Wyoming, part 3, Gardner Lake area, Wyoming: Geological Society of America Bulletin, v. 70, p. 1185-1216.

Henry, D. J., Mueller, P. A., Wooden, J. L., Warner, J. L., and Lee-Berman, R., 1982, Granulite grade supracrustal assemblages of the Quad Creek area, eastern Beartooth Mountains, Montana: Montana Bureau Mines and Geology Special Publication 84, p. 147-156.

Larsen, L. H., Poldervaart, A., and Kirchmayer, M., 1966, Geologic evolution of the Beartooth Mountains, Montana and Wyoming, part 7, Structural homogeneity of gneisses in the Lonesome Mountain area: Geological Society America Bulletin, v. 77, p. 1277-1292.

Mogk, D. W., 1982, The nature of the trondhjemitic gneiss-amphibolite basement complex in the North Snowy block, Beartooth Mountains, Montana: Montana Bureau of Mines and Geology Special Publication 84, p. 83-90.

Mogk, D. W., Mueller, P. A., and Wooden, J. L., 1988, Archean tectonics of the North Snowy block, Beartooth Mountains, Montana: Journal of Geology, *(in press).*

Montgomery, C., 1982, Preliminary U-Pb dating of biotite granodiorite from the South Snowy block, Beartooth Mountains: Montana Bureau of Mines and Geology Special Publication 84, p. 41-44.

Montgomery, D. W., and Lytwyn, J. N., 1984, Rb-Sr systematics and ages of principal Precambrian lithologies in the South Snowy block, Beartooth Mountains: Journal of Geology, v. 92, p. 103-112.

Mueller, P. A., and Wooden, J. L., 1976, Rb-Sr whole-rock age of the contact aureole of the Stillwater igneous complex, Montana: Earth and Planetary Science Letters, v. 29, p. 384-388.

______ *(compilers),* 1982, Precambrian geology of the Beartooth Mountains: Montana Bureau of Mines and Geology Special Publication 84, 167 p.

Mueller, P. A., Wooden, J. L., and Bowes, D. R., 1982, Precambrian evolution of the Beartooth Mountains, Montana and Wyoming, U.S.A.: Revista Brasileira de Geociencias, v. 12, p. 215-222.

Mueller, P. A., Wooden, J. L., Odom, A. L., and Bowes, D. R., 1982, Geochemistry of the Archean rocks of the Quad Creek and Hellroaring Plateau areas of the eastern Beartooth Mountains: Montana Bureau of Mines and Geology Special Publication 84, p. 69-82.

Mueller, P. A., Wooden, J. L., Schulz, K., and Bowes, D. R., 1983, Incompatible element rich andesitic amphibolites from the Archean of Montana and Wyoming: Evidence for mantle metasomatism: Geology, v. 11, p. 203-206.

Mueller, P. A., Wooden, J. L., Henry, D. J., and Bowes, D. R., 1985, Archean crustal evolution of the eastern Beartooth Mountains, Montana and Wyoming, *in* The Stillwater Complex, Montana: Geology and Guide: G. K. Czamanske, and M. L. Zientek, *(eds.)*: Montana Bureau of Mines and Geology Special Publication 92, p. 9-20.

Newton, R. C., and Perkins, D., 1982, Thermodynamic calibration of geobarometers based on the assemblages garnet-plagioclase-orthopyroxene (clinopyroxene)-quartz: American Mineralogist, v. 67, p. 203-222.

Nunes, P. D., and Tilton, G. R., 1971, Uranium-lead ages of minerals from the Stillwater igneous complex and associated rocks, Montana: Geological Society of American Bulletin, v. 82, p. 2231-2250.

Page, N. J., 1977, Stillwater complex, Montana: Rock succession, metamorphism and structure of the complex and adjacent rocks: U.S. Geological Survey Professional Paper 999, 79 p.

Page, N. J., and Nokleberg, W. J., 1972, Genesis of mesozonal granitic rocks below the base of the Stillwater Complex: U.S. Geological Survey Professional Paper 800 D, p. D127-D141.

Page N. J., and Zientek, M. L., 1985, Petrogenesis of the metamorphic rocks beneath the Stillwater

Complex: Lithologies and structures: Montana Bureau of Mines and Geology Special Publication 92, p. 55-69.

Peterman, Z. E., 1979, Geochronology and the Archean of the United States: Economic Geology, v. 74, p. 1544-1562.

Reid, R. R., McMannis, W. J., and Palmquist, J. C., 1975, Precambrian geology of the North Snowy block, Beartooth Mountains, Montana: Geological Society of America Special Paper 157, 135 p.

Richmond, D. P., 1987, Precambrian geology of Lake Plateau, Beartooth Mountains, Montana [M.S. thesis]: Montana State University, Bozeman, 43 p.

Richmond, D. P., and Mogk, D. W., 1985, Archean geology of the Lake Plateau area, Beartooth Mountains, Montana: Geological Society of America Abstracts with Programs, v. 17, p. 262.

Shuster, R. D., Mueller, P. A., Erslev, E. A., and Bowes, D. R., 1987, Age and composition of the pre-Cherry Creek metamorphic complex of the southern Madison Range, southwestern Montana: Geological Society of America Abstracts with Programs, v. 19, p. 843.

Thruston, P. B., 1986, Geochemistry and provenance of Archean metasedimentary rocks in the southwestern Beartooth Mountains [M.S. thesis]: Montana State University, Bozeman, 74 p.

Warner, J. L., Lee-Berman, R., and Simonds, C. H., 1982, Field and petrologic relations of some Archean rocks near Long Lake, eastern Beartooth Mountains, Montana and Wyoming: Montana Bureau of Mines and Geology Special Publication 84, p. 57-68.

Wooden, J. L., 1979, Geochemistry and geochronology of Archean gneissic rocks of the southwestern Beartooth Mountains—A preliminary study, *in* Field Conference Guidebook of the United States, P. A. Mueller and J. L. Wooden, *(eds.)*: National Committee on Archean Geochemistry, p. 10-17.

Wooden, J. L., and Mueller, P. A., 1988, Pb, Sr, and Nd isotopic compositions of a suite of Late Archean igneous rocks, eastern Beartooth Mountains: Implications for crust-mantle evolution: Earth Planetary Science Letters, v. 87, p. 59-72.

Wooden, J. L., Mueller, P. A., and Bowes, D. R., 1982a, An informal guidebook for the Precambrian rocks of the Beartooth Mountains, Montana-Wyoming, *in* Magmatic processes of early planetary crusts: Magma oceans and stratiform layered intrusions: Lunar Planetary Institute Technical Report No. 82-01, p. 195-234.

Wooden, J. L. Mueller, P. A., Hunt, D. K., and Bowes, D. R., 1982b, Geochemistry and Rb-Sr geochronology of Archean rocks from the interior of the southeastern Beartooth Mountains, Montana and Wyoming: Montana Bureau of Mines and Geology Special Publication 84, p. 45-56.

Wooden, J. L., Mueller, P A., Mogk, D. W., 1988, A review of the geochemistry and geochronology of the Archean rocks of the northern Wyoming province, *in* Metamorphism and Crustal Evolution in the Western United States (Rubey Volume VII), W. G. Ernst, *(ed.)*: Prentice-Hall, New York, p. 383-410.

Zartman, R. E., and Doe, B. R., 1981, Plumbotectonics—the model: Tectonophysics, v. 75, p. 135-162.

ARCHEAN ALLOCHTHONOUS UNITS IN THE NORTHERN AND WESTERN BEARTOOTH MOUNTAINS, MONTANA

David W. Mogk
Department of Earth Sciences
Montana State University
Bozeman, Montana 59717

Introduction

The western margin of the Beartooth Mountains lies along a fundamental discontinuity between two distinct terranes in the Archean basement of the northern Wyoming province (**Figure 1**). The central and eastern Beartooth Mountains and the Bighorn Mountains are comprised dominantly of Late Archean granitoids with inclusions of older supracrustal rocks (Peterman, 1981; Henry and others, 1982; Mueller and others, 1985). The granitoids in the Beartooth Mountains have been interpreted as the product of subduction along a continental margin (Mueller and others, 1985). The Archean basement exposed west of the Beartooth Mountains consists dominantly of medium- to high-grade metasupracrustal rocks as exposed in the Gallatin Range (Spencer and Kozak, 1975), Madison Range (Erslev, 1983), Tobacco Root Mountains (Vitaliano and others, 1979), and the Ruby Range (Garihan, 1979).

The boundary between these two terranes occurs along the western margin of the Beartooth Mountains (**Figure 2**) where there is direct evidence of tectonic intercalations of metaigneous and metasedimentary units. These relations are best seen in the North Snowy block (Mogk and Henry, 1988; Mogk and others, 1988). Other allochthonous units

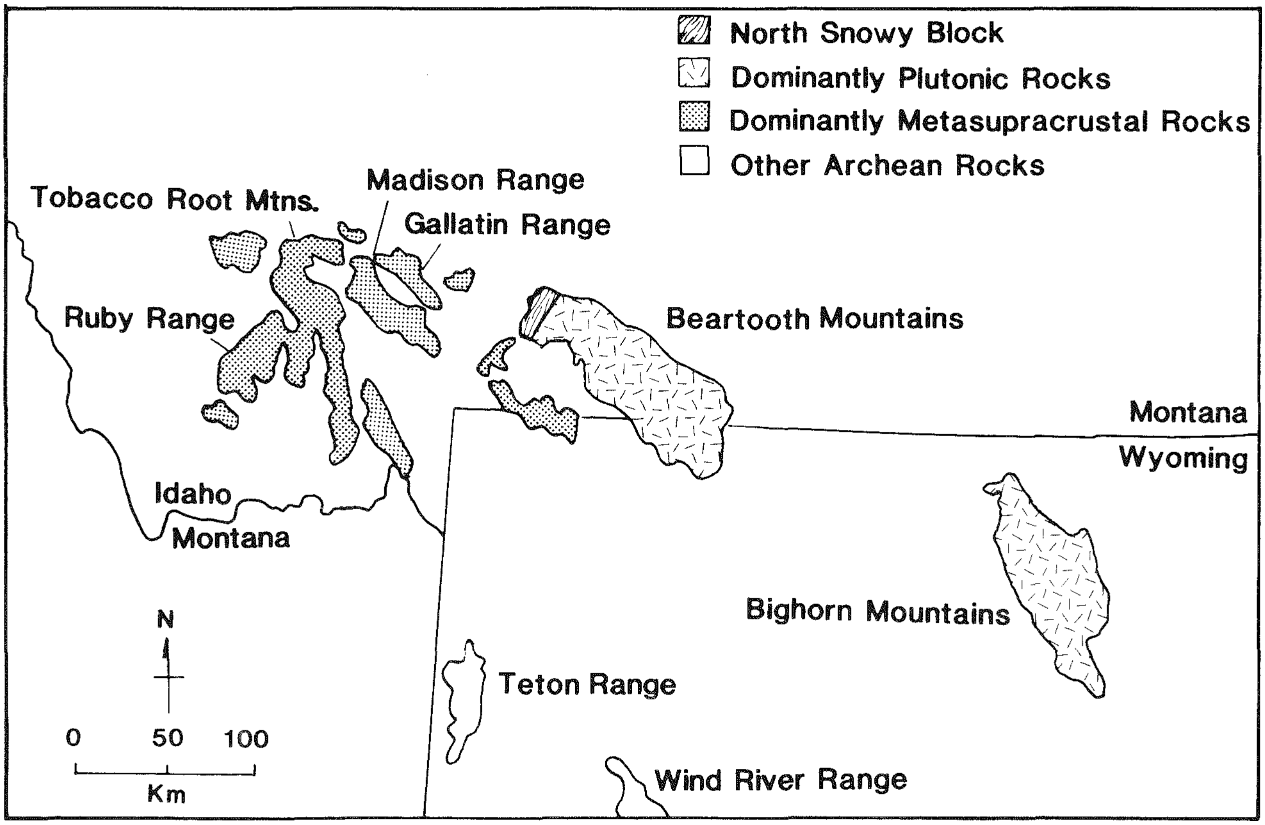
▨ North Snowy Block
☐ Dominantly Plutonic Rocks
▩ Dominantly Metasupracrustal Rocks
☐ Other Archean Rocks
Tobacco Root Mtns.
Madison Range
Gallatin Range
Ruby Range
Beartooth Mountains
Montana
Wyoming
Idaho
Montana
Bighorn Mountains
N
Teton Range
0 50 100
Km
Wind River Range

Figure 1—Sketch map of Archean exposures in the northern Wyoming province.

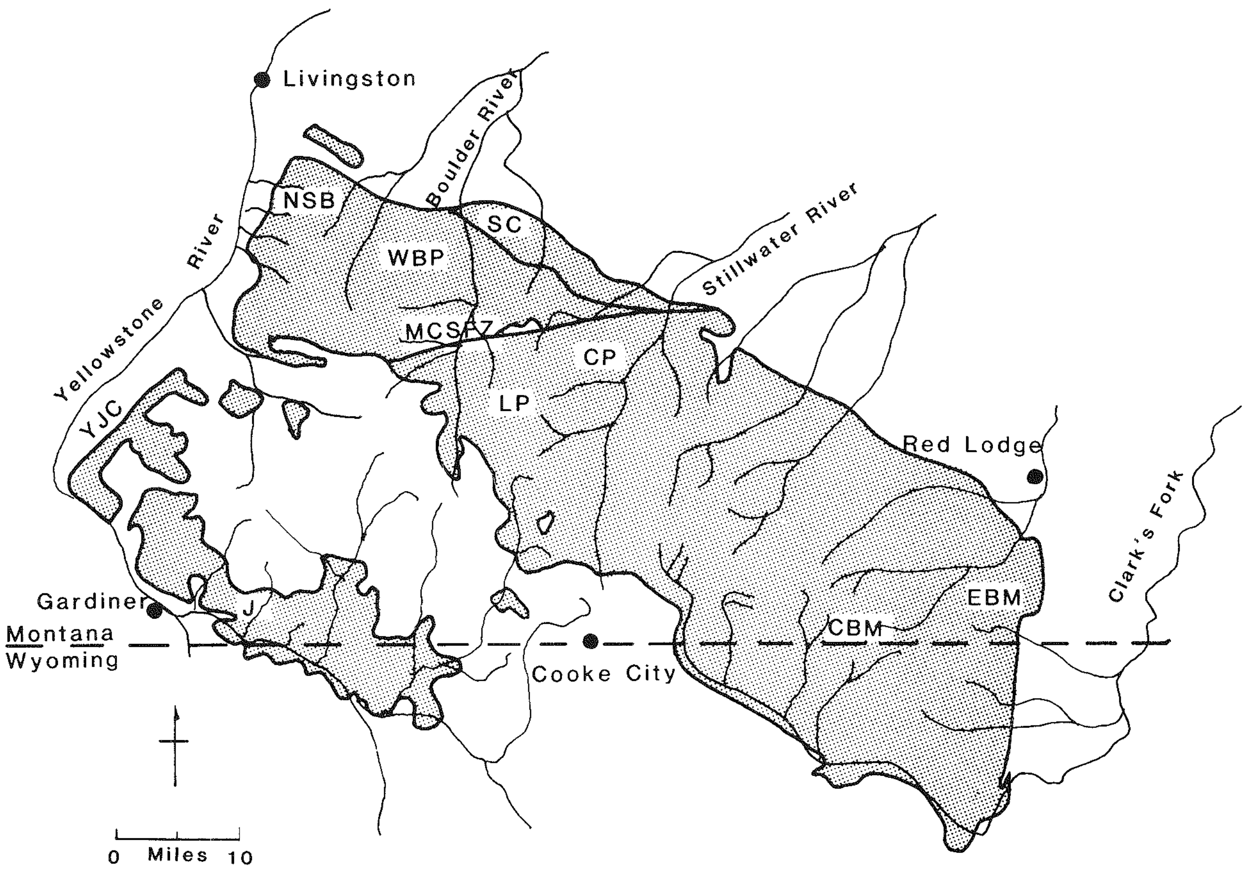

Figure 2—Sketch map of the Beartooth Mountains showing locations referred to in text: (NSB), North Snowy block; (WBP), West Boulder Plateau; (LP), Lake Plateau; (MCSFZ), Mill Creek-Stillwater fault zone; (SC), Stillwater Complex and hornfels aureole; (CP) Cathedral Peak area; (J), Jardine area; (YJC), Yankee Jim Canyon; (CBM), central Beartooth Mountains; (EBM), eastern Beartooth Mountains.

are recognized in the South Snowy block where low-grade metasedimentary rocks are tectonically juxtaposed against upper amphibolite facies rocks in the Jardine area (Thurston, 1986). In addition, the Stillwater Complex and its associated hornfels aureole were emplaced against mid-crustal granitoids of the main Beartooth Mountains (Geissman and Mogk, 1985). In each of these cases the tectonic emplacement of these units occurred in the Late Archean. Tectonic thickening of accreted allochthonous units is an important process in the evolution of this Archean continental crust. Evidence for accretion of allochthonous units in these three areas is presented in the following sections.

North Snowy block

The North Snowy block (NSB) is comprised of seven major lithologic units of Archean age: 1) the Mount Cowen granitic augen gneiss, 2) a paragneiss unit, 3) an augen-textured granitic sill, 4) the phyllitic Davis Creek schist, 5) a trondhjemitic gneiss-amphibolite complex, 6) the Pine Creek Nappe complex (**Figure 3**) which is a large-scale isoclinal structure with amphibolite core and symmetrically disposed marble and quartzite, and 7) a metasupracrustal-migmatite complex which consists of a quartzite-amphibolite unit with *lit-par-lit* injections of granitic rocks (Mogk and others, 1988). The contacts between these units are commonly mylonitic and each unit is distinguished by abrupt discontinuities in lithology, metamorphic grade and structural style. The tectonic juxtaposition of these units occurred after they had attained their peak metamorphism (i.e., the NSB is a small-scale collage of metamorphic terranes). The regional strike is northeast with a steep to moderate northwest dip. A brief description, as condensed from Mogk and others (1988), of each of these units in an east-west cross section follows:

1) The Mount Cowen granitic augen gneiss ranges in composition from granite to granodiorite. This unit contains subequal amounts of perthitic microcline, sodic oligoclase, quartz, with subordinate biotite, sphene, allanite, zircon and apatite, and retrograde chlorite, epidote, sericite and calcite. The

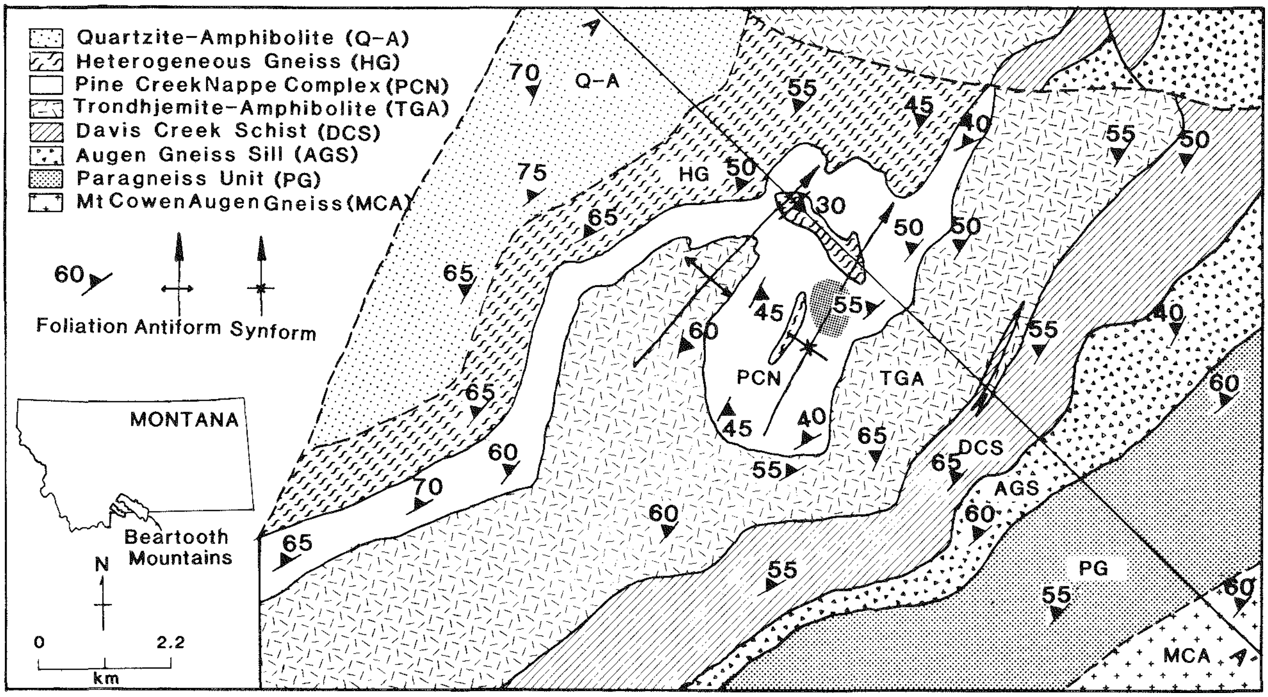

Figure 3—Geologic sketch map of part of the Pine Creek Lake area, North Snowy block. Shaded area in center of figure is Pine Creek Lake.

augen texture is characterized by anastomosing foliation defined by biotite and chlorite around K-spar porphyroclasts. The unit has a Rb-Sr whole-rock age of 2737 ± 52 Ma, and is a textural variant of the more massive granitoids exposed to the east on the West Boulder Plateau and Lake Plateau areas.

2) The paragneiss unit consists of a variety of quartzofeldspathic gneisses, psammitic schists, amphibolites and banded iron-formation. Individual compositional layers are discontinuous along strike; contacts between layers are strongly sheared and are typically retrograded suggesting a high degree of internal tectonic mixing. Anastomosing shear zones surround meter- to tens-of meter scale phacoidal pods of the various lithologies. The entire unit was metamorphosed in the upper (epidote free) amphibolite facies. Garnet-biotite temperatures are in the range of 650-700°C (Ferry and Spear, 1978). Retrograde temperatures calculated from garnet rims yield temperatures in the range of 550-650°C; the internal tectonic mixing of this unit most likely occurred under epidote-amphibolite to greenschist facies conditions. Rocks of similar composition, metamorphic grade and structural style occur to the south in the Yankee Jim Canyon area of the South Snowy block (Burnham, 1982).

3) The augen gneiss sill is compositionally and texturally identical to the Mount Cowen augen gneiss. However, recent geochronologic studies have determined a U-Pb zircon upper concordia intercept age of 2564 ± 13 Ma. This unit is in intrusive contact with the paragneiss unit and Davis Creek schist, and thus marks a minimum age for the juxtaposition of these units.

4) The Davis Creek schist is a phyllitic metapelite that contains the greenschist facies assemblage chlorite-muscovite-albite-quartz. Intrafolial isoclinal folds are locally preserved, and a late-stage disharmonic kinking folds the foliation. This unit is in tectonic contact with the overlying trondhjemitic gneiss-amphibolite complex as evidenced by mylonitic contacts, reduction of grain size, quartz ribbons, "ragged" chlorite, and anastomosing foliation around fractured albite porphyroclasts.

5) The trondhjemitic gneiss-amphibolite complex consists of trondhjemitic gneisses interlayered with discontinuous, tabular amphibolite bodies. Rb-Sr whole-rock data are scattered about a 3.4 Ga isochron and Sm-Nd whole-rock chondritic model ages of 3.55 and 3.26 Ga have been determined for the trondhjemitic gneiss. The entire unit is interpreted as a ductile shear zone. The amphibolite bodies are rotated as rigid bodies and flattened in the foliation in the relatively ductile trondhjemitic matrix. The gneisses are typically gray, and contain the major phases sodic oligoclase (45-50%), quartz (40-45%) and biotite (<10%). Accessory minerals include microcline, epidote, allanite, zircon, sphene, apatite, muscovite, chlorite and ilmenite. The texture is best described as blastomylonitic. Discrete shear zones are pervasive in the trondhjemitic gneisses and form an anastomosing foliation around plagioclase porphyroclasts. There is a marked reduction of grain size in the shear zones; quartz ribbons are well devel-

oped, and plagioclase grains have developed sub-domains, and bent or broken deformation twins. Neoblasts of both albite and oligoclase have formed around larger porphyroclasts of oligoclase indicating that dynamic recrystallization occurred at conditions below the crest of the peristerite solvus, approximately 500°C.

The amphibolites include coarse-grained varieties that are poorly foliated and finer-grained varieties with nematoblastic texture. The amphibolites have recrystallized in both the epidote-free and epidote-bearing amphibolite facies. The dominant mineral assemblage is hornblende-plagioclase-quartz ± epidote ± biotite ± sphene ± ilmenite. The amphibolites are locally crosscut by the trondhjemites; the foliation is truncated and a higher metamorphic grade is preserved in the amphibolites suggesting that they recrystallized in an earlier metamorphic cycle.

6) The Pine Creek nappe complex is an isoclinally folded thrust nappe, which structurally overlies the trondhjemitic gneiss-amphibolite complex. The core of the nappe consists of amphibolite; marble and quartzite are symmetrically disposed on the upper and lower limbs. The lower limb of the nappe is strongly attenuated, and quartzites at the contact with the trondhjemitic gneiss-amphibolite complex have developed a scaly mylonitic texture suggesting that the nappe was emplaced as a detached antiformal structure.

Metamorphism of all units in the Pine Creek nappe is in the upper (epidote free) amphibolite facies. The metamorphic mineral assemblage in the amphibolite is hornblende (Z = olive brown), oligoclase, quartz with subordinate biotite, garnet, apatite, sphene, ilmenite, zircon and pyrite. The marbles contain calcite-dolomite-quartz-diopside-phlogopite and retrograde tremolite. Garnet-biotite temperatures in the range of 600-650°C have been determined in rare schistose layers in the quartzites. The fabric in all of these units is a strong crystallization schistosity that is axial planar to intrafolial isoclinal folds. The ductile shearing observed in the underlying trondhjemitic gneiss-amphibolite complex is not present in the Pine Creek nappe. The age of the nappe rocks is difficult to determine. A single Sm-Nd chondritic model age of 3.2 Ga has been determined for the amphibolite, and a U-Pb sphene age of 2568 Ma was obtained from the same unit, indicating that the nappe has not been heated above 400°C since this time.

7) The supracrustal-migmatite complex consists of an upper quartzite-amphibolite unit (with minor schistose layers) and a lower heterogeneous gneiss unit in which granitic to tonalitic migmatites have injected the supracrustal rocks in *lit-par-lit* fashion. Evidence for injection includes crosscutting of foliation by pods of granitoids on a meter- to tens-of-meters scale, dilation of foliation planes, broken and rotated xenoliths of country rock, and partial assimilation of the country rock. The injected material consists of plagioclase, microcline and quartz in varying modal proportions, with subordinate biotite, hornblende, allanite, sphene, zircon, apatite, Fe-Ti-oxide and retrograde chlorite, epidote and sericite. The age of the migmatitic granitoids is poorly known, but six Rb-Sr whole-rock data points cluster around a 3.4 Ga reference isochron. (There is no implied genetic relationship with the trondhjemitic gneiss-amphibolite complex.) Metamorphism of the lower part of this complex is in the upper amphibolite facies. The metamorphic assemblage in pelitic layers is biotite-garnet-oligoclase-quartz with rare kyanite and late-stage fibrolitic sillimanite; garnet-biotite temperatures of these rocks is in the range of 650-700°C. The underlying Pine Creek nappe is in tectonic contact with the supracrustal-migmatite complex as evidenced by disharmonic folding, mechanical disruption of compositional layers, microcataclasis and retrogression under greenschist facies conditions of upper amphibolite facies mineral assemblages.

The North Snowy block consists of an aggregate of diverse metasedimentary and metaigneous units that have each experienced a unique metamorphic and deformational history prior to amalgamation in their present setting. The abrupt breaks in metamorphic grade between each unit can best be interpreted as the result of tectonic juxtaposition. There is a step-wise and discontinuous increase in metamorphic grade up section from the Davis Creek schist through the trondhjemitic gneiss-amphibolite complex, the Pine Creek nappe complex, and the supracrustal-migmatite complex. In addition, structural elements observed in one unit are not present in adjacent units (e.g., ductile shearing in the trondhjemitic gneiss is not present in the overlying Pine Creek nappe), and in the case of the supracrustal-migmatite complex the injection of the granitic material must have occurred in a different geologic setting because the underlying Pine Creek nappe shows no evidence of having been intruded by granitic material. Therefore, it is not appropriate to view the geologic history of this area in terms of a single chronology based on the cumulative evidence of all units as originally proposed by Reid and others (1975). Evidence presented above, and in more detail by Mogk and others (1988), leads to the interpretation that the North Snowy block formed by the tectonic interleaving of numerous diverse lithologic suites that were amalgamated in the Late Archean.

Field observations

Pine Creek Lake Trail: Access to the critical field relations in the North Snowy block can be gained via the Pine Creek Lake Trail which heads approximately 15 miles south of Livingston, Montana (Mt. Cowen 15′ quadrangle). The trail is five miles long (to Pine Creek Lake, elev. 9,032′) and is relatively steep, but it does provide the opportunity to view the units described above, as well as spectacular Alpine scenery. The first mile of the trail is in the Pine Creek valley; the outcrops to the north consist of the quartzite-amphibolite unit and injected granitic material of the migmatite complex. From the waterfall to the next creek crossing (2½ mi) the trail switchbacks across the Pine Creek nappe complex providing good exposures of amphibolite, marble and quartzite. The cliffs to the south of the trail at the 2½-mile creek crossing are the trondhjemite-amphibolite complex. From the creek crossing to Pine Creek Lake, the route is located primarily in the nappe complex. There are spectacular folded sequences in the marble and monomineralic tremolite bands (*Please do not abuse outcrops on the trail!*) The banded cliffs on the skyline are the supracrustal migmatite complex; blocks of these rocks can be seen in the talus. The cliff to the south of Jewel Lake (4 mi) shows an excellent overprinted, open, upright antiform.

The Pine Creek Lake cirque basin lies in the keel of the syncline of the overprinted open-fold system. At the east end of the lake one can walk across the sequence of quartzite-marble-amphibolite-marble-quartzite. There is a sheared schistose unit along the axial surface of the nappe. Excellent exposures occur on the divide between the Pine Creek Lake cirque and Lake McKnight where the scaly, mylonitic quartzite and attenuated lower limb of the nappe complex are exposed. The entire eastern ridge of the cirque basin is the trondhjemitic gneiss-amphibolite complex. For the intrepid hiker, a trip over Black Mountain (amphibolite in the nappe on the south side of the cirque) will cross the trondhjemitic gneiss-amphibolite complex, Davis Creek schist, granitic augen gneiss sill, and the paragneiss unit on a traverse along the ridge towards Martin Peak.

Jardine area of the South Snowy block

A thick sequence of metasedimentary rocks in the Jardine area is anomolous in the Archean basement of the Beartooth Mountains with respect to their metamorphic grade and composition. The petrology and geochemistry of these rocks were described by Thurston (1986), and Hallager (1980) described the gold mineralization of these rocks.

The rock types in the Yellowstone River canyon include quartz-biotite schists, biotite schists, metaconglomerate, banded iron-formation and felsic metavolcanic rocks. There is an overall fining of these rocks to the west, and their protoliths are interpreted as metagraywackes (quartz-biotite schist) and mudstones (biotite schists). Lithic fragments are locally preserved and these include tonalitic clasts and polycrystalline aggregates of quartz. Sedimentary structures are commonly preserved and these include compositional layering, graded bedding, low angle cross stratification, ripple cross stratification, wavy bedding, rip-up clasts and channel scour deposits; partial Bouma sequences have been recognized suggesting that these rocks were deposited by turbidity currents. The banded iron-formations include both oxide and silicate facies rocks. Metavolcanic rocks of dacitic composition are interbedded with the metasedimentary rocks. These rocks are interpreted as having been deposited along an active continental margin in a mid-to-distal fan geologic setting.

Metamorphism of this sequence is of anomolously low grade with respect to the surrounding schists and gneisses of the Beartooth Mountains. Andalusite is the stable aluminosilicate mineral; biotite, garnet, staurolite, quartz and plagioclase are the other major phases in these rocks. This paragenesis places maximum conditions of metamorphism at 3.8 kb and 550°C. The structural history of these rocks includes 1) development of S_1 foliation parallel to compositional layering, 2) development of small-scale intrafolial isoclinal folds (F_1), 3) open folds (F_2), and 4) disharmonic kink folds.

The composition of the schists is also unusual in that they contain unusually high Cr (up to 450 ppm) and Ni (up to 210 ppm) values, high MgO and FeO content and low total alkalies. This chemical signature indicates that there must have been a significant contribution of mafic or ultramafic detritus into this sedimentary sequence. A single U-Pb concordia intercept age of ca. 3.2 Ga has been determined for detrital zircons in these rocks (Paul Mueller, personal communication, 1988).

There are few rocks of appropriate age or composition currently exposed in the Beartooth Mountains that could have contributed to the deposition of this sedimentary sequence; there are small pods of ultramafic rocks in the Quad Creek, Hellroaring Plateau, and Highline Trail Lakes areas (Henry and others, 1982), but these are volumetrically insignificant in the voluminous younger granitoids of the Beartooth Mountains. The metasedimentary rocks of the Jardine area are anomolous in the Beartooth Mountains because they have lithologic and compositional similarities to sediments found in greenstone belts. The nearest exposures of similar rocks are found in central Wyoming in the Wind River and Rattlesnake Hills areas. In addition, the Jardine rocks have a metamorphic history and structural style not recognized in the surrounding Beartooth Mountains. Therefore, due to the unusual whole-rock chemistry, anomolously low metamorphic grade, and distinct structural history, it is most probable that this sequence was tectonically emplaced into its current setting after it developed its main metamorphic and structural fabric. Emplacement of the Jardine rocks occurred prior to 2.6 Ga, the age of the crosscutting Crevice quartz monzonite.

Access to low-grade metasedimentary rocks can be gained by vehicle on U.S. Forest Service roads east of Gardiner, Montana, and by hiking upstream from Gardiner along the Yellowstone River to the Bear Creek area, or by hiking in Yellowstone National Park along Blacktail Creek Trail down to the Yellowstone River canyon.

Stillwater Complex and its associated hornfels aureole

The Stillwater Complex has important tectonic implications both in its environment of formation and with respect to its current setting adjacent to the Beartooth Mountains. However, the tectonic setting of the origin of the Stillwater Complex, and its subsequent tectonic evolution has been largely overlooked; studies that have dealt with this aspect of the Stillwater Complex include Page (1977), and Page and Zientek (1985 a, b). Because of the layered nature of this intrusive body it should serve as a chronologic structural marker for Archean tectonics in the northern Wyoming province. However recent field, petrologic and paleomagnetic studies suggest that the Stillwater Complex was tectonically emplaced against the Beartooth Mountains during the Late Archean (Geissman and Mogk, 1986).

The Stillwater Complex and its associated hornfelses and the Archean schists and granitoids of the adjacent Beartooth Mountains represent two fundamentally different terranes. Evidence for the tectonic emplacement of the Stillwater Complex into its present structural setting lies in the abrupt discontinuities of metamorphic grade, structural style and geochemical signature of sedimentary rocks across the Mill Creek-Stillwater fault zone **(Figure 2)**. A full discussion of these differences is presented in Geissman and Mogk (1986); the following is a summary of the main lines of evidence:

1) The hornfelses of the Stillwater contact aureole experienced a static metamorphism, producing mineral assemblages of orthopyroxene-cordierite and anthophyllite-cordierite in pelitic rocks at temperatures of approximately 800°C and pressures of 2-3 Kb (Vaniman and others, 1980; Labotka, 1985). Metamorphism in the schists of the Beartooth Mountains is in the middle to upper amphibolite facies. The characteristic mineral assemblage is biotite-garnet-oligoclase-quartz, with local development of cordierite and late-stage fibrolitic sillimanite. Garnet-biotite temperatures (Ferry and Spear, 1978) are in the range 580-620°C, and pressures based on the garnet-cordierite barometer (Lonker, 1981) are 7-8 kb. In addition, the adjacent granitoids contain magmatic epidote, suggesting pressure of crystallization on the order of 8 kb (Zen and Hammarstrom, 1985). Butler (1969) originally suggested that the hornfelsic aureole merely overprinted the regional metamorphism recorded in the high-grade schists. However, Page (1977), and more recently Page and Zientek (1985b) recognized that these two sequences had experienced distinct geologic histories.

2) Primary sedimentary structures including graded bedding, cross bedding and cut-and-fill channels are locally preserved in the metasediments of the Stillwater aureole; rare isoclinal folds may be the result of soft sediment deformation (Page, 1977). The fabric of these rocks is granoblastic with no evidence of development of penetrative deformation. In contrast, the schists have developed a strong transposition foliation which is axial planar to mesoscopic isoclinal folds.

3) The metasediments of the Stillwater aureole are distinguished by their unusual composition. They characteristically have high MgO and FeO and low Na_2O and K_2O contents. In addition, their Cr (900-1400 ppm) and Ni (500-1000 ppm) content is extremely high. These compositions suggest a prominent component of ultramafic or mafic rocks in the source area (Page, 1977). The regionally metamorphosed schists have compositions more typical of pelitic rocks, and some of these rocks are andesitic in composition.

In addition, paleomagnetic data from the Banded series of the Stillwater Complex indicate a strong discordance with respect to nearly age equivalent rocks from the Superior province (Geissman and Mogk, 1986).

The timing of the tectonic juxtaposition of the Stillwater Complex against the granitoids and schists of the Beartooth Mountains is constrained by the following age relations: The age of the Archean Beartooth granitoids is 2735-2750 Ma (Mueller and others, 1985; Lafrenz and others, 1986), the age of the Stillwater Complex is 2700-2720 Ma (age dates summarized in Lambert and others, 1985), and the age of the Mouat quartz monzonite which is ca. 2700 to 2640 Ma (Nunes and Tilton, 1971; age recalculated using revised decay constants). The Mouat quartz monzonite crosscuts both the hornfels aureole and the Archean basement, thus placing a minimum age on the juxtaposition of these two sequences. This requires that the Stillwater Complex was intruded and crystallized at shallow levels, and was faulted along with part of its contact aureole in rapid succession. Paleomagnetic data on the Mouat quartz monzonite and Middle Proterozoic dikes are concordant with age-equivalent rocks in the Superior province, supporting the interpretation of large-scale tectonic displacement of the Stillwater Complex in the latest Archean (Geissman and Mogk, 1986).

The sense of displacement on the Mill Creek-Stillwater fault zone is problematic due to limited exposures. Geissman and Mogk (1986) have proposed that displacement occurred along an intracontinental wrench fault along the ancestral Nye-Bowler lineament. This interpretation is based on the significant gravity and magnetic anomolies located southwest of Billings, Montana known as the "Fromdorf high," which may indicate the location of the remainder of the Stillwater Complex. However, gravity modeling by Kleinkopf (1985), and the recognition of xenoliths of the Stillwater Complex in Late Cretaceous intrusive rocks in the Enos Mountain area just north of the Stillwater Complex (Brozdowski, 1985), indicate that at least some of the Stillwater Complex is buried by Phanerozoic cover northeast of present exposures.

The tectonic setting for the original emplacement of a layered mafic-ultramafic body such as the Stillwater Complex requires thick continental crust within a tensional, yet generally stable tectonic environment (Weiblen and Morley, 1980). Evidence for thick continental crust in the Beartooth Mountains is presented in Mueller and others (1985) and Mogk and Henry (1988). The tensional tectonic environment may have been established during wrench faulting within this thick continental crust. Formation of rift grabens is commonly associated with displacements along wrench faults (Molnar and Tapponier, 1975). The Stillwater Complex may have been intruded into a "pull-apart" basin along the recurrently active Nye-Bowler lineament, thus accounting for the original tensional environment, as well as the subsequent dismemberment and displacement of the complex.

The relationships discussed above demonstrate that the Stillwater Complex cannot be used as a structural chronologic marker due to its allochthonous nature. At this time it is not possible to document the transport distance of the Stillwater Complex. Whether it has experienced tens of kilometers of transcurrent displacement along the Nye-Bowler lineament as suggested by Geissman and Mogk (1986), or relatively local dismemberment and displacement, it is clear that there is on the order of 5 kb (15 km) vertical offset of the Stillwater Complex and the adjacent crystalline rocks of the Beartooth massif across the Mill Creek-Stillwater fault zone. The juxtaposition of these two rock sequences must have occurred prior to 2.7 Ga, the age of the crosscutting Mouat quartz monzonite.

There are similarities in lithology and whole-rock chemistry between the Stillwater Complex hornfels aureole and the metasediments of the Jardine area although they are on opposite sides of the Beartooth Mountains. It is not clear if there is a genetic relationship between these two sequences. However, these relationships do provide an interesting insight into the complexity of Late Archean tectonics in the northern Wyoming province. Access to the Stillwater Complex and the associated hornfels aureole is described in Czemanske and Zientek (1985); excellent exposures of the aureole can be found in the Bobcat Creek area south of Chrome Mountain.

Summary

The northern and western margins of the Beartooth Mountains contain lithologic sequences that are demonstrably allochthonous. It is difficult to reconstruct the original geometries of these units, or to determine the sense of displacement or distance of transport lacking the techniques of terrane analysis used in modern tectonic environments such as paleomagnetism, paleontology and stratigraphy. Nonetheless, discontinuities in metamorphic grade, structural style, unusual whole-rock chemistries and geochronologic constraints suggest that the northern and western part of the Beartooth Mountains are a collage of exotic units. Tectonic emplacement of these units must have occurred in the Late Archean, and is roughly contemporaneous with the development of a magmatic arc in the central and eastern Beartooth Mountains (Mueller and others, 1985; Mueller and Wooden, this volume). The western margin of the Beartooth Mountains (best seen in the North Snowy block) marks a fundamental boundary in the Archean basement between dominantly igneous rocks to the east and metasedimentary rocks to the west in the northern Wyoming province. A mechanical or accretionary boundary between these two terranes is compatible with previous studies (Mueller and others, 1985; Mogk and Henry, 1988) which suggests that plutonic rocks were produced by subduction-related magmatism. The contemporaneous development of a magmatic arc and accretion of allochthonous terranes suggests that the Beartooth Mountains experienced a collisional orogeny in the Late Archean, similar in many respects to modern convergent continental margins.

Acknowledgments

The ideas presented in this paper are the result of collaborative research with Paul Mueller, Joseph Wooden and Darrel Henry. Funding for field and analytical studies was provided by the Geological Society of America, Sigma Xi, Chevron Graduate Fellowship, NASA Early Crustal Genesis Program, and NSF (EAR-8618-327).

References

Brodzdowski, R. A., 1985, Cumulate xenoliths in the Lodgepole, Enos Mountain and Susie Peak intrusions: A guide, *in* The Stillwater Complex, Montana: Geology and guide, G. K. Czamanski and M. L. Zientek, *(eds.):* Montana Bureau of Mines and Geology Special Publication 92, p. 368-373.

Burnham, R. L., 1982, Mylonitic basement rocks in the Yankee Jim Canyon and Six Mile Creek areas, Park County, Montana: Geological Society of America Abstracts with Programs, v. 14, no. 6, p. 305.

Butler, J. R., 1966, Geologic evolution of the Beartooth Mountains, Montana and Wyoming, part 6, Cathedral Peak area, Montana: Geological Society of America Bulletin, v. 77, p. 45-64.

Czamanske, G. K., and Zientek, M. L. *(eds.),* 1985, The Stillwater Complex, Montana: Geology and guide, Montana Bureau of Mines and Geology Special Publication 92, 211 p.

Erslev, E. A., 1983, Pre-Beltian Geology of the southern Madison Range, southwestern Montana: Montana Bureau of Mines and Geology Memoir 55, 26 p.

Ferry, J. M., and Spear, F. S., 1978, Experimental calibration of the partitioning of Fe and Mg between biotite and garnet: Contributions to Mineralogy and Petrology, v. 66, p. 113-117.

Garihan, J. M., 1979, Geology and structure of the central Ruby Range, Madison County, Montana: Geological Society of America Bulletin, v. 90, part II, p. 695-788.

Geissman, J. G., and Mogk, D. W., 1986, Late Archean tectonic emplacement of the Stillwater Complex along reactivated basement structures, northern Beartooth Mountains, southern Montana, *in* Proceedings of the 6th International Conference on Basement Tectonics, p. 25-44.

Hallager, W. S., 1980, Geology of Archean gold-bearing metasediments near Jardine, Montana [Ph.D. dissertation]: University of California, Berkeley, 136 p.

Henry, D. J., Mueller, P. A., Wooden, J. L., Warner, J. L., and Lee-Berman, R., 1982, Granulite grade supracrustal assemblages of the Quad Creek area, eastern Beartooth Mountains, Montana: Montana Bureau of Mines and Geology Special Publication 84, p. 147-159.

Kleinkopf, M. D., 1985, Regional gravity and magnetic anomalies of the Stillwater Complex area, *in* The Stillwater Complex, Montana: Geology and guide: G. K. Czamanske and M. L. Zientek, *(eds.):* Montana Bureau of Mines and Geology Special Publication 92, p. 9-20.

Labotka, T. C., 1985, Petrogenesis of metamorphic rocks beneath the Stillwater Complex: Assemblages and conditions of metamorphism, *in* The Stillwater Complex, Montana: Geology and guide, G. K. Czamanske and M. L. Zientek, *(eds.):* Montana Bureau of Mines and Geology Special Publication 92, p. 70-76.

LaFrenz, W. B., Shuster, R. D., and Mueller, P. A., 1986, Archean and Proterozoic granitoids of the Hawley Mountain area, Beartooth Mountains, Montana, *in* Montana Geological Society-Yellowstone Bighorn Research Association Field Conference Guidebook, p. 79-89.

Lambert, D. D., Unruh, D. M., and Simmons, E. C., 1985, Isotopic investigations of the Stillwater Complex: A review, *in* The Stillwater Complex, Montana: Geology and guide, G. K. Czamanske and M. L. Zientek, *(eds.):* Montana Bureau of Mines and Geology Special Publication 92, p. 46-54.

Lonker, S. W., 1981, The P-T-X relations of the cordierite-garnet-sillimanite-quartz equilibrium: American Journal of Science, v. 281, p. 1056-1090.

Mogk, D. W., and Henry, D. J., 1988, Metamorphic petrology of the northern Archean Wyoming province, southwest Montana: Evidence for Archean collisional tectonics, *in* Metamorphism and Crustal Evolution in the Western United States (Rubey Volume VII), W. G. Ernst, *(ed.)*: Prentice-Hall, New York, p. 362-382.

Mogk, D. W., Mueller, P. A., and Wooden, J. L., 1988, Archean tectonics of the North Snowy block, Beartooth Mountains, Montana: Journal of Geology *(in press)*.

Molnar, P., and Tapponnier, P., 1975, Cenozoic tectonics of Asia: Effects of a continental collision: Science, v. 189, p. 419-426.

Mueller, P. A., Wooden, J. L., Henry, D. J., and Bowes, D. R., 1985, Archean crustal evolution of the eastern Beartooth Mountains, Montana and Wyoming, *in* The Stillwater Complex, Montana: Geology and guide, G. K. Czamanske and M. L. Zientek, *(eds.)*: Montana Bureau of Mines and Geology Special Publication 92, p. 9-20.

Nunes, P. D., and Tilton, G. R., 1971, Uranium-lead ages of minerals from the Stillwater Igneous Complex and associated rocks, Montana: Geological Society of America Bulletin v. 82, p. 2231-2250.

Page, N. J., 1977, Stillwater Complex, Montana: Rock succession, metamorphism, and structure of the complex and adjacent rocks: U.S. Geological Survey Professional Paper 999, 79 p.

Page, N. J., and Zientek, M. L., 1985a, Geologic and structural setting of the Stillwater Complex, *in* The Stillwater Complex, Montana: Geology and guide, G. K. Czamanske and M. L. Zientek, *(eds.)*: Montana Bureau of Mines and Geology Special Publication 92, p. 1-8.

______ 1985b, Petrogenesis of metamorphic rocks beneath the Stillwater Complex: Lithologies and structures, *in* The Stillwater Complex, Montana: Geology and guide, G. K. Czamanske and M. L. Zientek, *(eds.)*: Montana Bureau of Mines and Geology Special Publication 92, p. 55-69.

Peterman, Z. E., 1981, Dating of Archean basement in northeastern Wyoming and southern Montana: Geological Society of America Bulletin, part I, v. 92, p. 139-146.

Reid, R. R., McMannis, W. J., and Palmquist, J. C., 1975, Precambrian geology of the North Snowy block, Beartooth Mountains, Montana: Geological Society of America Special Paper 157, p. 1-135.

Spencer, E. W., and Kozak, S. V., 1975, Precambrian evolution of the Spanish Peaks, Montana: Geological Society of America Bulletin, v. 86, p. 785-792.

Thurston, P. B., 1986, Geochemistry and provenance of Archean metasedimentary rocks in the southwestern Beartooth Mountains [M.S. thesis]: Montana State University, Bozeman, p. 74.

Vaniman, D. J., Papike, J. J., and Labotka, T., 1980, Contact metamorphic effects of the Stillwater Complex, Montana: The concordant iron-formation: American Mineralogist, v. 65, p. 1087-1102.

Vitaliano, C. J., Cordua, W. S., Hess, D. F., Burger, H. R., Hanley, T. B., and Root, F. K., 1979, Explanatory text to accompany geologic map of southern Tobacco Root Mountains, Madison County, Montana: Geological Society of America Map and Chart Series MC-31.

Weiblan, P. W., and Morley, G. B., 1980, A summary of the stratigraphy, petrology and structure of the Duluth Complex: American Journal of Science, v. 280A, p. 88-113.

Zen, E-An, and Hammarstrom, J. M., 1984, Magmatic epidote and its petrologic significance: Geology, v. 12, p. 515-518.

©DIANE NUGENT 1988

PETROLOGY AND GEOCHEMISTRY OF ARCHEAN BASEMENT LITHOLOGIES IN THE YANKEE JIM AND LAMAR CANYON AREAS, MONTANA AND WYOMING

R. E. Guy
and
A. K. Sinha
Department of Geological Sciences
Virginia Polytechnical Institute and State University
Blacksburg, Virginia 24061

Introduction

The Beartooth uplift, located in southwestern Montana is composed of Precambrian gneisses, schists and crystalline rocks, which are mantled by Paleozoic sediments and Tertiary volcanics (**Figure 1**). The southwest portion of the Beartooth uplift, termed the South Snowy block, is bounded on the south by the Gardiner fault and on the north by the Mill Creek fault (Foose and others, 1961). The South Snowy block is primarily composed of Tertiary volcanics, with Archean gneisses and schists exposed along the western and southern edge of the block. Paleozoic sediments occur along the northern and southeastern edge of the block (Montgomery and Lytwyn, 1984). The southern part of the South Snowy block extends into the northern portion of Yellowstone National Park. To the south, lie the extensive basalts and rhyolites of the Yellowstone volcanic province. Extensive mapping along the northeastern margin of the Park has been done by Casella and others (1984), Montgomery (1984), Wooden and others (1984), and thesis studies by Huffman (1977); Lahti (1975); and Lytwyn (1982). Thurston (1986)

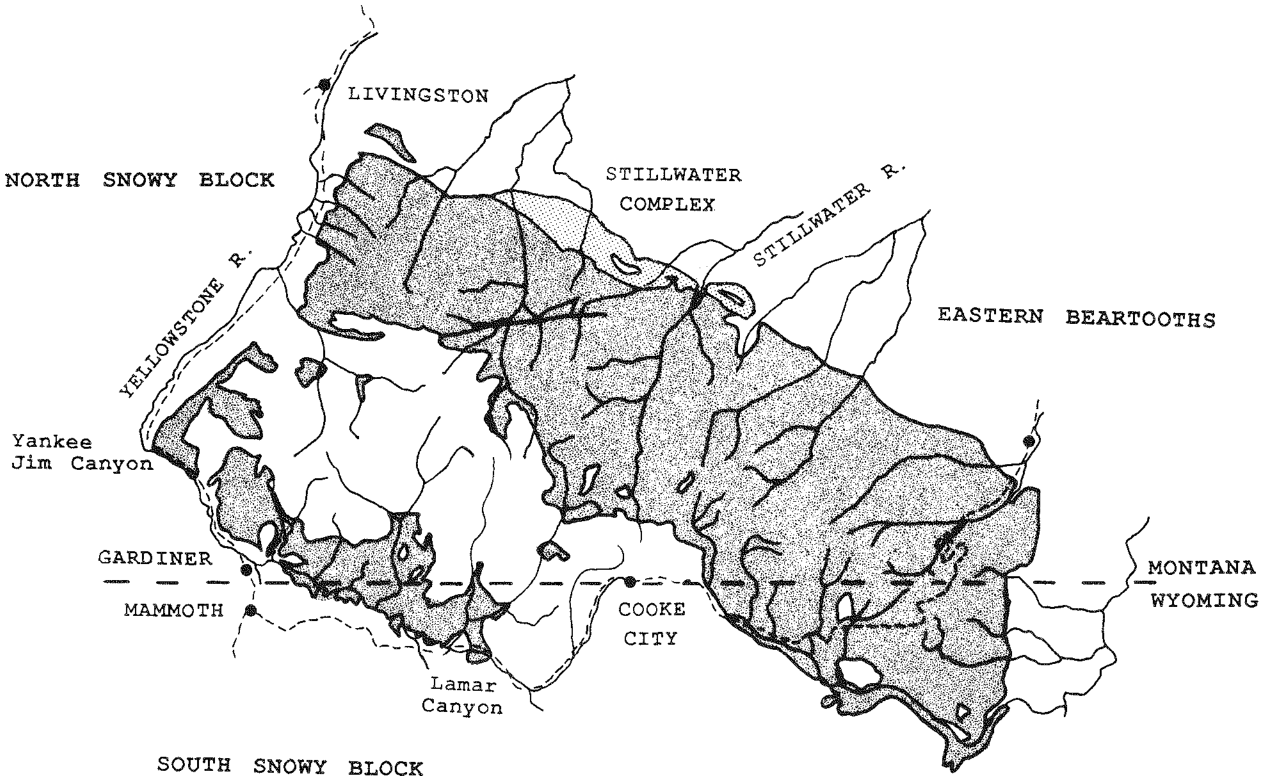
LIVINGSTON
NORTH SNOWY BLOCK
STILLWATER COMPLEX
STILLWATER R.
YELLOWSTONE R.
EASTERN BEARTOOTHS
Yankee Jim Canyon
GARDINER
MAMMOTH
COOKE CITY
MONTANA
WYOMING
Lamar Canyon
SOUTH SNOWY BLOCK

Figure 1—The Beartooth Mountains region, showing distribution of Archean rocks and the location of Yankee Jim Canyon and Lamar Canyon.

mapped in the northwestern region of the Park. In the Gardiner-Jardine areas investigations include Fraser and others (1969); Seager (1944); Hallager (1980), Thurston (1986) and a thesis study of the Yankee Jim Canyon area by Burham (1982).

This study was undertaken to investigate if the exposed basement lithologies could be modelled as source materials or contaminants for the rhyolites of nearby Yellowstone National Park. The extensive quartzofeldspathic gneisses exposed would appear as possible source rocks for the high-silica rhyolites, (Guy, *in progress*). Doe and others (1982) have suggested that the source region for the rhyolites is a deep-seated crustal keel that may not be related to the Archean rocks currently exposed at the surface.

Field relations

Exposure of crystalline basement rocks in the Gardiner area **(Figure 1)** result from uplift along N-NE trending normal faults (Holberg, 1940) along the eastern edge of Paradise Valley. A large mylonite zone in Yankee Jim Canyon and two mylonite zones in Sixmile Creek to the north have been described by Burnham (1982). Five kilometers south of Yankee Jim Canyon, the reverse high-angle Gardiner fault uplifts units to the north some 3,000 meters (Fraser and others, 1969). This fault represents the southernmost limit of the Beartooth uplift in the vicinity of Gardiner and Yankee Jim Canyon.

Samples for chemical, isotopic and petrological studies were collected in four areas along the northern edge of the Park **(Figure 1)**. Two regions, Yankee Jim Canyon (20 miles northwest of Gardiner) and Lamar Canyon (20 miles southeast of Gardiner), were sampled in detail for petrologic studies and radiometric dating by Pb, U-Pb, and Rb-Sr methods. Two other regions, Jardine (5 miles northeast of Gardiner) and Grayling Creek (10 miles north of West Yellowstone), were sampled to cover the range of basement compositions present in the region.

Yankee Jim Canyon offers excellent exposures in a 3-mile section along U.S. Highway 89 **(Figure 2)**. The lithologies include hornblende amphibolites, garnet-biotite-plagiogneisses, pegmatites, and quartzofeldspathic gneisses. The area shows a wide variation in lithologies and was sampled in detail to represent the total range of basement compositions.

The Lamar Canyon outcrops in the northeastern part of Yellowstone National Park are composed of quartzofeldspathic gneises of varying composition. This is the only basement locality sampled by Doe and others (1982) in a study on the isotopic compositions of the Yellowstone lavas. The lithologies are very similar in hand sample to the quartzofeldspathic gneisses of Yankee Jim Canyon. Iron-rich schists and gneisses are dominant lithologies in the Jardine area.

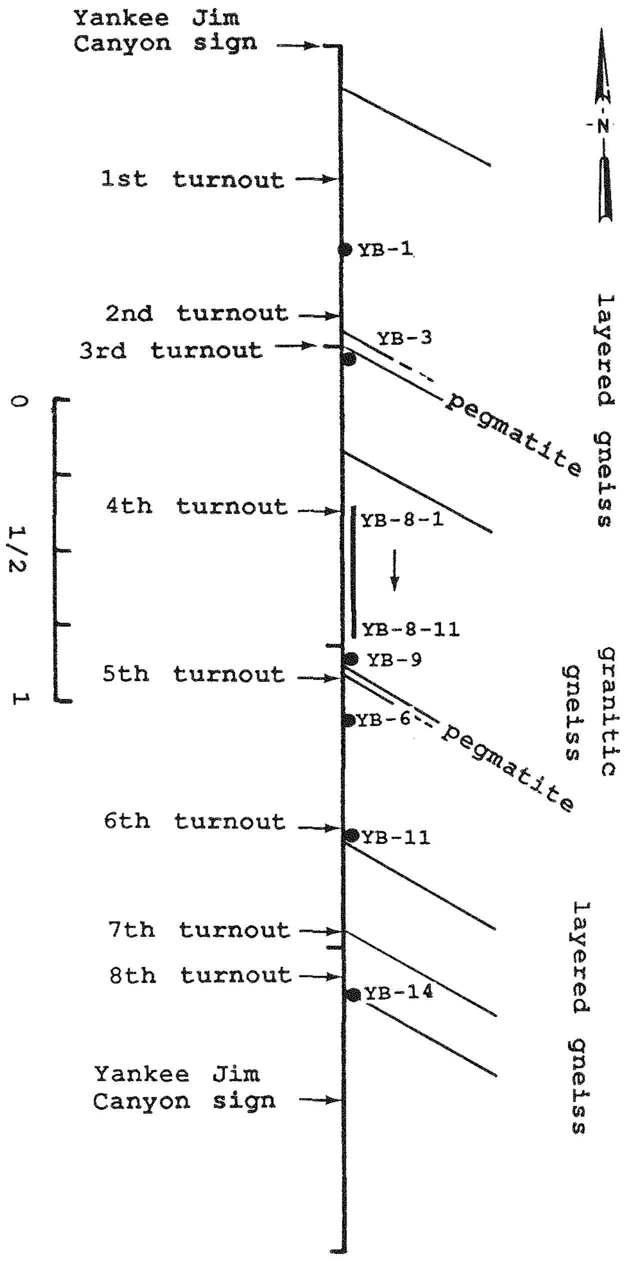

Figure 2—A traverse along Yankee Jim Canyon showing the localities of chemically analyzed samples.

Petrography

The lithologies in Yankee Jim Canyon are dominated by the quartzofeldspathic gneisses at the central and southern parts of the canyon, but also include garnet-biotite-cordierite gneisses, biotite gneisses and schists, amphibolites and pegmatites. The lithologies vary in thickness from a few centimeters (mafic layers) to hundred of meters (quartzofeldspathic gneisses). The contacts between lithologies are gradational, with extensive interfingering of schists, gneisses and mafic rocks. Because of the outcrop complexity, and the wide range in lithologies, only the four major rock types (which make up >95% of the outcrop) are described in detail.

The quartzofeldspathic gneiss unit dominates the central portion of Yankee Jim Canyon (4th turnout, **Figure 2, Table 1**). This unit ranges from a massive two feldspar gneiss to a foliated biotite-epidote gneiss (**Table 1**) and is predominantly pinkish in color. In thin section the samples have a seriate texture and are variably mylonitic. The plagioclase (An_{25-35}) grains are anhedral, reaching 10 millimeters in size, show albite twinning and typically lack zonation. Sericite alteration is generally present along the rim and fractures of a grain. The less common zoned crystals have extensive sericite alteration of the cores. Pseudomorphic replacement by microcline is common, producing an anhedral plagioclase grain displaying a euhedral microcline rim, with the microcline often forming more than half of the grain. Microcline grains reach 25 millimeters or more in size and exhibit extensive exsolution lamellae. Most grains show Carlsbad twinning, with minor cross-hatch twinning. The microcline megacrysts contain inclusions of small euhedral plagioclase grains, less commonly biotite, and rarely quartz. Biotite grains are large (up to 5 mm) and show green pleochroism. The grains are often corroded and altered to epidote, muscovite, and less commonly, chlorite and titanite. Allanite grains reach 5 millimeters in size and are commony rimmed by titanite and/or epidote. Titanite is present as subhedral grains (<2 mm) and as anhedral alteration grains associated with biotite and allanite. Most samples contain epidote grains; both as larger subhedral grains associated with biotite and as smaller grains formed by alteration of plagioclase and biotite. Numerous fine-grained aggregates of biotite and epidote are found, suggesting a replacement relationship with hornblende.

Biotite-garnet-cordierite gneiss occurs in the northern and southern sections of Yankee Jim Canyon (1st, 5th, 6th turnouts, **Figure 2, Table 1**). In hand sample, the gneiss is coarsely crystalline with biotite-garnet layers defining the foliation. In thin section, the rock shows a seriate texture. Plagioclase (An_{25-35}) occurs as anhedral to subhedral grains, approximately 2 millimeters in size, show albite twinning and contain inclusions of biotite and microcline. Minor sericite alteration is present, concentrated along small fractures in the grains. Quartz grains show undulatory extinction, mosaic textures, and serrated grain margins. They contain a few inclusions of biotite and are often encased in biotite sheaths. Microcline is present as fine-grained anhedral grains in the matrix and, less commonly, as larger phenocrysts. Myrmekite is common along microcline grain boundaries. Biotite is highly pleochroic (light to dark reddish brown), reaches 2 millimeters in size, and generally forms selvages of 1.0-2.5 millimeters, which define the foliation. Small biotite grains are often included in plagioclase and rarely in quartz. Muscovite replacement of biotite is common, though chlorite alteration is generally absent. Garnet forms large (10 mm) poikiloblasts with inclusions of quartz, biotite, and rarely sillimanite; feldspar inclusions are notably lacking. The garnet grains are often elongated rather than blocky, and do not show evidence of rolling or inclusion rings. Cordierite is present as large (2-7 mm) grains associated with biotite + garnet selvages. Cordierite contains inclusions of biotite and quartz and large secondary muscovite grains. The cordierite shows varying amounts of alteration from total replacement by pinite (muscovite + chlorite) to minor sillimanite alteration along the margins of the grains. Magnetite, ilmenite, zircon and apatite are the common accessory minerals. Sillimanite, although a minor accessory mineral, is present as inclusions in garnets and as an alteration product along the rims of cordierite grains.

Small mafic dikes or lenses are found throughout the canyon (4th, 6th 7th turnouts, **Figure 2, Table 1**). They are similar in appearance to those found in the Jardine area (Seager, 1944) and in the Buffalo Plateau area of Yellowstone National Park (Casella and others, 1982). In hand sample they are dark greenish gray with weak foliation. In thin section they are composed of hornblende, saussuritized plagioclase, augite and/or hypersthene, with traces of opaque minerals (**Table 1**). One outcrop (4th turnout, **Figure 2**) contains rare garnet crystals ($Al_{62}Py_{9}$-$Sp_{7}Gr_{22}$) intergrown with plagioclase. The unaltered samples are massive, equigranular and generally lack pervasive deformational features. In such samples the augite grains have exsolution lamellae, while the plagioclase (An_{55-70}) grains are coarsely twinned and contain inclusions of augite and opaque minerals. More typically, the samples show alteration of the mafic phases to hornblende or actinolite. With progressive development of foliation, plagioclase

Table 1—Chemical composition and model analyses of representative samples of the Archean complex in Yankee Jim Canyon. (GG), quartzofeldspathic gneiss; (CG), biotite-garnet-cordierite gneiss; (M), mafic lithologies; (BG), biotite-garnet gneiss.

	YB-1	YB-3	YB-5	YB-6	YB-8-1	YB-8-2	YB-8-3.5	YB-8-4	YB-8-5	YB-8-7	YB-8-9	YB-8-10	YB-8-11	YB-9	YB-11	YB-12	YB-13	YB-14
Sample	CG	BG	CG	BG	GG	GG	GG	GG	GG	GG	GG	GG	GG	GG	GG	M	CG	M
SiO_2	67.29	66.26	70.21	75.74	58.15	70.23	69.96	62.85	62.19	63.23	62.62	61.98	70.93	70.94	64.53	49.75	74.97	54.19
Al_2O_3	14.30	14.71	14.81	13.43	17.72	15.02	15.08	16.26	17.20	16.15	16.56	16.69	14.59	14.77	18.69	12.52	11.42	5.37
TiO_2	0.54	0.56	0.49	0.02	0.88	0.36	0.24	0.54	0.68	0.58	0.64	0.65	0.28	0.28	0.36	2.08	0.44	0.47
Fe_2O_3	7.12	6.29	4.61	0.61	5.23	2.64	1.81	4.13	5.08	4.95	4.11	4.39	2.06	2.10	2.28	17.09	4.44	11.12
MgO	3.20	3.46	3.27	0.66	2.19	1.64	0.75	1.26	2.27	1.30	1.20	1.35	1.03	1.41	2.09	4.84	1.88	14.73
MnO	0.11	0.13	0.09	0.05	0.10	0.06	0.02	0.04	0.09	0.05	0.05	0.05	0.06	0.07	0.05	0.24	0.08	0.24
CaO	1.92	1.60	1.62	1.10	3.61	2.44	2.23	2.48	3.91	2.86	2.68	3.08	1.94	2.21	4.32	8.92	2.49	11.33
Na_2O	2.45	3.46	2.46	3.29	3.49	3.83	3.16	3.11	3.31	3.84	3.67	3.73	3.68	3.63	5.21	1.32	2.32	0.00
K_2O	2.74	2.20	2.00	5.08	5.76	3.37	4.50	6.50	3.98	4.40	5.30	5.20	4.28	3.82	1.47	0.74	1.82	0.32
P_2O_5	0.08	0.03	0.05	0.07	0.29	0.14	0.19	0.46	0.27	0.37	0.39	0.40	0.07	0.05	0.08	0.25	0.09	0.16
BaO							0.31	0.76		0.48	0.60	0.55				0.04		0.06
LOI	0.01	0.85	0.63	0.18	1.68	0.39	0.78	0.63	1.15	0.81	0.99	1.01	1.23	0.94	0.79	0.30	0.39	1.10
Total	99.76	99.55	100.24	100.23	99.10	100.12	99.03	99.02	100.13	99.02	98.81	99.08	100.15	100.22	99.87	98.10	100.40	99.03
Ag	0.50	1.5	0.50	1.0	0.50	0.50	0.50	0.50	0.50	0.50	0.50	0.50	0.50	1.00	0.50	2.00	1.00	
Be	0.50	5.0	5.50	3.0	1.00	1.50	0.50	1.50	1.50	1.00	2.00	1.50	1.00	1.00	0.50	<0.50	<0.50	
Bi	<2.00	<2.0	<2.0	<2.0	<2.0	<2.0	<2.0	<2.0	<2.0	<2.0	<2.0	<2.0	<2.0	<2.0	<2.0	<2.0	<2.0	
Cd	0.50	.5	<0.5	1.0	<0.5	<0.5	0.50	<0.5	<0.5	<0.5	0.50	0.50	0.50	1.00	0.50	0.50	0.50	
Co	26.00	83.0	42.00	104.0	13.00	31.00	3.00	9.00	17.00	6.00	8.00	8.00	22.00	16.00	24.00	42.00	18.00	
Cr	121.00	264.0	212.00	11.0	5.00	6.00	81.00	41.00	12.00	55.00	40.00	51.00	22.00	19.00	10.00	122.00	287.00	
* Cu	34.00	18.0	40.00	<1.0	7.00	12.00	3.00	9.00	34.00	4.00	6.00	18.00	5.00	5.00	1.00	73.00	53.00	
Mo	<1.0	<1.0	<1.0	<1.0	1.00	<1.0	<1.0	<1.0	<1.0	<1.0	<1.0	<1.0	<1.0	<1.0	2.00	<1.0	<1.0	
Ni	55.0	123.0	85.0	3.0	3.00	6.00	8.00	6.00	8.00	1.00	3.00	1.00	8.00	8.00	9.00	48.00	78.00	
P	240.00	150.0	150.00	800.0	1,330.00	630.00	190.00	1,630.00	1,150.00	1,010.00	1,090.00	1,130.00	250.00	130.00	120.00	1,070.00	190.00	
V	76.00	90.0	76.00	<1.0	52.00	20.00	15.00	48.00	56.00	52.00	43.00	45.00	17.00	14.00	21.00	345.00	64.00	
W	120.00	650.0	240.00	1,080.0	60.00	240.00	<10.0	<10.0	110.00	<10.0	<10.0	<10.0	210.00	180.00	160.00	50.00	<10.00	
Zn	49.00	67.0	64.00	4.0	39.00	30.00	17.00	44.0	34.00	48.00	43.00	48.00	23.00	29.00	27.00	145.00	65.00	
Ba (XRF)	768.00	520.0	560.00	5,740.0	5,077.00	1,299.00	1,880.00	4,860.00	2,533.00	2,900.00	3,600.00	3,460.00	2,348.00	2,379.00	525.00	230.00	310.00	
Pb	28.00		24.00		36.00	40.00	22.00	40.00	32.00	48.00	48.00	50.00	34.00	34.00	26.00	52.00	42.00	
U (NAA)	4.70				<1.0		1.00	2.30	<1.0	1.70	4.30	2.10	<0.5	0.80	1.00			
Th (NAA)	8.00		27.00		30.00	50.00	17.00	14.00	18.00	46.00	57.00	43.00	6.00	3.00	11.00			
Rb (XRF)	91.00	72.00	68.00	27.00	131.00	111.00	120.00	100.00	122.00	170.00	120.00	130.00	100.00	98.00	52.00			7.00
Sr (XRF)	135.00	179.00	182.00	240.00	1,003.00	406.00	499.00	815.00	579.00	750.00	663.00	679.00	540.00	598.00	514.00	118.00	142.00	29.00
Quartz	35.60	36.60	38.80		15.20	32.30	25.50	35.70	23.80	24.90	29.60	20.70		39.3	17.60	7.40	35.70	8.30
K-Feldspar	4.40	13.50	5.60		27.20	22.20	8.00	20.80	38.60	20.60	7.70	21.60		14.4	15.20		3.70	
Plagioclase	21.60	11.40	20.20		22.20	29.00	41.20	14.60	20.20	28.90	26.30	32.70		25.3	38.80	28.80	20.90	2.60
Biotite	28.00	36.50	21.00		5.80	8.40	12.00	11.10	12.20	14.00	11.40	14.10		6.8	26.00	0.40	19.90	5.40
Garnet	1.80	0.60	4.20															
Cordierite	4.40		7.80															
Muscovite	1.20		1.40		3.60	4.20	trace	7.50	2.00	1.70	7.90	2.60		8.2	1.60		6.90	
Hornblende															83.50	45.40		83.50
Pyroxene																11.80		
Epidote		0.30	0.60		20.80	3.00	8.70	7.40	1.80	8.30	14.00	5.40		5.7				
Titanite					4.00	0.40	2.70		0.80	0.70	trace	1.10						
Apatite	1.20	trace				trace	trace	trace	trace		trace	0.40		trace	1.10	0.10	0.10	trace
Opaques	1.80	1.00	0.40		1.20	0.50	1.30	0.90	0.60	0.90	3.10	1.30		.1		6.00	0.90	0.20

---

*Trace-element data collected by Chemex Labs, Inc., Sparks, Nevada, using the intracoupled plasma (ICP) technique.

(An_{40-60}) grains reach 1 millimeter in size, are twinned and are often saussuritized to chlorite, mica and epidote. Augite and hypersthene grains are anhedral, 0.2-2.0 millimeters in size, and altered to fibrous actinolite. Hornblende grains are prismatic crystals ranging up to 4 millimeters in size, olive green in color, and are unaltered. Inclusions of quartz and opaque grains are common.

Biotite gneisses are commonly found along the margins of the pegmatites and quartzofeldspathic gneisses (3rd, 5th turnouts, **Figure 2**), where they occur as layers up to a few meters thick. In hand sample, the gneisses are coarse-grained and foliated, light gray in color and speckled with brown biotite. In thin section they consist of large plagioclase and quartz grains with interstitial biotite defining the foliation (**Table 1**). The plagioclase (An_{30-35}) grains are anhedral, contain inclusions of biotite, zircon, and rarely quartz, and show varying amounts of saussuritization. The grains are usually twinned, with the lamellae being bent or broken along fractures that are filled with alteration products. Fine-grained overgrowths of quartz and biotite often surround the plagioclase grains. The quartz grains range in size from <0.2 millimeters to 5 millimeters, are generally anhedral, and exhibit undulatory extinction or recrystallization. The biotite grains are dark brown, strongly pleochroic, and vary in size from 0.1-2.0 millimeters. They form layers of varying thickness (up to 5 mm) and generally rim the larger phenocrystic plagioclase and quartz grains. Muscovite, zircon, epidote and opaque minerals are common accessory minerals and are often found as inclusions in the biotite and plagioclase grains.

Analytical techniques

Mineral chemistry

Electron microprobe analyses of minerals were performed using an automated ARL SEMQ unit following the procedure of Solberg and Speer (1982). Mineral recalculation and H_2O content were computed by using the Fortran program SUPERRECAL (J. C. Rucklidge, personal communication, 1971).

Major and trace elements

Bulk samples were cleaned, crushed in a two-step shatter box (zirconia agate or steel lined) and split by the cone and quarter method for major and trace element analysis. Major elements were analysed using fused glass discs on a Philips Sequential X-ray Analysis System Model 1450 wave-length dispersive unit by utilizing the techniques of Norrish and Hutton (1969). Pressed powder pellets were analyzed for Ba, Rb, Sr and Na by applying the matrix correction methods of Reynolds (1963).

Isotopic analysis

Rb-Sr, Pb-Pb, and U-Pb (zircon) isotopic compositions were measured in a 35-cm solid-source mass spectrometer. Analytical procedures are given in Pettingill and others (1984) and Sinha and Bartholomew (1984). Regressions were calculated according to the method of York (1966); ages and MSRS values are quoted from regression Model II. All standard errors of the mean are quoted at the two sigma confidence level.

Mineral chemistry

Plagioclase

The plagioclase compositions in Yankee Jim Canyon differ widely with lithology, ranging from An_2 for a quartzofeldspathic gneiss sample to An_{92} for an unaltered gabbroic sample (**Figure 3**).

In the quartzofeldspathic gneiss, plagioclase compositions center around An_4, but range from An_{2-35}. Plagioclase composition can vary within a single outcrop depending on the degree of fabric developed in the sample. The more massive units have plagioclase compositions of An_{25-35}, while the more foliated samples have plagioclase compositions of An_{2-15}.

In the biotite-garnet-cordierite gneiss, plagioclase compositions are similar throughout the canyon, ranging from An_{25-35}. The samples from the northern part of the canyon show minor variation between units, but little variation within a unit. The samples from the southern end of the canyon have little compositional variation, averaging around An_{26}.

The compositional spread of plagioclase in mafic lithologies ranges from An_{50-92}, with the compositional spread within each unit ranging only 5-10% in An content. The plagioclase compositions cluster at An_{75-80} for the slightly altered rocks and An_{50-62} for the chloritized assemblages.

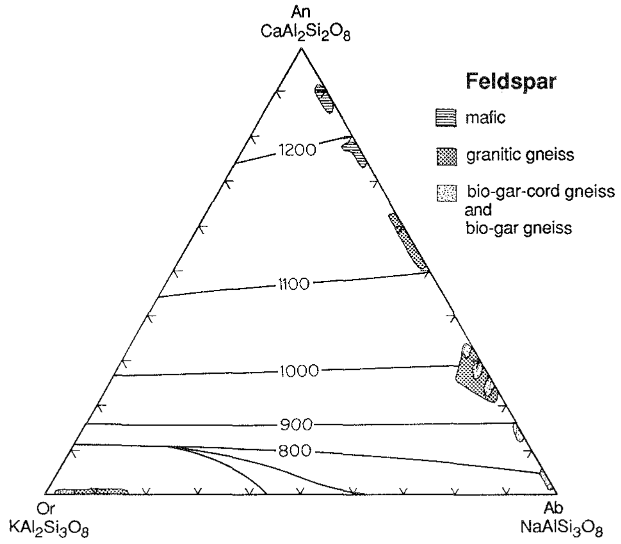

Figure 3—A plot of feldspar compositions in Yankee Jim Canyon showing An-Ab-Or content. (GG), feldspars from quartzofeldspathic gneiss; (MG), biotite-garnet and biotite-garnet-cordierite gneiss; (M), mafic lithologies.

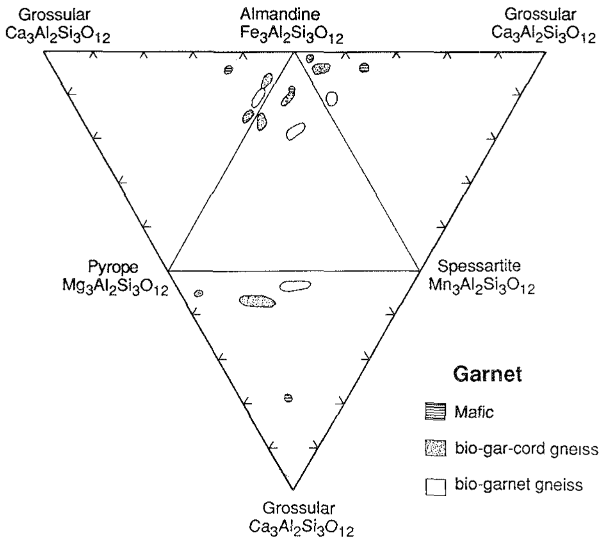

Figure 4—A plot of Yankee Jim Canyon garnet compositions. (CG), biotite-garnet-cordierite gneiss; (M), mafic lithologies; (BG), biotite-garnet gneiss.

Compositions in the biotite gneiss lithology are very similar to the quartzofeldspathic gneiss lithology, ranging from An_{25-30}. Compositional variation within biotite gneiss outcrops in the canyon is similar and variation within a single unit is very limited.

K-felspar

The K-feldspar compositions vary widely, ranging from Or_{77} to Or_{90} **(Figure 3)**. The K-feldspar compositions in the granitic gneiss lithology range from Or_{84-95}, although most compositions are in the range of Or_{90-93}.

In the biotite-garnet-cordierite gneisses, the K-feldspar grains contain a higher albite component than those in the quartzofeldspathic gneisses, with compositions ranging from Or_{81-91}.

The compositions of K-feldspars in the biotite gneiss vary slightly between the north and south ends of the canyon. The composition of grains in units at the north end range from Or_{84-91}, which is very similar to those in the granitic gneiss lithology. The composition of K-feldspars in units in the south end of the canyon are slightly more albitic, up to Or_{77} in composition.

Pyroxene

Pyroxene compositions from the two mafic units differ greatly between units, but are very similar within a single unit. In one mafic layer (4th turnout, **Figure 2**), the pyroxenes average $Wo_{44}En_{27}Fs_{29}$ in composition and range only 5% in Fs component. The second mafic unit (6th turnout, **Figure 2**) has pyroxenes of $Wo_2En_{37}Fs_{61}$ composition with a 5% variation in Fs component.

Garnet

Garnets are present in most units, except for the quartzofeldspathic gneiss. The garnet compositions are constant within any given outcrop **(Figure 4)**. The compositions, however, varied between lithologies and between outcrops of the same lithology. The garnets in the biotite-garnet-cordierite gneiss are almandine (65-75 mol. %) with less pyrope (13-28 mol. %), spessartine (3-7 mol. %), and grossular (3 mol. %) component.

A narrow mafic layer contains numerous garnets. The composition of the garnet is significantly different from other garnets in the area with 22 mol. % grossular and < 10% pyrope. This composition is consistent with the higher Ca content of the particular mafic layer.

Garnets from the biotite gneiss units differ from unit to unit through the section. One unit contains garnets with a significant pyrope (27 mol. %) but low spessartite (3 mol. %) component, while a unit one mile away contains garnets with high spessartite (18 mol. %) and lower pyrope (19 mol. %) components. This difference in mineral chemistry reflects the difference in bulk composition of the rocks in these two areas.

Epidote

Epidote grains are present only in the quartzofeldspathic gneiss lithology, where it occurs in two textural forms; as larger euhedral to anhedral grains or as wormy intergrowths in contact with plagioclase. The composition of the euhedral epidote grains (**Figure 5**) range from Ps 24.3-29.9% which is similar to compositions in granodiorites in the western United States cordillera (Zen and Hammarstrom, 1984). The wormy epidotes have compositions averaging Ps 18%, but range up to Ps 27%, which are similar to those reported by Tulloch (1979) for subsolidus breakdown of plagioclase + biotite.

Hornblende

Hornblende is found only in the more mafic lithologies in Yankee Jim Canyon. The composition of the hornblendes tend to be locally consistent, but vary greatly on the larger scale. The hornblendes in the pyroxene-bearing gabbroic lithology have the highest iron content, averaging $Gru_{44}Ant_{29}Caa_{29}$. The hornblendes in the hornblendite lithology have the lowest iron content, averaging $Gru_{19}Ant_{54}Caa_{27}$. The chloritized mafic lithology has hornblende of intermediate compositions, averaging $Gru_{26}Ant_{46}Caa_{28}$.

Biotite

Biotite compositions form two distinct groups; a tight cluster for the biotite gneiss and a second slightly scattered field for the quartzofeldspathic gneisses (**Figure 6**). The Fe/(Fe + Mg) ratios of these gneisses are 0.42-0.53, which are within the range of igneous biotites (Spear, 1984). The aluminum content shows a small range, 15-17%.

Biotites in the biotite-garnet-cordierite gneisses are significantly more aluminous than those of the granitic gneisses, averaging 20% Al_2O_3. The Fe/(Fe + Mg) ratios are in the same range as the quartzofeldspathic gneisses, with a spread of 5% (0.45-0.50).

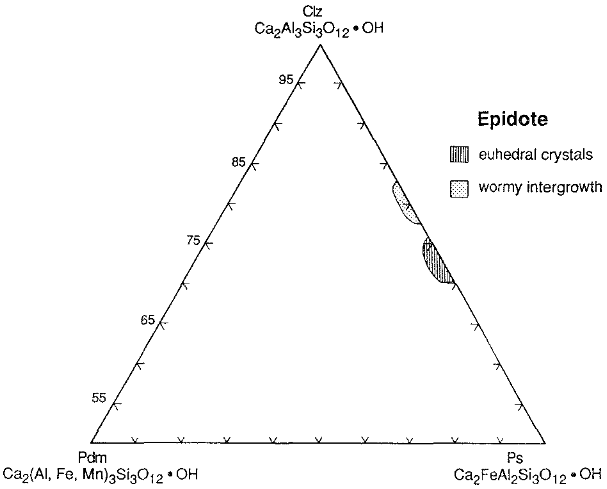

Figure 5—A plot of epidote compositions from the quartzofeldspathic gneisses of Yankee Jim Canyon. (EE), euhedral epidotes; (WE), wormy intergrowth epidotes.

The compositions of biotities in the biotite gneiss lithology are very similar to those in the biotite-garnet-cordierite lithology. The Al_2O_3 content average 18% while the Fe/(Fe + Mg) = 0.45.

Cordierite

Cordierite is present only in the biotite-garnet-cordierite lithology. The mineral grains have Fe/(Fe + Mg) ratios of 0.28-0.38 and are more Mg-rich than the coexisting biotites (0.45-0.55) and garnets ($Al_{75}Py_{13}Sp_7Gr_5$). One unit contains cordierite with varying amounts of alteration to muscovite and sillimanite. The less altered grains have a slightly higher Fe content (Fe/Fe + Mg = 0.31) than the more highly altered grains (0.28). The cordierite grains in a nearby unit do not show alteration and have an Fe/(Fe + Mg) ratio of 0.35-0.38. There is corresponding difference in Fe/(Fe + Mg) ratio for the whole-rock samples, with ratios varying from 0.55-0.70.

Pressure-temperature estimates

Epidote

Pressure-temperature results from epidotes are estimates due to the paucity of experimental data at appropriate compositions and pressures (**Table 2**). The temperature and pressure estimates can vary significantly with fO_2 (Liou, 1973), shifting by 100°C and 2.5 kb with a change from the nickle-nickle oxide buffer to the hematite-magnetite buffer. The presence of green biotite, titanite and magnetite indicates that the Yankee Jim and Lamar Canyon area gneisses are oxidized. Using the composition of the large euhedral crystals in the granitic gneiss (4th turnout, **Figure 2**) and the HM experimental data of Naney (1983), Liou (1973), and Holdaway (1972), yields a temperature of 600-700° and a pressure of 4-6 kb.

Biotite-garnet

The coexistence of garnet, biotite, quartz and K-feldspar can be used to estimate temperatures, using the data of Thompson (1976). The data for YB-3, a biotite gneiss, indicate temperatures of 620-635°C using Fe/(Fe + Mg) of 0.45-0.47 for biotite and 0.80-0.85 for garnet.

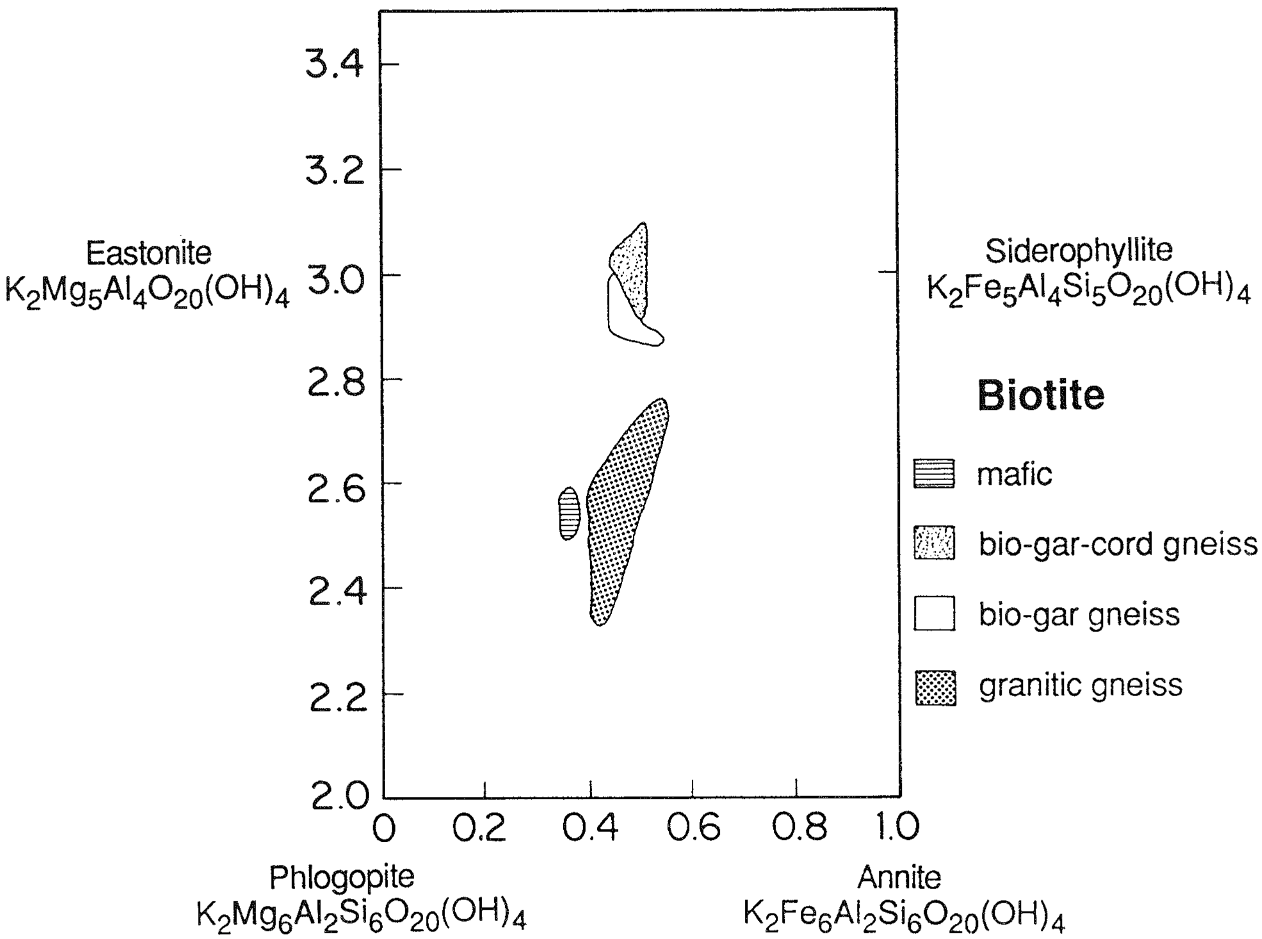

Figure 6—A plot of Yankee Jim Canyon biotite compositions. (GG), quartzofeldspathic gneiss; (CG), biotite-garnet-cordierite gneiss; (M), mafic lithologies; (BG), biotite-garnet gneiss.

Table 2—Temperature estimates in Yankee Jim Canyon from garnet-biotite and garnet-cordierite geothermometry.

	Geothermometry		
	Garnet-biotite	Garnet-cordierite	
Sample	Thompson, 1976	Thompson, 1976	Holdaway, 1977
YB-1 (core)	635°	640°	700°
YB-1 (core)	630°	610°	700°
YB-1 (rim)	575°	558°	700°
YB-3 (core)	619°		
YB-3 (core)	635°		
YB-3 (rim)	552°		
YB-5	795°	785°	725°
Yb-5	810°	800°	725°
YB-13	780°	775°	725°
YB-13	775°	760°	725°

The data for the biotite-garnet-cordierite gneiss indicate two different temperatures. The data for YB-1 (Fe/(Fe+Mg) of garnet = 0.80-0.85 and biotite = 0.50-0.55) indicate temperatures of 635°C for garnet core compositions and 575°C for garnet rim compositions. The data for YB-5 (Fe/(Fe+Mg) of garnet = 0.70 and biotite = 0.47-0.49) indicate a much higher temperature of 795-810°C. The cordierite in YB-1 has been considerably altered, while that in YB-5 shows very little alteration. This suggests that the temperatures calculated for YB-5 are closer to peak metamorphic temperatures, while those calculated for YB-1 are probably too low, due to later Fe/Mg redistribution.

Cordierite-garnet

The coexistence of cordierite, sillimanite and garnet can be used to estimate temperatures using the experimental data of Holdaway and Lee (1977) and Lonker (1981). Fe/(Fe+Mg) for garnet = 0.70-0.85 and cordierite, Fe/(Fe+Mg) = 0.4-0.5, indicated temperatures of ≥700°C and a pressure range of 3.5-4.0 kb ($P_{H_2O} = P_T$) (Holdaway and Lee, 1977) and 750°C and 4.5-5.5 kb (Lonker, 1981). The Fe/Fe + Mg ratios of 0.30-0.35 indicate temperatures of ≥700°C and a pressure range of 4.7-5.1 kb. The granite minimum melting curve places an effective temperature limit of 700-715°C (at 4-6 kb) on the mineral assemblage. Above this temperature, the K-feldspar, biotite and quartz assemblage melts to form a granitic liquid. The presence of small migmatitic veins (1st turnout, **Figure 2**) indicates that this melting temperature was probably, at least locally, exceeded. Re-equilibration during the cooling stage produced calculated temperatures using rim compositions approximately 65°C lower than those using core compositions.

Aluminosilicate

Sillimanite is only present in the biotite-garnet-cordierite gneisses of Yankee Jim Canyon. It occurs as a secondary alteration of cordierite and as inclusions in garnet. Kyanite has also been found in minor quantities (D. W. Mogk, personal communication 1988), although it was not found in the samples studied. Andalusite was not found, and no aluminosilicates were found in the Lamar Canyon gneisses. The presence of sillimanite indicates a lower temperature limit of 500°C (Holdaway, 1971) to 650°C (Richardson and others, 1969). The presence of both kyanite and sillimanite imply a minimum pressure of the aluminosilicate triple point; 3.75 kb (Holdaway, 1971) to 5.5 kb (Richardson and others, 1969).

Whole-rock chemistry

The range in silica content for the quartzofeldspathic gneisses is 56-75%*, with the Al_2O_3 content ranging from 15-19% (**Figure 7, Table 1**). There is an apparent increase in Al content with the increasing development of foliation. The Fe_2O_3 contents range from 2-5%. The foliated samples with higher alumina have higher Fe_2O_3 (5%) than the less foliated samples (2-3%). The MnO and MgO contents show

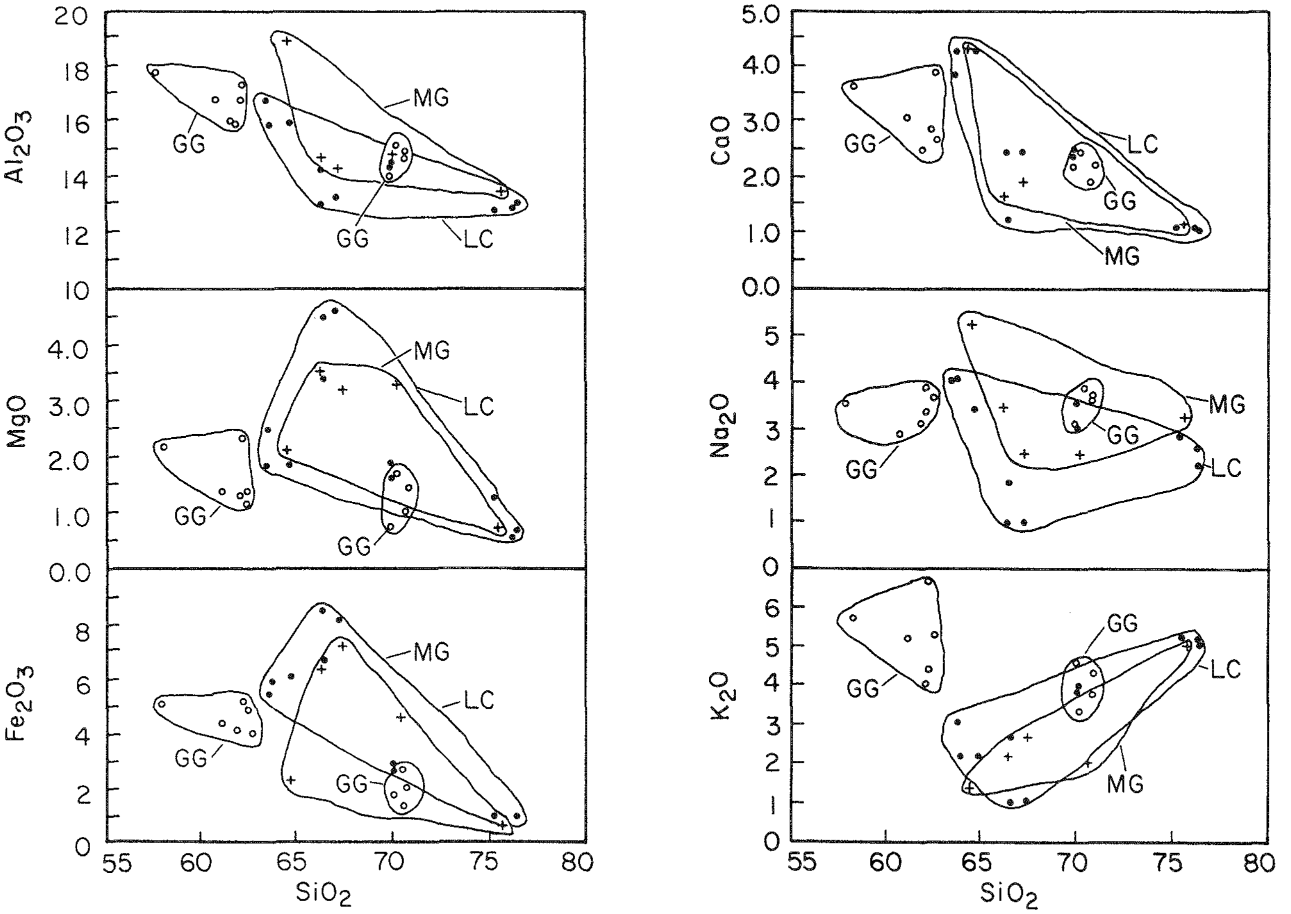

Figure 7—Major-element variation diagrams for Early Archean rock types in the Yankee Jim and Lamar Canyon areas. (GG), quartzofeldspathic gneiss of Yankee Jim Canyon; (MG), biotite-garnet gneiss and biotite-garnet-cordierite gneiss of Yankee Jim Canyon; (LC), Lamar Canyon quartzofeldspathic gneiss.

---

*All major-element data given in weight percent.

little variation with the total mafic content (Fe_2O_3 + MgO + MnO) being controlled by the variation in Fe_2O_3 content. CaO and K_2O contents show distinct compositional ranges for the foliated and unfoliated samples while the Na_2O values are constant. CaO and K_2O contents range from 3.5-4% for the foliated samples and 1.5-2.5% for the unfoliated samples. K_2O contents vary from 3.5% (unfoliated) to 6% (foliated), while the Na_2O contents vary little from the norm of 3.5%. TiO_2 values range from 0.3% (unfoliated) to 0.9% (foliated) and P_2O_5 values range from 0.05% (unfoliated) to 0.3% (foliated) following the local trend of bimodal distribution.

The gneisses show a wide range in trace-element compositions. The P content, although it ranges from 190 ppm to 1600 ppm, is generally above 1000 ppm. Pb content in the gneisses is relatively constant (22-50 ppm) while the U ($<$0.5-4.3 ppm) and Th (6-57 ppm) contents show more variation. The Rb concentration is relatively constant throughout the lithology, ranging from 100 to 170 ppm. Sr contents, however, range from 400-1000 ppm.

The biotite-cordierite-garnet gneisses have a more restricted compositional range than the quartzofeldspathic gneisses, with SiO_2 ranging from 67-70% **(Table 1)**. The Al_2O_3, CaO, Na_2O and K_2O contents are lower than in the quartzofeldspathic gneisses. Fe_2O_3 and MgO content are significantly higher than in the quartzofeldspathic gneisses, as is expected from the mafic mineral content.

The trace element contents of the biotite-garnet-cordierite gneisses differ from the quartzofeldspathic gneisses. Pb, U and Th contents show little variation and fall within the range of the quartzofeldspathic gneiss compositions, while the Rb (72-91 ppm) and Sr (135-182 ppm) concentrations show minimal variation and are significantly lower than in the quartzofeldspathic gneisses.

Biotite gneisses, from opposite ends of the canyon, have different compositions **(Table 1)**. SiO_2 contents are similar at 64-66%, but the Al_2O_3 content ranges from 14% at the north end of the canyon (YB-3) to 18% at the south end (YB-11). The finer-grained, foliated samples (3rd and 5th turnouts, **Figure 2**) have significantly higher Fe_2O_3 + MgO content (10% vs 4.5%), higher K_2O, and lower CaO and Na_2O contents. The average concentrations are similar to the quartzofeldspathic gneiss lithology, although the range in concentrations is slightly larger.

The Pb (26 ppm) and U (0.8 ppm) trace-element contents of the biotite gneisses are very similar to the granitic gneisses. The Rb (52-72 ppm), Sr (180-500 ppm), and Th (11 ppm) concentrations are similar to the biotite-garnet-cordierite gneisses and lower than in the granitic gneisses.

Age determinations

Yankee Jim Canyon

The whole-rock Rb-Sr isotope results are summarized in **Figure 8 and Table 3**. The data for the granitic gneiss samples do not yield an isochron. The errors on a regression through the data points (MSRS = 44) are larger than the analytical error, therefore the slope does not yield a geologically significant age. These results suggest that later metamorphic events such as at 1850 Ma (Casella and others, 1982; Montgomery and Lytwyn, 1984; Wooden and others, 1982; Brookins, 1968) have disturbed the Rb-Sr systematics.

The whole-rock Pb isotope data are shown in **Figure 9 and Table 4**. The data for the quartzofeldspathic gneisses indicate an age of 2620 Ma. The data for the biotite-cordierite and biotite gneisses have a similar slope and an age of 2647 Ma.

Resultant ages from the zircon U-Pb isotopic data **(Figure 10, Table 5)** indicate a complicated history. The quartzofeldspathic gneiss (YB-8) contained a single zircon population consisting of dark-pink, euhedral crystals. The crystals contain few inclusions, and cores are rarely visible. A discordia through two size splits indicate an age of approximately 2850 Ma, with a lower intercept of approximately 900 Ma. As there is little spread between the two data points, a small analytical error could alter this age significantly. If the regression is forced through the origin, then the data yields an intercept age of 2560 Ma. One split from the granitic gneiss was abraded and analyzed, which yielded a slightly older intercept age of 2642 Ma, suggesting that the zircons may have undergone some episodic lead loss.

A sample of coarse biotite gneiss (YB-11, **Figure 2**) contained a single zircon morphology of purplish euhedral crystals. The two size splits yielded data which was colinear with the granitic gneiss data, but with almost no spread between the points. The data yield an intercept age of 2570 Ma, similar to the age from the quartzofeldspathic gneiss.

A sample of biotite-garnet-cordierite gneiss (YB-1, **Figure 2**) contains two zircon morphologies; one group of dark-purplish euhedral crystals, and a second group of more acicular, light greenish-pink crystals. The greenish-pink crystals contain few in-

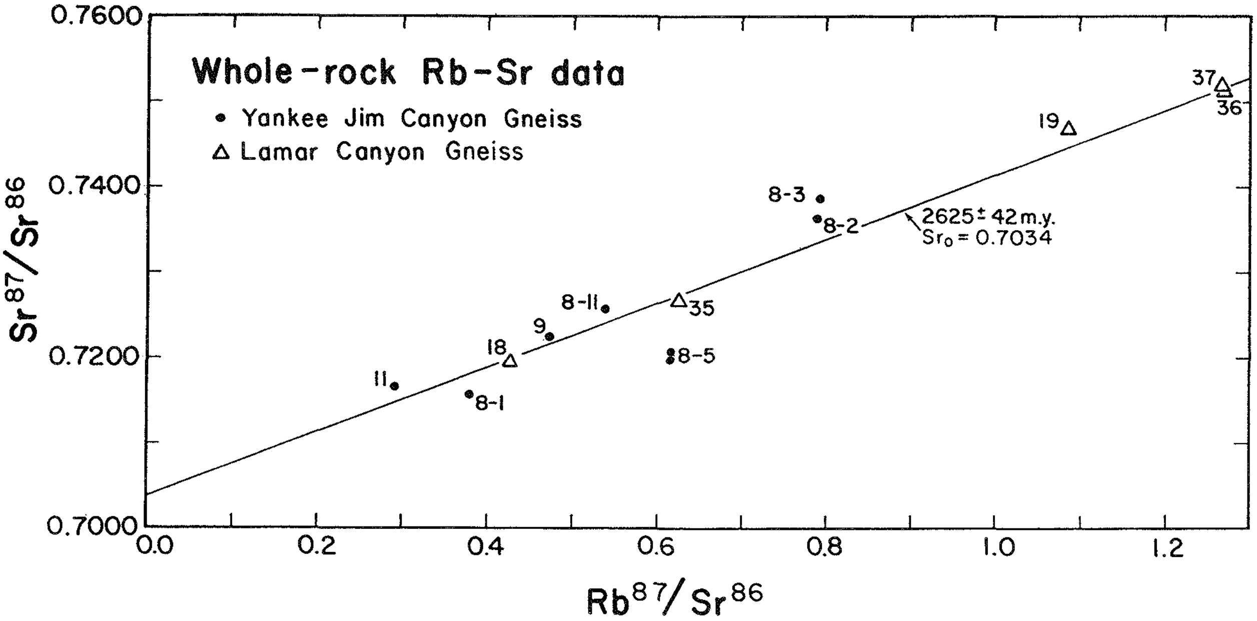

Figure 8—Whole-rock Rb-Sr isotope data for Yankee Jim Canyon (•) and Lamar Canyon (△). The Lamar Canyon data yields an age of 2625 ± 42 Ma, while Yankee Jim Canyon data yields a scatterchron.

Table 3—Whole-rock Pb isotope data for Yankee Jim Canyon and Lamar Canyon.

Whole-rock Lead Isotope Data

Yankee Jim Canyon

Sample	Pb 207/206	Pb 206/208	Pb 206/204	Pb 207/204	Pb 208/204
YB-1	0.87880	0.45694	17.90965	15.75659	39.23195
YB-3	1.00235	0.41058	15.70688	15.74838	38.28281
YB-5	0.92692	0.41127	16.75369	15.53118	40.74016
YB-6	0.98324	0.45875	15.65402	15.39111	34.11768
YB-8-1	0.99080	0.39879	15.46866	15.33215	38.79492
YB-8-2	0.93659	0.32586	16.52374	15.46250	50.91976
YB-8-5	0.99572	0.39718	15.37874	15.31393	38.73499
YB-8-11	0.96969	0.41644	15.80840	15.33015	37.95585
YB-9	1.01818	0.41050	14.89285	15.17220	36.30381
YB-11	0.79003	0.53157	20.58932	16.26284	38.72884

Lamar Canyon

Sample	Pb 207/206	Pb 206/208	Pb 206/204	Pb 207/204	Pb 208/204
YB-1	0.77777	0.53162	20.96032	16.31229	39.47490
YB-20	0.98354	0.30910	15.56457	15.31243	50.38871
YB-35	0.81483	0.51840	19.65006	16.03467	37.92561
YB-36	0.82968	0.49992	19.30279	16.01581	38.59779
YB-37	0.85972	0.48432	18.74900	16.12165	38.68356

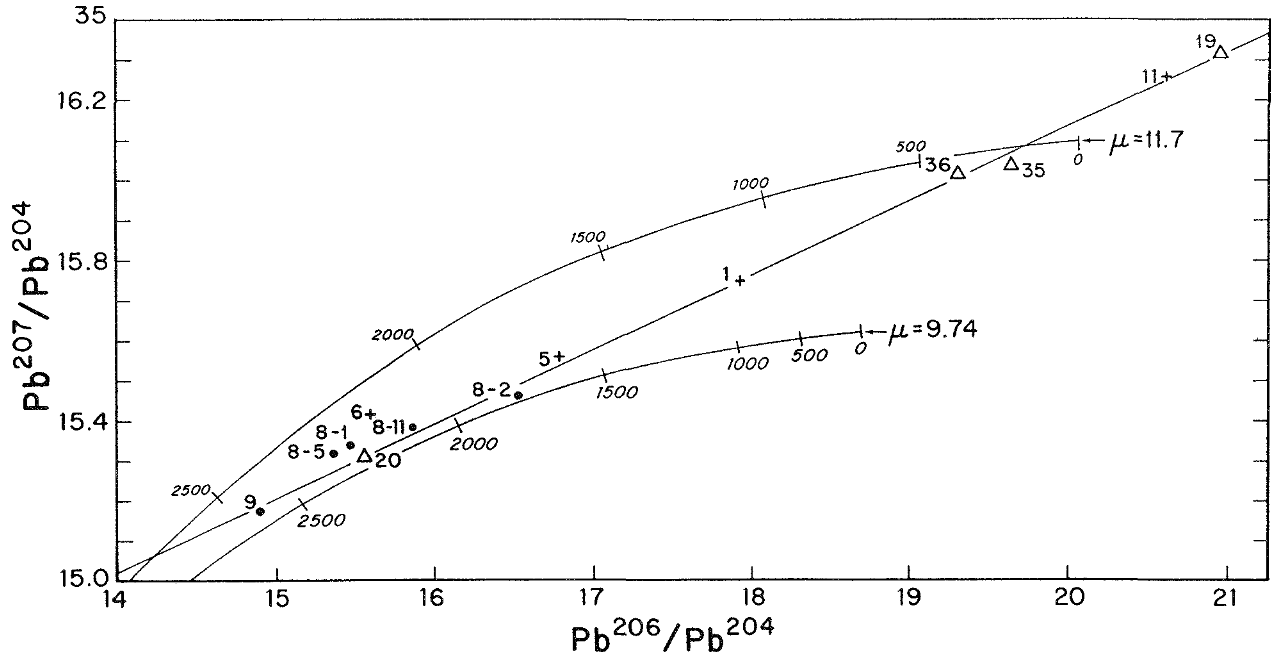

Figure 9—Whole-rock isotope for Yankee Jim Canyon and Lamar Canyon lithologies. (•) The Yankee Jim Canyon quartzofeldspathic gneiss; (+), Yankee Jim Canyon biotite-garnet and biotite-garnet-cordierite gneiss; (Δ), Lamar Canyon quartzofeldspathic gneisses. No radiogenic lead corrections have been made.

Table 4—Whole-rock Rb-Sr isotopic data for Yankee Jim Canyon and Lamar Canyon.

Whole-rock Rb-Sr Data

Yankee Jim Canyon

Sample	Rb (ppm)	Sr (ppm)	Rb^{87}/Sr^{86}	Sr^{87}/Sr^{86}
YB-1	91.4	135.0	1.9719	0.77580 (7)
YB-8-1	129.6	988.1	0.3798	0.71568 (11)
YB-8-2b	109.7	402.6	0.7906	0.73630 (5)
YB-8-3	110.3	406.3	0.7908	0.73853 (9)
YB-8-5	122.3	578.9	0.6105	0.72133 (7)
YB-8-11	99.0	533.6	0.5378	0.72569 (15)
YB-9	97.2	598.0	0.4709	0.72152 (7)
YB-11	51.9	513.9	0.2925	0.71676 (11)

Lamar Canyon

Sample	Rb (ppm)	Sr (ppm)	Rb^{87}/Sr^{86}	Sr^{87}/Sr^{86}
YB-18	68.3	457.5	0.4325	0.72011 (7)
YB-19	82.3	220.3	1.0850	0.74677 (10)
YB-20	41.7	113.4	1.0674	0.74110 (7)
YB-35	85.2	394.9	0.6254	0.72679 (8)
YB-36	107.9	246.6	1.2714	0.75136 (15)
YB-37	105.3	241.5	1.2670	0.75189 (7)

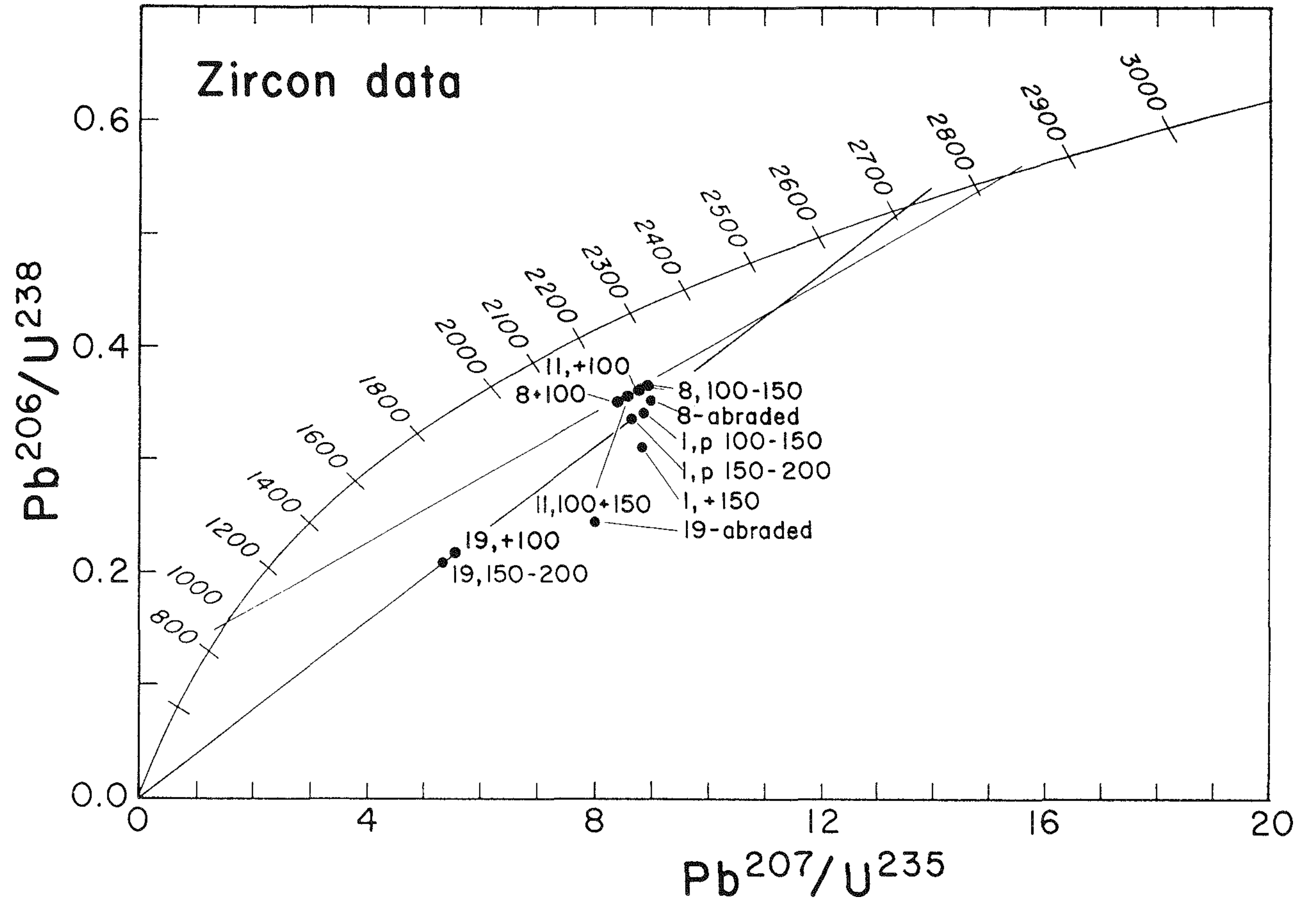

Figure 10—Zircon U-Pb data for Yankee Jim Canyon and Lamar Canyon. (1), biotite-garnet-cordierite gneiss of Yankee Jim Canyon; (8), quartzofeldspathic gneiss of Yankee Jim Canyon; (11), biotite gneiss of Yankee Jim Canyon; (9), quartzofeldspathic gneiss of Lamar Canyon. The following common lead corrections for 2750 Ma were used: $Pb^{206}/^{204}$ = 13.52, $Pb^{207};/^{204}$ = 14.639, and $Pb^{208}/^{204}$ = 33.262.

clusions and no visible cores, while the purplish population contains some inclusions and an occassional core. A single split from the greenish-pink group yielded data which indicate an age of 2857 Ma. This age is very similar to the upper intercept age from the quartzofeldspathic gneiss and biotite gneiss samples, which have a lower intercept of 900 Ma. Two size splits from the dark-pink population indicate an age of 2670 Ma.

Lamar Canyon

The data for Lamar Canyon (YB-19) yield a much clearer picture of the age relations for that region. The whole-rock Rb-Sr data (**Figure 8, Table 3**) yield an isochron age of 2625 ± 42 Ma. The whole-rock Pb-Pb data (**Figure 9, Table 4**) indicate an age of 2689 Ma, while the zircon splits (**Figure 10, Table 5**) indicate ages of 2664 Ma and 2712 Ma. These ages are all similar to other published Rb-Sr ages of 2640 ± 80 Ma (2692 Ma, Wooden and others, 1979; 2718 Ma, Montgomery and Lytwyn, 1984). One abraded zircon sample yielded a Pb^{207}/Pb^{206} age of 2975 Ma, suggesting the possibility of an inherited U-Pb component.

Summary

The lithologies in Yankee Jim Canyon are dominated by quartzofeldspathic gneisses, but also include biotite-garnet-cordierite gneisses, biotite gneisses, mafic units and pegmatites. The quartzofeldspathic gneisses show evidence of mylonitization along the contacts with the adjacent layered gneisses. Mineral chemistries show wide variation in the different lithologies. Solid solution minerals, such as plagioclase, range from An_2 (quartzofeldspathic gneiss) to An_{90} (mafic layers). Garnet and cordierite compositions vary slightly with the degree of alteration. The presence of cordierite, garnet, sillimanite and kyanite allow for good temperature-pressure estimates of 775-800°C and 4.5-6 kb.

The ages derived in Yankee Jim Canyon from

Table 5—Zircon U-Pb data for Yankee Jim Canyon and Lamar Canyon.

U-Pb (Zircon) Data

Sample (mesh)	Concentration (ppm)		Atom Ratios			Age (Ma)		
	Pb	U	Pb 206 / U 238	Pb 207 / U 235	Pb 207 / Pb 206	Pb 206 / U 238	Pb 207 / U 235	Pb 207 / Pb 206
Yankee Jim Canyon								
YB-1 (pale green split, +150)	250.2	703.2	0.30539	8.7929	0.20383	1718	2217	2857
YB-1 (purple split, +150)	280.2	679.5	0.34700	8.9295	0.18218	1920	2330	2672
YB-1 (purple split, 150-200)	284.7	691.4	0.34038	8.8347	0.18116	1889	2321	2669
YB-8 (100-150)	192.7	416.1	0.36534	8.9280	0.17301	2007	2330	2587
YB-8 (+100)	189.3	430.6	0.35040	8.4084	0.16987	1937	2276	2556
YB-11 (100-150)	224.2	582.0	0.35506	8.5865	0.17120	1959	2295	2569
YB-11 (+100)	216.6	551.1	0.36346	8.7929	0.17126	1999	2317	2570
Lamar Canyon								
YB-19 (+100)	262.1	1018.7	0.21591	5.5254	0.18117	1260	1904	2664
YB-19 (150-200)	250.7	1044.2	0.20036	5.2802	0.18657	1177	1865	2712
YB-19 (150-200, abraded)	240.7	769.2	0.25301	7.83323	0.21917	1454	2212	2975

whole-rock Pb isotope data center around 2625-2650 Ma for the various lithologies. The whole-rock Rb-Sr data indicate that the Rb-Sr systematics have been disturbed, most likely by a later metamorphic event. The zircon U-Pb data indicate a discordant age of 2850 Ma, with some indication of episodic lead loss.

The whole-rock Rb-Sr and whole-rock Pb isotopic data from Lamar Canyon indicate an intrusive period at 2625-2700 Ma, which is in agreement with other reported ages for the region. The zircon U-Pb data also indicate ages of 2650-2700 Ma. An abraded zircon sample with an age of 2975 Ma suggests an inherited U-Pb component.

Further detailed geochronologic work, coupled with structural data, is needed to clarify age relations in Yankee Jim Canyon and its relationship with the exposed gneisses to the east and southeast. Preliminary comparisons of isotopic and geochemical data from Archean lithologies with data from Yellowstone Plateau lavas eliminate exposed basement as a major source rock for the Yellowstone rhyolites.

Acknowledgements

The authors would like to thank Wayne Hamilton of the National Park Service for permission to sample within Yellowstone National Park boundaries. To M. C. Gilbert for his helpful discussions on various aspects of the field relationships. Hal Pendrak and Todd Solberg are acknowledged for their invaluable assistance with the geochemical, isotopic and microprobe facilities. Field work was partially funded through a Chevron Research Grant to R. Guy.

References

Brookins, D. G., 1968, Rb-Sr and K-Ar age determinations from the Precambrian rocks of the Jardine-Crevice Mountains area, southwestern Montana: Earth Science Bulletin, v. 1, p 5-9.

Burnham, R., 1982, Mylonite zones in the crystalline basement rocks of Sixmile Creek and Yankee Jim Canyon, Park County, Montana [M.S. thesis]: University of Montana, Missoula, 93 p.

Casella, C. J., Levay, J., Eble, E., Hirst, B., Huffman, K., Lahti, V., and Metzger, R., 1982. Precambrian geology of the southwestern Beartooth Mountains, Yellowstone National Park, Montana and Wyoming: Montana Bureau of Mines and Geology Special Publication 84, p. 1-24.

DePaolo, D. J., 1982, Sm-Nd age of the Stillwater Complex and evidence for Early Archean crust in the Beartooth Mountains: Montana Bureau of Mines and Geology Special Publication 94, p. 159-160.

Doe, B. R., Leeman, W. P., Christiansen, R. L., and Hedge, C. E., 1982, Lead and strontium isotopes and related trace elements as genetic tracers in the upper Cenozoic rhyolite-basalt association of the Yellowstone Plateau volcanic field: Journal of Geophysical Research, v. 87, p. 4785-4806.

Foose, R. M., Wise, D. U., and Garbarini, G. S., 1961, Structural geology of the Beartooth Mountains, Montana and Wyoming: Geological Society of America Bulletin, v. 72, p. 1143-1172.

Fraser, G. D., Waldrop, H. A., and Hayden, H. J., 1969, Geology in the Gardiner area, Park County, Montana: U.S. Geological Survey Bulletin 1277, 118 p.

Hallager, W. S., 1980, Geology of Archean gold-bearing metasediments near Jardine, Montana [Ph.D. dissertation]: University of California, Berkeley, 136 p.

Holberg, L., 1940, Geomorphic problems and glacial geology of the Yellowstone valley, Park County, Montana: Journal of Geology, v. 48, p. 275-303.

Holdaway, M. J., 1971. Stability of andalusite and the aluminum silicate phase diagram: American Journal of Science, v. 271, p. 97-131.

______ 1972, Thermal stability of Al-Fe epidote as a function of fO_2 and Fe content: Contributions to Mineralogy and Petrology, v. 37, p. 307-340.

Holdaway M. J. and Lee, S. M., 1977, Fe-Mg cordierite stability in high-grade pelitic rocks based on experimental, theoretical and natural observations: Contributions to Mineralogy and Petrology, v. 63, p. 175-198.

Huffman, K., 1977, The Precambrian geology of the Coyote Creek area, Montana [M.S. thesis]: Northern Illinois University, De Kalb, 104 p.

Lahti, V. R., 1975, Precambrian and structural geology of the Crevice Lake area, southwestern Beartooth Mountains, Montana and Wyoming [M.S. thesis]: Northern Illinois University, De Kalb, 72 p.

Liou, J. G., 1973, Synthesis and stability relations of epidote, $Ca_2Al_2FeSi_3O_{12}(OH)$: Journal of Petrology, v. 14, p. 381-413.

Lonker, S. W., 1981, P-T-X relations of the cordierite-garnet-sillimanite-quartz equilibrium: American Journal of Science, v. 281, p. 1056-1090.

Lytwyn, J. N., 1982, Geochemistry and ages of Precambrian plutonic rocks from the southwest Beartooth Mountains, Yellowstone National Park, Wyoming and Montana [M.S. thesis]: Northern Illinois University, De Kalb, 111 p.

Mehnert, K. R., 1968, Migmatites and the Origin of Granitic Rocks: Elsevier, Amsterdam, 398 p.

Montgomery, C., 1982, Preliminary zircon U-Pb dating of biotite granodiorite from the South Snowy block, Beartooth Mountains: Montana Bureau of Mines and Geology Special Publication 84, p. 41-44.

Montgomery, C. and Lytwyn, J. N., 1984, Rb-Sr systematics and ages of principal Precambrian lithologies in the South Snowy block, Beartooth Mountains: Journal of Geology, v. 92, p. 103-112.

Naney, M. T., 1983, Phase equilibria of rock-forming ferromagnesian silicates in granitic systems: American Journal of Science, v. 283, p. 993-1033.

Norrish, K. and Hutton, J. T., 1969, An accurate x-ray spectrographic method for the analysis of a wide range of geological samples: Geochimica et Cosmochimica Acta, v. 33, p. 431-453.

Pettingill, H., Sinha, A. K., and Tatsumoto, M., 1984, Age and origin of anorthosites, charnockites and granulites in the central Virginia Blue Ridge: Nd and Sr isotopic evidence: Contributions to Mineralogy and Petrology, v. 85, p. 279-291.

Reynolds, R. C., 1963, Matrix corrections in trace element analysis by x-ray fluorescence: Estimation of the mass absorption coefficient by Compton scattering: American Mineralogist v. 48, p. 1133-1143.

Richardson, S. W., Gilbert, M. C., and Bell, P. M., 1969, Experimental determination of the kyanite-andalusite and andalusite-sillimanite equilibria: The aluminum silicate triple point: American Journal of Science, v. 267, p. 259-277.

Seager, G. F., 1944, Gold, arsenic and tungsten deposits of the Jardine-Crevice Mountain district, Park County, Montana: Montana Bureau of Mines and Geology Memoir 23, 110 p.

Sinha, A. K., and Bartholomew, M. J., 1984, Evolution of the Grenville terrane in the central Virginia Appalachians: Geological Society of America Special Paper 194, p. 175-186.

Solberg, T. N., and Speer, J. A., 1982, QALL, a 16-element analytical scheme for efficient petrologic work on an automated ARL-SEMQ: Application to mica reference samples: Microbeam Analysis, p. 422-426.

Speer, J. A., 1984, Micas in igneous rocks, *in* Reviews in Mineralogy Micas; S. W. Bailey, *(ed.)*: v. 13, p. 299-356.

Streckeisen, A. L. and others, 1973, Plutonic rocks: Classification and nomenclature recommended by the International Union of Geological Sciences Subcommittee on the Systematics of Igneous Rocks: Geotimes, v. 18, p. 26-30.

Thompson, A. B., 1976, Mineral reactions in pelitic rocks: Calculation of some P-T-X(Fe-Mg) phase relations: American Journal of Science, v. 276, p. 425-454.

Thruston, P. B., 1986, Geochemistry and provenance of Archean metasedimentary rocks in the southwestern Beartooth Mountains [M.S. thesis]: Montana State University, Bozeman, 74 p.

Tulloch, A. J., 1979, Secondary Ca-Al silicates as low-grade alteration products of granitoid biotite: Contributions to Mineralogy and Petrology, v. 69, p. 105-117.

Wooden, J. L., Mueller, P. A., Hunt, D. K., and Bowes, D. R., 1982, Geochemistry and Rb-Sr geochronology of Archaean rocks from the interior of the southeastern Beartooth Mountains, Montana and Wyoming: Montana Bureau of Mines and Geology Special Publication 84, p. 45-56.

York, D., 1969, Least-squares fitting of a straight line with correlated errors: Earth and Planetary Science Letters, v. 5, p. 320-324.

Zen, E. and Hammarstrom, J. M., 1984, Magmatic epidote and its petrologic significance: Geology, v. 12, p. 515-518.

©DIANE NUGENT
1988

LATE ARCHEAN THIN-SKINNED THRUSTING OF THE CHERRY CREEK METAMORPHIC SUITE IN THE HENRY'S LAKE MOUNTAINS, SOUTHERN MADISON RANGE, MONTANA AND IDAHO

Wendolyn Sumner and Eric A. Erslev
Department of Earth Resources
Colorado State University
Fort Collins, Colorado 80523

Introduction

The nature and driving mechanisms of Archean tectonic regimes are highly debated due to the fragmentary rock record preserved in Precambrian shields. Many workers have proposed a substantial change in the crust-mantle system between the Archean and the Proterozoic based on differences in tectonic style and rock composition from the two periods (Taylor and McLennan, 1985). Archean provinces are characterized by an abundance of high-grade gneiss and greenstone belts and a corresponding dearth of continental margin and shelf associations. The increased occurrence of stable shelf suites through geologic time is an important yet unexplained temporal pattern with major implications for the evolution of the earth (Taylor and McLennan, 1985; Gibbs and others, 1986).

In the northwestern Wyoming province, the Cherry Creek metamorphic suite is an anomalously well-preserved (by Archean standards) carbonate-quartzite-pelite shelf association. Massive dolomite marbles form up to 27% of the stratigraphic section and contain a Sr isotopic composition more consistent with Phanerozoic carbonates than Archean carbonates (Gibbs and others, 1986). Similarly, the abundant pelitic rocks of the sequence contain post-Archean geochemical signatures quite different from those of typical Archean greenstone belt pelites, including negative europium anomalies and steep LREE patterns. This anomalous Archean sequence clearly points to a greater diversity of Archean petrogenetic environments than those encompassed by the traditional greenstone belt-gneiss belt classifications. Ongoing investigations are focused on the petrogenesis and subsequent preservation of the Cherry Creek metamorphic suite to evaluate its significance to Archean tectonic processes.

This study documents the earliest stage of deformation in the Cherry Creek metamorphic suite, in an area with minimal subsequent deformational events. Precise determination of deformational history in crystalline terranes is often complicated by several episodes of deformation and metamorphism. In the northwestern Wyoming province, a clear understanding of the tectonic processes which preserved the suite requires the characterization and subtraction of Phanerozoic and Proterozoic deformations from the overall rock fabric. The study area in the Henrys Lake Mountains portion of the southern Madison Range (**Figure 1**) was chosen for this investigation because it shows the least effects of Early Proterozoic crustal reworking which reset K-Ar clocks along the northwest rim of the Wyoming province (Giletti, 1962).

Phanerozoic deformation of the crystalline rocks is limited to block faulting with minimal penetrative deformation during Laramide thrusting and Recent basin and range extension (Schmidt and Garihan, 1983; Erslev, 1983). Early Proterozoic (1.9 Ga) deformation in the southern Madison Range is characterized by epidote-amphibolite facies assemblages and ductile shearing concentrated within the Madison mylonite zone north of the study area. The Cherry Creek metamorphic suite south of the shear zone is relatively unaffected by Proterozoic shearing, as seen by the lack of reset ^{40}Ar-^{39}Ar ages which are the rule in all other exposures of the suite. An Archean age (2.7 Ga) is indicated for the pervasive middle-amphibolite facies assemblages south of the shear zone based on ^{40}Ar-^{39}Ar analyses of hornblende from amphibolites. Thus, a study of the deformation south of the Madison mylonite zone provides the clearest view of Archean structures of the Cherry Creek metamorphic suite.

Erslev (1983) suggested minor structural repetitions of the Cherry Creek metamorphic suite on thrusts with tectonic transport opposite that of the

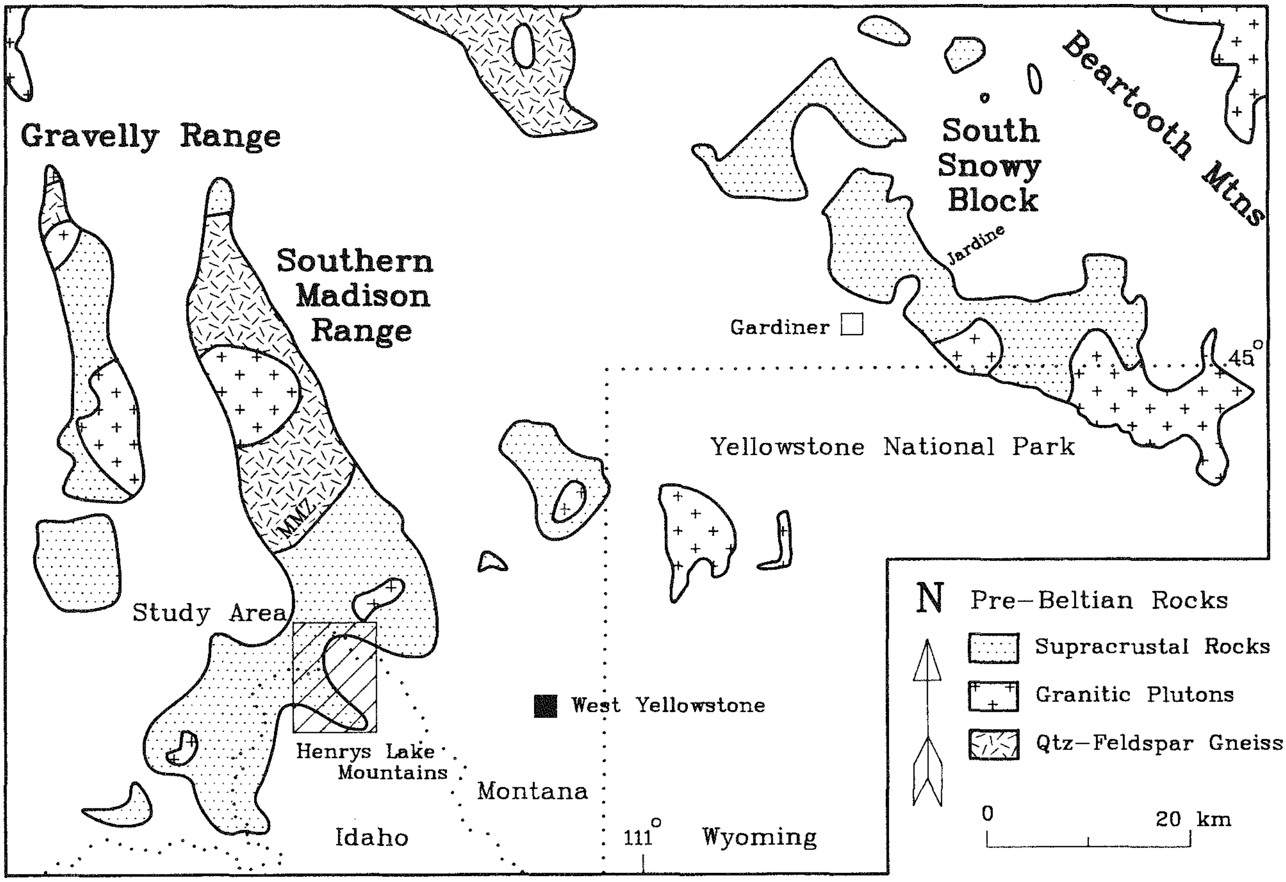
Gravelly Range
Southern Madison Range
MMZ
Study Area
Henrys Lake Mountains
Montana
Idaho
West Yellowstone
111°
Wyoming
Gardiner
Yellowstone National Park
South Snowy Block
Beartooth Mtns
Jardine
45°
N
Pre–Beltian Rocks
Supracrustal Rocks
Granitic Plutons
Qtz–Feldspar Gneiss
0
20 km

Figure 1—Archean exposures in the northwestern Wyoming province and location of the southern Madison Range and Henrys Lake Mountains.

Madison mylonite zone. The association of prograde mineral assemblages within these zones and their rotation during shearing in the Madison mylonite zone suggests an older age of deformation, which has been confirmed by ^{40}Ar-^{39}Ar studies. The faults can be projected into a zone of complex structural and lithologic relationships mapped by Witkind (1972). This study tests whether the complex zone is due to Archean thrusting and if recent stratigraphic hypotheses are consistent with and could aid in the deciphering of the area. It also defines the structural geometry of the Archean deformation in the Cherry Creek metamorphic suite of the southern Madison Range through reconstruction of the stratigraphic sequence, petrofabric analyses, strain data, and a down-plunge projection across the study area.

Cherry Creek stratigraphy

Reconstruction of the local Cherry Creek stratigraphic sequence imposes important constraints on the large-scale structural geometry of the southern Madison Range. Detailed field traverses along ridge crests trending perpendicular to regional foliation reveal a coherent stratigraphy. The stratigraphic column of the Cherry Creek metamorphic suite (**Figure 2**) was constructed by measuring unit thicknesses (dip corrected) (Erslev, 1983), which is in the same strike belt as the study area. In the northern portion, major unit contacts are laterally continuous, undisrupted by folding, and lack obvious unit repetition. The lithologic sequence in this area apparently represents primary stratigraphy with bedding-parallel thrusts. These thrusts appear to be entirely contained within individual map units, causing an increase in thickness in both the major marble and pelite units. The thrusts are equivalent to flats in a thin-skinned thrust belt.

Relict graded bedding, minor cross beds and scour casts in the biotite schist (meta-turbidite) provided 153 stratigraphic-up directions. Local graded beds in pebbly quartzites (3) and graded-volcanic lapilli in amphibolites (5) all suggest regional stratigraphic up to the southeast.

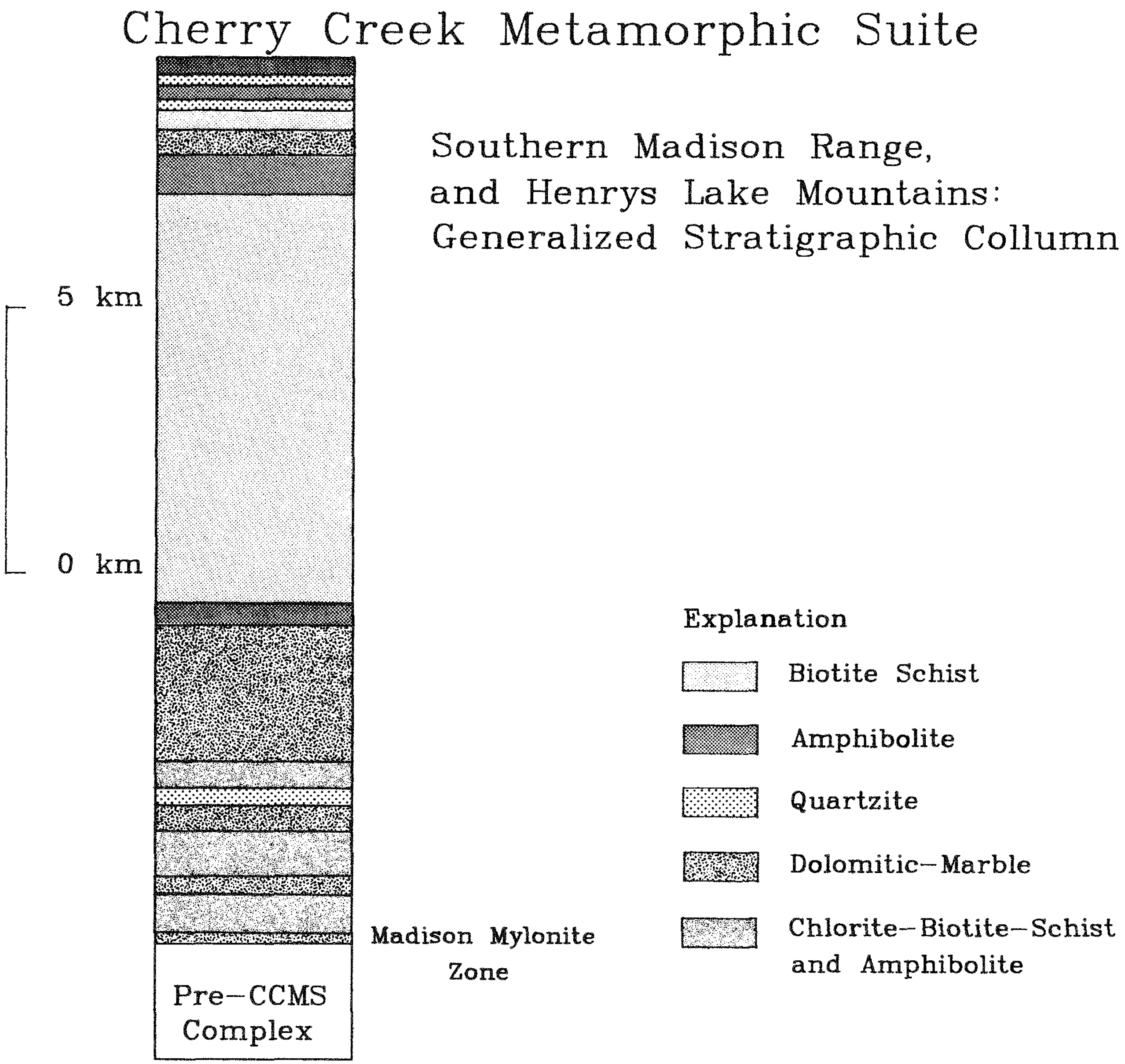
Cherry Creek Metamorphic Suite
Southern Madison Range,
and Henrys Lake Mountains:
Generalized Stratigraphic Collumn
5 km
0 km
Explanation
Biotite Schist
Amphibolite
Quartzite
Dolomitic–Marble
Chlorite–Biotite–Schist and Amphibolite
Madison Mylonite Zone
Pre–CCMS Complex

Figure 2—Generalized stratigraphic column of the Cherry Creek metamorphic suite for the Henrys Lake Mountains.

From 161 measurements of sedimentary structures, 65% give regional stratigraphic up to the southeast (**Figure 3**). The Sheep and Coffin Lake areas gives evenly contradictory tops directions, with 50 to the southeast and 44 to the northwest. This area is directly in line with projected traces of thrusts cutting the marble-bearing part of the sequence, suggesting that the discordance of these measurements reflects thrust-generated folding, generating the anomalous thickness of biotite schist unit. If these readings are omitted, 82% of the measurements give tops to the southeast, which is consistent with the stratigraphic interpretation of Erslev (1983).

Map-scale geometry

The Archean lithologies were mapped on a scale of 1:24,000 during the summer of 1985 and fall of 1986. The geologic map (**Figure 3**) pattern reveals a series of stratigraphic repetitions and truncations along strike. Similar relationships were noted in the Gravelly Range (Heinrich and Rabbitt, 1960) and in the central Madison Range (Erslev, 1983). Heinrich and Rabbitt (1960) reported marked variation in unit thickness and petrology along strike from the type locality of the Cherry Creek metamorphic suite in the Gravelly Range.

A good example of unit repetition and truncation along strike is the repeated dolomite-amphibo-

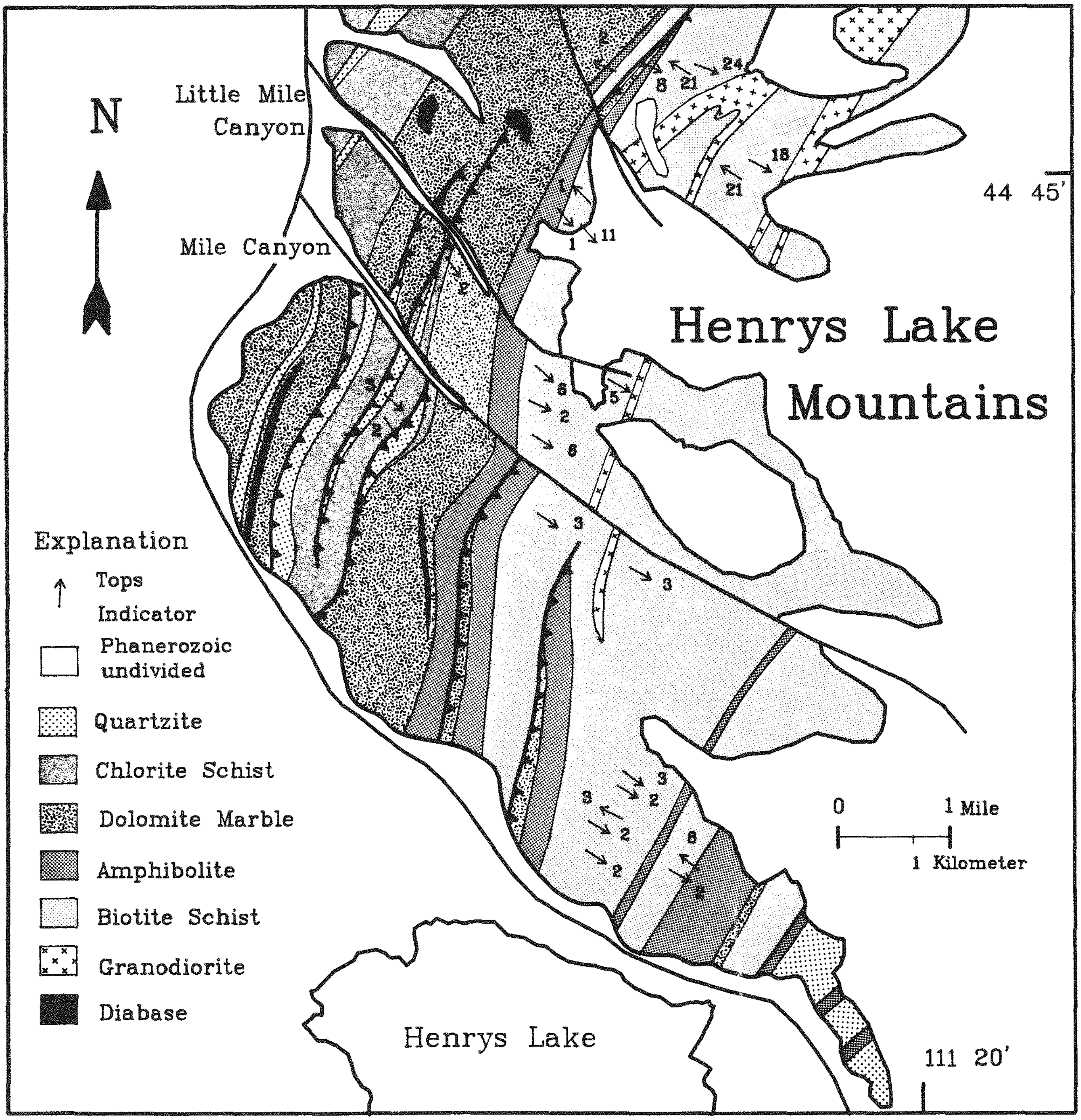
N
Little Mile Canyon
Mile Canyon
Henrys Lake Mountains
44 45'
Explanation
Tops Indicator
Phanerozoic undivided
Quartzite
Chlorite Schist
Dolomite Marble
Amphibolite
Biotite Schist
Granodiorite
Diabase
0
1 Mile
1 Kilometer
Henrys Lake
111 20'

Figure 3—Geologic map of the Henrys Lake Mountains showing stratigraphic tops indicators. *Modified from* Witkind (1972).

lite-biotite schist sequence along the southwestern flank of the range (**Figure 3**). In general, the total thickness of the lithologies increases to the southwest. For example, from northeast to southwest (**Figure 3**) the thickest dolomite unit is split by a chlorite-schist/quartzite sequence. Duplication of the marble unit and three repetitions of the chlorite-schist/quartzite assemblage occurs to the southwest along this complex zone. The apparent individual unit thicknesses actually increases to the northeast, with the major marble increasing from 0.8 to 2.0 kilometers and the major biotite schist increasing from 3.2 to 5.5 kilometers, suggesting thrusting within the units.

Detailed examinations of unit contacts reveal that unit duplications and truncations occur along a series of generally concordant, SE-dipping mylonite zones, varying in thickness from centimeters to meters. **Figure 4A** shows a photograph of a protomylonite zone at a lithologic contact. Repetition of Cherry Creek lithologic sequences along these ductile shear zones is either the result of thrust duplexing, strike-slip faulting, or a combination of both.

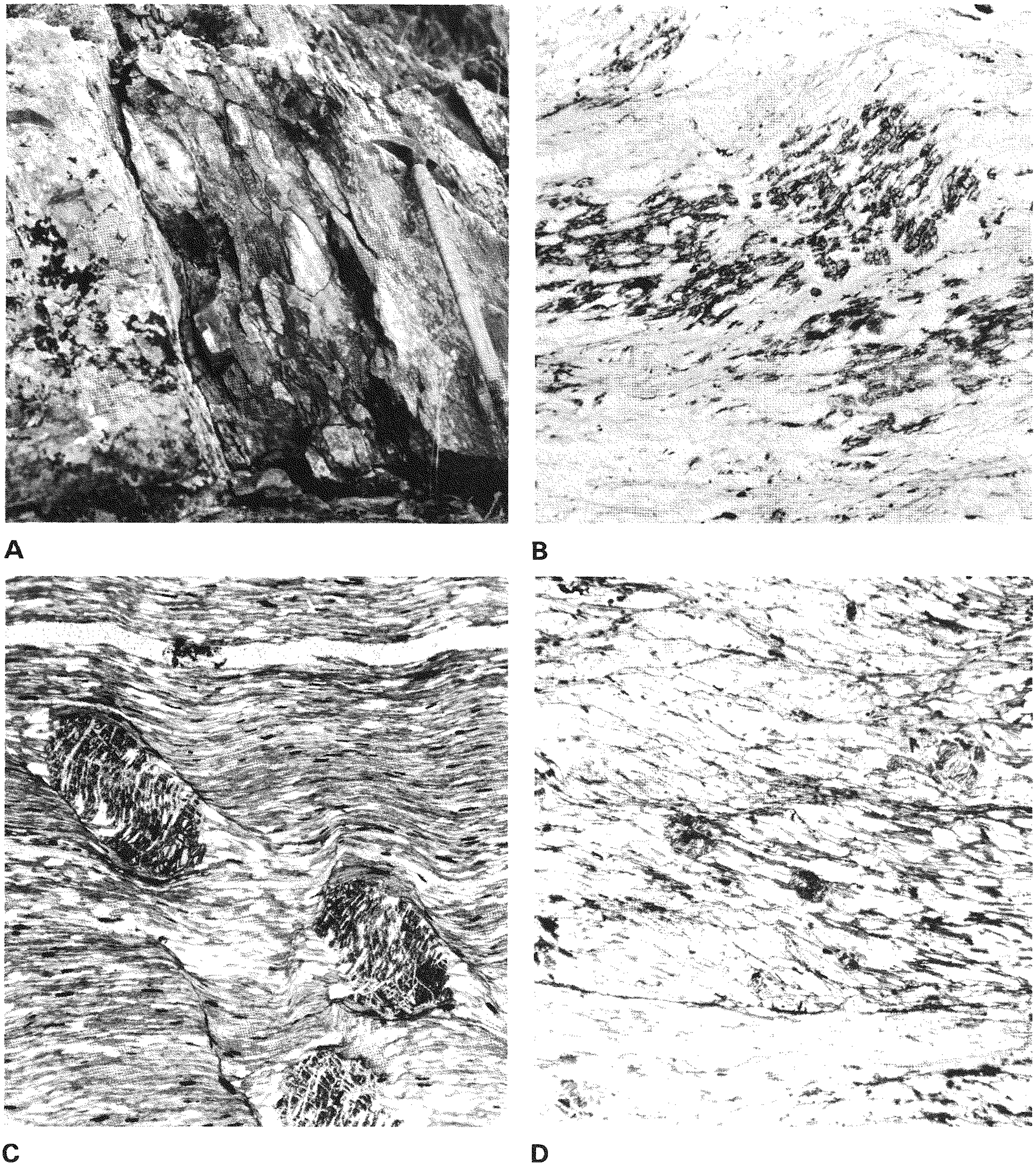

Figure 4—Mylonitic fabrics of the X-Z plane from oriented samples. (A), protomylonite between dolomite-marble (on left) and chlorite-schist/quartzite unit; (B), photomicrograph (plane polarized light) of sheared kyanite from protomylonite zone shown in A; (C), photomicrograph (plane polarized light) of rotated porphyroblastic garnet in hornblende-biotite-garnet schist showing sinistral shear *(after* Simpson and Schmid, 1983); (D), sheared biotite-schist with C-S surfaces indicating sinistral shear. Photomicrographs are 4.4 millimeters in horizontal dimension.

Fabric and strain data

Metamorphic assemblages (e.g., quartz + biotite + garnet + staurolite + kyanite in pelitic schists) are consistent with moderate grade, amphibolite facies metamorphism (600°C, >6 kb) based on garnet-biotite geothermometry and aluminosilicate stability in rocks to the north (Erslev, 1983). Regional foliation strikes northeasterly, paralleling compositional layering and relict bedding surfaces, with generally moderate dips to the southeast (**Figure 5A**). Rotation of some of the foliations about a horizontal axis to NW-dipping orientations is the result of subsequent ductile shearing in the Madison mylonite zone to the north.

Mineral growth lineations defined by biotite, muscovite, hornblende and staurolite trend northeast-southwest and are parallel to small-scale fold axes (**Figures 5B, 5C**). Mineral stretching lineations (X) are subparallel to the dip direction of the regional foliation, with an average trend and plunge of S50E,65.

Many small-scale, isolated intrafolial folds suggest heterogeneous deformation localized in zones of intense shear. The fact that mineral growth lineations parallel fold axes in these zones suggests mineral growth concurrent with deformation. Axial planar cleavage parallels regional foliation and is probably related to regional foliation development.

Strain analysis

Eighty-two oriented thin sections were prepared to evaluate the finite strain. Deformed quartz and plagioclase grains in clastic portions of the biotite schist were measured to determine the type, amount

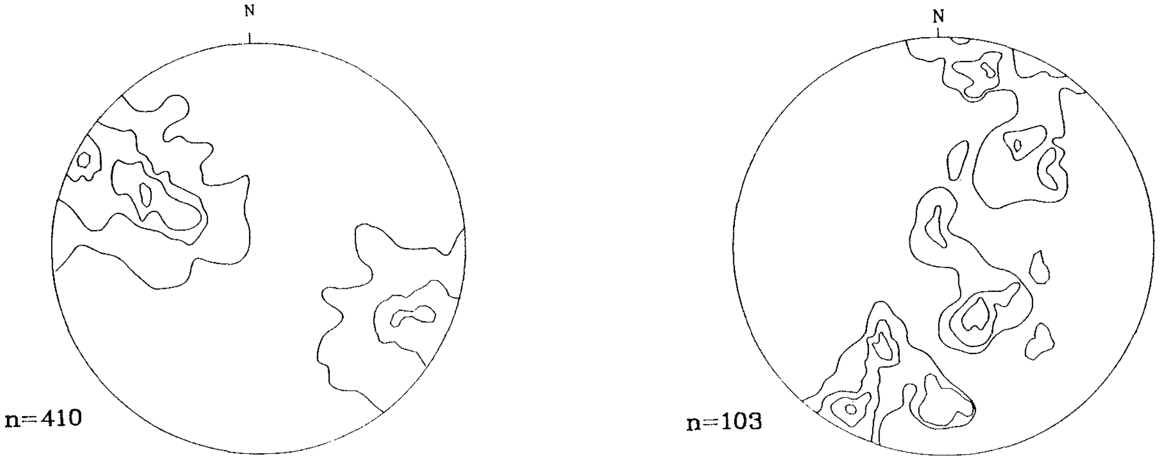

all lithologies

A

mineral growth and stretching lineations

B

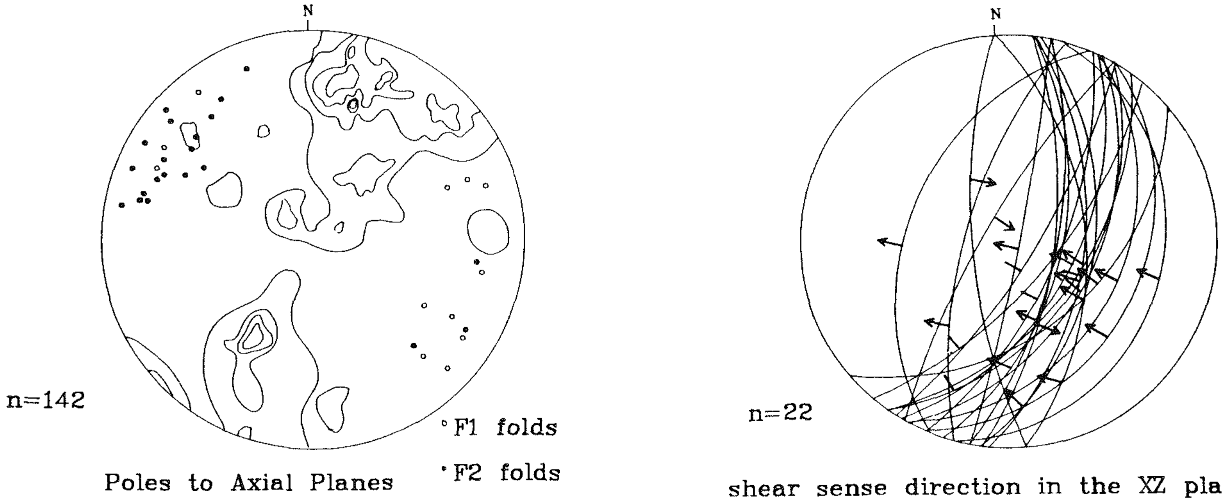

Poles to Axial Planes

C

shear sense direction in the XZ plane plotted here perpendicular to foliation

D

Figure 5—Fabric data. Contours represent 1, 3, 5 and 7% per 1% area for (A), poles to foliation; (B), fold axes; (C), lineations; (D), S-surface orientations (X-Y planes) and shear-sense indicators are plotted at X, with arrows showing displacement of the hanging wall relative to the footwall.

and shear sense associated with Archean deformation of the Cherry Creek metamorphic suite. Detailed strain measurements were made from 12 biotite schists, two quartzites, and one pebbly meta-siltstone. For each thin section, the mean axial ratio was determined by the Fry (1979) method, normalized Fry method (Erslev, 1988) and the Rf/Phi (Ramsay, 1967) method. A minimum of 150 elliptical grains were digitized and input into INSTRAIN, an integrated strain analysis program, which generated the analyses (**Figure 6**).

Most samples indicate largely flattening strains produced by bulk shortening, with X:Y:Z strain of 2.15:2.13:1 in a representative sample. The strain in two samples collected from mylonite zones, and a quartzite and a pebbly-siltstone, plot close to the

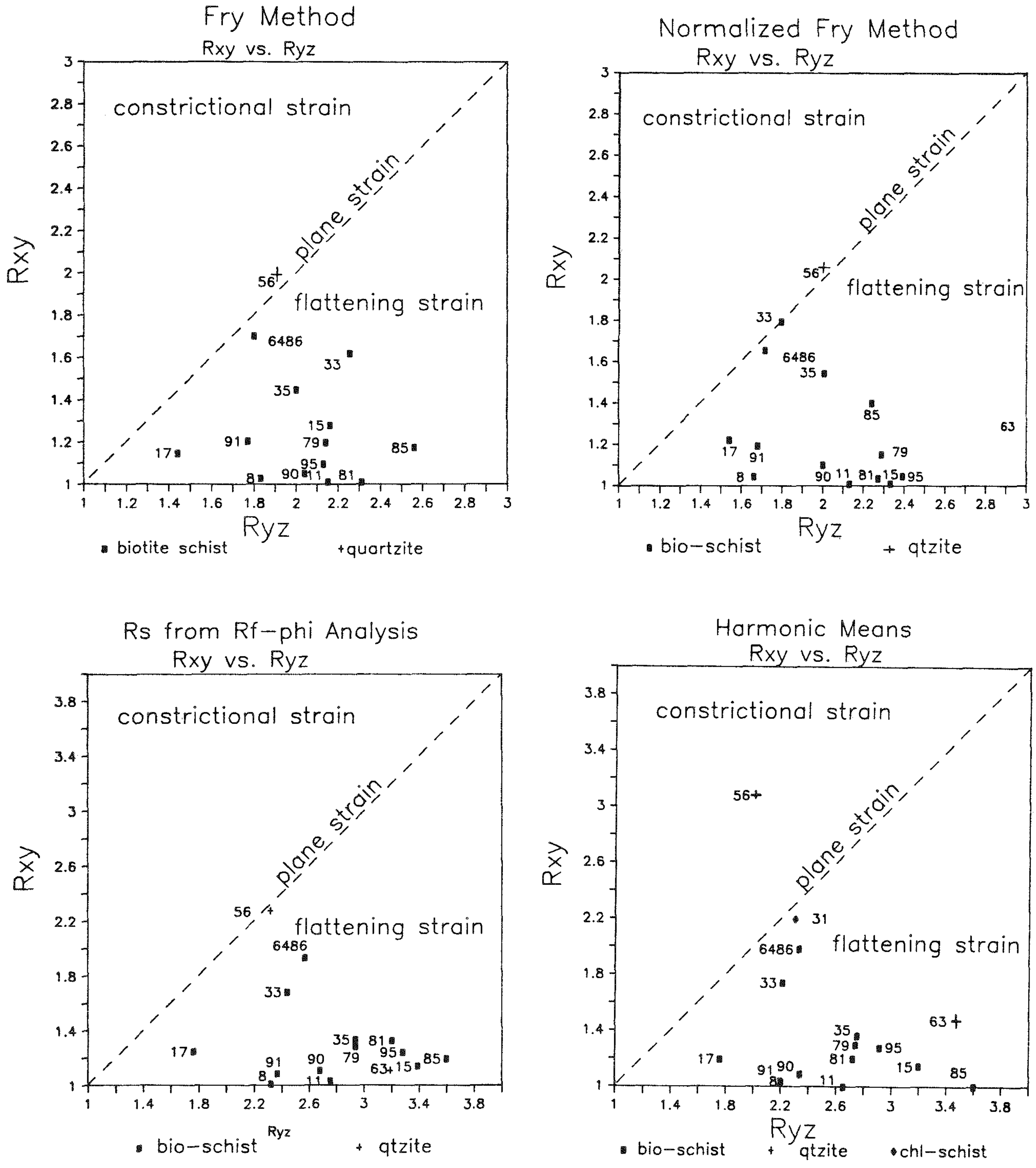

Figure 6—Flinn diagrams showing results of three-dimensional strain analyses. Numbers correspond to sample numbers.

plane strain line, possibly indicating simple shear in the mylonite zones. Deformed quartz clasts from one of these mylonite zones has X:Y:Z strain of 3.1:2.4:1.0.

Shear-sense determinations

To determine the shear sense in the mylonite zones, the asymmetry of mineral grains was measured directly in three outcrops and in the X-Z plane of 22 oriented thin sections. Shear-sense determinations from prograde mineral assemblages using the criteria of Simpson and Schmid (1983) are summarized in (**Figure 5D**), a stereonet plot of X-Y planes with shear sense (parallel to X, measured in the X-Z plane).

In thin sections cut parallel to the X-Z plane, shear-sense determinations were measured from asymmetric porphyroclasts of quartz, feldspar, staurolite and kyanite, C-S surfaces, oblique and elongate mineral grains, and rolled garnets (**Figure 4**). Mineral stretching lineations paralleling the X strain direction are generally subparallel or oblique to the foliation dip direction. Shear-sense criteria indicate dominantly reverse (high-angle thrust) motion with tectonic transport toward the northwest (**Figure 5D**).

Structural model and interpretations

A structural model was developed by constructing a down-plunge projection (Mackin, 1950) incorporating regional stratigraphic and structural data. The data was compiled from eight parallel cross sections oriented perpendicular to the regional fold axis trend. In the down-plunge view, exposures in the southwest represent structurally lower levels, while exposures along unit strikes to the northeast represent structurally higher levels. Data for each section include lithologies, facing directions, contact relationships (mylonitic versus stratigraphic) and strain data.

The down-plunge cross section (**Figure 7**) shows tectonic thickening along an imbricate thrust zone due to thin-skinned thrusting during a compressional orogenic event. When viewed perpendicular to the cross section line, the geologic map (**Figure 3**) resembles a longitudinal cross section across a thrust belt (Woodward and others, 1985). From this vantage point, it is apparent that many unit truncations along lithologic strike are the result of lateral ramps in thrusts cutting up section to the northeast. The complex regional map pattern shows an original depositional sequence duplicated by thrust faulting along generally SE-dipping mylonite zones with northwest vergence.

Sequential deformation model

The sequential deformation model exhibited (**Figure 8**) is based on the regional geology constrained by the necessity to approach cross section balance or restorability (Woodward and others 1985). It should be noted that variations in strain have not been rigorously incorporated into the sections shown here. The model is analogous to interpretations of thin-skinned thrusting and duplexing along many post-Archean continental margins (Boyer and Elliott, 1982; Elliott and Johnson, 1980; Suppe, 1983).

The restored primary stratigraphy compiled from the regional stratigraphic column is shown in **Figure 8A**. Thrusting during a Late Archean compressional orogeny formed horses (thrust-bounded blocks) due to bifurcation of faults in ramp areas, forming a duplex structure (Suppe, 1983). The fact that continued thrusting in the hinterland often rotates the early thrusts to higher angles provides a possible explanation of the steep dips in the southern Madison Range. Thrusting events depicted in **Figure 8B** are interpreted to be synkinematic with prograde, mid-amphibolite facies metamorphism of Late Archean (2.7Ga) age. **Figure 8C** shows Proterozoic (1.9 Ga) thrusting of the pre-Cherry Creek metamorphic complex (the basement upon which the Cherry Creek units were deposited), over the Cherry Creek metamorphic suite in the Madison mylonite zone. This event rotated the regional foliation within the ductile shear zone through the vertical, forming a NW-dipping zone of Proterozoic basement reworking.

Conclusions

Mapping in the Henrys Lake portion of the southern Madison Range reveals a coherent stratigraphic sequence which constrains the large-scale structural geometry of the Cherry Creek metamorphic suite. The study concludes that the complex map pattern, with repetitions and truncations of the Cherry Creek stratigraphy, is the result of Archean thin-skinned thrusting along a series of narrow, generally SE-dipping mylonite zones. Increases in individual unit bulk thickness to the northeast is the

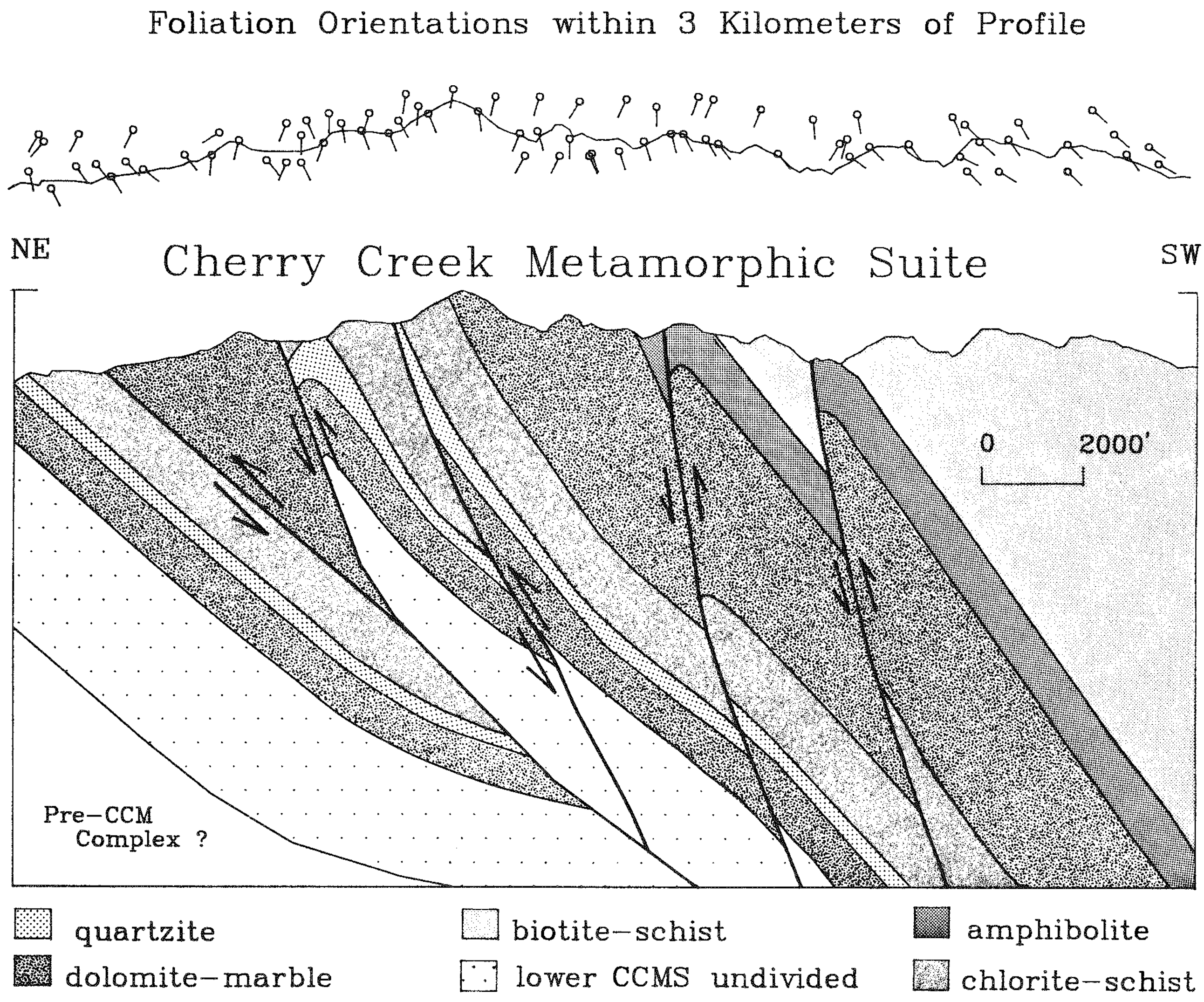
Foliation Orientations within 3 Kilometers of Profile
NE
Cherry Creek Metamorphic Suite
SW
0 2000'
Pre-CCM Complex ?
quartzite
dolomite-marble
biotite-schist
lower CCMS undivided
amphibolite
chlorite-schist

Figure 7—Cross section of regional structure constructed using the down-plunge method (Mackin, 1950) of the Henrys Lake Mountains.

result of intraformational fold and thrust thickening, forming zones of opposing facing directions and isoclinal folding.

The strain analysis of psammitic portions of metaturbidites indicates largely flattening strains and bulk shortening of the Cherry Creek metamorphic suite. However, mylonitic zones contain plane-strain fabrics consistent with ductile simple shear. Fabric asymmetries reveal reverse (high-angle thrust) motion along these SE-dipping mylonite zones with northwest tectonic transport. Prograde mineral growth lineations parallel fold axes in zones of shear folding and suggest mineral growth (middle-amphibolite facies metamorphism) concurrent with deformation.

This study documents the earliest stage of deformation in the Cherry Creek metamorphic suite during the 2.7 Ga middle-amphibolite facies metamorphism, and has important implications for the crustal development of the northwestern Wyoming province. The deformation is characterized by imbricate thrust stacking and shortening of the Cherry Creek metamorphic suite, and is analogous to thin-skinned thrusting traditionally recognized in many post-Archean convergent belts. This would suggest that this type of tectonic process was also operative in the Archean.

Acknowledgements

This research was supported by a grant from Chevron Oil Company. The authors wish to thank Gregg Campbell, Ana Vargo and James Rogers for a helpful reviews of an early draft of the manuscript.

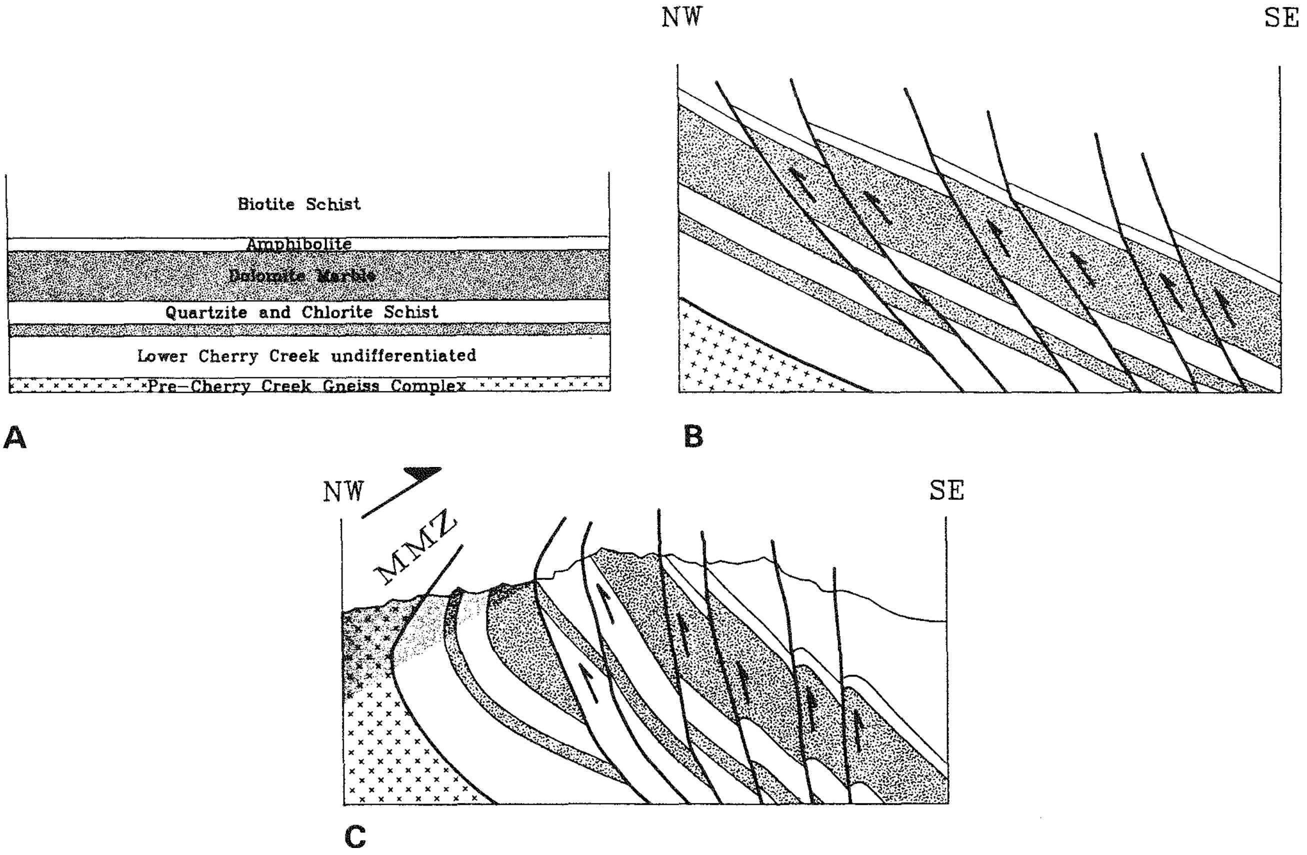
NW
SE
Biotite Schist
Amphibolite
Dolomite Marble
Quartzite and Chlorite Schist
Lower Cherry Creek undifferentiated
Pre-Cherry Creek Gneiss Complex
A
B
NW
MMZ
SE
C

Figure 8—Sequential deformation model. (A), original stratigraphic sequence of the Cherry Creek metamorphic suite; (B), Archean (2.7 Ga) thrusting synkinematic with middle-amphibolite facies metamorphism, showing thrust vergence toward the northwest; (C), Proterozoic thrusting (1.9 Ga) of opposite shear sense along the Madison mylonite zone and associated epidote-amphibolite facies metamorphism.

References

Boyer, S. E., and Elliott, D., 1982, Thrust systems: American Association of Petroleum Geologists Bulletin, v. 66, p. 1196-1230.

Condie, K. C., 1982, Plate-tectonic model for Proterozoic continental accretion in the southwestern United States: Geology, v. 10, p. 37-42.

Elliott, D., and Johnson, M. R. W., 1980, Structural Evolution in the northwestern part of the Moine thrustbelt, northwestern Scotland: Transactions of the Royal Society of Edinborough, v. 71, p. 69-96.

Erslev, E. A., 1983, Pre-Beltian geology of the southern Madison Range, southwestern Montana, Montana Bureau of Mines and Geology Memoir 55, 26 p.

______ 1986, Basement balancing of Rocky Mountain foreland uplifts: Geology, v. 14, p. 259-262.

______ 1988, Normalized center-to-center strain analysis of packed aggregates: Journal of Structural Geology *(in press)*.

Fry, W., 1979, Random point distributions and strain measurement in rocks: Tectonophysics, v. 60, p. 89-105.

Gibbs, A. K., Montgomery, C. W., O'Day, P., and Erslev, E. A., 1986, The Archean-Proterozoic transition: Evidence from the geochemistry of the metasedimentary rocks of Guyana and Montana: Geochimica et Cosmochimica Acta, v. 50, p. 2151-2141.

Giletti, B. J., 1966, Isotopic ages from southwestern Montana: Journal of Geophysical Research, v. 71, p. 4029-4036.

Heinrich, E. W., and Rabbitt, J. C., 1960, Pre-Beltian geology of the Cherry Creek and Ruby Mountain areas, southwestern Montana: Montana Bureau of Mines and Geology Memoir 38, 48 p.

Karlstrom, K. E., and Houston, R. S., 1984, The Cheyenne belt: Analysis of a Proterozoic suture in southern Wyoming: Precambrian Research, v. 25, p. 415-446.

Korsch, R. J., Lindsay, J. F., O'Brien, P. E., Sexton, M. J., and Wake-Dyster, K. D., 1986, Deep crustal seismic reflection profiling, New England orogen, eastern Australia: Telescoping of the crust and a hidden, deep, layered sedimentary sequence: Geology, v. 14, p. 982-985.

Mackin, J. H., 1950, The down-structure method of viewing geologic maps: Journal of Geology, v. 58, p. 55-72.

Ramsay, J. G., 1967, Folding and fracturing of rocks: McGraw-Hill, New York, 568 p.

Simpson, C., and Schmid, S. M., 1983, An evaluation of criteria to deduce the sense of movement in sheared rocks: Geological Society of America Bulletin, v. 94, p. 1281-1288.

Schmidt, C. J., and Garihan, J. M., 1983, Laramide tectonic development of the Rocky Mountain foreland of southwest Montana, *in* Rocky Mountain Foreland Basins and Uplifts, J. D. Lowell *(ed.)*: Rocky Mountain Assocation of Geologists Symposium, p. 271-294.

Suppe, J., 1983, Geometry and kinematics of fault-bend folding: American Journal of Science, v. 283, p. 648-721.

Taylor, S. R., and McLennan, S. M., 1985, The continental crust: Its composition and evolution: Blackwell Scientific Publications, Boston, 312 p.

Witkind, I. J., 1972, Geologic map of the Henrys Lake Quadrangle, Idaho and Montana, U.S. Geological Survey Map I-781-A. Scale 1:62,500.

Woodward, N. B., Boyer, S. E., and Suppe, J., 1985, An outline of balanced cross sections: University of Tennessee Studies in Geology No. 11, *(2nd ed.)*, Knoxville, 170 p.

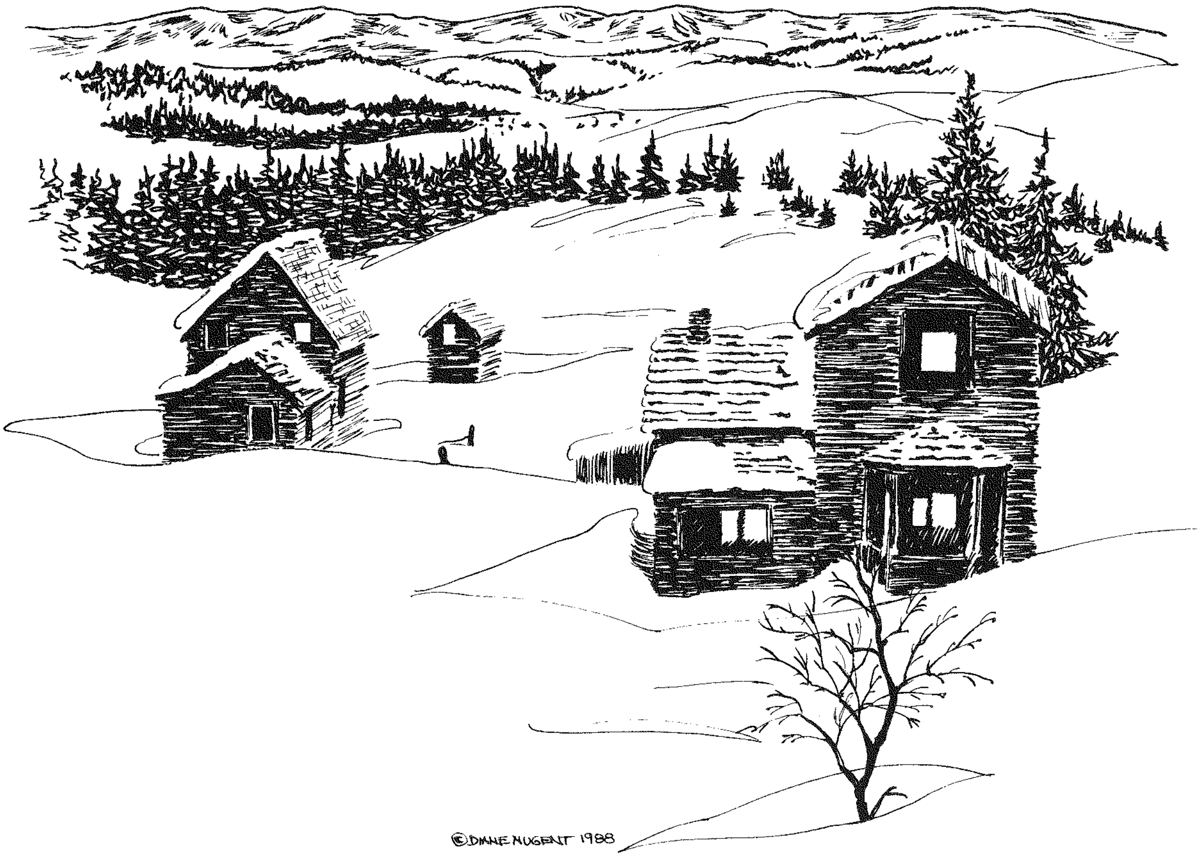

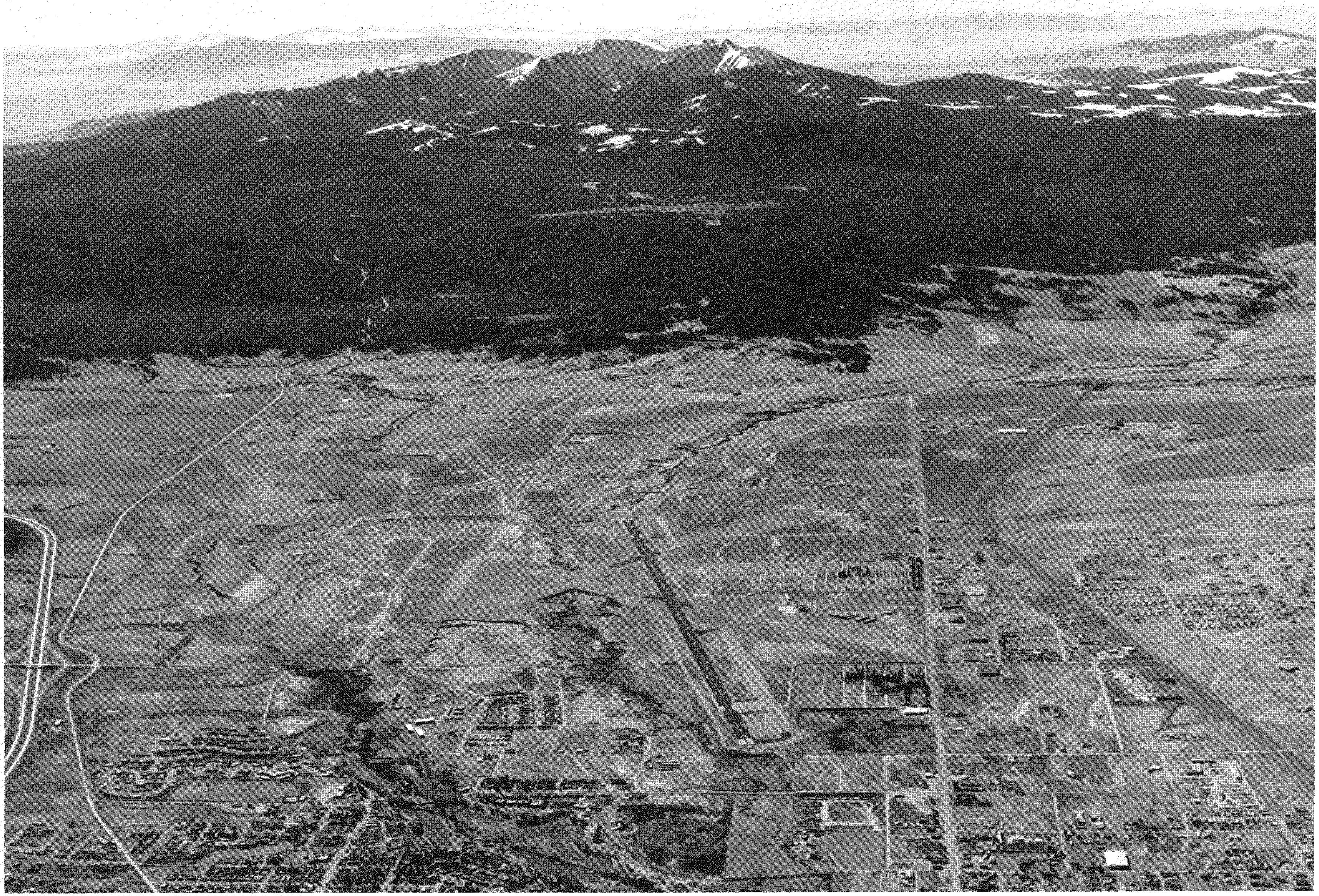

Highland Mountains overlooking southern city limits of Butte, Montana. (Hugh Dresser photo.)

AN EARLY PROTEROZOIC GNEISS DOME IN THE HIGHLAND MOUNTAINS, SOUTHWESTERN MONTANA

J. Michael O'Neill
U.S. Geological Survey
Denver, Colorado 80225

Mack S. Duncan
127 Woodcrest Court
Macon, Georgia 31210
and
Robert E. Zartman
U.S. Geological Survey
Denver, Colorado 80225

Introduction

The southern part of the Highland Mountains contains the largest of the northwesternmost exposures of crystalline basement rocks in southwestern Montana (**Figure 1**). The cratonic rocks of this region, a part of the Archean Wyoming province, consist of a multilithologic assemblage of metasedimentary, mixed metavolcanic and metasedimentary, and quartzofeldspathic and granitic lithologies. Abundant exposures of dolomitic marble, quartzite, pelitic schist, and aluminous gneiss and schist are the main components of the metasedimentary sequence (James and Weir, 1972; Vitaliano and others, 1979; Hadley, 1969). Thick successions of migmatitic biotite- and hornblende-rich gneiss probably represent interlayered metasedimentary and metavolcanic rocks (Garihan, 1979; Karasevich and others, 1981). In addition to these well-layered sequences, thick, complexly deformed quartzofeldspathic gneiss that includes pods of younger granite (Heinrich, 1960; James and Hedge, 1980; Karasevich and others, 1981) occupy large parts of some southwest Montana ranges. The crystalline basement rocks of the Ruby Range, southeast of the Highland Mountains, are well studied and described. In this range, an interpretative stratigraphic succession places the hornblende- and biotite-rich gneiss at the base, overlain by quartzofeldspathic and granitic gneiss, which in turn, is capped by the metasedimentary sequence (Karasevich and others, 1981; H. L. James, written communication, 1987).

The age of most cratonic core rocks exposed in southwestern Montana is Archean; a minimum Rb-Sr age of about 2.7 Ga was established for rocks in the Tobacco Root and Ruby ranges by Mueller and Cordua (1976) and James and Hedge (1981). Other crystalline basement rocks exposed in the northwestern part of the Beartooth Mountains yield an Pb-Pb age in excess of 3 Ga (Reid and others, 1975). Studies of metamorphic rocks in most of these ranges suggest that the amphibolite-grade metamorphism that pervades these Archean rocks is superimposed on an even higher-grade metamorphic event (Reid, 1957; Vitaliano and others, 1979; Erslev, 1980). Based mainly on Rb-Sr ages of biotite, all of the Archean rocks were later affected by an Early Proterozoic thermal event, about 1.6-1.8 Ga (Giletti, 1966). In addition to evidence that most of the basement rocks of the region are Archean in age, crystalline rocks of limited exposure in the Pioneer Mountains, west of the Highland Mountains, have yielded a Rb-Sr whole rock age of 1.7-1.8 Ga (Arth and others, 1986). A preliminary U-Pb zircon geochronologic study of the crystalline basement rocks of the Highland Mountains document a major 1.8 Ga penetrative metamorphic event. The primary age of these rocks is less well constrained, but apparently they are at least as old as those of the adjacent Tobacco Root and Ruby ranges.

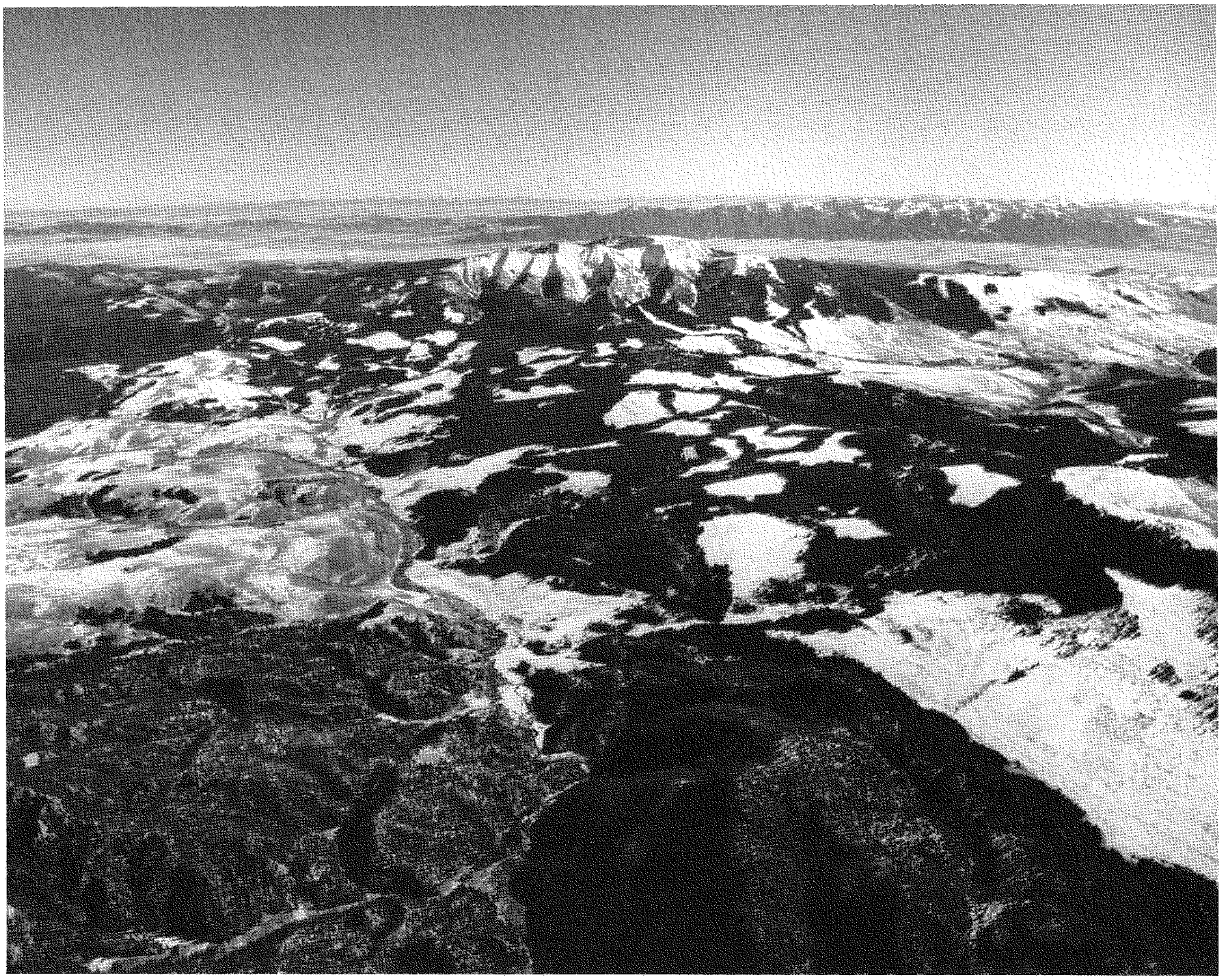

Figure 1—Eastward view of the Highland Mountains, with Tobacco Root Mountains visible on right horizon. The drainage line of Moose Creek runs diagonally (from top to bottom) across left center of the scene. (Hugh Dresser photo.)

Precambrian metamorphic and igneous rocks

Precambrian amphibolite-grade, regionally metamorphosed rocks are the oldest lithologic units exposed in the southern Highland Mountains (Duncan, 1976, Ruppel and others, 1983; (**Figure 2**). These layered metamorphic rocks define a large, doubly plunging antiform that trends northeast to east and is herein referred to as the Highland Mountain dome (equivalent to the Rochester antiform of Duncan, 1976). The gneisses and related rocks that comprise the dome (**Figure 2**) consist principally of three major rock types. Massive to well-foliated quartzofeldspathic gneiss of unknown thickness is restricted to the central part of the dome and is overlain by 0-100 meters of garnetiferous gneiss, which in turn is capped by more than 3 kilometers of biotite gneiss. The quartzofeldspathic gneiss and biotite gneiss compose over 90 per cent of the exposed rocks. Also present in the area are igneous rocks of Precambrian age that consist of metabasite dikes and sills, aplite and granitic pegmatite sills and minor dikes and, youngest of all, diabase dikes.

Metamorphic rocks

Quartzofeldspathic gneiss exposed in the Highland Mountain dome can be divided into two major types: (1) massive leucocratic gneiss exposed in the core of the dome, and (2) the overlying, well-foliated quartz-feldspar-biotite gneiss.

Leucocratic gneiss

The leucocratic gneiss is structurally the lowest unit and is well exposed in the central parts of the dome. The dominant rock type consists of massive,

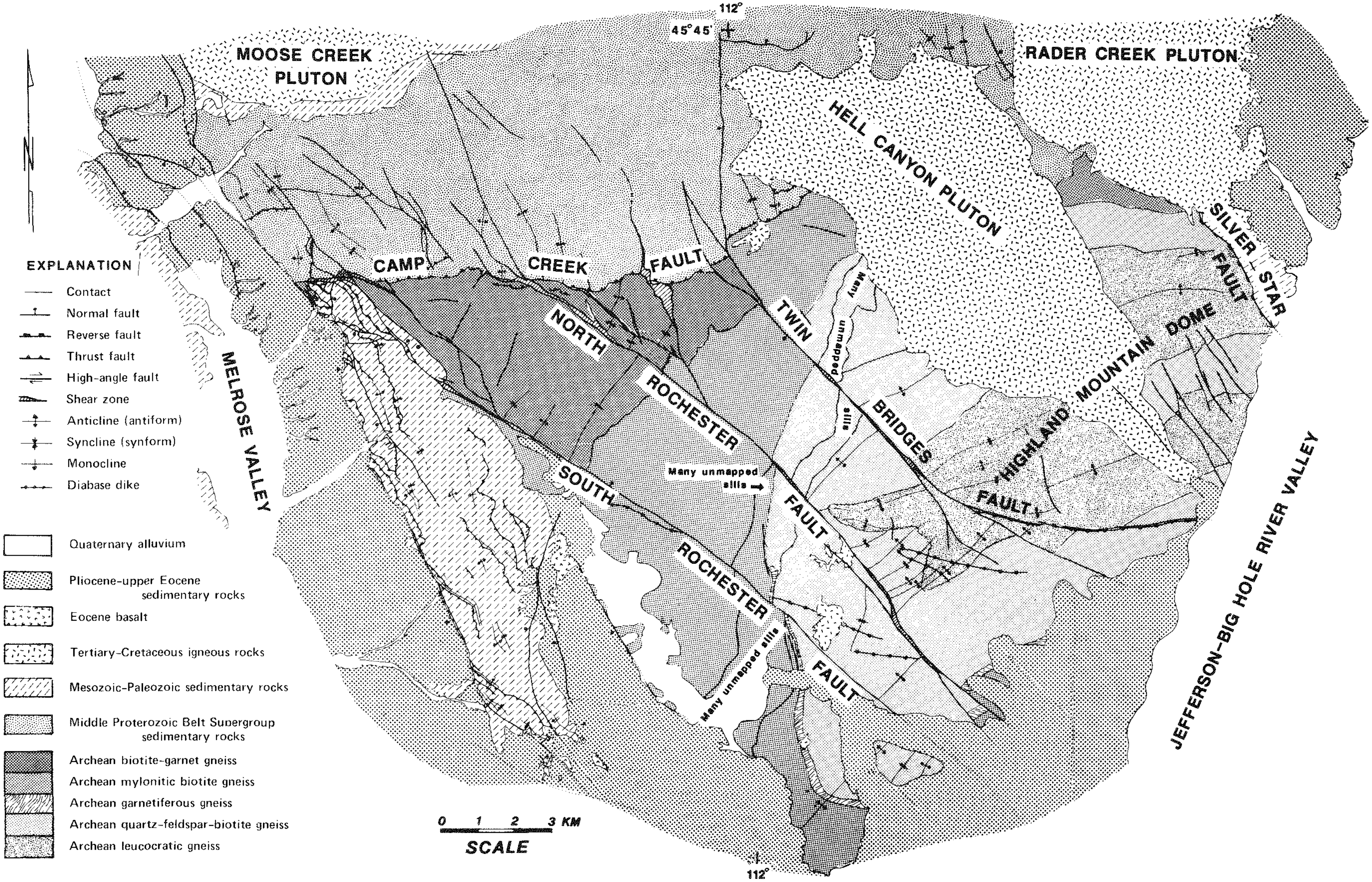
112°
45°45'
MOOSE CREEK PLUTON
RADER CREEK PLUTON
HELL CANYON PLUTON
CAMP CREEK FAULT
NORTH ROCHESTER FAULT
SOUTH ROCHESTER FAULT
TWIN BRIDGES FAULT
HIGHLAND MOUNTAIN DOME
SILVER STAR FAULT
MELROSE VALLEY
JEFFERSON-BIG HOLE RIVER VALLEY
Many unmapped sills
Many unmapped sills →
Many unmapped sills
N
EXPLANATION
Contact
Normal fault
Reverse fault
Thrust fault
High-angle fault
Shear zone
Anticline (antiform)
Syncline (synform)
Monocline
Diabase dike
Quaternary alluvium
Pliocene-upper Eocene sedimentary rocks
Eocene basalt
Tertiary-Cretaceous igneous rocks
Mesozoic-Paleozoic sedimentary rocks
Middle Proterozoic Belt Supergroup sedimentary rocks
Archean biotite-garnet gneiss
Archean mylonitic biotite gneiss
Archean garnetiferous gneiss
Archean quartz-feldspar-biotite gneiss
Archean leucocratic gneiss
0 1 2 3 KM
SCALE
112°

Figure 2—Generalized geologic map of southern part of the Highland Mountains. Most Tertiary sedimentary rocks of Pliocene to Eocene age are capped by thin gravels of Quaternary age.

strongly deformed and lineated quartz-feldspar gneiss that contains only sparse biotite or muscovite. The rock mainly is equigranular, but commonly contains augen of potassium feldspar 1-3 centimeters in diameter. The gneiss is strongly migmatized; quartz and feldspar contribute much to the leucocratic character of the rock.

In the field, many variations of ideal leucocratic gneiss are present. Commonly, sugary-textured leucogneiss grades into very strongly contorted and folded, augen-bearing leucogneiss that is strongly lineated and displays an overall planar foliation that is locally deformed into low amplitude folds. In other places, quartz-feldspar-biotite and amphibolitic gneiss is strongly injected by augen-bearing leucogranitic gneiss displaying well-developed mylonitic texture. Locally, leucogranite encloses chaotically invaded lenses of amphibolite that were boudinaged, brecciated, magmatically injected and recrystallized.

Quartz-feldspar-biotite gneiss

Quartz-feldspar-biotite gneiss is in gradational contact with the underlying leucocratic gneiss. The gneiss is fine- to medium-grained and displays a distinct, platy foliation defined by a regular alternation of leucocratic and biotite-bearing layers. The gneiss locally grades into seams of finely layered mylonitic leucogneiss or into graphic granite sills. The contact with the underlying leucogneiss is difficult to define. The well-layered quartz-feldspar-biotite gneiss grades downward into increasingly migmatitic, less platy, augen-bearing, biotite-poor leucogneiss over an interval of several tens of meters or more. The contact is placed where the well-defined platy character of the gneiss gives way to more massive, strongly lineated, biotite-poor gneiss. The contact is approximate because of the absence of marker beds or gross lithologic changes. One of the most difficult areas in which to map this contact is near Silver Star, where migmatitic injection into the overlying quartz-feldspar-biotite gneiss is very common.

Garnetiferous gneiss

The garnetiferous gneiss is an extremely diverse, garnet-rich unit that, for the most part, separates the underlying quartz-feldspar-biotite gneiss from biotite gneiss. The unit consists of quartzofeldspathic and biotite gneiss similar to the underlying and overlying rocks, but also includes amphibolite, quartz-plagioclase-garnet gneiss, anthophyllite-garnet gneiss, magnetite gneiss and marble. Foliation is well developed in most rock types and is parallel to individual lithologic contacts.

Biotite gneiss

Biotite-rich gneiss, the structurally highest metamorphic sequence exposed in the Highland Mountains, is divided into two mappable units—a lower mylonitic biotite gneiss, and an upper biotite-garnet gneiss. The biotite gneiss is medium- to coarse-grained, is composed of essential biotite, quartz and plagioclase, and contains conspicuous porphyroblasts of plagioclase and garnet. Biotite-garnet gneiss, characterized by bold outcrops of generally strongly folded and contorted rock, is coarsest where it is injected by numerous thin, quartz-feldspar sills up to 4 centimeters thick. Plagioclase porphyroblasts, 0.5-2 centimeters across, are ubiquitous in the biotite-garnet gneiss. Plagioclase porphyroclasts are typical of the mylonitic biotite gneiss; these crystals are anhedral and broken, or may be sheared and drawn out in the plane of foliation, or may occur as augen. Quartz commonly occurs as long, relatively thin ribbons 2-3 centimeters in length, separated by thin seams rich in biotite. The mylonitic gneiss locally contains abundant, tectonically distended fragments of amphibolite up to 1 meter across. Strong shearing in these mylonitic rocks has resulted in an extremely planar, nonfolded fabric that, in addition to texture, serves to distinguish it from the overlying, more massive and contorted, biotite-garnet gneiss. The contact between these two varieties of biotite gneiss is gradational over several hundred meters.

Amphibolite

Well-layered amphibolite, present in all major rock units of the southern Highland Mountains, occurs as concordant lenses 0.5-3 meters in thickness and generally less than 100 meters in length. Composition of amphibolite is variable; all rocks carry essential hornblende and plagioclase and may include garnet, quartz, cummingtonite and biotite.

Igneous rocks

Aplite and pegmatite

Granitic aplite to pegmatite occurs as sills and minor dikes in well-foliated gneisses that cap the core of the Highland Mountain dome; these rocks are absent from the more massive leucocratic core rocks. Most of these rocks are medium- to coarse-grained quartz monzonite, and most are present as a major swarm of sills along the northwestern edge of the dome (**Figure 2**). This intrusive swarm of sills can be divided into two zones: Massive, non-layered granitic aplite and pegmatite sills occur structurally above a zone of non-layered quartz monzonite to well-foliated, leucocratic augen gneiss and finely laminated leucocratic sills. In the upper zone, sills converge and diverge, are interconnected by short, near vertical dikes, and commonly contain small rafts or xenoliths of host mylonitic biotite gneiss. Aplitic sills less than 3 meters thick are non-foliated, fine- to medium-grained, inequigranular, and weakly porphyritic. Sills thicker than 3 meters have coarse-grained pegmatitic cores that may contain crystal aggregates of potassium feldspar and/or quartz greater than 1 meter across.

In the lower zone, many of these felsic intrusive rocks appear to be smeared out in the plane of foliation. Here the felsic rocks are composed of quartz ribbons, potassium feldspar augen, and very minor muscovite and biotite. Locally these rocks grade into graphic granite sills. In one locality, a vertical granite pegmatite dike is associated with thin stringers of mylonitic and augen gneiss 0.2-1 meter in thickness that have been injected into the wall rock. Upwards, the dike thins and the branches of leucocratic sills increase in number, thickness and length, culminating in a sill of mylonitic and augen gneiss where the dike pinches out.

Metabasite

Metabasite occurs as weakly foliated, dark-brown to black dikes and sills that range in thickness from less than 1 meter to 10-15 meters. All metabasites contain essential hornblende, garnet, augite and plagioclase. The metabasite occurs solely as dikes in the leucocratic core rocks of the Highland Mountain dome. The dikes are subvertical and branch and split into multiple, subparallel dikes at the highest structural levels in the core rocks. Where these dikes encounter well-foliated quartz-feldspar-biotite gneiss that overlies the leucocratic core of the dome, they occur as sills or concordant, irregularly shaped pods that pinch and swell along strike, locally creating a very sinuous outcrop pattern where the rock was complexly injected into the foliated gneiss.

Diabase

Diabase in the southern Highland Mountains occurs as subvertical, 3 to 100 m-thick, NW-W-trending dikes. In many places the intrusion of these dikes is structurally controlled by major NW-trending faults that cut obliquely across the range (O'Neill and others, 1986). The mineral assemblage in all diabase dikes consists of plagioclase, augite, opaque oxide and minor hornblende. Similar dikes mapped and described from the Tobacco Root Mountains to the east have been dated at 1.1 and 1.4 Ga (Wooden and others, 1979).

Geochronology

Samples of leucocratic gneiss from the core of the Highland Mountain dome and of mylonitic biotite gneiss from the northwest flank of the dome were collected for U-Pb zircon age determination. Both rock types contain two distinct populations of zircon: (1) gray to brown, subhedral to anhedral grains, which appear to predate the final metamorphism and deformation of the rock, and (2) pink to red, euhedral grains, whose external morphology suggests growth during metamorphism. Preliminary analysis of the pink, euhedral population in conjunction with analyses of similar zircons collected from gneisses exposed in the Armstead anticline and the Tendoy Mountains (southeast of the Highland Mountains) reveal a complex isotopic pattern on a concordia diagram. These data suggest metamorphic growth of zircon at about 1.8 Ga, in part nucleating upon cores of an older generation of crystals. These data suggest that the quartzofeldspathic gneisses of the Highland Mountains are at least as old as the 2.7 Ga crystalline basement rocks of the adjacent Tobacco Root and Ruby ranges; however, subsequent Early Proterozoic penetrative deformation associated with the development of the Highland Mountain dome has thoroughly recrystallized the rocks, and now gives them a structural attribute quite different from the Archean rocks immediately to the east.

Structural geology

Structural setting

The elongate domal feature defined in the crystalline rocks of the southern Highland Mountains is exposed in the northern part of the Laramide-age Highland uplift. The dome is truncated on the east by Tertiary-Quaternary basin-bounding faults (Ruppel and others, 1983; Hanneman and O'Neill, 1986) and covered on the east and south by Tertiary and Quaternary sedimentary deposits. On the northeast, the nose of the dome is cut by the NW-trending, Laramide-age, Silver Star fault that marks the partly exposed edge of the Cretaceous Highland uplift. On the north, metasedimentary rocks of the Middle Proterozoic Belt Supergroup overlie basement rocks along the N-dipping Camp Creek fault of small displacement that cuts obliquely across the dome **(Figure 1)**. Nevertheless, the domal architecture of the basement rocks is largely intact; the distinctive garnetiferous and mylonitic gneiss that mantle the dome can be traced about 40 percent of the way around the structure. The most informative exposures are present on the northwest side of the dome, where one can traverse across the core into overlying mylonitic and strongly folded biotite gneiss.

Macroscopic structure

The dominant structural aspects of the crystalline basement rocks of the Highland Mountains are threefold: (1) an elongate dome on the southeast, (2) an adjacent synform on the northwest, and (3) an intervening zone of mylonitic gneiss **(Figure 2)**. The antiform or elongate dome is slightly asymmetric, arcuate in plan, trends northeast in the south, and curving to a more easterly trend in the north. The dip of the foliation on the northwest flank of the dome rarely exceeds 30 degrees, whereas the foliation on the southeast side is variable, ranging from 35 degrees to nearly vertical. The metamorphic core of the dome is characterized by leucocratic, augen-bearing gneiss whose general attitude conforms to the overall antiformal aspect of the feature. The antiformal architecture of the structure is doubly plunging. The axial plunge reverses south of the Hell Canyon pluton **(Figure 2)**. To the south, the axial core is split by a complexly folded, medial synform separating antiforms exposing core rocks along their axes. These folds plunge gently to the southwest beneath the overlying quartz-feldspar-biotite gneiss; core rocks are not exposed south of the North Rochester fault. On the north, the core rocks inclose a major, infolded slice of multilithologic strata of the overlying quartz-feldspar-biotite gneiss. Core rocks are overlain by quartz-feldspar-biotite gneiss and mylonitic biotite gneiss that outline the elongate domal shape of the structure.

The elongate dome is bounded on the northwest by a NE-trending, 3 km-thick succession of mylonitic biotite gneiss that is strongly injected by sills of aplite, pegmatite, and finely layered to augen-bearing leucocratic orthogneiss in its lower part. The mylonitic biotite gneiss is overlain by biotite-garnet gneiss that defines a major NE-trending synform. Dips of foliation on the limbs of the synform are relatively shallow, rarely exceeding 30 degrees; the fold plunges gently southwest. The trace of the axial surface of the fold lies directly west of the mylonitic gneiss-biotite-garnet gneiss contact; however, the underlying mylonitic gneiss does not reemerge on the opposite side of the synform, as it should if these lithologies were part of a pre-existing layered sequence. Rather, the mylonitic gneiss must (1) extend beneath the synform, and (2) represent a major NW-dipping, planar zone of shear that formed in conjunction with the macroscopic folding event. Asymmetric folds, rotated augen, and extension fractures in the mylonitic and underlying quartz-feldspar-biotite gneiss on the northwest limb of the dome indicate that these rocks were transported northwestward (down dip) relative to the underlying rocks.

Mesoscopic structure

Outcrop-scale folds are present in all gneisses throughout the Highland Mountains. Similar folds are a main characteristic of the core rocks and concentric folds are most common in rocks that lie above the core of the dome. Folds in the leucocratic gneiss are typically disharmonic, similar, intrafolial and isoclival. They are locally rootless, commonly sheared and drawn out in the plane of the foliation. This axial planar foliation may be very strongly contorted, and locally merges with and becomes tangential to subvertical shear zones in the gneiss.

Similar folds are also present in the quartz-feldspar-biotite gneiss that overlies the leucocratic core rocks. Here also, the foliation is axial planar, but the fold limbs are less commonly sheared out and instead define asymmetric isoclines. Associated with these isoclines are small, asymmetric folds that are clearly younger and that fold the axial planar foliation. The orientation of the fold axes of the intrafolial folds and of the non-intrafolial, asymmetric folds, are colinear. They are parallel to the axis of the dome proper, even though one fold set is obviously older than the other. In the majority of outcrops examined, folds verge down dip, regardless of which side of the dome they are located.

Concentric folds are best developed in all of the rocks overlying the leucocratic core of the dome. Wave length ranges from 20 centimeters to near 50 meters. Foliation is folded around the axial planes of these folds, but no evidence was found of a cleavage subparallel to these axial planes.

Planar and linear tectonite fabric elements are observed in hand samples. The overall schistosity and foliation in rocks that overlie the leucocratic core rocks is probably parallel to the pre-metamorphic layering. This is best expressed by the regular, geometric encirclement and conformity in attitude of the garnetiferous gneiss to the main plan of the dome. However, intrafolial folds are common and foliation in many exposures appears to be axial planar. Lineations are common in all rocks and are delineated by mesoscopic fold axes, by elongate laths of micaceous minerals, by parallel alignment of individual micaceous and prismatic minerals, and by the boudins axes. Mylonitic gneiss is well developed and common in rocks that directly overlie the leucocratic core of the dome. Mylonite and boudinage is best developed in only the lower part of the biotite gneiss that directly overlies the quartz-feldspar-biotite gneiss.

Conclusions

The major structures of the crystalline rocks of the Highland Mountains are, from southeast to northwest: (1) a dome cored with quartzofeldspathic gneiss, (2) an overlying, strongly sheared and mylonitic interval of biotite gniess, more than 3 kilometers thick that contains conspicuous sills of aplite to pegmatite and leucocratic mylonitic orthogneiss in its lower part, and (3) a structurally higher synform composed of coarsely cystalline, strongly folded biotite-garnet gneiss. Minor structures in these rocks, from small-scale folds to fabric elements, indicate that all rocks were affected by the doming event; there does not appear to have been a non-mobile, rigid infrastructure upon which the metamorphic tectonites rest, nor does there appear to be preserved in the Highlands a non-metamorphosed carapace that was distended by brittle fracture during denudation. Mesoscopic folds and rotated augen in the gneisses overlying the core of the dome almost always show down-dip tectonic transport, regardless of which side of the dome they are located.

The Highland Mountain dome apparently formed by: (1) differential vertical rise of a mobile leucocratic core, (2) penetrative metamorphism of the mantling rocks and injection into these rocks of quartz monzonite sills and orthogneisses, and (3) extension and down-dip shearing of the overlying mylonitic gneiss off of the hinge zone. The dome is interpreted to be a gneiss dome similar to those described from orogenic zones elsewhere in the world. The dome may be a reflection of a major NE-trending Precambrian orogenic zone that crosses western Montana, as postulated by O'Neill and Lopez (1985).

References

Arth, J. G., Zen, E., Sellers, G., and Hammerstrom, J., 1986, High initial Sr isotopic ratios and evidence for magma mixing in the Pioneer batholith of southwest Montana: Journal of Geology, v. 94, p. 419-430.

Erslev, E. A., 1980, Geology of the Precambrian metamorphic rocks of the southern Madison Range, southwestern Montana: Geological Society of America Abstracts with Programs, v. 12, no. 6, p. 272.

Duncan, M. S., 1976, Structural analysis of the pre-Beltian metamorphic rocks of the southern Highland Mountains, Madison and Silver Bow counties, Montana [Ph.D. thesis]: Indiana University, Bloomington, 222 p.

Garihan, J. M., 1979, Geology and structure of the central Ruby Range, Madison County, Montana: Summary: Geological Society of America Bulletin, part 1, v. 90, no. 4, p. 323-326.

Garihan, J. M. and Okuma, A. F., 1974, Field evidence suggesting a non-igneous origin for the Dillon quartzo-feldspathic gneiss, Ruby Range, southwestern Montana: Geological Society of America Abstracts with Programs, v. 6, p. 510.

Giletti, B. J., 1966, Isotopic ages from southwestern Montana: Journal of Geophysical Research, v. 71, p. 4029-4036.

Hadley, J. B., 1969, Geologic map of the Cameron quadrangle, Madison County, Montana: U.S. Geological Survey Geologic Quadrangle Map GQ-813. Scale 1:62,500.

Hanneman, D. L., and O'Neill, J. M., 1986, Late Tertiary-Quaternary collapse of a Laramide-age foreland uplift, southwestern Montana: Geological Society of America Abstracts with Programs, v. 18, no. 5, p. 359.

Heinrich, E. W., 1960, Pre-Beltian geology of the Cherry Creek and Ruby Mountains areas, southwestern Montana, part 2, Geology of the Ruby Mountains: Montana Bureau of Mines and Geology Memoir 38, p. 1-14.

James, H. L., and Weir, K. L., 1972, Geologic map of the Carter Creek iron deposit: U.S. Geological Survey Miscellaneous Field Studies Map MF-359. Scale 1:3,000.

James, H. L., and Hedge, C. E., 1980, Age of the basement rocks of southwest Montana: Geological Society of America Bulletin, part 1, v. 91, p. 11-15.

Karasevich, L. P., Garihan, J. M., Dahl, P. S., and Okuma, A. F., 1981, Summary of Precambrian metamorphic and structural history, Ruby Range, southwest Montana, *in* Guidebook of Southwest Montana, Thomas E. Tucker *(ed.)*: Montana Geological Society p. 225-237.

Mueller, P. A., and Cordua, W. S., 1976, Rb-Sr whole-rock age of gneisses from the Horse Creek area, Tobacco Root Mountains, Montana: Isochron/West, no. 16, p. 33-36.

O'Neill, J. M., and Lopez, D. A., 1985, Character and regional significance of the Great Falls tectonic zone of east-central Idaho and west-central Montana: American Association of Petroleum Geologists Bulletin, v. 69, p. 437-447.

Reid, R. R., 1957, Bedrock geology of the north end of the Tobacco Root Mountains, Madison County, Montana: Montana Bureau of Mines and Geology Memoir 36, 27 p.

Reid, R. R., McMannis, W. J., and Palmquist, J. C., 1975, Precambrian geology of the North Snowy block, Beartooth Mountains, Montana: Geological Society of America Special Paper 157, 135 p.

Ruppel, E. T., O'Neill, J. M., and Lopez, D. A., 1983, Preliminary geologic map of the Dillon 1° x 2° quadrangle, Montana: U.S. Geological Survey Open-File Report 83-168. Scale 1:250,000.

Vitaliano, C. J., Cordua, W. S., Burger, H. R., Hanley, T. B., Hess, D. F., and Root, F. K., 1979, Geology and structure of the southern part of the Tobacco Root Mountains, southwestern Montana: Map summary: Geological Society of America Bulletin, part. 1, v. 90, no. 8, p. 712-715.

Wooden, J. L., Vitaliano, C. J., Koehler, S. W., and Ragland, P. C., 1978, The late Precambrian mafic dikes in the southern Tobacco Root Mountains, Montana: Geochemistry, Rb-Sr geochronology, and relationship to Belt tectonics: Canadian Journal of Earth Sciences, v. 15, p. 467-479.

© DIANE NUGENT 1988

SEDIMENTATION AND TECTONIC SETTING OF THE MIDDLE PROTEROZOIC LAHOOD FORMATION, BELT SUPERGROUP, SOUTHWESTERN MONTANA

James G. Schmitt
Department of Earth Sciences
Montana State University
Bozeman, Montana 59717

Introduction

The LaHood Formation of the Middle Proterozoic Belt Supergroup is a thick (3500 m) wedge of arkosic conglomerate, arkose and interbedded arkose, argillite and limestone which crops out along the southern margin of the Belt basin in southwestern Montana (**Figure 1**). LaHood Formation outcrops are contained in an area 130 kilometers long by 15 kilometers wide extending from the Highland Mountains eastward to the Bridger Range (**Figure 2**).

Strata belonging to the LaHood Formation were originally defined as the North Boulder River Group by Ross (1949) for exposures along the Boulder River just north of Cardwell, Montana. Alexander (1955) later proposed that the name LaHood Formation be assigned to this sequence of strata for exposures in a drainage 1 kilometer east of LaHood Park in Jefferson Canyon (**Figure 2**). McMannis (1963) redefined the LaHood and established a reference section 9.6

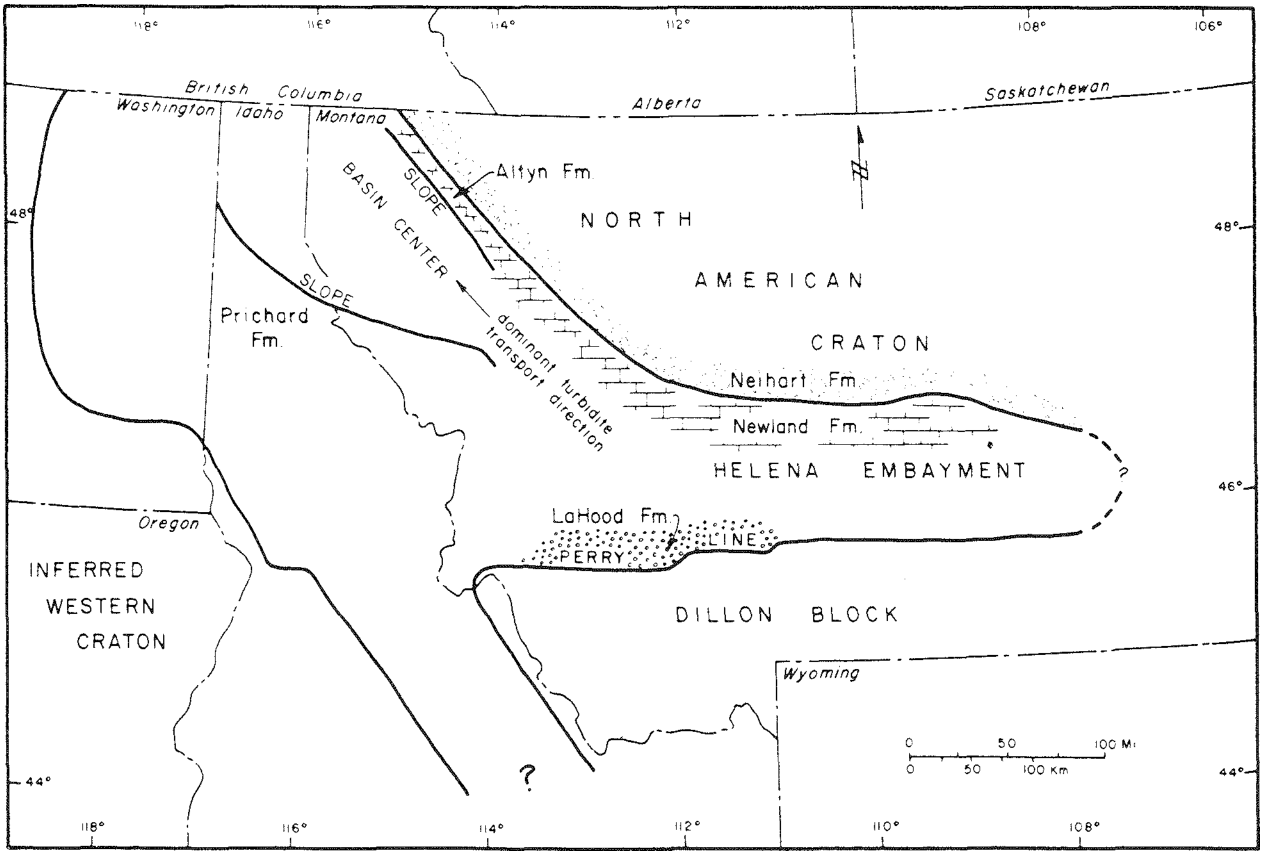
118°
116°
114°
112°
108°
106°
British Columbia
Alberta
Saskatchewan
Washington
Idaho
Montana
Altyn Fm.
NORTH
AMERICAN
CRATON
BASIN CENTER
SLOPE
SLOPE
Prichard Fm.
dominant turbidite transport direction
Neihart Fm.
Newland Fm.
HELENA EMBAYMENT
LaHood Fm.
PERRY LINE
DILLON BLOCK
INFERRED WESTERN CRATON
Oregon
Wyoming
48°
46°
44°
0 50 100 Mi
0 50 100 Km
?
118°
116°
114°
112°
110°
108°

Figure 1—Generalized facies map of the lower Belt Supergroup (*from* Winston, 1986a).

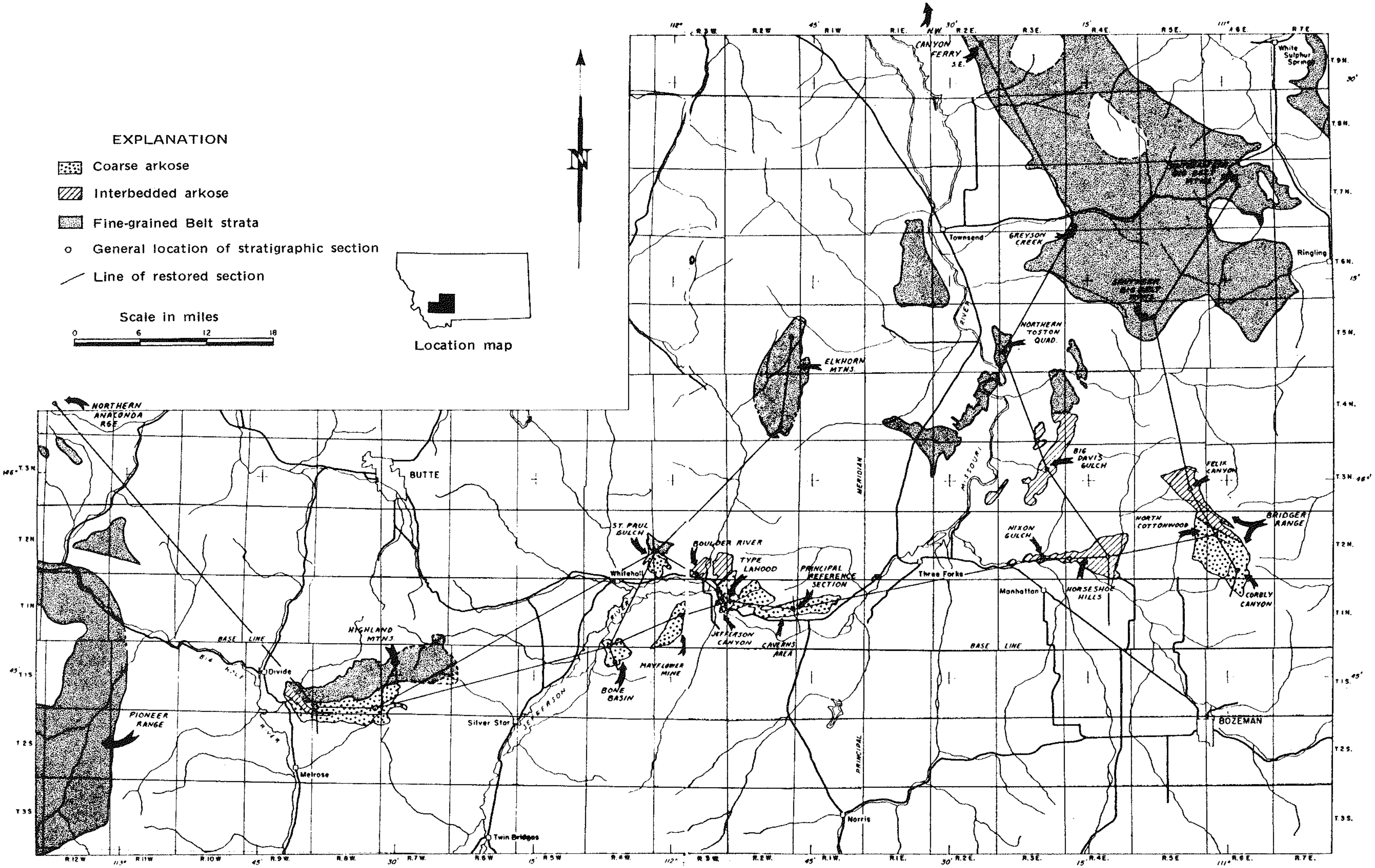
EXPLANATION
Coarse arkose
Interbedded arkose
Fine-grained Belt strata
General location of stratigraphic section
Line of restored section
Scale in miles
0
6
12
18
Location map
N
CANYON FERRY S.E.
White Sulphur Springs
Townsend
GREYSON CREEK
Ringling
NORTHERN TOSTON QUAD.
ELKHORN MTNS.
MISSOURI RIVER
BIG DAVIS GULCH
FELIX CANYON
BRIDGER RANGE
NORTH COTTONWOOD
NIXON GULCH
Three Forks
Manhattan
HORSESHOE HILLS
CORBLY CANYON
BOZEMAN
NORTHERN ANACONDA RGE.
BUTTE
ST. PAUL GULCH
Whitehall
BOULDER RIVER
TYPE LAHOOD
PRINCIPAL REFERENCE SECTION
JEFFERSON CANYON
CAVERNS AREA
MAYFLOWER MINE
BONE BASIN
HIGHLAND MTNS.
Divide
BIG HOLE RIVER
BASE LINE
PIONEER RANGE
Silver Star
JEFFERSON
Melrose
Twin Bridges
Norris
PRINCIPAL MERIDIAN
T. 9 N.
T. 8 N.
T. 7 N.
T. 6 N.
T. 5 N.
T. 4 N.
T. 3 N.
T. 2 N.
T. 1 N.
T. 1 S.
T. 2 S.
T. 3 S.
R. 12 W.
R. 11 W.
R. 10 W.
R. 9 W.
R. 8 W.
R. 7 W.
R. 6 W.
R. 5 W.
R. 4 W.
R. 3 W.
R. 2 W.
R. 1 W.
R. 1 E.
R. 2 E.
R. 3 E.
R. 4 E.
R. 5 E.
R. 6 E.
R. 7 E.
113°
112°
111°
46°
45°

Figure 2—Distribution of LaHood Formation outcrops and generalized facies distribution (*from* McMannis, 1963).

kilometers east of Alexander's (1955) type section (**Figure 2**). According to McMannis (1963, p. 409), the LaHood consists of ... *all dominantly coarse Belt strata along the southern margin of the central Montana embayment of the Belt geosyncline* [and the term applies] *arbitrarily, ... where Belt strata contain less than 75 per cent of fine-grained rocks and greater than 25 per cent of coarse arkosic debris.*

Stratigraphy

Stratigraphic relations indicate that the LaHood Formation is equivalent to the lower Belt (**Figure 3**), and that it fines abruptly to the north as it grades into the Chamberlain Shale, Newland Limestone and Greyson Shale (Winston, 1986a). The rapid northward fining of the LaHood is best exemplified by a northeast to south cross section from the Big Belt Mountains to the Bridger Range (**Figure 3**). Even within the Bridger Range, the abundance of fine-grained interbeds increases markedly toward the north with concomitant decrease in coarse-grained arkosic strata (**Figure 3**). In contrast, coarseness of the LaHood Formation along the east-west trend of the southern margin of the Belt basin is relatively uniform (**Figure 4**).

The LaHood Formation also becomes finer grained up section. Lower portions of the unit are well exposed in Jefferson Canyon and near LaHood Park (**Figure 2**) and are characterized by approximately 1,400 meters of chaotic boulder and cobble conglomerate with distinct zones of crudely bedded imbricated and aligned pebble and cobble conglomerate and some finer-grained interbeds. Contacts between conglomerate, pebbly arkose, and mudrock units are both abrupt and gradational. Conglomerate clast populations include amphibolite, gneiss, schist and marble.

The upper part of the lower LaHood Formation is exposed approximately 1 kilometer north of the Jefferson Canyon section and 1.25 kilometers south of LaHood Park along the east side of Montana Route 2, and is characterized by near-vertical beds of bouldery and pebbly arkose. This section is faulted against pre-Belt crystalline rocks and contains more silty and shaly interbeds than the Jefferson Canyon section (McMannis, 1963). To the east in Corbly Canyon in the Bridger Range, the lower LaHood Formation is also faulted against pre-Belt crystalline rocks

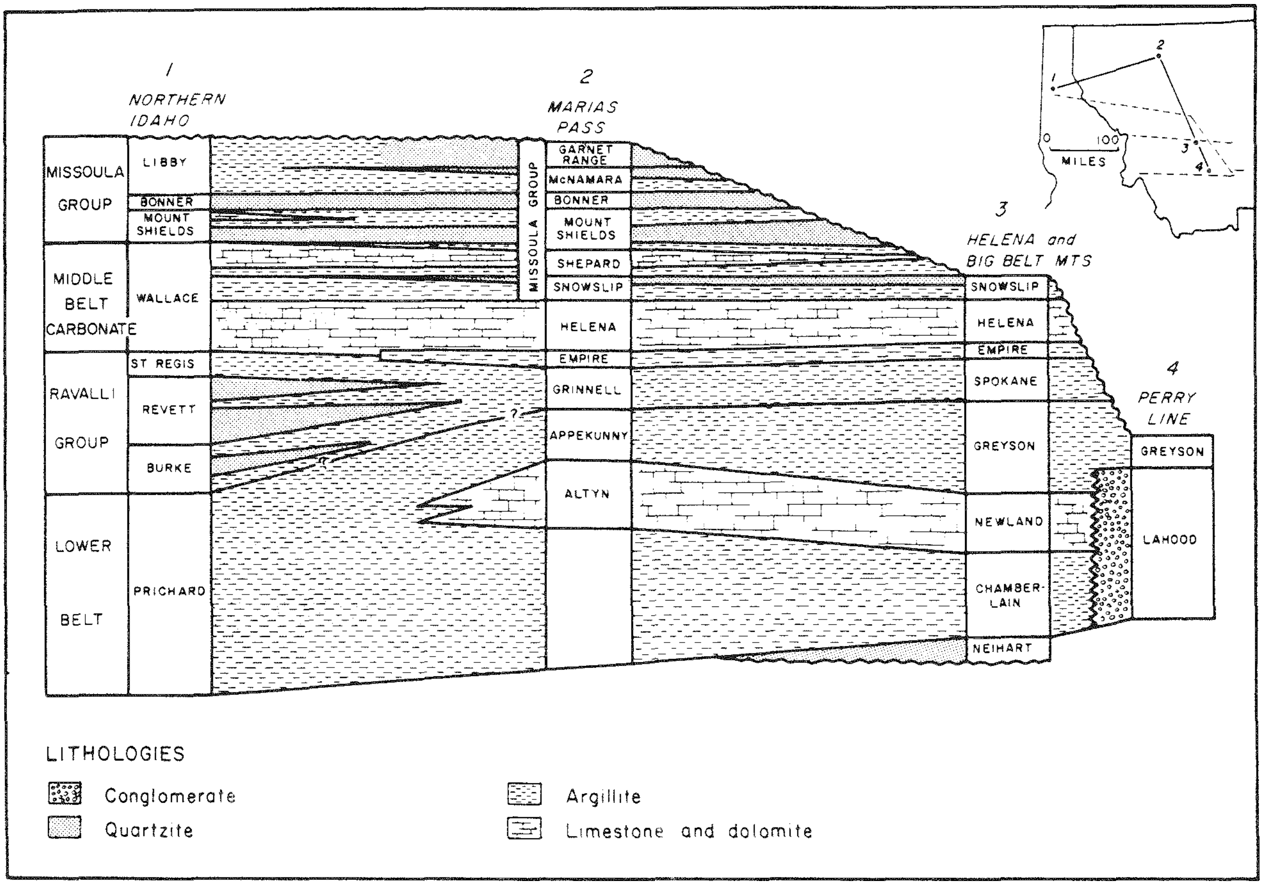
1
NORTHERN IDAHO
2
MARIAS PASS
3
HELENA and BIG BELT MTS
4
PERRY LINE
MISSOULA GROUP
MIDDLE BELT CARBONATE
RAVALLI GROUP
LOWER BELT
LIBBY
BONNER
MOUNT SHIELDS
WALLACE
ST REGIS
REVETT
BURKE
PRICHARD
MISSOULA GROUP
GARNET RANGE
McNAMARA
BONNER
MOUNT SHIELDS
SHEPARD
SNOWSLIP
HELENA
EMPIRE
GRINNELL
APPEKUNNY
ALTYN
SNOWSLIP
HELENA
EMPIRE
SPOKANE
GREYSON
NEWLAND
CHAMBERLAIN
NEIHART
GREYSON
LAHOOD
0 100 MILES
LITHOLOGIES
Conglomerate
Quartzite
Argillite
Limestone and dolomite

Figure 3—Stratigraphic section showing principal formations of the Belt Supergroup, (*from* Winston, 1986a).

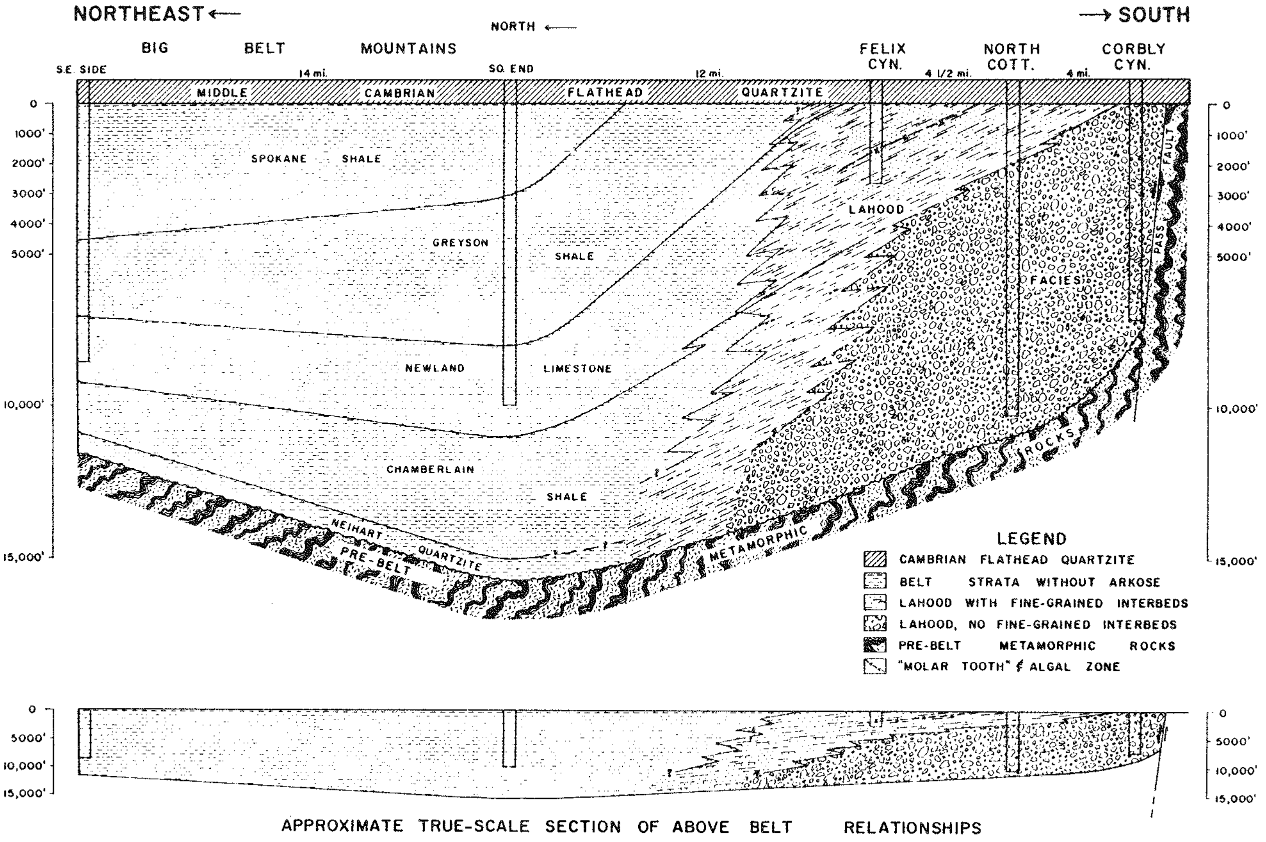
NORTHEAST←
NORTH ←
→ SOUTH
BIG BELT MOUNTAINS
S.E. SIDE
14 mi.
SO. END
12 mi.
FELIX CYN.
4 1/2 mi.
NORTH COTT.
4 mi.
CORBLY CYN.
MIDDLE CAMBRIAN FLATHEAD QUARTZITE
SPOKANE SHALE
GREYSON SHALE
NEWLAND LIMESTONE
CHAMBERLAIN SHALE
NEIHART QUARTZITE
PRE-BELT METAMORPHIC ROCKS
LAHOOD FACIES
PASS FAULT
0
1000'
2000'
3000'
4000'
5000'
10,000'
15,000'
LEGEND
CAMBRIAN FLATHEAD QUARTZITE
BELT STRATA WITHOUT ARKOSE
LAHOOD WITH FINE-GRAINED INTERBEDS
LAHOOD, NO FINE-GRAINED INTERBEDS
PRE-BELT METAMORPHIC ROCKS
"MOLAR TOOTH" ∮ ALGAL ZONE
0
5000'
10,000'
15,000'
APPROXIMATE TRUE-SCALE SECTION OF ABOVE BELT RELATIONSHIPS

Figure 4—Restored stratigraphic section showing relationships of LaHood facies from Corbly Canyon in the southern Bridger Range north to the Big Belt Mountains. See Figure 2 for location of section line, (*from* McMannis, 1963).

and contains approximately 2,500 meters of pebbly arkose with rare conglomeratic or fine-grained interbeds (**Figure 5**).

The upper portion of the LaHood Formation is well exposed northwest of LaHood Park, 2.5 kilometers north of the intersection of Montana Routes 2 and 359, where arkose is rhythmically interbedded with shale. Similar facies relations for the upper LaHood are also present in the Horseshoe Hills, northern Bridger Range, and at St. Paul Gulch (**Figure 2**), where a 100-m thick limestone interval is also present. It is thought that this limestone interval, which interfingers southward with coarser-grained arkose, is correlative with the Newland Limestone to the north (McMannis, 1963).

Deposition of the coarse-grained LaHood facies has been viewed as syntectonic by numerous workers, including McMannis (1963), Boyce (1975), and Hawley and others (1982). LaHood sedimentation was in response to Proterozoic faulting along the Perry line, an E-W-trending normal fault zone, referred to locally as the Willow Creek or Pass fault zone, which has been interpreted as the southern margin of the Belt basin (Winston, 1986a). Major uplift of the Dillon block south of the Perry line exposed a rugged, mountainous terrain of Archean Wyoming province crystalline rock which served as source for the northward dispersal of coarse-grained, arkosic LaHood sediments. Transition of the conglomeratic LaHood Formation upward into fine-grained calcareous argillite of the Newland Formation to terrigeneous argillite of the Greyson Formation was interpreted by McMannis (1963) to represent a decrease in motion along the Perry line and possible southward onlap of Belt sediments across the line. Alternatively, Reynolds (1984) has suggested, based upon Belt facies relations and thickness trends, that the southern margin of the Belt basin did not coincide with the Willow Creek fault zone (Perry line), but was farther south, perhaps near the site of the Madison and Gravelly ranges.

Belt basin paleogeography

The paleogeography of the Belt basin has proven to be an issue of debate between various workers in the area. Winston (1986b) provides a historical summary of the evolution of Belt basin paleogeography, which concentrates on a marine basin interpretation versus an enclosed, intracratonic basin inter-

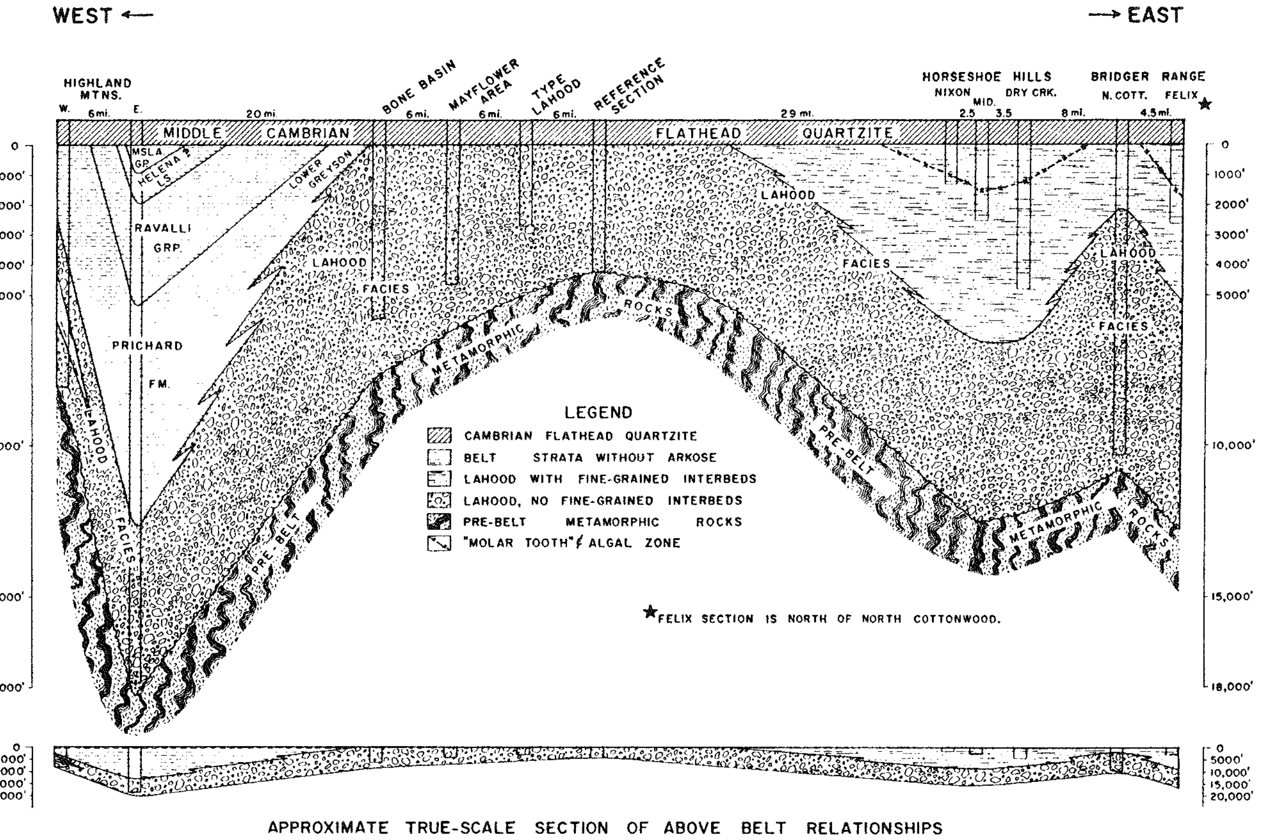
WEST ←
→ EAST
HIGHLAND MTNS.
W. 6mi. E.
20 mi
BONE BASIN
6mi.
MAYFLOWER AREA
6mi.
TYPE LAHOOD
6mi.
REFERENCE SECTION
29 mi.
HORSESHOE HILLS
NIXON
MID.
DRY CRK.
2.5 3.5
8 mi.
BRIDGER RANGE
N. COTT.
FELIX
4.5mi.
MIDDLE CAMBRIAN
FLATHEAD QUARTZITE
MSLA GP.
HELENA LS.
RAVALLI GRP.
LOWER GREYSON
PRICHARD FM.
LAHOOD FACIES
LAHOOD
FACIES
PRE-BELT METAMORPHIC ROCKS
PRE-BELT
METAMORPHIC ROCKS
0
1000'
2000'
3000'
4000'
5000'
10,000'
15,000'
18,000'
LEGEND
CAMBRIAN FLATHEAD QUARTZITE
BELT STRATA WITHOUT ARKOSE
LAHOOD WITH FINE-GRAINED INTERBEDS
LAHOOD, NO FINE-GRAINED INTERBEDS
PRE-BELT METAMORPHIC ROCKS
"MOLAR TOOTH"¢ ALGAL ZONE
★FELIX SECTION IS NORTH OF NORTH COTTONWOOD.
0
5000'
10,000'
15,000'
20,000'
APPROXIMATE TRUE-SCALE SECTION OF ABOVE BELT RELATIONSHIPS

Figure 5—Restored stratigraphic section showing relationships of LaHood facies from the Highland Mountains east to the Bridger Range. See Figure 2 for location of section line, (*from* McMannis, 1963).

pretation. Initially, Walcott (1914) interpreted Belt strata as lacustrine in origin. The study by Fenton and Fenton (1937) of Belt (Helena Formation) stromatolites in Glacier National Park led them to suggest that much of the Belt was marine in origin, albeit deposited in a severely restricted sea. Beginning in the 1960s, various workers including Price (1964), Gabrielse (1972), and McMechan (1981) contributed to the view that the Belt (and Purcell) Supergroups represented craton-derived deltaic continental margin strata which graded westward into a thickening miogeoclinal sequence of shallow marine shelf deposits. Harrison (1972) proposed that a landmass to the southwest of the Belt basin (termed Belt island) shed sediments to the northeast during deposition of the Revett Formation. This island restricted the Belt basin to being an epicontinental reentrant into the North American continent from an inferred Proterozoic cordilleran miogeocline (Harrison and others, 1974). Boyce (1975) modified this interpretation and viewed the Belt basin as an aulacogen formed during Proterozoic rifting of western North America.

Stratigraphic analysis of the Prichard Formation led Cressman (1985) to the conclusion that a source area of continental proportions existed to the west of the Belt basin in what is now southeastern Washington and northeastern Oregon at approximately 1.6 Ma. Recent Sm-Nd isotopic studies of Belt strata by Frost and Winston (1987) have led them to conclude that the LaHood Formation was indeed sourced by rocks in the Archean Wyoming province, but that much of the remainder of Belt strata was derived from erosion of a large western continent. Various workers have suggested that this continent could have been Siberia (Sears and Price, 1978), Australia (Jefferson, 1980), or a combination of Siberia and Australia (Eisbacher, 1985).

Further sedimentologic and stratigraphic work by Winston and others (1984) led also to the conclusion that the Belt basin was a large intracratonic basin which contained a landlocked sea. Winston and Woods (1986) later suggested that the Belt basin was lacustrine in nature with no marine influence. Thus, the full circle has been made back to the original intracontinental nonmarine basin interpretation of Walcott (1914).

Interpretations of LaHood Formation depositional environment

Several investigations have been made of the stratigraphy and sedimentology of the LaHood Formation in southwestern Montana. The results of these studies have not been in agreement, and as a result, two differing depositional models have emerged. These include submarine fan and alluvial fan/fan-delta interpretations. The criteria used to develop each of these models are summarized below.

Submarine fan interpretation

Alexander (1955) originated the origin of the submarine interpretation for LaHood Formation sedimentation and inferred that an absence of shallow-water sedimentary structures including ripple marks and mudcracks required deposition below wave base and in water depths below the effects of tidal influence. McMannis (1963) developed this view further by noting an apparent absence of cross bedding, mudcracks and other shallow water structures such as rain drop imprints and salt crystal casts combined with presence of normally graded bedding and intraformational slump features. These characteristics were interpreted as evidence for rapid subaqueous deposition by turbidity currents. The interbedding of algal and laminated carbonate rocks with graded arkose (turbidites) in the Horseshoe Hills and elsewhere led McMannis (1963) to conclude that deposition probably occurred in moderate water depths, although shallow water conditions could not be conclusively ruled out. In this scenario, unstable accumulations of coarse-grained arkosic debris were thought to have accumulated in nearshore areas along the topographically rugged southern margin of the Belt basin. Subsequent slumping and generation of turbidity currents resulted in transport of this debris northward to more stable positions on the sea floor.

Development of a submarine fan model for LaHood deposition was initiated by Hawley (1973) who interpreted graded bedding as the dominant sedimentary structure. He suggested that this bedding style was a component of incomplete Bouma sequences generated by turbidity flows. Soft-sediment slump structures were interpreted as submarine slides and some massive sandstones as subaqueous sand flows. The absence of load casts, flute marks, and other sole marks characteristic of turbidite bases was viewed by Hawley (1973, p. 77) as *disappointing*. The complete picture of LaHood deposition which emerged from Hawley's (1973) work was one of a steep source terrain directly bordering a marine basin into which eroded arkosic debris was transported and deposited nearby as submarine fans in relatively deep water.

Somewhat more detailed stratigraphic and sedimentologic analyses of the finer-grained LaHood facies, especially the limestone-bearing upper portion, were employed by Bonnet (1979) and Hawley and others (1983) to strengthen the submarine fan interpretation. Bonnet (1979) interpreted the arkosic and conglomeratic portions of the LaHood as proximal to medial submarine fan-channel facies. Evidence to support this interpretation for coarser-grained intervals includes abrupt lateral thickness changes, amalgamation of sandstone beds, graded bedding and what were interpreted as incomplete Bouma sequences. Interchannel facies are dominated by siltstone and mudrock intervals with lesser amounts of arkosic sandstone. Mudrocks were interpreted to indicate deposition from suspension; ripple cross-laminated horizons represent reworking by bottom currents. Turbidity flows which occassionally spilled out of fan channels also contributed sandy sediment to the interchannel areas. Evidence of syndepositional slumping is confined to these fine-grained interchannel sequences.

Algal limestones in the LaHood were interpreted by Bonnet (1979) as allochthonous. Because of deep water conditions suggested by the submarine fan interpretation and the deformed nature of some of the algal limestone intervals, it was suggested that the limestones were deposited in shallow water and slumped or slid downslope onto the fans along with other terrigeneous clastic shallow water facies in response to seismic events along the Belt basin margin.

Alluvial fan/fan-delta interpretation

The alluvial fan/fan-delta model proposed by Boyce (1975) is based upon detailed stratigraphic and sedimentologic analyses of the LaHood Formation. The focus is somewhat different than that of other workers since efforts were devoted to the coarser-grained conglomeratic basin margin facies of the formation. The analyses revealed the presence of massive, normally and inversely graded beds, medium- to large-scale cross stratification, scoured bases, intraclast zones, imbricated clast fabrics, and well-sorted tops of massive beds which were collectively interpreted as evidence for debris flow and streamflow deposition on the proximal portion of subaerial alluvial fans.

To the north, where pebble conglomerates and arkose are most prevalent, dominant sedimentary structures include medium-scale, trough cross stratification, horizontal stratification, and occassional graded bedding with pebble lenses, mudchip breccias and channel-like sequences. According to Boyce (1975), these strata represent deposition in mid- to distal-fan areas below the intersection point in ephemeral braided stream channels characterized by development of longitudinal bars.

Farther to the north, these fan deposits grade into finer-grained sequences characterized by interbedded mudrock, arkose and stromatolitic limestone. Deposition of these sequences is attributed to a complex of braided fluvial, alluvial flood plain, lacustrine and tidal flat environments. In the western part of the LaHood outcrop belt (Highland Mountains and St. Paul Gulch), Boyce (1975) interpreted interbedded sandstone and mudrock intervals as deposits of a high-constructive delta complex. The close proximity to the south of alluvial fan facies led to the suggestion that this may have been a fan-delta environment of deposition.

Suggestions for future investigation

The question of which model best accounts for deposition of the LaHood Formation is critical to the understanding of the paleogeographic setting and tectonic significance of the Belt basin. Belt researchers are now at the threshold of reevaluating their approach concerning the setting of the Belt basin, with respect to the Proterozoic tectonic evolution of western North America (Winston, 1986a), as well as the nature of Belt depositional environments. The time is ripe for a major sedimentologic reinvestigation of the LaHood. Principally, definitive interpretation of the environment of deposition will contribute significantly to improving the overall knowledge of Belt basin paleogeography and will add evidence to the continuing marine versus intracratonic debate. In addition, detailed stratigraphic, sedimentologic and provenance analysis of the LaHood Formation has the potential to provide a better understanding of the structural setting of the southern Belt basin margin. The LaHood Formation is an important stratigraphic unit in the Belt Supergroup since it represents the only preserved basin margin facies recognized to date; thus, it has significant potential of recording the tectonic style which characterized basin margins.

Additionally, from a sedimentologic perspective, reinvestigation of the LaHood Formation is necessitated by major advances in lithofacies analysis made during the past 10 years. The evolution of alluvial fan, fluvial, fan-delta, and submarine fan facies models in particular, has been particularly dramatic. The vastly increased knowledge which sedimentologists now possess of most modern depositional systems and the characteristics of their deposits will facilitate resolution of conflicting models of LaHood Formation deposition.

References

Alexander, R. G., 1955, Geology of the Whitehall area, Montana: Yellowstone-Bighorn Research Association Project Contribution 195, 111 p.

Bonnet, A. T., 1979, Lithostratigraphy and depositional setting of the limestone-rich interval of the LaHood Formation (Belt Supergroup), southwestern Montana [M.S. thesis]: Montana State University, Bozeman, 87 p.

Boyce, R. L., 1975, Depositional systems in the LaHood Formation, Belt Supergroup, southwestern Montana [Ph.D. dissertation]: University of Texas, Austin, 247 p.

Cressman, E. R., 1985, The Prichard Formation of the lower part of the Belt Supergroup (Middle Proterozoic), near Plains, Sanders County, Montana: U.S. Geological Survey Bulletin 1553, 64 p.

Eisbacher, G. H., 1985, Late Proterozoic rifting, glacial sedimentation, and sedimentary cycles in the light of Windermere deposition, western Canada: Palaeogeography, Palaeoclimatology, and Palaeoecology, v. 51, p. 231-254.

Fenton, C. L., and Fenton, M. A., 1937, Belt series of the north; stratigraphy, sedimentation, paleontology: Geological Society of America Bulletin, v. 48, p. 1873-1969.

Frost, C. D., and Winston, D., 1987, Nd isotope systematics of coarse-and fine-grained sediments: Examples from the Middle Proterozoic Belt-Purcell Supergroup: Journal of Geology, v. 95, p. 309-327.

Gabrielse, H., 1972, Younger Precambrian of the Canadian cordillera: American Journal of Science, v. 272, p. 521-536.

Harrison, J. E., 1972, Precambrian Belt basin of northwestern United States—its geometry, sedimentation and copper occurrences: Geological Society of America Bulletin, v. 83, p. 1215-1240.

Harrison J. E., Griggs, A. G., and Wells, J. D., 1974, Tectonic features of the Precambrian Belt basin and their influence on post-Belt structures: U.S. Geological Survey Professional Paper 866, 15 p.

Hawley, D., 1973, Sedimentary environment of the LaHood Formation, a southeastern facies of the Belt Supergroup, Montana: Belt Symposium: University of Idaho and Idaho Bureau of Mines and Geology, Moscow, p. 322.

Hawley, D., Bonnet-Nicolaysen, A., and Coppinger, W., 1982, Stratigraphy, depositional environments, and paleotectonics of the LaHood Formation: Geological Society of America, Rocky Mountain Section Field Trip Guidebook: Montana State University, Bozeman 20 p.

Jefferson, C. W., 1980, Correlation of Middle and upper Proterozoic strata between northeastern Canada and south and central Australia: International Geological Congress Abstracts, v. 2, p. 594.

McMannis, W. J., 1963, LaHood Formation—a coarse facies of the Belt Series in southwestern Montana: Geological Society of America Bulletin, v. 74, p. 407-436.

McMechan, M. E., 1981, The Middle Proterozoic Purcell Supergroup in the southwestern Purcell Mountains, British Columbia, and the initiation of the cordilleran miogeocline, southern Canada and adjacent United States: Bulletin of Canadian Petroleum Geologists, v. 29, p.583-621.

Price, R. A., 1964, The Precambrian Purcell system in the Rocky Mountains of southern Alberta and British Columbia: Bulletin of Canadian Petroleum Geologists, v. 12, p. 399-426.

Reynolds, M. W., 1984, Tectonic setting and development of the Belt basin, northwestern United States, *in* The Belt: Abstracts with Summaries, Belt Symposium II, S. Warren Hobbs *(ed.)*, Montana Bureau of Mines and Geology Special Publication 90, p. 44-46.

Ross, C. P., 1949, The Belt problem (Montana) (abs.): Washington Academy of Sciences Journal, v. 39, p. 111-113.

Sears, J. W., and Price, R. A., 1978, The Siberian connection: A case for Precambrian separation of the North American and Siberian cratons: Geology, v. 6, p. 267-270.

Walcott, C. D., 1914, Pre-Cambrian Algonkian algal flora: Smithsonian Miscellaneous Collections, v. 64, no. 2, p. 77-156.

Winston, D., 1986a, Sedimentation and tectonics of the Middle Proterozoic Belt basin, and their influence on Phanerozoic compression and extension in western Montana and northern Idaho, *in* Paleotectonics and sedimentation in the Rocky Mountain region, United States: J. Peterson, *(ed.)*: American Association of Petroleum Geologists Memoir 41, p. 87-118.

______ 1986b, Sedimentology of the Ravalli Group, middle Belt carbonate and Missoula Group, Middle Proterozoic Belt Supergroup, Montana, Idaho and Washington, *in* Belt Supergroup: A Guide to Proterozoic Rocks of Western Montana and Adjacent Areas: Sheila M. Roberts, *(ed.)*, Montana Bureau of Mines and Geology Special Publication 94, p. 85-124.

Winston, D., and Woods, M., 1986, Alluvial apron, sandflat, mudflat and shallow water sediment types of the intracratonic, Middle Proterozoic Belt basin, Montana and Idaho: Geological Society of America Abstracts with Programs, v. 18, no. 5, p. 423.

Winston, D., Woods, M., and Byer, G., 1984, The case for an intracratonic Middle Proterozoic Belt-Purcell basin: Tectonic, stratigraphic, and stable isotopic considerations, *in* Northwest Montana and Adjacent Canada; J. D. McBane and P. B. Garrison, *(eds.)*: Montana Geological Society Field Conference Guidebook, p. 103-118.

THE NORTHERN IDAHO BATHOLITH AND ITS ASSOCIATED HIGH-GRADE METAMORPHIC ROCKS

Donald W. Hyndman
and
David A. Foster*
Department of Geology
University of Montana
Missoula, Montana 59812

Introduction

The following paper characterizes the westernmost margin of Precambrian North America, which was subjected to high-grade regional metamorphism and intrusion of granites of the Idaho batholith in Cretaceous time. The present exposures are at mid-crustal levels, perhaps transitional in characteristics to those exposed at somewhat deeper levels in Archean basement terranes.

Idaho batholith environment

General aspects and regional tectonics

The Idaho batholith was emplaced into the Precambrian continental crust of North America, just east of a major collisional suture zone bounding the Seven Devils/Wallowa terrane or micro-continent to the southwest (**Figure 1**). Beginning about 120 Ma, the Seven Devils/Wallowa terrane arrived in western Idaho, colliding with the Precambrian rifted margin of old North America, and completing docking with plugging by quartz dioritic plutons 85 to 82 Ma (Lund and others, 1985; Snee and others, 1987). The boundary is marked by a major mylonitic suture zone, the western Idaho suture zone, that trends northward in western Idaho near the western edge of the Idaho batholith, then curves westward near the town of Orofino at latitude 46°30'N, and disappears under Miocene Columbia River basalts. At the bend, the microcontinent was being underthrust northeastward at a 50° plunge under North America. At least 80 kilometers of transport are documented in deformed dikes in the mylonite zone. The suture closely follows the boundary between generally mafic rocks of oceanic affinity on the west and generally felsic rocks of continental affinity on the east, and between $^{87}Sr/^{86}Sr$ initial ratios of less than 0.704 on the west and greater than 0.706 on the east (Armstrong and others, 1977; Fleck and Criss, 1985).

Proterozoic semipelitic to quartzose and impure calcareous sedimentary rocks of the Belt Supergroup, underlying most of northwestern Montana and northern Idaho, were subjected to regional burial metamorphism to the greenschist facies. Metamorphism reached lower grades higher in the stratigraphic section. During Mesozoic time, rocks adjacent to the northern Idaho batholith were deformed and subjected to regional-dynamothermal metamorphism grades reaching as high as the sillimanite zones (cf., Hyndman and others, 1988), an effect that extends as much as 70 kilometers from the batholith contact (**Figure 1**). In contrast to the massive, spotted fabric of Precambrian burial metamorphism, the Mesozoic regional metamorphism formed well-foliated schists and gneisses. Metamorphic grades increase progressively, in most areas, towards the batholith. However, locally isograds are cut at low angles by the batholith contact, demonstrating that at least the latest effects of intrusion postdated regional metamorphism. Mineral assemblages that include quartz, muscovite, biotite, staurolite, sillimanite and kyanite suggest that rocks north and northwest of the batholith were formed at depths greater than 25 kilomet-

---

*Present address: Department of Geology, State University of New York, Albany, New York 12222.

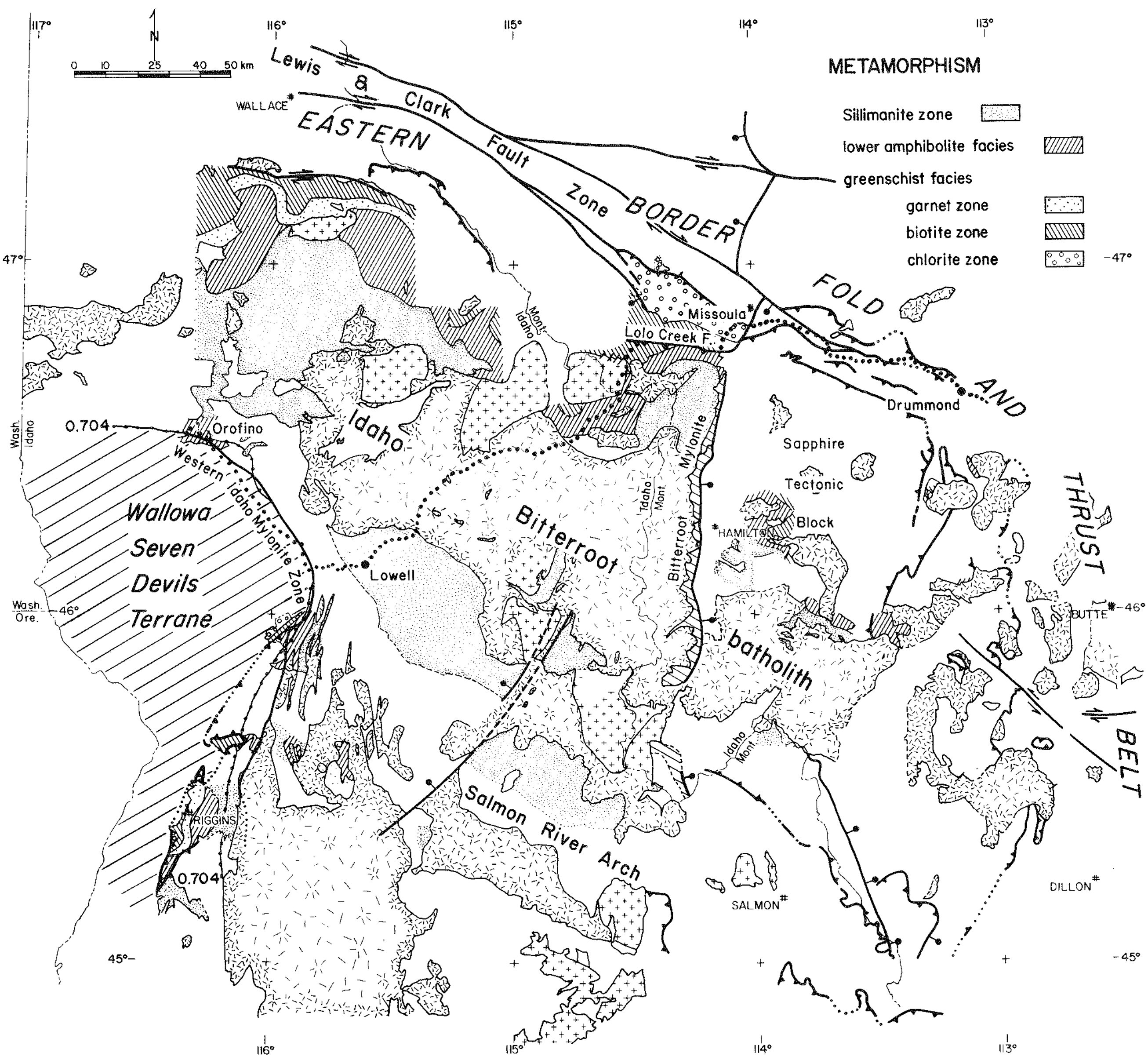
117°
116°
115°
114°
113°
N
0 10 25 40 50 km
Lewis & Clark Fault Zone
WALLACE
EASTERN BORDER
FOLD AND THRUST BELT
METAMORPHISM
Sillimanite zone
lower amphibolite facies
greenschist facies
garnet zone
biotite zone
chlorite zone
47°
46°
45°
Missoula
Lolo Creek F.
Drummond
Sapphire Tectonic Block
HAMILTON
BUTTE
DILLON
SALMON
Mont. Idaho
Idaho Mont.
Bitterroot Mylonite
Idaho Bitterroot batholith
Salmon River Arch
Orofino
Lowell
Western Idaho Mylonite Zone
Wallowa Seven Devils Terrane
0.704
RIGGINS
Wash. Idaho
Wash. Ore.

Figure 1—Tectonic and regional metamorphic map of the Idaho batholith region. Dotted line indicates field guide location (see Hyndman and Foster, this volume). Stronium isotope ratio boundary is labelled 0.704. Kamiah pluton occupies northern part of Wallowa-Seven Devils terrane. Areas with random hachures are Late Cretaceous granite-granodiorite. Plus pattern marks Eocene granite plutons. *Modified from* Hyndman and others, 1988.

ers, somewhat less to the southeast (Rice, 1987; Hyndman and others, 1988). Melting formed anatectic migmatites at the highest metamorphic grades, suggesting that the regional metamorphism accompanied crustal melting to form the Idaho batholith.

Main-phase units of the northern Idaho batholith, or Idaho-Bitterroot batholith (**Figure 2**), are granite to granodiorite emplaced in Late Cretaceous time between about 65 and 80, or possibly 85 Ma. The timing, immediately after collision along the western Idaho suture zone, and proximity of the batholith to that zone, suggest that subduction that formed the batholith lay west or southwest of the western Idaho suture zone. The 14,000 km² Idaho-Bitterroot batholith was apparently emplaced into a broad synclinorium trending southeastward in the Proterozoic Belt Supergroup. The batholith rocks are felsic, medium-grained, and for the most part, are massive. Much of the granite along the deep line of section along the Lochsa River is relatively homogeneous mineralogically and chemically (Hyndman, 1984), but elsewhere the batholith shows considerable variation within the range of granite and granodiorite (Hyndman, 1983; Toth, 1987; Reid, 1987). The western border zone, about 20 percent of the width of the Idaho batholith, consists of somewhat earlier intrusions of biotite-hornblende quartz diorite to tonalite. The rocks are massive and generally foliated on steep surfaces trending approximately parallel to the west-

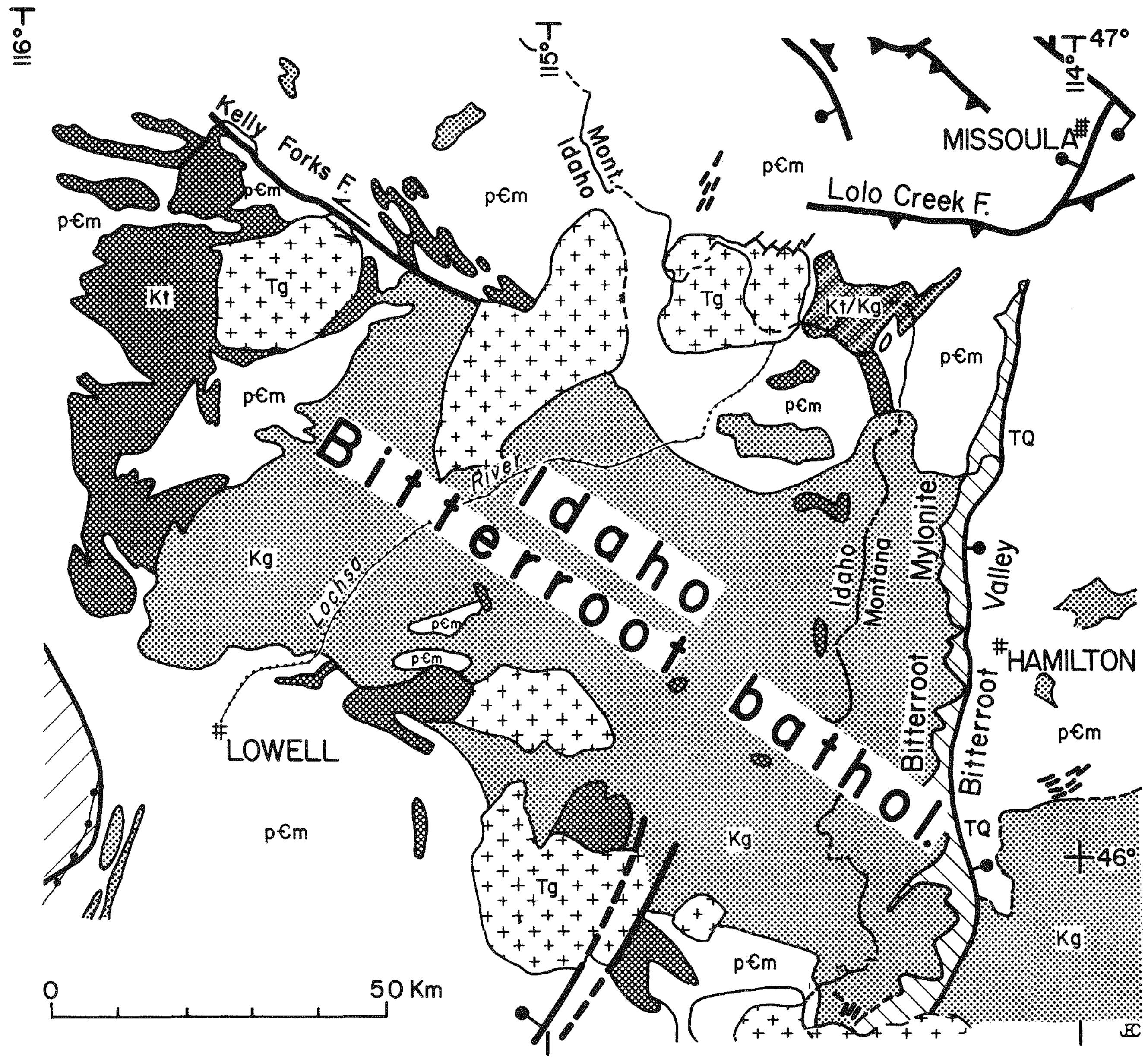
116°
115°
114°
47°
46°
Kelly Forks F.
Mont.
Idaho
MISSOULA
Lolo Creek F.
pꞒm
Kt
Tg
Kt/Kg
Kg
TQ
River
Lochsa
Bitterroot Idaho batholith
Idaho
Montana
Bitterroot
Mylonite
Bitterroot
Valley
HAMILTON
LOWELL
0
50 Km
JE

Figure 2—Intrusive map of the northern Idaho batholith. (pꞒm), metamorphosed Precambrian metasedimentary rocks; (Kt), Cretaceous tonalite/quartz diorite; (Kg), Cretaceous granodiorite/granite main-phase units of the batholith; (Tg), Eocene plutons emplaced at shallow depths; (TQ), Tertiary-Quaternary valley-fill sediments (*after* Hyndman and Foster, 1988).

ern Idaho suture zone. These lie on the oceanic (southwest) side of the Sr-isotope boundary. Sheets and other bodies of tonalitic and quartz diorite orthogneiss occur elsewhere in the deeper and border zones of the batholith (Taubeneck, 1971; Chase, 1973; Wiswall and Hyndman, 1986; Hyndman and Foster, 1988). These mafic-rich rocks may mark the deepest levels of the Idaho batholith, as also inferred for the Sierra Nevada batholith (Ross, 1985).

Large, voluminous swarms of synplutonic basaltic andesite to andesite dikes, and small areas of gabbroic complex, cut the batholith (Hyndman and Foster, 1988). In one ten-kilometer-wide section along the Lochsa River valley, 20% dikes (by volume) were measured. Mafic synplutonic dikes are also widespread in the tonalite/quartz diorite of the western border zone of the batholith.

Intrusive relations indicate that the mafic dikes in the Idaho-Bitterroot batholith were emplaced in the same time period as the main-phase granites (**Figure 3**). Evidence for such a synplutonic nature (Hyndman and Foster, 1988) includes the following:

1. Mafic dikes cut the host granite as tabular, sharply-bounded bodies; some are stretched, thinned, segmented, or dismembered, or are folded in undeformed granite.
2. Many of the mafic dikes show foliation, lineation and mylonitic texture imposed by post-emplace-

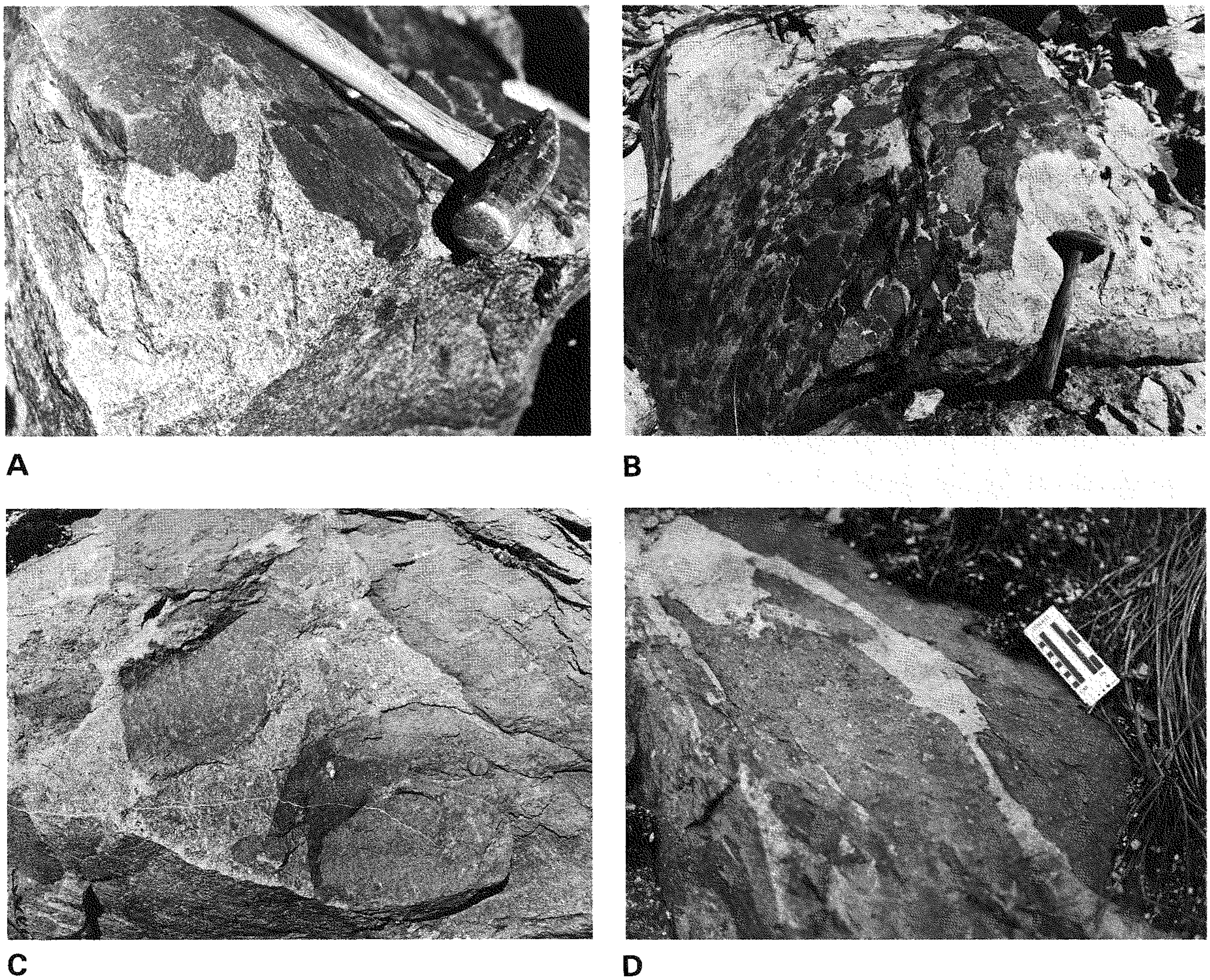

Figure 3—Photographs taken along U.S. Highway 12 (Lochsa River canyon) illustrating magma mingling and mixing relationships between synplutonic mafic dikes and granite-granodiorite of the Idaho-Bitterroot batholith. (A), Sharply bounded, fine-grained mafic dike with rounded, bulbous contact to granite. Foliated schlieren of intermediate composition at left. Location is 150 meters downstream from milepost 125 (below road level); (B), dike of fine-grained mafic blobs surrounded by coarser intermediate-composition (mixed) phase that is enclosed in and cut by granite. Location same as A; (C), rounded masses of mafic dike in contaminated granodiorite. View is 0.5 meters wide. Location is at milepost 122.3; (D) fine-grained, relatively mafic and felsic phases in sharp, rounded to cuspate contact. Location is near milepost 122.5.

ment movement of the granite. Some are foliated oblique to the walls of the dike.

3. Mafic dikes grade into rounded blobs, or mafic schlieren, in the granite.
4. Mafic dikes are cut by tabular or ptygmatic dikes of the host granite, and are metamorphosed by heat from the host granite, or contain late alkali feldspar megacrysts like those in the granite.
5. Granite within a meter or so of some of the dikes is contaminated and becomes more mafic than normal Idaho batholith granite.
6. Granite and andesite in composite dikes show small-scale intermingling, or rounded blobs of basalt with thin leucogranite rims.
7. The complete range of chemical composition of the synplutonic dikes, from basaltic andesite to dacite, lies along a linear, major-element mixing trend which includes the composition of the enclosing granite to granodiorite. Magma mingling and mixing is supported by megascopic to abundant microscopic disequilibrium textures in intermediate rock types.

Given the nature of their interaction with the enclosing granite, synplutonic mafic magmas appear to have been injected at early, intermediate, and late stages during crystallization of the granite. Since voluminous, high-temperature, mafic magmas apparently were emplaced throughout crystallization of the granite of the Idaho-Bitterroot batholith, they must have added considerable heat. As suggested by Hyndman and Foster (1988), the mafic magmas, rising above the subduction zone, probably provided the additional heat required to melt the lower continental crust to form the granitoid magmas of the Idaho batholith.

Pegmatites and minor aplites occur in several environments. A few early concordant muscovite-biotite-quartz-feldspar pegmatites pinch and swell and show 1 to 3 millimeter biotite selvages in pelitic to quartzofeldspathic country rocks. These probably formed by anatexis during regional metamorphism. Most of the pegmatitic dikes were emplaced by injection (Chase and Johnson, 1977) after regional metamorphism; many were probably associated with emplacement of the main-phase units of the batholith.

Many tabular, post-metamorphic muscovite-quartz-feldspar pegmatites 5 to 25 centimeters thick have injected planar fractures. Another group of tabular pegmatites or aplites, 1 centimeter to 2 meters thick, dips 5 to 25°W, NW, or N, regardless of the dip or degree of deformation of the enclosing rock. These subhorizontal pegmatitic sheets are emplaced only into granodiorites and granites of the western 16 kilometers of the Lochsa River valley section (see Hyndman and Foster, this volume), and extend for only 1.3 kilometers into the country rocks (Hyndman, 1983). The surfaces of the pegmatite dikes are marked by slickenside striae plunging down dip to the northwest, indicating post-emplacement slip and probably shear-surface control of emplacement.

Several stages of deformation are recognized in the Idaho batholith environment (Hietanen, 1961; Chase, 1973; Reid and others, 1973; Nold, 1974; Childs, 1982; Wiswall and Hyndman, 1986; Rice, 1987; Hyndman and others, 1988). Tight isoclinal folds with strong axial-plane schistosity were formed in deformation D1, but they are difficult to find. A few large folds verging away from the batholith have been described. The major amphibolite-facies regional metamorphism surrounding the batholith, and described above, produced the axial-plane schistosity of D1 folds. Open to nearly isoclinal folds deformed the dominant schistosity during D2 deformation; they developed a new weak to locally strong axial-plane schistosity with muscovite and biotite. These folds tend to have nearly vertical plunges near the batholith contacts, perhaps as a result of rise of the batholith magmas during D3. Upright and relatively open concentric and flexural slip folds of the earlier metamorphic schistosity formed during D3 deformation, probably during the final stages of forceful emplacement of the batholith. No new axial plane schistosity formed. Rapid rise of the batholith terrain may have accompanied emplacement.

Summary

An overall model for formation of the northern Idaho batholith is as follows. The Seven Devils/Wallowa terrane of eastern Oregon and western Idaho docked in Late Cretaceous time near the present western edge of the Idaho batholith, a boundary marked by a major mylonite zone and the Sr-isotope initial-ratio boundary. Subduction on a separate zone southwest of the terrane, between about 120 to 80, and 80 to 65 m.y. ago, gave rise to the mafic western border and the felsic main-phase magmas, respectively, of the batholith. Partial melting formed basaltic andesite magmas in the mantle wedge above the subducted oceanic plate, and those high-temperature magmas rose into the overlying crust. Outboard of old continental North America, they crystallized to form tonalite and quartz diorite plutons. Where the mafic magmas rose into the old granitoid continental crust, they heated the crust to cause regional metamorphism and ultimately caused secondary melting to form the granodiorite and granite magmas of the batholith. The synplutonic mafic dikes now preserved in the batholith formed by continued rise of the same mafic magmas.

References

Armstrong, R. L., Taubeneck, W. H., and Hales, P. O., 1977, Rb-Sr and K-Ar geochronometry of Mesozoic granitic rocks and their Sr isotopic composition, Oregon, Washington and Idaho: Geological Society of America Bulletin, v. 88, p. 397-441.

Chase, R. L., 1973, Petrology of the northeast border zone of the Idaho batholith, Bitterroot Range, Montana: Montana Bureau of Mines and Geology Memoir 43, 28 p.

Chase, R. L., and Johnson, B. R., 1977, Border-zone relationships of the northern Idaho batholith: Northwest Geology, v. 6-1, p. 38-50.

Childs, J. F., 1982, Geology of the Precambrian Belt Supergroup and the northern margin of the Idaho batholith, Clearwater County, Idaho, [Ph.D. dissertation]: University of California, Santa Cruz, 419 p.

Fleck, R. J., and Criss, R. E., 1985, Strontium and oxygen isotope variations in Mesozoic and Tertiary plutons of central Idaho: Contributions to Mineralogy and Petrology, v. 90, p. 291-308.

Greenwood, W. R., and Morrison, D. A., 1973, Reconnaissance geology of the Selway-Bitterroot Wilderness area: Idaho Bureau Mines and Geology Pamphlet 154, 30 p.

Hietanen, A., 1961, Relationship between deformation, metamorphism, metasomatism, and intrusion along the northwest border zone of the Idaho batholith, Idaho: U.S. Geological Survey Professional Paper 424-D, p. 161-164.

Hyndman, D. W., 1983, The Idaho batholith and associated plutons, Idaho and western Montana, *in* Circum-Pacific Batholiths, J. A. Roddick (*ed.*): Geological Society of America Memoir 159, p. 213-240.

______ 1984, A petrographic and chemical section through the northern Idaho batholith: Journal of Geology, v. 92, p. 83-102.

Hyndman, D. W. and Foster, D. A., 1988, The role of tonalites and mafic dikes in the generation of the Idaho batholith: Journal of Geology, v. 96, p. 31-46.

Hyndman, D. W., Alt, D., and Sears, J. W., 1988, Post-Archean metamorphic and tectonic evolution of western Montana and northern Idaho, *in* Metamorphism and Crustal Evolution of the Western United States, W. G. Ernst (*ed.*): Prentice-Hall, Englewood Cliffs, New Jersey p. 332-361.

Jens, J. C., 1974, A layered ultramafic intrusion near Lolo Pass, Idaho: Northwest Geology, v. 3, p. 38-46.

Lund, K., Snee, L. W., and Sutter, J. F., 1985, Style and timing of suture-related deformation in island arc rocks of western Idaho: Geological Society of America Abstracts with Programs, v. 17, p. 367.

Nold, J. L., 1974, Geology of the northeastern border zone of the Idaho batholith: Northwest Geology, v. 3, p. 47-52.

Reid, R. R., 1987, Structural geology and petrology of a part of the Bitterroot lobe of the Idaho batholith, *in* Geology of the Blue Mountains Region of Oregon, Idaho and Washington: The Idaho Batholith and its Border Zone, T. L. Vallier and H. C. Brooks, (*eds.*): U.S. Geological Survey Professional Paper 1436, p. 37-58.

Reid, R. R., Morrison, D. A., and Greenwood, W. R., 1973, The Clearwater orogenic zone: A relict of Proterozoic orogeny in central and northern Idaho: Belt Symposium, University of Idaho and Idaho Bureau of Mines and Geology, v. 1, p. 10-56.

Reid, R. R., Bittner, E., Greenwood, W. R., Luddington, S., Lund, K., Motzer, W., and Toth, M., 1979, Geologic section and road log across the Idaho batholith: Idaho Bureau Mines and Geology Information Circular 34, 20 p.

Rice, J. M., 1987, Polymetamorphism in northern Idaho: A schistose scenario of Belt and batholith, *in* Geological Society of America Abstracts with Program, v. 19, no. 7, p. 818.

Ross, D. C., 1985, Mafic gneiss complex (batholith root?) in the southernmost Sierra Nevada, California: Geology, v. 13, p. 288-291.

Schuster, R. D., and Bickford, M. E., 1985, Chemical and isotopic evidence for the petrogenesis of the northeastern Idaho batholith: Journal Geology, v. 93, p. 727-742.

Snee, L., Lund, K., and Davidson, G., 1987, Ages of metamorphism, deformation, and cooling of juxtaposed oceanic and continental rocks near Orofino, Idaho: Geological Society of America Abstracts with Programs, v. 19, p. 335.

Strayer, L. M., IV, Hyndman, D. W., and Sears, J. W., 1987, Movement direction and displacement estimate in the western Idaho suture zone mylonite: Dworshak Dam/Orofino area, west-central Idaho: Geological Society of America Abstracts with Programs, v. 19, no. 7, p. 857.

Taubeneck, W. H., 1971, Idaho batholith and its southern extension: Geological Society of America Bulletin, v. 82, p. 1899-1928.

Toth, M. I., 1987, Petrology and origin of the Bitterroot Lobe of the Idaho batholith, *in* Geology of the Blue Mountains Region of Oregon, Idaho and Washington: The Idaho batholith and its border zone, T. L. Vallier and H. C. Brooks (*eds.*), U.S. Geological Survey Professional Paper 1436, p. 9-35.

Wehrenberg, J. P., 1972, Geology of the Lolo Peak area, northern Bitterroot Range, Montana: Northwest Geology, v. 1, p. 25-32.

Whitney, J. A., 1975, The effects of pressure, temperature, and X_{H_2O} on phase assemblages in four synthetic rock compositions: Journal of Geology, v. 83, p. 1-81.

Wiswall, G., and Hyndman, D. W., 1986, Emplacement of the main plutons of the Idaho batholith, *in* Geology of the Blue Mountains Region of Oregon, Idaho and Washington: The Idaho Batholith and its Border Zone, T. L. Vallier and H. C. Brooks (*eds.*): U.S. Geological Survey Professional Paper 1436, p. 59-72.

THE SALMON RIVER SUTURE, WESTERN IDAHO: AN ISLAND ARC-CONTINENT BOUNDARY

Karen Lund
U.S. Geological Survey
Denver, Colorado 80255

Introduction

The Salmon River suture zone forms the western edge of the Paleozoic and Mesozoic North American continent for more than 500 kilometers in western Idaho. Along this truncated margin, allochthonous oceanic island arc rocks are juxtaposed directly against continental rocks; no continental margin or ocean basin transitional rocks intervene. Isotope and trace-element geochemical data (Armstrong and others, 1977; Fleck and Criss, 1985; Hoover and others, 1985; Manduca and others, 1986) and aeromagnetic data (U.S. Geological Survey, 1978) also define the abrupt boundary between terranes. This boundary trends about 015° for more than 400 kilometers from the South Mountain area (southwestern Idaho) to near Orofino where it abruptly trends west for about 100 kilometers. In eastern and central Washington, the boundary is covered by the Columbia River Basalt Group (**Figure 1**).

Stratigraphy

In much of west-central Idaho, the age and correlation of metamorphic rocks of pre-Cretaceous North America are imperfectly understood. In areas that are 70 kilometers or more east of the suture, metasedimentary rocks at greenschist facies or lower metamorphic grade are equivalent to the Middle Proterozoic Belt Supergroup (Hietanen, 1962; Harrison, 1972; Ruppel and others, 1983). In addition, several metamorphosed Middle Proterozoic plutons have been dated in central Idaho (Evans, 1986; Evans and Fischer, 1986). However, closer to the suture zone, metamorphic grade progressively increases from greenschist facies at distances of more than 50 kilometers to amphibolite facies along the suture; the age of the metasedimentary rocks is not known. Common lithologies of continental rocks in central Idaho include mica schist, calc-silicate gneiss, quartzite, quartzite pebble conglomerate, and marble (Stop 6 of Lund, this volume). Most of these rocks are probably correlative with the Belt Supergroup; however, a distinct group of metasedimentary rocks along the western side of the continental terrane is probably Late Proterozoic to Paleozoic (Lund, 1984a; Lund and Snee, 1988). Although it has been suggested that many of the metasedimentary rocks in central Idaho are older than the Middle Proterozoic Belt Supergroup (Harrison and others, 1974; Armstrong, 1975; Ruppel, 1975), this has not been demonstrated by field or subsequent dating studies. The absence of detailed mapping and geochronologic studies in large parts of central Idaho leaves the correlation of the majority of continental metasedimentary rocks open to question.

Allochthonous oceanic rocks in Idaho west of the Salmon River suture form composite fault-bounded slices (**Figure 2**; Lund, Figure 1; and Aliberti and Manduca, Figure 1, this volume), all of which contain island arc-related volcanic, volcaniclastic and plutonic rocks. The westernmost rocks are greenschist- to amphibolite-facies, Permian to Triassic rocks of the Wallowa terrane (**Figure 2**; Hietanen, 1962; Hamilton, 1963, 1969b; Vallier, 1977; Myers, 1982). Rocks of the Wallowa terrane have been correlated to Wrangellia (Silberling and Jones, 1984) or to Stikinia (Mortimer, 1985). The rocks of the Wallowa terrane are structurally overlain by another slice of upper-greenschist- to amphibolite-facies island arc rocks (Rapid River plate of Lund, this volume; Hamilton, 1963; Onasch, 1977, 1988; Aliberti and others, 1987); the age of these rocks, that are named the Riggins Group, is unknown (**Figure 2**; Hamilton, 1963).

Another wedge of amphibolite-facies mafic rocks of unknown age lies structurally above and to the east of both the Wallowa terrane and the Rapid River plate (Riggins Group); this includes the Pollock Mountain plate of Aliberti and Manduca, this volume; Aliberti and others (1987); Aliberti and Manduca (1988); and the North Fork plate of Lund, this volume

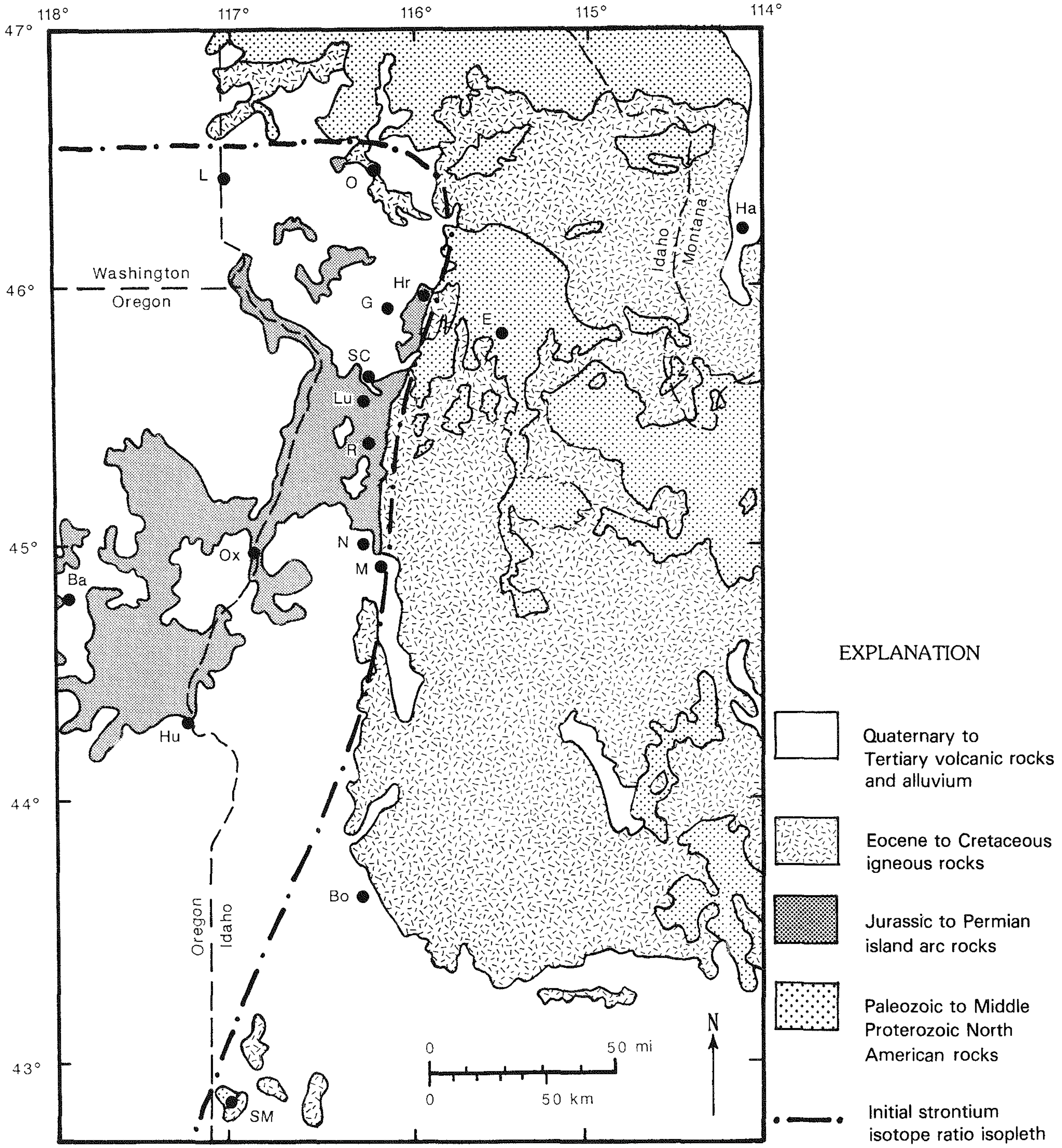
118°
117°
116°
115°
114°
47°
46°
45°
44°
43°
L
O
Ha
Washington
Oregon
Hr
G
E
SC
Lu
R
Idaho
Montana
N
M
Ox
Ba
Hu
Bo
Oregon
Idaho
SM
0
50 mi
0
50 km
N
EXPLANATION
Quaternary to Tertiary volcanic rocks and alluvium
Eocene to Cretaceous igneous rocks
Jurassic to Permian island arc rocks
Paleozoic to Middle Proterozoic North American rocks
Initial strontium isotope ratio isopleth

Figure 1—Generalized geologic map of Salmon River suture zone. Locations: (Ba), Baker; (Bo), Boise; (E), Elk City; (G), Grangeville; (Ha), Hamilton; (Hr), Harpster; (Hu), Huntington; (L), Lewiston; (Lu), Lucile; (M), McCall; (N), New Meadows; (O), Orofino; (Ox), Oxbow; (R), Riggins; (SC), Slate Creek; (SM), South Mountain. Geology *from* Bond (1978), Brooks and Vallier (1978), Lund (1984a), and McCollough (1984). Strontium isotope data approximated from Armstrong and others (1977) and Fleck and Criss (1985); oceanic values of <0.704 west of the line and continental values of >0.706 east of the line.

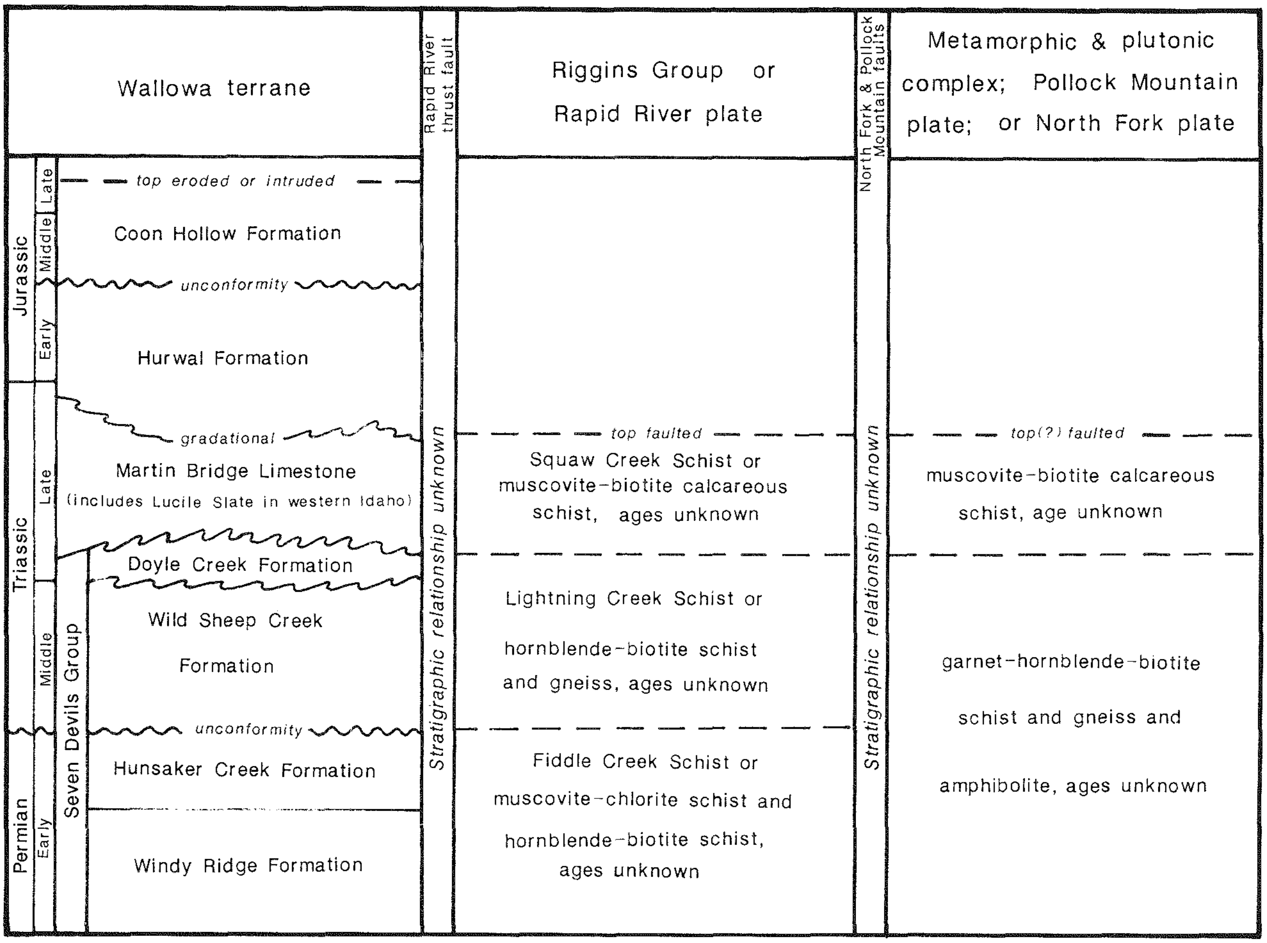
Wallowa terrane
Rapid River thrust fault
Riggins Group or Rapid River plate
North Fork & Pollock Mountain faults
Metamorphic & plutonic complex; Pollock Mountain plate; or North Fork plate
Jurassic
Late
Middle
Early
top eroded or intruded
Coon Hollow Formation
unconformity
Hurwal Formation
gradational
Triassic
Late
Middle
Martin Bridge Limestone (includes Lucile Slate in western Idaho)
Doyle Creek Formation
Wild Sheep Creek Formation
unconformity
Permian
Early
Seven Devils Group
Hunsaker Creek Formation
Windy Ridge Formation
Stratigraphic relationship unknown
top faulted
Squaw Creek Schist or muscovite-biotite calcareous schist, ages unknown
Lightning Creek Schist or hornblende-biotite schist and gneiss, ages unknown
Fiddle Creek Schist or muscovite-chlorite schist and hornblende-biotite schist, ages unknown
Stratigraphic relationship unknown
top(?) faulted
muscovite-biotite calcareous schist, age unknown
garnet-hornblende-biotite schist and gneiss and amphibolite, ages unknown

Figure 2—Generalized correlation diagram for oceanic rocks of western Idaho. ***Compiled from*** **Vallier, 1977; Follo, 1986; Hamilton, 1963; Onasch, 1977; Lund, this volume; Aliberti and Manduca, this volume. Age of units in columns 2 and 3 are unknown; stratigraphic relationships of units among columns is uncertain.**

(**Figure 2**). Alternative suggestions for the origin of these fault-bounded slices are: 1) they represent fragments of separate exotic terranes (Hamilton, 1963; Vallier and others, 1977; Brooks and Vallier, 1978); or 2) the slices are parts of a single, dismembered island arc that have undergone progressively greater metamorphism and deformation near the suture and were imbricated (Lund, 1984a; Lund and others, 1985; Lund and Snee, 1988).

Geologic history

It is only near the suture zone that evidence for the final suturing of arc to continent can be observed; only metamorphism in island arc rocks less than 15 kilometers distant and in continental rocks less than 65 kilometers distant from the suture zone have been related to this Late Cretaceous suturing event (Lund and others, 1985; Lund and Snee, 1988). Metamorphic grade and deformational intensity increase toward the Salmon River suture from both sides (Lund, 1984a, b). The increase in grade occurs across faults that brought higher-grade rocks up and over, or up and along side of, lower-grade rocks and thereby formed an inverted metamorphic gradient (Hietanen, 1962; Hamilton, 1963; Myers, 1982; Lund, 1984a; Onasch, 1987; Lund and Snee, 1988; Aliberti and Manduca, 1988). Several episodes of metamorphism punctuated by deformation took place in metamorphic rocks near the suture zone (Lund, 1984a, b; Lund and others, 1985; Selverstone and others, 1987; Lund and Snee, 1988).

Dating by ^{40}Ar/^{39}Ar age-spectrum methods of metamorphic minerals in the lowest grade, simplest island arc metamorphic rocks shows that metamorphic events began at about 120 Ma (Sutter and others, 1984; Snee and others, 1987; Lund and Snee, 1988). Locally, the first pulses of tonalitic magma were also emplaced at about this time (Manduca, 1987; Snee and others, 1987; Lund and Snee, 1988); these plutons include those at Stop 2 of Davidson (this volume) and the Hazard Creek complex (Stop 6) of Aliberti and Manduca, this volume. Metamorphic ages of higher-grade, more complex rocks nearer the suture zone form two age groups around 109 and 101 Ma (Lund and Snee, 1988). Based on crosscutting relationships among dated rocks, macroscopic deformation in the metamorphic rocks culminated between 105 and 95 Ma. Macroscopic structures, preserved in pre-95 Ma rocks, verge away from the suture (Hamilton, 1963; Myers, 1982; Onasch, 1977, 1987) and also steepen both at depth and toward the center of the zone (Lund, 1984a, b; Hoover, 1986; Manduca and Kuntz, 1987; Lund and Snee, 1988; Aliberti and Manduca, 1988).

Following the above described dynamothermal events, voluminous quartz dioritic, tonalitic and granodioritic plutons intruded into the eastern part of the regionally metamorphosed oceanic rocks and into vast areas of continental metamorphic rocks. These plutons include plutonic rocks at Stop 1 of Davidson (this volume); in the suture zone near Dworshak Dam, Strayer (this volume); at Stop 4, Lund (this volume); and at Stop 7 of Aliberti and Manduca, this volume). These intrusions include epidote-bearing plutons that were emplaced at depths of 25-30 kilometers (Zen, 1985). In less than a 10 kilometers-wide belt within the suture zone, these plutons and included xenoliths and roof pendants were deformed during a final amphibolite-facies dynamothermal event (Lund, 1984a, b). Foliation that formed during this event parallels the suture zone, and associated lineations are steep (Lund, 1984a, b; Hoover and others, 1985; Manduca and Kuntz, 1987; Manduca, 1987; Lund and Snee, 1988). L-tectonites and mylonitic shear zones occur in these rocks (Stop 1 of Davidson, Stops 3 and 4 of Lund, and Stop 7 of Aliberti and Manduca, this volume). The equivalent quartz dioritic to granodioritic plutons, which were emplaced outside (primarily to the east) of the suture zone, contain less strong planar or nondirectional fabrics (Lund, 1984a; Lund and Snee, 1985; Hoover, 1986; Aliberti and Manduca, 1988; Stop 1 Davidson; Stop 5 of Lund; and Stop 8 of Aliberti and Manduca, this volume). Based on combined ^{40}Ar/^{39}Ar age-spectrum dating and U/Pb (zircon and sphene) techniques, the ages of these plutons are approximately 93 to 85 Ma. ^{40}Ar/^{39}Ar data from metamorphic and plutonic rocks in the suture zone show that the final (suture zone parallel) dynamothermal deformation was superimposed at about 90 to 80 Ma (Sutter and others, 1984; Lund and Snee, 1985, 1988; Snee and others, 1987).

Along the N-NE-trending segment of the Salmon River suture, initiation of uplift coincided with emplacement of the youngest tonalitic to granodioritic plutons. Based on cooling data from detailed ^{40}Ar/^{39}Ar data, uplift of as much as 15 kilometers on the continental side of the boundary occurred along N-NE-trending normal faults between 85 and 75 Ma and facilitated cooling of the intrusive and metamorphic rocks (Lund and Snee, 1985, 1988; Snee and others, 1985). Along the W-trending segment of the suture, a longer period of slower uplift and cooling and/or perhaps a later structural event is recorded (Snee and others, 1987; Davidson and others, 1988). At present, the origin of ubiquitous brittle and ductile faults and fabrics in quartz dioritic to granodioritic rocks near and parallel to the suture zone is unclear. These features may be related to: 1) transpression along the suture after emplacement of the approximately 90 Ma plutons or to uplift, both of which would produce vertical fabrics (Lund, 1984a; Lund and others, 1986; Lund and Snee, 1988); 2) diapiric emplacement (Myers, 1972, 1982; Myers and Carlson, 1982); or 3) reactivation in a compressional regime (Manduca, 1987).

Voluminous muscovite-biotite granite plutons were emplaced passively into older metamorphic and plutonic rocks on the continental side of the suture zone (Stop 6 of Lund, this volume). Cooling information from ^{40}Ar/^{39}Ar data indicate that these plutons were emplaced between 75 and 70 Ma at depths of 6-9 kilometers. Slow uplift and cooling continued into the Tertiary (Snee and others, 1984; Lund and others, 1986; Lund and Snee, 1988).

After most of the uplift had occurred, basalt flows of the Miocene Columbia River Basalt Group may have been moated against scarps along these steep faults. These flows were later cut and displaced by post-Miocene faults that are parallel to the earlier formed steep faults (Lund, 1984a).

Geometry of suture zone

Probably the first widely recognized novelty about the Salmon River suture zone was the abrupt change in initial strontium isotope ratios in plutonic rocks from oceanic to continental values (Armstrong and others, 1977). More detailed work substantiated this isotopic boundary and showed the transition from oceanic to continental values to be less than 5 kilometers wide across several transects (Fleck and Criss, 1985). Although these workers concluded that the change in initial ratios is due to contamination by country rocks, it has also been suggested that the change in values may represent different magma source areas (Lund, 1984a; Lund and Snee, 1988). Subsequent rare-earth element study of the plutonic rocks across the suture zone (Hoover, 1986) showed that samples of plutonic rocks known to have oceanic strontium isotopic signatures (Fleck and Criss, 1985) were derived from an oceanic source, whereas those with continental signatures were derived from a continental source. The change between source rock affinities is as sharp as indicated by the Fleck and Criss (1985) strontium isotope data and evidence for contamination by upper crustal rocks or widespread mixing of source rocks was not found (Hoover and others, 1985; Hoover, 1986). These data strongly suggest that the Salmon River suture is a sharp and near vertical crustal boundary (Lund, 1984a, b; Hoover and others, 1985; Hoover, 1986; Lund and Snee, 1988).

Structural and metamorphic geometry, geochemical and geophysical characteristics, plutonic suites, and timing of events are remarkably consistent along the length of the suture. Although less is known about the W-trending segment of the suture, preliminary data suggest that the general features are the same as along the better known N-trending segment (Hietanen, 1962). Miogeoclinal and other transitional rocks that were originally between the oceanic and continental rocks were tectonically removed and are not present within the suture zone. Other features that are commonly associated with suture zones, such as tectonic melange, high-pressure low-temperature metamorphic rocks, ophiolites, and overall structural asymmetry, are not found along the length of the Salmon River suture zone. The direct, apparently simple, juxtaposition of oceanic and continental rocks is unique in comparison with the broad, stratigraphically and structurally complex transitions in Canada and Nevada (**Figure 3**). Because of the volume of post-accretionary plutons, the contact between the terranes is obscured and the only direct evidence for relative motion between them is for late-stage, post-plutonic, Late Cretaceous movement. A comprehensive explanation for the tectonic history of this suture, which includes the W-trending segment, has not been attempted and further work is necessary.

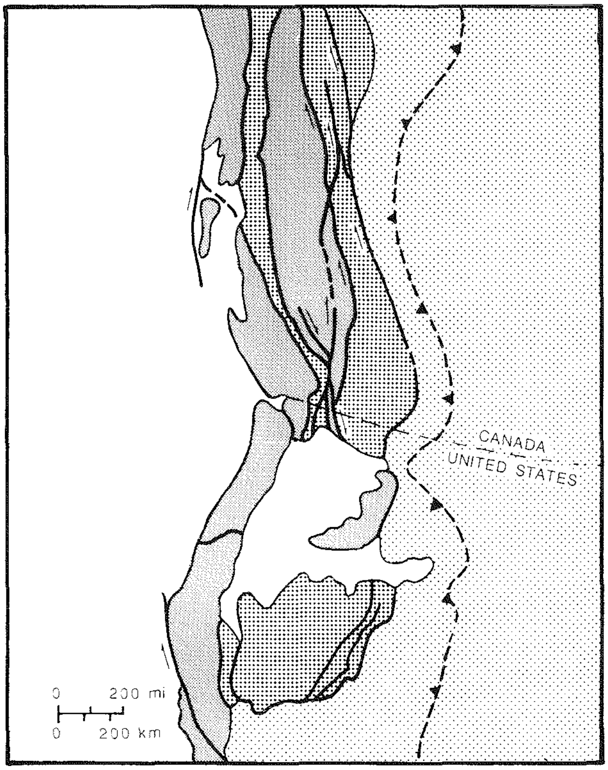

EXPLANATION

□ Quaternary to Tertiary cover rocks

▩ Allochthonous oceanic rocks

▦ Allochthonous transitional or mixed rocks

░ Autochthonous or parautochthonous North American rocks

— Faulted terrane boundary

⇀ Transcurrent fault boundary

▲ Approximate limit of Cenozoic to Mesozoic thrust faulting

Figure 3—Generalized tectonic map of part of North America showing general composition of terranes and location of Cretaceous to Eocene faults. *Modified after* Coney and others (1980); Silberling and Jones (1984); and Gabrielse (1985).

Models

Despite the incomplete data, several models for formation of the Salmon River suture zone have been proposed. The earliest plate tectonic models for the formation of the N-NE-trending segment of this suture suggested that this was the site of a subduction zone that caused accretion of the arc sometime between Triassic and Cretaceous time (Hamilton, 1969a, 1976, 1978; Talbot and Hyndman, 1975; Hyndman and Talbot, 1976; Onasch, 1977; Davis and others, 1978; Myers, 1982). Hamilton (1978) and Davis and others (1978) suggested that the Paleozoic to early Mesozoic passive western margin of North America was rifted during the Mesozoic prior to the onset of subduction. More detailed study of the suture, consideration of regional plate motions, and comparison with better known tectonic settings have resulted in proposals that the Salmon River suture formed by: 1) right-lateral transpression that truncated the continental margin, translated transitional rocks to the north, and caused final accretion of the oceanic terranes to North America between 120 and 90 Ma (Lund, 1984a, b; Sutter and others, 1984;

Lund and Snee, 1988); or 2) mid-Jurassic to mid-Cretaceous collision-penetration of oceanic terranes into North America in the general present-day location of Idaho, and tectonic escape of the transitional rocks (Wernicke, 1984; Klepacki and Wernicke, 1985; Aliberti and Wernicke, 1986).

Field observations

The purpose of the field guides in this volume is to view features of the Salmon River suture along almost half of its length. Rocks of the island arc terrane are most readily observed because the highways follow rivers that are cut into such rocks. To observe the suture zone and some of the structures and metamorphic lithologies of the continental terrane, the trip will involve traverses across the structural grain into continental rocks. The traverses along the South Fork of the Clearwater River and along the Little Salmon River and its headwaters (Aliberti and Manduca, this volume) cross from high structural levels in island arc rocks into deep structural levels where large amounts of Cretaceous plutonic rock can be observed. The most revealing cross section of the metamorphic rocks, the structural geometries, and particularly the higher level units and structures in the continental rocks is along the east-trending canyon of Slate Creek (Lund, this volume). The road log from Peck to Dworshak Reservoir (Davidson, this volume) constrasts styles of earlier deformation with late-stage, suture-zone-restricted deformation and shows the complexity of lithologies of metamorphic rocks along this boundary. The field observations described in this volume help illustrate the history of accretion along the western margin of Mesozoic North America and will show the striking continuity of structures, geometries and plutonic units along this suture zone.

References

Aliberti, E., and Wernicke, B., 1986, Occluded terrane boundaries: An example from an island arc-craton contact in west-central Idaho: Eos, Transactions of the American Geophysical Union, v. 67, p. 1226-1227.

Aliberti, E., and Manduca, C. A., 1988, A transect across an island arc—continent boundary in west-central Idaho, *in* Guidebook to the Geology of Central and Southern Idaho, Paul Karl Link and William R. Hackett *(eds.)*: Idaho Geological Survey Bulletin 27, p. 99-107.

Aliberti, E., Jacobsen, S., and Wernicke, B., 1987, Nd and Sr constraints on the tectonic evolution of the arc-continent collision in west-central Idaho: Geological Society of America Abstracts with Programs, v. 19, p. 569.

Armstrong, R. L., 1975, Precambrian (1500 my old) rocks of central Idaho—The Salmon River arch and its role in cordilleran sedimentation and tectonics: American Journal of Science, v. 275-A, p. 437-467.

Armstrong, R. L., Taubeneck, W. H., and Hales, P. O., 1977, Rb-Sr and K-Ar geochronometry of Mesozoic granitic rocks and their Sr isotopic composition, Oregon, Washington and Idaho: Geological Society of America Bulletin, v. 88, p. 397-411.

Bond, J. G., 1978, Geologic map of Idaho: Idaho Bureau of Mines and Geology. Scale 1:500,000.

Brooks, H. C., and Vallier, T. L., 1978, Mesozoic rocks and tectonic evolution of eastern Oregon and western Idaho, *in* Mesozoic paleogeography of the western United States, D. G. Howell, and K. S. McDougall, *(eds.)*: Society of Economic Paleontologists and Mineralogists, Pacific Coast Section, Pacific Coast Paleogeography Symposium II, p. 133-146.

Coney, P. J., Jones, D. L., and Monger, J. W. H., 1980, Cordilleran suspect terranes: Nature, v. 288, p. 329-333.

Davidson, G. F., Snee, L. W., and Lund, K., 1988, Complex tectonic history along the island arc—continent boundary near Peck and Ahsahka, western Idaho: Geological Society of America Abstracts with Programs, v. 20, p. 411.

Davis, G. A., Monger, J. W. H., and Burchfiel, B. C., 1978, Mesozoic construction of the cordilleran "collage," central British Columbia to central California, *in* Mesozoic paleogeography of the western United States; D. G. Howell, and K. A. McDougall, *(eds.)*: Society of Economic Paleontologists and Mineralogists, Pacific Section, Pacific Coast Paleogeography Symposium II, p. 1-32.

Evans, K. V., 1986, Middle Proterozoic deformation and plutonism in Idaho, Montana and British Columbia, Belt Supergroup, *in* Belt Supergroup: A Guide to Proterozoic Rocks of Western Montana and Adjacent Areas, Sheila M. Roberts *(ed.)*:

Montana Bureau of Mines and Geology Special Publication 94, p. 237-244.

Evans, K. V., and Fischer, L. G., 1986, U-Pb geochronology of two augen gneiss terranes, Idaho—New data and tectonic implications: Canadian Journal of Earth Sciences, v. 23, p. 1919-1927.

Fleck, R. J., and Criss, R. E., 1985, Strontium and oxygen isotopic variations in Mesozoic and Tertiary plutons of central Idaho: Contributions to Mineralogy and Petrology, v. 90, p. 291-308.

Follo, M. F., 1986, Sedimentology of the Wallowa terrane, northeastern Oregon [Ph.D. dissertation]: Harvard University, Cambridge, Massachusetts, 292 p.

Gabrielse, H., 1985, Major dextral transcurrent displacements along the northern Rocky Mountain trench and related lineaments in north-central British Columbia: Geological Society of America Bulletin, v. 96, p. 1-14.

Hamilton, W., 1963, Metamorphism in the Riggins region, western Idaho: U.S. Geological Survey Professional Paper 436, 95 p.

______ 1969a, Mesozoic California and the underflow of the Pacific mantle: Geological Society of America Bulletin, v. 80, p. 2409-2430.

______ 1969b, Reconnaissance geologic map of the Riggins quadrangle, west-central Idaho: U.S. Geological Survey Miscellaneous Geologic Investigations Map I-597. Scale 1:125,000.

______ 1976, Tectonic history of west-central Idaho: Geological Society of America Abstracts with Programs v. 8, p. 378.

______ 1978, Mesozoic tectonics of the western United States, *in* Mesozoic Paleogeography of the western United States; D. G. Howell, and K. A. McDougall, *(eds.)*: Society of Economic Paleontologists and Mineralogists, Pacific Coast Section, Pacific Coast Paleogeography Symposium II, p. 33-70.

Harrison, J. E., 1972, Precambrian Belt basin of northwestern United States: Its geometry, sedimentation, and copper occurrences: Geological Society of America Bulletin, v. 83, p. 1215-1240.

Harrison, J. E., Griggs, A. B., and Wells, J. D., 1974, Tectonic features of the Precambrian Belt basin and their influence on post-Belt structures: U.S. Geological Survey Professional Paper 866, 15 p.

Hietanen, A., 1962, Metasomatic metamorphism in western Clearwater County Idaho: U.S. Geological Survey Professional Paper 344-A, 116 p.

Hoover, A. L., 1986, Transect across the Salmon River suture, South Fork of the Salmon River, western Idaho: Rare-earth element, geochemical, structural, and metamorphic study [M.S. thesis]: Oregon State University, Corvallis, 138 p.

Hoover, A. L., Lund, K., and Snee, L. W., 1985, Tectonic model for the island arc—continent suture zone, west-central Idaho: Structural and geochemical constraints: Geological Society of America Abstracts with Programs, v. 17, p. 613.

Hyndman, D. W., and Talbot, J. L., 1976, The Idaho batholith and related subduction complex: Geological Society of America, Cordilleran Section Field Guide No. 4, 15 p.

Jones, D. L., Silberling, N. J., and Hillhouse, J. W., 1978, Wrangellia—a displaced terrane in northwestern North America: Canadian Journal of Earth Sciences, v. 14, p. 2565-2577.

Klepacki, D. W., and Wernicke, B., 1985, Escape hypothesis for the Stikine block: Geological Society of America Abstracts with Programs, v. 17, p. 365.

Lund, K., 1984a, Tectonic history of a continent—island arc boundary, west-central Idaho [Ph.D. dissertation]: The Pennsylvania State University, University Park, 207 p.

______ 1984b, The continent-island arc juncture in west-central Idaho—A missing link in cordilleran tectonics: Geological Society of America Abstracts with Programs, v. 16, p. 580.

Lund, K., and Snee, L. W., 1985, Structural and metamorphic setting of the central Idaho batholith: Geological Society of America Abstracts with Programs, v. 17, p. 253.

______ 1988, Metamorphic and structural development of the continent— island arc juncture in west-central Idaho, *in* Metamorphism and Crustal Evolution, Western Conterminous United States, (Rubey Volume VII), W. G. Ernst, *(ed.)*: Prentice-Hall, New York, p. 296-331.

Lund, K., Snee, L. W., and Sutter, J. F., 1985, Style and timing of suture-related deformation in island arc rocks of western Idaho: Geological Society of America Abstracts with Programs, v. 17, p. 367.

Lund, K., Snee, L. W., and Evans, K. V., 1986, Age and genesis of precious metals deposits, Buffalo Hump district, central Idaho: Economic Geology, v. 81, p. 990-996.

Manduca, C. A., 1987, Multi-stage formation of arc-continent boundary in western Idaho: Geological Society of America Abstracts with Programs, v. 19, p. 758.

Manduca, C. A., and Kuntz, M. A., 1987, Deformed plutonic rocks on the western edge of the Idaho batholith near McCall, Idaho: Geological Society of America Abstracts with Programs, v. 19, p. 318.

Manduca, C. A., Silver, L. T., and Taylor, H. P., 1986, Study of an abrupt change in Sr and ^{18}O in granodiorite in the western border of the Idaho batholith: Eos, Transactions of the American Geophysical Union, v. 67, p. 1268.

Mortimer, N., 1986, Later Triassic, arc-related, potassic igneous rocks in the North American cordillera: Geology, v. 14, 1035-1038.

Myers, P. E., 1972, Batholith emplacement in the Harpster region, Idaho: Geological Society of America Abstracts with Programs, v. 4, p. 206.

______ 1982, Geology of the Harpster area, Idaho County, Idaho: Idaho Bureau of Mines and Geology Bulletin 25, 46 p.

Myers, P. E., and Carlson, D. H., 1982, Tectonic elements and plutonic evolution of the Mesozoic cratonic margin, South Fork of the Clearwater River, Idaho: Geological Society of America Abstracts with Programs, v. 15, p. 343.

Onasch, C. M., 1977, Structural evolution of the western margin of the Idaho batholith in the Riggins, Idaho area [Ph.D. dissertation]: The Pennsylvania State University, University Park, 196 p.

______ 1987, Temporal and spatial relations between folding, intrusion, metamorphism, and thrust faulting in the Riggins area, west-central Idaho, *in* Geology of the Blue Mountains region of Oregon, Idaho and Washington, T. L. Vallier, and H. C. Brooks, *(eds.)*: U.S. Geological Survey Professional Paper 1436, p. 139-150.

Ruppel, E. T., 1975, Precambrian Y sedimentary rocks in east-central Idaho: U.S. Geological Survey Professional Paper 889-A, 23 p.

Ruppel, E. T., O'Neill, J. M., and Lopez, D. A., 1983, Preliminary geologic map of the Dillon 1° x 2° quadrangle, Montana: U.S. Geological Survey Open-File Report 83-168. Scale 1:250,000.

Selverstone, J., Aliberti, E., and Wernicke, B., 1987, Petrologic constraints on the tectonic evolution of the arc-continent collision zone in west-central Idaho: Geological Society of America Abstracts with Programs, v. 19, p. 837.

Silberling, N. J., and Jones, D. L., 1984, Lithotectonic terrane maps of the North American cordillera: U.S. Geological Survey Open-File Report 84-523, part C, 43 p.

Snee, L. W., Lund, K., and Evans, K. V., 1984, Age and depth of formation of gold deposits using $^{40}Ar/^{39}Ar$ age-spectrum techniques: Geologic implications in central Idaho: Geological Society of America Abstracts with Programs, v. 16, p. 662.

Snee, L. W., Lund, K., and Gammons, C. H., 1985, Mineralization history of the central Idaho batholith: Importance of fracture-controlled Cretaceous activity: Geological Society of America Abstracts with Programs, v. 17, p. 265-266.

Snee, L. W., Lund, K., and Davidson, G. F., 1987, Ages of metamorphism, deformation, and cooling of juxtaposed oceanic and continental rocks near Orofino, Idaho: Geological Society of America Abstracts with Programs, v. 19, p. 335.

Snee, L. W., Sutter, J. F., Lund, K., Balcer, D. E., and Evans, K. V., 1987, $^{40}Ar/^{39}Ar$ age-spectrum data for metamorphic and plutonic rocks from west-central Idaho: U.S. Geological Survey Open-File Report 87-0052, 19 p.

Sutter, J. F., Snee, L. W., and Lund, K., 1984, Metamorphic, plutonic, and uplift history of a continent-island arc suture zone, west-central Idaho: Geological Society of America Abstracts with Programs, v. 16, p. 670-671.

Talbot J. L., and Hyndman, D. W., 1975, Consequence of subduction along the Mesozoic continental margin of the Idaho batholith: Geological Society of America Abstracts with Programs, v. 7, p. 1290.

U.S. Geological Survey, 1978, Aeromagnetic map of Idaho: U.S. Geological Survey Geophysical Investigation Map GP-919. Scale 1:500,000.

Vallier, T. L., 1977, The Permian and Triassic Seven Devils Group, western Idaho and northeastern Oregon: U.S. Geological Survey Bulletin 1437, 58 p.

Vallier, T. L., Brooks, H. C., and Thayer, T. P., 1977, Paleozoic rocks of eastern Oregon and western Idaho, *in* Paleozoic Paleogeography of the western United States, J. H. Stewart, C. H. Stevens, and A. E. Fritsche, *(eds.)*: Society of Economic Paleontologists and Mineralogists, Pacific Cost Section, Pacific Coast Paleogeography Symposium I, p. 455-466.

Wernicke, B., 1984, A working hypothesis for Jurassic and Cretaceous terrane accretion in the Pacific northwest: Eos, Transactions of the American Geophysical Union, v. 65, p. 1095.

Zen, E., 1985, Implications of magmatic epidote-bearing plutons on crustal evolution in the accreted terranes of northwestern North America: Geology, v. 13, p. 266-269.

GEOLOGY OF THE IRON DYKE MINE, BAKER COUNTY OREGON

Steven Bussey
Colorado School of Mines
Golden, Colorado 80401

Introduction

The Iron Dyke mine is a volcanogenic copper-gold deposit hosted in Permian island arc volcanic rocks. The mine is located just south of Hells Canyon on the west side of the Snake River near Oxbow, Oregon **(Figure 1)**. It was discovered in 1897 and reached peak production during World War I and through the early 1920s when it became Oregon's top copper producer. Low copper prices forced the mine to shut down in 1928. The Butler Ore Company attempted to reopen the mine in the early 1940s but was unsuccessful. In 1979, Texasgulf, Inc. purchased the property and entered into an agreement with Silver King Mines, Inc. as a joint venture. Silver King Mines acquired the mine from Texasgulf, Inc. in 1983 and has operated it intermittently since that time. From 1910 to 1928 the total recorded production was 34,967 ounces of gold, 258,489 ounces of silver and 14,417,920 pounds of copper (Brooks and Ramp, 1968). Since 1979 exploration by Texasgulf, Inc. and Silver King Mines, Inc. has resulted in the definition of additional reserves that average 2.5% copper, 0.25 ounces per ton gold and 0.5 ounces per ton silver (B. E. Wise, personal communication, 1983).

Regional geologic setting

The Iron Dyke mine is located in the southeast part of the Permian-Triassic Wallowa terrane **(Figure 1)**, one of four pre-Tertiary allochthonous terranes recognized in the Blue Mountains province of eastern Oregon and western Idaho (Silberling and others, 1984). The province formed in the mid-Pacific at a latitude of about 18° north or south (Hillhouse and others, 1982) during the Early Permian and appears to have been separate from the allochthonous Wrangellia terrane which apparently lay to the south (Pessango and Blome, 1986; Hillhouse and others, 1982; Debiche and others, 1987; Stanley, 1986). The four terranes that make up the Blue Mountains province are, from northwest to southeast, the Wallowa, Baker, Izee and Olds Ferry terranes. The Wallowa terrane consists of a Late Paleozoic oceanic arc basement complex overlain by Permian and Triassic volcanic rocks, clastic sedimentary rocks and limestone (Vallier, 1977; Brooks and Vallier, 1978; Walker, 1986; LeAnderson and Richey, 1985). The four terranes were assembled west of the North American continent by 160 Ma and were accreted in the Columbia embayment about 120 Ma (Sutter and others, 1984). Following a period of erosion, most of the province was covered by Columbia River Basalt flows which were erupted in Miocene time. Recent downcutting by the Snake River and its tributaries has exposed the underlying Blue Mountains province.

Wallowa terrane

The Wallowa terrane represents the product of Early Permian to Late Triassic arc volcanism that resulted from subduction of oceanic crust since Pennsylvanian time (Walker, 1986). In the southeastern part of the arc, near the Iron Dyke mine, the overlying volcanic rocks are the Permian Windy Ridge and Hunsaker Creek formations and the Triassic Wild Sheep Creek and Doyle Creek formations (Vallier, 1977).

The Permian Windy Ridge and Hunsaker Creek formations **(Figure 2)** constitute a bimodal basalt-rhyolite volcanic pile with minor andesite and abundant clastic sedimentary rocks and limestone.

Structural geology

In the mine area **(Figure 3)** the rocks have been folded into a series of NE-SW-trending anticlines and synclines. A syncline is the most prominent structure on the mine property and plunges 20-30 degrees

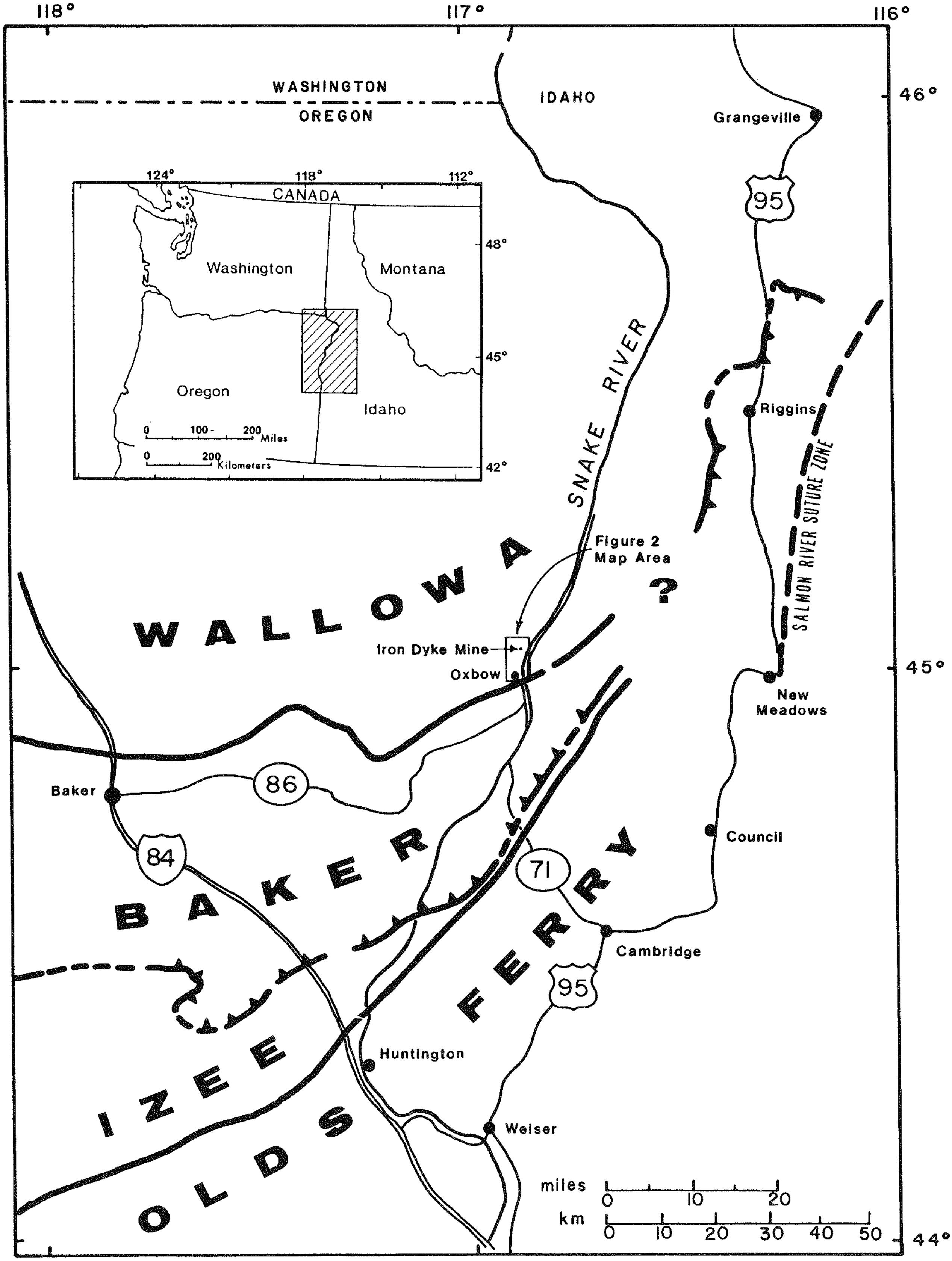
118°
117°
116°
46°
45°
44°
WASHINGTON
OREGON
IDAHO
Grangeville
95
124°
118°
112°
CANADA
48°
45°
42°
Washington
Montana
Oregon
Idaho
0 100 200 Miles
0 200 Kilometers
SNAKE RIVER
Riggins
SALMON RIVER SUTURE ZONE
Figure 2 Map Area
?
WALLOWA
Iron Dyke Mine
Oxbow
New Meadows
Baker
86
84
BAKER
71
Council
Cambridge
95
FERRY
IZEE
OLDS
Huntington
Weiser
miles 0 10 20
km 0 10 20 30 40 50

Figure 1—Map showing location of the Iron Dyke mine near Oxbow, Oregon. Also shown are the boundaries of the allochthonous Wallowa, Baker, Izee and Olds Ferry terranes in eastern Oregon and western Idaho. Terrane boundaries *from* Brooks and Vallier (1978). Terrane names *from* Silberling and others (1984).

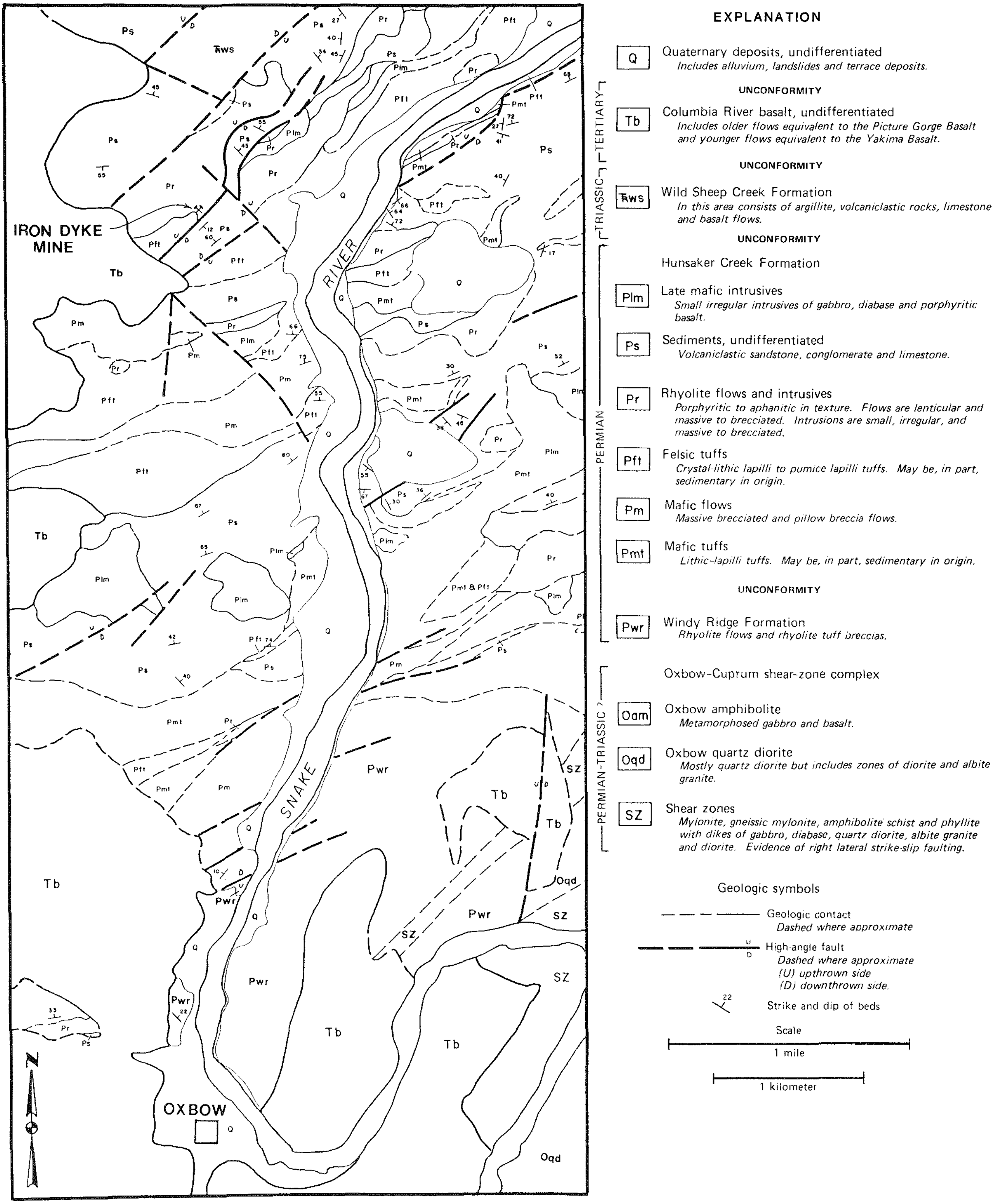
IRON DYKE MINE
OXBOW
SNAKE RIVER
EXPLANATION
Q Quaternary deposits, undifferentiated
Includes alluvium, landslides and terrace deposits.
UNCONFORMITY
Tb Columbia River basalt, undifferentiated
Includes older flows equivalent to the Picture Gorge Basalt and younger flows equivalent to the Yakima Basalt.
UNCONFORMITY
TERTIARY
TRIASSIC
₸ws Wild Sheep Creek Formation
In this area consists of argillite, volcaniclastic rocks, limestone and basalt flows.
UNCONFORMITY
Hunsaker Creek Formation
Plm Late mafic intrusives
Small irregular intrusives of gabbro, diabase and porphyritic basalt.
Ps Sediments, undifferentiated
Volcaniclastic sandstone, conglomerate and limestone.
Pr Rhyolite flows and intrusives
Porphyritic to aphanitic in texture. Flows are lenticular and massive to brecciated. Intrusions are small, irregular, and massive to brecciated.
Pft Felsic tuffs
Crystal-lithic lapilli to pumice lapilli tuffs. May be, in part, sedimentary in origin.
Pm Mafic flows
Massive brecciated and pillow breccia flows.
Pmt Mafic tuffs
Lithic-lapilli tuffs. May be, in part, sedimentary in origin.
UNCONFORMITY
Pwr Windy Ridge Formation
Rhyolite flows and rhyolite tuff breccias.
PERMIAN
Oxbow-Cuprum shear-zone complex
Oam Oxbow amphibolite
Metamorphosed gabbro and basalt.
Oqd Oxbow quartz diorite
Mostly quartz diorite but includes zones of diorite and albite granite.
SZ Shear zones
Mylonite, gneissic mylonite, amphibolite schist and phyllite with dikes of gabbro, diabase, quartz diorite, albite granite and diorite. Evidence of right lateral strike-slip faulting.
PERMIAN-TRIASSIC ?
Geologic symbols
Geologic contact
Dashed where approximate
High-angle fault
Dashed where approximate
(U) upthrown side
(D) downthrown side.
Strike and dip of beds
Scale
1 mile
1 kilometer
N

Figure 2—Geologic map of the Snake River Canyon, Idaho-Oregon. The location of units in the Oxbow-Cuprum shear-zone complex are *from* Vallier (1974).

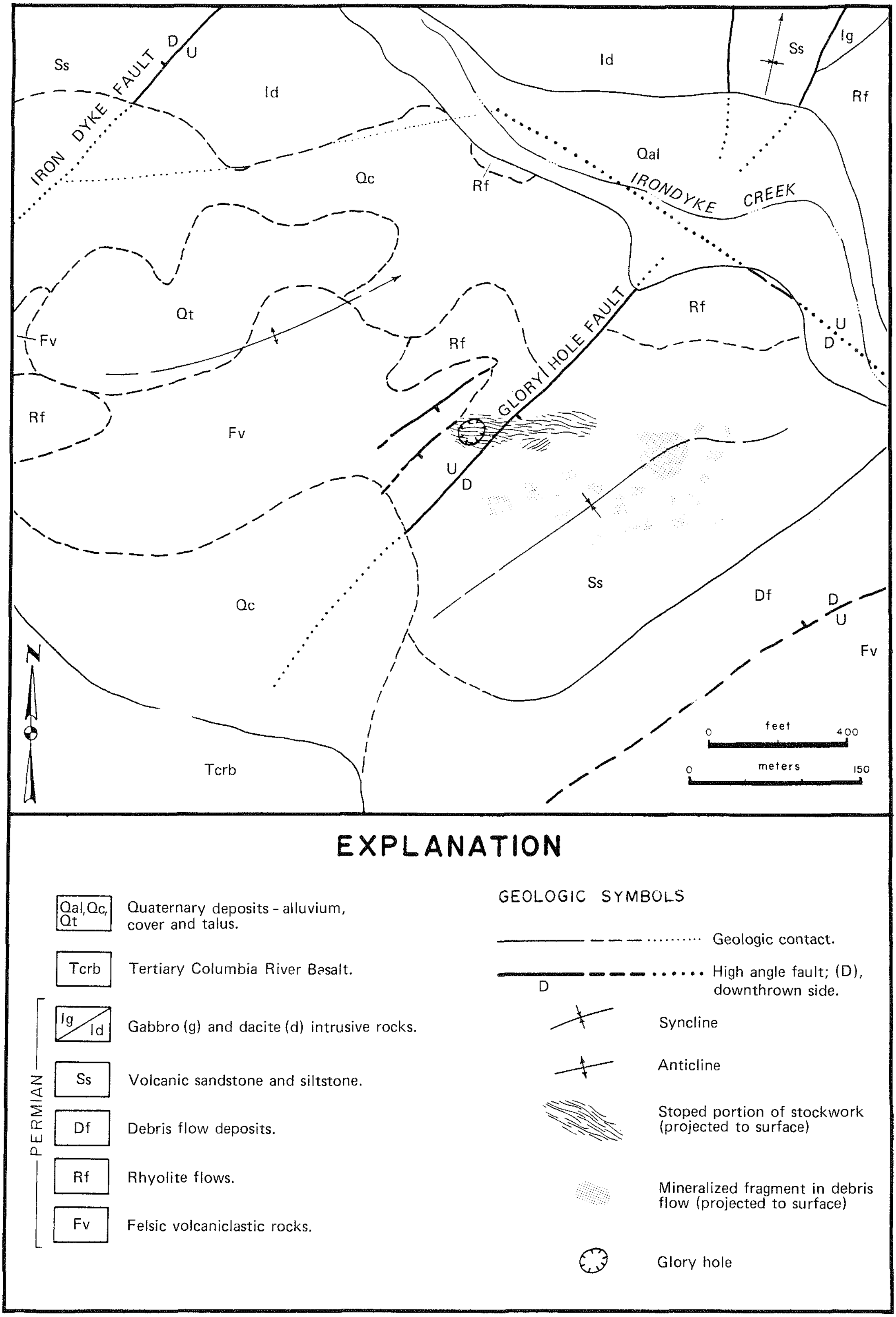
Ss
D
U
IRON DYKE FAULT
Id
Id
Ss
Ig
Rf
Qal
Qc
Rf
IRONDYKE CREEK
Qt
Fv
Rf
Rf
GLORY HOLE FAULT
U
D
Rf
Fv
U
D
Ss
Df
D
U
Fv
Qc
Tcrb
N
feet
0
400
meters
0
150
EXPLANATION
Qal, Qc, Qt
Quaternary deposits - alluvium, cover and talus.
Tcrb
Tertiary Columbia River Basalt.
PERMIAN
Ig / Id
Gabbro (g) and dacite (d) intrusive rocks.
Ss
Volcanic sandstone and siltstone.
Df
Debris flow deposits.
Rf
Rhyolite flows.
Fv
Felsic volcaniclastic rocks.
GEOLOGIC SYMBOLS
Geologic contact.
D
High angle fault; (D), downthrown side.
Syncline
Anticline
Stoped portion of stockwork (projected to surface)
Mineralized fragment in debris flow (projected to surface)
Glory hole

Figure 3—Geologic map in the vicinity of the Iron Dyke mine. The locations of stockwork and mineralized fragments are projected to the surface from depth. The stockwork is exposed in the "glory hole" at the surface from depth.

northeast (R. S. Fredrickson, written communication, 1977). The youngest rock exposed in the syncline is a sequence of fine-grained volcanic sandstones. A broad anticline northwest of the syncline exposes a sequence of felsic-bedded tuffs and volcaniclastic rocks along its axis. Both fold structures are bounded by NE-SW-trending faults. The faults are vertical to steeply dipping and show normal displacement. The Glory Hole fault zone, which separates the syncline and anticline, is a complex series of closely spaced normal faults that dip steeply to the southeast. The northwest side of the anticline is bounded by the Iron Dyke fault, a normal fault that dips steeply to the west. Younger northwest-southeast faults are sharp and have displacement of 10 to 50 meters. Other faults in the area are difficult to identify due to poor exposure, abrupt lithologic changes, and a lack of reliable marker horizons.

Mineralization

Mineralization at the Iron Dyke mine **(Figure 3)** can be divided into two fundamental styles which are spatially and morphologically distinct (Stevens, 1981). Stockwork mineralization is present immediately northwest of the Glory Hole fault where quartz-sulfide veins and associated alteration form a pipe-like body that cuts through a rhyolite flow and underlying felsic volcaniclastic rocks. Southeast of the Glory Hole fault, mineralization occurs as fragments and clasts in a debris flow deposit. The fragments of mineralization range in size from pebbles to enormous boulders and consist of stockwork as well as other types of mineralization not recognized in the stockwork.

Quartz-sulfide veins

Quartz-pyrite-chalcopyrite veins **(Figure 4)** form a stockwork that developed in highly silicified and altered rhyolite and underlying felsic volcaniclastic rocks **(Figure 4)**. Sphalerite and galena are present in minor amounts, with traces of tetrahedrite, bornite and gold. Veins are epithermal in character and typically range in size from a few millimeters to 10 centimeters in width with one observed vein a meter in width. They consist of early euhedral quartz with later crustiform banded quartz and sulfides and late euhedral quartz in vugs and open cavities.

The original near-surface workings have caved and subsided, forming a small "glory hole." Early mining stoped a lense-shaped body up to two meters wide within the vein system that dipped 60 degrees east and extended to a depth of 125 meters below the "glory hole" (Swartley, 1914). High-grade ore from this body was reported to contain 15 to 20% copper (Lindgren, 1901). At a point about 130 meters below the "glory hole," stockwork mineralization is truncated by the Glory Hole fault. The continuation of the stockwork zone presumably occurs in the hanging wall at depth in the Stewart syncline.

Alteration is centered on the stockwork and consists of a central chloritic zone confined to the stockworks, and an outer sericitic zone that occurs in the upper part of the stockwork and extends over an area 300 x 1000 meters that is elongated in a northeast-southwest direction.

Another body of quartz-sulfide veins is located about 350 meters west of the "glory hole" **(Figure 3)**. Mineralization and alteration in this body are similar to that at the "glory hole," but are less intense and less extensive. Widely spaced quartz veins and weak alteration can also be found along the ridge between the two vein systems.

Mineralized fragments in the Iron Dyke lahar

The greatest production at the mine has been from fragments in the Iron Dyke lahar. These fragments are typically silicified and display stockwork mineralization consisting primarily of quartz, pyrite, chalcopyrite and sphalerite. They are thought to have been derived from the stockwork body and transported into an adjacent basin along with other coarse-grained debris flows. In addition to the stockwork fragments, other types of mineralization are present which are not found in the "glory hole" area. These include massive sphalerite, massive chalcopyrite, chalcopyrite-chlorite breccias, hematitic quartz breccias, and massive hematitic barite **(Figures 5, 6)**. Although present in only minor amounts, fragments of these types are found throughout the Iron Dyke lahar along with the stockwork fragments.

The size and distribution of known fragments and their spatial relationship to the original stockwork ore body is shown in **(Figure 3)**. Some fragments are unusually large, from tens of meters in diameter to a fragment reported to contain 150,000 tons of ore (Stevens, 1981). They have sharp contacts with the lahar and are quite angular. Their presence in a debris flow that originated in the vicinity of the stockwork implies uplift and erosion of the stockwork shortly after its formation. The intimate spatial association between the various types of ore fragments found in the Iron Dyke lahar suggests a

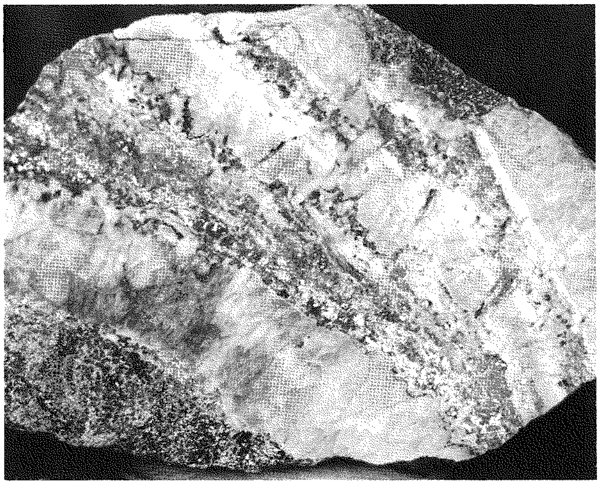

Figure 4—Quartz-pyrite-chalcopyrite vein with dark green chlorite halo from the stockwork. The vein shows early euhedral rose quartz along its walls, a brecciation event, followed by deposition of fine-grained sulfides, chlorite and quartz.

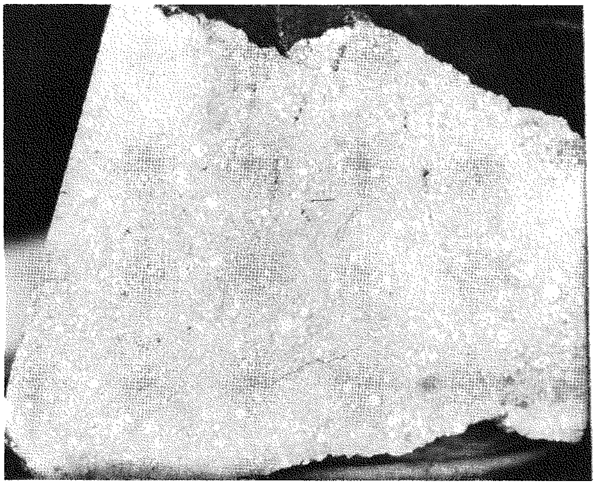

Figure 5—Massive chalcopyrite-pyrite collected from the Iron Dyke lahar shows clastic texture with large chalcopyrite-pyrite fragments in a matrix of fine-grained pyrite and chalcopyrite.

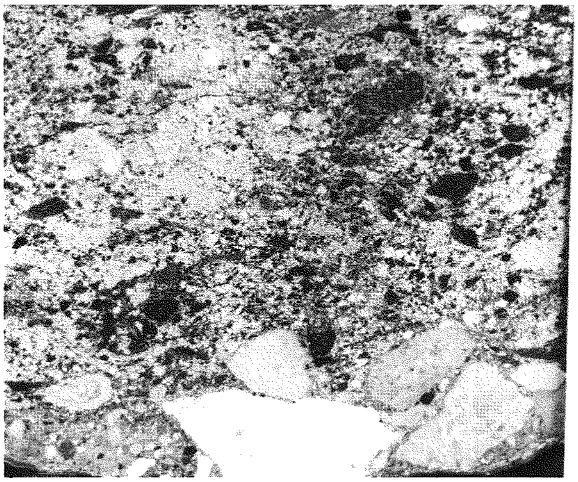

Figure 6—Chalcopyrite-pyrite-chlorite breccia collected from the Iron Dyke lahar. Elongate fragments of chlorite and pyrite-chalcopyrite mineralization exhibit subparallel alignment.

common origin for all of the fragments. Mineralized fragments, whose character is distinctly different from that of the stockwork zone, probably represent those parts of the ore system vertically above the exposed stockwork zone. The position of these ore types (e.g., massive sphalerite, massive chalcopyrite-pyrite, hematitic quartz breccias and massive hematitic barite) above the exposed stockwork is consistent with the present understanding of vertical zonation in massive sulfide ore systems.

Conclusions

Footwall rocks consist of felsic lavas intruded into, and extruded on top of, previously deposited pyroclastic material. As the eruptive center expanded felsic lavas were intruded into, and extruded on top of, previously deposited pyroclastic material. Subsequent hydrothermal activity resulted in widespread alteration, brecciation and silicification of these felsic flows and small intrusives. Fracturing of the silicified zones focused hydrothermal activity into open channelways and formed the veins now exposed in the "glory hole" (**Figure 7A**). Normal movement along the fracture system created a fault scarp that uplifted part of the deposit and exposed it to more oxidizing conditions (**Figure 7B**). Movement along the fault zone enhanced hydrothermal activity and formed complex breccias by repeated fracturing and resealing. Massive sulfides that formed at the rock-water interface periodically slumped off of the vent area to

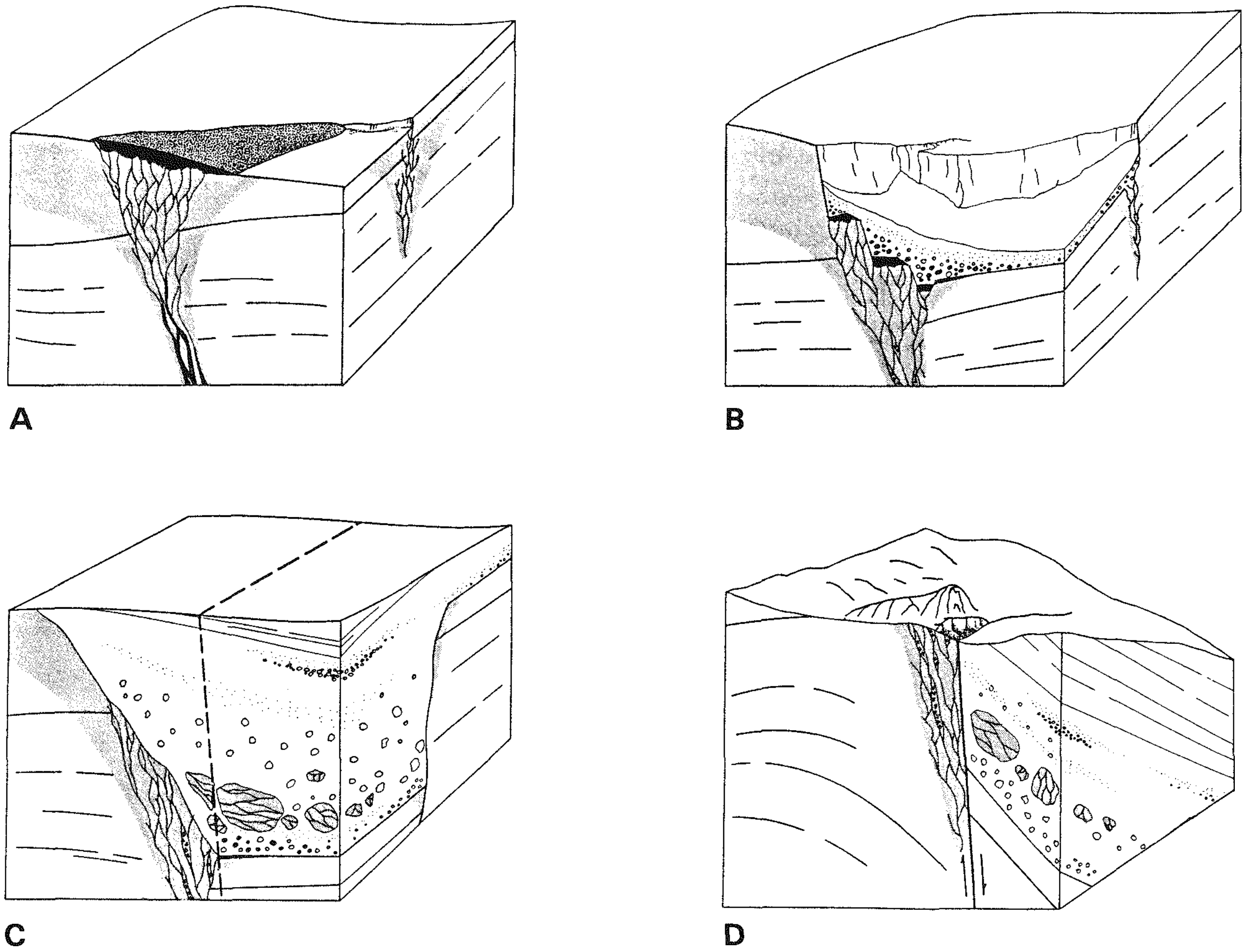

Figure 7—Schematic diagrams illustrating the geologic history of the Iron Dyke deposit. (A), initial hydrothermal activity; (B), movement along stockwork fracture zone and formation of transported sulfides; (C), continued uplift and collapse of stockwork and burial by fine-grained sediments; (D), present configuration following movement on the Glory Hole fault.

form massive sulfides with clastic textures. Volcanic debris that accumulated along the base of the scarp was altered by venting hydrothermal fluids. When the scarp became unstable, it slumped, disrupted the uplifted part of the deposit, and formed a debris flow rich in mineralized fragments. Continued sedimentation buried the fragments with coarse conglomerates and associated fine-grained sediments **(Figure 7C)**. Additional faulting and folding occurred during accretion of the Wallowa-Seven Devils volcanic arc to the North American craton **(Figure 7D)**. Erosion has removed the mineralization that must have extended above the level of the stockwork now exposed at the "glory hole."

Acknowledgements

The author would like to thank the Fogarty Fellowship, Coulter Scholarship, and the Geology Department of the Colorado School of Mines for support during this study. The guidance of Dr. Jim LeAnderson is particularly appreciated. In addition, grateful acknowledgement is made to Stuart Havenstrite and the management of Silver King Mines, Inc. for access to drill core and underground workings as well as field support during the summers of 1984, 1985 and 1986. Particularly helpful were discussions of Iron Dyke geology with exploration manager Carl Pesicio and modification by the author of previous mapping **(Figure 3)** supplied by geologist B. E. Wise.

References

Brooks, H. C., and Ramp, Len, 1968, Gold and silver in Oregon: Oregon Department of Geology and Mineral Industries Bulletin 61, 337 p.

Brooks, H. C. and Vallier, T. L., 1978, Mesozoic rocks and tectonic evolution of eastern Oregon and western Idaho, *in* Mesozoic Paleogeography of the Western United States, D. G. Howell, and K. A. McDougall, *(eds.):* Society of Economic Paleontologists and Mineralogists, Pacific Coast Section, Pacific Coast Paleogeography Symposium II, p. 133-145.

Debiche, M. G., Cox, Allan, and Engebretson, D. C., 1987, The motion of allochthonous terranes across the North Pacific basin: Geological Society of America Special Paper 207, 49 p.

Hillhouse, J. W., Gromme, C. S., and Vallier, T. L., 1982, Geomagnetism and Mesozoic tectonics of the Seven Devils volcanic arc in northeastern Oregon: Journal of Geophysical Research, v. 87, p. 3777-3794.

LeAnderson, P. J., and Richie, Scott, 1985, Geology of the Wallowa-Seven Devils volcanic (island) arc terrane between the Snake and Salmon rivers near Lucile, Idaho: U.S. Geological Survey Open-File Report 85-0611, 30 p.

Lindgren, W., 1901, The gold belt of the Blue Mountains of Oregon: U.S. Geological Survey Annual Report No. 22, p. 560-576.

Pessango, E. A., Jr., and Blome, C. D., 1986, Faunal affinities and tectogenesis of Mesozoic rocks in the Blue Mountains province of eastern Oregon and western Idaho, *in* Geology of the Blue Mountains region of Oregon, Idaho and Washington: Geological implications of Paleozoic and Mesozoic paleontology and biostratigraphy, Blue Mountains province, Oregon and Idaho, T. L. Vallier, and H. C. Brooks, *(eds.):* U.S. Geological Survey Professional Paper 1435, p. 549-579.

Silberling, N. J., Jones, D. L., Blake, Jr., M. C., and Howell, D. G., 1984, Lithotectonic terrane maps of the North American cordillera: U.S. Geological Survey Open-File Report 84-523.

Stanley, G. D., Jr., 1986, Late Triassic coelenterate faunas of western Idaho and northeastern Oregon: Implications for biostratigraphy and paleogeography, *in* Geology of the Blue Mountains region of Oregon, Idaho and Washington: Geological implications of Paleozoic and Mesozoic paleontology and biostratigraphy, Blue Mountains province, Oregon and Idaho, T. L. Vallier, and H. C. Brooks, *(eds.):* U.S. Geological Survey Professional Paper 1435, p. 53-58.

Stevens, M. G., 1981, Geology of the Iron Dyke mine, Homestead, Oregon [M.S. thesis]: University of Utah, Salt Lake City, 78 p.

Sutter, J. F., Snee, L. W., and Lund, Karen, 1984, Metamorphic, plutonic and uplift history of a continent-island arc suture zone, west-central Idaho: Geological Society of America Abstracts with Programs, v. 16, no. 6, p. 670-671.

Swartley, A. M., 1914, Ore deposits in northeastern Oregon: Oregon Bureau of Mines and Geology of Mineral Resources, v. 1, 229 p.

Vallier, T. L., 1974, A preliminary report on the geology of part of the Snake River Canyon, Oregon and Idaho: Oregon Department of Geology and Mineral Industries Geological Map Series No. 6, 15 p.

______ 1977, The Permian and Triassic Seven Devils group, western Idaho and northeastern Oregon: U.S. Geological Survey Bulletin 1437, 58 p.

Walker, N. W., 1986, U/Pb geochronology and petrologic studies in the Blue Mountains terrane, northeastern Oregon and westernmost-central Idaho: Implications for pre-Tertiary tectonic evolution [Ph.D. dissertation]: University of California, Santa Barbara, 214 p.

©DIANE NUGENT 1988

INDEX MAP TO FIELD GUIDES

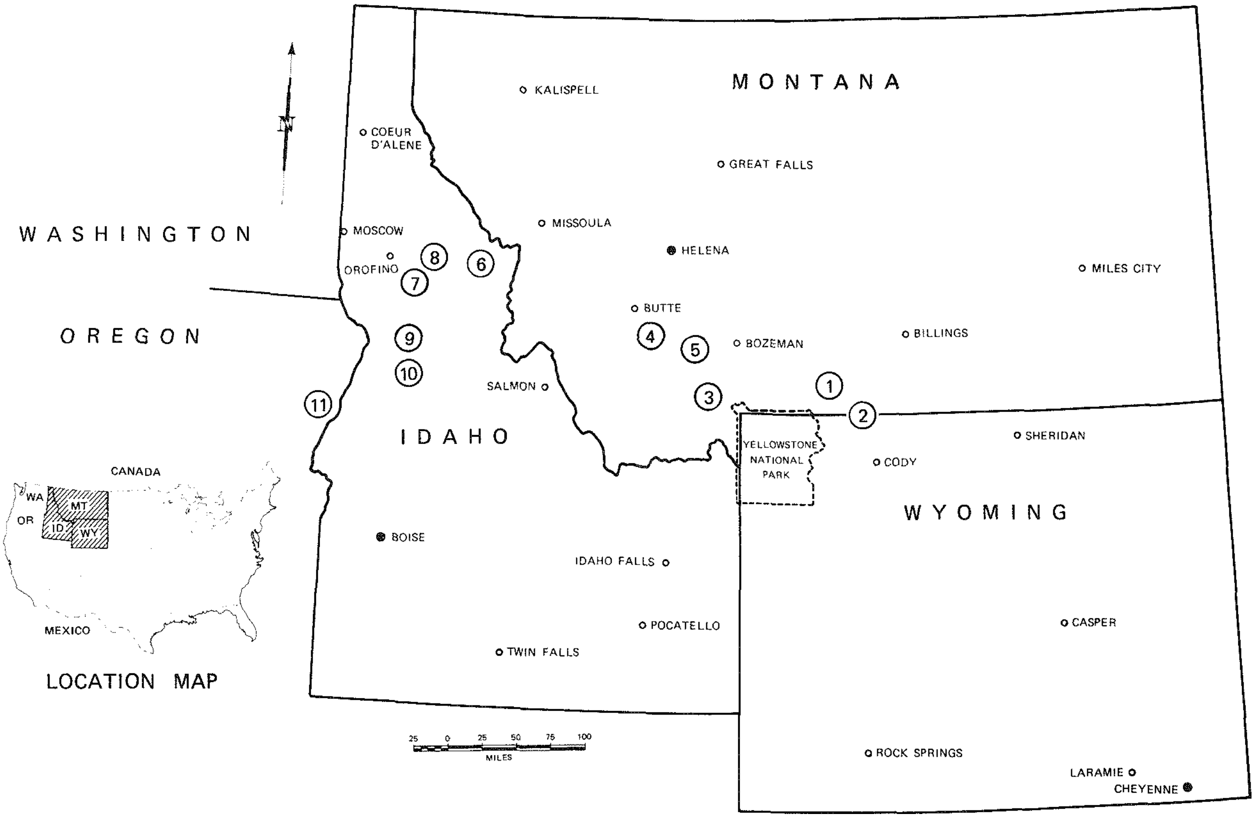
MONTANA
KALISPELL
COEUR D'ALENE
GREAT FALLS
WASHINGTON
MOSCOW
MISSOULA
HELENA
OROFINO
MILES CITY
OREGON
BUTTE
BOZEMAN
BILLINGS
SALMON
IDAHO
YELLOWSTONE NATIONAL PARK
SHERIDAN
CODY
WYOMING
BOISE
IDAHO FALLS
POCATELLO
CASPER
TWIN FALLS
ROCK SPRINGS
LARAMIE
CHEYENNE
CANADA
WA
MT
OR
ID
WY
MEXICO
LOCATION MAP
1
2
3
4
5
6
7
8
9
10
11
25 0 25 50 75 100
MILES

Field guides

An overview of some of the Precambrian crystalline rocks of southwestern Montana and northwestern Wyoming

(1) Field guide to the Mountain View and West Fork areas, Stillwater Complex, Montana .... *I. S. McCallum* 121
(2) Field guide to an Archean transect, eastern Beartooth Mountains, Montana-Wyoming .... *Paul A. Mueller and Joseph L. Wooden* 131
(3) Field guide to pre-Beltian geology of the southern Madison and Gravelly ranges, southwest Montana .... *Eric A. Erslev* 141
(4) Field guide to the Highland Mountains, southwest Montana .... *J. Michael O'Neill* 151
(5) Field guide to mesoscopic features in the LaHood Formation, Jefferson Canyon area, southwest Montana .... *Sharon E. Lewis* 155

An overview from the continent into the Mesozoic suture zone, central Idaho and northeastern Oregon

(6) Field guide to a section through the northern Idaho batholith and surrounding high-grade metamorphic rocks .... *Donald W. Hyndman and David A. Foster* 159
(7) Field guide to deformation and sense of displacement in mylonitic rocks near Orofino, Idaho .... *Luther M. Strayer, IV* 165
(8) Field guide to variations in lithologies and deformation styles of metamorphic and plutonic rocks west of Orofino, Idaho .... *Gary F. Davidson* 171
(9) Field guide to a traverse (Slate Creek) across the Salmon River suture zone, west-central Idaho ..... *Karen Lund* 175
(10) Field guide to a transect across an island-arc continent boundary in west-central Idaho .... *Elaine A. Aliberti and Cathryn Allen Manduca* 181
(11) Field guide to the Iron Dyke mine, Baker County Oregon .... *Steven Bussey* 191

FIELD GUIDE TO THE MOUNTAIN VIEW AND WEST FORK AREAS, STILLWATER COMPLEX, MONTANA

I. S. McCallum
Department of Geological Sciences
University of Washington
Seattle, Washington 98195

Introduction

The Mountain View area of the Stillwater Complex, which is exposed on the west side of the Stillwater River valley, contains a well exposed, easily accessible section through the Ultramafic series. In this area the ultramafic cumulates have, for the most part, escaped the serpentinization common in other parts of the complex. The Basal series rocks and the lowermost ultramafic cumulates, however, have suffered extensive alteration. The hornfels and the sill/dike complex are reasonably fresh and well exposed in the Verdigris Creek area, the site of intensive exploration for Cu/Ni sulfides. The Banded series rocks are well exposed along the mine road leading to the abandoned Mouat chromite mine, although only Lower Banded series cumulates are present in this area. Extensive geological, exploration and mining efforts over the better part of a century have resulted in the accumulation of an enormous amount of information, much of which is summarized by Page and others (1985). Among the many contributions to the geology of this area, notable are those of Jackson (1961), Page (1977, 1979), Zientek (1983), and Raedeke and McCallum (1984).

The rocks of the complex are bounded by the Bluebird thrust on the south and the Horseman thrust on the north (**Figure 1**). A major fault within the complex, the Lake fault, separates the block containing the Ultramafic and Basal series (Mouat block) from the block containing the Banded series. The strike of the layering in the Banded series is conformable with that in the rest of the complex whereas the strike of the layering in the Ultramafic series indicates that the Mouat block has been rotated about 90 degrees relative to the rest of the intrusion. Several high-angle faults, most notably the Verdigris fault, have caused small offsets in the rocks of the Mouat block. In the northern block, the South Prairie fault has locally caused repetition or loss of part of the Lower Banded series section. In the eastern part of the map area, Late Archean quartz monzonite has intruded the hornfels and sill/dike complex. Several mafic dikes chilled against the complex and presumed to be of Proterozoic age, cut the complex and the quartz monzonite. Two large landslides cover much of the area between the Lake fault and the Horseman thrust.

Parts of the Ultramafic series and Lower Banded series are exposed along the West Fork of the Stillwater River between the Bluebird thrust on the south and the Horseman thrust on the north (Mann and others, 1985). Olivine cumulates of the lowermost Ultramafic series, containing chromitite seams A and B, are exposed close to the trail about 2 miles southwest of the parking lot which marks the end of the road. In the prominent cliffs north and west of the parking lot, a section through the Lower Banded series is very well exposed. The OB-I zone, which contains the J-M/Howland reef, is fully developed in this area. This area is of historical interest since it contains the first outcrop discoveries of platinum group element (PGE) mineralization (1974). The portal of the West Fork adit is visible at the base of the cliffs north of the river.

Field guide

Mountain View area (Stops 1-8)

The field guide begins at the end of the Mouat mine road (**Figure 1**), 6.4 miles from the main office of the Stillwater Mining Company. Stop 1 is located at the end of the road near the No. 2 portal of the Mouat chrome mine at an elevation of 7,460 feet.

Stop 1: *Cyclic units in the Peridotite zone.* This stop involves a traverse along the Mountain View

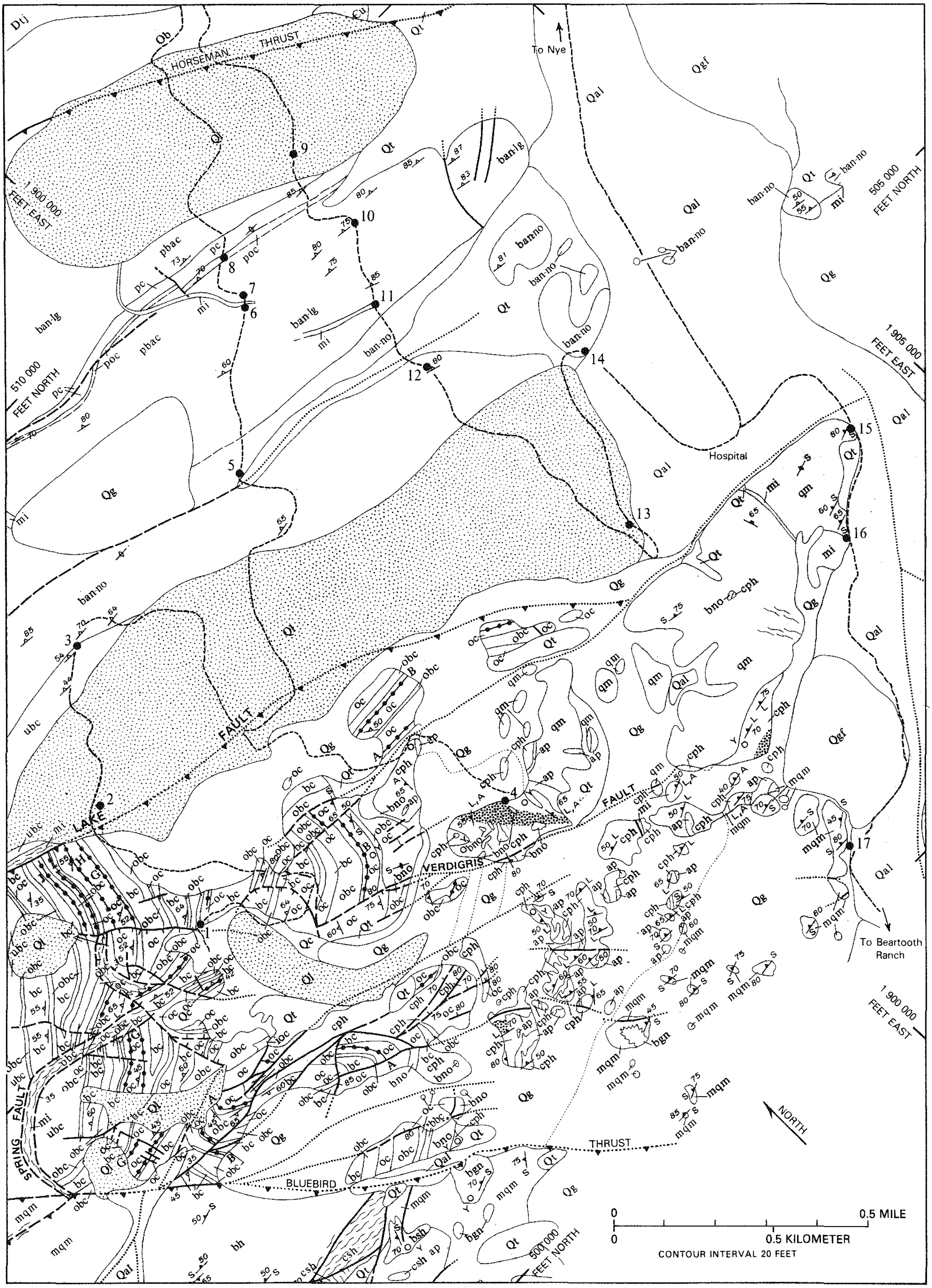
HORSEMAN THRUST
To Nye
Hospital
LAKE
FAULT
VERDIGRIS
FAULT
SPRING FAULT
BLUEBIRD
THRUST
To Beartooth Ranch
1 900 000 FEET EAST
510 000 FEET NORTH
505 000 FEET NORTH
1 905 000 FEET EAST
1 900 000 FEET EAST
500 000 FEET NORTH
NORTH
0
0.5 MILE
0
0.5 KILOMETER
CONTOUR INTERVAL 20 FEET
1
2
3
4
5
6
7
8
9
10
11
12
13
14
15
16
17
Qal
Qgf
Qg
Qt
Ql
ban-lg
ban-no
pbac
poc
pc
mi
ubc
obc
oc
bc
cph
ap
qm
mqm
bno
bgn
bh
csh
Dtj
Ob
Cu

Figure 1—Geologic map of the Mountain View area and the west side of the Stillwater River valley, showing stops discussed in this guide. *Reproduced from* Page and others (1985), which was *modified from* Page and Nokleberg (1974).

EXPLANATION

Age			Map unit	Description
QUATERNARY			Qal Qt Qc	ALLUVIUM; TALUS DEPOSITS; COLLUVIUM
			Ql Qgf	LANDSLIDE DEPOSITS; GLACIAL FAN DEPOSITS
			Qg	GLACIAL DEPOSITS
DEVONIAN			Dtj	THREE FORKS SHALE AND JEFFERSON DOLOMITE
ORDOVICIAN			Ob	BIGHORN DOLOMITE
CAMBRIAN			€u	UNDIVIDED LIMESTONE AND SHALE
PRECAMBRIAN			mi	MAFIC INTRUSIVE ROCKS
			ap	APLITE
			mqm	MEDIUM-GRAINED QUARTZ MONZONITE
			qm	COARSE-GRAINED QUARTZ MONZONITE
	Stillwater Complex	Banded series	ban-lg	LOWER GABBRO ZONE—-poc, plagioclase-olivine cumulate; -pc, plagioclase cumulate; -pbac, plagioclase-bronzite-augite cumulate
			ban-no	NORITE ZONE
		Ultramafic series	ubc	BRONZITITE ZONE
			bc obc oc	PERIDOTITE ZONE—-bc, bronzite cumulate; -obc, olivine-bronzite cumulate; -oc, olivine cumulate; line and balls, chromite seam
		Basal series	bbc	BASAL BRONZITE CUMULATE ZONE
			bno	BASAL NORITE ZONE
			cph bh csh	HORNFELS—cph, cordierite-orthopyroxene biotite hornfels; stippled pattern, diamictite; csh, chlorite schist; bh, biotite-cordierite hornfels
			bgn ggn bsh	REGIONALLY METAMORPHOSED ROCKS—ggn, granitic gneiss; bsh, biotite schist; bgn, biotite gneiss

Symbol	Explanation
———	CONTACT—Approximately located, dotted where concealed. Y, younger intrusive rock; O, wallrock
———	FAULT—Showing dip, dashed where approximately located or inferred; dotted where concealed
▲▲▲	THRUST FAULT—Showing dip, dashed where approximately located or inferred; dotted where concealed; sawteeth on upper plate
≈≈≈	SHEAR ZONE
┴┴┴┴┴	LOW-ANGLE GRAVITY FAULTS—Dashed where approximately located. Hachures on downthrown side
	Planar and linear features—Symbols may be combined
	STRIKE AND DIP OF CUMULATE LAYERS
60	Inclined
—◇—	Vertical
	STRIKE AND DIP OF METAMORPHIC FOLIATION
55	Inclined
—◆—	Vertical
	A, axial plane of minor fold
	S, parallel inequant minerals
	L, discontinuous lenses of varying composition
	STRIKE AND DIP OF JOINTS
50	Inclined
● 2	STOPS—Described in text
- - - - -	ROAD

cliffs following a trail worn by countless geologists. The trail crosses two complete cyclic units and the lower part of a third, and covers the stratigraphic interval from 770 to about 1,000 meters as shown in Figure 3 (McCallum, this volume). The trail and the units traversed are shown in **Figure 2.** A steel post marks the beginning of the traverse. A section through the first cyclic unit was studied in detail by Raedeke and McCallum (1984) and is shown here as **Figure 3.**

The first rock type encountered is an olivine cumulate containing minor chromite. Bronzite occurs as oikocrysts up to 5 cm in diameter. This unit is overlain by a relatively thin olivine-bronzite cumulate with a distinctive, knobbly, weathered surface. Thin section analysis reveals that the ratio of cumulus oli-

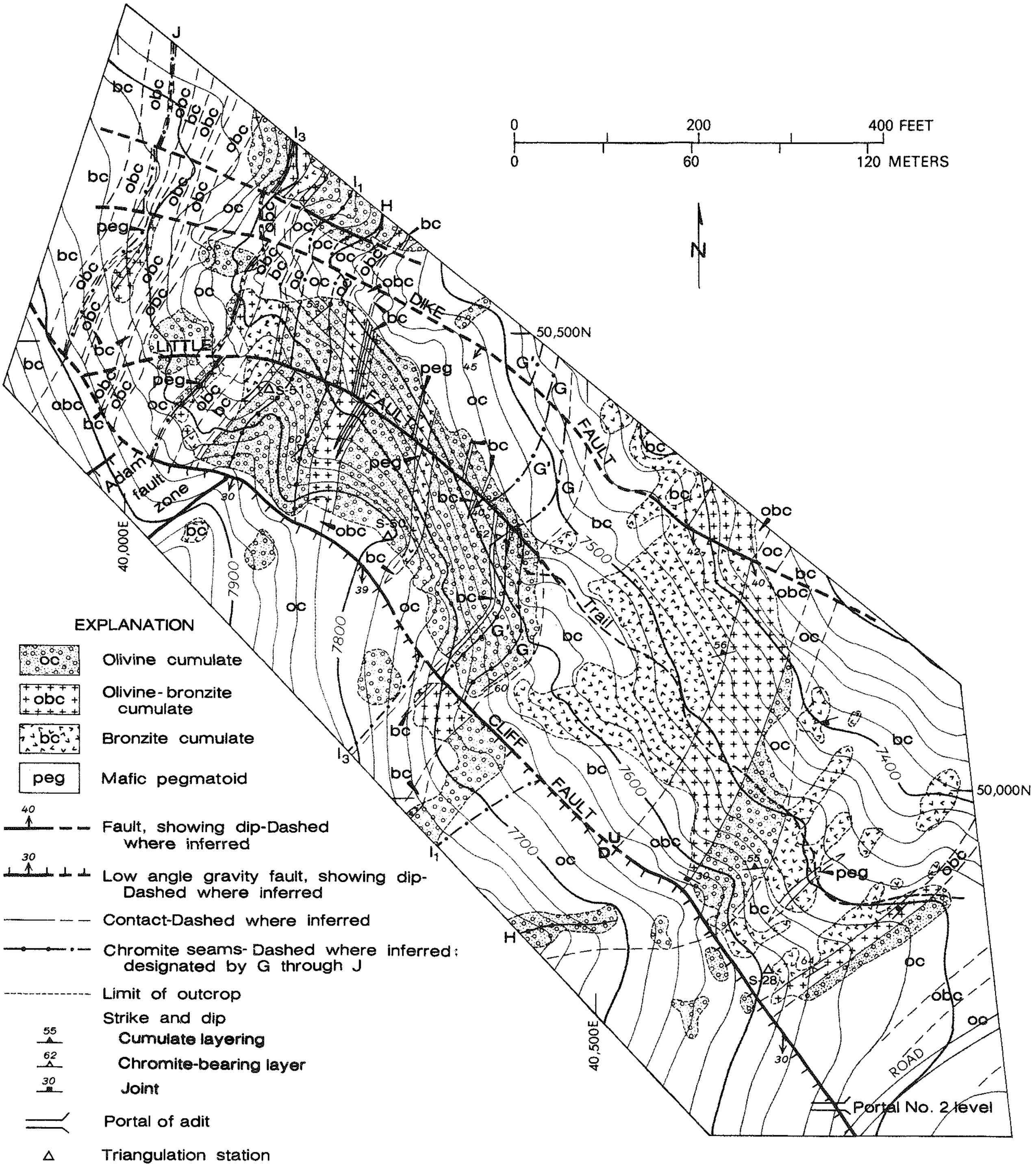
0
200
400 FEET
0
60
120 METERS
N
50,500N
50,000N
40,000E
40,500E
LITTLE
DIKE
FAULT
Adam
fault
zone
CLIFF
FAULT
Trail
ROAD
Portal No. 2 level
J
H
G
G'
I3
I1
U
D
S-51
S-50
S-28
7900
7800
7700
7600
7500
7400
oc
obc
bc
peg
EXPLANATION
oc Olivine cumulate
obc Olivine-bronzite cumulate
bc Bronzite cumulate
peg Mafic pegmatoid
40 Fault, showing dip-Dashed where inferred
30 Low angle gravity fault, showing dip-Dashed where inferred
Contact-Dashed where inferred
Chromite seams-Dashed where inferred; designated by G through J
Limit of outcrop
Strike and dip
55 Cumulate layering
62 Chromite-bearing layer
30 Joint
Portal of adit
△ Triangulation station

Figure 2—Geologic map of part of the Ultramafic series exposed in the cliffs above the Mouat chromite mine, showing trail from the road to the G chromitite. *Reproduced from* Page and others (1985), which was *modified from* Peoples and others (1954).

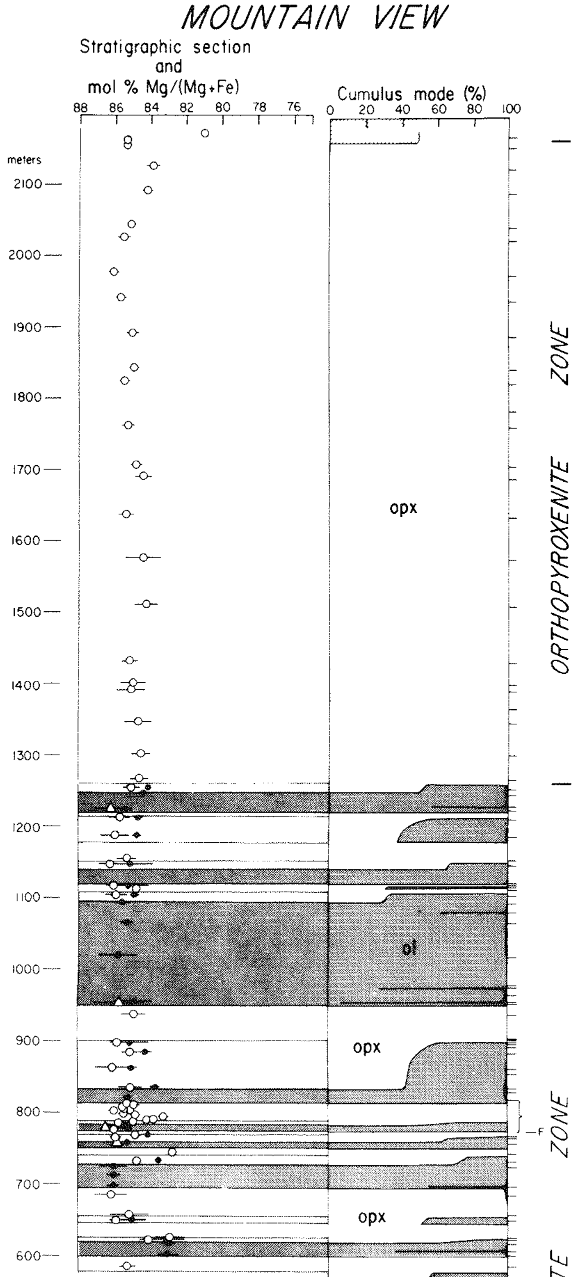

Figure 3—Detailed stratigraphic section through the cyclic unit that begins at 775 meters at Mountain View. "F" indicates a probable fault. Closed circles are cumulus olivine compositions, open circles are cumulus orthopyroxene compositions, and open triangles are postcumulus orthopyroxene compositions (*from* Raedeke and McCallum, 1984).

vine to cumulus bronzite decreases up section. This member is, in turn, overlain by a bronzite cumulate which shows variations in grain size, friability, and intercumulus mineral content. Intercumulus minerals in both obC and bC members are plagioclase and augite, the latter forming distinctive bright green oikocrysts. The second cyclic unit is also complete and well exposed along the trail. As shown in Figure 3 (McCallum, this volume) there is very little variation in composition of the cumulus minerals in these cyclic units.

The trail ends at the base of the third cyclic unit which contains the famous G chromitite, the thickest chromitite seam in the complex, and the subject of investigations by Jackson (1961). The G chromitite, which occurs several meters above the base of the cyclic unit, varies in thickness between ~1 and ~5 meters when traced along strike. It is made up of massive chromitite (cC) interlayered with chromite-olivine cumulate (coC) and olivine-chromite cumulate (ocC). The lower contact is sharp while the upper contact tends to be gradational. About 14 meters stratigraphically above the G is a satellite seam, the G′, which is about half a meter in thickness.

Olivine in the oC beneath the G chromitite is coarser grained than normal but within and above the main chromitite seam, the rock is very coarse grained and locally pegmatitic. Phlogopite is relatively abundant in the pegmatitic zones suggesting that crystallization under an increased fugacity of water may have contributed to the formation of pegmatitic textures. A detailed study of this part of the complex has recently been completed by Murck (1985).

Stop 2: *Mouat mine dump.* Intrepid souls can scramble down the talus slope to Stop 2 while others may prefer to retrace their steps back along the trail and follow the road to Stop 2.

Fresh samples of all ultramafic lithologies can be picked up on the mine dump. Portal No. 5 of the Mouat mine is at this level. The mine was active for less than a year during World War II. Mining was resumed in 1953 by The American Chrome Company and close to one million tons of chromite concentrate were produced and stockpiled before mining was terminated in 1961.

Stop 3: *Ultramafic series—Banded series contact.* The contact between the Bronzitite zone and the Norite I zone of the Lower Banded series is well exposed at this locality. This contact, which is marked by the first appearance of cumulus plagioclase, is traceable across the entire complex. The bronzitite shows variations in grain size and in the modal abundances of interstitial plagioclase and oikocrysts of green augite. The norite ranges from massive to layered and also contains large augite oikocrysts.

The simplest explanation for this cumulate sequence is that it represents a normal fractional crystallization sequence with the magma reaching the plagioclase-orthopyroxene cotectic at this horizon. However, several factors suggest that this explanation is not totally adequate. For example, there is a change in the composition of orthopyroxene across the contact (McCallum and others, 1980) and the magmas that formed the bronzitites have a different trace element pattern than those from which the norite crystallized (Lambert and Simmons, 1987). In addition, initial Sr isotopic ratios also change across the contact (Don DePaolo, personal communication, 1988).

Stop 4: *Verdigris Creek.* Detailed descriptions of the geology of this area are described by Page and others (1985, p. 179-188). The area can be reached by a side road that leads from the mine road on the eastern side of Mountain View Lake and heads towards Verdigris Creek and the Mouat Nickel mine (0.7 miles). Verdigris Creek provides excellent exposures of hornfels, the sill/dike complex, the Basal series, Cu/Ni sulfides, the lowermost cyclic units of the Ultramafic series, and the younger quartz monzonite intrusion.

Stop 5: *Traverse through the Lower Banded series.* Beginning at the adit where the road turns east, norites (pbC) of the N-I zone are exposed along the western side of the horseshoe bend in the road. As the road turns northeast it crosses a drainage that follows the trace of the South Prairie fault system. Neither the GN I zone nor the OB I zone, which should be present at this part of the section, are exposed. North of the fault trace, the rocks cropping out above the road are modally graded norites, with occasional layers of spotted anorthosite (pC), belonging to the N II zone of the LBS. A short distance down the road an anorthosite is overlain by a modally graded gabbronorite (pbaC) which, in turn, is overlain by a norite. The appearance of gabbronorite marks the base of GN II.

The contact between N II and GN II can be traced across the entire complex and it marks the horizon at which the magma reached augite saturation during fractional crystallization. There is no evidence to suggest that this contact is other than a normal sequence, although it should be noted that the cumulate sequence, when viewed in detail, shows alternations and reversals that are not well understood.

Stops 6 and 7: *Mafic dike and gabbronorite.* This mafic dike is one of many that intrude the complex. Although its precise age is unknown, it is most likely Proterozoic. Note the chilled margins. The gabbronorite at this locality contains clots of polycrystalline plagioclase set in a matrix of plagioclase + orthopyroxene + augite. Similar textures have been described by McCallum and others (1980) from the Middle Banded series on Contact Mountain.

Most of the Beartooth dikes in the vicinity of the Stillwater Complex are believed to be Proterozoic although some may be coeval with the complex. The latter dikes are commonly MgO-rich and contain orthopyroxene phenocrysts (Longhi and others, 1983) and may have been derived from the same source as the primary Stillwater magma.

Stop 8: *Gabbronorite-troctolite-anorthosite layers in GN II.* In the type section of GN II on Contact Mountain, olivine-bearing layers have not been observed. However, such layers are relatively common in GN II in the eastern part of the complex. In this particular set of outcrops, the layering is near vertical with tops of units facing north, and contacts between units are sharp.

The gabbronorite (pbaC) occurs as the footwall unit to the troctolite. It contains green augite, brown orthopyroxene, and white plagioclase. All three minerals are cumulus. A lamination defined by plagioclase crystals is well developed. The troctolite (poC) contains two modally-graded units with decreasing olivine up section. Olivine is almost totally altered to serpentine plus magnetite or to fibrous amphibole. The troctolite is overlain by a 40 meter-thick anorthosite (pC) containing coarse-grained oikocrysts of augite. A thin sulfide zone occurs about midway through the anorthosite.

The occurrence of troctolitic and anorthositic layers within gabbronorite presents some interesting petrologic problems. The most likely cause for the reappearance of olivine as a liquidus mineral is the influx of batches of fresh olivine-saturated magma which crystallized to some extent before mixing with the magma resident in the chamber. Plausible as it may appear, this hypothesis is unable to provide a totally satisfactory explanation for all of the petrological and geochemical details.

Three quarters of a mile beyond Stop 8 is the junction with Forest Service Road 846. **Take left fork** which leads past the Initial Creek campground to the West Fork trailhead, a distance of 6 miles. Following discussions at the West Fork adit section, the guide returns to this junction where an examination of outcrops along the lower part of the road will be made.

West Fork adit section

A detailed description of the rocks in the West Fork area is provided by Mann and others (1985, p. 231-246). Most of the information in this guide is summarized from that article.

The discovery outcrop of the J-M Reef occurs in the cliffs on the west side of the river. The steep cliffs, ~300 meters west of the portal of the adit, expose a section through OB I of the Lower Banded series. The layering strikes N 80° W and dips ~45 degrees into the hill. The surface geology in this area is summarized in **Figure 4**. The terminology used by Johns-Manville geologists is slightly different from that used in this guide. The troctolite-anorthosite zone I (TAZ I) of Johns-Manville geologists corresponds to OB I of McCallum and others (1980), except that the latter authors include the gabbro subzone in GN I rather than in OB I.

The lower half of the cliff outcrop is composed of gabbronorite (pbaC) with subordinate interlayers of norite (pbC) and anorthosite (pC) belonging to the GN I zone. The upper part of the cliff section is more leucocratic and contains several conspicuous layers. Most of the visible layering in this section is due to the weathering of olivine-bearing units. In this area olivine-bearing layers O5A, O5B, O6, O7, and O8 (J-M terminology) have been recognized. Olivine-bearing layers O1 through O4, which are present in the Contact Mountain area, are apparently absent from this section. This points up some of the problems of attempting to correlate units over long distances. On the cliff face, olivine-bearing layers are recognizable because they sustain more vegetation. Layer O5B, which hosts the J-M Reef, is visible about half way up the cliff. It is overlain and underlain by leucocratic anorthosite. Layers of O6, O7 and O8 are visible as vegetated bands separated by anorthosite which contains pyroxene oikocrysts. In most of the olivine-bearing layers, the lowermost member is a peridotite (oC) which grades upwards to a troctolite (poC). Pegmatitic textures are widespread in the oC units and phlogopite and chromite are common accessory minerals.

Excellent samples of all lithologies can be collected on the West Fork adit rock dump. Many of the rocks have suffered some alteration. This is particularly true of the olivine-bearing samples in which the olivine has been replaced by serpentine plus magnetite or a fibrous amphibole. In searching for sulfides, samples showing surface limonitic alteration are usually the best source for sulfides. The rock type at the portal to the adit is an unusually fresh gabbronorite. A sample dated by DePaolo and Wasserburg (1979) was collected from this outcrop.

A trail ("of sorts") leads to outcrops of the J-M Reef package exposed above the adit portal. This trail passes through the lowermost gabbronorite which is in sharp contact with the overlying anorthosite (~7 m thick). Layer O5A, which in reality is a pegmatitic olivine-bearing gabbronorite, is sporadically developed in this anorthosite but is absent in the section above the adit. The contact between the anorthosite and O5B is sharp. The base of O5B is an altered, coarse-grained peridotite (oC) about 1 meter thick containing pyroxene oikocrysts, interstitial plagioclase, minor phlogopite and chromite, and sporadic sulfides. This unit is overlain by a troctolite (poC) with anorthositic patches, about 4 meters thick, and contains pyroxene oikocrysts, phlogopite, chromite and sulfides. This unit is the host of PGE mineralization which takes the form of disseminated sulfides recognizable on the surface by their alteration to limonite. Several trenches dug across the reef in this locality provide good exposures of the mineralized zone. The troctolite is overlain by a mottled anorthosite containing pyroxene oikocrysts and sparse olivine grains.

Retrace route back to junction of the West Fork road with the Mouat mine road and return to the Stillwater valley.

Mountain View area (Stops 9-17)

Stop 9: *Inch-scale layering in landslide block.* Inch-scale layering, originally described by Hess (1960) is quite common in the norites and gabbronorites of the Lower Banded series, but in this much photographed outcrop, inch-scale layering reaches its most spectacular development. The layers are formed by alternations of pyroxene and plagioclase. The plagioclase is present as cumulus grains whereas the pyroxenes have the oikocrystic habit usually associated with intercumulus growth. Whether the pyroxenes have a cumulus core is a matter of some debate. In this outcrop the layers are arranged in doublets although singlets and other groupings are also common. Inch-scale layers tend to be coarser grained than associated non-layered rocks.

Stop 10: *More fine-scale layering.* In this outcrop, layering is defined by alternations of cumulus orthopyroxene and cumulus plagioclase. Some parts of the outcrop show two superimposed layering patterns.

Many hypotheses have been advanced to explain the origin of inch-scale layering, the most plausible being that recently proposed by Boudreau (1987), who showed that layer spacing was proportional to crystal grain size and that pattern development, in the form of honeycomb arrangements, also occurred within the plane of layering. Boudreau (1987) presented a computer model in which layer development was simulated during textural coarsening. An assemblage of crystals plus liquid is inherently unstable to minor perturbations in crystal size. Large grains will grow at the expense of smaller grains to diminish the total free energy of the system. Such a process can produce layering when a gradient of grain size is present across the system, as might be expected in an advancing front of nucleation and growth in a solidifying magma.

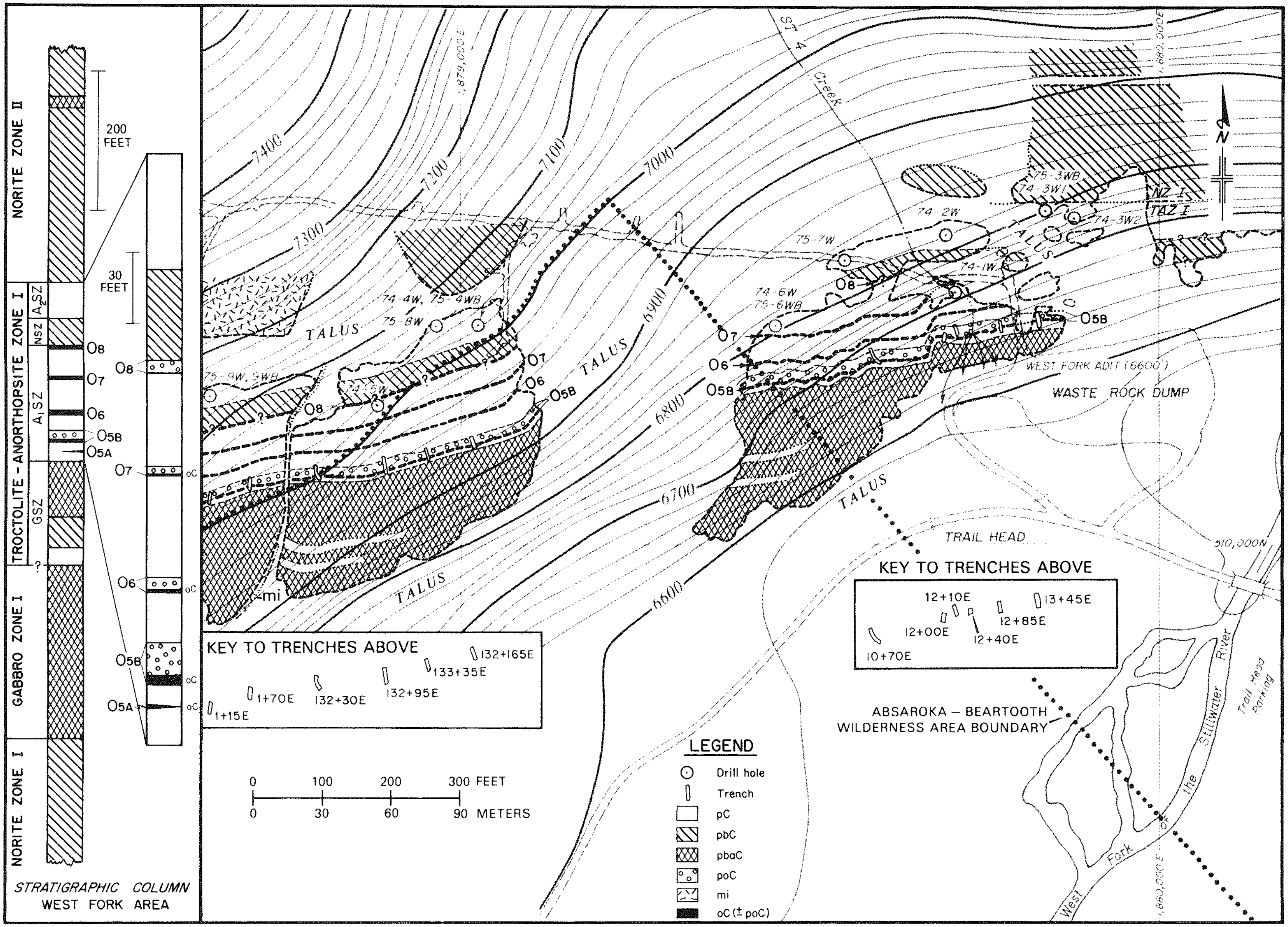
NORITE ZONE II
TROCTOLITE - ANORTHOSITE ZONE I
A2SZ
NSZ
A1SZ
GSZ
GABBRO ZONE I
NORITE ZONE I
200 FEET
30 FEET
O8
O7
O6
O5B
O5A
oC
STRATIGRAPHIC COLUMN
WEST FORK AREA
7400
7300
7200
7100
7000
6900
6800
6700
6600
1,879,000 E
1,880,000 E
510,000 N
ST 4
Creek
TALUS
mi
74-4W, 75-4WB
75-8W
75-9W, 9WB
74-5W
74-6W
75-6WB
75-7W
74-2W
74-1W
75-3WB
74-3W1
74-3W2
NZ I
TAZ I
N
WEST FORK ADIT (6600')
WASTE ROCK DUMP
TRAIL HEAD
KEY TO TRENCHES ABOVE
12+10E
13+45E
12+85E
12+00E
12+40E
10+70E
KEY TO TRENCHES ABOVE
132+165E
133+35E
132+95E
1+70E
132+30E
1+15E
ABSAROKA – BEARTOOTH WILDERNESS AREA BOUNDARY
West Fork of the Stillwater River
Trail Head Parking
0 100 200 300 FEET
0 30 60 90 METERS
LEGEND
Drill hole
Trench
pC
pbC
pbaC
poC
mi
oC (± poC)

Figure 4—Geologic map and detailed stratigraphic column of the West Fork adit area. *Reproduced from* Mann and others (1985).

Stop 11: *Olivine-bearing zone I.* **Park at road intersection** where a mafic dike is exposed and walk along the upper road for about 300 meters to an outcrop that exposes a section of OB-I containing the J-M reef. In this area the reef package is significantly different from the reef exposed at the West Fork and Contact Mountain, again emphasising the difficulty of correlation. At this locality, the rocks beneath OB-I are mainly gabbronorites containing layers of norite and anorthosite. OB-I is composed of a sequence of pegmatitic anorthosite, norite, peridotite and troctolite. Patches showing typical cumulate structures and textures are in irregular contact with the pegmatitic patches. The PGE mineralized zone occurs within a 3 meter-thick peridotite/troctolite with a very distinctive "ameboidal" texture. Phlogopite, chromite and apatite are present in addition to disseminated sulfides. This unit is overlain by a modally graded troctolite which passes upwards into a mottled anorthosite.

The reef package in this area is affected by a major Laramide structure, the South Prairie fault, a high-angle reverse-fault system which dips steeply north in the Mountain View area. This fault is roughly conformable with the reef package, although in places it has resulted in removal of the reef.

The origin of the reef package and the associated mineralization is matter of great controversy at the present time. The model with the greatest support holds that the OB-I sequence formed in response to the addition of batches of olivine-and sulfide-saturated magma that mixed in a turbulent fashion with the magma in the chamber. Turbulent mixing is required for the immiscible sulfide droplets to come in contact with the large volume of magma required to generate the high concentrations of PGE (Campbell and others, 1983). The alternative hypothesis, vigorously advocated by Boudreau (1988), holds that the PGE were concentrated by a hydrothermal mechanism in which hydrous fluids, exsolved from the interstitial melt lower in the cumulate pile, scavenged PGE from existing sulfides and deposited them at a major lithologic discontinuity in the OB-I zone. This hypothesis has the advantage of explaining the pegmatitic textures and the widespread occurrence of phlogopite and chlorapatite in the mineralized zones.

Stops 12 through 17:

Current mining activities may limit access to some of these areas. A complete description is provided by Page and others (1985).

Acknowledgements

This work was supported by Grant NAG 9-84 from the National Aeronautics and Space Administration. The author is indebted to Norm Page and Bob Mann for permission to reproduce Figures 1, 2 and 4.

References

Boudreau, A. E., 1987, Pattern formation during crystallization and the formation of fine-scale layering, *in* Origins of Igneous Layering, I. Parsons, *(ed.)*: Reidel Publishing Company, Dordrecht, Holland, p. 453-471.

______ 1988, Investigations of the Stillwater Complex: Part IV. The role of volatiles in the petrogenesis of the J-M Reef, Minneapolis adit section: Canadian Mineralogist, *(in press)*.

Campbell, I. H., Naldrett, A. J., and Barnes, S. J., 1983, A model for the origin of platinum-rich sulfide horizons in the Bushveld and Stillwater complexes: Journal of Petrology, v. 24, p. 133-165.

DePaolo, D. J., and Wasserburg, G. J., 1979, Sm-Nd age of the Stillwater Complex and the mantle evolution curve for neodymium: Geochimica et Cosmochimica Acta, v. 43, p. 999-1008.

Hess, H. H., 1960, Stillwater Igneous Complex, Montana—a quantitative mineralogical study: Geological Society of America Memoir 80, 230 p.

Jackson, E. D., 1961, Primary textures and mineral associations in the Ultramafic zone of the Stillwater Complex, Montana: U.S. Geological Survey Professional Paper 358, 106 p.

Lambert, D. D., and Simmons, E. C., 1987, Magma evolution in the Stillwater Complex, Montana, part I. Rare-earth element evidence for the formation of the Ultramafic series: American Journal of Science, v. 287, p. 1-32.

Longhi, J., Wooden, J. L., and Coppinger, K. D., 1983, The petrology of high-Mg dikes from the Beartooth Mountains, Montana: A search for the parent magma of the Stillwater Complex, *in* Proceedings of the Fourteenth Lunar and Planetary Science Conference, part 1: Journal of Geophysical Research, v. 88, supplement, p. B53-B69.

Mann, E. L., Lipin, B. R., Page, N. J., Foose, M. P., and Loferski, P. J., 1985, Guide to the Stillwater Complex exposed in the West Fork area, *in* The Stillwater Complex, Montana: Geology and guide, G. K. Czamanske and M. L. Zientek, *(eds.)*: Montana Bureau of Mines and Geology Special Publication 92, p. 231-246.

McCallum, I. S., Raedeke, L. D., and Mathez, E. A., 1980, Investigations of the Stillwater Complex, Montana, part I. Stratigraphy and structure of the Banded zone: American Journal of Science, v. 280A, p. 59-87.

Murck, B. W., 1985, Factors influencing the formation of chromite seams [Ph.D. dissertation]: University of Toronto, Canada, 334 p.

Page, N. J., 1977, Stillwater Complex, Montana: Rock succession, metamorphism, and structure of the complex and adjacent rocks: U.S. Geological Survey Professional Paper 999, 79 p.

______ 1979, Stillwater Complex, Montana: Structure, mineralogy, and petrology of the Basal zone with emphasis on the occurrence of sulfides: U.S. Geological Survey Professional Paper 1038, 69 p.

Page, N. J., and Nokleberg, W. J., 1974, Geologic map of the Stillwater Complex, Montana: U.S. Geological Survey Miscellaneous Investigations Series I-797. Scale 1:12,000.

Page, N. J., Zientek, M. L., Lipin, B. R., Raedeke, L. D., Wooden, J. L., Turner, A. R., Loferski, P. J., Foose, M. P., Moring, B. C., and Ryan, M. P., 1985, Geology of the Stillwater Complex exposed in the Mountain View area and on the west side of the Stillwater canyon, *in* The Stillwater Complex, Montana: Geology and guide, G. K. Czamanske and M. L. Zientek, *(eds.)*: Montana Bureau of Mines and Geology Special Publication 92, p. 147-209.

Raedeke, L. D., and McCallum, I. S., 1984, Investigations in the Stillwater Complex, part II, Petrology and petrogenesis of the Ultramafic series: Journal of Petrology, v. 25, p. 395-420.

Zientek, M. L., 1983, Petrogenesis of the Basal zone of the Stillwater Complex, Montana [Ph.D. dissertation]: Stanford University, Palo Alto, California, 246 p.

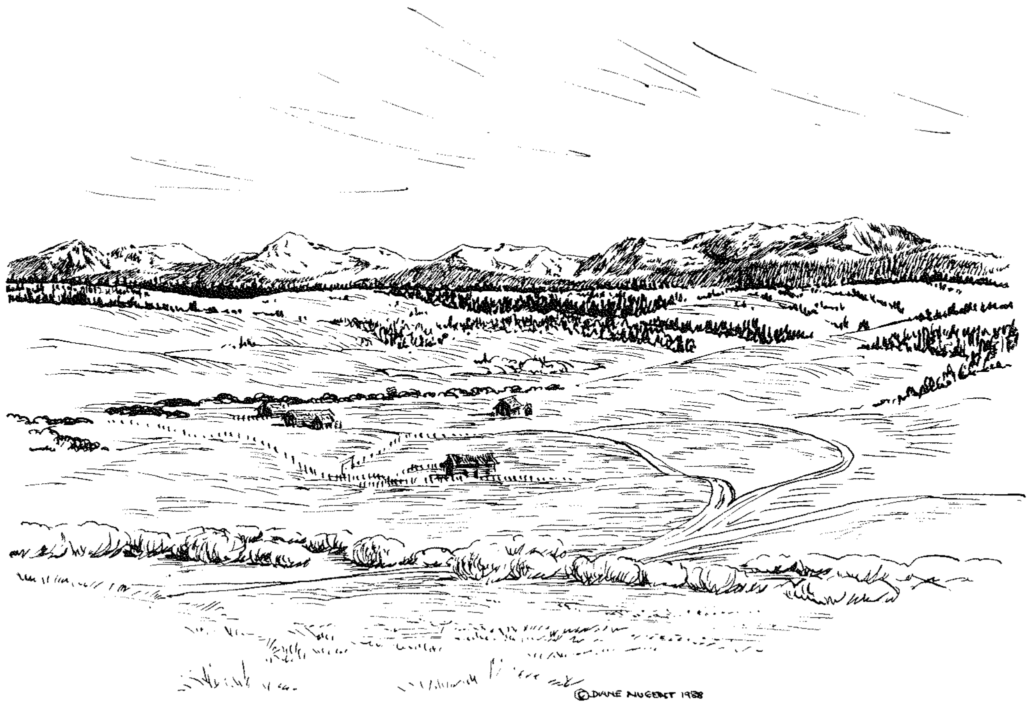

FIELD GUIDE TO AN ARCHEAN TRANSECT, EASTERN BEARTOOTH MOUNTAINS, MONTANA-WYOMING

Paul A. Mueller
Department of Geology
University of Florida
Gainesville, Florida 32611
and
Joseph L. Wooden
U.S. Geological Survey
Menlo Park, California 94025

Introduction

The eastern Beartooth Mountains of Montana and Wyoming (**Figure 1**) contain a record of crustal evolution that spans almost 1000 Ma and culminates in a major episode of crustal growth 2700-2800 Ma. The earlier record is sparse and complex as a result of extensive magmatism and intense metamorphism associated with Late Archean activity. In general, however, it appears that continental material was present in this area by roughly 3600 Ma, and that a stable continental shelf accumulated quartzites, iron-formation, and lesser amounts of pelitic to psammitic units interspersed with small volumes of mafic to silicic volcanic rocks. This cycle of accumulation was apparently terminated by an episode of granulite facies metamorphism 3300-3400 Ma, perhaps as a result of continent-continent collision.

Little activity is recorded between 3300 and 2800

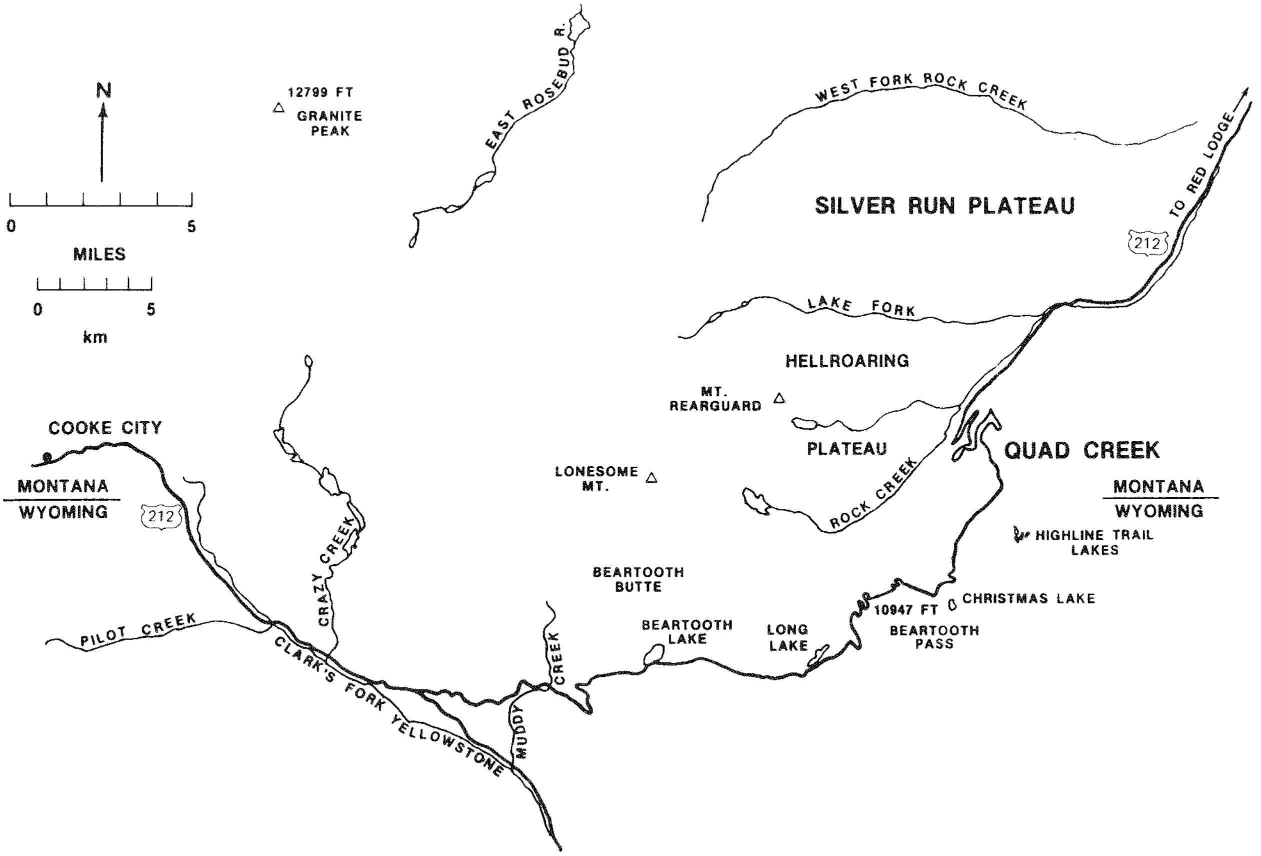
N
0 5
MILES
0 5
km
12799 FT
GRANITE PEAK
EAST ROSEBUD R.
WEST FORK ROCK CREEK
TO RED LODGE
SILVER RUN PLATEAU
212
LAKE FORK
HELLROARING
MT. REARGUARD
PLATEAU
QUAD CREEK
COOKE CITY
MONTANA
WYOMING
212
LONESOME MT.
ROCK CREEK
MONTANA
WYOMING
HIGHLINE TRAIL LAKES
CRAZY CREEK
BEARTOOTH BUTTE
CHRISTMAS LAKE
10947 FT
BEARTOOTH PASS
BEARTOOTH LAKE
LONG LAKE
PILOT CREEK
CLARK'S FORK YELLOWSTONE
CREEK
MUDDY

Figure 1—Map of the eastern Beartooth Mountains showing location of areas referenced in text.

Ma in any geochronologic system. About 2800-2900 Ma, a second major cycle of crustal growth began that bears some resemblence to those associated with modern continent-ocean subduction zones. This cycle may have begun with a period of high-grade metamorphism 2800-2900 Ma, but no igneous rocks appear to have been generated at that time. The first igneous rocks produced during this cycle were andesitic or dioritic rocks, both coarse and fine grained, that were subsequently metamorphosed to amphibolite facies. The oldest protoliths for these andesitic amphibolites were emplaced about 2792 Ma and metamorphosed within about 10 Ma. This interval is restricted by the presence of a granodioritic series (Long Lake granodiorite) that was intruded late in the kinematic cycle. This interpretation is favored because this rock is rather consistently foliated, but retains its igneous mineralogy and texture in many cases. The series was probably intruded about 2779 Ma and marks the lower limit for the last major episode of regional metamorphism. The last and most volumetrically important rock produced during this cycle was the Long Lake granite. This unit composes approximately 80-90% of the eastern portion of the range and engulfs all older rock types. This series of rocks varies from tonalite to granite, but is generally characterized by high Na_2O and SiO_2 contents. It appears to have been intruded about 2740 Ma.

Road log

This excursion will attempt to view the evidence of these two major cycles in four main stops: 1) Hellroaring Plateau, 2) Lower Quad Creek, 3) Upper Quad Creek, and 4) Long Lake. Late Archean mafic dikes (at Beartooth Lake) will also be examined.

Mileage

0.0 Red Lodge, Montana. **Proceed southwest** on U.S. Highway 212 toward Cooke City.
9.0
9.0 Lake Fork turnoff; **continue straight ahead.**
1.7
10.7 **Turn right** (at signs) leading to Greenough Lake and Hellroaring Plateau.
0.4
11.1 Junction with road to right; **continue straight ahead.**
0.5
11.6 **Bear right** on road to Hellroaring Plateau; Greenough Lake turnoff to the west.
5.3
16.9 Follow road to Wilderness boundary (marked by large boulders placed across road). **Park vehicles; proceed on foot** on pack trail for approximately 1.5 kilometers to knoll overlooking cirque opening into Rock Creek drainage. The best exposures of the lithologies described at Stop 1 are located in the vicinity of this knoll and the canyon wall to the south. *Caution: Loose material in canyon walls is deceptively unstable.*

Stop 1: Hellroaring Plateau. The Hellroaring Plateau contains some of the best examples of Middle to Early Archean rocks in the Beartooth Mountains (James 1946; Mueller and others, 1982). These studies provide a general picture of layered Archean rocks trending parallel to the canyon walls until they reach the head of the valley where they were engulfed by younger granitoids. The layered sequence contains metamorphic equivalents of orthoquartzites, banded iron-formation, small quantities of pelitic rocks, mafic to intermediate volcanic rocks, and quartzofeldspathic rocks that may have had volcanic protoliths.

Intercalated within this sequence are pods of ultramafic rocks that have been mined in the past (World War II) for chromite (James, 1946; Loferski and Lipin, 1983). All of these rocks have been multiply deformed and metamorphosed as high as granulite grade. At the head of the canyon the younger granitoids have intruded and partially assimilated members of the layered sequence as well as other apparently older tonalitic and trondhjemitic rocks (F. Barker, personal communication, 1987). These rocks have all experienced the strong Late Archean thermo-tectonic cycle and, in some cases, underwent partial melting at that time. Later folding and fracturing continued up until about 2500 Ma as evidenced by mafic dikes and pegmatites.

Geochronologic data for this area is principally restricted to two units within the older, layered sequence that are informally referred to as the Hellroaring migmatite and the Hellroaring quartzite. The Hellroaring migmatite is of overall rhyodacitic composition in zones that have not undergone partial melting. Remobilized zones are very K-rich. The unit has a distinctive REE pattern characterized by (La/Yb) of 5-10 with strong Eu depletion indicating a probable crustal origin **(Figure 2)**. The age of the protolith is somewhat problematic, but Rb-Sr and Sm-Nd model ages suggest 3.5-3.6 Ga. The remobilized zones are

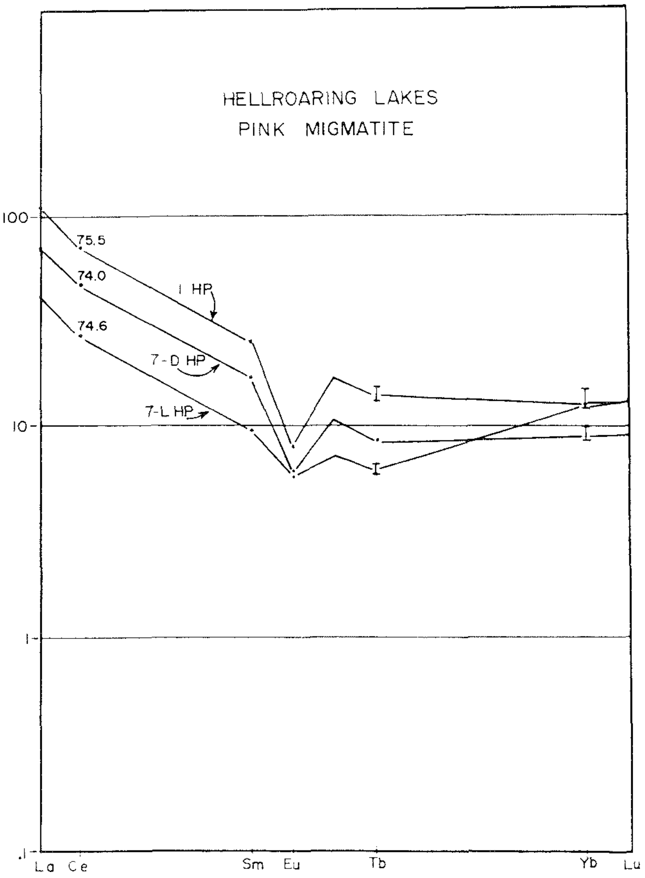

Figure 2—Chrondrite normalized REE patterns for pink migmatite (metarhyodacite) from the Hellroaring Plateau.

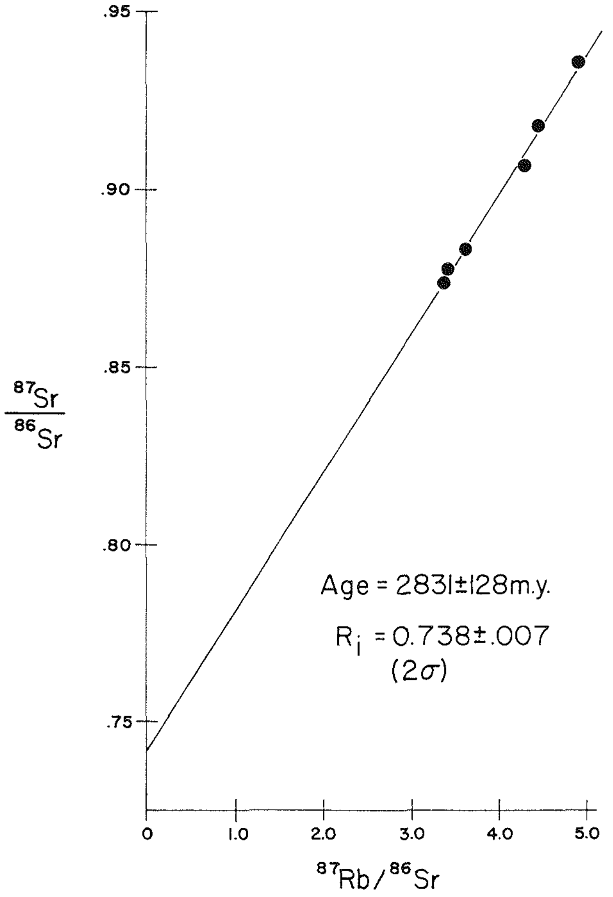

Figure 3—$^{87}Rb/^{86}Sr$ vs $^{87}Sr/^{86}Sr$ for whole-rock samples of pink migmatite from Hellroaring Plateau. Model age based upon average Rb/Sr and a 0.700 initial is about 3.6 Ga.

~2800 Ma by Rb-Sr with an initial ratio of 0.738 (**Figure 3**). Zircons from the unit are highly disturbed and yield poorly defined ages in the range of 3.0-3.2 Ga. These data suggest a geologic history that began at least 3.5 Ga and was followed by a granulite facies metamorphism at about 3.35 Ga. The Late Archean event (~2800 Ma) severely affected all isotopic systems, including resetting of the Rb-Sr systematics in the K-rich zones of the migmatite.

The quartzite(s) from the Hellroaring Plateau are orthoquartzites that are greater than 90-95% SiO_2, but with relatively high Cr and Ni contents (**Figures 4, 5**). These rocks contain zircon and are clearly detrital in origin. Zircons separated from the quartzite fall into two populations. One is composed of clear, acicular grains that are nearly concordant at about 2800 Ma while the other consists of fractured, rounded, overgrown grains thought to be of detrital origin. U-Pb studies of these grains yield similar results to those of the migmatite with maximum upper intercept ages of 3.2 Ga (Mueller and others, 1982). As in the case of the migmatite, the authors feel that these ages must be minimum ages and that the scatter seen in the data reflects the intensity of the metamorphic events to which they have been exposed.

In addition to these two units, one will also see a variety of amphibolites exposed along the edge of the plateau. These rocks constitute an extremely variable group compositionally (**Figure 6**). They range from ultramafic to intermediate compositions and appear to have also experienced upper amphibolite to granulite grade metamorphism. Some of the mafic types still retain unfractioned REE patterns despite their metamorphic history (**Figure 7**). A more detailed discussion of these rocks may be found in Wooden and others, this volume, and Mueller and others, (1982).

6.2

23.1 **Retrace route** back to U.S. Highway 212, **turn right** toward Cooke City.

2.1

25.2 Turnout to right (at opening in guardrail) below first switchback in highway. A mafic

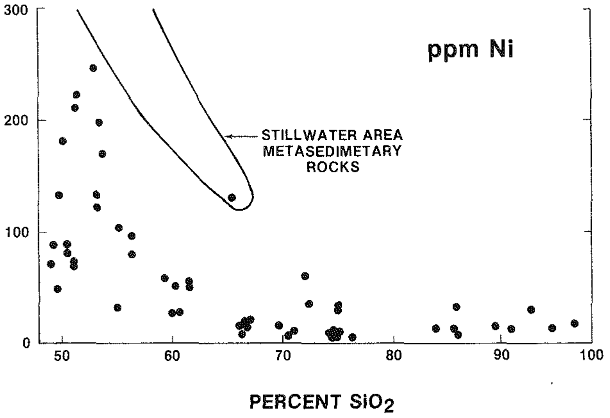

Figure 4—Plots of Ni vs SiO_2 for Middle Archean metasedimentary rocks of the eastern Beartooth Mountains.

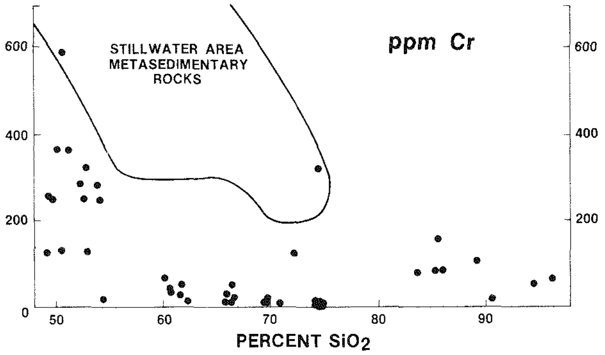

Figure 5—Plots of Cr vs SiO_2 for Middle Archean metasedimentary rocks of the eastern Beartooth Mountains.

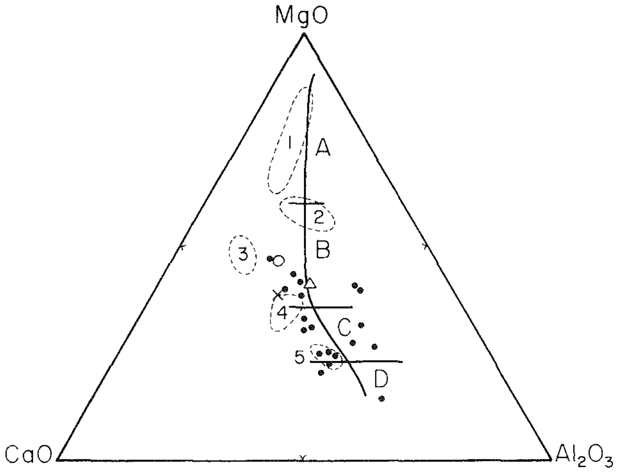

Figure 6—Normalized plot of CaO, MgO, and Al_2O_3 for mafic rocks of the Hellroaring Plateau. Differentiation trend (solid line) is for komatiite rocks from Munro township, A, (peridotitic komatiites); B, (pyroxenitic komatiites); C, (basaltic komatiites); and D, (tholeiitic komatiites). Fields are for komatiites from South Africa, 1, (ultramafic); 2, (Geluk high Al_2O_3 type); 3, (Badplaas type); 4, (Barberton type); and 5, (tholeiitic basalts). Others are: (O), komatiite from Wawa, Ontario; (X), komatiite from Ely, Minnesota; (△), komatiite from western Australia (*after* Mueller and others, 1982).

dike and quartzofeldspathic gneisses are prominent here.

Stop 2: Lower Quad Creek. The exposures of Archean rocks around Quad Creek were mapped by Eckelmann and Polvervaart (1956) and, in part, by Rowan (1969). These outcrops expose some of the same lithologies found on Hellroaring Plateau (e.g., quartzite, iron-formation) as well as tonalitic and trondhjemitic to granitic gneisses that are dissimilar to those across the canyon. In addition, Late Archean granitoids have more pervasively affected the older Archean rocks in this area, particularly their isotopic systematics. The rocks are exposed in the walls of Rock Creek Canyon along the switchbacks of the Beartooth Highway (U.S. 212), particularly adjacent to Quad Creek proper where two localities will be examined and discussed (**Figure 8**). These rocks are also described in Wooden and others, this volume, Mueller and others (1982), and Mueller and others (1985).

This outcrop is composed of an interlayered sequence of metaquartzite and quartzofeldspathic gneisses with minor mafic rocks. Although the protolith of the quartzite was probably sedimentary, the protoliths of the gneisses are enigmatic. They range in composition from tonalite to trondhjemite and granite, but show no consistent major or trace-element relations that suggest they represent a coherent suite of rocks. Geochronologically they show disturbed whole-rock Rb-Sr and Pb-Pb systematics on a large sample scale and disturbed U-Pb systematics in zircon. In general, whole-rock studies suggest an age of about 3.3-3.4 Ga with considerable scatter. U-Pb data from zircons suggest that the rocks have suffered severe metamorphism because small grains consistently yield younger ages than larger grains. If this interpretation is correct, these data indicate that the zircons originally formed sometime before 2900 Ma and were metamorphosed sometime after 2830 Ma. These data suggest a high-grade metamorphic event prior to the intrusion/extrusion of the first of the major Late Archean rock series—the andesitic amphibolites.

4.8

30.0 Turnout inside guardrail (before Forest Service lookout). Base of metanorite is well exposed at this location.

Stop 3: Upper Quad Creek. These outcrops are adjacent to Quad Creek immediately below the Forest Service lookout (**Figure 9**).

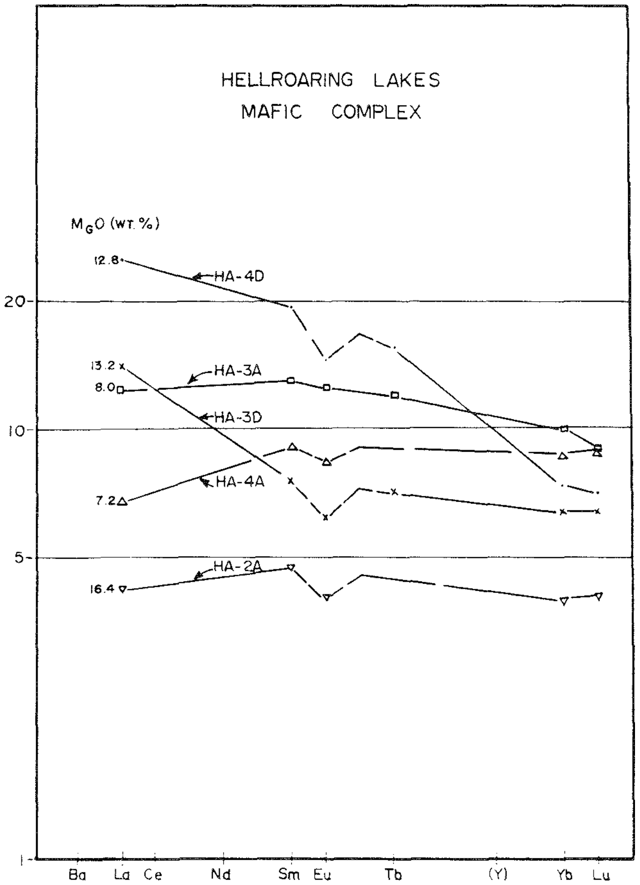

Figure 7—Chondrite normalized REE patterns for a variety of mafic amphibolites from the Hellroaring Plateau.

Here, orthoquartzites are intercalated with more feldspathic quartz-rich rocks of probable sedimentary origin (iron-formation, mafic amphibolites, and minor amounts of more pelitic rocks). This sequence, as well as a block of mafic-ultramafic agmatite, is surrounded by quartzofeldspathic gneisses. These gneisses are of two distinct types. One is a trondhjemitic (70-75% SiO_2) gneiss while the other is a granitic gneiss, also with high SiO_2 **(Figure 10)**. These two types are geochemically, isotopically and petrographically distinct (Rowan, 1969; Mueller and others, 1985). The iron-formation here retains granulite facies mineral assemblages in part **(Figure 11)** and suggests that perhaps all rocks have reached granulite grade.

Compositions and isotopic systematics of these rocks are discussed in Henry and others (1982), Wooden and Mueller (1988), and Wooden and others, this volume. In brief, whole-rock Rb-Sr and Pb-Pb data for the gneisses are scattered, but generally suggestive of isotopic equilibration roughly 2.8 Ga during metamorphism(s). As was the case for the rocks from the Hellroaring Plateau, zircon ages are generally intermediate between 2.8 and 3.2, probably a result of metamorphism as well. The sequence of older rocks was also

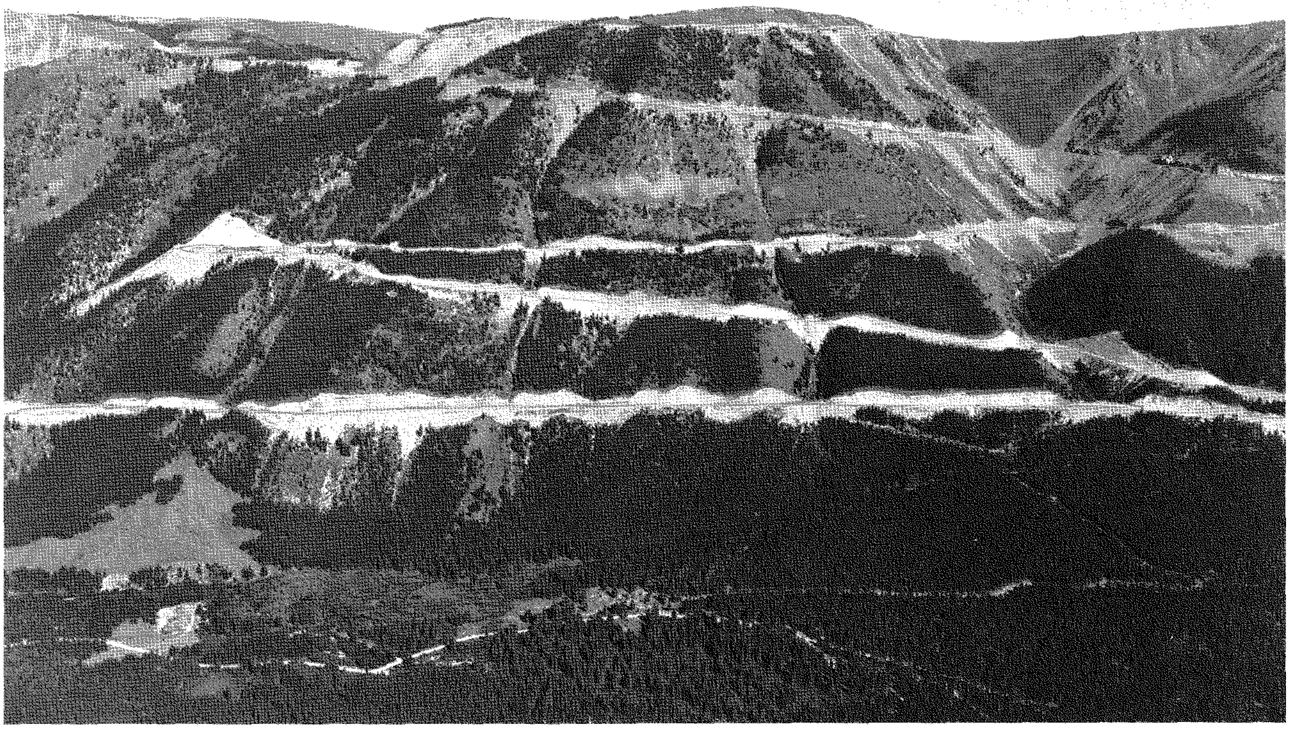

Figure 8—Switchbacks on the Beartooth Highway (U.S. 212) exposing Late Archean granitoids. (H. L. James photo.)

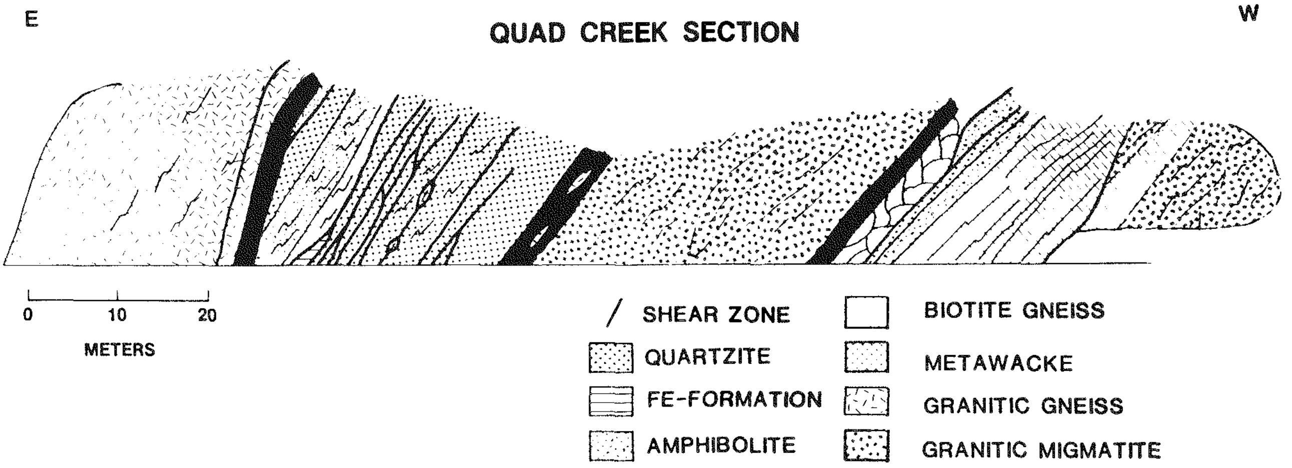
E
QUAD CREEK SECTION
W
0
10
20
METERS
/ SHEAR ZONE
QUARTZITE
FE-FORMATION
AMPHIBOLITE
BIOTITE GNEISS
METAWACKE
GRANITIC GNEISS
GRANITIC MIGMATITE

Figure 9—Schematic drawing of outcrop adjoining Quad Creek (Stop 2).

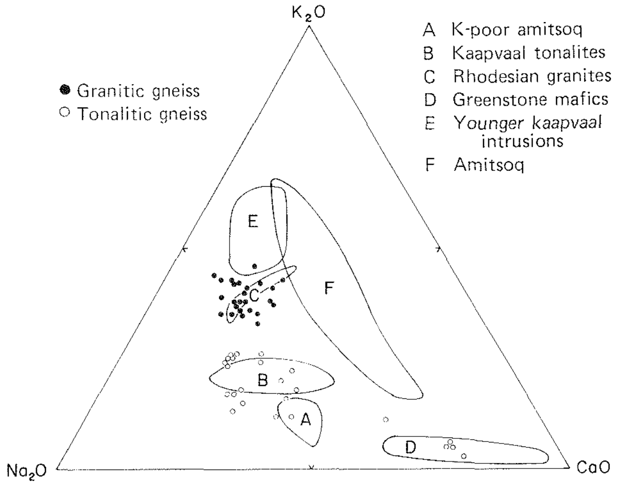

Figure 10—Comparison of normalized compositions of silicic gneisses at Quad Creek.

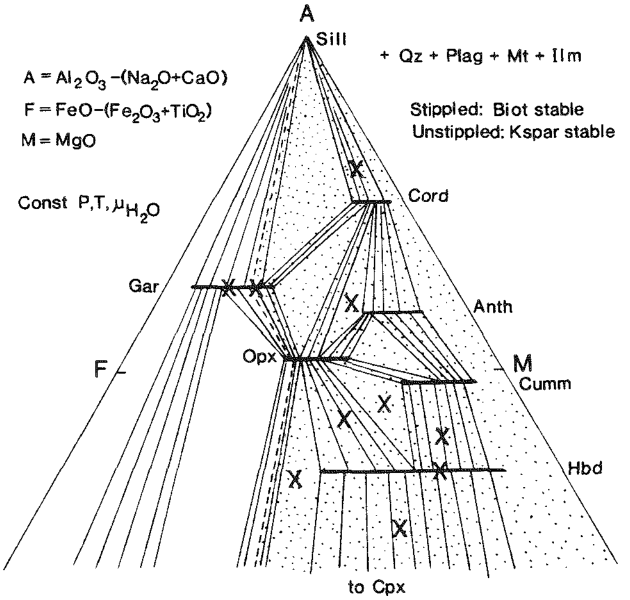
A
Sill
+ Qz + Plag + Mt + Ilm
$A = Al_2O_3-(Na_2O+CaO)$
$F = FeO-(Fe_2O_3+TiO_2)$
$M = MgO$
Stippled: Biot stable
Unstippled: Kspar stable
Const P, T, μ_{H_2O}
Cord
Gar
Anth
Opx
M
Cumm
F
Hbd
to Cpx
X

Figure 11—Mineral paragenesis (X) found in iron-formation and other non-K_2O bearing rocks at Quad Creek that suggest granulite facies. This is a schematic AFM projection.

intruded by members of the Late Archean suite and perhaps were also structurally interlayered with them. From an isotopic point-of-view, this magmatic and structural mixing compounds the problems of isolating the effects of the Late Archean metamorphism(s). Consequently, isotopic systems are more disturbed in this section than in the layered sequence from the Hellroaring Plateau, and it has not been possible to ascertain the relation between the protoliths of the earlier Archean rocks from the two areas.

1.2

31.2 Highway crosses narrow saddle at Forest Service lookout and roadside park.

4.6

35.8 Montana-Wyoming state line.

11.9

47.7 **Stop 4: Long Lake.** Along U.S. Highway 212, immediately southwest of the snow gate (just above Long Lake), is a large outcrop of Long Lake granite, which contains inclusions of a widespread amphibolite unit (andesitic amphibolite) and a granodiorite (Long Lake granodiorite) that are found throughout this part of the range (Mueller and others, this volume; Warner and others, 1982). A late mafic dike (approximately 2.5 to 2.7 Ga) that has been quarried for road metal is also exposed here. The importance of these three main phases is that they represent the last major episode of crustal growth in this area and were produced over a time span of only about 50 Ma. This short period, in conjunction with trace-element and isotopic data, suggest that these rocks were produced along an Archean subduction zone. If this interpretation is correct, these rocks represent the Archean equivalent of a modern magmatic arc, and the

Beartooth Mountains must lie along a paleocontinental margin of Archean age. (For more detailed discussion of ages and geochemistry, see Mueller and others, this volume.)

The oldest unit is the andesitic amphibolite (AA). This amphibolite is composed of plagioclase, hornblende, biotite and quartz, and has an overall andesitic composition. It varies from coarse to fine grained and occurs as inclusions in the Long Lake granite and Long Lake granodiorite. Though small in size, larger (kilometer-sized) blocks are also present in the region. This unit has a distinctive geochemistry highlighted by very high incompatible element contents (e.g., REE, Ba, Sr) as discussed in Mueller and others (1983). Field relations (intrusive contacts) suggest the oldest member of the Late Archean complexes is approximately 2,792 Ma (U-Pb zircon).

The Long Lake granodiorite (LLGd) is extremely difficult to recognize consistently in the field. The best exposures are among the small outcrops on the north side of the U.S. Highway 212 directly across from the borrow pit. In general, this unit appears to have been a late synkinematic intrusion that varies from unfoliated to moderately foliated (as in this outcrop). Less foliated varieties are difficult to distinguish from the more abundant Long Lake granite series. The only consistent mineralogic difference is the higher abundance of sphene in the granodiorite. Geochemically, the unit is also enriched in incompatible elements, though the rock itself does not appear to be related directly to the andesitic amphibolite. Chronologically, U-Pb zircon determinations suggest a crystallization age of 2,780 Ma.

The Long Lake granite (LLG) varies in composition from true granite to tonalite, with the major felsic minerals being quartz, plagioclase and K-feldspar; biotite is the only mafic mineral. This unit is the most voluminous rock in the eastern Beartooth Mountains and is the principal unit exposed at this outcrop. Because bulk compositions of the LLG and LLGd overlap, the LLG is most easily distinguished from the Long Lake granodiorite because it is generally less foliated and possesses a much lower incompatible element content despite its higher average SiO_2 content. Both units contain varying amounts of coarse-grained allanite, which is clearly visible in this area. U-Pb zircon analyses yield an age of 2,738 ± 21 Ma. The generally less foliated nature of the granite and its intrusive relationship to the granodiorite suggest that it is a postkinematic intrusion.

In summary, the Long Lake outcrop contains evidence for an early volcanic-plutonic phase (AA) that was subjected to amphibolite facies metamorphism at about 2,785 Ma and then injected by an incompatible element enriched granodiorite (LLGd). These two rocks were then intruded by the Long Lake granite. This sequence of magmatic and metamorphic events represents the last major crust-forming event in this region and the second major event in the Beartooth Mountains. The presence of rocks representing both of these crust-forming cycles is unique to the Beartooth Mountains. Recent summaries of the Archean geology may be found in Mueller and Wooden (1982), Mueller and others (1985), and Mueller and others, this volume. A detailed map of rocks from the general area of Long Lake is included in Warner and others (1982).

5.0

52.7 **Beartooth Lake.**

Stop 5: Mafic dikes. The eastern Beartooth Mountains have been extensively intruded by mafic dikes since the intrusion of the Late Archean magmatic complex (Long Lake granite). A variety of dikes have been identified (Prinz, 1964; Mueller and Rogers, 1973; Baadsgaard and Mueller, 1973; Wooden, 1975). At this location (exposed along the west shore of Beartooth Lake) is one of the most distinctive members of the Late Archean suite (2.5-2.6 Ga). It is locally referred to as "Leopard rock." In most cases, the dike is composed of a central portion containing large (normally 2-5 cm) saussuritized plagioclase phenocrysts set in an altered groundmass that was originally pyroxene and plagioclase. The net effect of the alteration gives the rocks a spotted appearance of white pseudophenocrysts set in a dark green groundmass, hence the name. The border zones of these dikes are phenocryst free and the concentration of larger crystals in the central portion of the dikes is most likely the result of flow differentiation. Similar rocks are found in other Archean terranes in the Wyoming province.

"Leopard rock" at this outcrop is unusual in that it is relatively unaltered. The phenocrysts here are ~An 80 and their black color is the result of finely disseminated magnetite. The groundmass and the chill zone have essentially the same composition. The following composition is from Prinz (1964):

Plagioclase phenocrysts (An 80)	57.3%
Groundmass	42.7%

quartz	0.4
plagioclase	17.1
pyroxene	23.0
hornblende	0.3
ores	1.9

In addition, chemical analysis of the phenocrysts (Mueller, 1971) shows:

Rb = 12 ppm, Sr = 230 ppm, K_2O = 0.5%.

The chill zone composition (Wooden, 1975; Mueller, 1971) is:

SiO_2	49.0%	Y	27 ppm
TiO_2	1.1	Rb	9
Al_2O_3	15.3	Sr	109
FeO	12.9	Ba	79
MnO	0.2	Zr	89
MgO	7.7	V	266
CaO	11.5	Cr	349
Na_2O	2.6	Ni	146
K_2O	0.2	Cu	109
		Zn	109

This dike is classified as one of the Archean metadolerites of Prinz (1964), Group I of Mueller and Rogers (1973), and probably has an age of 2.5-2.6 Ga (Baadsgaard and Mueller, 1973; Wooden, 1975).

The Precambrian dikes of the Beartooth Mountains have been more extensively studied than those of any other mountain range in the Wyoming-Montana area. The earliest studies were those of Prinz (1964, 1965). These studies were followed by more regional works of Condie and others (1969). Mueller and Rogers (1973), and Baadsgaard and Mueller (1973) presented a detailed study of the major element chemistry and K-Ar and Rb-Sr systematics of the eastern Beartooth dikes. Wooden (1975) extended the major element and Rb-Sr studies to the central and western Beartooth dikes and determined trace element data for dikes from all three regions. In the course of these studies, approximately 400 individual samples have been analyzed. The agreement is good between the earliest analyses done by wet chemical methods and those done later by rapid instrumental methods. Because so many data exist for the Beartooth dikes, they can be used as the type example for the Wyoming province dikes, although they may not be typical in all respects.

There are numerous fracture sets in the Beartooth Mountains, and dikes can be found occupying most of the orientations represented by the fractures. A general classification based on TiO_2 and FeO_T/MgO (**Figure 12**) is used in the following discussion. The 2800-2500 Ma group (groups 1, 2, 3, 4, 5, 8, 9, 11, 13, 16, 17), as might be expected from the varied chemical groups found in it, shows the most diverse set of orientations. The 2000-2100 Ma group (groups 6, 7, 12 ?) con-

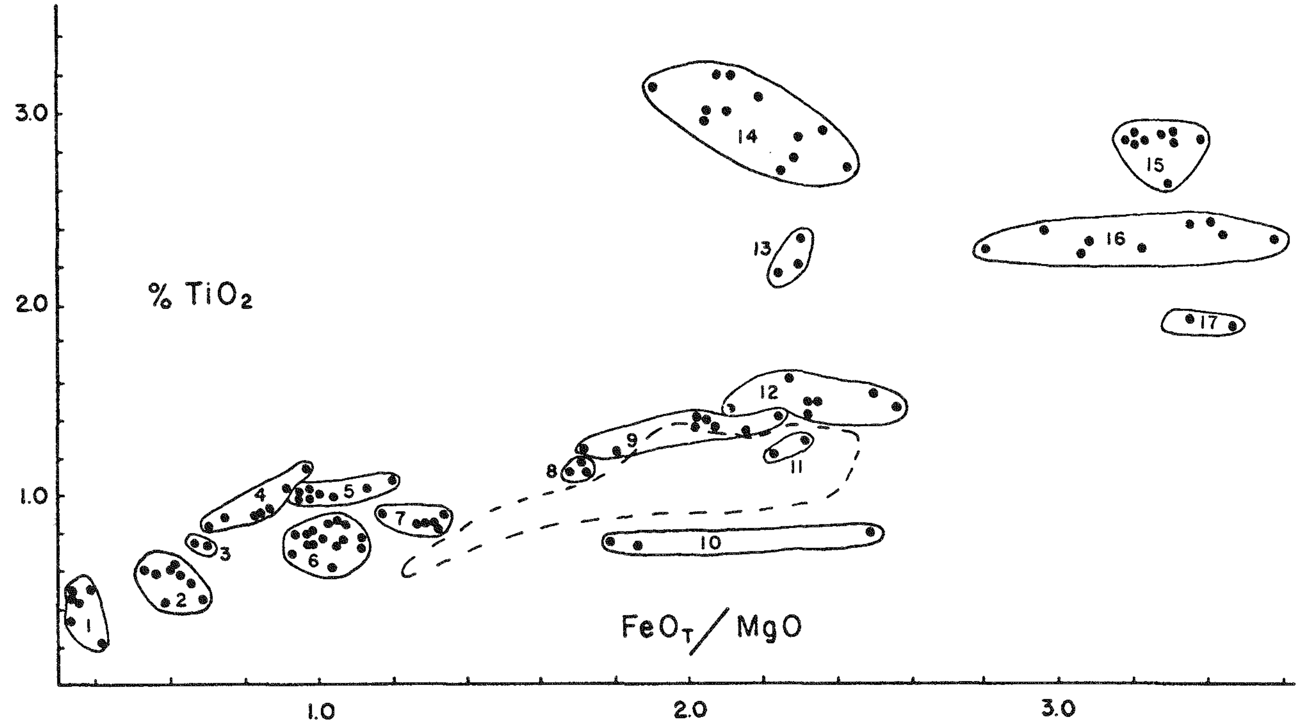

Figure 12—Plot of TiO_2 vs total Fe as FeO/MgO for a variety of mafic dikes of the eastern Beartooth Mountains.

tains 2-3 chemical types, but are all generally oriented north-south. The 1300 Ma (14) and the 740 Ma (15) groups have one chemical type each and very consistent orientations of N 30°W and N 75°W respectively. As a general rule, one chemical grouping is restricted to a limited geographic area and consistently oriented fractures. Only the 1300 Ma alkali-olivine diabases have been found across the entire Beartooth Mountains. Some chemical groups are represented by a single-known dike. (Although a large number of dikes have been sampled, there still remain many that are unsampled.) It is not unusual for different chemical types to occupy the same fracture with segments placed end-to-end, but not side-by-side.

The variety of chemical groups and the variously oriented fractures that they occupy suggest that the 2800-2500 Ma group represents a number of distinct magmas intruded over a period of time during which the orientation of the stress field changed. The 2200-2100 Ma event encompasses 2 or 3 magma types, but the stress field seems to have remained constant. The two younger events represent single pulses of magma. The pattern of intrusion in the Beartooth Mountains appears to range from the complex to the simple with decreasing age; a pattern that might be correlated with a gradual stabilization of crust in the Wyoming province since 2800 Ma. The extensive nature of the 1300 Ma event is probably related to the tectonics of the Belt basin which was active between 1450 Ma and 900 Ma and the main axis of which is oriented parallel to the trend of the 1330 Ma dike swarm (Wooden and others, 1978).

References

Baadsgaard, H. and Mueller, P. A., 1973, K-Ar and Rb-Sr ages of the intrusive Precambrian mafic rocks, southern Beartooth Mountains, Montana and Wyoming: Geological Society of America Bulletin, v. 84, p. 3635-3643.

Condie, K. C., Barsky, C. K., and Mueller, P. A., 1969, Geochemistry of Precambrian diabase dikes from Wyoming: Geochimica et Cosmochimica Acta 33, p. 1371.

Eckelmann, F. D., and Poldervaart, A., 1957, Geologic evolution of the Beartooth Mountains, Montana and Wyoming, part 1, Archean history of the Quad Creek area: Geological Society of America Bulletin, v. 58, p. 1125-1262.

Henry, D. J., Mueller, P. A., Wooden, J. L., Warner, J. L., and Lee-Berman, R., 1982, Granulite grade supracrustal assemblages of the Quad Creek area, eastern Beartooth Mountains, Montana: Montana Bureau Mines and Geology Special Publication 84, p. 147-156.

James, H. L., 1946, Chromite deposits near Red Lodge, Carbon County, Montana: U.S. Geological Survey Bulletin 945, p. 151-189.

Loferski, P. J., and Lipin, B. R., 1983, Exsolution in metamorphosed chromite from the Red Lodge district, Montana: American Mineralogist, v. 68, p. 777-789.

Mueller, P. A., and Rogers, J. J. W., 1973, Secular chemical variation in a series of Precambrian mafic rocks, Beartooth Mountains, Montana and Wyoming: Geological Society of America, v. 84, p. 3645-3652.

Mueller, P. A., and Wooden, J. L. *(compilers)*, 1982, Precambrian geology of the Beartooth Mountains, Montana and Wyoming: Montana Bureau of Mines and Geology Special Publication 84, 167 p.

Mueller, P. A., Wooden, J. L., Odom, A. L., and Bowes, D. R., 1982, Geochemistry of the Archean rocks of the Quad Creek and Hellroaring Plateau areas of the eastern Beartooth Mountains: Montana Bureau of Mines and Geology Special Publication 84, p. 69-82.

Mueller, P. A., Wooden, J. L., Schulz, K., and Bowes, D. R., 1983, Incompatible element-rich andesitic amphibolites from the Archean of Montana and Wyoming: Evidence for mantle metasomatism: Geology, v. 11, p. 203-206.

Mueller, P. A., Wooden, J. L., and Bowes, D. R., 1985, Archean crustal evolution of the eastern Beartooth Mountains, Montana-Wyoming. Montana Bureau of Mines and Geology Special Publication 92, p. 9-21.

Prinz, M., 1964, Geologic evolution of the Beartooth Mountains, Montana and Wyoming, part 5, Mafic dike swarms of the southern Beartooth Mountains: Geological Society of America Bulletin, v. 75, p. 1217-1248.

______ 1965, Structural relationships of mafic dikes in the Beartooth Mountains, Montana-Wyoming: Journal of Geology, v. 73, p. 165-179.

Rowan, L. C., 1969, Structural geology of the Quad-Wyoming-Line Creek areas, Beartooth Mountains, Montana: Geological Society of America Memoir 115, p. 1-18.

Warner, J. L., Lee-Berman, R., and Simonds, C. H., 1982, Field and petrologic relations of some Archean rocks near Long Lake, eastern Beartooth Mountains, Montana and Wyoming: Montana Bureau of Mines and Geology Special Publication 84, p. 57-68.

Wooden, J. L., 1975, Geochemistry and Rb-Sr geochronology of Precambrian mafic dikes from the Beartooth, Ruby Range, and Tobacco Root Mountains, Montana [Ph.D. dissertation]: University of North Carolina, Chapel Hill, 194 p.

Wooden, J. L., and Mueller, P. A., 1988, Pb, Sr, and Nd isotopic compositions of a suite of Late Archean igneous rocks, eastern Beartooth Mountains: Implications for crust-mantle evolution: Earth Planetary Science Letters, v. 87, p. 59-72.

©DIANE NUGENT
1988

FIELD GUIDE TO PRE-BELTIAN GEOLOGY OF THE SOUTHERN MADISON AND GRAVELLY RANGES, SOUTHWEST MONTANA

Eric A. Erslev
Department of Earth Resources
Colorado State University
Fort Collins, Colorado 80523

Introduction

Southwest Montana exposes an unusual Archean metasedimentary sequence which provides a new perspective on the diversity of crustal processes and environments during the Archean. Since the rock record is biased by preferential recycling of vulnerable tectonic environments (Veizer and Jansen, 1985), the study of anomalous Archean terranes, such as are exposed in southwestern Montana, is essential to understanding the full spectrum of Archean petrogenetic environments.

As a whole, the northwestern Wyoming province has many of the characteristics of intermediate P-T gneiss belts, including kyanite-bearing amphibolite and granulite facies rocks and a predominance of quartzofeldspathic gneiss **(Table 1)**. The region also contains abundant carbonate-and pelite-rich metasedimentary domains, an unusual sedimentary association in greenstone belts (Condie, 1981), but not uncommon in gneiss terranes. These metasedimentary domains are unusually well preserved and stratigraphically coherent for an Archean gneiss terrane, locally containing phyllitic slates with excellent tops indicators.

This field guide will concentrate on the geology of the least-metamorphosed region in the northwestern Wyoming province—the southern Madison and Gravelly ranges. These ranges expose a wide variety of lithologies, from granulite facies tonalitic gneiss of Middle Archean age to greenschist facies mylonites and metasedimentary rocks of uncertain age. Excellent, if discontinuous, exposures have been provided by the combination of thrusting and uplift of basement blocks during the Laramide orogeny followed by the current phase of basin and range extension. The superb quality and freshness of exposures give unusually well-defined, three-dimensional geologic control relative to most Archean shields. **Figure 1** shows the general pre-Beltian geology of the area traversed during the field day.

Road log

Mileage

0.0 West Yellowstone, Montana (north side of town); **proceed north** on U.S. Highway 87.

8.3

8.3 Junction with U.S. Highway 191, **turn left** (west) on U.S. Highway 287 toward Hebgen Lake.

3.0

11.3 Turnout on right; view of Coffin Mountain to southwest across Hebgen Lake.

10.2

Stop 1: *Overview of the southern Madison Range*. The southern Madison Range provides a crucial link between the pelite-granite association of the Beartooth Mountains and the carbonate-dominated metasedimentary rocks of southwest Montana. This vantage point shows the southeastern margin of the range. The Precambrian rocks of the Madison Range to the west were thrust to the east over the Phanerozoic section on the Cabin Creek fault zone **(Figure 2)**. Recent backsliding on this fault has opened the Madison valley on the west side of the range, splitting an originally coherent Laramide uplift into the southern Madison and Gravelly ranges. This extension continues today, forming the Hebgen and Red Mountain faults on the northeast side of the lake which slipped during the 1959 Hebgen Lake earthquake.

To the west, across Hebgen Lake, is a

Table 1—Provenance characteristics of Archean gneiss belts.

Sequence	Age(Ga)	Grade(P&T)	%Carbonate	%Quartzite	%Metapelite	%Volcanics	Sedimentary Structure	References
Western gneiss terrain, Western Australia	3.6-3.4	amp. & gran. (5-6.5Kb, 750--840°C)	Present	Present	Very Abundant	Trace	preserved x-beds	Blight, 1978 Gee and others, 1981 Myers and Williams, 1985
Limpopo, South Africa	3.5-3.3	amp. & gran. 10Kb, 800°C)	15%	17%	50%	15%	none reported	Coward and others, 1976 Eriksson and Kidd, 1985 Horrocks, 1983
Labrador	3.8-3.6	predominately amphibolite & granulite	Present	Present	Abundant (<20%)	Abundant (< 50%)	none reported	Collerson and others, 1976 Windley, 1984
Atlantic granulite belt, Brazil	2.7	amp. & gran. (4-7Kb, 780-850°C)	Present	Present	Present	Present	none reported	Wernick, 1981
Napier complex, Australia/Antarctic Territory	3.8-3.3	amp. & gran. (8-10Kb, 900°C)	Trace (<1%)	Trace (<3%)	Present (10%)	Abundant (<80%)	none reported	Sandiford and Wilson, 1986
South India	3.4	amp. & gran. (9-10Kb, 720-840°C)	Present	Present	Abundant	Abundant	none reported	Beckinsale and others, 1980 Harris and others, 1982 Weaver and others, 1978
Kapuskasing, Canada	2.8-2.6	amp. & gran. (5.4-8.4, 600-800°C)	None	None	Present	Abundant	none reported	Taylor and others, 1986
Northwest Wyoming province	3.4-2.6	gs. & amp. (3-8Kb, 500-800°C)	27%	3%	57%	12%	x-beds graded beds	Gibbs and others, 1986 Erslev, 1983

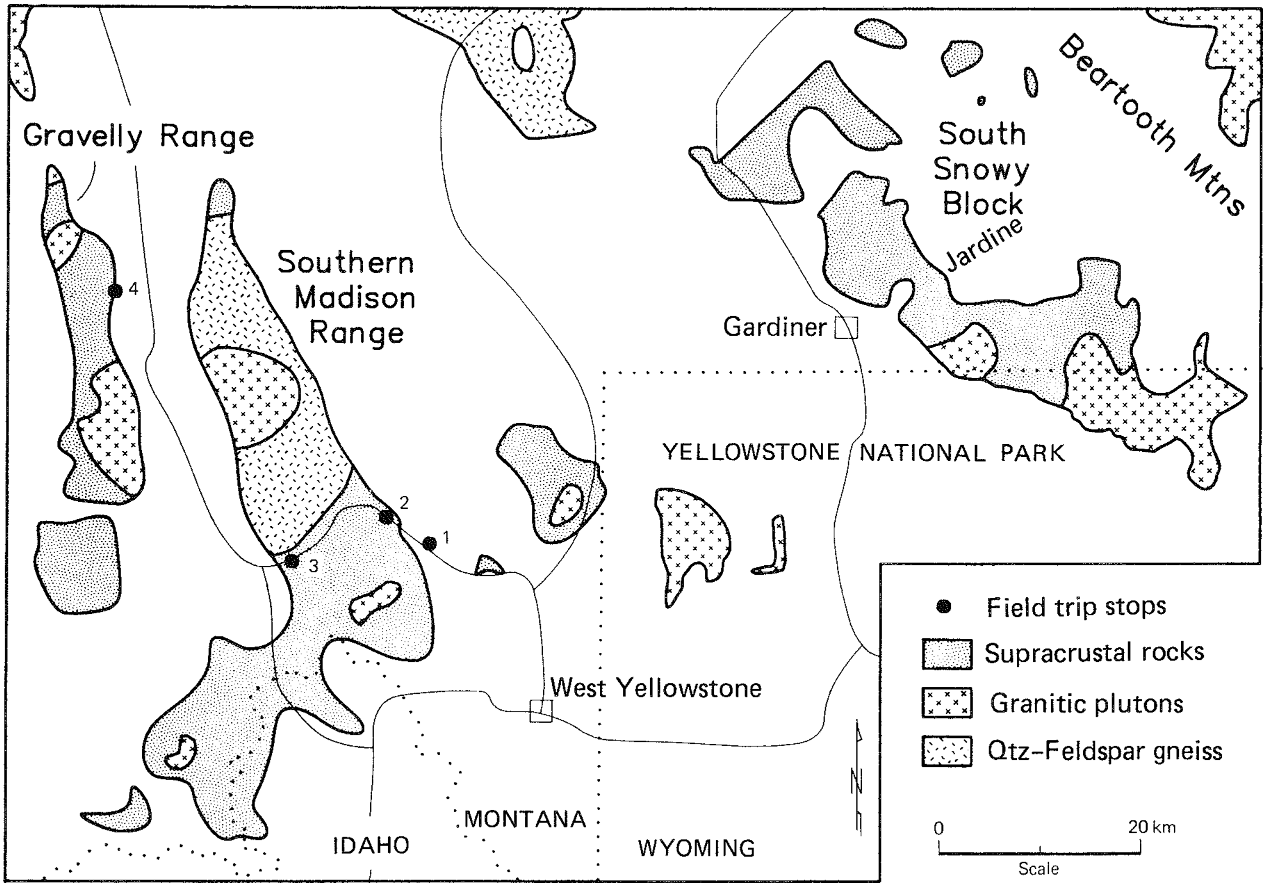
Gravelly Range
Southern Madison Range
South Snowy Block
Beartooth Mtns
Jardine
Gardiner
YELLOWSTONE NATIONAL PARK
West Yellowstone
MONTANA
IDAHO
WYOMING
N
1
2
3
4
Field trip stops
Supracrustal rocks
Granitic plutons
Qtz-Feldspar gneiss
0
20 km
Scale

Figure 1—Basement map of part of southwest Montana showing field stop locations.

complete stratigraphic section through the Cherry Creek metamorphic suite (Erslev, 1983). From south to north, a thick section of biotite-garnet schist is followed by a three-kilometer-thick unit of dolomite marble. This unit is followed by more finely interlayered marble, schist, greenschist/amphibolite and quartzite. These rocks were deposited on an older basement, the pre-Cherry Creek metamorphic complex, consisting of tonalitic migmatite-gneiss and intercalcated metasedimentary rocks cut by granitic plutons. These units form the rugged peaks to the northwest.

The biotite-garnet schist shows excellent graded bedding with tops to the southeast. Biotite-garnet geothermometry and assemblages containing staurolite and kyanite indicate metamorphic conditions of 615°C and greater than 6 kilobars. Accompanying deformation resulted in minor duplication of the stratigraphy on NW-vergent thrust faults. ^{40}Ar-^{39}Ar data from an amphiolite in the schists give a metamorphic age of 2.7 Ga. These rocks are cut by a 2.58 Ga granodiorite sills (Schuster and others, 1987).

Strong textural and metamorphic similarities between these schists and those in the Jardine area further east suggest that they are correlative (**Figure 3**). Recent rare earth (Gibbs and others, 1986) and major element (**Table 2**) analyses of these rocks support this correlation. Note that the average CaO, K_2O and Na_2O contents of pelites from the southern Madison and Beartooth ranges (**Table 2**) fall outside of the 95% confidence limits given by Taylor and McLennan (1985) for Archean clastic rocks. This apparent compositional singularity further supports the idea of contiguous sedimentation in the northwestern Wyoming province during Late Archean Time. The fact that the rare-earth chemistry of the metapelites and the ^{87}Sr-^{86}Sr isotopic composition of the marbles more closely resemble post-Archean sequences than Archean sequences led Gibbs and others (1986) to suggest that many of the proposed changes in earth composition at the Archean-Proterozoic boundary may be more a function of sampling bias than true temporal changes.

21.5 Turnoff on left to Hebgen Dam.

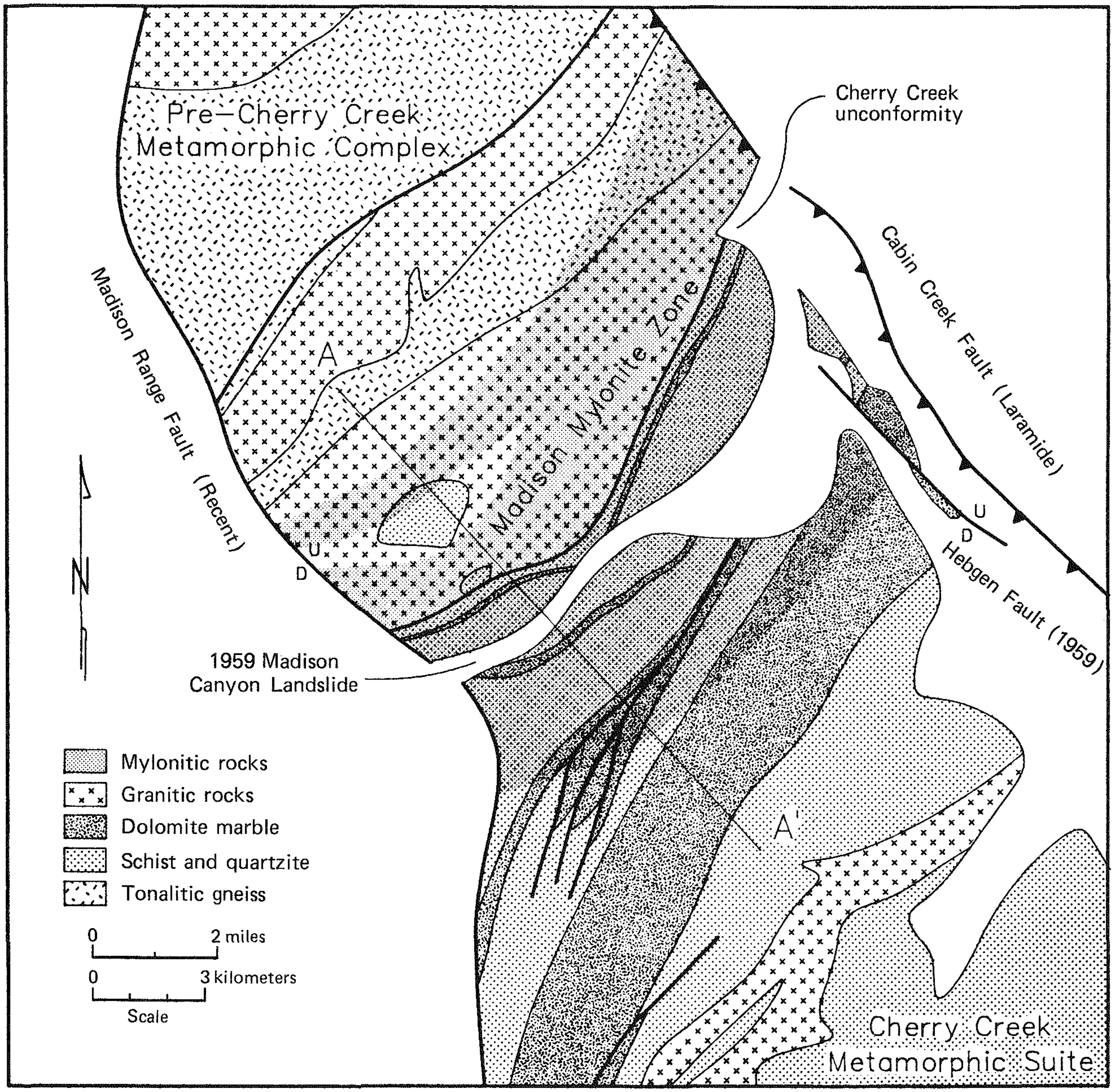
Pre–Cherry Creek Metamorphic Complex
Cherry Creek unconformity
Cabin Creek Fault (Laramide)
Madison Range Fault (Recent)
Madison Mylonite Zone
A
A'
U
D
Hebgen Fault (1959)
N
1959 Madison Canyon Landslide
Mylonitic rocks
Granitic rocks
Dolomite marble
Schist and quartzite
Tonalitic gneiss
0
2 miles
0
3 kilometers
Scale
Cherry Creek Metamorphic Suite

Figure 2—Generalized map of the Precambrian geology of part of the southern Madison Range (*after* Erslev, 1983).

0.6

22.1 **Stop 2:** *Hebgen Dam.* The thickest dolomite marble unit in the Cherry Creek metamorphic suite is exposed across the dam. The lack of calc-silicates in these dolomite + qtz (± phlogopite ± chlorite) marbles suggest relatively high P_{CO_2} during metamorphism (615°C, > 6kb from associated pelites). Retrograde metamorphism due to fluids circulating in the Madison mylonite zone to the north becomes apparent here, resulting in abundant secondary chlorite.

On the evening of August 17, 1959, this portion of U.S. Highway 287 was severed by landslides triggered by the 7.5 magnitude Hebgen Lake earthquake (**Figure 4**). The Hebgen Dam was repeatedly overtopped by seiches and the spillway was badly damaged (**Figure 5**). The Hebgen fault scarp of 1959 is exposed above the highway. Collapse grabens and fissures immediately adjacent to the fault suggest a curved fault plane at depth.

22.1 Cabin Creek campground and earthquake scarp exhibit on right.

2.0

24.1 Madison County line.

3.4

27.5 **Turn right** (north) to U.S. Forest Service Earthquake Visitor's Center (**Figure 6**).

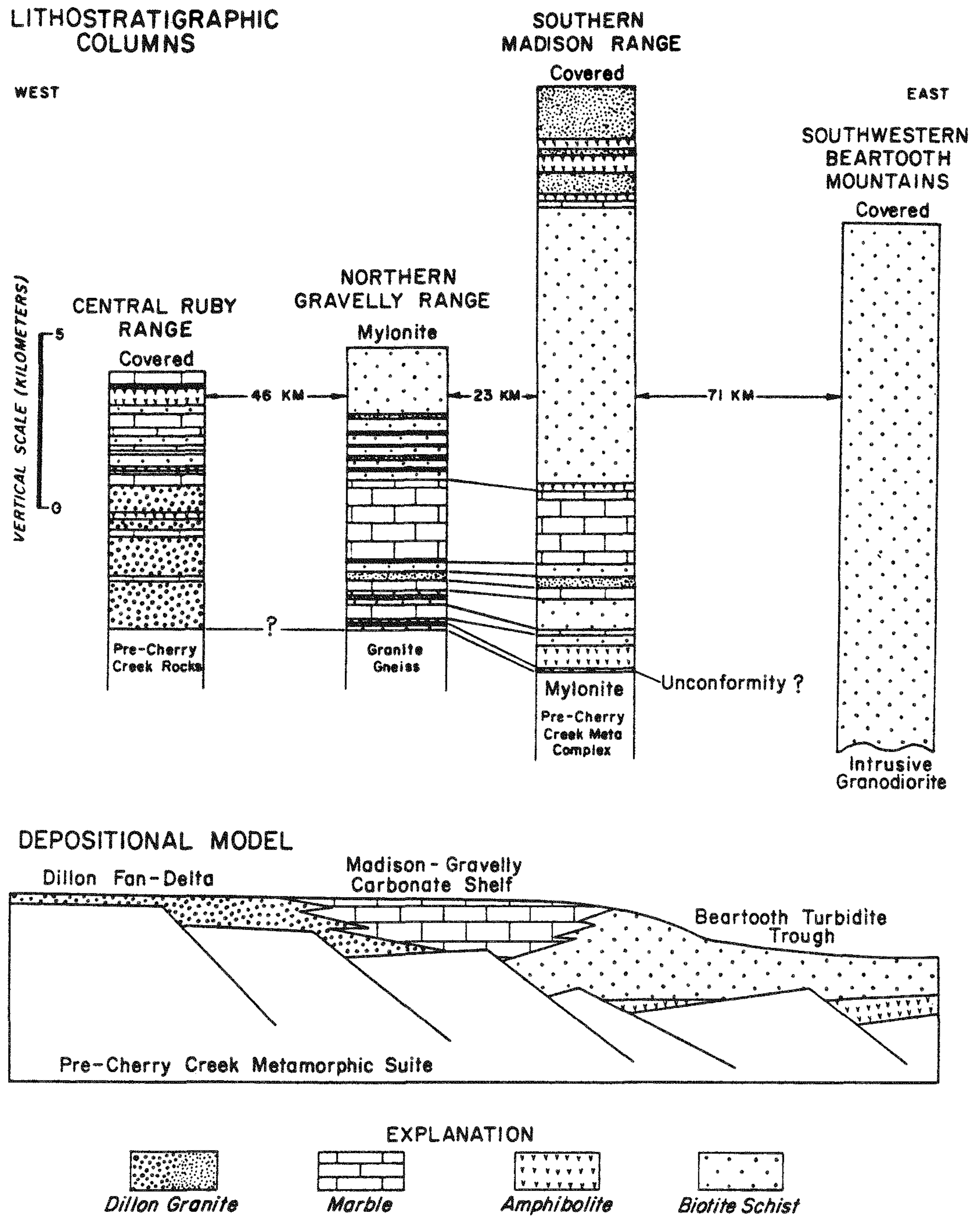
LITHOSTRATIGRAPHIC COLUMNS
WEST
EAST
VERTICAL SCALE (KILOMETERS)
5
0
CENTRAL RUBY RANGE
Covered
Pre-Cherry Creek Rocks
46 KM
NORTHERN GRAVELLY RANGE
Mylonite
Granite Gneiss
23 KM
SOUTHERN MADISON RANGE
Covered
Mylonite
Pre-Cherry Creek Meta Complex
Unconformity ?
71 KM
SOUTHWESTERN BEARTOOTH MOUNTAINS
Covered
Intrusive Granodiorite
?
DEPOSITIONAL MODEL
Dillon Fan-Delta
Madison - Gravelly Carbonate Shelf
Beartooth Turbidite Trough
Pre-Cherry Creek Metamorphic Suite
EXPLANATION
Dillon Granite
Marble
Amphibolite
Biotite Schist

Figure 3—Dip-corrected lithostratigraphic columns and depositional model of metasedimentary sequences in southwest Montana. No correction for internal strain has been attempted.

10.4

Stop 3: *Upper parking lot of Visitor Center.* The Madison Canyon landslide occurred due to a combination of an over-steepened, unstable slope and the sudden acceleration of the seismic event. Units on the southern side of the canyon consist of a phyllonitic schist overlain by a thinner unit of dolomite marble. This marble acted as a retaining wall for the weaker schist, allowing the slope to be over-steepened by erosion prior to the landslide. The breakage of this wall caused the landslide. The slide moved as a coherent mass, preserving the relative stratigraphy of the original bedrock. The stratigraphic coherence of the slide mass, its transport far up the northern slope, and reports of high-velocity wind gusts adjacent to the slide, suggest that the sliding was facilitated by a layer of trapped, compressed air.

Table 2—Compositions of clastic metasedimentary rocks from the Wyoming province (weight percent).

	Southwest Montana				Wyoming	Worldwide
	1	2	3	4	5	6
SiO_2	65.4	59.7	66.6	66.6	65.6	65.9 ± 2.2
TiO_2	0.7	0.8	0.5	0.5	0.6	0.6 ± 0.1
Al_2O_3	14.8	17.5	13.9	16.0	15.8	14.9 ± 1.3
FeO	6.9	8.2	6.9	7.6	6.0	6.4 ± 1.5
MgO	3.3	3.9	3.2	3.6	3.2	3.6 ± 1.0
CaO	1.6	1.9	1.2	1.1	2.3	3.3 ± 1.1
Na_2O	2.0	1.9	2.1	2.0	3.8	2.9 ± 0.5
K_2O	2.6	3.0	2.5	2.8	2.5	2.2 ± 0.3
K_2O/Na_2O	1.3	1.6	1.5	1.4	0.7	0.76
$FeO+MgO$	10.2	12.1	10.1	11.2	9.2	10.0

1. *Average of 14 schists, southern Madison Range, Montana*
2. Average of 3 schists, western South Snowy block
3. Average of 13 schists, central South Snowy block, Montana (Thurston, 1986)
4. Average of 6 schists, central South Snowy block (Gibbs and others, 1986)
5. Average of 23 greywackes, Wind River Mountains, Wyoming (Condie, 1967)
6. Average Archean clastic sedimentary composition ±95% confidence limit (Taylor and McLennan, 1985)

The unconformable, conglomeratic contact between the Late Archean Cherry Creek metamorphic suite and the Middle Archean pre-Cherry Creek metamorphic complex is exposed midway up the north canyon wall. This contact is complicated by a zone of ductile shearing and retrograde metamorphism several kilometers in thickness, the Madison mylonite zone (**Figure 7**). In this shear zone, foliations are rotated about a horizontal, NE-trending axis until they dip at moderate angles to the northwest. Rotations of foliation, stretching directions, fabric asymmetry, minor fold axes and rock strain all indicate up-dip thrusting in this ductile fault zone. This motion brought older pre-Cherry Creek rocks over the younger Cherry Creek units. ^{40}Ar-^{39}Ar hornblende analyses of mylonitic rocks show pervasive argon-loss at 1.9 Ga, with muscovite ^{40}Ar-^{39}Ar totally reset to 1.9 Ga, the inferred age of shearing.

Exposures along the road to the north contain a variety of mylonitic schists and amphibolites. Amphibolitic rocks typically contain hornblende augen surrounded by finer-grained epidote, chlorite and needle-like actinolite. Some of these rocks have lenses of amphibolite stretched to a 20 to 1 axial ratio in the vertical, XZ plane containing the dip direc-

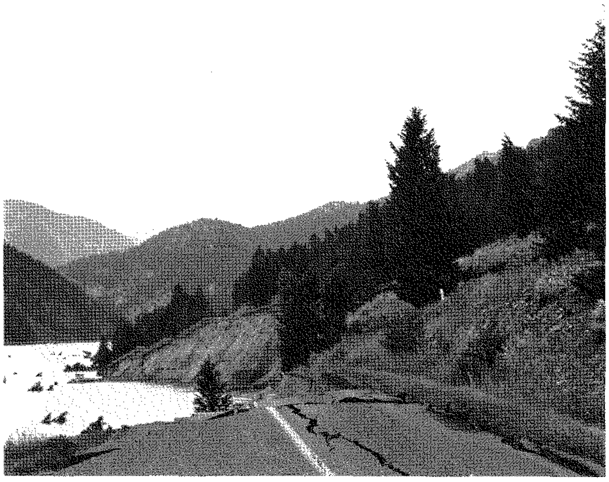

Figure 4—Severed U.S. Highway 287 along north shore of Hebgen Lake, August 18, 1959. (I.J. Witkind photo, courtesy U.S. Geological Survey.)

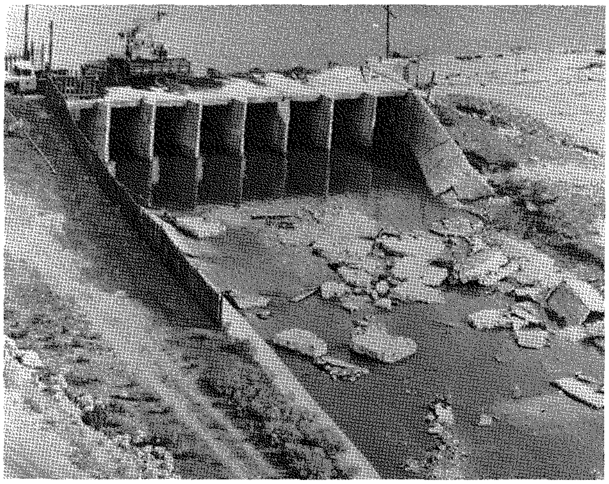

Figure 5—Spillway damage at Hebgen Dam. (Montana Power Company photo.)

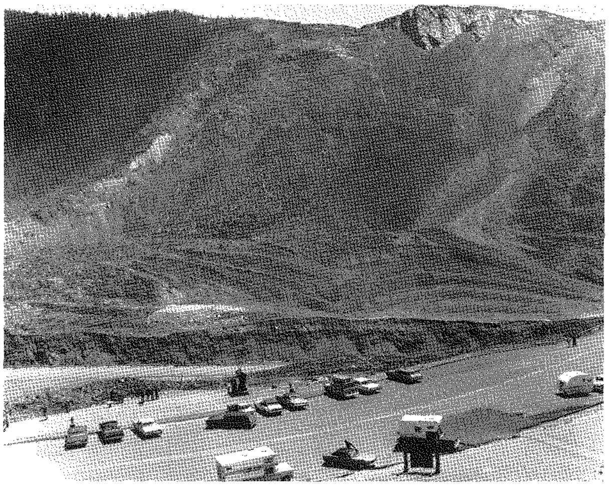

Figure 6—View of Madison Canyon landslide area from visitor's center. (U.S. Forest Service photo.)

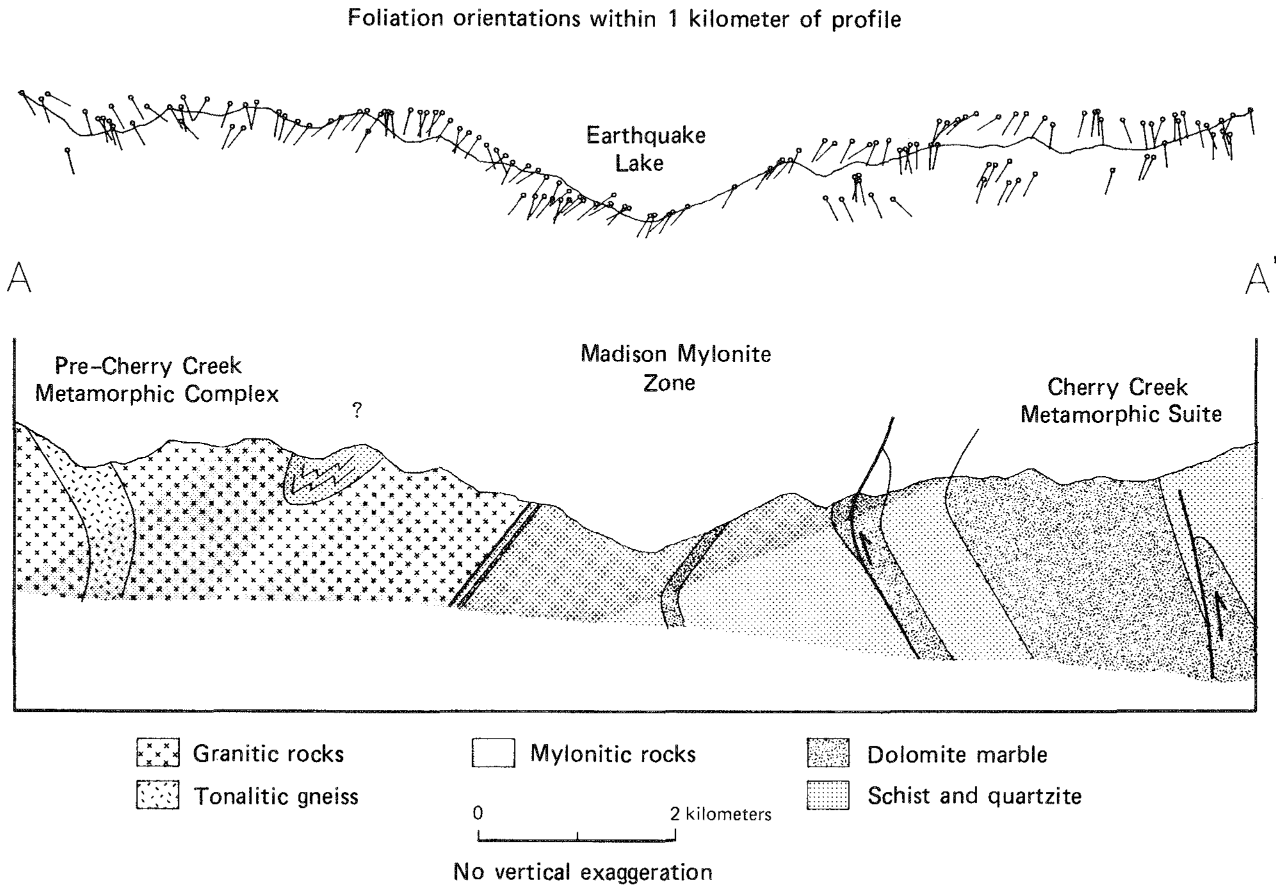
Foliation orientations within 1 kilometer of profile
Earthquake Lake
A
A'
Pre-Cherry Creek Metamorphic Complex
?
Madison Mylonite Zone
Cherry Creek Metamorphic Suite
Granitic rocks
Tonalitic gneiss
Mylonitic rocks
0
2 kilometers
Dolomite marble
Schist and quartzite
No vertical exaggeration

Figure 7—Structure section through A-A' in Figure 2 showing foliation orientations within 1 kilometer of the structure section.

tion. These pods may have originated as pillow basalts. In the talus, fine-grained quartzite, garnet-muscovite schist, partially sheared gabbro and feldspathic gneiss can be found.

While it is tempting to use this shear zone as a suture, the excellent stratigraphic correlation between the Cherry Creek sequences south of the shear zone in the southern Madison Range and north of the shear zone in the central Madison and Gravelly ranges makes this unlikely **(Figure 3)**. In addition, lithologic units within the shear zone show remarkable continuity, suggesting continuous, penetrative ductile shearing during a Late Proterozoic compressional event.

To the northwest, K-Ar analyses give predominantly Proterozoic ages, indicating that the southern Madison Range is on the margin of a major Proterozoic orogenic belt (Giletti, 1966). The Archean rocks northwest of the southern Madison and Gravelly ranges become progressively more highly metamorphosed, suggesting that Proterozoic thrusting has exposed successively deeper levels in the Archean crust to the northwest. The documentation and differentiation of Proterozoic and Archean events throughout southwest Montana will be essential to the interpretation of the northwestern Wyoming province.

37.9 Rest area on south side of U.S. Highway 287.

2.0

39.9 Pinedale moraine on north side of highway.

12.7

52.6 **Turn left** (west) on McAtee Road, just before Indian Creek bridge.

0.8

53.4 Intersection with Ruby Creek campground road (to south). **Proceed straight ahead** on Johnny Gulch Road.

2.0

55.4 Cattleguard. Facilities on north side of road owned by Cyprus Industrial Minerals. **Turn left** (south) on dirt track. *Please close gate!* Dirt tracks ahead; follow track between fence rows.

1.3

56.7 Entrance to Wall Creek Wildlife Management Area. *(Be advised on seasonal closure to motor vehicles.)*

0.5

57.2 **Turn right** (west) into Ruby Creek drainage and park. Geologic traverse extends 3 to 4 kilometers up Ruby Creek drainge.

Stop 4: *Structural repetition of Gravelly Range metasedimentary rocks.* To the east, the rugged peaks of the Hilgard and Taylor Peak areas of the southern Madison Range expose the Middle Archean pre-Cherry Creek metamorphic complex and associated intrusive granitic rocks. Cherry Creek rocks with clearly correlative stratigraphy are exposed below the distinctive Sphinx Mountain, which is composed of a Laramide synorogenic conglomerate. The same stratigraphic sequence is exposed north of Johnny Gulch (**Figure 8**). The large dolomite unit to the north, which is correlative with the marble seen at Stop 2, hosts the largest talc production in the western hemisphere in two mines operated by Cyprus Industrial Minerals and Westmont Mining Company.

The field trip ends with a walk to the northwest through a mixed pelitic-psammitic-iron-formation-carbonate sequence which is duplicated by a series of thrust nappes. These rocks differ from those of the pelitic sequence in the southern Madison Range in several important ways. Lithologically, they are much more varied, with abundant marble, trough cross-bedded quartzite and iron-formation lacking in equivalent strata. Structural fabrics indicate a predominance of southeast-vergent tectonic transport, a characteristic of the 1.9 Ga Madison mylonite zone. The occurrence of low-grade phyllites recording only one stage of metamorphism suggest that some of these rocks may not have undergone Archean amphibolite-facies metamorphism. Either the prograde event during the Proterozoic exceeded the Archean metamorphic imprint, or this sequence may be Proterozoic in age. Current investigations are attempting to unravel the structural and metamorphic chronology of this area.

Retrace route to U.S. Highway 287. Turn left (north) to Ennis.

Acknowledgements

The author is indebted to Wendolyn Sumner and Ana Vargo of Colorado State University for the use of preliminary geochemical data (W.S.) and the Gravelly Range map (A.V.). Whole-rock XRF analyses were provided by John C. Reed, Jr. of the U.S. Geological Survey.

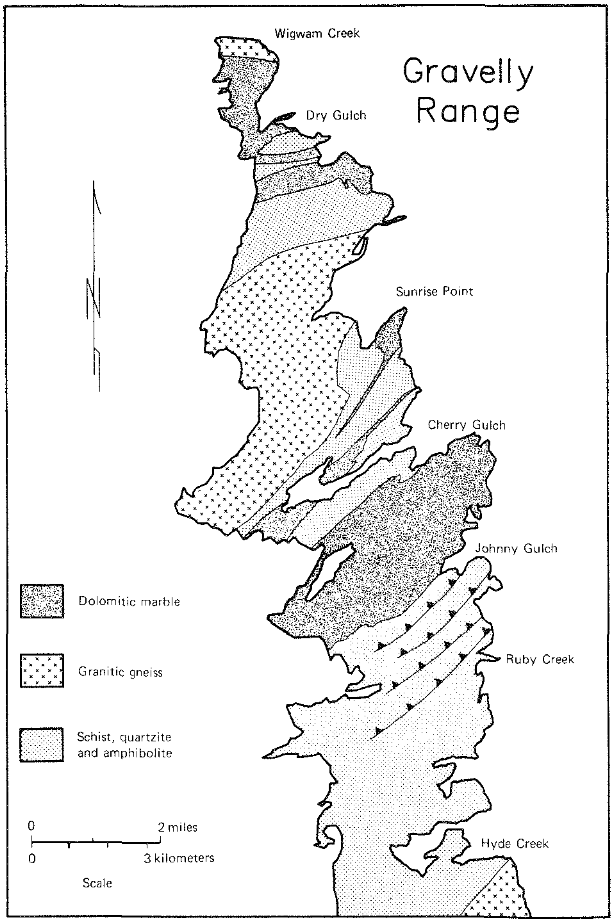

Figure 8—**Precambrian geology of the central Gravelly Range** ***(modified after*** **Millholland, 1976).**

References

Beckinsel, R. D., Drury, S. A., and Holt, R. W., 1980, 3360 Ma old gneisses of South Indian Craton: Nature, v. 283, p. 469-470.

Blight, D. F., 1878, Petrological evidence for an unusually high Archean geothermal gradient in the Wonger Hills area, Western Australia; Annual Report: *Geological Survey of West Australia for* 1977, p. 64-65.

Collerson, K. D., Jesseau, C. W., and Bridgewater, P., 1976, Crustal development of the Archean gneiss complex—eastern Labrador, *in* The Early History of the Earth, B. F. Windley *(ed.):* John Wiley & Sons, New York, p. 237-253.

Condie, K. C., 1967, Geochemistry of early Precambrian greywackes from Wyoming: Geochimica et

Cosmochimica Acta, v. 31, p. 2135-2149.

______ 1981, Archean Greenstone Belts: Elsevier, Amsterdam, 434 p.

Coward, M. P., Lintern, B. C., and Wright, L. I., 1976, The pre-cleavage deformation of the sediments and gneisses of the northern part of the Limpopo belt, *in* The Early History of the Earth; B. F. Windley *(ed.)*: John Wiley & Sons, New York, p. 323-330.

Eriksson, K. A., and Kidd, W. S. F., 1985, Sedimentologic and tectonic aspects of the Archean Limpopo belt: Geological Society of America Abstracts with Programs, v. 17, p. 575.

Erslev, E. A., 1982, The Madison mylonite zone: A major shear zone in the Archean basement of southwestern Montana, *in* Geology of the Yellowstone Park area, Steven G. Reid, and David J. Foote, *(eds.)*: Wyoming Geological Association Guidebook, p. 213-222.

______ 1983, Pre-Beltian geology of the southern Madison Range, southwestern Montana, Montana Bureau of Mines and Geology Memoir 55, 26 p.

Gee, R. D., Baxter, J. L., Wilde, S. A., and Williams, I. R., 1981, Crustal development in the Archean Yilgarn block, Western Austrialia, *in* Archean Geology; J. E. Glover, and D. I. Groves, *(eds.)*: Geological Society of Australia, Inc., p. 43-56.

Gibbs, A. K., Montgomery C., O'Day, P. A., and Erslev, E. A., 1986, Geochemistry of Archean and Proterozoic sedimentary rocks and the record of continental crust formation: Geochimica et Cosmochimica Acta, v. 50, p. 2125-2141.

Giletti, B. J., 1966, Isotopic ages from southwestern Montana: Journal of Geophysical Research, v. 71, p. 4029-4036.

Hallager, W. S., 1980, Geology of Archean gold-bearing metasediments near Jardine, Montana [Ph.D. dissertation]: University of California, Berkeley, 140 p.

Harris, N. B. W., Holt, R. W., and Drury, S. A., 1982, Geobarometry, geothermometry and Late Archean geotherms from the granulite facies terrane of southern India: Journal of Geology, v. 90, p. 509-527.

Horrocks, P. C., 1983, A corundum and sapphirine paragenesis from the Limpopo mobile belt, South Africa: Journal of Metamorphic Geology, v. 1, p. 13-23.

Millholland, M. A., 1976, Mineralogy and petrology of Precambrian metamorphic rocks of the Gravelly Range, southwestern Montana [M.A. thesis]: Indiana University, Bloomington, 134 p.

Montgomery, C. W., and Lytwyn, J. N., 1984, Rb-Sr systematics and ages of principal Precambrian lithologies in the South Snowy block, Beartooth Mountains: Journal of Geology, v. 92, p. 103-112.

Myers, J. S., and Williams, I. R., 1985, Early Precambrian crustal evolution at Mt. Barryer, Western Australia: Precambrian Research, v. 27, p. 153-163.

Sandiford, M., and Wilson, C. J. L., 1986, The orgin of Archean gneisses in the Fyfe Hills region: Enderby Land, Field occurrence, petrography and geochemistry: Precambrian Research, v. 31, p. 37-68.

Shuster, R. D., Mueller, P. A., Erslev, E. A., and Bowes, D. R., 1987, Age and composition of the pre-Cherry Creek metamorphic complex of the southern Madison Range, southwestern Montana: Geological Society of America Abstracts with Programs, v. 19, p. 843-844.

Taylor, S. R., and McLennan, S. M., 1985, The continental crust: Its composition and evolution: Blackwell Scientific Publications, Boston, Massachusetts, 312 p.

Taylor, S. R., Rudnick, R. L., McLennan, S. M., and Eriksson, L. A., 1986, Rare-earth elements patterns in Archean high-grade metasediment and their tectonic significance: Geochimica et Cosmochimica Acta, v. 50, p. 2267-2279.

Thurston, P. B., 1986, Geochemistry and provenance of Archean metasedimentary rocks in the southwestern Beartooth Mountains [M.S. thesis]: Montana State University, Bozeman, 74 p.

Veizer, J., and Jansen, S. L., 1985, Basement and sedimentary recycling 2: Time dimension to global tectonics: Journal of Geology, v. 93, p. 625-643.

Weaver, B. L., Tarney, J., Windley, B. F., Sagavanam, E. B., and Venkate, R. V., 1978, Madras granulites: Geochemistry and PT conditions of crystallization, *in* Archean Geochemistry, B. F. Windley, and S. M. Naqvi, *(eds.)*: Elsevier, Amsterdam, p. 177-204.

Windley, B. F., 1984, The Evolving Continents: John Wiley & Sons, New York, 399 p.

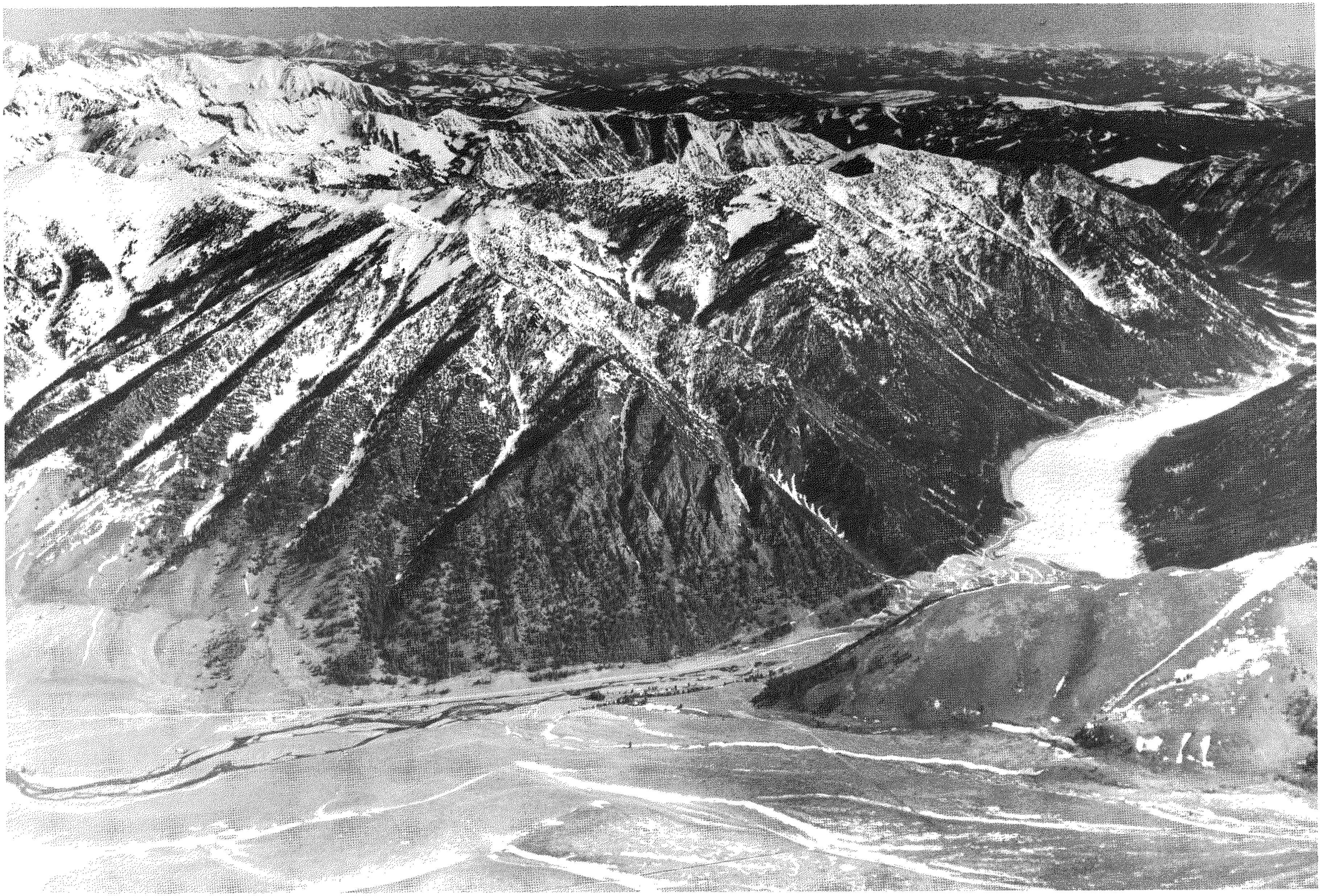

Aerial oblique of the southern Madison Range, Montana. Madison Canyon landslide and Quake Lake are seen in lower right of photograph. (Hugh Dresser photo.)

FIELD GUIDE TO THE HIGHLAND MOUNTAINS, SOUTHWEST MONTANA

J. Michael O'Neill
U.S. Geological Survey
Denver, Colorado 80225

Introduction

The basement rocks in the southern part of the Highland Mountains are exposed in the Twin Bridges 15-minute quadrangle and adjacent Wickiup Creek and Nez Perce 7½-minute quadrangles. This field guide begins in Twin Bridges, located in the southeast quarter of the quadrangle and proceeds northwestward across the southern and northern parts of the mountains to Butte, **(Figure 1)** . The purpose of the field trip is: (1) to visit outcrops on the southeast side of the Highland Mountain dome to examine quartz-feldspar-biotite gneiss, garnetiferous gneiss, and biotite gneiss; (2) make a 5-mile foot traverse across the southwestern part of the dome; (3) make an auto traverse across the uppermost biotite gneiss; and (4) to view a complete section of metasedimentary rocks of the Middle Proterozoic Belt Supergroup, as well as travel across the southern part of the Boulder batholith.

Road log

Mileage

0.0 Twin Bridges. Intersection of Montana routes 287 and 41; **proceed west** on Montana Route 41. Cross Beaverhead River.

0.6

0.6 **Turn right** on paved, non-designated county (Melrose) road.

1.2

1.8 Cross Big Hole River.

Stop 1: *Overview of the Highland Mountains.* Outcrops of crystalline rocks in the Highland Mountains outline a roughly triangular area of low-lying terrane, ranging in elevation from 5,000-8,800 feet. These crystalline rocks are part of a partially collapsed, basement-cored uplift of Laramide age. The uplift is a large, doubly plunging, N-NW-trending Laramide anticline. The crystalline basement rocks are bounded on the west mainly by homoclinally dipping Paleozoic rocks that, on the north and south, are folded into synclinal bends overturned to the west-southwest and faulted against crystalline rocks along NW-trending faults. On the northeast, the NW-trending, SW-dipping Silver Star reverse fault with structural relief near 8,000 feet has juxtaposed, overturned and thrust-faulted Devonian through Pennsylvanian sedimentary rocks against basement crystalline rocks. Crystalline rocks in the central part of the uplift are also cut by conspicuous NW-trending faults that first formed in Precambrian time and which have been reactivated during the Mesozoic and Cenozoic. On the north the cratonic rocks are overlain by homoclinally dipping Proterozoic through Mesozoic sedimentary rocks. The highest parts of the range, visible from this point, are underlain by Belt quartzites and siltites that are present near the base of this sedimentary succession. The basement rocks consist of penetratively deformed, amphibolite-grade metamorphic rocks that define a large, doubly plunging antiform that trends northeast to east and herein is referred to as the Highland Mountain dome.

0.8

2.6 Junction; **bear right** (northwest) on Rochester road.

1.8

4.4 Junction; **turn right** and ascend steep incline onto pediment surface cut on basement rocks of the Highland Mountains.

1.1

5.5 **Stop 2**: *Southeast limb of Highland Mountains dome*. (After passing through gate, descend about 20 meters into the first dry gulch.) Outcrops in this gulch are on the southeast

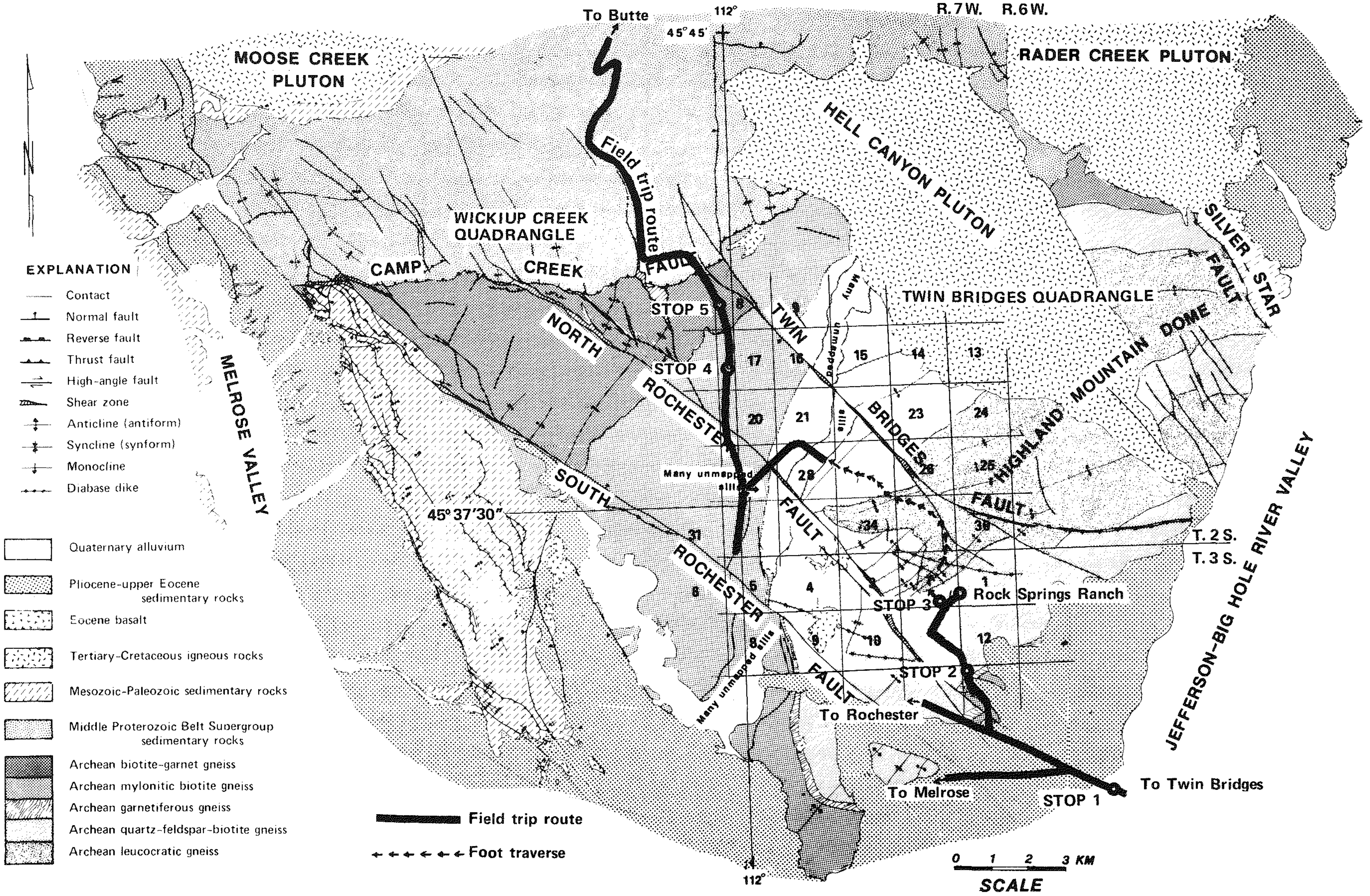
To Butte
112°
45°45'
R.7W.
R.6W.
MOOSE CREEK PLUTON
RADER CREEK PLUTON
HELL CANYON PLUTON
Field trip route
WICKIUP CREEK QUADRANGLE
CAMP CREEK FAULT
SILVER STAR FAULT
TWIN BRIDGES QUADRANGLE
HIGHLAND MOUNTAIN DOME
STOP 5
STOP 4
NORTH ROCHESTER FAULT
TWIN BRIDGES FAULT
MELROSE VALLEY
Many unmapped sills
SOUTH ROCHESTER FAULT
45°37'30"
JEFFERSON-BIG HOLE RIVER VALLEY
T. 2 S.
T. 3 S.
Rock Springs Ranch
STOP 3
STOP 2
To Rochester
To Melrose
STOP 1
To Twin Bridges
0 1 2 3 KM
SCALE
EXPLANATION
Contact
Normal fault
Reverse fault
Thrust fault
High-angle fault
Shear zone
Anticline (antiform)
Syncline (synform)
Monocline
Diabase dike
Quaternary alluvium
Pliocene-upper Eocene sedimentary rocks
Eocene basalt
Tertiary-Cretaceous igneous rocks
Mesozoic-Paleozoic sedimentary rocks
Middle Proterozoic Belt Supergroup sedimentary rocks
Archean biotite-garnet gneiss
Archean mylonitic biotite gneiss
Archean garnetiferous gneiss
Archean quartz-feldspar-biotite gneiss
Archean leucocratic gneiss
Field trip route
Foot traverse

Figure 1—Generalized geologic map of southern part of Highland Mountains showing location of field guide and foot traverse.

limb of the dome. The rocks that overlie the core of the dome consist principally of quartz-feldspar-biotite gneiss and biotite gneiss. These rocks are separated from one another by a garnet-rich horizon of gneiss and schist that includes anthophyllite-garnet gneiss, mica schist, marble, amphibolite and magnetite gneiss. Here, these three rock sequences dip southeast, away from the axial part of the dome. Note the very platy character of the quartz-feldspar-biotite gneiss and the sheared, augen-bearing character of the overlying biotite gneiss. Small folds and rotated augen indicate that tectonic transport was down dip to the southeast.

Continue northwestward on narrow dirt road.

1.5

6.5 Junction; **bear right** (northeast) on trail road toward the ruins of Rock Springs Ranch.

0.6

7.1 Junction. **Park vehicles** on south side of gate leading to Rock Springs Ranch.

Stop 3: Begin 5-mile foot traverse which commences along a dirt road from this point, crossing through section 2, T3S, R7W.* The traverse begins in the lower part of the quartz-feldspar-biotite gneiss, through the rather broad contact zone between these well-layered rocks and the underlying leucocratic augen gneiss, across the axis of the dome, and down the northwest limb of the dome. Follow the road northward to the crest of the high ridge. The best outcrops are west of the road, along the south-trending spur that leads to the ridge crest. The axial part of the dome crosses the highest part of the traverse. South of the ridge crest, the axis of the dome bifurcates, resulting in a complexly folded, medial synform separating two antiforms exposing core rocks along their axes. These folds plunge gently southwest beneath the overlying quartz-feldspar-biotite gneiss. At the west side of the axis of the dome, core rocks consist of massive, strongly sheared and folded granitic gneiss to quartz-feldspar-biotite gneiss. Foliation in these rocks is axial planar and widely variable. The northwest side of the dome is more complex than the southeast side.

The quartz-feldspar-biotite gneiss and amphibolite that rest above the core rocks are gently folded into open synforms and antiforms and are strongly injected with pegmatite, augen gneiss, finely layered leucogneiss, and foliated granitic gneiss. Minor folds and rotated augen indicate relative tectonic transport down dip to the northwest. At the end of the traverse, in the northeast quarter of section 28, a coarse-grained, vertical granitic pegmatite intrudes quartz-feldspar-biotite gneiss. The dike is associated with thin sills of augen gneiss that appear to have been derived from the pegmatite, and injected into the wall rock; these sills thin and pinch out away from the dike. The dike, 10-12 feet thick in its lower parts, thins upward and terminates in pods of leucoaugen gneiss.

4.8

11.9 Big Bonanza mine. **Proceed southwest** downhill to Rochester road.

0.9

12.8 Junction; **turn right** (north).

2.0

14.8 **Stop 4**: *Dougherty Butte*. (Mylonitic biotite gneiss and diabase dike). The biotite-rich gneiss is the structurally highest metamorphic sequence in the Highland Mountains. The gneiss is divided into two mappable units—a lower mylonitic biotite gneiss and an upper biotite-garnet gneiss. The composition of both units is essentially biotite, quartz, plagioclase and garnet. Plagioclase porphyroblasts are common in the biotite-garnet gneiss, but in the mylonitic gneiss these crystals are anhedral and broken, or may be sheared and drawn out in the plane of foliation, or may occur as augen. The mylonitic gneiss is also characterized by a very planar foliation, and locally contains abundant boudins and tectonically distended fragments of amphibolite up to 1 meter in diameter. In contrast, the foliation in the overlying biotite-garnet gneiss is strongly folded and contorted, and is not sheared. The biotite-garnet gneiss is folded into a NE-trending synform that plunges gently southwest. The trace of the axis of the fold lies directly west of the mylonitic biotite and biotite-garnet gneiss contact; however, the mylonitic biotite gneiss does not reemerge on the opposite side of the synform, as it should if these lithologies were a part of a pre-existing layered sequence. The mylonitic gneiss is interpreted to have formed synchronously with the Highland Mountain dome and the adjacent synform, and represents a major zone of shear along which rocks slid off the axis of the dome.

1.7

16.5 **Stop 5**: Low pass. Biotite-garnet gneiss.

---

* For pickup at end of traverse, vehicles should **turn right** at trail road junction and proceed northwestward 4.5 miles to the Big Bonanza mine (**Figure 1**). At a dirt road junction, **turn right** for 1.5 miles to a cattle watering trough in the NE corner of section 28.

Camp Creek fault (0.3 miles to the north) separates biotite gneiss from coarse clastic facies of the LaHood Formation of the Belt Supergroup (Figure 1, O'Neill and others, this volume).

2.1

18.6 Junction; **turn right** onto Camp Creek road. (Road to left follows drainage of same name that ultimately leads to Melrose.) The route in this area traverses more that 8,000 feet of Proterozoic Belt sedimentary rocks, passing through the lowermost LaHood Formation into Newland, Greyson, Spokane, and Helena (middle Belt carbonate) formations, and through a thin section of the Missoula Group in the upper part of the Belt Supergroup.

0.2

20.3 Moffet Gulch to left.

0.3

20.6 **Bear right** (uphill).

1.7

22.3 **Turn left**; follow switchbacks uphill. (*Note:* Road is not shown on Wickiup Creek 7½-minute quadrangle.)

2.2

24.5 Leave Wickiup Creek 7½-minute quadrangle

0.6

25.1 Pass. Camp Creek drainage basin to the south, Moose Creek drainage basin to the north. The route is situated on part of the Spokane Formation at this location. Gold Hill (11:00) is underlain by the Helena Formation and a small stock related to the Boulder batholith.

8.0

29.1 Junction; **turn right** on Benton Park/Highland road.

0.4

29.5 Highland mine. Mine is in skarns associated with fault wedges of metasedimentary rocks surrounding the Burton Park pluton, satellite of the Boulder batholith.

8.0

37.5 Junction with Montana Route 2; **turn left.**

13.6

51.1 Intersection with Harrison Avenue, southern city limits of Butte.

©DIANE NUGENT 1988

FIELD GUIDE TO MESOSCOPIC FEATURES IN THE LAHOOD FORMATION, JEFFERSON RIVER CANYON AREA, SOUTHWESTERN MONTANA

Sharon E. Lewis
Montana Bureau of Mines and Geology
Butte, Montana 59701

Introduction

The Jefferson River Canyon south of LaHood Park in Madison County, Montana, is the site of spectacular, scenic exposures of Proterozoic to Mesozoic rocks, but perhaps the most distinctive unit exposed in the canyon is the Middle Proterozoic LaHood Formation of the Belt Supergroup. The distinctive and compelling well-exposed lithologies have attracted numerous geologists. The type section of the LaHood Formation is at this locality (Alexander, 1955; McMannis, 1963), although within the larger outcrop area of the formation, the rocks in the canyon may be somewhat anomalous. (See Schmitt, this volume for a summary of interpretations of LaHood Formation depositional environments and tectonic settings.)

This field guide is limited to observations of three well-exposed outcrops along or near Montana Route 2 in the LaHood Formation at the northwest end of Jefferson River Canyon. Other field guide coverages to the canyon and the LaHood Formation include Schmidt and others (1987), and Hawley and others (1982). Lithologies exposed here are sandstones; lithic sandstones; pebble, cobble, and boulder conglomerates (the most immediate attraction); and sparse fine- grained siltstone or argillaceous layers. Sedimentary features such as graded bedding (both normal and reversed), cross stratification, pebble imbrication, and channels and scours (large and small scale) are readily observable in one or the other of the three exposures. The conglomerates are polymictic, and clast lithologies include quartzofeldspatic gneisses and granitoids, amphibolites (ranging from fine to coarse grained, occasionally garnet bearing), limestone/marble (commonly with light-brown weathering calc-silicate layers), pegmatites, quartzites, and other minor lithologic types. Inasmuch as the clasts are generally reminiscent of southwestern Montana Archean lithologies presently exposed to the south and west, the age of the clasts is presumed to be Archean.

Road log

Mileage

0.0 LaHood Park: **proceed south and east** on Montana Route 2. (*Note:* The field stops in the narrow confines of Jefferson Canyon are in hazardous locations along the highway. Please use caution in parking and be advised of traffic.)

0.5

0.5 **Stop 1**: Gulch on the east side of the highway. Parking is ample in the immediate area. *Stay Alert!* In the appropriate season, the rattlesnake population may locally exceed the geologist population. Ticks are also seasonally abundant.

This site is the second stop in the field guide of Schmidt and others (1987) and adjacent to the gulch location of the original type section of Alexander (1955) (**Figure 1**). Bedding dips very steeply to the east, and the most prominent feature is a greater than 1 m-wide pegmatite boulder in a conglomerate on the east end of the outcrop. Viewed from the road, or slightly closer, another prominent feature is a 10^{+} m-thick, chaotically bedded, boulder conglomerate layer. Its basal contact is offset several meters in an apparently sinistral sense along the principal thrust of a minor fault zone approximately 30 centimeters wide. Subparallel faults which offset cobbles and narrow argilliceous beds show a lesser, but compatible movement sense. Fractures

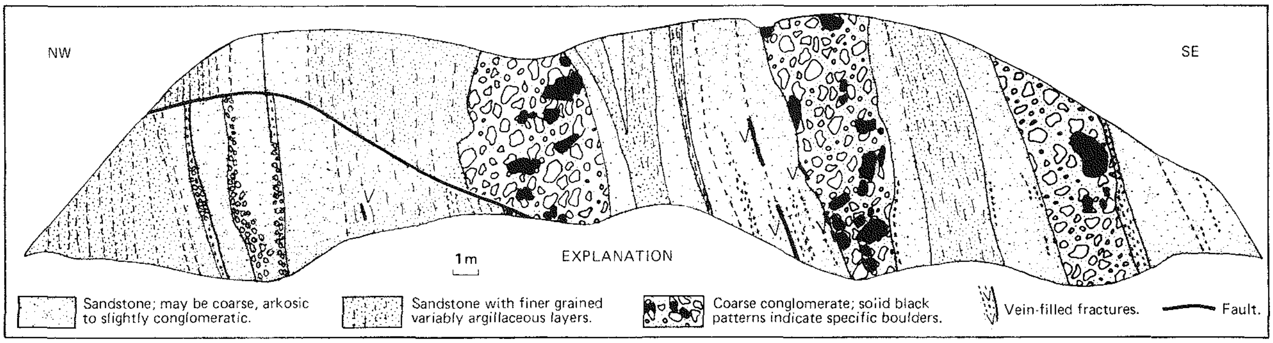
NW
SE
1 m
EXPLANATION
Sandstone; may be coarse, arkosic to slightly conglomeratic.
Sandstone with finer grained variably argillaceous layers.
Coarse conglomerate; solid black patterns indicate specific boulders.
Vein-filled fractures.
Fault.

Figure 1—Sketch of roadcut face at Stop 1.

veined with calcite (**Figure 1**) dip very steeply (parallel or subparallel) to bedding at this location.

Sedimentary features dominate this outcrop. Two large cobble conglomerate beds, the easternmost of which contains the large pegmatite boulder, occur east of the above described chaotic boulder bed. Coarse sandstone and conglomeratic sandstone form the largest volume of the outcrop. Graded bedding is observable in several layers. Zones with thinner-bedded layers increase to the west of the chaotic boulder bed, although a very prominent zone of thin-bedded sandstones, silty and argillaceous sandstone wedges, occurs just east of the boulder bed. Three irregularly bedded conglomerates can be traced from exposure level up to the fault on the west end of the outcrop.

0.3

0.8 **Stop 2**: Roadcut; parking space is available at both ends of the cut. Although not as coarse and obviously chaotic as the preceding location, conglomerates are a significant feature of this exposure. Toward the southeast, very irregularly bedded conglomerates show interdigitating relationships with sandstones. The northwestern end of the exposure is generally finer grained and more regularly bedded than the southeastern portion. **Figure 2** shows some of the few fine-grained argillaceous layers interbedded with finer sandstone and siltstone. This zone "feathers out" into the coarser material up dip several meters west of the view seen in **Figure 2**. Conglomeratic lenses are also visible above the finer beds.

Compared to the previous exposure, mesoscopic structural features are also more numerous at this location. Gently to moderately dipping shear zones (an example of which can be seen in the center of **Figure 2**) are interspersed throughout this roadcut. Some of these shears have 15 to 30 cm-thick zones of deformation. The low-angle faults locally parallel bedding, but more commonly are at some angle to the bedding. The lower-angle faults offset very steeply to vertically dipping, vein-filled fractures, in a sinistral sense as displayed in the offset shown in **Figure 2.** En echelon vein-filled fractures are locally common in this exposure.

0.2

1.0 **Stop 3**: Roadcut; parking is adequate at either end of the cut. Coarse clastic rocks are the major lithology at this location. Conglomerates form a significant proportion, although similar to the preceding locality, clasts larger than 30 centimeters are uncommon. Good examples of pebble imbrication are present at the northwest end of the exposure. Large channels and graded bedding also may be observed here.

Mesoscopic structural features are much more abundant at this stop than in the preceding locations. Gently to moderately dipping faults similar to those at Stop 2, and shown in **Figure 2**, are much more numerous. Steeply dipping, vein-filled fractures, and steeply dipping shear zones also occur more frequently at this location. One of the most intriguing mesoscopic features to be seen along this cut are offsets involving numerous cobbles within the conglomerates. Some cobbles are simply sheared off along faults with no remnant of the matching portion, but a few show movements of a few millimeters to several centimeters with respect to the same cobble. The cobbles are cut by both low-angle and steeply dipping faults, in a few instances within the same cobble. Lower-angle, E-dipping faults consistently show an apparent sinistral sense of offset, conversely W-dipping faults exhibit an apparent dextral offset (**Figures 3, 4, 5**). In most cases, higher-angle faults and vein-filled fractures are offset or terminated by the lower-angle faults. At least two 1 m-wide

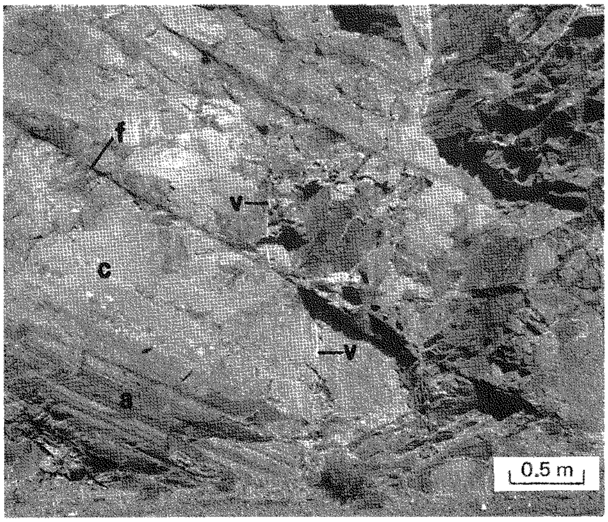

Figure 2—Argillaceous (a) and conglomeratic (c) sandstone of the LaHood Formation exposed in roadcut at Stop 2. Note offset of vein (v) by bedding plane fault (f). View is toward the northeast.

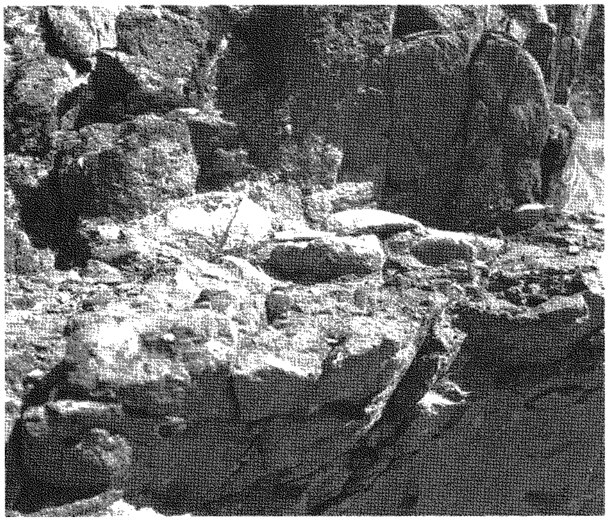

Figure 3—Marble clast showing dextral offset along W-dipping fault. Pocket knife for scale rests on plane of offset. View is toward the northeast.

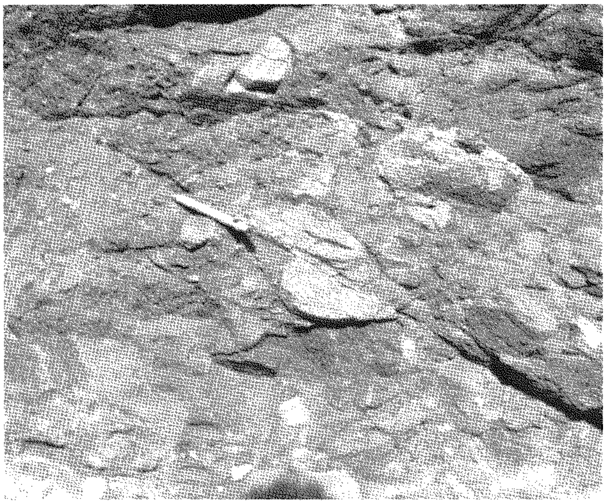

Figure 4—Quartzofeldspathic gneiss cobble showing sinistral offset along E-dipping fault.

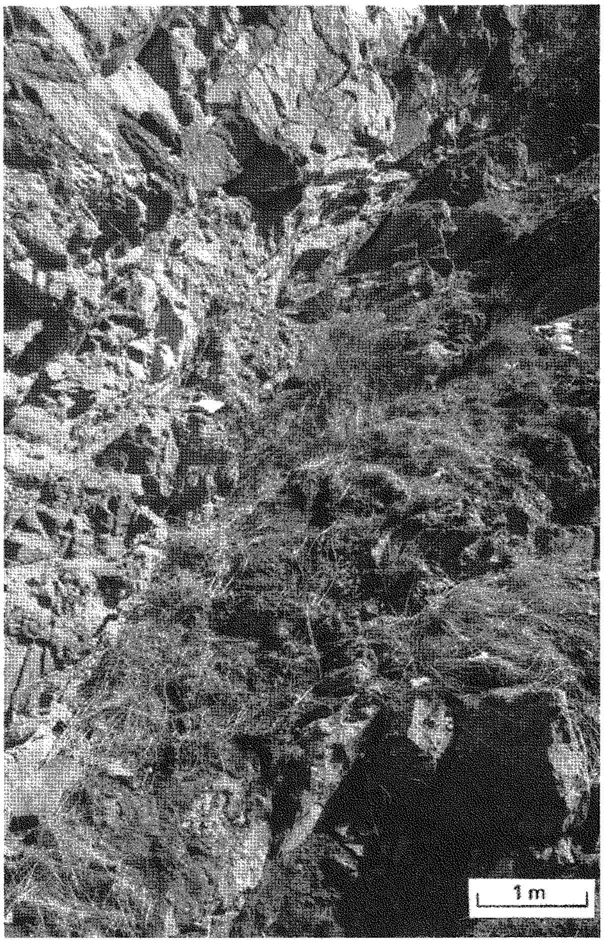

Figure 5—Zone of deformation along moderately dipping fault, parallel or sub-parallel to the thrust which places LaHood Formation over Paleozoic rocks.

zones of relatively significant offset are observable along this cut. Both faults dip moderately to the northwest.

The zone of deformation along the westernmost fault is shown in **Figure 5**. These faults roughly parallel the main fault which terminates the LaHood Formation exposures on the far eastern end of the roadcut and displaces Middle Proterozoic rocks over Paleozoic, and locally, Mesozoic rocks (Schmidt and others, 1987). Near the eastern end of the cut, a large vertically dipping shear zone, approximately one meter wide, shows some local offsets by lower-angle faults. This feature is roughly parallel to, but much larger than, the vein-filled fractures. Small veins within this shear zone and the lower-dipping zone immediately to the southeast contain talc, calcite and quartz (R. B. Berg, personal communication, 1988).

Discussion

A tentative sequence of formation of small-scale structures in Jefferson Canyon can be derived from the rocks exposed at the three field stops. **Figure 6** shows an equal area plot of poles to bedding surfaces (measured, mostly at road level, from northwest to southeast), which suggest that these rocks have been folded. The fold axis would be approximately N40E @ 20 NE. This is consistent with the slightly variable fold axes trends depicted by Schmidt and others (1987). Steeply dipping, vein-filled fractures maintain a consistent orientation over all three locations, and, if they represent a single generation of fracture filling, do not appear to have been affected by the folding event. These fractures are demonstrably offset by lower-angle faults, which are the classic conjugate set which would be associated with thrust faults (cf:, Ramsay and Huber, 1987). The smaller-scale conjugate faults are probably related to the major thrust which plots compatibly with the lesser faults on an equal area plot. The fault which displaces the steeply dipping chaotic boulder bed at Stop 1 has the same movement sense (sinistral) as the other E-dipping conjugate faults and is likely related to them. The offset of the vertical bedding indicates that the fault is post-folding, which may be the case for the major thrust as well.

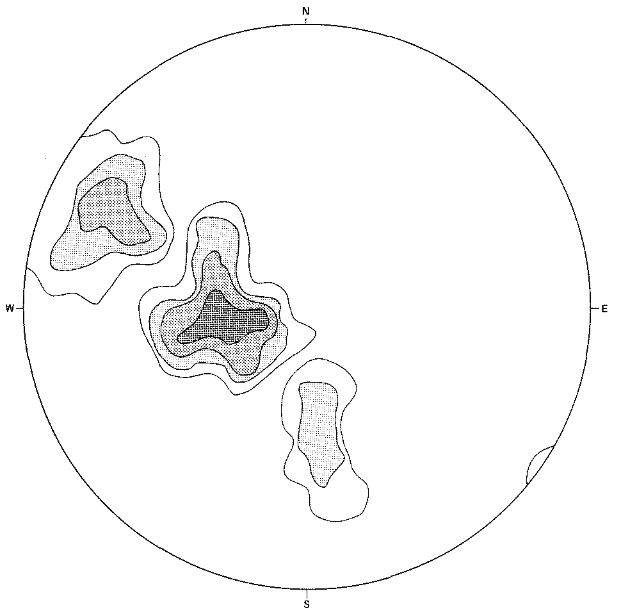

Figure 6—Equal area plot of 33 poles to bedding measured from road level between Stops 1 and 3. Contours are 3%, 6%, 9% and 12%.

Although penetrative cleavage is common in Belt Supergroup rocks throughout southwestern Montana, it is rudimentary to nonexistent in these outcrops. This is most likely a function of lithologic composition because such a high percentage of these rocks are phyllosilicate poor. Brittle fractures abound, with minor brittle-ductile behavior occurring along major shear zones. Most of the strain appears to be accommodated by brittle fracturing and interfault regions are likely zones of low to zero strain. Pure shear (irrotational strain) is the dominant mode of deformation. The few scattered vein-filled fractures may serve as local pressure solution sinks, but that process appears to be minor.

This preliminary study suggests that a considerable amount of interesting work could be accomplished, both by looking at a greater spectrum of the LaHood Formation in the Jefferson Canyon area, and by comparing minor structural features in the adjacent Phanerozoic section with those in the formation.

References

Alexander, R. G., 1955, Geology of the Whitetail area, Montana: Yellowstone-Bighorn Research Project Contribution 195, 111 p.

Hawley, D., Bonnet-Nicolaysen, A., and Coppinger, W., 1982, Stratigraphy, depositional environments, and paleotectonics of the LaHood Formation: Geological Society of America, Rocky Mountain Section Field Trip Guidebook: Montana State University, Bozeman, 20 p.

McMannis, W. J., 1963, LaHood Formation—a coarse facies of the Belt Series in southwestern Montana: Geological Society of America Bulletin, v. 74, p. 407-436.

Ramsay, J. G., and Huber, M. I., 1987, The Techniques of Modern Structural Geology: Folds and Fractures: Academic Press, v. 2, 700 p.

Schmidt, C. S., Aram, R., and Hawley, D., 1987, The Jefferson River Canyon area: Geological Society of America Centennial Field Guide, Rocky Mountain Section, v. 2, p. 63-68.

FIELD GUIDE TO A SECTION THROUGH THE NORTHERN IDAHO BATHOLITH AND SURROUNDING HIGH-GRADE METAMORPHIC ROCKS*

Donald W. Hyndman and David A. Foster**
Department of Geology
University of Montana
Missoula, Montana 59812

Introduction

This field trip traverses a well-exposed cross section of the northern Idaho batholith and briefly examines the broad aspects of this deep-seated granitoid body and its regional metamorphic country rocks. It also considers the role of synplutonic mafic magmas from the mantle in providing heat for melting of continental crustal rocks to form the more-felsic main-phase units of the batholith. The route of the field guide provides an opportunity to study the following:

1. Low- to high-grade regional metamorphic rocks of the eastern border zone.
2. Main-phase granodiorite to granite of the batholith.
3. Fine-grained synplutonic dikes of basaltic andesite to andesite which cut the batholith and make up about 20% of the total batholith volume; their complex mixing relationships with the batholith magmas.
4. High- to medium-grade regional metamorphic rocks and sheet-like intrusions of the western border zone.
5. Injection migmatites in the border zone rocks.
6. Some of the structures which relate to emplacement of the batholith.
7. Early western border zone tonalites.

Road log

Mileposts

90.1 Missoula, Montana to Lowell, Idaho via U.S. Highways 12 and 93. Bridge across Bitterroot River at south edge of Missoula.

88.4 to 87.4 Roadcuts in red to pale-brownish to pale-green, well-layered mudstones of Proterozoic Missoula Group of the Belt Supergroup. These rocks show ripple marks and mudcracks indicative of deposition in shallow water, perhaps a tidal flat or river flood plain. Similar, poorly exposed rocks continue to the proximity of Lolo.

83.4/ 32.6 Junction: Lolo, Montana; **turn right** on U.S. Highway 12. This route follows the Lolo Creek fault, a steep reverse fault with the south side up. Wallace Formation (underlies Missoula Group) sedimentary rocks of the biotite zone of the greenschist facies are on the north or downthrown side; Ravalli Group quartzite (underlies Wallace Formation) in the amphibolite facies is on the south or upthrown side. Prichard Formation semipelitic metasedimentary rocks of the lower Belt Supergroup, underlying the Ravalli Group farther south, are in the sillimanite zones bordering the northern Idaho batholith. Along the highway (for 25 miles) between Lolo and Lolo Hot Springs, are exposures of pale-gray to white, poorly bedded quartzite of the Ravalli Formation alternating with dark, rusty weathering, thin-bedded dolomitic siltstone of the Wallace Formation.

**Modified from* material prepared for the International Geological Congress (1989) and International Association of Volcanology and Chemistry of the Earth's Interior (1989).

**Present address: Department of Geology, State University of New York, Albany, New York 12222.

26.0 to 25.1 Lolo Peak (elev. 9,075′), visible on the skyline to the south, is in sillimanite zone of Prichard Formation metasediments (Wehrenberg, 1972). The northeast corner of the Idaho batholith is 15 kilometers farther south.

22.0 Pale-gray quartzite of the Ravalli Group in roadcut.

18.1 to 8.1 Roadcuts are mostly in thinly layered Wallace Formation sedimentary rocks with variable degrees of rusty weathering.

7.5 Large exposure of the Eocene Lolo batholith at Lolo Hot Springs (just inside contact of the batholith). It is a shallow, hypersolvus, A-type granite with miarolitic cavities.

0.0/174.35 Lolo Pass. Montana-Idaho border (elev. 5,233′).

170.8 Small metamorphosed gabbroic layered intrusion in roadcut; studied by Jens (1974). The black ultramafic layers of diopside and hornblende alternate with gray mafic layers of foliated amphibolite. The intrusion is faulted and cut by many discordant pegmatites, but its age, though pre-metamorphic, is uncertain.

169.75 Immediately northeast of bridge across Crooked Fork Creek, exposure of quartz diorite or granodiorite of the Brushy Fork stock (Nold, 1974), is cutting metaBelt quartzite. It is a medium-grained biotite quartz diorite or tonalite with about 20% biotite. The foliation is oriented about 113°/71°NE. The granitoid rock is cut by a discordant muscovite granite pegmatite/aplite dike. A 1 m-long xenolith of muscovite-biotite quartzite has foliation and layering concordant to the contact and to the foliation in the granitoid intrusion. Crosswarps of the schistosity are at about 90°.

165.8 Calc-silicate paragneiss, probably meta-Wallace Formation of the Belt Supergroup, has been regionally metamorphosed to the amphibolite-facies. Layering oriented 074/45°N is cut by a concordant muscovite-biotite-quartzofeldspathic alaskite dike about 15 centimeters thick and a discordant dike 45 centimeters thick. A vertical granite dike 3 or 4 meters thick, has reacted with diopside to form black hornblende. Several fine-grained mafic dikes about 60 centimeters to 1 meter thick dip gently northeast. These are internally foliated and contain small biotite porphyroblasts.

165.05 A rockslide made up of large blocks of well-layered meta-Wallace Formation with actinolite-diopside-plagioclase layers and biotite quartzite layers. The largest block above the highway shows a well-developed dilational pegmatite with thin aplite and pegmatite borders. Smaller blocks just below highway and slightly east show a rippled-looking surface: Are these preserved ripple marks or the intersection of a spaced cleavage cutting layering and schistosity?

159.5 Papoose Creek. Located 0.1 miles to the northeast, nearly vertical dark-gray synplutonic mafic dikes cut granite and metasedimentary rocks of the Idaho batholith border zone. The dikes trend nearly parallel to the roadcut. The dikes are metamorphosed and now consist of biotite-plagioclase rock. Strong foliation and slight lamination in the dikes are essentially parallel to the dike walls. Granite and pegmatite dikes up to 1.2 meters thick cut the mafic dikes.

156.45 **Stop 1: Park in small turnout** just east of curve on south side of highway. Megacryst-rich biotite granodiorite, apparently an early complexely deformed phase of the Idaho batholith, shows complex veining by granitic dikes; the most-photogenic exposures are in blocks below highway and slightly east of turnout. K-feldspar megacrysts average about 2.5 x 4 centimeters, and have white plagioclase rims. They are subhedral and make up 5 to 10% of the rock, though locally they make up 15 to 20 cm-zones with up to 35% megacrysts. The groundmass contains no K-feldspar. Considered alternative origins for the K-feldspar megacrysts are:

a. Early-formed phenocrysts? Consider magma/rock composition on an An-Ab-Or ternary (no apparent peritectic relationship to eliminate K-feldspar)?

b. Are late-magmatic grains (crystallization order plausible from experimental $T\text{-}X_{H_2O}$ diagrams of Whitney, 1975) large because of higher water content of magma in late stages? Consider why they are subhedral and some have concentrically enclosed inclusions of other minerals in the rock. Are they a replacement of a pre-existing groundmass?

c. Post-magmatic porphyroblasts. Note that one or two straddle granodiorite/country rock contacts. If isochemical metamorphic porphyroblasts, why is only the K-feldspar so coarse? Why the concentric inclusions? If metasomatic porphyroblasts, why are K-feldspar porphyroblasts essentially confined to the granodiorite and not in the country rocks?

Foliation is oriented 140°/74°SW and is marked by K-feldspar megacrysts, plagioclase and biotite. Irregular criss-crossing veins of biotite-quartz-feldspar pegmatite and alaskite are 1 to 10 centimeters thick. Dikes of layered medium-grained granite are up to 1 meter thick and locally up to 6 meters thick. The subtly graded layers have variable mafic content and grain size with tops up.

156.6 to 148.9 A large roadcut in dark gray, biotite-rich quartz diorite orthogneiss is cut by many criss-crossing pegmatite and alaskite dikes 1 to 60 centimeters wide. Plagioclase making up about 40% of the rock occurs as 4 to 7 mm-subhedral, white grains. Scattered translucent megacrysts of K-feldspar have more opaque white rims of plagioclase 1 or 2 millimeters thick. Quartz diorite orthogneiss cuts layered paragneiss (metaBelt?). One planar, subhorizontal fine-grained mafic dike 30 to 60 centimeters thick cuts the other rocks.

141.9 Main-phase biotite granite with 1 to 2% K-feldspar megacrysts. A few faint schlieren are at N 55° W/37° NE. Very fine-grained, dark gray mafic dikes 15 to 30 centimeters thick cut the granite. The mafic dike at southwest end of outcrop (near milepost 141.85) shows foliation oblique to its borders.

141.85 Essentially massive megacryst-bearing, main-phase granite. Faintly visible are 2 to 5 cm-schlieren which are oriented N40°W/45°NE. Very irregular 15 to 60 cm-mafic dikes cut the granite on curved fractures. One mafic dike contains a 2 x 5 cm-xenolith of medium-grained granite.

139.1 Exposed granodiorite complex shows complex interactions between magmas. Medium-grained biotite granodiorite is inhomogeneous, has more felsic zones, more mafic zones, and granitic pegmatites. Zones rich in pink K-feldspar appear to be associated with cross-cutting joints and are probably alteration zones imposed in Tertiary time. The granodiorite is cut by a mafic dike and contains angular mafic xenoliths resembling the dike. The granodiorite, in a curving, irregular contact with a finer-grained more-mafic phase, is in turn cut by pod-shaped masses and dikes of granite. The more-mafic phase contains angular xenoliths of fine-grained mafic dike material that are, in turn, cut by fine-grained, light-gray felsic dikelets 1 to 6 millimeters thick. The granodiorite has more mafic areas, swirled more-mafic granodiorite, and granitic patches (some rounded and some swirled with granodiorite).

Another sheet of mafic rock less than 1 meter thick and 5 meters long, is cut by pegmatites higher in the outcrop. Masses of mafic rock and granitic areas become larger and more defined; most of the mafic xenoliths are cut by ptygmatic veins of granite. Below the highway, at the stream edge (behind "anglers" sign), a large, light-colored block about 2 meters across, shows white, medium-grained granite cutting 15 cm-layers of meso-type medium-grained biotite granodiorite that is foliated obliquely to the granite. The granite is also weakly foliated subparallel to layers in the granodiorite. Both granite and granodiorite are cut by planar joints oriented about 80° to the foliation, that show pink medium-grained K-feldspar alteration zones about 2 centimeters wide. This alteration was probably associated with Tertiary intrusions nearby. Oblique diffuse shears about 30° to the layers, combined with the foliation resemble mylonitic S-C surfaces.

134.3 **Stop 2: Park in turnout** on south side of highway. A sample of quartz monzodiorite at milepost 134.15 has been dated at 66 Ma.; U-Pb zircon lower intercept of 66 Ma. (Schuster and Bickford, 1985).

There are three dikes in the roadcut that show synplutonic mafic-dike relationships. The dike to the southwest is thin, poorly exposed, and mylonitic. The thick (3.2 m) dike in the center of the roadcut is fine-grained, gray basaltic andesite to andesite with some areas containing 1 to 2 mm-mafic spots. The dike is very inhomogeneous, consists of many rounded inclusions, or blobs of andesite, with thin rims of felsic material and a matrix of andesite. It contains one 5 cm-rounded inclusion of granite. The mafic dike to the northeast curves and steepens upward into a thick sheet or sill which shows clear synplutonic relationships with the host granite. It is somewhat finer-grained and chilled against the intruded granite. Numerous granitic dikes and ptygmatic granitic pods injected into the thick mafic sheet are contorted, pinch and swell, and some seem to surround blobs of andesite. Below the mafic sheet, the granitic rock is contaminated to a very inhomogeneous granodiorite to quartz diorite with many felsic and mafic inclusions. The more mafic granitoid rocks from high on the outcrop can be sampled in the loose material in the borrow pit. A loose block halfway down to the river and 5 or 6 meters downstream from the thickest dike, shows fine-grained dark-gray dike rock laced with medium-gray more-felsic dikelets. Several other blocks nearby show the same relationship.

128.55 to 128.7 Synplutonic gabbroic/peridotite complex. The brownish weathering peridotite or hornblende pyroxenite in the central part of the long exposure may be a differentiated magma chamber of the "mafic dike magma" (?). Also hornblende-rich (50%) metagabbro.

To the southwest is a hornblende diorite to biotite granodiorite injection zone, probably a zone of mixing between mafic and felsic magmas. It possesses a highly variable mafic mineral content, and the lighter-colored phases contain darker inclusions. Sharply bounded xenoliths of more-mafic diorite are enclosed in a nearly massive hornblende diorite. Farther to the southwest these rocks are cut by granodiorite to granite.

128.45 State of Idaho highway maintenance shop.

125.0 **Stop 3: Park in turnout** on south side of highway. **Walk** from milepost 125.0 to 124.9 and consider the total percentage of mafic dike material. There are numerous dikes and many dike-granite relationships. The mafic dikes show sharp to moderately sharp, but irregular to planar contacts with the granitoid rock. Some dikes are foliated and veined at a large angle to the contacts; the 3 mm-mafic "phenocrysts" are now altered. The granodiorite is inhomogeneous. Some dikes are lineated, have streaks of granitoid material, and numerous small mafic spots—pseudomorphs of small mafic phenocrysts. Angular xenoliths of meta-andesite contain 1-2 mm-mafic spots in the granodiorite. Some dikes show intermingling of andesite and granite. Granitoid areas in some dikes are more mafic—contaminated by mafic dike magma. One dacite dike shows veins, streaks, spots, megacrysts, inclusions of felsic material, and a xenolith of a mafic dike. One area of small dikes grades out into schlieren. Note that boulders near the river at milepost 124.95 show mafic dikes that grade into rounded blobs and schlieren.

About 400 meters downstream from milepost 125 (23 m downstream from a tributary creek flowing beneath the highway in a large pipe) and below road level, is a loose block showing medium-grained granite in contact with fine-grained, dark gray, elongate inclusions of mafic dike material, which are surrounded by a "mixed zone" of intermediate composition and grain size.

122.4 **Stop 4**: Near big pine tree on outside bend of highway); **park in turnout** on south side of road at milepost 122.5. This large area of mafic dike rock is marginally exposed, but shows much interaction with the granite. Upslope (approximately 8 m) are some good exposures of comingled mafic and felsic magmas. The granite contains a few 2 to 10 cm-subrounded xenoliths of mafic dike rock. Many excellent (clean) exposures are in loose blocks on the midslope between the highway and river—particularly 30 meters upstream to 45 meters downstream from the big pine tree.

118.6 to 116.0 Mafic dikes with xenocrysts(?). Massive, intermediate-composition mafic dikes have very small gabbroic xenoliths, now altered white. One dike has chilled margins. The mafic dikes cut biotite granite with some K-feldspar megacrysts. Country rock to the west across a steeply dipping fault is a foliated migmatitic calc-silicate gneiss containing much diopside. Alaskite dikes 1 to 8 centimeters thick crisscross the outcrop of gneiss, the most prominent set dipping 15° to the northwest.

Exposure of massive main-phase granite at milepost 116.0. A large, irregular xenolith of contorted biotite-rich gneiss is enclosed in the granite which also shows faint but distinct schlieren. A few gently dipping pegmatite dikes 2 to 45 centimeters thick cut the granite and are discordant to the mafic schlieren. A steeply dipping, dark-gray, fine-grained andesite dike 8 to 12 centimeters thick cuts the granite. Another basaltic dike appears as a large angular "patch," with a chilled border on one side and sheared on the other side. A pod of fine-grained rhyolite (Eocene?), about 2 meters thick dips, 10 to 20°NE and has a wavy contact with the granite.

112.5 Biotite quartzofeldspathic gneiss and veined gneiss with foliation oriented 107°/78°NE is cut by a subhorizontal layered granite sheet. The sheet shows grading with mafic grains concentrated towards the base of each 2 to 30 cm-thick layer. The sheet extends from milepost 112.4 to 112.75 and is about 1 to 3 meters thick and cuts main-phase granite. It may represent movement on a subhorizontal shear in the late stages of crystallization of the granite (a late-magmatic "mylonite zone"). At milepost 112.65 the layered granite sheet is cut by a gently dipping 2 to 5 cm-thick muscovite-quartz-feldspar pegmatite. A fine-grained greenish white rhyolitic dike about 5 meters thick cuts both the layered granite sheet and the thin later pegmatite at milepost 112.70.

111.3 to 110.5 Main-phase granite of the Idaho batholith contains about 10% megacrysts of K-feldspar; most of the megacrysts are about 1 x 2 or 3 centimeters. The rock is rather inhomogeneous in places; some gneissic schlieren contain steeply plunging folds (milepost 110.5) intruding breccia at pluton contact of granodiorite cutting biotite-rich country rock. The country rock has somewhat contorted, near-vertical foliation; the folds plunge on very steep axes. A gently SW-dipping pegmatite dike about 2 meters thick cuts the intrusion breccia. Just to the east is a massive fine- to medium-grained granodiorite containing many wavy, streaky xenoliths and schlieren. Several pegmatite dikes 5 to 75 centimeters thick dip gently to the northwest.

109.3 Calc-silicate gneiss of the Wallace Formation(?) metaBelt with steep foliation is cut by subconcordant, irregular, veins of streaky hornblende granodiorite and a few 8 cm-thick veins of aplite.

104.75 **Stop 5**: Early megacryst-rich tonalitic unit. The best exposures are in blocks between the highway and river. This megacryst-rich biotite granodiorite is a tonalitic rock with K-feldspar megacrysts. K-feldspar megacrysts also exist in some granitic dikes that cut the megacryst granodiorite. This unit cuts and locally contains xenoliths of biotite-quartz schist that may be metaBelt. Megacrysts and biotite define a steep foliation; small folds in the schist plunge 63° → 125°. Foliation of megacrysts is crenulated on a decimeter scale and becomes strongly sheared and even mylonitic on some limbs; the megacrysts become augen in the sheared areas. Undeformed discordant granitic dikes up to 40 centimeters thick cut the megacryst granodiorite parallel to the axial planes of the crenulations. A few mafic dikes show mutually crosscutting relationships with megacryst granodiorite and approximately parallel (most-attenuated or sheared limbs) of crenulations of granodiorite. The mafic dikes are themselves foliated.

The sequence of events appears to be intrusion and foliation of the megacryst granodiorite, overlapping with intrusion of mafic dikes, and probably overlapping with crenulation of the megacryst granodiorite. These events are followed by intrusion of the granitic dikes parallel to the crenulations. If the biotite-quartz schist is metaBelt, the megacryst granodiorite cannot be pre-Belt basement and is presumed to be early-phase Idaho batholith.

103.4 Eocene dikes containing euhedral phenocrysts of quartz.

103.15 Foliated biotite-tonalitic orthogneiss shows mafic schlieren, xenoliths and diffusely bounded pegmatitic phases.

102.1 High-grade migmatite. A medium-grained laminated biotite-quartz-feldspar gneiss with foliation oriented 116°/76°NE is cut by a concordant biotite-quartz-feldspar pegmatite 2 meters or more thick, and by a steeply dipping, dark-gray fine-grained 60 cm-thick andesite dike with 30% plagioclase phenocrysts.

96.85 Bridge across Lochsa River at Lowell. A medium-grained kyanite-biotite-quartzofeldspathic gneiss is foliated at 145°/52°SW. The schistosity is crenulated on the scale of 1 to 3 millimeter grains.

Metasedimentary rocks in this region (west of the contact of the Idaho-Bitterroot batholith) have been described by Greenwood and Morrison (1973) and Reid and others (1979). Farther west, the flood basalts of the Columbia River Plateau, have filled the ancestral valley of the Clearwater River and are, in places, exposed near the highway. Still farther northwest, towards Orofino, long roadcuts on the south side of the Clearwater River expose diorites and tonalites of the Cretaceous Kamiah pluton.

References

Greenwood, W. R., and Morrison, D. A., 1973, Reconnaissance geology of the Selway-Bitterroot Wilderness area: Idaho Bureau Mines and Geology Pamphlet 154, 30 p.

Jens, J. C., 1974, A layered ultramafic intrusion near Lolo Pass, Idaho: Northwest Geology, v. 3, p. 38-46.

Nold, J. L., Geology of the northeastern border zone of the Idaho batholith: Northwest Geology, v. 3, p. 47-52.

Reid, R. R., Bittner, E., Greenwood, W. R., Luddington, S., Lund, K., Motzer, W., and Toth, M.,1979, Geologic section and road log across the Idaho batholith: Idaho Bureau Mines and Geology Information Circular 34, 20 p.

Schuster, R. D., and Bickford, M. E., 1985, Chemical and isotopic evidence for the petrogenesis of the northeastern Idaho batholith: Journal of Geology, v. 93, p. 727-742.

Wehrenbert, J. P., 1972. Geology of the Lolo Peak area, northern Bitterroot Range, Montana: Northwest Geology, v. 1, p. 25-32.

Whitney, J. A., 1975, The effects of pressure, temperature, and X_{H_2O} on phase assemblages in four synthetic rock compositions: Journal of Geology, v. 83, p. 1-81.

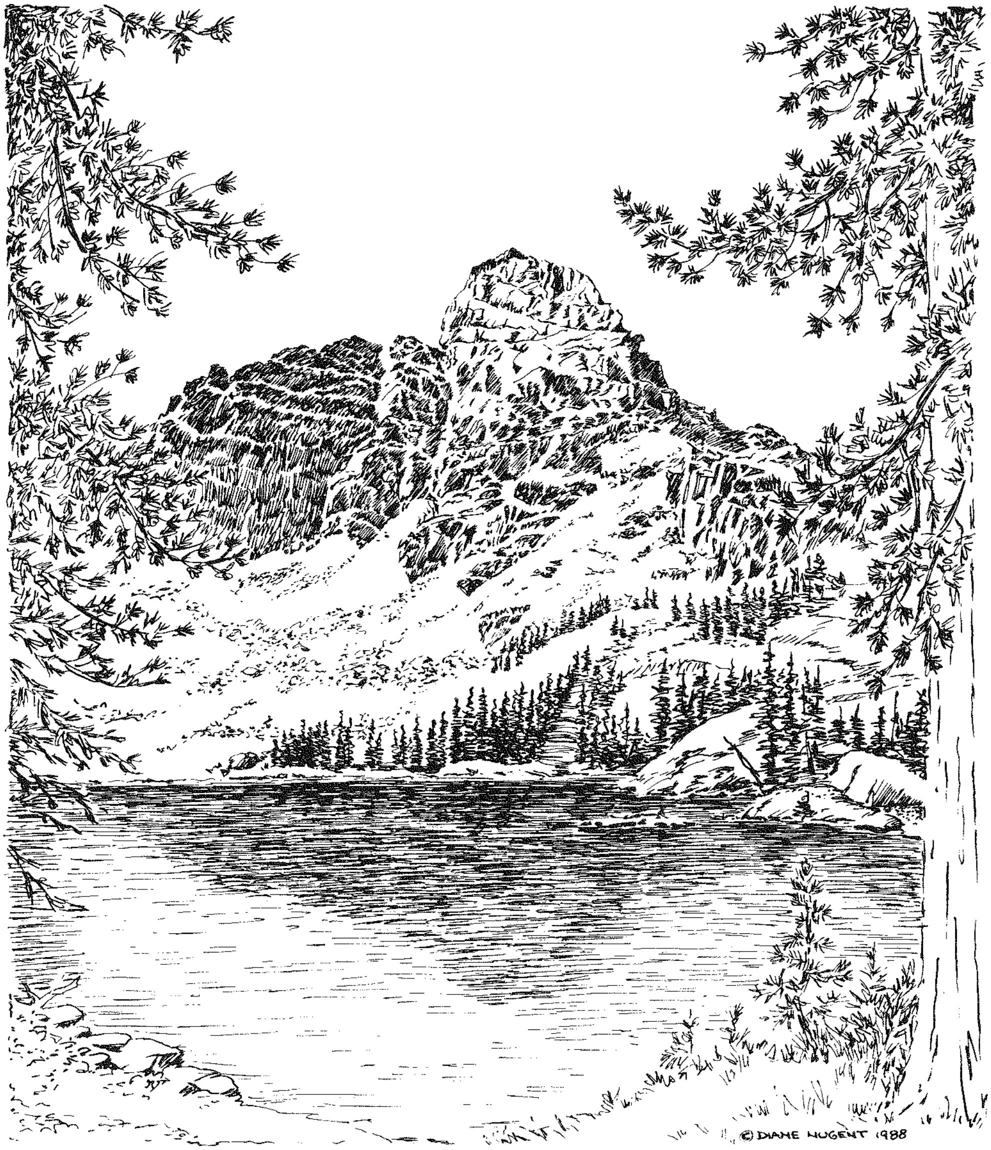

FIELD GUIDE TO DEFORMATION AND SENSE OF DISPLACEMENT IN MYLONITIC ROCKS NEAR OROFINO, IDAHO

Luther M. Strayer, IV
Department of Geology
University of Montana
Missoula, Montana 59812

Introduction

Kinematic analysis of strained synplutonic dikes in the mylonitic Kamiah pluton documents large scale (top-to-the-southwest) thrusting along the western Idaho suture zone (WISZ). Dip-slip movement of at least 85 kilometers placed mid-crustal levels of North America over the Kamiah pluton (Strayer and others, 1987) along a 1.5 km-thick, NE-dipping mylonite zone (**Figure 1**), which coincides with the boundary between Sr isotope initial ratios of about 0.704 or less to the west and 0.706 or greater to the east (Armstrong and others, 1977; Fleck and Criss, 1985).

The Kamiah pluton is a 83-81 Ma (Snee and others, 1987) tonalite/quartz diorite body laced with synplutonic mafic and pegmatitic dikes. It apparently intruded along a pre-existing boundary between continental North America and the Wallowa/Seven Devils terrane (Manduca, 1987); it was mylonitized near magmatic solidus temperatures.

Shear within the mylonite zone translated the synplutonic dikes into virtual parallelism with the mylonitic foliation (cf., Strayer and others, 1987; Strayer and others, 1988). Offset of late-stage pegmatite dikes across the concordant mafic dikes shows that shear was concentrated in the mafic dikes, and large-scale symmetry relationships indicate that displacement was dominantly down plunge at least for this section of the WISZ.

Road log

Proceed north from Kamiah on U.S. Highway 12 to historical markers for Long Camp and Asa Smith Mission (milepost 65.8). This is 1.8 miles from the bridge across the Clearwater River on the east side of Kamiah.

Stop 1: Located here is the southernmost exposure of the Late Cretaceous Kamiah pluton. From this point, and continuing to about the town of Greer, are numerous synplutonic mafic dikes; from Greer to Orofino the pluton becomes increasingly more foliated and the mafic dikes become less obvious. These dikes tend to be nearly vertical throughout the host quartz diorite and tonalite of the Kamiah pluton, but are without any regular trend (Hietanen 1962). Other excellent examples of these mafic dikes can be seen at mileposts 63.5, 62.5 and 61.8.

At this location, in outcrop and float, the mafic dikes and quartz diorite can be seen to be mutually crosscutting, indicating that both lithologies were emplaced at the same time. Undeformed plutonic rock along this portion of the highway consists of plagioclase, quartz, blue-green amphibole euhedral epidote (often with allanite cores) ± biotite. The euhedral nature of the epidote in isolation from plagioclase indicates the epidote may be of magmatic origin. Magmatic epidote can crystallize only at depths greater than about 25 kilometers (Zen and Hammarstrom, 1984; Zen, 1985). The mafic dikes are basaltic in composition with local grains of biotite. Extensive networks of pegmatitic dikes lace the undeformed quartz diorite pluton and mafic dikes. These pegmatites appear to be randomly oriented and are composed primarily of variable amounts of plagioclase, orthoclase, quartz and biotite. These are assumed to be the latest-stage differentiates of the Kamiah pluton. Observations within the shear zone (Stops 2, 3) indicate that injection of the pegmatites overlap the later stages of mylonitic deformation.

Continue on U.S. Highway 12 to Orofino.

Mileage

0.0 **Turn right** into Orofino, crossing bridge over Clearwater River. **Turn left** onto Idaho State Route 7 at "T" intersection and continue west along north side of Clearwater River (**Figure 2**).

4.0

4.0 Cross North Fork of Clearwater River; **turn right** at first intersection past bridge.

0.2

4.2 **Stop 2**: **Pull off** the highway to right in parking area beneath power lines.

This exposure is typical of the 1.5 km-thick body of mylonitized quartz diorite/tonalite of the area. The mineralogy of the unsheared and sheared quartz diorite in and adjacent to the suture zone are identical as determined by microprobe analysis, although the sheared quartz diorite is completely recrystallized in most samples. The stable metamorphic mineral assemblage is hornblende-plagioclase-±biotite-quartz. Rare mica 'fish' have the stair-stepping asymmetry of a type II S-C mylonite (Lister and Snoke 1984). These show top-to-the-southwest sense of displacement. In samples where the plagioclase has not been completely recrystallized, asymmetric composite tails of recrystallized plagioclase show a similar sense of displacement.

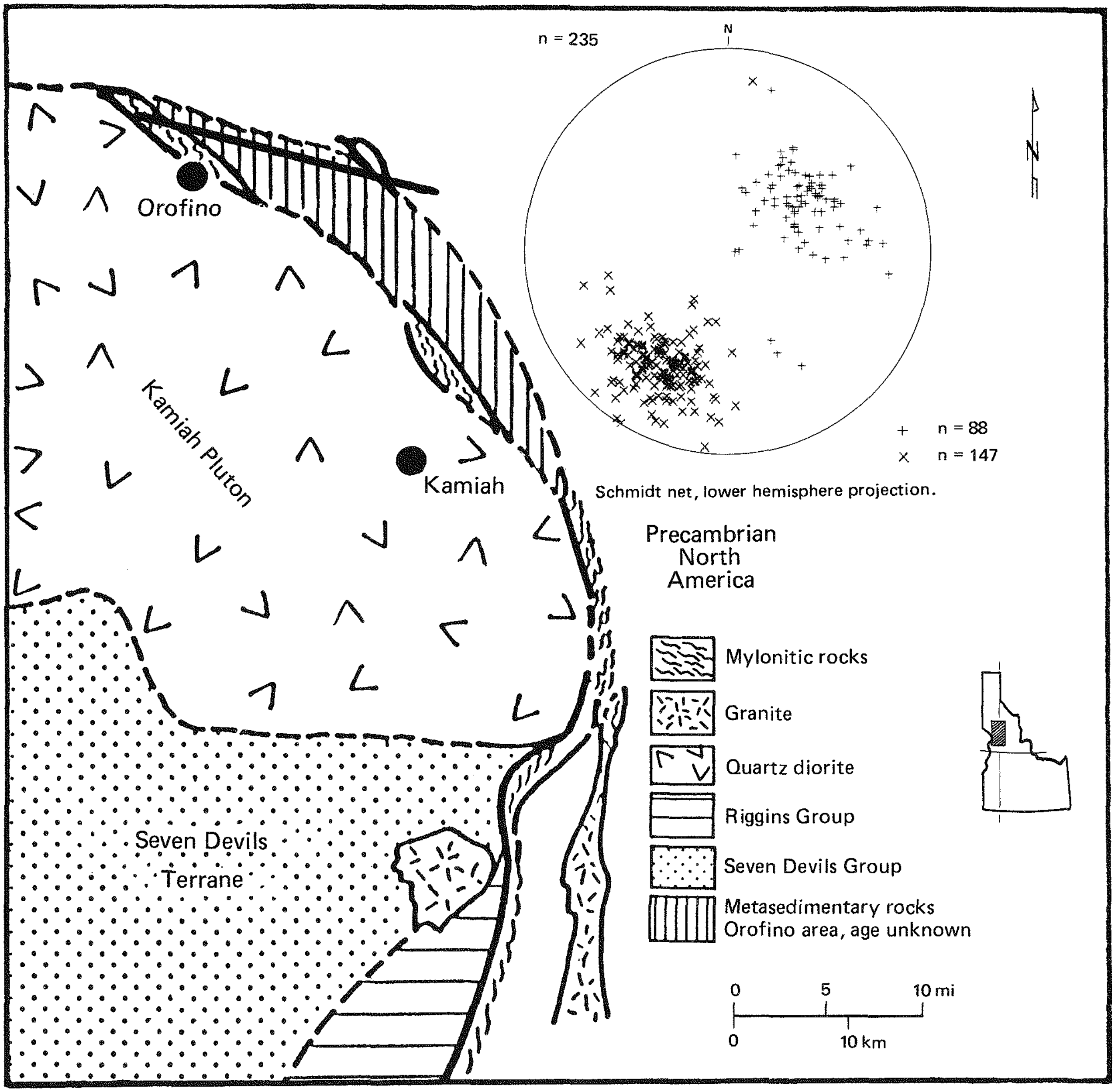
n = 235
N
+ n = 88
× n = 147
Schmidt net, lower hemisphere projection.
N
Orofino
Kamiah Pluton
Kamiah
Precambrian North America
Seven Devils Terrane
Mylonitic rocks
Granite
Quartz diorite
Riggins Group
Seven Devils Group
Metasedimentary rocks Orofino area, age unknown
0
5
10 mi
0
10 km

Figure 1—Geologic sketch map of northern part of the western Idaho suture zone (WISZ). Stereonet shows NE-plunging lineations (points) and the NW-SE-striking foliations (poles plotted as +) in the area of Ahsahka, northwest of Orofino. The ^{87}Sr/^{86}Sr initial isotopic ratio line is coincident with the boundary between Precambrian North American (white) and the western accreted terranes (patterned). Miocene Columbia River Plateau Basalts not shown.

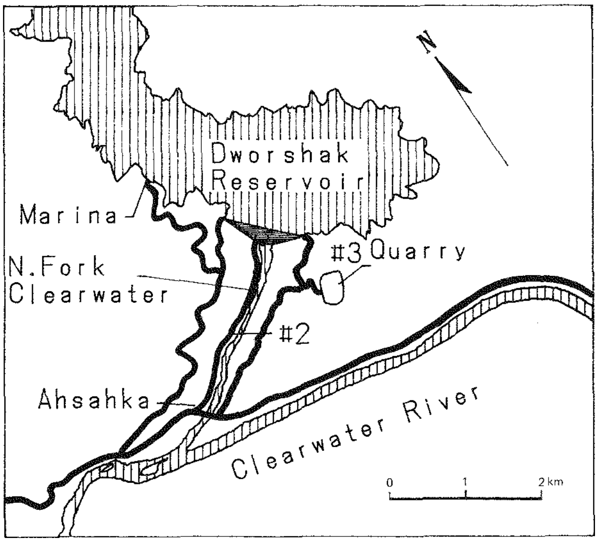

Figure 2—Sketch map of location of Stops 2 and 3 within the shear zone northwest of Orofino.

This outcrop also contains all of the features necessary to model the displacement that has occurred on this segment of the suture zone.

The most obvious feature of the outcrop is the mylonitic foliation. It has a mean strike and dip of 116°/54°NE, although this has probably been over-steepened by the pervasive latest-stage, SW-dipping, high-angle-reverse shear zones that are evident throughout this area, especially in the quarry at Stop 3.

Lying upon the foliation surface is a variably developed mylonitic lineation made up of aligned amphibole, biotite, or feldspar augen (the latter from sheared pegmatites). The mean lineation direction is 49°/055°, which in mylonites, is the direction of movement (Hanmer, 1982).

The synplutonic mafic dikes from outside the shear zone are observed here as sheared bodies, essentially concordant to the mylonitic foliation (**Figure 3**). The large-scale displacement can be modelled here by transposing the originally sub-vertical synplutonic mafic dikes from outside the shear zone to within virtual parallelism of the mylonitic foliation within the shear zone. For example; transposition of an initially vertical dike, to within 1° of the mylonitic lineation plunging at 49°, yields a very large shear strain γ of 56 by the equation of Ramsay (1967).

$$\gamma = \cot(\alpha') - \cot(\alpha)$$

where: α is the initial orientation of the dike with respect to the shear zone, and α' is the final orientation (**Figure 4**).

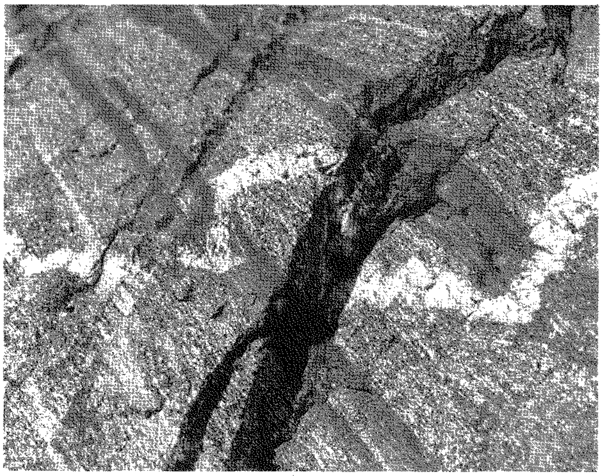

Figure 3—Outcrop photograph of transposed mafic dikes (dark material) that is virtually concordent to the mylonitic foliation. The two dark bands are actually from one folded mafic dike, now seen as two limbs of a northeast (right) plunging isocline. A later stage pegmatite dike (white material) crosscuts the transposed mafic dike and is offset in a top-to-the-southwest (left) sense. The pegmatite dike is approximately 3 centimeters across. (D. W. Hyndman photo.)

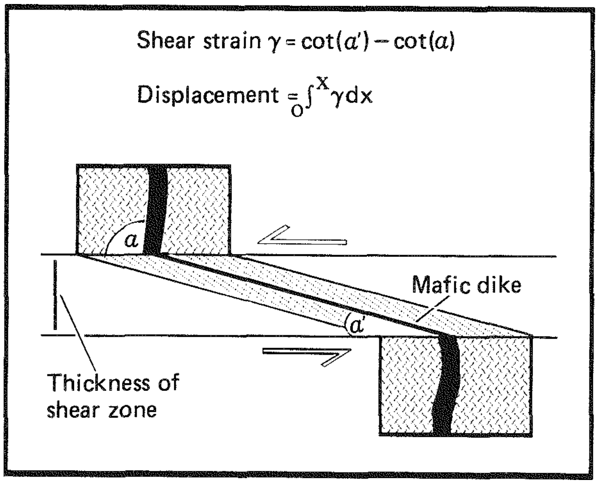
Shear strain $\gamma = \cot(\alpha') - \cot(\alpha)$
Displacement $= \int_0^X \gamma dx$
α
α'
Mafic dike
Thickness of shear zone

Figure 4—Large-scale displacement model shows an unsheared, nearly vertical mafic dike, transposed to within a small angle α' of the shear zone. Shear strain γ is calculated using α and α'. Displacement is calculated by integrating γ over the thickness of the shear zone.

Displacement can therefore be estimated to be about 85 kilometers by integrating over γ the 1.5-kilometer width of the shear zone (Ramsay and Graham 1970). Due to the large errors that can occur with small values of α' in the above equation, it is important to establish that the value of 1° is valid. Using a chalk line to accurately measure the angle between the dike and foliation, it was found that a maximum angle of 3°, and in most cases it was less than 1°, and too small to measure. Since the shear strain γ approaches infinity as α' approaches zero, the 1° angle used in the displacement calculation yields a conservative minimum estimate of displacement.

In this outcrop the sense of displacement is readily determined. Pegmatitic dikes that appear to be the latest-stage differentiates of the pluton are present within the shear zone; they range from undeformed, to boudinaged into series of discrete augen trains. Here, along the lower road and in the quarry at Stop 3, relatively undeformed pegmatites are seen to crosscut the sheared mafic bands where they display a top-to-the-southwest sense of shear (**Figure 5**). Also visible along this lower road are NE-plunging isoclines made up of transposed mafic bands and pegmatites that have been progressively deformed with the mylonitic foliation. In some locations, and especially in the quarry at Stop 3, these approach the geometry of sheath folds with plunges that plot on a stereonet parallel to the mineral lineations. This is consistent with the large shear strains previously determined.

Stop 3: Dworshak Dam quarry, near the east end of the dam. (*NOTE*: Access to this quarry is restricted and prior permission is necessary.)

This Stop affords a 360° view of the mylonitic deformation. The northeast wall of the quarry strikes almost perpendicular to the plunge direction and therefore gives an excellent down-plunge view of the mylonite. The large southeast wall of the quarry shows well-developed mylonitic foliation that is also visible at Stop 2. Symmetry relationships exhibited here show clear evidence of displacement along the plunge. Viewed along strike of the mylonitic foliation, deformed synkinematic pegmatites show strong overall monoclinic symmetry, with the mylonitic lineation lying in the plane of symmetry (**Figure 6**). Viewed down plunge however, the pegmatites are poorly oriented (**Figure 7**). In this direction the pegmatites, which act as passive markers, have been stretched in the plunge direction. A small granodioritic mass about 10 meters in diameter at the northeast end of the quarry (uppermost level) shows an almost rounded cross section when viewed down plunge, but appears streaked out into the foliation when viewed normal to the plunge. The combination is compatible with monoclinic symmetry and indicates that recorded shear along this segment of the suture was dip slip.

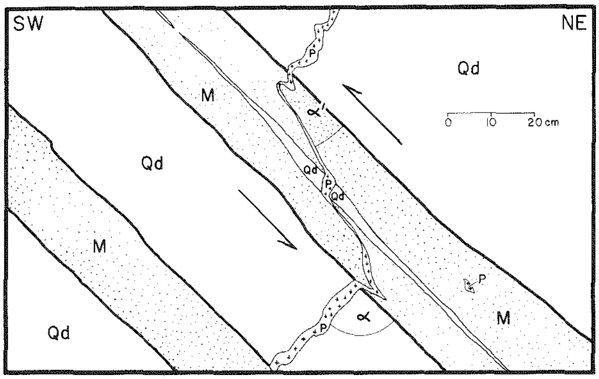

Figure 5—Tracing of outcrop photograph of transposed mafic dike. The dike is virtually parallel to the mylonitic foliation and contains a stretched quartz diorite inclusion. Late-stage pegmatitic dikes are shown crosscutting sheared mafic dikes and are consistently off-set in a top-to-the-southwest sense by simple shear. Shear strain γ is calculated using α and α' with the average = 3.2. Note the competency contrast between the mafic (M) and plutonic material (Qd) indicated by the less intense shearing of the pegmatite (P) within the quartz diorite inclusion.

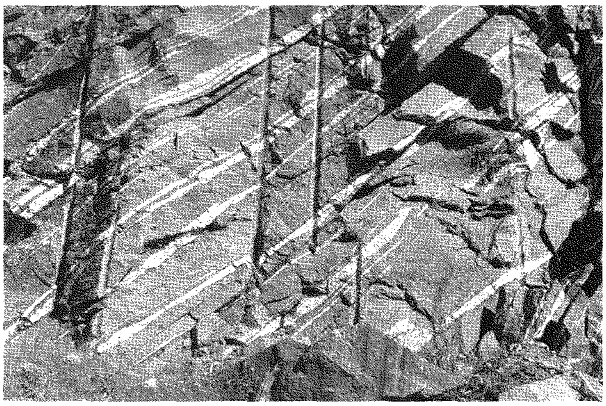

Figure 6—Outcrop photograph showing symmetry relationships of pegmatitic dikes from the quarry adjacent to Dworshak Dam. Viewed perpendicular to the mylonitic lineation direction, the well-developed NE-dipping foliation is marked by transposed late-stage pegmatitic dikes (white material) showing monoclinic symmetry. The vertical lines are 9 cm-diameter drill holes used in excavation. (D. W. Hyndman photo.)

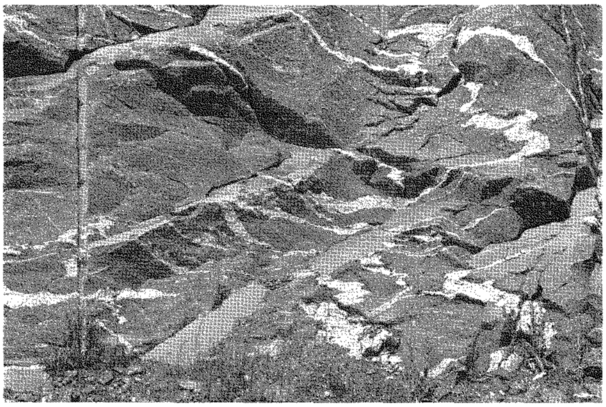

Figure 7—Outcrop photograph showing down-plunge direction (90° from Figure 6). The foliation is poorly defined and the pegmatites are poorly orientated in this exposure in the quarry adjacent to Dworshak Dam. In this view some of the pegmatites appear to have been passively deformed into folds which approach the geometry of sheaths. The vertical lines are 9 cm-diameter drill holes used in excavation. (D. W. Hyndman photo.)

Conclusions

Since the pegmatites are variably deformed in the mylonite zone and are the latest phase of the pluton, mylonitic deformation must have occurred as the pluton was at magmatic solidus temperatures. The pluton was emplaced into the Wallowa/Seven Devils terrane, as it was underthrust northeastward beneath continental North America. Kyanite- and sillimanite-bearing migmatites in the lower part of the Precambrian Belt Supergroup northeast of the suture (Hietanen, 1962), and apparently magmatic epidote in the Kamiah pluton, indicates that this part of the WISZ may be the deepest exposure of a structural and metamorphic culmination formed by underthrusting. The Rapid River and associated thrusts may be shallow level splays, rooting from the WISZ mylonites **(Figure 8)**.

Rise of arc basaltic magmas, presumably from the evolving Kamiah pluton, may have initiated melting of hanging-wall continental crust and caused the subsequent formation of the Idaho batholith (Hyndman and others, 1988; Hyndman and Foster, 1988).

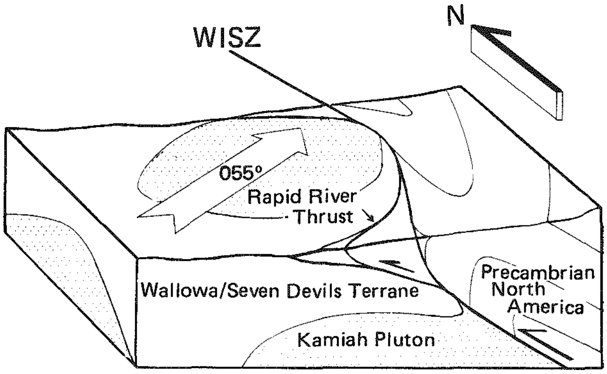

Figure 8—Simplified block diagram shows underthrusting of the western Wallowa/Seven Devils terrane beneath Precambrian North America along the western Idaho suture zone (WISZ).

References

Armstrong, R. E., Taubeneck, W. H., and Hales, P. O., 1977, Rb-Sr and K-Ar geochronometry of Mesozoic granitic rocks and their Sr isotopic composition, Oregon, Washington and Idaho: Geological Society of America Bulletin, v. 88, p. 397-411.

Fleck, R. J., and Criss, R. E., 1985, Strontium and oxygen isotopic variations in Mesozoic and Tertiary Plutons of central Idaho: Contributions to Mineralogy and Petrology, v. 90, p. 291-308.

Hanmer, S. K., 1982, Microstructure and geochemistry of plagioclase and microcline in naturally deformed granite: Journal of Structural Geology, v. 4, no. 1, p. 197-213.

Hietanen A., 1962, Metasomatic metamorphism in western Clearwater County Idaho: U.S. Geological Survey Professional Paper 344-A, 116 p.

Hyndman, D. W., and Foster, D. A. 1988, The role of tonalites and mafic dikes in the generation of the Idaho batholith: Journal of Geology, v. 96, p. 31-46.

Hyndman, D. W., Strayer, IV, L. M., and Sears, J. W., 1988, The western Idaho suture zone (II): Implications from the Kamiah pluton: Geological Society of America Abstracts with Programs, v. 20, no. 6, p. 422.

Lister G. S., and Snoke A. W., 1984, S-C mylonites: Journal of Structural Geology, v .6, no. 6, p. 617-638.

Manduca, C. A., 1987, Multi-stage formation of arc-continent boundary in western Idaho: Geological Society of America Abstracts with Programs 1987, v. 19, no. 7, p. 758.

Ramsay, J. G., 1967, Folding and Fracturing of Rocks. McGraw-Hill, New York, 568 p.

Ramsay, J. G., and Graham, R. H., 1970, Strain variations in shear belts: Canadian Journal of Earth Science, v. 7, p. 786-813.

Snee, L. W., Lund, K., and Davidson, G., 1987, Ages of metamorphism, deformation, and cooling of juxtaposed oceanic and continental rocks near Orofino, Idaho: Geological Society of America Abstracts with Programs, v. 19, no. 5, p. 335.

Strayer, IV, L. M., Hyndman, D. W., and Sears, J. W., 1987, Movement direction and displacement estimate in the western Idaho suture zone mylonite: Dworshak Dam/Orofino area, west-central Idaho: Geological Society of America Abstracts with Programs, v. 19, no. 7, p. 857.

Strayer, IV, L. M., Sears, J. W. and Hyndman, D. W., 1988, The western Idaho suture zone (I): Evidence for a structural and metamorphic culmination: Geological Society of America Abstracts with Programs, v. 20, no. 6, p. 471.

Zen, E., 1985, Implications of magmatic epidote-bearing plutons on crustal evolution in the accreted terranes of northwestern North America: Geology, v. 13, p. 266-269.

Zen, E., and Hammarstrom J. M., 1984, Magmatic epidote and its petrologic significance: Geology, v. 12, p. 515-518.

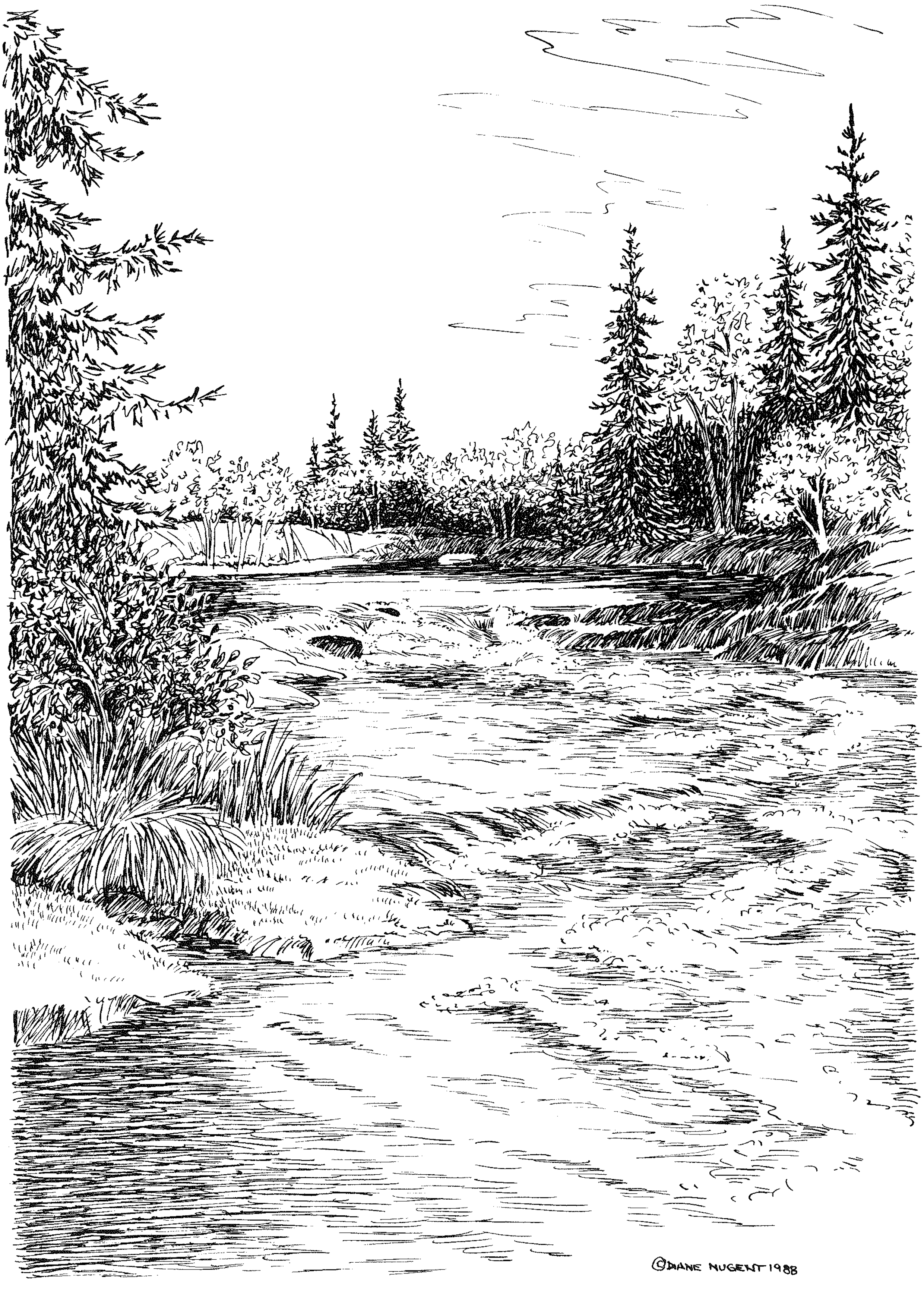

©DIANE NUGENT 1988

FIELD GUIDE TO MYLONITIC ROCKS WEST OF OROFINO, IDAHO

Gary F. Davidson
Department of Geology
Oregon State University
Corvallis, Oregon 97331

Introduction

In the Orofino area, the oceanic island arc-continent boundary occurs as a W-trending zone defined by strontium initial ratios (Armstrong and others, 1977; Fleck and Criss, 1985) in deformed plutonic rocks along the lower part of the North Fork of the Clearwater River. Metamorphic rocks in the area can be divided into three distinct lithologic domains. To the north, aluminosilicate-rich schist and quartzite have been correlated with continentally-derived Middle Proterozoic rocks of the Belt Supergroup (Hietanen, 1962). In the southwestern part of the area, near Peck, amphibolite and biotite and biotite-hornblende schist and gneiss are probably island arc-derived metavolcanic or metavolcaniclastic rocks (Hietanen, 1962). Separating these rocks, and overlapping the boundary as defined by strontium intitial ratios, is a mixed sequence of biotite and hornblende schist and gneiss, amphibolite, calc-silicate rocks and marble called the Orofino series (Anderson, 1930; Hietanen, 1962). The age and origin of the Orofino series rocks are unknown. It has been suggested that these rocks may correlate with Middle Proterozoic rocks of the Belt Supergroup, or they may be much younger, possibly Paleozoic or Mesozoic in age (Anderson, 1930; Johnson, 1947; Hietanen, 1962). Alternatively, the Orofino series may represent a sequence of high-grade metamorphic rocks of differing origins that were tectonically juxtaposed and mixed along the boundary.

Several scattered bodies of quartz diorite and tonalite intrude the metasedimentary rocks in the northern part of the area. Most of these plutonic bodies crosscut structures in the metasedimentary rocks indicating that intrusion generally post-dates deformation of the country rocks (Hietanen, 1962). To the south, metasedimentary rocks of the Orofino series and metamorphic rocks near Peck are strongly disrupted by plutonic rocks, the most abundant being quartz diorite and tonalite. These plutonic rocks are variably deformed. Within the boundary zone near Ahsahka, quartz diorite, tonalite and granodiorite contain a pentrative mylonitic foliation and lineation with nearly complete transposition of all early formed structures (Strayer and others, 1987). In contrast, deformation in the plutonic rocks along the Clearwater River west of Ahsahka is characterized by discrete ductile shear zones, ranging from 1-2 millimeters up to ten's of meters in thickness, which cut parts of the rock containing only a weak, commonly linear fabric. In some places, these shear zones appear to have undergone later brittle deformation with the formation of fault gouge.

The objectives of the following field trip are to: 1) observe the complex structural relationships and lithologies in rocks of probable island arc origin; 2) contrast lithologies and possible origins of island arc metamorphic rocks with metasedimentary rocks of the Orofino series; 3) contrast the style of deformation in plutonic rocks outside the boundary zone with that in plutonic rocks within the zone.

Road log

Mileage

0.0 Orofino City Park, located at west end of town across the bridge (Clearwater River) from U.S. Highway 12. **Drive west** on U.S. Highway 12 towards Lewiston **(Figure 1)**. Outcrops along the highway are primarily variably deformed hornblende and biotite-hornblende quartz diorite and gabbro/diorite.

7.5

7.5 **Stop 1: Pull off the highway** and park at turnout on right side of road in the middle of a large curve about 400 meters past Snells Island (large island in the river) and just east of house with yard art. **On foot**, cross the highway and walk approximately 400 meters to the west to

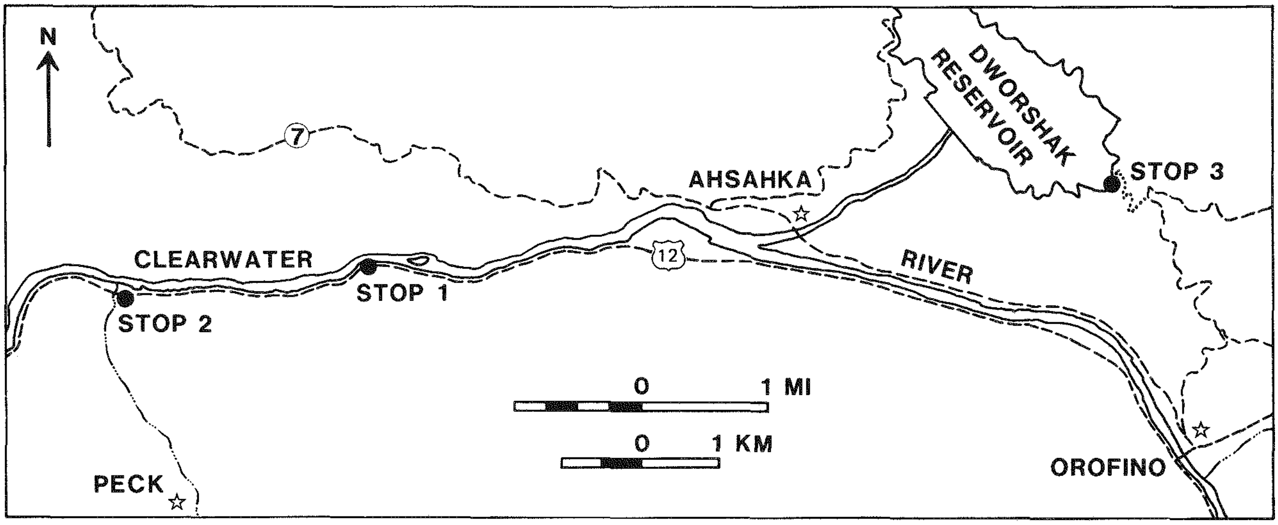

Figure 1—Route map showing location of field stops.

a small culvert in the ditch (Yes, there are rocks at this stop—don't give up!).

Although the exposure is poor, for the *next 400 meters to the west, outcrops of gab*bro/diorite contain structures typical of the plutonic rocks outside of the mylonite zone near Ahsahka. Weakly to moderately foliated/lineated plutonic rock are cut by discrete, commonly anastomozing, mylonitic shear zones. Locally developed S-C fabrics, an approximately down-dip hornblende lineation (to the northeast), and bending of an earlier-formed fabric towards parallelism with shear zones suggest a northeast-over-southwest sense of motion. However, more detailed work is needed (*in progress*) before it can be confidently stated that this represents the overall sense of motion across these shear zones.

Approximately 150 meters west of the culvert, a larger shear zone (uphill) contains schistose rocks and asymmetrically folded and sheared pegmatite veins. Within this zone, very non-resistant rock gives the appearance that the ductiley sheared rocks may have been overprinted by brittle faulting. Whether the brittle deformation represents changing conditions during the same event that produced the ductile structures or a later superimposed event is not clear.

Continue walking west along the highway to the first well-exposed massive outcrop. The sheared eastern margin of the outcrop represents the western margin of the section of discontinuously sheared gabbro that has been observed enroute to this point. On close inspection of the massive-looking gabbro, an early formed fabric (dipping to the west) is cut by thin (1-2 mm) discrete, E-dipping, planar shears. The W-dipping foliation, found only rarely, is distinctly discordant to the dominant NE-dipping foliation in the area. Work is in progress to examine the possibility that these discordant early-formed structures may represent remnants of an earlier deformation event that has been largely obscured. Such evidence for possible early deformation events is critical in determining whether or not the northeast-over-southwest sense of motion on late-stage structures actually represents the relative motions between the island arc and continental terranes during their early interaction.

2.1

9.6 **Stop 2: Pull off the highway** at the grain silo, at the mouth of Big Canyon Creek. The large roadcut across from the grain silo provides an excellent view of the complex structural relations and lithologies in rocks of probable island arc affinity. Rocks at the west end of the outcrop are thinly interlayered biotite schist and amphibolite in which compositional layering has been transposed into parallelism with the foliation. More massive amphibolite structurally overlies the layered rocks. Based on the lithology and layering in the biotite schist/amphibolite section and the lack of compositional layering in the massive amphibolite, these rocks are interpreted to be metamorphosed volcaniclastic and volcanic rocks, respectively. Moving east along the outcrop, coarse-grained metagabbro and garnet-bearing biotite tonalite are in sheared contact with the amphibolite. The occurence of sheared lenses of gabbro within the tonalite suggests that the tonalite intruded the gabbro and that both were subsequently ductilely deformed. At the east end of the outcrop, biotite schist structurally overlies the gabbro and tonalite. All of the above rocks are cut by both low and high-angle faults. Also present is a nearly vertical light-colored dike composed primarily of quartz, plagioclase, muscovite and epidote. Although the dike clearly cuts across the earlier ductilely deformed rocks, it contains a strong foliation and lineation parallel to its margins, suggesting that it may have intruded along a fault/shear zone.

Preliminary Ar^{40}/Ar^{39} age-spectrum dating of hornblende from the amphibolite and gabbro indicates that the rocks have undergone at least two periods of deformation (Snee and others, 1987; Davidson and others, 1988). A plateau age on synkinematic hornblende from amphibolite indicates that the amphibolite and biotite schist underwent metamorphism and deformation at about 121 Ma. A 114 Ma plateau age (an intrusive age?) on hornblende from the gabbro suggests that the gabbro was emplaced after the 121 Ma event, with subsequent intrusion of the tonalite followed by a second episode of ductile deformation. Dating of muscovite from the felsic dike (*in progress*) should give a lower limit for the age of this second deformation event.

After completion of this stop, return to Orofino via U.S. Highway 12.

0.0 At the first intersection after crossing the railroad tracks, **turn left** onto Idaho Route 7. Immediately after turn, **turn right** toward Dent Bridge. Route passes through poorly exposed tonalitic and quartz dioritic gneissic plutonic rocks, as well as biotite schist and calc-silicate gneiss; layers of white marble are also present in places. The metasedimentary rocks are part of the Orofino series as mapped by Hietanen (1962).

1.0

1.0 Sharp switchback just after passing power substation, **turn left** onto dirt road that leads to top of ridge.

1.9

2.9 **Turn left** at the ridge summit and follow dirt road downhill to the picnic area at Merry's Bay on Dworshak Reservoir. **Caution:** This is a 14% grade and muddy during wet weather.

0.9

3.8 **Stop 3:** Parking is available at picnic area. **Walk south and west** along shoreline of Dworshak Reservoir. Exposed along the shore between the picnic area and the first point is a sequence of layered metasedimentary rocks of the Orofino series, including white marble, calc-silicate gneiss, biotite schist and biotite gneiss interlayered with amphibolite. These rocks are intruded by abundant pegmatites. Near the point, three sets of small-scale folds are visible; isoclinal F1 folds are themselves isoclinally folded, with a later set of close folds superimposed on the earlier formed folds.

Rocks of the Orofino series differ from the metamorphic rocks near Peck, in the southwestern part of the area (Stop 1), primarily by the abundance of carbonate-rich lithologies in the Orofino series. They also distinctly differ from the metamorphosed Belt rocks to the north (Anderson, 1930; Hietanen, 1962) by the abundance of biotite and hornblende gneiss and lack of aluminosilicate-rich rocks in the Orofino series (Hietanen, 1962).

References

Anderson, A. L., 1930, The geology and mineral resources of the region about Orofino, Idaho: Idaho Bureau of Mines and Geology Pamphlet No. 34, 65 p.

Armstrong, R. L., Taubeneck, W. H., and Hales, P. L., 1977, Rb/Sr and K/Ar geochronometry of Mesozoic granitic rocks and their Sr isotopic composition, Oregon, Washington and Idaho: Geological Society of America Bulletin, v. 88, p. 397-411.

Davidson, G. F., Snee, L. W., and Lund, K., 1988, Complex tectonic history along the island arc-continent boundary near Peck and Ahsahka, western Idaho: Geological Society of America Abstracts with Programs, v. 20, no. 6, p. 411-412.

Fleck, R. J., and Criss, R. E., 1985, Strontium and oxygen isotopic variations in Mesozoic and Tertiary plutons of central Idaho: Contributions to Mineralogy and Petrology, v. 90, p. 281-308.

Hietanen, A.. 1962, Metasomatic metamorphism in western Clearwater County, Idaho: U.S. Geological Survey Professional Paper 344-A, p. A1-A116.

Johnson, C. H., 1947, Igneous metamorphism in the Orofino region, Idaho: Journal of Geology, v. 55, no. 6, p. 490-501.

Snee, L. W., Lund, K., and Davidson, G. F., 1987, Ages of metamorphism, deformation, and cooling of juxtaposed oceanic and continental rocks near

Orofino, Idaho: Geological Society of America Abstracts with Programs, v. 19, no. 7, p. 335.

Strayer, IV, L. M., Hyndman, D. W., and Sears, J. W., 1987, Movement direction and displacement estimate in the western Idaho suture zone mylonite: Dworshak Dam/Orofino area, west-central Idaho: Geological Society of America Abstracts with Programs, v. 19, no. 7, p. 857.

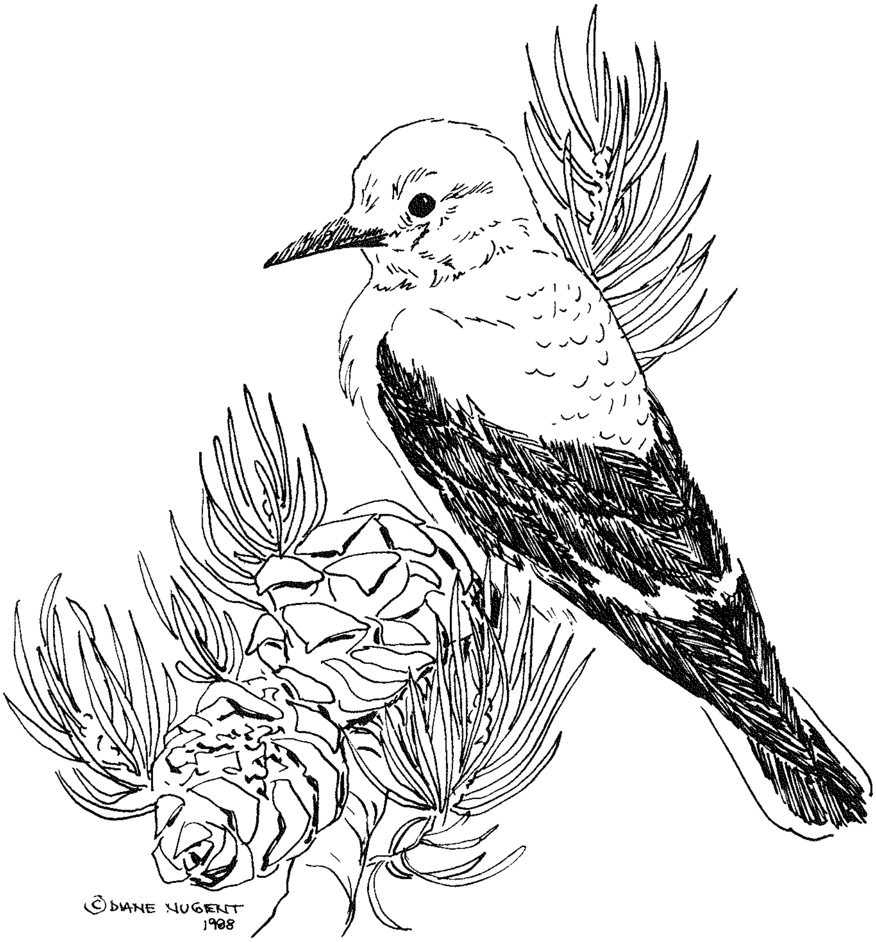

FIELD GUIDE TO A TRAVERSE (SLATE CREEK) ACROSS THE SALMON RIVER SUTURE ZONE, WEST-CENTRAL IDAHO

Karen Lund
U.S. Geological Survey
Denver, Colorado 80225

Introduction

The objectives of this traverse are to: 1) observe the stratigraphy of metamorphic rocks across the Salmon River suture; 2) view the metamorphic grade and structural complexity near the suture; 3) consider the problems of stratigraphy vs. dynamothermal features in the creation and use of map units; 4) discuss the origin of the dynamothermal processes; and 5) consider the relationship between plutonism and dynamothermal processes. The road log begins at Slate Creek Ranger Station on U.S. Highway 95 approximately 26 miles south of Grangeville, Idaho (**Figure 1**). From Grangeville to Slate Creek, roadcuts are in rocks of the Miocene Columbia River Basalt Group.

Road log

Mileage

0.0 **Proceed south** on U.S. Highway 95 from Slate Creek Ranger Station and enter Box Canyon which cuts greenschist-facies metavolcanic rocks of the Permian to Triassic Seven Devils Group (part of the Wallowa terrane). Greenschist-facies tonalite dikes, sills and small stocks cut the metavolcanic rocks, particularly at the southern end of Box Canyon.

3.0

3.0 **Turn left** onto road that leads around oxbow lake (just past sign indicating geological site). At the turn, metatonalite is exposed in roadcut on left; the isotopic age of this pluton is about 259 Ma as determined by U/Pb zircon methods on 2 splits (Walker, 1986). **Turn left** and pass through gate and continue up Long Gulch.

0.5

3.5 **Stop 1**: The outcrop on the south side of the road is greenschist-facies metavolcanic rocks of the Seven Devils Group interbedded with calcareous slate of probable Triassic age, which is traceable continously along strike from type locality of the Triassic(?) Lucile Slate of Hamilton (1963), but probably is correlative with the Martin Bridge Limestone of the southern Wallowa Mountains of Follo (1986). Uphill to the south, McCollough (1984) showed that a thick marble band, which is visible from this point, stratigraphically interfingers with and overlies the slate. These primary layering characteristics illustrate the complex stratigraphic relationships in this volcanic arc and point out problems with stratigraphy in the higher-grade metamorphic rocks to the east.

These low-grade metamorphic rocks are the farthest from the suture zone to be seen on the Slate Creek traverse. They are at the lowest structural level, are the lowest metamorphic grade, and are the least deformed. Metavolcanic rocks that crop out about 10 miles to the south are approximately the same grade; in these rocks non-lineated hornblende reveals $^{40}Ar/^{39}Ar$ dates of about 118 Ma. This date is probably near the age of onset of metamorphism because the hornblende should have formed near the lower limits of hornblende stability and had little or no cooling history (Lund and Snee, 1988; Snee and others, 1988).

Retrace route, to U.S Highway 95, and

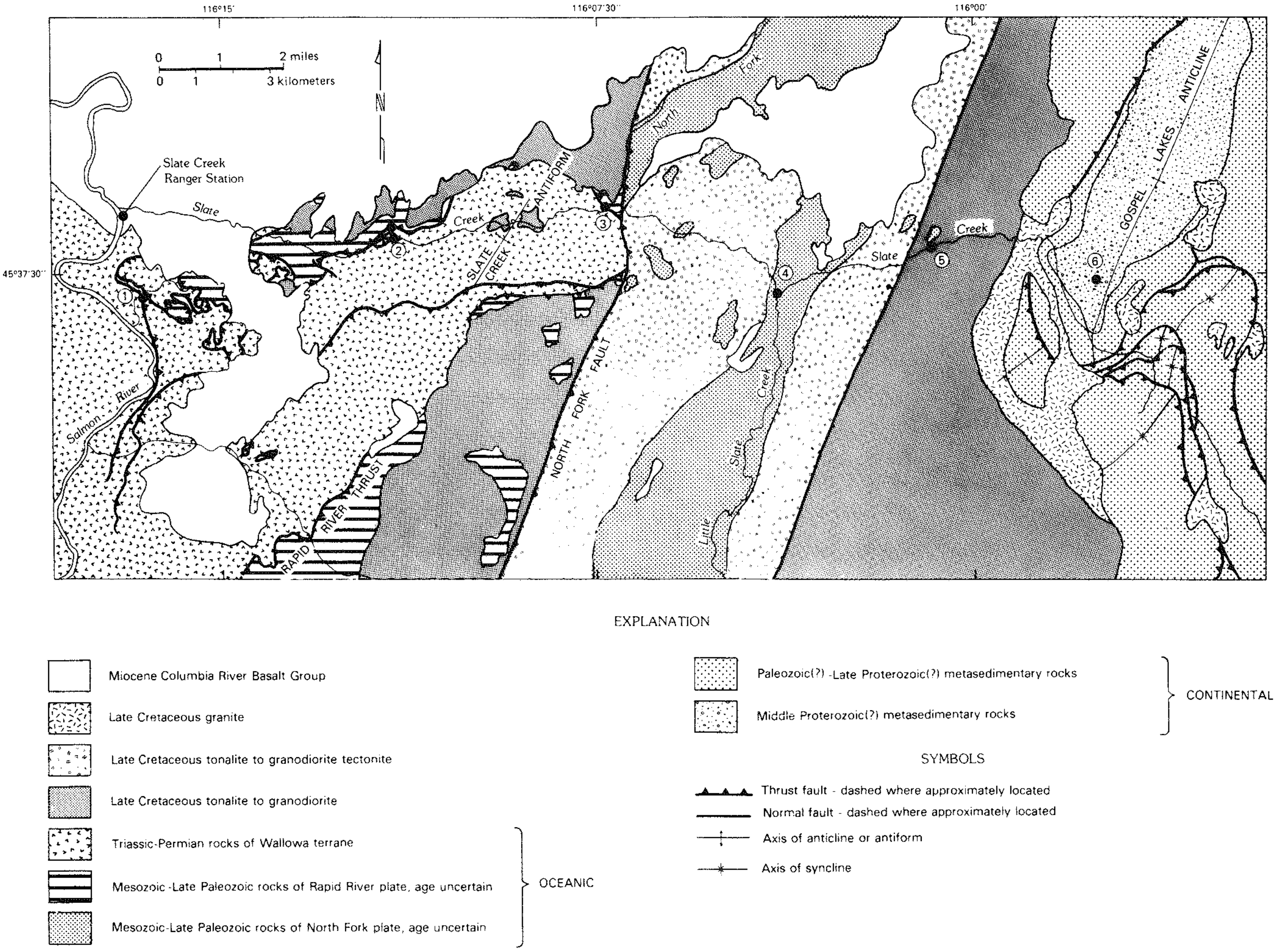
116°15'
116°07'30"
116°00'
45°37'30"
0 1 2 miles
0 1 3 kilometers
N
Slate Creek Ranger Station
Slate
Creek
Salmon River
Rapid River Thrust
Slate Creek Antiform
North Fork
North Fork Fault
Little Slate Creek
Gospel Lakes Anticline
1
2
3
4
5
6
EXPLANATION
Miocene Columbia River Basalt Group
Late Cretaceous granite
Late Cretaceous tonalite to granodiorite tectonite
Late Cretaceous tonalite to granodiorite
Triassic-Permian rocks of Wallowa terrane
Mesozoic-Late Paleozoic rocks of Rapid River plate, age uncertain
Mesozoic-Late Paleozoic rocks of North Fork plate, age uncertain
OCEANIC
Paleozoic(?)-Late Proterozoic(?) metasedimentary rocks
Middle Proterozoic(?) metasedimentary rocks
CONTINENTAL
SYMBOLS
Thrust fault - dashed where approximately located
Normal fault - dashed where approximately located
Axis of anticline or antiform
Axis of syncline

Figure 1—Generalized tectonic map of the Slate Creek area showing location of stops discussed in text. *Compiled from* Lund (1984) and McCollough (1984).

continue north to the mouth of Slate Creek.

0.0 **Turn right** at ranger station on Forest Service Road 354 and continue up Slate Creek through rocks of the Miocene Columbia River Basalt Group. (*NOTE*: Roads in the Slate Creek traverse are passable by car up to Windy Saddle (between Stops 5 and 6). The road beyond Windy Saddle is extremely rough and travel by four-wheel drive vehicles is advised.)

2.5

2.5 Road crosses into pre-Tertiary rocks. A thin sliver of calcareous schist (metamorphosed volcaniclastic sedimentary rock of the Wallowa terrane, probable equivalent to the Triassic slate at Stop 1) is structurally overlain by hornblende-biotite schist and gneiss (metamorphosed volcanic rock that is probably equivalent to the Lightning Creek schist of the Riggins Group of Hamilton (1963), or possibly a high-grade equivalent of the Seven Devils Group) that is part of a structurally overlying slice of higher-grade metamorphic rocks called the Rapid River plate. The concealed fault between these slices is a post-metamorphic thrust fault that is probably equivalent to the Rapid River thrust fault to the south (Hamilton, 1963; Aliberti and Manduca, this volume).

Canyon narrows; beyond the cattleguard a pre-metamorphic pluton that cuts the hornblende-biotite gneiss and, locally, muscovite schist is exposed on the left. The pluton is altered biotite tonalite with accessory apatite and secondary pyrite, calcite, muscovite and epidote. Foliations in the metavolcanic rocks and the pluton are parallel, but the intrusive contact is discordant to the fabrics.

3.0

3.0 Slate Creek Canyon broadens slightly. Road crosses back into hornblende-biotite gneiss and schist.

0.5

3.5 Road crosses unexposed post-metamorphic Rapid River thrust fault where the hornblende-biotite gneiss (Rapid River plate) structurally overlies marble (Wallowa terrane, probably part of the Triassic Martin Bridge Limestone). A small outcrop of marble is exposed in the hillside on the north side of the road, but the majority of this large unit lies on the south side of the creek.

1.5

5.0 **Stop 2: Pull off road** after bridge to abandoned Slate Creek guard station. **Walk** up creek on main road to first roadcut. Dark gray, hornblende-biotite gneiss (Rapid River plate), which contains plagioclase-rich, lighter colored, elongated patches is exposed. This rock is interpreted to be a metavolcaniclastic conglomerate.

The second roadcut is mostly metavolcaniclastic conglomerate, but in the lower west corner of the roadcut, the clast-bearing hornblende-biotite gneiss of the metavolcaniclastic conglomerate structurally overlies biotite calcareous schist of the Wallowa terrane (Triassic Martin Bridge Limestone of Follo, 1986, or Triassic(?) Lucile Slate of Hamilton, 1963). The hornblende-biotite gneiss has an overprinting, retrograde chlorite fabric. Biotites in the calcareous schist are randomly oriented. $^{40}Ar/^{39}Ar$ age-spectrum dates on the metamorphic hornblende (from the biotite-hornblende gneiss) show argon loss from 109 to 94 Ma, and dates on biotite give cooling ages of about 90 Ma (Lund and Snee, 1988; Snee and others, 1987). Both the age of prograde metamorphism that formed the hornblende fabric (about 110 Ma as determined from other samples) and a later reheating event (about 94 Ma), probably retrograde, are shown by these dates. About 2 miles east of this stop, the randomly oriented biotite porphyroblasts from the calcareous schist of the lower plate give dates of about 84 Ma, indicating still later reheating at that time.

The W-vergent thrust fault in this outcrop is part of the post-metamorphic Rapid River thrust fault (**Figure 2**). The thrust fault can be traced discontinuously from this roadcut on the western limb of the Slate Creek antiform, around the nose of the fold; therefore, the fault must have pre-dated folding. This exposure illustrates the relative timing of: 1) amphibolite facies metamorphism during which the foliation was formed, 2) thrust faulting that cut metamorphic fabrics, and 3) macroscopic folding of the thrust fault in the Slate Creek area; $^{40}Ar/^{39}Ar$ dating shows that the thrust faulting and folding are younger than 109 Ma.

Slate Creek road continues into the core of the Slate Creek antiform, through the structurally lowest unit (calcareous biotite schist from Stop 2). Tonalite seen in some roadcuts is part of a major plutonic suite dated about 93 to 87 Ma. Tonalite cuts the prograde metamorphic fabric, Rapid River thrust fault, and Slate Creek antiform; therefore, macroscopic structures (Rapid River thrust fault and Slate Creek antiform) formed before 93 Ma, but after 109 Ma.

4.5

9.5 **Stop 3: Turn into** North Fork campground at the mouth of North Fork of Slate Creek. **Walk back** (downstream) to roadcut in rocks on the east limb of the Slate Creek antiform. Coarse-grained, pyrite-phlogopite marble (probably part of Triassic Martin Bridge Limestone) forms the majority of the exposure, but the east corner of the roadcut is in hornblende schist (metavolcanic rock) that is structurally above the post-metamorphic, pre-folding thrust fault (Rapid River thrust fault) seen at Stop 2. Tonalite dikes cutting the marble are younger than the Slate Creek antiform, but some dikes are deformed along reverse faults that cut the antiform.

In outcrops and in the roadcut on the west side of North Fork, weakly deformed granodiorite and tonalite cut the Rapid River thrust fault and Slate Creek antiform. The North Fork fault, a major high-angle reverse fault along the North Fork and Waterspout Creek (across Slate Creek to the south), is the

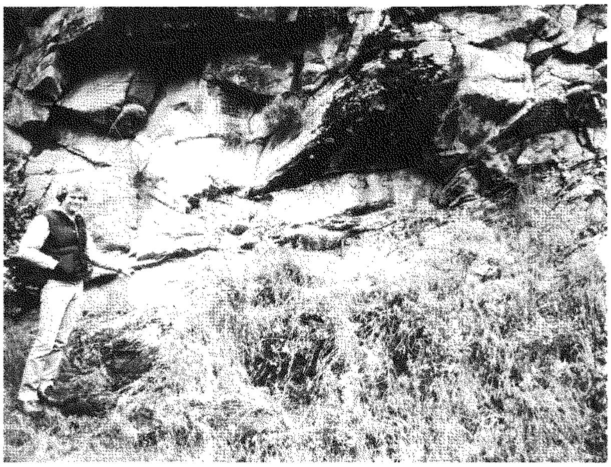

Figure 2—Rapid River thrust fault at Stop 2. Rapid River plate (hanging wall) is amphibolite-facies volcaniclastic conglomerate (hornblende-biotite gneiss with retrograde chlorite possibly correlative with the Permian to Triassic Seven Devils Group) and footwall is calcareous biotite schist (correlative with the Triassic Martin Bridge Limestone of the Wallowa terrane). Fault plane indicated by person's hand.

western boundary of the North Fork plate, a structural wedge composed of amphibolite-facies metamorphic rocks and strongly deformed tonalite, that structurally cuts out the Slate Creek anticline and less deformed, crosscutting plutonic rocks.

Continue on the Slate Creek road through complexly deformed Upper Cretaceous tonalitic to granodioritic and metavolcanic rocks of the North Fork plate. These rocks are characterized by a strong N-NE-trending steep foliation and near-vertical lineations that were superposed on pre-existing fabrics. Some of the deformed plutonic rocks are L-tectonites indicating intense unidirectional flow (in this case, vertical flow) during deformation.

3.5

13.0 **Stop 4: Pull off** road at the mouth of Little Slate Creek. This location, in the North Fork plate, is approximately where initial strontium isotope ratios from plutonic rocks change from oceanic values of < 0.704 to continental values of > 0.706 (Fleck and Criss, 1985). Along Slate Creek, the transition from oceanic initial strontium ratios to continental ratios occurs across an interval of less than 0.5 miles (R.J. Fleck, personal communication, 1982), although xenoliths of possible metavolcanic rocks are found up to 2.5 miles east of this stop.

This roadcut illustrates the concordant deformation of tonalitic and metamorphic rocks in the North Fork plate; foliation in both igneous and metamorphic rocks is parallel. Steep foliation and lineation in tonalite are deformational fabrics. A complex paragenetic sequence of metamorphic minerals is preserved in metavolcanic screens and xenoliths; many samples have ragged hornblende porphyroblasts that were rolled during formation of the new foliation that contains younger medium-grained hornblendes. ^{40}Ar/^{39}Ar dates from this area suggest that the tonalite was emplaced about 93 Ma (Snee and others, 1988); dates on hornblende from deformed tonalite are about 90 Ma and indicate the age of deformation (Lund and Snee, 1988; Snee and others, 1987). ^{40}Ar/^{39}Ar age-spectrum dates on hornblende from the metavolcanic rocks exhibit argon loss from about 101 to 90 Ma or reset ages of about 90 Ma. These data indicate that the metavolcanic rocks cooled to below 530°C by 101 Ma and were subsequently reheated and then deformed and cooled together with the tonalitic plutons at about 90 Ma (Lund and Snee, 1988).

Continue on the main Slate Creek road through poor exposures of deformed tonalite and probable metavolcanic xenoliths. Some Miocene Columbia River Basalt Group occurs at milepost 15.

4.5

17.5 **Turn right** onto main gravel road, Forest Service Road 221.

1.0

18.5 **Stop 5**: After crossing Slate Creek, **turn left** onto road that leads to Rocky Bluff campground. Primary epidote-bearing, sphene-hornblende-biotite tonalite that crops out here is only weakly foliated. Muscovite-biotite granite dikes in roadcut south of creek are part of a large granite pluton that is exposed about 2 miles to the east. U/Pb dates on the tonalite are concordant at 90.4 ± 3.0 Ma (5 zircon splits and 1 sphene split); ^{40}Ar/^{39}Ar age-spectrum dates on hornblende form a plateau at 84 Ma, on biotite form a plateau at 81 Ma, and on microcline show slow cooling from 78 to 75 Ma. ^{40}Ar/^{39}Ar dates on muscovite from the granite pluton are about 78 Ma (Snee and others, 1987). Data on the tonalite indicates that the pluton was emplaced at deep crustal levels—from primary epidote, Zen (1985); from hornblende geobarometry, Hammarstrom and Zen, (1988); and from ^{40}Ar/^{39}Ar cooling information, Snee and others (1987), but the pluton was uplifted and cooled by 81 Ma. The microcline data from the tonalite indicate that the crosscutting granite was emplaced after the tonalite had cooled below 150°C and that the granite magma did not significantly heat the country rocks (Lund and Snee, 1988; Snee and others, 1987).

Turn around and retrace route on Forest Service Road 221.

5.0

23.5 **Turn right** on Forest Service Road 444 to Gospel Peaks and the Gospel-Hump Wilderness Area. Proceed about 4 miles (through granodiorite and quartzite float) to the Sawyer Ridge lookout road. At this junction, road crosses into the Gospel Peaks roof pendant and into a well-preserved sequence of North American continental rocks. Coarse-grained sillimanite quartzite (possibly Late Proterozoic to Paleozoic) is exposed from here to top of ridge **(Figure 3)**. At Windy Saddle, the road crosses a covered, E-vergent post-metamorphic thrust fault that cuts the Gospel Lakes anticline. Rocks in the saddle are muscovite-biotite schist of probable Middle Proterozoic

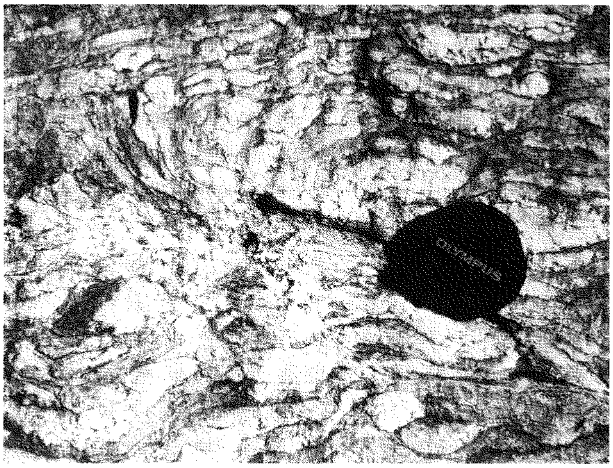

Figure 3—Stretched and folded quartzite pebble conglomerate of probable Late Proterozoic to Paleozoic age located about 2 miles south-southeast of Stop 6. Lens cap for scale.

age that are on the west limb of the Gospel Lakes anticline (**Figure 4**). **Continue up the ridge** into well-layered sillimanite-muscovite quartzite (also probably Middle Proterozoic). Note lithologies of rocks on east side of route; "don't look out west side at 3,000-foot drop into oceanic rocks."

6.5

30.0 **Stop 6: Pull off** road at the saddle overlooking Upper Gospel Lake. Layered sillimanite-muscovite quartzite is at the core of the Gospel Lakes anticline. This fold is part of an anticline-syncline pair in which more than 5 kilometers of stratigraphic section are preserved; younger rocks (possibly Late Proterozoic to Paleozoic) in the syncline to the east contain primary sedimentary features that determine stratigraphic facing. As in the island arc rocks, metamorphic grade is highest in rocks near the suture zone; quartzite units in this location contain sillimanite whereas the same units only a few miles to the east do not.

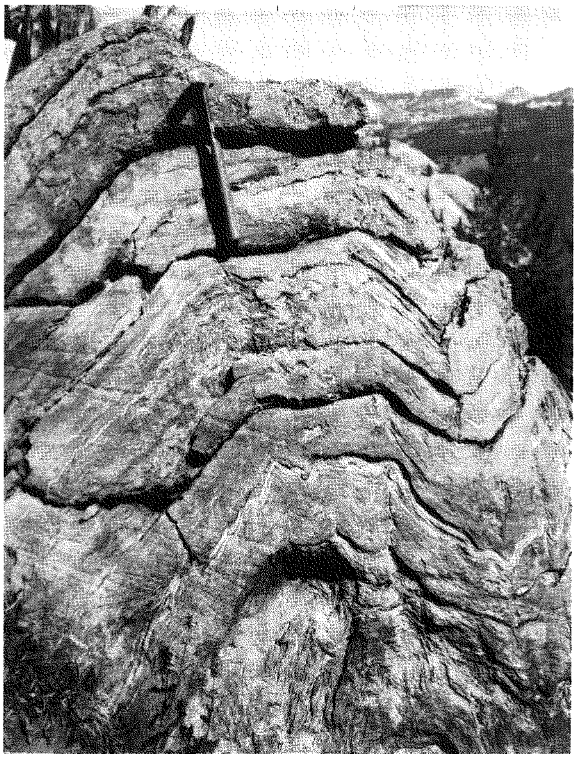

Figure 4—Conjugate kink-band folding in probable Late Proterozoic to Paleozoic thrust plate in Gospel Peaks about 3 miles south-southeast of Stop 6. Hammer for scale.

Undeformed muscovite-biotite granite of the core of the Idaho batholith cut the folded rocks after metamorphism and deformation, but before the metasedimentary rocks had cooled significantly. Retrograde or contact metamorphic effects are rare.

Retrace route back to U.S. Highway 95 and then south for approximately 52 miles to Riggins.

References

Fleck, R. J., and Criss, R. E., 1985, Strontium and oxygen isotopic variations in Mesozoic and Tertiary plutons of central Idaho: Contributions to Mineralogy and Petrology, v. 90, p. 1919-1927.

Follo, M. F., 1986, Sedimentology of the Wallowa terrane, northeastern Oregon [Ph.D. dissertation]: Harvard University, Cambridge, Massachusetts, 292 p.

Hamilton, W., 1963, Metamorphism in the Riggins region, western Idaho: U.S. Geological Survey Professional Paper 436, 95 p.

Hammarstrom, J. M., and Zen, E., 1988, Petrology and mineral chemistry of magmatic epidote-bearing rocks from the suture zone near Round Valley, western Idaho: Geological Society of America Abstracts with Programs, v. 20, p. 419.

Lund, K., 1984, Tectonic history of a continent—island arc boundary: west-central Idaho [Ph.D. dissertation], The Pennsylvania State University, University Park, 207 p.

Lund, K., and Snee, L. W., 1988, Metamorphic and structural development of the continent—island arc juncture in west-central Idaho, *in* Metamorphism and Crustal Evolution, Western Conterminous United States (Rubey Volume VII), W. G. Ernst, *(ed.)*: Prentice-Hall, New York, p. 296-331.

Lund, K., Scholten, R., and McCollough, W. F., 1984, Consequences of interfingered lithologies in the Seven Devils island arc: Geological Society of America Abstracts with Programs, v. 15, p. 284.

McCollough, W. F., 1984, Stratigraphy, structure, and metamorphism of Permo-Triassic rocks along the western margin of the Idaho batholith, John Day Creek, Idaho [M.S. thesis]: The Pennsylvania State University, University Park, 141 p.

Snee, L. W., Sutter, J. F., Lund, K., Balcer, D. E., and Evans K. V., 1987, ^{40}Ar/^{39}Ar age-spectrum data for metamorphic and plutonic rocks from west-central Idaho: U.S. Geological Survey Open-File Report 87-0052, 20 p.

Walker, N. W., 1986, U/Pb geochronologic and petrologic studies in the Blue Mountains terrane, northeastern Oregon and westernmost-central Idaho: Implications for pre-Tertiary tectonic evolution [Ph.D. dissertation]: University of California, Santa Barbara, 214 p.

Zen, E., 1985, Implications of magmatic epidote-bearing plutons on crustal evolution in the accreted terranes of northwestern North America: Geology, v. 13, p. 266-269.

Running Lake in Seven Devils Peaks area, north-central Idaho. (Roy M. Breckenridge photo, courtesy Idaho Division of Tourism.)

FIELD GUIDE TO A TRANSECT ACROSS AN ISLAND ARC-CONTINENT BOUNDARY IN WEST-CENTRAL IDAHO*

Elaine A. Aliberti
Department of Earth and Planetary Sciences
Harvard University
Cambridge, Massachusetts 02138
and
Cathryn Allen Manduca
Department of Earth and Planetary Sciences
California Institute of Technology
Pasadena, California 91125

Introduction

One of the most striking paleogeographic anomalies of the western United States cordillera is exposed in west-central Idaho where Permian and Triassic island arc volcanics of the Wallowa terrane are juxtaposed against rocks with cratonic affinities across a narrow transition zone of metamorphic and plutonic rocks. In this area much or all of the Paleozoic miogeoclinal section present elsewhere along the western edge of the craton is missing, as are commonly intervening belts of melange and eugeoclinal sedimentary rocks of mixed provenance between the oceanic arc terrane and the cratonic margin (Davis and others, 1978; Hamilton, 1978; Lund, 1984). The preserved transition zone records an Early to Middle Cretaceous period of compressional deformation. This event appears to postdate the truncation of the Paleozoic miogeoclinal section and the removal of transitional assemblages between the arc and continental margin.

The original nature of the boundary between accreted arc material and the continental margin has been obscured by Cretaceous compressional deformation and by the emplacement of voluminous intrusives. No evidence of the event that truncated the continental margin and removed the transitional assemblages is preserved. The boundary is recognized by an abrupt change in the lithology of metamorphic pendants within the plutonic rocks. Pendants of metavolcanic and volcaniclastic schists and gneisses give way to quartzites and metapelites of continental affinity suggesting the plutons were emplaced across a steeply dipping boundary between arc and continent (Lund, 1984; Manduca and Kuntz, 1987). Geochemical studies in this area have revealed a rapid change in the strontium and oxygen isotopic ratios of the rocks, which generally corresponds with the change in abundance of pendants (Armstrong and others, 1977; Fleck and Criss, 1985; Manduca and others, 1986).

The transition zone between rocks of the Wallowa terrane and the continental margin as preserved within the Cretaceous intrusives of the Idaho batholith is illustrated schematically in **(Figure 1)**. The transition zone consists of a series of lithotectonic packages which are, from west to east: The Wallowa terrane, the Rapid River thrust plate, the Pollock Mountain plate, the Little Goose Creek complex and the Payette River complex. The Wallowa terrane consists of Permian and Triassic Seven Devils Group arc volcanics, and overlying limestone of the Martin Bridge Formation and slate of the Lucile (or Hurwal) Formation. These rocks have been relatively unaffected by deformation and metamorphism along the transition zone. The Rapid River thrust system emplaces Riggins Group schists and lesser amounts of Martin Bridge, Lucile and Seven Devils lithologies over the Wallowa terrane. The Riggins Group is an assemblage of metavolcanic and volcaniclastic schists thought to represent a portion of an island arc terrane. These schists have been correlated with either the Wallowa terrane or the Olds Ferry terrane and adjacent flysch and melange sequences in eastern Oregon (Hamilton, 1978; Brooks and Vallier, 1978; Lund, 1984; Silberling and others, 1984). The Rapid River thrust plate increases in metamorphic grade from lower greenschist facies in the west to uppermost greenschist or lower amphibolite facies in the east, and is penetratively deformed throughout. The Pollock Mountain fault emplaces the Pollock Mountain Amphibolite and the Hazard Creek complex over the Rapid River thrust plate. Both the Rapid River thrust system and Pollock Mountain fault are

---

*Reprinted and *modified from* Aliberti and Manduca, 1988.

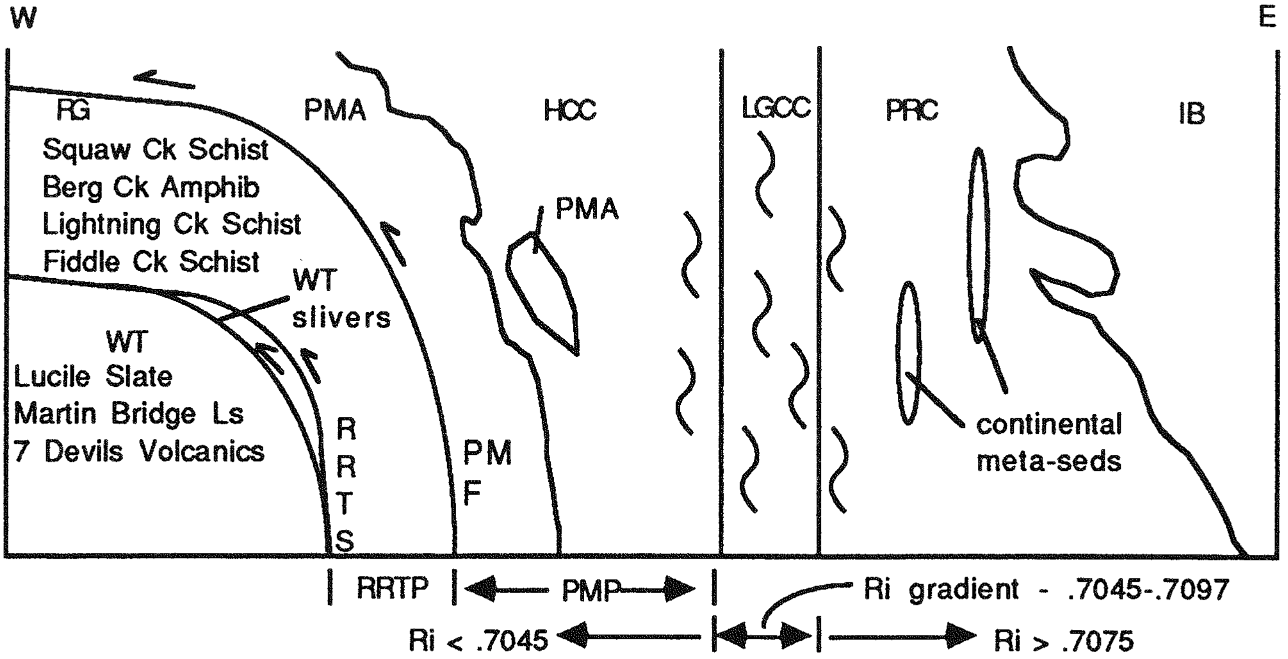

Figure 1—Schematic cross section of the transition zone: (WT), Wallowa terrane; (RG), Riggins Group; (PMA), Pollock Mountain Amphibolite; (HCC), Hazard Creek complex; (LGCC), Little Goose Creek complex; (PRC), Payette River complex; (IB), two-mica core of the Idaho batholith; (RRTS), Rapid River thrust system; (PMF), Pollock Mountain fault; (RRTP), Rapid River thrust plate; (PMP), Pollock Mountain plate; (Ri), calculated initial ^{87}Sr/^{86}Sr values (Manduca and others, 1986).

shallowly dipping, NW-directed thrusts at high structural levels, which steepen into vertical shear zones at depth.

The Hazard Creek complex, Little Goose Creek complex and the Payette River complex are all composed primarily of Cretaceous plutonic rocks. The Hazard Creek complex consists of variably deformed epidote-bearing intrusives and gneissic country rocks emplaced during the Early to Middle Cretaceous compressional deformation. The westernmost plutons in the Hazard Creek complex intrude metamorphosed island arc volcanics of the Pollock Mountain Amphibolite. The Little Goose Creek complex consists primarily of strongly mylonitized porphyritic granodiorite orthogneiss. This mylonitization is the youngest penetrative deformation in the area, postdating the emplacement of all three intrusive complexes. It affects the eastern margin of the Hazard Creek complex and the western margin of the Payette River complex, obscuring the original nature of these contacts. The transition in wall rocks from arc-related to continentally derived material, and the rapid change in strontium and oxygen isotopic ratios, occur within the Little Goose Creek complex. The Payette River complex consists primarily of undeformed tonalite, containing abundant screens and inclusions of continentally derived metamorphosed sedimentary rocks.

This field trip traverses the transition zone from west to east, beginning in rocks of the Wallowa terrane and ending in rocks of the continental margin preserved as pendants within the Cretaceous Payette River complex (**Figure 2**). Although the transition occurs within a 25 mile (40 km)-wide zone, roads that are nearly parallel to the strike of the transition zone require a longer trip.

Road log

Mileage

0.0 Salmon River Inn at Riggins, Idaho. **Drive south** on U.S. Highway 95 to Rapid River turnoff.

4.4

4.4 Junction; **turn right** on Rapid River Road. Outcrops along the road comprise the type section of the Squaw Creek Schist member of the Riggins Group. The Squaw Creek Schist is a gray, compositionally layered schist which typically weathers rusty brown. The schists are dominantly composed of sodic plagioclase and quartz with abundant carbonate, biotite, muscovite, and carbon dust with minor amounts of epidote, clinozoisite, garnet, hornblende and chlorite. Compositional layering of the schists has been transposed by per-

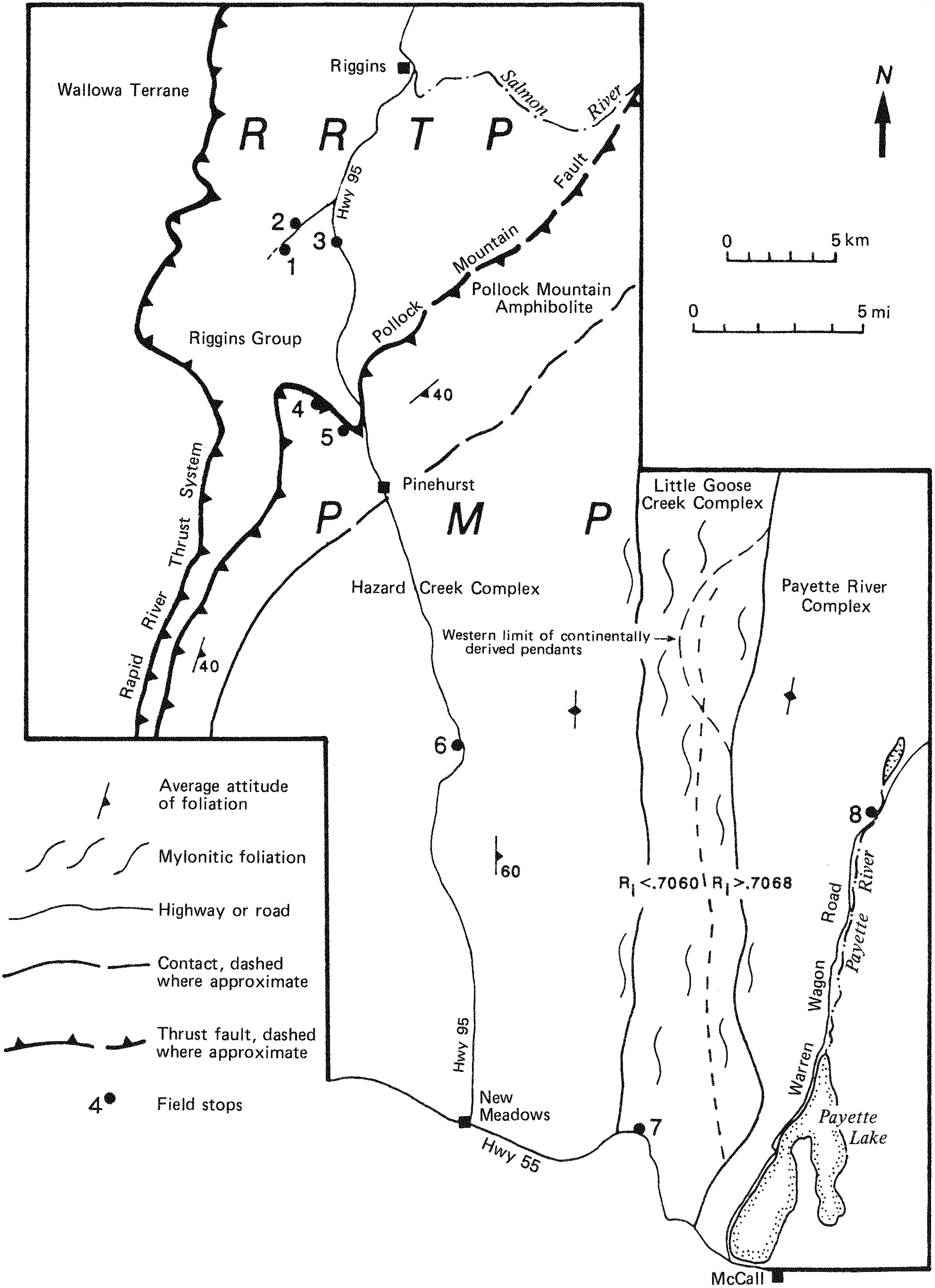
Wallowa Terrane
Riggins
Salmon River
R R T P
N
Hwy 95
Fault
2
3
1
Mountain
0 5 km
Pollock Mountain Amphibolite
0 5 mi
Pollock
Riggins Group
40
4
5
Rapid River Thrust System
Pinehurst
P M P
Little Goose Creek Complex
Hazard Creek Complex
Payette River Complex
Western limit of continentally derived pendants
40
6
Average attitude of foliation
Mylonitic foliation
Highway or road
Contact, dashed where approximate
Thrust fault, dashed where approximate
4 Field stops
60
Ri <.7060
Ri >.7068
8
Warren Wagon Road
Payette River
Hwy 95
New Meadows
7
Hwy 55
Payette Lake
McCall

Figure 2—Generalized basement map of the transition zone between the Wallowa terrane and continental margin showing field stops covered in text. The Miocene Columbia River Basalt has been removed for simplicity. (RRTP), Rapid River thrust plate; (PMP), Pollock Mountain plate; (Ri), calculated initial $^{87}Sr/^{86}Sr$ values (Manduca and others, 1986); thin short dashes-isotopic step; thin long dashes-western limit of continentally derived pendants. *Complied from* mapping by E. A. Aliberti, M. A. Kuntz, and C. A. Manduca.

vasive deformation of this unit. Hamilton (1963) described the schists as marine sediments with a volcanic provenance.

0.8

5.2 Junction; **continue straight ahead** on unpaved Rapid River Road.

1.4

6.6 Junction; **stay left** on main Rapid River Road.

0.4

7.0 **Stop 1: Park near** the Rapid River fish hatchery dam. At this locality one can view a portion of the Rapid River thrust system. The Rapid River thrust was originally mapped by Hamilton (1963, 1969) as a major post-metamorphic thrust which emplaces Riggins Group schists over the Seven Devils Group volcanics and the overlying Martin Bridge Formation and Lucile Slate. The Rapid River thrust actually consists of a system of faults which dip shallowly to the east at high structural levels, but steepen rapidly into a vertical shear zone with depth (Aliberti and Wernicke, 1986a). Here the basal thrust of the Rapid River thrust system emplaces Riggins Group schists, as well as blue-gray calcite marbles of the Martin Bridge Formation and black phyllites of the Lucile Slate, over Seven Devils Group volcanics.

Walk up the Rapid River trail to look at basal thrust of the Rapid River thrust system. Rattlesnakes, poison ivy, and steelhead salmon are seasonally abundant in the vicinity of the trail. Steep outcrops in the canyon consist of pervasively deformed marbles of the Martin Bridge Formation above the basal Rapid River thrust. Approximately 0.25 mile (0.4 km) up the trail (on the right side) there is a shallow cave in blue marble. The lower slab of marble shows excellent calcite stretching lineations **(Figure 3A)**. Mineral stretching lineations collected above the Rapid River thrust south of Riggins indicate northwest movement along the Rapid River thrust system **(Figure 3B**; Aliberti and Wernicke, 1986a). The Martin Bridge Formation and the Lucile Slate intercalated with Riggins Group schists above the thrust suggest that all three units were tectonically interleaved before or during thrusting.

Continue west along the Rapid River trail to an unsigned trail junction; **bear left** on lower trail. Small-scale duplexing in the Martin Bridge Formation is observed in the cliff face across the river. The Seven Devils Group metavolcanic tuffs and breccias crop out at the top of the next small hill approximately 0.5 mile (0.8 km) from the parking area. The mottled green and red colors are characteristic of these volcanics below the thrust. Steep foliations typical of the lower plate volcanics are present. Locally, tectonic slivers of Seven Devils Group volcanics are incorporated along

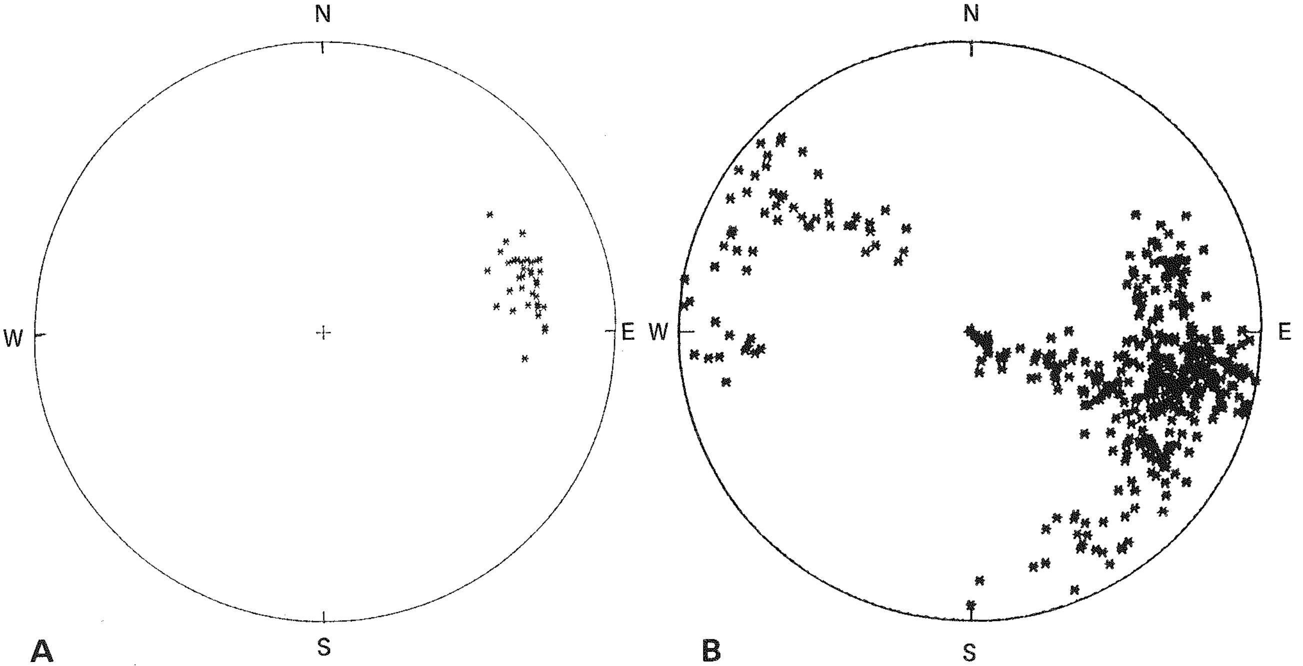

Figure 3—Equal-area projections of mineral stretching lineations. (A), calcite-stretching lineations from Stop 1; (B), compilation of mineral stretching lineations above the Rapid River thrust system south of Riggins, indicating northwest movement along the thrust system.

the basal thrust. Looking back down river, the low-angle thrust contact between the Martin Bridge Formation and the Seven Devils Group is clearly visible where the Rapid River crosses it.

Return to parking area. Along the edge of the pool above the dam there are a few boulders of deformed volcanic breccias. These are typical of the Seven Devils Group volcanics, deformed in the root zone of the Rapid River thrust system upstream. Strain analysis of oriented breccias within the root zone shows that they have been flattened by pure shear and pressure solution along vertical foliation planes, which strike approximately N15°E. The subparallel attitude of the plane of flattening to the arc-continent boundary at this latitude suggests that the maximum shortening direction was at a high angle to the continental margin (Aliberti and Wernicke, 1986b). **Retrace route** on Rapid River Road toward U.S. Highway 95.

0.4

7.4 **Stop 2**: Intersection of Shingle Creek and Rapid River roads. A silicified talc schist tectonite pod is present on the contact between the Lucile Slate and the Lightning Creek Schist. Such pods are volumetrically very minor, but they are the only material within the transition zone that may represent ocean floor or oceanic crust.

2.0

9.4 Outcrops along the road expose the Lightning Creek Schist member of the Riggins Group, unconformably overlain by Quaternary gravels.

The Lightning Creek Schist member of the Riggins Group is a green to grayish-green schist composed of chlorite, sodic plagioclase, quartz, actinolite and epidote with local occurrences of biotite, hornblende, garnet, clinozoisite and carbonate. Along the roadside, chlorite schists are dipping gently eastward, with E-plunging mineral stretching lineations. Hamilton (1963) recognized this unit as a sequence of metavolcanic tuffs and flows with local agglomerate horizons. However, specific correlation of these schists with either the Olds Ferry terrane or the Wallowa terrane remains unresolved.

0.1

9.5 U.S. Highway 95; **turn right** and continue south.

2.3

11.8 **Stop 3:** Rest area. Squaw Creek Schist is a member of the Riggins Group exposed in the roadcuts on the opposite side of the highway. The rock is typically a banded quartz-rich biotite schist or phyllite with variable amounts of carbonate. The metamorphic grade of Riggins Group schists increases eastward from the Rapid River thrust, where rocks are metamorphosed to lower greenschist facies (to the Pollock Mountain fault), where rocks reach upper greenschist to lower amphibolite facies. This increase in grade is interpreted to reflect a vertical section of the crust that was brought up along the steeply dipping Rapid River thrust system.

5.1

16.9 **Turn right** on Whitebird Ridge Road. (*Note:* Road, 2.5 miles beyond this point, is closed between December 1-June 15; inquiries are advised).

0.1

17.0 Junction; **bear right** on Whitebird Ridge Road.

0.4

17.4 Junction; **bear left** and continue uphill.

1.8

19.2 Junction; **bear left** and continue uphill.

0.5

19.7 **Stop 4**: This location affords a good view of the Pollock Mountain fault on the hillside across the Little Salmon River. The trace of this low-angle fault cuts below resistant outcrops on the hilltops and extends down through the upper terraces. It is offset slightly by a high-angle fault and steepens into the river. The Pollock Mountain fault separates high-grade, garnet-bearing amphibolitic gneisses of the Pollock Mountain plate above, from lower-grade Riggins Group schists of the the Rapid River thrust plate below. These two plates record radically different metamorphic histories. Two-stage garnets within the amphibolites suggest burial of the Pollock Mountain plate to pressures of 8 to 10 kb and temperatures of 600 to 650°C (Selverstone and others, 1987). In contrast, single-stage garnets from the Rapid River thrust plate suggest isothermal decompression to 6 kb at 500 to 550°C (Selverstone and others, 1987). The importance of burial metamorphism in the Pollock Mountain plate and the dramatic change in history across the Pollock Mountain fault both suggest that metamorphism is related to regional tectonism and is not primarily the result of heat advected by batholithic intrusives as suggested by Hamilton (1963). Small bodies of epidote biotite tonalite are locally present in tectonic slivers along the fault and show evidence of brittle deformation. Hornblende stretching lineations in amphibolite along the fault indicate north-northwest movement. To the north, the low rolling hills and grassy slopes are all within the lower plate. Note the flat-lying lava flows in the distance (Miocene Columbia River Basalt). **Turn around** and retrace route back toward U.S. Highway 95.

1.6

21.3 **Stop 5**: The Pollock Mountain Amphibolite is composed of garnet-bearing amphibolite and interlayered felsic gneisses. Variable microscopic to mesoscopic layering within the mafic amphibolites is characterized by alternating hornblende-rich, plagioclase-rich, and epidote-rich layers. The abundance of epidote associated with layered amphibolite is suggestive of calcic layers in a volcanic pile. Nd and Sr isotope systematics of the Pollock Mountain Amphibolite have been studied by Aliberti and others (1987). Whole-rock samples of both mafic and felsic layers are isotopically indistinguishable and show a small range in ^{147}Sm/^{144}Nd from 0.15 to 0.22. Data scatter about a reference isochron of 200 Ma and suggests a roughly Late Triassic crystallization age. Initial epsilon Nd values range from 6.65 to 8.09 and initial epsilon Sr values range from -6 to +22 (^{87}Sr/^{86}Sr = 0.7041 to 0.7061), suggesting these rocks were island arc volcanics that interacted with sea water either prior to or during metamorphism. Both compositional characteristics and isotopic constraints indicate that the Pollock Mountain Amphibolite is a metamorphosed pile of Triassic island arc volcanics (Aliberti and others, 1987). A preliminary garnet-whole rock isochron from single-stage synkinematic garnets within the Pollock Mountain Amphibolite near Pollock Mountain gives a metamorphic age of 144 Ma, interpreted to be the earliest stage of metamorphism and deformation associated with the arc-continent collision (Aliberti and others, 1988). Early deformation of the Pollock Mountain Amphibolite was followed by synkinematic intrusion of the Hazard Creek complex to the east. ^{40}Ar/^{39}Ar ages ranging from 118 to 95 Ma (Snee and others, 1987) may be related to deformation and uplift along the Pollock Mountain fault and Rapid River thrust system, as well as increased magmatic activity.

This locality is typical of high-grade injection gneisses of the Pollock Mountain Amphibolite above the Pollock Mountain fault, with garnet-bearing amphibolites pervasively injected by tonalite. Folded concordant sills of hornblende-biotite tonalite are coarse grained and contain xenocrystic garnets from the amphibolites. Deformation is syn- to post-intrusive. Younger but compositionally similar dikes are discordant to foliation, and these intrusives may be correlative with the oldest members of the Hazard Creek complex. Sets of post-Miocene high-angle faults and joints are superimposed on earlier structures. **Retrace route** to U.S. Highway 95.

1.2

22.5 U.S. Highway 95; **turn right** and continue south.

1.9

24.4 Pinehurst; **continue south.** The outcrops along the highway are primarily Columbia River Basalt.

6.4

30.8 Roadcuts in the Hazard Creek complex. This Hazard Creek complex is the westernmost of the units which are composed primarily of Cretaceous intrusive rocks. The major members of the complex are variably deformed and recrystallized epidote-bearing quartz diorite to trondhjemite orthogneisses. These orthogneisses, intruded during ongoing deformation, are the oldest intrusives emplaced into the suture zone. (Older Permian and Triassic intrusives are an intergal part of the Wallowa terrane.) The structural style of the Hazard Creek complex is very asymmetric. On the east, the complex has a steeply dipping, N-NW-striking foliation. The plutons are elongate bodies with pervasive ductile folding around their margins. On the west, as seen in the following outcrops, dips are generally more shallow with diverse strike directions. The plutons are relatively equant with stoped blocks of wall rocks abundant along their margins. This asymmetry suggests the intrusives were emplaced within and to the west of an active zone of flattening and vertical flow.

1.1

31.9 Layered mafic gneisses seen along the highway are a minor component of the Hazard Creek complex. (The best access to these roadcuts is gained by parking in a pullout on the west side of the highway about 100 meters south of milepost 175 and walking back north to the roadcut.) They are surrounded by intrusive material and are inferred to be a pendant within the intrusive rocks. Smaller blocks of layered gneiss are also common as inclusions within the intrusive rocks. The presence of the gneisses as pendants and inclusions, as well as the irregular contact between the Pollock Mountain Amphibolite and the Hazard Creek complex, suggest that the contact is intrusive rather than tectonic.

The most abundant gneisses are andesitic in composition, containing andesine, hornblende, biotite, quartz + clinozoisite, epidote, garnet, diopside and cummingtonite. Amphibolites, calcsilicate-and quartzofeldspathic gneisses are interlayered with andesitic gneisses on scales from tens of centimeters to tens of meters. Amphibolites locally contain pyroxene. Calcsilicate gneisses contain varying proportions of hornblende, epidote, tremolite, plagioclase, quartz and sphene. These gneisses, interpreted as metamorphosed volcanic and volcaniclastic rocks of an oceanic volcanic arc, strongly resemble the Pollock Mountain Amphibolite. Quartzofeldspathic layers, composed of plagioclase, quartz, biotite, clinozoisite, muscovite and garnet, contain large relict, zoned plagioclase grains and are interpreted as metamorphosed tonalite or trondhjemite sills. Compositionally, they strongly resemble early intrusives from the Hazard Creek complex. Younger crosscutting biotite granodiorite dikes are probably related to younger intrusives in the complex.

1.1

33.0 **Stop 6: Turnout** on west. The Hazard Creek complex contains several generations of intrusive rocks which have been variably deformed into gneisses. At this locality a variety of older orthogneisses within the complex can be observed. The oldest is fine grained, of quartz diorite composition, and contains abundant folded leucocratic veins. It occurs both as blocks and as elongate pods within the epidote-biotite-hornblende tonalite orthogneiss, which makes up most of the outcrop. Minor amounts of epidote-biotite-trondhjemite orthogneiss are interlayered and deformed with the tonalite orthogneiss. Magmas of these compositions were injected throughout an ongoing deformational episode, since these lithologies occur as crystalloblastic gneisses, as gneissic intrusives and as little-deformed intrusives. Tonalite and trondhjemite dikes crosscutting the orthogneisses represent one of the youngest intrusions in this series.

0.8

33.8 Outcrops in the upper portion of this canyon contain abundant epidote-biotite tonalite and trondhjemite. These are part of one of the younger intrusive bodies in the complex and are only slightly deformed. The intrusive style of the pluton varies locally. In some outcrops a flow foliation is well developed and inclusions of older material are concordant. Elsewhere, foliation is weak and crosscutting relationships are more abundant. Related trondhjemite dikes crosscut the foliation and show no prefered orientation. The youngest crosscutting dikes are granitic and are related to the youngest intrusive in the area, a granitic body which crops out in Round Valley at the south end of the canyon.

12.1

45.9 New Meadows; **turn left** on Idaho Route 55 toward McCall.

5.7

51.6 **Stop 7**: The Little Goose Creek complex is composed primarily of this distinctive mylonitic, porphyritic biotite granodiorite orthogneiss. The porphyritic orthogneiss is tectonically interlayered with other intrusives ranging in composition from granite to gabbro. Epidote-free tonalites similar to those in the western portions of this outcrop are the most abundant interlayers. Layered mafic gneisses similar to those seen in the Hazard Creek complex are also intercalated with the porphyritic orthogneiss and can be observed in the upper part of the canyon. In the eastern portion of the Little Goose Creek complex, metamorphosed continentally derived sediments are interlayered with the porphyritic orthogneiss. Thus, the orthogneiss contains inclusions of both arc-related and continentally derived material. Strontium and oxygen isotopes within this unit have been studied by Manduca and others (1986). The isotopic ratios change dramatically from west to east. Calculated initial $^{87}Sr/^{86}Sr$ values range from 0.7045 in the west to 0.7097 in the east; ^{18}O values range from 8.0 to 10.9. Ratios generally increase from west to east, with a step in the central part of the complex. This step does not coincide in detail with the change in composition of metamorphic pendants (**Figure 2**). The gradient is inferred to reflect an eastward-increasing contribution of evolved crustal material (with elevated $^{87}Sr/^{86}Sr$ and ^{18}O) to the melt which formed the porphyritic orthogneiss. The changes in both pendant compositions and isotopic ratios within the orthogneiss suggest it intruded a steeply dipping lithospheric boundary, along which continental and oceanic arc lithologies were juxtaposed.

The Little Goose Creek complex has been pervasively deformed into a mylonitic gneiss. Mylonitization appears to have occurred under dry conditions at amphibolite facies, since amphibolite facies mineral assemblages have not been retrograded and oxygen isotope variations are preserved. Mylonitization also affected the western margin of the Payette River complex to the east, and the eastern margin of the Hazard Creek complex to the west. Deformation postdates the emplacement of the Payette River tonalite and is the youngest penetrative deformational event in the area. Mylonitic foliations strike north-south, and dips are steep to vertical. (Foliation at this outcrop dips more shallowly than average.) A well-developed mineral stretching lineation plunges down dip, and fold axes generally parallel the lineation. Movement is inferred to have been vertical with a strong flattening component.

5.4

57.0 McCall; **turn left** on Warren Wagon Road and **continue north** along the west shore of Payette Lake through rocks of the Payette River complex.

7.7

64.7 Junction; **stay left** on Warren Wagon Road.

7.3

72.0 **Stop 8**: Tonalite forming the western portion of the Payette River complex is part of a belt of tonalite which crops out on the west side of the Idaho batholith along much of its length. Here the body is approximately 6 miles (10 km) wide and has a strong N-striking igneous flow foliation that dips steeply to the east. A steeply NE-plunging flow lineation is also commonly present. Mylonitization of the western margin is the only post-emplacement penetrative deformation observed in this body.

Concordant screens and pods of metasedimentary rocks, inferred to be metamorphosed continentally derived clastic rocks, are present throughout the complex. In this outcrop they are composed of calcsilicate gneiss and biotite schist; quartzite and sillimanite-bearing schist are also common. Inclusions of metasedimentary rocks vary in size from a meter to several kilometers in width; the largest body is greater than 6 miles (10 km) in length. The metasedimentary material is intimately associated with granitic to tonalitic material, suggesting partial melting and local assimilation occurred during intrusion of the tonalite. Structures and fabrics in the metasedimentary rocks are generally parallel to those in the tonalite and appear to be due to deformation which transposed compositional layering during intrusion of the tonalites. Older structures and fabrics may have been obliterated. The crosscutting granitic dikes at this outcrop are related to the two-mica granitic core of the Idaho batholith which crops out 4 miles (6.5 km) to the east.

Retrace route to New Meadows.

Acknowledgments

The work of Aliberti has been supported by N.S.F. Grants EAR-84-51181 and EAR-87-96198, and by Geological Society of America Research Grants 3379-85 and 3531-86. The field work of Manduca has been supported by the U.S. Geological Survey in collaboration with M. A. Kuntz. The field guide stems from the Ph.D. dissertation of Aliberti (Harvard University) under the supervision of B. P. Wernicke, and the Ph.D. dissertation of Manduca (California Institute of Technology) under the direction of L. T. Silver. The manuscript was reviewed by D. W. Rodgers and V. E. Chamberlain.

References

Aliberti, E. A., and Wernicke, B. P., 1986a, Late-stage processes in the growth of new continental crust: Observations from the eastern margin of the Seven Devils terrane, west-central Idaho: Geological Society of America Abstracts with Programs, v. 18, no. 6, p. 524-525.

______ 1986b, Occluded terrane boundaries: An example from an island arc-craton contact in west-central Idaho [abs.]: Eos, Transactions of the American Geophysical Union, v. 67, no. 44, p. 1226-1227.

Aliberti, E., and Manduca, C. A., 1988, A transect across an island arc—continent boundary in west-central Idaho, *in* Guidebook to the Geology of Central and Southern Idaho, Paul Karl Link and William R. Hackett, *(eds.)*: Idaho Geological Survey Bulletin 27, p. 99-107.

Aliberti, E. A., Jacobsen, S. B., and Wernicke, B. P., 1987, Nd and Sr isotopic constraints on the tectonic evolution of the arc-continent collision in west-central Idaho: Geological Society of America Abstracts with Programs, v. 19, no. 7, p. 569.

Aliberti, E. A., Selverstone, J., Jacobsen, S., and Wernicke, B. P., 1988, The Pollock Mountain Amphibolite: Isotopic and petrologic constraints on the evolution of an island arc-continent boundary: Geological Society of America Abstracts with Programs, Rocky Mountain Section, v. 20, no. 6, p. 403.

Armstrong, R. L., Taubeneck, W. H., and Hales, P. O., 1977, Rb-Sr and K-Ar geochronometry of Mesozoic granitic rocks and their Sr isotopic composition, Oregon, Washington and Idaho: Geological Society of America Bulletin, v. 88, p. 397-411.

Bonnichsen, Bill, 1987, Pre-Cenozoic geology of the West Mountain-Council Mountain-New Meadows area, west-central Idaho: U.S. Geological Survey Professional Paper 1436, p. 151-170.

Brooks, H. C., and Vallier, T. L., 1978, Mesozoic rocks and tectonic evolution of eastern Oregon and western Idaho, *in* Mesozoic paleogeography of the western United States: D. G. Howell, and K. A. McDougall, *(eds.)*: Society of Economic Paleontologists and Mineralogists, Pacific Coast Section, Pacific Coast Paleogeography Symposium II, p. 133-146.

Davis, G. A., Monger, J. W. H., and Burchfiel, B. C., 1978, Mesozoic construction of the cordilleran "collage," central British Columbia to central California, *in* Mesozoic paleogeography of the western United States: D. G. Howell, and K. A. McDougall, *(eds.)*: Society of Economic Paleontologists and Mineralogists, Pacific Coast Section, Pacific Coast Paleogeography Symposium II, p. 1-32.

Fleck, R. J., and Criss, R. E., 1985, Strontium and oxygen isotopic variations in Mesozoic and Tertiary plutons of central Idaho: Contributions to Mineralogy and Petrology, v. 90, p. 291-308.

Hamilton, W. R., 1963, Metamorphism in the Riggins region, western Idaho: U.S. Geological Survey Professional Paper 436, 95 p.

______ 1969, Reconnaissance geologic map of the Riggins quadrangle, west-central Idaho: U.S. Geological Survey Miscellaneous Investigations Map I-579. Scale 1:125,000.

______ 1978, Mesozoic tectonics of the western United States, *in* Mesozoic paleogeography of the western United States: D. G. Howell, and K. A. McDougall, *(eds.)*: Society of Economic Paleontologists and Mineralogists, Pacific Coast Section, Pacific Coast Paleogeography Symposium II, p. 33-70.

Lund, K., 1984, Tectonic history of a continent-island arc boundary, west-central Idaho [Ph.D. dissertation]: The Pennsylvania State University, University Park, 207 p.

Manduca, C. A., and Kuntz, M. A., 1987, Deformed plutonic rocks on the western edge of the Idaho batholith near McCall, Idaho: Geological Society of America Abstracts with Programs, v. 19, no. 5, p. 318.

Manduca, C. A., Silver, L. T., and Taylor, H. P., 1986, Study of an abrupt change in Sr_i and $\delta^{18}O$ in granodiorite in the western border of the Idaho batholith [abs.]: Eos, Transactions of the American Geophysical Union, v. 67, no. 44, p. 1268.

Selverstone, J., Aliberti, E., and Wernicke, B., 1987, Petrologic constraints on the tectonic evolution of the arc-continent collision zone in west-central Idaho: Geological Society of America Abstracts with Programs, v. 19, no. 7, p. 837.

Silberling, N. J., Jones, D. L., Blake, Jr., M. C., and Howell, D. C., 1984, Lithotectonic terrane map of the western conterminous United States, *in* Tectonic terrane map of the northern cordillera, N. J. Silberling, and D. L. Jones, *(eds.)*: U.S. Geological Survey Open-File Report OF-84523, part C, p. C1-C43.

Snee L. W., Sutter, J. F., Lund, K., Balcer, B. E., and Evans, K. V., 1987, $^{40}Ar/^{39}Ar$ age-spectrum data for metamorphic and plutonic rocks from west-central Idaho: U.S. Geological Survey Open-File Report 87-0052, 20 p.

Hells Canyon on the Snake River, Idaho-Oregon. (Roy M. Breckenridge photo, courtesy Idaho Division of Tourism.)

FIELD GUIDE
TO THE IRON DYKE MINE, BAKER COUNTY, OREGON

Steven Bussey
Colorado School of Mines
Golden, Colorado 80401

Introduction

On the road from Oxbow, Oregon to the Iron Dyke mine, the first mile is in the Windy Ridge Formation, a sequence of massive rhyolitic flows and flow breccias. Here it is in fault contact with mafic flows of the Hunsaker Creek Formation. To the northeast the contact appears to be depositional, with sediments and felsic pumice-lapilli tuffs overlying the Windy Ridge. Once into the Hunsaker Creek Formation, the road passes rapidly from one lithology to another. Lithologies representative of the Hunsaker Creek Formation are exposed in all of the small tributary canyons heading west from the Snake River. Bedding can be observed in sediments and volcaniclastic units while most other units are massive. The mine is situated in the upper part of the Hunsaker Creek Formation, which consists of tuff epiclastic volcanic breccia, conglomerate, sandstone, siltstone, minor limestone, with lava flows and sills of dacite and basalt.

Road log

Mileage

0.0 Cambridge, Idaho, **Proceed west** on Idaho State Route 71.

28.6

28.6 Cross Snake River bridge into Oregon, downstream from Brownlee Dam.

10.9

39.5 **Turn right** at "T" intersection at Copperfield Park (Oxbow, Oregon).

0.1

39.6 **Turn left** onto gravel road leading to Homestead and Iron Dyke mine.

3.5

43.1 **Stop 1: Park along road** and proceed on foot up Holbrook Creek to examine Hunsaker Creek Formation (Figures 1, 2, Bussey, this volume).

Lithologies typical of the Hunsaker Creek Formation can be seen in exposures along Holbrook Creek which heads west from the Snake River one half-mile south of the Iron Dyke mine office. Four exposures are briefly described. The farthest one is about one half-mile from the road.

1. Good exposures are present in the powerline roadcut just north of the entrance to Holbrook Creek. Lithologies include interbedded sandstone and mafic lapilli tuff. Mafic breccia with vesicular fragments are associated with mafic lapilli tuff and dark-colored hematite-rich sandstones. Bedding strikes east-west and dips 74°N.
2. Monolithic mafic lapilli tuffs with crude bedding and fossil fragments suggest an origin as a subaqueous pyroclastic flow or debris flow which gathered fossil fragments during transport. Upstream from this point the mafic lapilli tuff is transitional to a debris flow and contains large blocks of mixed lithologies. Exposures of felsic pumice lapilli tuffs also become more common.
3. Light-colored exposures of flow banded, aphanitic rhyolite occur on both sides of the creek. The origin of this unit is uncertain, but it may be a large block within the debris flow, which also contains frag-

ments of vesicular basalt and red siltstone.

4. A *lens of massive, heterolithic conglomerate* is overlain by sandstone which, in turn, is overlain by a felsic flow breccia with large, flow-banded blocks at its base. The local occurrence of the conglomerate suggests that it filled a small depression or channel along the flank of the submerged island arc. This rock type is typical of the Hunsaker Creek Formation.

0.3

43.4 **Turn left and park** at entrance to Iron Dyke mine property. (For further descriptions of the Iron Dyke mine, see Bussey, this volume.)

APPENDIX

ACCESS ROAD LOGS TO FIELD GUIDES

An overview of some of the Precambrian crystalline rocks of southwestern Montana and northwestern Wyoming

Columbus, Montana to Butte, Montana

Mileage

0.0 Exit 408 from Interstate 90 to Columbus; **proceed south.**

0.9

0.9 Columbus; **turn right** (west) on Montana Route 78 toward Absarokee.

0.3

1.2 **Turn left** and cross Yellowstone River; **continue southwest** on Montana Route 78.

13.8

15.0 Absarokee; **proceed south** on Montana Route 78.

2.8

17.8 Junction: County Route 419; **turn right** (west) to Fishtail and Nye.

3.4

21.2 Fishtail; **proceed southwest** on County Route 419 toward Nye.

1.0

22.2 Intersection with West Rosebud road; **bear right** on County Route 419.

9.5

31.7 Benbow Mine road to left; **continue on** County Route 419 toward Nye.

5.9

37.6 Cross Stillwater River.

0.2

37.8 Nye Post Office.

0.3

38.1 Junction with West Fork Stillwater River road to north; **continue straight ahead.**

5.0

43.1 Office of Stillwater Mining Company (in old Nye hospital) on north side of highway. Access to Mountain View and West Fork areas; gate is usually locked. *INQUIRE AT STILLWATER MINING COMPANY OFFICES FOR ACCESS PERMISSION AND INFORMATION.* Field stops begin at the end of the Mouat mine road, approximately 6.4 miles from the Stillwater Mining Company office.

Field guide to Mountain View and West Fork area, Stillwater Complex, Montana by I. S. McCallum

0.0 From Stillwater Mining Company office, **retrace route** back to junction of County Route 419 with Montana Route 78. **Turn right** (south) on Montana Route 78 toward Red Lodge.

10.0

10.0 Roscoe junction; **continue southeast** on Montana Route 78.

19.4

29.4 Enter town limits of Red Lodge.

0.4

29.8 Junction; **turn right** (south) on U.S. Highway 212.

Red Lodge to Beartooth Lake

Field guide to an Archean transect, eastern Beartooth Mountains, Montana by Paul A. Mueller and Joseph L. Wooden. Total distance 52.7 miles.

From Stop 4 (of the above field guide), follow U.S. Highway 212 to Cooke City (approximately 19 miles).

Cooke City. Silver Gate and Yellowstone National Park northeast entrance (approximately 4 miles).

In Yellowstone National Park, follow highway across northern part of Park, (approximately 29 miles to Tower Junction).

Next road log begins at West Yellowstone.

At this point two choices of routes through Yellowstone National Park are available.

1) **Turn right** (northwest) to Mammoth Hot Springs (approximately 18 miles). At Mammoth Hot Springs, **turn south** to Norris Junction (approximately 21 miles).

2) **Turn left** (southwest) to Canyon Junction (via Dunraven Pass, approximately 19 miles). At Canyon Junction **turn right** (west) to Norris Junction (approximately 12 miles).

From Norris Junction, **proceed southwest** to Madison Junction (approximately 14 miles).

At Madison Junction **turn right** (west) to the western Yellowstone National Park boundary and the town of West Yellowstone (approximately 14 miles).

West Yellowstone to Indian Creek

Field guide to pre-Beltian geology of the southern Madison and Gravelly ranges, southwest Montana by Eric A. Erslev. Total distance 57.2 miles.

Follow U.S. Highway 287 north to Ennis from Indian Creek (approximately 18 miles).

On north side of Ennis, **bear left** (west) on Montana Route 287 to Alder (via Virginia City and Nevada City, approximately 24 miles).

At Alder, **turn right** (northwest) on Montana Route 287 to Twin Bridges (via Sheridan, approximately 20 miles).

Field guide to the Highland Mountains, southwest Montana by J. Michael O'Neill. Total distance one way 51.1 miles, including 5-mile foot traverse.

An overview from the continent into the Mesozoic suture zone, central Idaho and northeastern Oregon

Missoula, Montana to Lowell, Idaho

0.0 Exit from Interstate 90 at Orange Street Exit in Missoula (Exit 104); **proceed south** on Orange Street following signs to U.S. Highway 93.
0.8
0.8 West Broadway
0.1
0.9 Cross Clark Fork River
0.6
1.5 Stephens Street; **bear right**
0.7
2.2 Mount Avenue; **bear left** following U.S. Highway 93.
0.3
2.5 Brooks Street; **turn right.**
2.4
4.9 Cross Bitterroot River.

Field guide to a section through the northern Idaho batholith and surrounding high-grade metamorphic rocks by Donald W. Hyndman and David A. Foster. Total distance 167 miles.

From Lowell continue westerly on U.S. Highway 12 through Syringa (past Kooskia) to Kamiah (approximately 30 miles from Lowell).

Kamiah to Orofino area

Field guide to mylonitic deformation and sense of displacement in mylonitic rocks near Orofino, Idaho by Luther M. Strayer, IV. Approximately 32 miles, including return to Orofino.

Field guide to variations in lithologies and deformation styles west of Orofino, Idaho by Gary F. Davidson. Approximately 27 miles, including return to Orofino.

From Orofino **proceed southeast** 30 miles on U.S. Highway 12 to junction with U.S. Highway 95 just east of Kooskia. **Turn right** (south) on U.S. Highway 95 and continue 26 miles to Grangeville. **Continue south** on U.S. Highway 95 along the Salmon River to Slate Creek Ranger Station, approximately 26 miles south of Grangeville.

Slate Creek area

Field guide to a traverse (Slate Creek) across the Salmon River suture zone, west-central Idaho by Karen Lund. Approximately 67 miles, including retracing of route to Slate Creek Ranger Station.

From Slate Creek Ranger Station **continue south** 52 miles on U.S. Highway 95 to Riggins.

Riggins to New Meadows to Boise, Idaho

Field guide to a transect across an island arc-continent boundary in west-central Idaho by Elaine A. Aliberti and Cathryn Allen Manduca. Total mileage, including retracing of route to New Meadows is 99.3 miles.

New Meadows; **turn left** (west) on U.S. Highway 95 and proceed southerly 45 miles to Cambridge.

Field guide to the Iron Dyke Mine, Baker County, Oregon by Steven Bussey. Total mileage, including retracing of route to Cambridge is 86.8 miles.

0.0 Cambridge; **turn right** and proceed southerly on U.S. Highway 95.

32.0

32.0 Weiser, Idaho

18.0

50.0 Payette, Idaho

4.0

54.0 Enter Interstate Highway 84 and proceed southeasterly.

49.0

103.0 Boise, Idaho

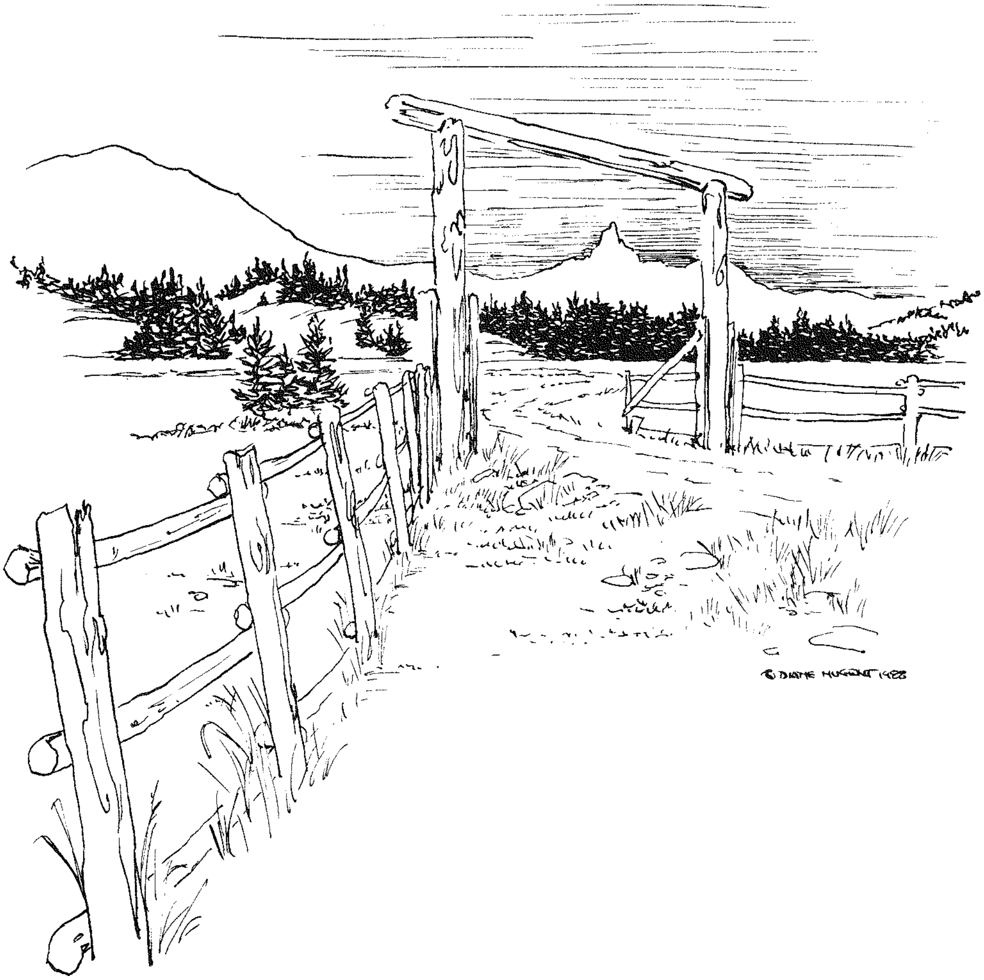

Production Information

Camera-ready copy prepared on EditWriter 7500 by MBMG.

Stock:	Cover —	17 pt. Kivar Chrome
	Text —	70 lb. Dixon Matte
Ink:	Cover —	PMS 160 (Brown)
Composition:	*Univers* type	
	Heads —	1st order—18 pt. theme, leaded 2 pt.
		2d order—14 pt. theme, leaded 2 pt.
		3d order—12 pt. theme, leaded 2 pt.
	Text —	10 pt. theme, leaded 2 pt.
Presswork:	Heidelberg Sorkz 25½"	
Binding:	Perfect Bind	
Press run:	1,500 copies	